Mathematical Problems in Engineering

Control Problems of Nonlinear Systems with Applications 2021

Lead Guest Editor: Rongwei Guo
Guest Editors: Yi Qi, Renming Yang, and Cuimei Jiang

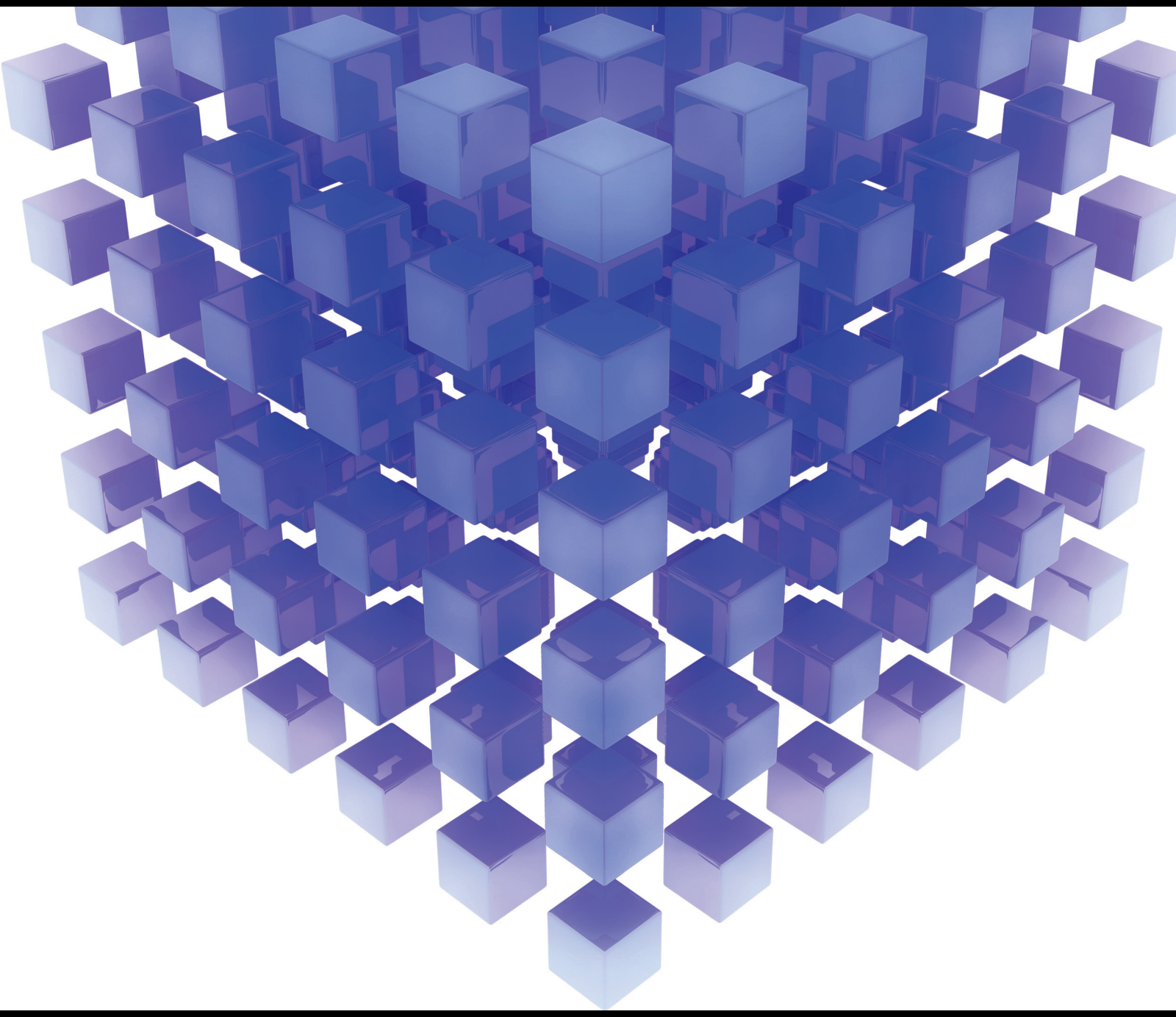

Control Problems of Nonlinear Systems with Applications 2021

Mathematical Problems in Engineering

Control Problems of Nonlinear Systems with Applications 2021

Lead Guest Editor: Rongwei Guo
Guest Editors: Yi Qi, Renming Yang, and Cuimei Jiang

Contents

Contents

Hindawi
Mathematical Problems in Engineering
Volume 2023, Article ID 5748824, 13 pages
https://doi.org/10.1155/2023/5748824

Research Article

Robust Control for Stochastic Nonlinear Delay Systems with Jumps

Linlin Zhang[1] and Xingzhen Bai[2]

[1]*College of Mathematics and Systems Science, Shandong University of Science and Technology, Qingdao 266590, China*
[2]*College of Electrical Engineering and Automation, Shandong University of Science and Technology, Qingdao 266590, China*

Correspondence should be addressed to Xingzhen Bai; xzbai@163.com

Received 6 May 2021; Revised 9 July 2021; Accepted 7 October 2021; Published 27 May 2023

Academic Editor: Yi Qi

The problem of infinite horizon H_∞ control for general delayed nonlinear stochastic Markov jump systems with the infinite jumping parameters is considered in this paper, in which the noise is dependent on the state, control, and external disturbance. The coupled Hamilton–Jacobi inequalities (HJIs)-based sufficient condition is given to ensure the existence of the H_∞ controller. As a corollary, infinite horizon H_∞ controllers are designed for nonlinear stochastic time-delay systems without jumps by solving a series of coupled HJIs. Besides, the effectiveness of the proposed method is verified by a numerical example.

1. Introduction

As we all know, Markov jump systems have been used widely both in theory and in engineering over the past decades [1]. In the practical life, the occurrence of parts failures and the change of the relationship between subsystems, as well as the sudden environmental disturbances, will cause the jump of systems structure or parameters. The Markov jump system may be a prefect model in describing these phenomena. As perturbations are unavoidable in practical systems [2], in recent years, many researchers have paid attention to the problem of stability and control for It $\hat{o}$-type Markov jumps stochastic systems; see [3–6] and the references therein.

It is noteworthy that most of the existing works on jump systems have been carried out in the finite state Markov process, that is, its state space is a finite set. In fact, some physical variables may be described more appropriately with infinite jump states. For instance, in the solar heat receiver model proposed in [7], the atmospheric parameters take the values in a Borel measurable infinite set. It is needed to emphasize that there are essential differences in performance between finite and infinite Markov jump systems (IMJSs), and the causal and anticausal Lyapunov operators of infinite Markov jump systems being no more adjoint is the reason. The authors [8] have pointed out that exponential stability and stochastic stability for IMJSs are no longer equivalent. In addition, IMJSs have attracted an increasing interest; see [9–16].

On the other hand, time delay and nonlinearity, which often occur in engineering, biological, and economic systems, are the important reasons for systems to be instable or performance being destroyed [17]. Notice that the robust stability and H_∞ control have been investigated a little for nonlinear stochastic systems with jumps and delay. The authors in [18] solved the infinite horizon H_∞ control for nonlinear IMJSs with disturbance-, control-, and state-dependent noise, but the effects of time delay is neglected. For the nonlinear delayed system with finite Markov jump, the authors in [19] designed its H_∞ controller. In conclusion, the research on stability and control of nonlinear stochastic systems with infinite Markov jumps and time delay has important theoretical meaning. However, as far as we know, these issues have not been fully investigated so far, which greatly inspires our research interest.

The problem of H_∞ control is mainly solved in this paper for general nonlinear delay stochastic systems with infinite Markov jumps and (x, u, v)-dependent noise. The main contributions are concluded as follows: First, we

develop an infinite horizon asymptotically mean square stable H_∞ controller design method based on the complete square technique and Itô's formula. A numerical example shows the effectiveness of the proposed method. Second, a nonlinear stochastic bounded real lemma is derived as a byproduct. Compared with the previous work, our results have a wider range of applications. The work reported in [19], for example, is a special case of this paper.

The following notations are used in this study: R^n: the n-dimensional Euclidean space; $\|x\|$: the Euclidean norm of n-dimensional real vector x; $L^2_{\mathscr{F}}(R^+;R^l)$: the space of all nonanticipative stochastic processes $y(t)\in R^l$ with respect to an increasing σ-algebra $\mathscr{F}_t$ satisfying $\|y(t)\|_{L^2_{\mathscr{F}}(R^+;R^l)} = E(\int_0^\infty \|y(t)\|^2 dt)^{1/2} < \infty$; I: the identity matrix; A': the transpose of matrix A; $A\geq 0\,(A>0)$: A is positive semi-definite (positive definite); $C^{2,1}(U;T)$: the class of functions $V(x,t)$ which are twice continuously differentiable with respect to $x\in U$ and once continuously differentiable with respect to $t\in T$ except possibly at the point $x=0$; $C([-\delta,0];R^n)$: the vector space of all continuous R^n-valued functions defined on $[-\delta,0]$; $col(x_1,x_2,\ldots,x_n) := [x_1,x_2,\ldots,x_n]'$; and S_n: the set of symmetric matrices.

2. Preliminaries

Consider the following nonlinear delay system with infinite jumps:

$$\begin{cases} dx(t) = [f(x,x_\delta,t,\theta_t) + k(x,x_\delta,t,\theta_t)u + s(x,x_\delta,t,\theta_t)v]dt, \\ +[g(x,x_\delta,t,\theta_t) + h(x,x_\delta,t,\theta_t)u + q(x,x_\delta,t,\theta_t)v]d\omega(t), \\ z(t) = \mathrm{col}(m(x,x_\delta,t,\theta_t),u) := \begin{pmatrix} m(x,x_\delta,t,\theta_t) \\ u \end{pmatrix}, \\ x(t) = \Phi(t) \in \mathscr{C}^b_{\mathscr{F}_0}([-\delta,0];R^n), \end{cases} \tag{1}$$

where $x_\delta = x(t-\delta)$ is the time delay state, $x(t)\in R^n$ is the system state, $u(t)\in R^{n_u}$ is the control input, $v(t)\in R^{n_v}$ represents the multiplicative noise, and $z(t)\in R^{n_z}$ is the measured output. $\omega(t)$ is the standard one-dimensional Wiener process on a complete filtered space $(\Omega,\mathscr{F},\{\mathscr{F}_t\}_{t\in R^+},P)$, and the filtration $\{\mathscr{F}_t\}_{t\in R^+}$ satisfies usual conditions. $\mathscr{C}^b_{\mathscr{F}_0}([-\delta,0];R^+)$ defines all $\mathscr{F}$-measurable bounded $\mathscr{C}([-\delta,0];R^+)$-valued random variable $\varphi = \{\varphi(\xi): -\delta\leq\xi\leq 0\}$ with $E\|\varphi\|^2<\infty$, where $\|\varphi\| = \sup_{-\delta\leq\xi\leq 0}\|\varphi(\xi)\|$. The jumping process θ_t is a continuous-time discrete-state Markov process which takes values in an infinite set $D=\{1,2,\cdots\}$ with the generator $\Gamma = (\pi_{rh})_{r,h\in D}$, that is,

$$P\{\theta_{t+k} = h \mid \theta_t = r\} = \begin{cases} \pi_{rh}k + o(k), & \text{if } r\neq h, \\ 1+\pi_{rr}k + o(k), & \text{if } r = h, \end{cases} \tag{2}$$

where $k>0$, $\lim_{k\longrightarrow 0}(o(k)/k) = 0$, $\pi_{rh}\geq 0\,(r,h\in D, r\neq h)$ is the switching rate from mode r at time t to mode h at time $t+k$ and $\pi_{rh} = -\sum_{h\in D, r\neq h}\pi_{rh} < \infty$ for all $r\in D$. The processes θ_t and $\omega(t)$ are supposed to be independent in this paper. For every $\theta_t = r\in D$, the local Lipschitz condition and the linear growth condition are satisfied for f,k,s,g,h,q, and m, which can ensure that system (1) has a unique strong solution [6].

Let $f(0,0,t,r)\equiv 0$, $g(0,0,t,r)\equiv 0$, and $\forall(t,r)\in R\times D$. For $V\in\mathscr{C}^{2,1}(R^n\times R\times D;R)$, the following infinitesimal generator $\mathscr{L}V$: $R^n\times R^n\times R\times D\longrightarrow R$ associated with (1) is denoted [6]:

$$\begin{aligned} \mathscr{L}V(x,y,t,r) = {} & \frac{\partial V(x,t,r)}{\partial t} + \frac{\partial V'(x,t,r)}{\partial x}[f(x,y,t,r) + k(x,y,t,r)u + l(x,y,t,r)v] \\ & + \frac{1}{2}[g(x,y,t,r) + h(x,y,t,r)u + q(x,y,t,r)v]'\frac{\partial V^2(x,t,r)}{\partial x^2} \\ & \times[g(x,y,t,r) + h(x,y,t,r)u + q(x,y,t,r)v] + \sum_{h=1}^{\infty}\pi_{rh}V(x,t,r). \end{aligned} \tag{3}$$

To design the infinite horizon H_∞ controller for system (1), the internal stability requirement is needed. Thus, the definition of stochastic stability is introduced as follows.

Definition 1 (see [6]). The nonlinear stochastic delayed system given by

$$\begin{cases} dx(t) = f(x,x_\delta,t,\theta_t)dt + g(x,x_\delta,t,\theta_t)d\omega, \\ x(t) = \Phi(t)\in\mathscr{C}^b_{\mathscr{F}_0}([-\delta,0];R^n), \end{cases} \tag{4}$$

is stable in probability (SIP) if

$$\lim_{x_0\longrightarrow 0} P\left(\sup_{t\geq 0}\|x(t)\| > \varepsilon\right) = 0, \quad \forall\varepsilon>0. \tag{5}$$

If system (4) is SIP and

$$P\left\{\lim_{t\longrightarrow\infty} x(t)=0\right\}=1, \tag{6}$$

then it is called to be globally asymptotically stable in probability (GASIP). System (4) is asymptotically stable in mean square (ASMS) if

$$\lim_{t\longrightarrow\infty} E\|x(t)\|^2=0. \tag{7}$$

Definition 2. For given $\gamma>0$, $u(t)=u^*(t)\in L^2_{\mathscr{F}}(R^+;R^{n_u})$ is called an infinite horizon H_∞ controller for system (1), if the following conditions are met:

(i) When $v=0$, system (1) with $u(t)=u^*(t)$ is internally stable, i.e., the system

$$\begin{aligned}\mathrm{d}x(t)=&\left[f(x,x_\delta,t,\theta_t)+h(x,x_\delta,t,\theta_t)u^*(t)\right]\mathrm{d}t\\&+\left[g(x,x_\delta,t,\theta_t)+h(x,x_\delta,t,\theta_t)u^*(t)\right]\mathrm{d}\omega,\end{aligned} \tag{8}$$

is ASMS.

(ii) For $\forall v\in L^2_{\mathscr{F}}(R^+;R^{n_v})\neq 0$,

$$\|z\|_{L^2_{\mathscr{F}}(R^+;R^{n_z})}\le\gamma\|v\|_{L^2_{\mathscr{F}}(R^+;R^{n_v})},\quad x(0)=0. \tag{9}$$

Remark 3. Let the perturbation operator $\|\mathscr{L}^{u^*}_\infty\|$ be denoted by $\mathscr{L}^{u^*}_\infty$: $L^2_{\mathscr{F}}(R^+;R^{n_v})\mapsto L^2_{\mathscr{F}}(R^+;R^{n_z})$ as

$$\mathscr{L}^{u^*}_\infty(v)=z(x(t,u^*,v,\theta_t)),\quad t\ge 0. \tag{10}$$

Its norm is

$$\left\|\mathscr{L}^{u^*}_\infty\right\|=\sup_{\substack{v\in L^2_{\mathscr{F}}(R^+;R^{n_z})\\ v\neq 0,x_0=0,\theta_0\in D}}\frac{\|z\|_{L^2_{\mathscr{F}}(R^+;R^{n_z})}}{\|v\|_{L^2_{\mathscr{F}}(R^+;R^{n_v})}}. \tag{11}$$

It is easy to verify that (9) is equivalent to $\|\mathscr{L}^{u^*}_\infty\|\le\gamma$.

Lemma 4 (see [20]). *If there exists a positive Lyapunov function $V(x,t,r)\in C^{2,1}(R^n\times R\times D;R)$ satisfying $\mathscr{L}V(x,t,r)<0$ for $x\neq 0$ and $V(x,t,r)$ being radially unbounded, i.e.,*

$$\lim_{\|x\|\longrightarrow\infty}\inf_{t>0}V(x,t,r)=\infty, \tag{12}$$

then the point $x\equiv 0$ of (8) is GASIP.

Lemma 5 (see [21]). *For $z,b\in R^n$, $\mathscr{B}\in S_n$, and $\mathscr{B}^{-1}$ exists, we have*

$$z'\mathscr{B}z+b'z+z'b=\left(z+\mathscr{B}^{-1}b\right)'\mathscr{B}\left(z+\mathscr{B}^{-1}b\right)-b'\mathscr{B}^{-1}b. \tag{13}$$

3. Main Results

A sufficient condition is obtained for the infinite horizon H_∞ control of system (1) as follows.

Theorem 6. *For a given disturbance attenuation level $\gamma>0$, assume that there exist a set of positive functions $V(x,t,\theta_t)\in C^{2,1}(R^n\times R\times D;R)$ which have an infinitesimal upper limit (i.e., $\lim_{\|x(t)\|\longrightarrow\infty t>0}\inf V(x,t,\theta_t)=\infty$), $V(0,0,r)=0$, and $\partial^2V(x,t,\theta_t)/\partial x^2\ge 0$ for all nonzero $x\in R^n$, $r\in D$. Besides, one assumes that $V(x,t,\theta_t)>a\|x(t)\|^2$ for some $a>0$. If $V(x,t,\theta_t)$ solves the following HJIs:*

$$\begin{cases}\Pi_r:=\dfrac{\partial V_r}{\partial t}+\dfrac{\partial V_r'}{\partial x}f_r+\dfrac{1}{2}g_r'\dfrac{\partial^2V_r}{\partial x^2}g_r+m_r'm_r+\displaystyle\sum_{h=1}^{\infty}\pi_{rh}V_h\\[2ex] +\dfrac{1}{4}\left(g_r'\dfrac{\partial^2V_r}{\partial x^2}q_r+\dfrac{\partial V_r'}{\partial x}s_r\right)\left(\gamma^2I-q_r'\dfrac{\partial^2V_r}{\partial x^2}q_r\right)^{-1}\left(q_r'\dfrac{\partial^2V_r}{\partial x^2}g_r+s_r'\dfrac{\partial V_r}{\partial x}\right)\\[2ex] -\dfrac{1}{4}\left(g_r'\dfrac{\partial^2V_r}{\partial x^2}h_r+\dfrac{\partial V_r'}{\partial x}k_r\right)\left(I+h_r'\dfrac{\partial^2V_r}{\partial x^2}h_r\right)^{-1}\left(h_r'\dfrac{\partial^2V_r}{\partial x^2}g_r+k_r'\dfrac{\partial V_r}{\partial x}\right)<0,\\[2ex] \gamma^2I-q_r'\dfrac{\partial^2V_r}{\partial x^2}q_r>0,\quad r\in D,\end{cases} \tag{14}$$

where

$$\begin{aligned}&[V_r,f_r,k_r,s_r,g_r,h_r,q_r,m_r]=\\&\quad[V(x,t,\theta_t),f(x,y,t,\theta_t),k(x,y,t,\theta_t),s(x,y,t,\theta_t),g(x,y,t,\theta_t),h(x,y,t,\theta_t),q(x,y,t,\theta_t),m(x,y,t,\theta_t)],\end{aligned} \tag{15}$$

for all $x, y \in R^n$, $t \geq 0$, and $r \in D$, then

$$u_r^* = -\frac{1}{2}\left(I + h_r'\frac{\partial^2 V_r}{\partial x^2}h_r\right)^{-1}\left(h_r'\frac{\partial^2 V_r}{\partial x^2}g_r + k_r'\frac{\partial V_r}{\partial x}\right), \tag{16}$$

is an asymptotically mean square H_∞ control for system (1).

Proof. First, we prove that system (8) is ASMS. For $r \in D$, we have the infinitesimal operator $\mathscr{L}_{u^*}$ of system (8).

$$\begin{aligned}
&\mathscr{L}_{u^*}V(x, y, t, \theta_t)\mid_{v=0} \\
&= \frac{\partial V_r}{\partial t} + \frac{\partial V_r'}{\partial x}(f_r + k_r u_r^*) + \sum_{h=1}^{\infty}\pi_{rh}V_h + \frac{1}{2}(g_r + h_r u_r^*)'\frac{\partial^2 V_r}{\partial x^2}(g_r + h_r u_r^*) \\
&= \frac{\partial V_r}{\partial t} + \frac{\partial V_r'}{\partial x}f_r + \frac{\partial V_r'}{\partial x}k_r u_r^* + \sum_{h=1}^{\infty}\pi_{rh}V_h + \frac{1}{2}g_r'\frac{\partial^2 V_r}{\partial x^2}g_r \\
&\quad + \frac{1}{2}u_r^{*'}h_r'\frac{\partial^2 V_r}{\partial x^2}g_r + \frac{1}{2}g_r'\frac{\partial^2 V_r}{\partial x^2}h_r u_r^* + \frac{1}{2}u_r^{*'}h_r'\frac{\partial^2 V_r}{\partial x^2}h_r u_r^* \\
&= \frac{\partial V_r}{\partial t} + \frac{\partial V_r'}{\partial x}f_r + \frac{1}{2}g_r'\frac{\partial^2 V_r}{\partial x^2}g_r + \sum_{h=1}^{\infty}\pi_{rh}V_h + \Gamma_{1r} + \Gamma_{2r},
\end{aligned} \tag{17}$$

where

$$\begin{aligned}
\Gamma_{1r} &= \frac{\partial V_r'}{\partial x}k_r u_r^* + \frac{1}{2}u_r^* h_r'\frac{\partial^2 V_r}{\partial x^2}g_r + \frac{1}{2}g_r'\frac{\partial^2 V_r}{\partial x^2}h_r u_r^* \\
&= -\frac{1}{2}\frac{\partial V_r'}{\partial x}k_r\left(I + h_r'\frac{\partial^2 V_r}{\partial x^2}h_r\right)^{-1}\left(h_r'\frac{\partial^2 V_r}{\partial x^2}g_r + k_r'\frac{\partial V_r}{\partial x}\right) \\
&\quad - \frac{1}{4}\left(g_r'\frac{\partial^2 V_r}{\partial x^2}h_r + \frac{\partial V_r'}{\partial x}k_r\right)\left(I + h_r'\frac{\partial^2 V_r}{\partial x^2}h_r\right)^{-1}h_r'\frac{\partial^2 V_r}{\partial x^2}g_r \\
&\quad - \frac{1}{4}g_r'\frac{\partial^2 V_r}{\partial x^2}h_r\left(I + h_r'\frac{\partial^2 V_r}{\partial x^2}h_r\right)^{-1}\left(h_r'\frac{\partial^2 V_r}{\partial x^2}g_r + k_r'\frac{\partial V_r}{\partial x}\right) \\
&= -\frac{1}{2}\left(\frac{\partial V_r'}{\partial x}k_r + g_r'\frac{\partial^2 V_r}{\partial x^2}h_r\right)\left(I + h_r'\frac{\partial^2 V_r}{\partial x^2}h_r\right)^{-1}\left(h_r'\frac{\partial^2 V_r}{\partial x^2}g_r + k_r'\frac{\partial V_r}{\partial x}\right),
\end{aligned} \tag{18}$$

and

$$\begin{aligned}
\Gamma_{2r} &= \frac{1}{2}u_r^{*'}h_r'\frac{\partial^2 V_r}{\partial x^2}h_r u_r^* \\
&= \frac{1}{8}\left(g_r'\frac{\partial^2 V_r}{\partial x^2}h_r + \frac{\partial V_r'}{\partial x}k_r\right)\left(I + h_r'\frac{\partial^2 V_r}{\partial x^2}h_r\right)^{-1}h_r'\frac{\partial^2 V_r}{\partial x^2}h_r \\
&\quad \times\left(I + h_r'\frac{\partial^2 V_r}{\partial x^2}h_r\right)^{-1}\left(h_r'\frac{\partial^2 V_r}{\partial x^2}g_r + k_r'\frac{\partial V_r}{\partial x}\right) \\
&\leq \frac{1}{8}\left(g_r'\frac{\partial^2 V_r}{\partial x^2}h_r + \frac{\partial V_r'}{\partial x}k_r\right)\left(I + h_r'\frac{\partial^2 V_r}{\partial x^2}h_r\right)^{-1}\left(h_r'\frac{\partial^2 V_r}{\partial x^2}g_r + k_r'\frac{\partial V_r}{\partial x}\right).
\end{aligned} \tag{19}$$

Substituting (18) and (19) into (17), and considering (14), one gets

$$
\begin{aligned}
&\mathscr{L}_{u^*}V(x,y,t,\theta_t)|_{v=0}\\
&=\frac{\partial V_r}{\partial t}+\frac{\partial V_r'}{\partial x}f_r+\frac{1}{2}g_r'\frac{\partial^2 V_r}{\partial x^2}g_r+\sum_{h=1}^{\infty}\pi_{rh}V_h\\
&\quad-\frac{1}{2}\left(\frac{\partial V_r'}{\partial x}k_r+g_r'\frac{\partial^2 V_r}{\partial x^2}h_r\right)\left(I+h_r'\frac{\partial^2 V_r}{\partial x^2}h_r\right)^{-1}\left(h_r'\frac{\partial^2 V_r}{\partial x^2}g_r+k_r'\frac{\partial V_r}{\partial x}\right)\\
&\quad+\frac{1}{8}\left(g_r'\frac{\partial^2 V_r}{\partial x^2}h_r+\frac{\partial V_r'}{\partial x}k_r\right)\left(I+h_r'\frac{\partial^2 V_r}{\partial x^2}h_r\right)^{-1}\left(h_r'\frac{\partial^2 V_r}{\partial x^2}g_r+k_r'\frac{\partial V_r}{\partial x}\right)\\
&\le\frac{\partial V_r}{\partial t}+\frac{\partial V_r'}{\partial x}f_r+\frac{1}{2}g_r'\frac{\partial^2 V_r}{\partial x^2}g_r+\sum_{h=1}^{\infty}\pi_{rh}V_h\\
&\quad-\frac{1}{4}\left(g_r'\frac{\partial^2 V_r}{\partial x^2}h_r+\frac{\partial V_r'}{\partial x}k_r\right)\left(I+h_r'\frac{\partial^2 V_r}{\partial x^2}h_r\right)^{-1}\left(h_r'\frac{\partial^2 V_r}{\partial x^2}g_r+k_r'\frac{\partial V_r}{\partial x}\right)\\
&<-m_r'm_r-\frac{1}{4}\left(g_r'\frac{\partial^2 V_r}{\partial x^2}g_r+\frac{\partial V_r'}{\partial x}s_r\right)\left(\gamma^2 I-q_r'\frac{\partial^2 V_r}{\partial x^2}q_r\right)^{-1}\left(g_r'\frac{\partial^2 V_r}{\partial x^2}q_r+\frac{\partial V_r'}{\partial x}s_r\right)\\
&\le 0.
\end{aligned}
\tag{20}
$$

Based on Lemma 4, (8) is GASIP. Besides, by using It $\hat{o}'s$ formula, for $t\ge s\ge 0$, one obtains

$$
\begin{aligned}
EV(x(t),t,\theta_t)&=EV(x(s),s,\theta_s)+E\int_s^t \mathscr{L}_{u^*}V(x(\tau),\tau,\theta_\tau)\Big|_{v=0}\mathrm{d}\tau\\
&\quad+E\int_s^t[g(x(\tau),\tau,\theta_\tau)+h(x(\tau),\tau,\theta_\tau)u^*(\tau)]V(x(\tau),\tau,\theta_\tau)\mathrm{d}\omega(\tau)\\
&=EV(x(s),s,\theta_s)+E\int_s^t \mathscr{L}_{u^*}V(x(\tau),\tau,\theta_\tau)\Big|_{v=0}\mathrm{d}\tau\\
&\le EV(x(s),s,\theta_s).
\end{aligned}
\tag{21}
$$

It is easy to find that $E|V(x(t),t,\theta_t)|<\infty$. Setting $\tilde{\mathscr{F}}_t=\mathscr{F}_t\cup\sigma(y(s),0\le s\le t)$, then (21) yields

$$
\begin{aligned}
E\left[V(x(t),t,\theta_t)|\tilde{\mathscr{F}}_s\right]&\le E\left[V(x(s),s,\theta_s)|\tilde{\mathscr{F}}_s\right]\\
&\le V(x(s),s,\theta_s)\ a.s.
\end{aligned}
\tag{22}
$$

Accordingly, considering $\left\{\tilde{\mathscr{F}}_t\right\}_{t\in R^+}$, $\left\{V(x(s),s,\theta_s),\tilde{\mathscr{F}}_t,\right.$ $\left.0\le s\le t\right\}$ is a non-negative supermartingale. By Doob's convergence theorem [22], it deduces that $V(x(\infty),\infty,\theta_\infty)=\lim_{t\longrightarrow\infty}V(x(t),t,\theta_t)=0$ $a.s.$ Moreover, $\lim_{t\longrightarrow\infty}EV(x(t),t,\theta_t)=EV(x(\infty),\infty,\theta_\infty)=EV(0,\infty,\theta_\infty)=0.$

Because of $V(x(t),t,\theta_t) \geq a\|x(t)\|^2$ for some $a>0$, then $\lim_{t\longrightarrow\infty} E\|x(t)\|^2 = 0$.

Next, we will prove that (9) holds for system (1). For the initial state $x_0 = 0$, $\theta_0 = r$, and any $T>0$, by using It $\hat{o}'s$ formula, we have

$$
\begin{aligned}
&E\left[V\left(x_T,T,\theta_T\right) - V\left(x(0),0,\theta_0\right)|\theta_0 = r\right] \\
&= E\left\{\int_0^T \mathscr{L}V\left(x,x_\delta,t.\theta_t\right)\mathrm{d}t|\theta_0 = r\right\} \\
&= E\left\{\int_0^T \left[\frac{\partial V_{\theta_t}}{\partial t} + \frac{\partial V_{\theta_t}'}{\partial x}\left(f_{\theta_t} + k_{\theta_t}u + s_{\theta_t}v\right) + \sum_{h=1}^{\infty}\pi_{rh}V_h\right.\right. \\
&\quad \left.\left. + \frac{1}{2}\left(g_{\theta_t} + h_{\theta_t}u + q_{\theta_t}v\right)'\frac{\partial^2 V_{\theta_t}}{\partial x^2}\left(g_{\theta_t} + h_{\theta_t}u + q_{\theta_t}v\right)\right]dt|\theta_0 = r\right\} \\
&= E\left\{\int_0^T \left[\frac{\partial V_{\theta_t}}{\partial t} + \frac{\partial V_{\theta_t}'}{\partial x}\left(f_{\theta_t} + k_{\theta_t}u + s_{\theta_t}v\right) + \sum_{h=1}^{\infty}\pi_{rh}V_h\left\|m_{\theta_t}\right\|^2 + \|u\|^2 - \gamma^2\|v\|^2\right.\right. \\
&\quad \left.\left. + \frac{1}{2}\left(g_{\theta_t} + h_{\theta_t}u + q_{\theta_t}v\right)'\frac{\partial^2 V_{\theta_t}}{\partial x^2}\left(g_{\theta_t} + h_{\theta_t}u + q_{\theta_t}v\right) - \left\|z^2 + \gamma^2\right\|v^2\right]dt|\theta_0 = r\right\} \\
&= E\left\{\int_0^T \left[\frac{\partial V_{\theta_t}}{\partial t} + \frac{\partial V_{\theta_t}'}{\partial x}f_{\theta_t} + \frac{1}{2}g_{\theta_t}'\frac{\partial^2 V_{\theta_t}}{\partial x^2}g_{\theta_t} + m_{\theta_t}'m_{\theta_t} + \sum_{h=1}^{\infty}\pi_{rh}V_h\right.\right. \\
&\quad + v'\left(-\gamma^2 I + \frac{1}{2}q_{\theta_t}'\frac{\partial^2 V_{\theta_t}}{\partial x^2}q_{\theta_t}\right)v + \frac{1}{2}\left(g_{\theta_t}'\frac{\partial^2 V_{\theta_t}}{\partial x^2}q_{\theta_t} + \frac{\partial V_{\theta_t}'}{\partial x s_{\theta_t}}\right)v \\
&\quad + \frac{1}{2}v'\left(s_{\theta_t}'\frac{\partial V_{\theta_t}}{\partial x} + q_{\theta_t}'\frac{\partial^2 V_{\theta_t}}{\partial x^2}g_{\theta_t}\right) + u'\left(I + \frac{1}{2}h_{\theta_t}'\frac{\partial^2 V_{\theta_t}}{\partial x^2}h_{\theta_t}\right)u \\
&\quad + \frac{1}{2}u'\left(h_{\theta_t}'\frac{\partial^2 V_{\theta_t}}{\partial x^2}g_{\theta_t} + k_{\theta_t}'\frac{\partial V_{\theta_t}}{\partial x}\right) + \frac{1}{2}\left(\frac{\partial V_{\theta_t}'}{\partial x}k_{\theta_t} + g_{\theta_t}'\frac{\partial^2 V_{\theta_t}}{\partial x^2}h_{\theta_t}\right)u \\
&\quad \left.\left. + \frac{1}{2}v'q_{\theta_t}'\frac{\partial^2 V_{\theta_t}}{\partial x^2}h_{\theta_t}u + \frac{1}{2}u'h_{\theta_t}'\frac{\partial^2 V_{\theta_t}}{\partial x^2}q_{\theta_t}v - \left\|z^2 + \gamma^2\right\|v^2\right]dt|\theta_0 = r\right\} \\
&= E\left\{\int_0^T \left[\Pi_1\left(x,x_\delta,t,\theta_t\right) + \Pi_2\left(v,x,x_\delta,t,\theta_t\right) + \Pi_3\left(u,x,x_\delta,\theta_t\right)\right.\right. \\
&\quad \left.\left. + \frac{1}{2}v'q_{\theta_t}'\frac{\partial^2 V_{\theta_t}}{\partial x^2}h_{\theta_t}u + \frac{1}{2}u'h_{\theta_t}'\frac{\partial^2 V_{\theta_t}}{\partial x^2}q_{\theta_t}v - \left\|z^2 + \gamma^2\right\|v^2\right]dt|\theta_0 = r\right\},
\end{aligned}
\tag{23}
$$

where

$$\Pi_1(x, x_\delta, t, \theta_t) = \frac{\partial V_{\theta_t}}{\partial t} + \frac{\partial V_{\theta_t}'}{\partial x} f_{\theta_t} + \frac{1}{2} g_{\theta_t}' \frac{\partial^2 V_{\theta_t}}{\partial x^2} g_{\theta_t} + m_{\theta_t}' m_{\theta_t} + \sum_{h=1}^{\infty} \pi_{rh} V_h, \Pi_2$$

$$(v, x, x_\delta, t, \theta_t) = v' \left(-\gamma^2 I + \frac{1}{2} q_{\theta_t}' \frac{\partial^2 V_{\theta_t}}{\partial x^2} q_{\theta_t} \right) v + \frac{1}{2} \left(g_{\theta_t}' \frac{\partial^2 V_{\theta_t}}{\partial x^2} q_{\theta_t} + \frac{\partial V_{\theta_t}'}{\partial x s_{\theta_t}} \right) v$$

$$+ \frac{1}{2} v' \left(s_{\theta_t}' \frac{\partial V_{\theta_t}}{\partial x} + q_{\theta_t}' \frac{\partial^2 V_{\theta_t}}{\partial x^2} g_{\theta_t} \right), \tag{24}$$

$$\Pi_3(u, x, x_\delta, t, \theta_t) = u' \left(I + \frac{1}{2} h_{\theta_t}' \frac{\partial^2 V_{\theta_t}}{\partial x^2} h_{\theta_t} \right) u + \frac{1}{2} u' \left(h_{\theta_t}' \frac{\partial^2 V_{\theta_t}}{\partial x^2} g_{\theta_t} + k_{\theta_t}' \frac{\partial V_{\theta_t}}{\partial x} \right)$$

$$+ \frac{1}{2} \left(\frac{\partial V_{\theta_t}'}{\partial x} k_{\theta_t} + g_{\theta_t}' \frac{\partial^2 V_{\theta_t}}{\partial x^2} h_{\theta_t} \right) u.$$

Considering $\partial^2 V(x, t, \theta_t)/\partial x^2 \geq 0$ and $r \in D$, we assert

$$\frac{1}{2} \left(h_{\theta_t} u - q_{\theta_t} v \right)' \frac{\partial^2 V_{\theta_t}}{\partial x^2} \left(h_{\theta_t} u + q_{\theta_t} v \right) \geq 0, \tag{25}$$

which shows that

$$\frac{1}{2} v' q_{\theta_t}' \frac{\partial^2 V_{\theta_t}}{\partial x^2} h_{\theta_t} u + \frac{1}{2} u' h_{\theta_t}' \frac{\partial^2 V_{\theta_t}}{\partial x^2} q_{\theta_t} v$$
$$\leq \frac{1}{2} u' h_{\theta_t}' \frac{\partial^2 V_{\theta_t}}{\partial x^2} h_{\theta_t} u + \frac{1}{2} v' q_{\theta_t}' \frac{\partial^2 V_{\theta_t}}{\partial x^2} q_{\theta_t} v. \tag{26}$$

Therefore,

$$E\left[V(x_T, T, \theta_T) - V(x_0, 0, \theta_0) | \theta_0 = r \right]$$
$$\leq E\left\{ \int_0^T \left[\Pi_1(x, x_\delta, t, \theta_t) + \Pi_2(v, x, x_\delta, t, \theta_t) + \Pi_3(u, x, x_\delta, t, \theta_t) \right.\right.$$
$$\left.\left. + \frac{1}{2} u' h_{\theta_t}' \frac{\partial^2 V_{\theta_t}}{\partial x^2} h_{\theta_t} u + \frac{1}{2} v' q_{\theta_t}' \frac{\partial^2 V_{\theta_t}}{\partial x^2} q_{\theta_t} v - \|z\|^2 + \gamma^2 \|v\|^2 \right] \mathrm{d}t \,\middle|\, \theta_0 = r \right\} \tag{27}$$
$$= E\left\{ \int_0^T \left[\Pi_1(x, x_\delta, t, \theta_t) + \widetilde{\Pi}_2(v, x, x_\delta, t, \theta_t) + \widetilde{\Pi}_3(u, x, x_\delta, t, \theta_t) \right.\right.$$
$$\left.\left. - \|z\|^2 + \gamma^2 \|v\|^2 \right] \mathrm{d}t \,\middle|\, \theta_0 = r \right\},$$

where

$$\begin{aligned}\widetilde{\Pi}_2(v,x,x_\delta,t,\theta_t) &= v'\left(-\gamma^2 I + q_{\theta_t}'\frac{\partial^2 V_{\theta_t}}{\partial x^2}q_{\theta_t}\right)v + \frac{1}{2}\left(g_{\theta_t}'\frac{\partial^2 V_{\theta_t}}{\partial x^2}q_{\theta_t} + \frac{\partial V_{\theta_t}'}{\partial x}s_{\theta_t}\right)v \\ &\quad + \frac{1}{2}v'\left(s_{\theta_t}'\frac{\partial V_{\theta_t}}{\partial x} + q_{\theta_t}'\frac{\partial^2 V_{\theta_t}}{\partial x^2}g_{\theta_t}\right), \\ \widetilde{\Pi}_3(u,x,x_\delta,t,\theta_t) &= u'\left(I + h_{\theta_t}'\frac{\partial^2 V_{\theta_t}}{\partial x^2}h_{\theta_t}\right)u + \frac{1}{2}u'\left(h_{\theta_t}'\frac{\partial^2 V_{\theta_t}}{\partial x^2}g_{\theta_t} + k_{\theta_t}'\frac{\partial V_{\theta_t}}{\partial x}\right) \\ &\quad + \frac{1}{2}\left(\frac{\partial V_{\theta_t}'}{\partial x}k_{\theta_t} + g_{\theta_t}'\frac{\partial^2 V_{\theta_t}}{\partial x^2}h_{\theta_t}\right)u.\end{aligned} \tag{28}$$

Applying Lemma 5 to $\widetilde{\Pi}_2(v,x,x_\delta,t,\theta_t)$ and $\widetilde{\Pi}_3(u,x,x_\delta,t,\theta_t)$, we arrive at

$$\begin{aligned}&\widetilde{\Pi}_2(v,x,x_\delta,t,\theta_t) \\ &= (v+\Lambda_1)'\left(-\gamma^2 I + q_{\theta_t}'\frac{\partial^2 V_{\theta_t}}{\partial x^2}q_{\theta_t}\right)(v+\Lambda_1) \\ &\quad - \frac{1}{4}\left(\frac{\partial V_{\theta_t}'}{\partial x}s_{\theta_t} + g_{\theta_t}'\frac{\partial^2 V_{\theta_t}}{\partial x^2}q_{\theta_t}\right)\left(-\gamma^2 I + q_{\theta_t}'\frac{\partial^2 V_{\theta_t}}{\partial x^2}q_{\theta_t}\right)^{-1}\left(s_{\theta t}'\frac{\partial V_{\theta_t}}{\partial x} + q_{\theta_t}'\frac{\partial^2 V_{\theta_t}}{\partial x^2}g_{\theta_t}\right),\end{aligned} \tag{29}$$

and

$$\begin{aligned}\widetilde{\Pi}_3(u,x,x_\delta,t,\theta_t) &= (u+\Lambda_2)'\left(I + h_{\theta_t}'\frac{\partial^2 V_{\theta_t}}{\partial x^2}h_{\theta_t}\right)(u+\Lambda_2) \\ &\quad - \frac{1}{4}\left(g_{\theta_t}'\frac{\partial^2 V_{\theta_t}}{\partial x^2}h_{\theta_t} + \frac{\partial V_{\theta_t}'}{\partial x}k_{\theta_t}\right)\left(I + h_{\theta_t}'\frac{\partial^2 V_{\theta_t}}{\partial x^2}h_{\theta_t}\right)^{-1}\left(k_{\theta_t}'\frac{\partial V_{\theta_t}}{\partial x} + h_{\theta_t}'\frac{\partial^2 V_{\theta_t}}{\partial x^2}g_{\theta_t}\right),\end{aligned} \tag{30}$$

where

$$\Lambda_1 = \frac{1}{2}\left(\gamma^2 I + q_{\theta_t}{}'\frac{\partial^2 V_{\theta_t}}{\partial x^2} q_{\theta_t}\right)^{-1}\left(q_{\theta_t}{}'\frac{\partial^2 V_{\theta_t}}{\partial x^2} g_{\theta_t} + s_{\theta_t}{}'\frac{\partial V_{\theta_t}}{\partial x}\right),$$

$$\Lambda_2 = \frac{1}{2}\left(I + h_{\theta_t}{}'\frac{\partial^2 V_{\theta_t}}{\partial x^2} h_{\theta_t}\right)^{-1}\left(h_{\theta_t}{}'\frac{\partial^2 V_{\theta_t}}{\partial x^2} g_{\theta_t} + k_{\theta_t}{}'\frac{\partial V_{\theta_t}}{\partial x}\right). \tag{31}$$

Substituting (29) and (30) into (27), and considering (14), one infers that

$$\begin{aligned} &E\left[V\left(x_T, T, \theta_T\right) - V\left(x_0, 0, \theta_0\right)|\theta_0 = r\right] \\ &\le E\left\{\int_0^T \left[\left(v + \Lambda_1\right)'\left(-\gamma^2 I + q_{\theta_t}{}'\frac{\partial^2 V_{\theta_t}}{\partial x^2} q_{\theta_t}\right)\left(v + \Lambda_1\right)\right.\right. \\ &\left.\left. +\left(u + \Lambda_2\right)'\left(I + h_{\theta_t}{}'\frac{\partial^2 V_{\theta_t}}{\partial x^2} h_{\theta_t} h_{\theta_t}\right)\left(u + \Lambda_2\right) - \|z\|^2 + \gamma^2\|v\|^2\right]\mathrm{d}t \,\middle|\, \theta_0 = r\right\}. \end{aligned} \tag{32}$$

In view of (14), if one takes $u = u^* = -\Lambda_2$, then (32) becomes

$$\begin{aligned} &E\left(\int_0^T \|z\|^2 \mathrm{d}t \,\middle|\, \theta_0 = r\right) \\ &\le -E\left[V\left(x_T, T, \theta_T\right)|\theta_0 = r\right] + \gamma^2 E\left[\int_0^T \|v\|^2 \mathrm{d}t \,\middle|\, \theta_0 = r\right] \\ &\quad - E\left[\int_0^T \left(v + \Lambda_1\right)'\left(\gamma^2 I + q_{\theta_t}{}'\frac{\partial^2 V_{\theta_t}}{\partial x^2} q_{\theta_t}\right)\left(v + \Lambda_1\right)\mathrm{d}t \,\middle|\, \theta_0 = r\right] \\ &< \gamma^2 E\left(\int_0^T \|v\|^2 \mathrm{d}t \,\middle|\, \theta_0 = r\right). \end{aligned} \tag{33}$$

Letting $T \longrightarrow \infty$, it can be seen that (9) is established, which achieves the desired result. □

Setting $u(t) \equiv 0$, then (1) becomes the following unforced nonlinear system:

$$\begin{cases} dx(t) = \left[f\left(x, x_\delta, t, \theta_t\right) + s\left(x, x_\delta, t, \theta_t\right)v\right]\mathrm{d}t + \left[g\left(x, x_\delta, t, \theta_t\right) + q\left(x, x_\delta, t, \theta_t\right)v\right]\mathrm{d}\omega(t), \\ z(t) = m\left(x, x_\delta, t, \theta_t\right), \\ x(t) = \Phi(t) \in \mathscr{C}^b_{\mathscr{F}_0}\left([-\delta, 0]; R^n\right). \end{cases} \tag{34}$$

Remark 7. It is generally HJIs (14) that are not easy to be solved. Maybe we can try getting the approximate solution by a fuzzy method.

The nonlinear stochastic bounded real lemma for system (34) will be obtained by Theorem 6.

Corollary 8. *For $\gamma > 0$, assume that there exist a set of positive functions $V(x, t, \theta_t) \in C^{2,1}(R^n \times R \times D; R)$ which satisfy $\lim_{\|x(t)\| \longrightarrow \infty} \inf_{t>0} V(x, t, \theta_t) = \infty$, $V(0, 0, r) = 0$, and $\partial^2 V(x, t, \theta_t)/\partial x^2 \ge 0$ for all nonzero $x \in R^n$, $r \in D$, as*

well as $V(x,t,\theta_t) > a\|x(t)\|^2$ *for some* $a > 0$. *If* $V(x,t,\theta_t)$ *satisfies the following HJIs:*

$$\begin{cases} \dfrac{\partial V_r}{\partial t} + \dfrac{\partial V_r'}{\partial x} f_r + \dfrac{1}{2} g_r' \dfrac{\partial^2 V_r}{\partial x^2} g_r + m_r' m_r + \displaystyle\sum_{h=1}^{\infty} \pi_{rh} V_h \\ + \dfrac{1}{4}\left(g_r' \dfrac{\partial^2 V_r}{\partial x^2} q_r + \dfrac{\partial V_r'}{\partial x} s_r \right)\left(\gamma^2 I - q_r' \dfrac{\partial^2 V_r}{\partial x^2} q_r \right)^{-1} \left(q_r' \dfrac{\partial^2 V_r}{\partial x^2} g_r + s_r' \dfrac{\partial V_r}{\partial x} \right) < 0, \\ \gamma^2 I - q_r' \dfrac{\partial^2 V_r}{\partial x^2} q_r > 0, r \in D, t \geq 0, \end{cases} \tag{35}$$

then system (34) is internally stable and $\|\mathscr{L}_{\infty}^{u^*}\| \leq \gamma$.

More particularly, consider the following nonlinear time-delay system with (x,u,v)-dependent noise but without Markov jumps:

$$\begin{cases} \mathrm{d}x(t) = [f_1(x, x_\delta, t) + k_1(x, x_\delta, t)u + s_1(x, x_\delta, t)v]\mathrm{d}t \\ +[g_1(x, x_\delta, t) + h_1(x, x_\delta, t)u + q_1(x, x_\delta, t)v]\mathrm{d}\omega(t), \\ z(t) = col(m_1(x, x_\delta, t), u) := \begin{pmatrix} m_1(x, x_\delta, t), \\ u \end{pmatrix}, \\ x(t) = \Phi(t) \in \mathscr{C}_{\mathscr{F}_0}^b([-\delta, 0]; R^n). \end{cases} \tag{36}$$

For $\widetilde{V} \in \mathscr{C}^{2,1}(R^n \times R; R)$, an infinitesimal generator $\mathscr{L}\widetilde{V}$: $R^n \times R^n \times R \longrightarrow R$ associated with (36) is defined as follows [23]:

$$\begin{aligned} \mathscr{L}\widetilde{V}(x,y,t) = {} & \frac{\partial \widetilde{V}(x,t)}{\partial t} + \frac{\partial \widetilde{V}'(x,t)}{\partial x}[f_1(x,y,t) + k_1(x,y,t)u + l_1(x,y,t)v] \\ & + \frac{1}{2}[g_1(x,y,t) + h_1(x,y,t)u + q_1(x,y,t)v]' \frac{\partial \widetilde{V}^2(x,t)}{\partial x^2} \\ & \times [g_1(x,y,t) + h_1(x,y,t)u + q_1(x,y,t)v]. \end{aligned} \tag{37}$$

For system (36), according to Theorem 6, we can directly obtain the following corollary.

Corollary 9. *For a given* $\gamma > 0$, *assume that there exist a set of positive functions* $\widetilde{V}(x,t) \in C^{2,1}(R^n \times R; R)$ *which satisfy* $\lim_{\|x(t)\| \longrightarrow \infty} \inf_{t>0} \widetilde{V}(x,t) = \infty$, $V(0,0) = 0$, *and* $\partial^2 \widetilde{V}(x,t)/\partial x^2 \geq 0$ *for all nonzero* $x \in R^n$, *as well as* $\widetilde{V}(x,t) > a\|x(t)\|^2$ *for some* $a > 0$. *If* $\widetilde{V}(x,t)$ *solves the following HJIs:*

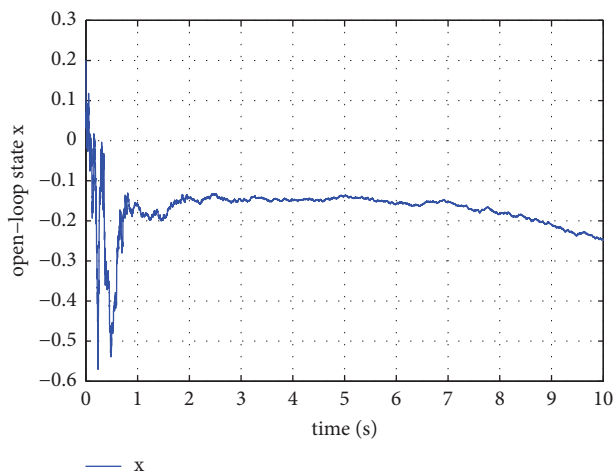

Figure 1: State trajectories of the unforced system.

$$\begin{cases} \Pi_r := \dfrac{\partial \widetilde{V}}{\partial t} + \dfrac{\partial \widetilde{V}'}{\partial x} f_1 + \dfrac{1}{2} g_1' \dfrac{\partial^2 \widetilde{V}}{\partial x^2} g_1 + m_1' m_1 \\ + \dfrac{1}{4}\left(g_1' \dfrac{\partial^2 \widetilde{V}}{\partial x^2} q_1 + \dfrac{\partial \widetilde{V}'}{\partial x} s_1 \right)\left(\gamma^2 I - q_1' \dfrac{\partial^2 \widetilde{V}}{\partial x^2} q_1 \right)^{-1} \left(g_1' \dfrac{\partial^2 \widetilde{V}}{\partial x^2} q_1 + \dfrac{\partial \widetilde{V}'}{\partial x} s_1 \right) \\ - \dfrac{1}{4}\left(g_1' \dfrac{\partial^2 \widetilde{V}}{\partial x^2} h_1 + \dfrac{\partial \widetilde{V}'}{\partial x} k_1 \right)\left(I + h_1' \dfrac{\partial^2 \widetilde{V}}{\partial x^2} h_1 \right)^{-1} \left(h_1' \dfrac{\partial^2 \widetilde{V}}{\partial x^2} g_1 + k_1' \dfrac{\partial \widetilde{V}}{\partial x} \right) < 0, \\ \gamma^2 I - q_1' \dfrac{\partial^2 \widetilde{V}}{\partial x^2} q_1 > 0, t \geq 0, \end{cases} \tag{38}$$

then

$$u^* = -\frac{1}{2}\left(I + h_1' \frac{\partial^2 \widetilde{V}}{\partial x^2} h_1 \right)^{-1} \left(h_1' \frac{\partial^2 \widetilde{V}}{\partial x^2} g_1 + k_1' \frac{\partial \widetilde{V}}{\partial x} \right), \tag{39}$$

is an asymptotically mean square H_∞ control for system (36).

4. A Simulation Example

A simulation example is presented to indicate the correctness of the results obtained in this paper.

Example 10. Consider a one-dimensional nonlinear stochastic delayed system with infinite Markov jumps, and the following parameters are listed:

$$\begin{gathered} f_\rho = -\frac{\rho x x_\delta}{\xi} - \frac{x}{2(\xi)}, k_\rho = \frac{7}{\xi}, s_\rho = \frac{1}{\xi}, \\ g_\rho = \frac{x}{\xi}, h_\rho = 1, q_\rho = 1, m_\rho = \frac{\rho x x_\delta}{\xi}, \end{gathered} \tag{40}$$

where $\xi = \rho + 1$. Let $\gamma = \sqrt{2}$. The transition rate of $\{\theta_t\}_{t \geq 0}$ is given by $-\pi_{\rho\rho} = \pi_{\rho,\xi} = 1$ and $\pi_{\rho h} = 0, \rho \in D, h \in D/\{\rho, \xi\}$. Setting $V(x, t, \rho) = \rho x^2 / 2\xi$, the coupled HJIs (14) become

$$\begin{aligned} \Pi = {} & \frac{\rho x}{\xi} \cdot \left(-\frac{\rho x x_\delta}{\xi} - \frac{x}{2\xi} \right) + \frac{1}{2} \frac{x}{\xi} \cdot \frac{\rho}{\xi} \cdot \frac{x}{\xi} + \frac{\rho x x_\delta}{\xi} \cdot \frac{\rho x x_\delta}{\xi} - \frac{\rho x^2}{2\xi} \cdot \frac{\xi x^2}{2\xi} \\ & + \frac{1}{4}\left(\frac{x}{\xi} \cdot \frac{\rho}{\xi} + \frac{\rho x}{\xi} \cdot \frac{1}{\xi} \right)\left(2 - \frac{\rho}{\xi} \right)^{-1} \left(\frac{\rho}{\xi} \cdot \frac{x}{\xi} + \frac{1}{\xi} \cdot \frac{\rho x}{\xi} \right) \end{aligned}$$

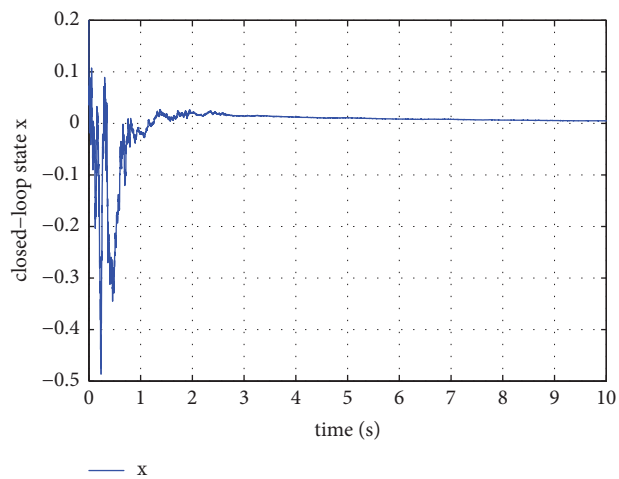

Figure 2: State trajectories of the controlled system.

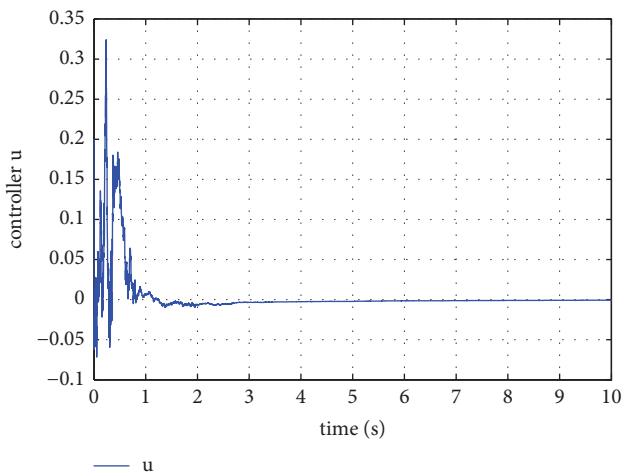

Figure 3: State trajectories of the controller.

$$-\frac{1}{4}\left(\frac{x}{\xi}\cdot\frac{\rho}{\xi}+\frac{\rho x}{\xi}\cdot\frac{7}{\xi}\right)\left(1+\frac{\rho}{\xi}\right)^{-1}\left(\frac{\rho}{\xi}\cdot\frac{x}{\xi}+\frac{7}{\xi}\cdot\frac{\rho x}{\xi}\right)$$
$$=\frac{\left(-24\rho^3-50\rho^2+9\rho+2\right)x^2}{2(\xi)^3(\rho+2)(2\xi-1)}<0, \tag{41}$$
$$\gamma^2 I-q_\rho'\frac{\partial' V_\rho}{\partial x^2}q_\rho=2I-\frac{\rho}{\xi}=\frac{2+\rho}{\xi}>0.$$

According to Theorem 6, the H_∞ controller of system (1) is

$$u_\rho^*=-\frac{4\rho}{\xi(2\xi-1)}x. \tag{42}$$

Select the initial condition $\Phi(t)=0.15$ for any $t\in[-\delta,0]$ with $\delta=0.15$ and $v(t)=e^{-(\rho-1)}\sin(0.1\rho\pi)$. Figures 1–3 show the trajectories of the states of the unforced system $(u(t)=0)$, the states of the controlled system $(u(t)=u_\rho^*)$, and the control input $u(t)$, respectively. It can be seen from the simulation results that the controlled system can not only achieve stability but also satisfy the attenuation performance by using the H_∞ controller.

5. Conclusion

This paper has solved the problem of infinite horizon H_∞ control for general nonlinear stochastic jump systems with (x,u,v)-dependent noise and delay. And the asymptotic mean square H_∞ controller has been designed by solving

a series of coupled HJIs. Finally, the validity of the obtained results has been demonstrated by a numerical example. Some more difficult and meaningful topics need to be studied in the future, including infinite horizon H_2/H_∞ control and filter problems for nonlinear stochastic systems with infinite Markov jumps and time-varying delays.

Data Availability

No data were used to support this study.

Conflicts of Interest

The authors declare that they have no conflicts of interest.

Acknowledgments

This work was supported by the Natural Science Foundation of Shandong Province (no. ZR2020MF071).

References

[1] G. Yin and X. Zhou, "Markowitzs mean-variance portfolio selection with regime switching: from discrete-time models to their continuous-time limits," *IEEE Transactions on Automatic Control*, vol. 49, no. 3, pp. 349–360, 2004.

[2] X. Mao, *Stochastic Differential Equations and Applications*, Horwood Publishing Limited, Horwood, UK, 1997.

[3] F. Deng, Q. Luo, and X. Mao, "Stochastic stabilization of hybrid differential equations," *Automatica*, vol. 48, no. 9, pp. 2321–2328, 2012.

[4] T. Hou, W. Zhang, and H. Ma, "A game-based control design for discrete-time Markov jump systems with multiplicative noise," *IET Control Theory & Applications*, vol. 7, no. 5, pp. 773–783, 2013.

[5] T. Hou, W. Zhang, and H. Ma, "Finite horizon H_2/H_∞control for discrete-time stochastic systems with Markovian jumps and multiplicative noise," *IEEE Transactions on Automatic Control*, vol. 55, no. 5, pp. 1185–1191, 2010.

[6] X. Mao and C. Yuan, *Stochastic Differential Equations with Markovian Switching*, Imperial College Press, London, UK, 2006.

[7] O. L. V. Costa and D. Z. Figueiredo, "Stochastic stability of jump discrete-time linear systems with Markov chain in a general Borel space," *IEEE Transactions on Automatic Control*, vol. 59, no. 1, pp. 223–227, 2014.

[8] T. Hou and H. Ma, "Exponential stability for discrete-time infinite Markov jump systems," *IEEE Transactions on Automatic Control*, vol. 61, no. 12, pp. 4241–4246, 2016.

[9] Q. Zhu and B. Song, "Exponential stability of impulsive nonlinear stochastic differential equations with mixed delays," *Nonlinear Analysis: Real World Applications*, vol. 12, no. 5, pp. 2851–2860, 2011.

[10] E. F. Costa, J. B. R. do Val, and M. D. Fragosa, "On a detectability concept of discrete-time infinite Markov jump linear systems," *Stochastic Analysis and Applications*, vol. 23, no. 1, pp. 1–14, 2005.

[11] I. Kordonis and G. P. Papavassilopoulos, "On stability and LQ control of MJLS with a Markov chain with general state space," *IEEE Transactions on Automatic Control*, vol. 59, no. 2, pp. 535–540, 2014.

[12] O. Costa and M. D. Fragoso, "Discrete-time LQ-optimal control problems for infinite Markov jump parameter systems," *IEEE Transactions on Automatic Control*, vol. 40, no. 12, pp. 2076–2088, 1995.

[13] C. Li, M. Chen, J. Lam, and X. Mao, "On exponential almost sure stability of random jump systems," *IEEE Transactions on Automatic Control*, vol. 57, no. 12, pp. 3064–3077, 2012.

[14] T. Morozan and V. Dragan, "An H_2-type norm of a discrete-time linear sotchastic systems with periodic coefficients simultaneously affected by an infinite Markov chain and multiplicative white noise perterbations," *Stochastic Analysis and Applications*, vol. 32, no. 5, pp. 776–801, 2014.

[15] T. Hou, Y. Liu, and F. Deng, "Stability for discrete-time uncertain systems with infinite Markov jump and time-delay," *Science China Information Sciences*, vol. 64, no. 5, p. 11, Article ID 152202, 2021.

[16] Y. Liu and T. Hou, "Robust H_2/H_∞ fuzzy filtering for nonlinear stochastic systems with infinite Markov jump," *Journal of Systems Science and Complexity*, vol. 33, no. 4, pp. 1023–1039, 2020.

[17] S. Niculescu, *Delay Effects on Stability: A Robust Control Approach*, Springer, New York, NY, USA, 2001.

[18] Y. Liu and T. Hou, "H_∞ control for nonlinear infinite Markov jump systems," *Mathematical Problems in Engineering*, vol. 2018, Article ID 2904521, 9 pages, 2018.

[19] Y. Wang, Z. Pan, Y. Li, and W. Zhang, "H_∞ control for nonlinear stochastic Markov systems with time-delay and multiplicative noise," *Journal of Systems Science and Complexity*, vol. 30, no. 6, pp. 1293–1315, 2017.

[20] W. Zhang, L. Xie, and B. S. Chen, *Stochastic H_2/H_∞ Control: A Nash Game Approach*, CRC Press, London, UK, 2017.

[21] W. Zhang, B. S. Chen, H. Tang, L. Sheng, and M. Gao, "Some remarks on general nonlinear stochastic H_∞ control with state, control, and disturbance-dependent noise," *IEEE Transactions on Automatic Control*, vol. 59, no. 1, pp. 237–242, 2014.

[22] J. L. Doob, *Stochastic Processes*, Wiley, New York, NY, USA, 1953.

[23] X. Mao, "LaSalle-type theorems for stochastic differential delay equations," *Journal of Mathematical Analysis and Applications*, vol. 236, no. 2, pp. 350–369, 1999.

Hindawi
Mathematical Problems in Engineering
Volume 2021, Article ID 7808565, 10 pages
https://doi.org/10.1155/2021/7808565

Research Article

Containment Control of Heterogeneous Discrete-Time Multiagent Systems with Time Delay

Jiawei Wu, Yongguang Yu, and Guojian Ren

Department of Mathematics, Beijing Jiaotong University, Beijing 100044, China

Correspondence should be addressed to Guojian Ren; gjren@bjtu.edu.cn

Received 7 May 2021; Accepted 23 August 2021; Published 30 September 2021

Academic Editor: Rongwei Guo

In this paper, the containment control of heterogeneous MASs with multi-interactional leaders is addressed. The objective of the containment control is of two layers. The leaders converge to an expected form; subsequently, the followers enter the convex hull spanned by the leader's final position. To achieve the goal, the dynamics of the leaders and the followers are modeled by a single integrator and a double integrator, respectively. A reduced-order transformation is employed to obtain the sufficient conditions for realizing the follower agents' control. In this manner, the maximum allowed time delay is given. Moreover, based on the topological structure and matrix, it confirms that the followers are able to enter the expected convex hull. Finally, the numerical simulation reveals the effectiveness of the control strategy.

1. Introduction

Over the past years, inspired by the work in [1–3], a lot of researchers began the research on multiagent systems (MASs) with cooperative control. The reasons lie on its widespread application in different disciplines [4–6]. In those works, the cooperative control in networks for MAS has been studied in the group behaviors. As one of the cooperative control, the containment control law, inspired from numerous natural and social phenomena, has attracted lots of researchers to continue developing it with the agents' neighbor information. Considering that the double-order controller dynamics has a good interpretation of the complex processes in the reality, its consensus control is of great interest, thus has been deeply studied [7–9]. More recently, the stabilization and consensus problem of systems has received much attention [10–12].

According to the number of leaders in the formation, the algorithm for its cooperative control can be demarcated into two categories: the case of one leader and the one with multiple leaders. As for the previous case, it is a consensus control problem. The corresponding algorithm will track the trajectory of each agents. Among these agents, one of them is called a leader, However, it is not able to receive any feedback from the other agents. There already exists many studies in the literature. In [13], the fixed-time leader-following consensus of second-order MASs with delay is investigated. In [14], a high-dimensional leader for neuroadaptive consensus tracking of MASs is discussed. In [15], a dynamic leader for bipartite tracking consensus of linear MASs is studied.

As for the case with several leaders, it focuses on the formation containing a group of leaders and followers. It is essentially a containment control problem. Different from the main idea in the consensus control problem, the control law in the containment control problem is supposed to force the followers to get into the convex hull formed by the leaders. In recent years, the containment control has received great population [16–18]. In [16], a dynamic output approach is investigated to study the containment of higher-order multileaders' MASs. In [17], a distributed containment law is proposed to study the double-integrator controllers for the multiple dynamic leaders by only using their position measurement. In [18], a distributed finite-time containment control is developed for the double-integrator MASs.

Many researchers have studied a group of leaders and followers. In recent years, the containment control problems [16–18] have been intensively studied, aiming at designing

control laws to force followers into the convex hull formed by leaders. In [16], a dynamic output approach is investigated to study containment of higher-order multileaders MASs. In [17], distributed containment law is investigated to study multiple dynamic leaders for double-integrator dynamics and only using position measurement. In [18], a distributed finite-time containment control is investigated for double-integrator MASs.

However, the abovementioned algorithms only apply to the consensus problems with homogeneous MASs, in which the dynamics for all agents are modeled by the same order. Meanwhile, it should be mentioned that variety of phenomena for consensus problem cannot be described by the homogeneous dynamics systems [7, 19]. Indeed, the containment control problem of heterogeneous MASs has already been investigated in [20–22]. In [20], the asynchronous group consensus is investigated for heterogeneous MASs. In [21], a containment law is studied for heterogeneous MASs. In [22], a distributed containment law is studied for heterogeneous MASs.

Nevertheless, the protocols devised in the abovementioned references do not consider time-vary delay. Quan et al. and Dong et al. [23, 24] investigated MASs with time delay, but they are not for heterogeneous MASs. So, inspired by the above progress, the containment control problem of heterogeneous discrete-time MASs with time delay is considered in this manuscript. To be more specific, the leaders designed to form the formation are interactional. That is to say, the positions of leaders form the first layer of the MASs. Followers are controlled to enter the convex hull of the leaders' final position, in which the leaders are first-order agents and the followers are second-order agents. In view of the different goals of the leaders and the followers, this paper designs a leader position formation control protocol which is independent of the positions of the followers. Moreover, a consensus method based on the agents' neighbor information is proposed. The upper bound of time delay is given which depends on the topology, the control parameters, and the sampling time.

The paper is organized as follows. In Section 2, some important definitions on topology are given. In Section 3, the dynamics equation and control law are described and some basic lemmas are given. In Section 4, the stability of containment control law involving multiple leaders is studied. In Sections 5 and 6, the numerical simulation and conclusions are presented, respectively.

2. Preliminaries

In this section, some basic knowledge about graph, concerned definition, and notations is given.

2.1. Graph Theory. In the study of MASs, the directed graph is always employed for modeling the communication between agents. The graph offers an intuitive glance of the switching topology, and it also facilitates the control analysis. Basically, the network consists of n agents (m leaders and $n-m$ leaders), and its graph can be described by $\mathscr{G} = \{\mathscr{V}, \mathscr{E}\}$. Here, $\mathscr{V} = \{1, 2, \ldots, m, m+1, \ldots, n\}$, and it represents the set containing the followers and leaders. $\mathscr{E} = \{(i, j) \in \mathscr{V} \times \mathscr{V}\}$; it embodies the undirected edges between the leader and the followers and neighboring relations among leaders and followers. Denote the set of leaders as $f = \{1, 2, \ldots, m\}$ and the set of followers as $l = \{m+1, m+2, \ldots, n\}$. Define the adjacency matrix as $\mathscr{A} = [a_{ij}] \in \mathbb{R}^{(n)\times(n)}$, $a_{ij} > 0$, if $(j, i) \in \mathscr{E}$, otherwise $a_{ij} = 0$.

The Laplacian matrix of the graph is given by $L = [L_{ij}] \in \mathbb{R}^{(N)\times(N)}$, where $l_{ii} = \sum_{j=1, j\neq i}^{N} a_{ij}$ and $l_{ij} = -a_{ij}$, $i \neq j$.

2.2. Definition and Notations. In this paper, 1_n, I_m, and 0 are designed as $n \times 1$ column vector of all ones, the identity matrix with order m, and zero matrix, respectively. $\mathrm{diag}\{x_1, x_2, \ldots, x_n\}$ denotes the block-diagonal matrix constructed by $x_1, x_2, \ldots, x_n$. $\otimes$ is the Kronecker product.

Definition 1. A set $\mathscr{C} \subseteq \mathbb{R}^{(N)\times(N)}$ is convex if, for all $x, y \in \mathscr{C}$ and any $\mu \in [0, 1]$, we can have $(1-\mu)x + \mu y \in \mathscr{C}$. Define the minimal convex set encompassing all points $\mathscr{X} = \{x_1, x_2, \ldots, x_M\}$ as $Co(\mathscr{X})$. In detail,

$$Co(\mathscr{X}) = \left\{ \sum_{i=1}^{M} \mu_i x_i | x_i \in \mathscr{X}, \mu_i \in \mathbb{R}, \mu_i \geq 0, \sum_{i=1}^{M} \mu_i = 1 \right\}. \tag{1}$$

3. Problem Formulation

In this part, the containment law with the dynamic leader for the heterogeneous MASs is introduced, while each follower agent receives the relative information of its neighbors with time delays $\tau(t)$.

Definition 2. If, for each tracking node, at least one guide node has a directed path to the following node, the directed graph $\mathscr{G}$ has a spanning tree [25].

We consider the discrete-time MASs. Each leader's dynamics is described as follows:

$$x_i(k+1) = x_i(k) + Tu_i(k), \quad i = 1, \ldots, m. \tag{2}$$

The dynamics of the followers are given as follows:

$$\begin{cases} x_i(k+1) = x_i(k) + Tv_i(k), & i = m+1, \ldots, n, \\ v_i(k+1) = v_i(k) + Tu_i(k), \end{cases} \tag{3}$$

where T is the sample time.

The Laplacian matrix $\mathscr{L}$ can be written as

$$L = \begin{bmatrix} L_{ll} & L_{fl} \\ 0 & L_{ff} \end{bmatrix}, \tag{4}$$

where L_{ll} is the corresponding Laplacian matrix among leaders, L_{ff} is the Laplacian matrix among followers, and L_{fl} represents the connection between leaders and followers. Note that the last $n-m$ rows and the first m columns of $\mathscr{L}$ are equal to zero because the last $n-m$ rows are for the

followers and the first m columns represent the leaders, who do not receive the information from any other agents.

In order to solve the containment problem for heterogeneous agents, a distributed controller is designed. The control protocol is illustrated as follows:

$$\begin{cases} u_i(k) = \sum_{j=1}^{m} a_{ij}\left[x_j(k-\tau(k)) - \eta_j - \left(x_i(k-\tau(k)) - \eta_i\right)\right], & i = 1,\ldots,m, \\ u_i(k) = \sum_{j=1}^{n}\left[x_j(k-\tau(k)) - x_i(k-\tau(k))\right] + \gamma^{-1}\sum_{j=1}^{n} a_{ij}\left[v_j(k-\tau(k)) - v_i(k-\tau(k))\right] - \gamma v_i(k), & i = m+1,\ldots,n, \end{cases} \tag{5}$$

where $\gamma = k_1^{-1}$, $k_1 > 0$, is an unknown feedback gain which awaits for later determination.

Letting $y_i(t) = x_i(t) + \gamma^{-1}v_i(t)$, we have

$$\begin{cases} x_f(k+1) = x_f(k) + T\gamma\left[y_f(k) - x_f(k)\right], & \text{(4a)}, \\ y_f(k+1) = y_f(k) - T\left[\gamma^{-1}L_{ff}y_f(k-\tau(k)) + \gamma^{-1}L_{fl}y_l(k-\tau(k))\right], & \text{(4b)}, \\ x_l(k+1) = x_l(k) - TL_{ll}x_l(k-\tau(k)) + TL_{ll}\eta_l(k), & \text{(4c)}, \end{cases} \tag{6}$$

where $x_f = [x_{m+1}, x_{m+2}, \ldots, x_n]$, $y_f = [y_{m+1}, y_{m+2}, \ldots, y_n]$, $x_l = [x_1, x_2, \ldots, x_m]$, and $y_l = [y_1, y_2, \ldots, y_m]$. $y_i(t), i = m+1, \ldots, n$, is considered as virtual followers corresponding to $x_i(t), i = m+1, \ldots, n$.

Noting that the Laplacian matrix of a directed graph is asymmetrical, thus its corresponding eigenvalues are complex. For the convenience, we state the following lemma to provide a rational for further demonstration.

Lemma 1 (see [26]). *Suppose that the digraph $\mathcal{G}$ has a directed spanning tree. Then, all the eigenvalues of L_{ff} have positive real parts, each element of $L_{ff}^{-1}l_{fl}$ is nonnegative, and the sum of each row of $L_{ff}^{-1}l_{fl}$ is 1.*

Lemma 2 (see [27]). *Given the polynomial with complex coefficients,*

$$F_n(s) = s^n + (\alpha_1 + i\beta_1)s^{n-1} + \cdots + (\alpha_{n-1} + i\beta_{n-1})s + \alpha_n + i\beta_n. \tag{7}$$

The polynomial is stable if and only if $F_{n-1}(s)$ (see equation (11)) is stable:

$$F_{n-1}(s) = \alpha_1 s^{n-1} + \left(\alpha_1\alpha_2^{(1)} + \beta_1^{(1)}\beta_2 + i\beta_2\right)s^{n-1} + \cdots + \left[\alpha_{n-1} + i\left(\alpha_1\beta_{n-1}^{(1)} - \beta_1^{(1)}\alpha_{n-1}\right)\right]s + \alpha_1\alpha_n^{(1)} + \beta_1^{(1)}\beta_n + i\beta_n, \tag{8}$$

where $\beta_1^{(1)} = \alpha_1\beta_1 - \beta_2$, $\alpha_2^{(1)} = \alpha_1\alpha_2 - \alpha_3, \ldots, \beta_{n-1}^{(1)} = \alpha_1\beta_n - 1 - \beta_n, \alpha_n^{(1)} = \alpha_1\alpha_n$.

Corollary 1. *It is not difficult to verify that Lemma 2 works well for a second-order polynomial $s^2 + ps + q$, whose conditions can be induced as*

$$\begin{cases} \mathrm{Re}(p) > 0, \\ (\mathrm{Re}(p))^2\mathrm{Re}(q) + \mathrm{Re}(p)\mathrm{Im}(p)\mathrm{Im}(q) - (\mathrm{Im}(q))^2 > 0. \end{cases} \tag{9}$$

4. Main Results

The sufficient condition proves that law (6) is competent with the consensus objective of heterogeneous MAS (3) and (5).

Theorem 1. *Suppose that the sampling time T satisfies $T < 1/\max_{i=1,\ldots,n} d_{ii}$. Using (6) for (3) and (5), the heterogeneous MASs reach consensus, for any initial condition, if $\mathcal{G}$ contains a directed spanning tree, feedback gain γ^{-1} and sample time T satisfy*

$$\begin{cases} T < \gamma^{-1}, \\ 4|\mu_i|^4\left(T - \gamma^{-1}\right)^4 - \left[4\gamma^{-2}|\mu_i|^4 - 12\mathrm{Re}(\mu_i)|\mu_i|^2\right]\left(T - \gamma^{-1}\right)^2 - 9\mathrm{Im}^2(\mu_i) > 0, \end{cases} \tag{10}$$

and time delay,

$$\tau \in [0, \overline{\tau}), \quad \overline{\tau} = \min_{\mu_i, i \in f}\{\tau \| Z| \geq 1, \Psi(z, \tau) = 0\}. \tag{11}$$

Proof. Taking the Z transform of x_l in equation (2); then, we can obtain

$$X_f(z) = (z - 1 + T\gamma)^{-1}\left[T\gamma Y(z) + zx_f(0)\right]. \tag{12}$$

Similarly, applying the Z transform to equation (3), we can obtain

$$\left[\left(z^2 - 2z + 1\right)I_m + \left(T^2 - T\gamma^{-1}\right)L_{ff}z^{-\overline{\tau}} + \left(T\gamma^{-1}\right)L_{ff}z^{-\overline{\tau}+1}\right]Y_f(z)$$
$$= z(z - 1 + T\gamma)y(0) - T\gamma x_f(0) - \left(T\gamma^{-1}\right)(z - 1 + T\gamma)L_{fl}\frac{z^{-\overline{\tau}+1}}{z - 1x_l}, \tag{13}$$

where $X_f(z)$ and $Y_f(z)$ are the Z transforms of $x_f(k)$ and $y(k)$, respectively.

Firstly, we show that the convergence of the state of real followers will reach to the state of their own virtual followers. We have $T - \gamma^{-1} < 0$. The condition and final value theorem guarantee the response of (13), i.e., $x_f(k)$, where the initial condition $x_f(0)$ will be 0 at $t \longrightarrow \infty$. Besides, (14) indicates that the poles of $Y(z)$ are the zeros of the transfer matrix:

$$\left(z^2 - 2z + 1\right)I_m + \left(T^2 - \frac{T}{\gamma}\right)L_{ff}z^{-\overline{\tau}} + \frac{T}{\gamma}L_{ff}z^{-\overline{\tau}+1}. \tag{14}$$

It can be completed by calculating characteristic equation in the following:

$$\prod_{i=1}^{m}\left(z^2 - 2z + 1 + \left(T^2 - \frac{T}{\gamma}\right)\mu_i z^{-\overline{\tau}} + \frac{T}{\gamma}z^{-\overline{\tau}+1}\right) = 0. \tag{15}$$

Case 1: $\tau = 0$.

Assume that there is no time delay; equation (15) will be reduced to

$$z^2 + \left(\frac{T}{\gamma}\mu_i - 2\right)z + 1 + \left(T^2 - \frac{T}{\gamma}\right)\mu_i = 0. \tag{16}$$

All the roots of the polynomial,

$$z^2 + \left(\gamma^{-1}T\mu_i - 2\right)z + 1 + \left(T^2 - \gamma^{-1}T\right)\mu_i = 0, \tag{17}$$

site in the unit circle if and only if the sample time T satisfies the following inequality:

$$\begin{cases} T < \gamma^{-1}, \\ 4|\mu_i|^4\left(T - \gamma^{-1}\right)^4 - \left[4\gamma^{-2}|\mu_i|^4 - 12\mathrm{Re}(\mu_i)|\mu_i|^2\right]\left(T - \gamma^{-1}\right)^2 - 9\mathrm{Im}^2(\mu_i) > 0, \end{cases} \tag{18}$$

The proof is as follows. In order to keep the roundness of the polynomial equation, the value out of the unit circle is mapped to its right, and we substitute z in equation (17) by adopting a Mobius transformation, i.e., $z \longrightarrow s + 1/s - 1$; then, multiplying $(s - 1)^2$ to the two sides of equation (17), subsequently, equation (17) becomes

$$\left(T^2\mu_i\right)s^2 + 2\mu_i\left(\gamma^{-1}T - T^2\right)s + \left[\left(T^2 - 2\gamma^{-1}T\right)\mu_i + 3\right] = 0. \tag{19}$$

It can be derived that equation (19) follows the conditions in equation (18). Then, use Lemma 1, if and only if equation (19) is stable, which is equivalent to equation (17) which has roots inside the unit circle.

All the roots of characteristic polynomial are inside the unit circle. Hence, this system is asymptotically stable based on the final value theorem.

Case 2: $\tau \neq 0$.

When $T < \gamma^{-1}$, we can have [28]

$$\Psi(z, \tau) = \prod_{i=1}^{m}\left(z^2 - 2z + 1 + \left(T^2 - \frac{T}{\gamma}\right)\mu_i z^{-\overline{\tau}} + \frac{T}{\gamma}\mu_i z^{-\overline{\tau}+1}\right) = 0. \tag{20}$$

It has no root locating inside the unit circle for $\forall \tau \in \mathbb{Z}$.

It can be easily found that the roots of (22) never stay over the unit circle for $\forall \tau \in \mathbb{Z}$. Therefore, one can guarantee that the system never makes the oscillation behavior cross the convex hull spanned by the leaders' states. Hence, the maximum time delay can be reckoned by τ. Therefore, when the delay satisfies τ, (12) and (22) are stable.

Thus, it is sufficient to prove the convergence of virtual follower to the convex hull crossed by the leader as $t \longrightarrow \infty$; it further demonstrates that the real followers are able to converge to the convex hull which is spanned by the leaders.

Supposing that

$$\xi(k) = \left[x(k), x(k-1), \ldots, x\left(k - \left\lceil\frac{\overline{\tau}}{T}\right\rceil\right)\right]^T,$$
$$x(k-j) = \left[x_1(k-j), \ldots, x_m(k-j), y_{m+1}(k-j), \ldots, y_n(k-j)\right]^T, \tag{21}$$

the equation of the system can be summarized as follows:

$$\xi(k+1) = \Phi\xi(k) + Y, \tag{22}$$

where

$$\Phi = \begin{bmatrix} I_n - T\gamma^{-1}D + T\gamma^{-1}A_0 & T\gamma^{-1}A_1 & \dots & T\gamma^{-1}A_{\lceil \overline{\tau}/T \rceil - 1} & T\gamma^{-1}A_{\lceil \overline{\tau}/T \rceil} \\ I_n & & & & \\ & I_n & & & \\ & & \ddots & & \\ & & & I_n & 0 \end{bmatrix},$$
$$\Upsilon = \begin{bmatrix} 0 \\ TL_{ll}\eta_l \\ 0 \\ \vdots \\ 0 \end{bmatrix}, \tag{23}$$

where the Laplacian matrix $L = D - \sum_{k=0}^{\lceil \tau/T \rceil} A_k$.

Meanwhile, from the definitions of the leaders and the followers, it is easy to attain the following partitions:

$$D = \begin{bmatrix} D_f & \\ & D_l \end{bmatrix},$$
$$A_k = \begin{bmatrix} A_{ffk} & A_{flk} \\ \mathbf{0} & A_{llk} \end{bmatrix}. \tag{24}$$

Denote $\xi_f(k) = [y_f^T(k), y_f^T(k-1), \dots, y_f^T(k - \lceil \overline{\tau}/T \rceil)]^T$ and $\xi_l(k) = [x_l^T(k), x_l^T(k-1), \dots, x_l^T(k - \lceil \overline{\tau}/T \rceil)]^T$. Afterwards, the dynamics of the leaders can be transformed to

$$\xi_l(k+1) = \Phi_{ll}\xi_l(k) + Y_l, \tag{25}$$

where

$$\Phi_{ll} = \begin{bmatrix} I_m - TD_l + TA_{ll0} & TA_{ll1} & \dots & TA_{ll(\lceil \overline{\tau}/T \rceil - 1)} & TA_{ll\lceil \overline{\tau}/T \rceil} \\ I_m & & & & \\ & I_m & & & \\ & & \ddots & & \\ & & & I_m & 0 \end{bmatrix},$$
$$\Upsilon_l = \begin{bmatrix} TL_{ll}\eta_l \\ 0 \\ 0 \\ \vdots \\ 0 \end{bmatrix}. \tag{26}$$

Likewise, the dynamics of the followers become

$$\xi_f(k+1) = \Phi_{ff}\xi_f(k) + \Phi_{fl}\xi_l(k), \tag{27}$$

where

$$\Phi_{ff} = \begin{bmatrix} I_{n-m} - TD_f + TA_{ff0} & TA_{ff1} & TA_{ff(\lceil \overline{\tau}/T \rceil - 1)} & TA_{ff\lceil \overline{\tau}/T \rceil} \\ I_{n-m} & & & \\ I_{n-m} & & & \\ \ddots & & & \\ I_{n-m} & 0 & & \end{bmatrix},$$
$$\Phi_{ff} = \begin{bmatrix} TA_{fl0} & TA_{fl1} & \dots & TA_{fl(\lceil \overline{\tau}/T \rceil - 1)} & TA_{fl\lceil \overline{\tau}/T \rceil} \\ 0 & 0 & \dots & 0 & 0 \\ 0 & 0 & \dots & 0 & 0 \\ \vdots & \vdots & \ddots & \vdots & \vdots \\ 0 & 0 & \dots & 0 & 0 \end{bmatrix}. \tag{28}$$

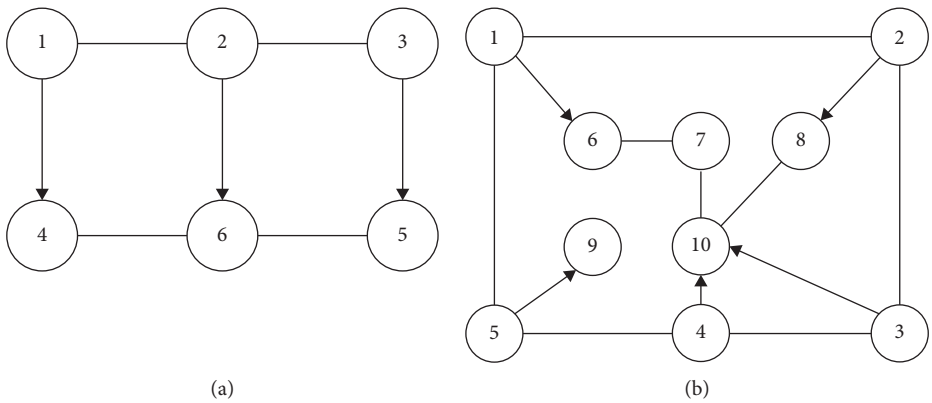

Figure 1: The communication topology of two examples. (a) Example 1. (b) Example 2.

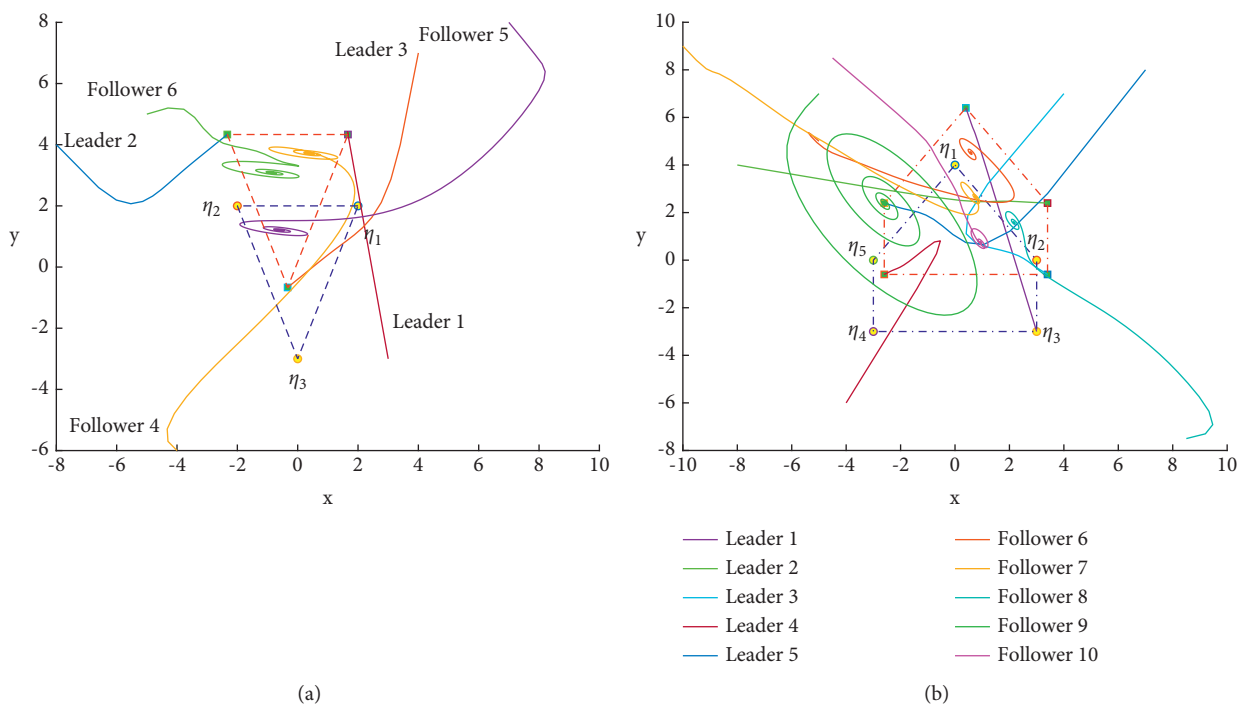

Figure 2: State trajectories of all agents in the phase plane. (a) Example 1. (b) Example 2.

It is worth mentioning that $T < 1/\max_{i=1,\ldots,n} d_{ii}$; therefore, $\rho(\Phi_{ff}) \leq 1$. Assume that 1 is an eigenvalue of Φ_{ff}; it can be concluded that there exists an eigenvector,

$$\alpha = \left[\alpha_0^T, \alpha_1^T, \ldots, \alpha_{\lceil \bar{\tau}/T \rceil}^T\right]^T \neq 0, \tag{29}$$

such that $\Phi_{ff}\alpha = 1 \cdot \alpha$, i.e.,

$$\left(I_{n-m} - TD_f + TA_{ff0}\right)\alpha_0 + TA_{ff1}\alpha_1 + \cdots + TA_{ff\lceil \bar{\tau}/T \rceil}\alpha_{\lceil \bar{\tau}/T \rceil} = \alpha_0, \tag{30a}$$

$$\alpha_0 = \alpha_1, \tag{30b}$$

$$\vdots \tag{30c}$$

$$\alpha_{\lceil \bar{\tau}/T \rceil - 1} = \alpha_{\lceil \bar{\tau}/T \rceil}. \tag{30d}$$

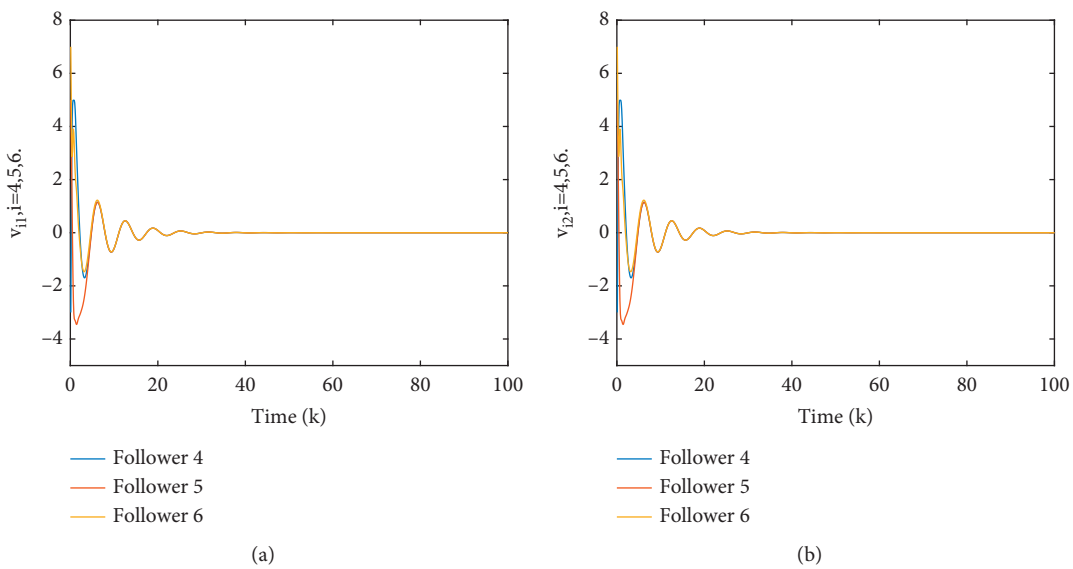

Figure 3: Velocity trajectories of all followers in Example 1. (a) Case 1. (b) Case 2.

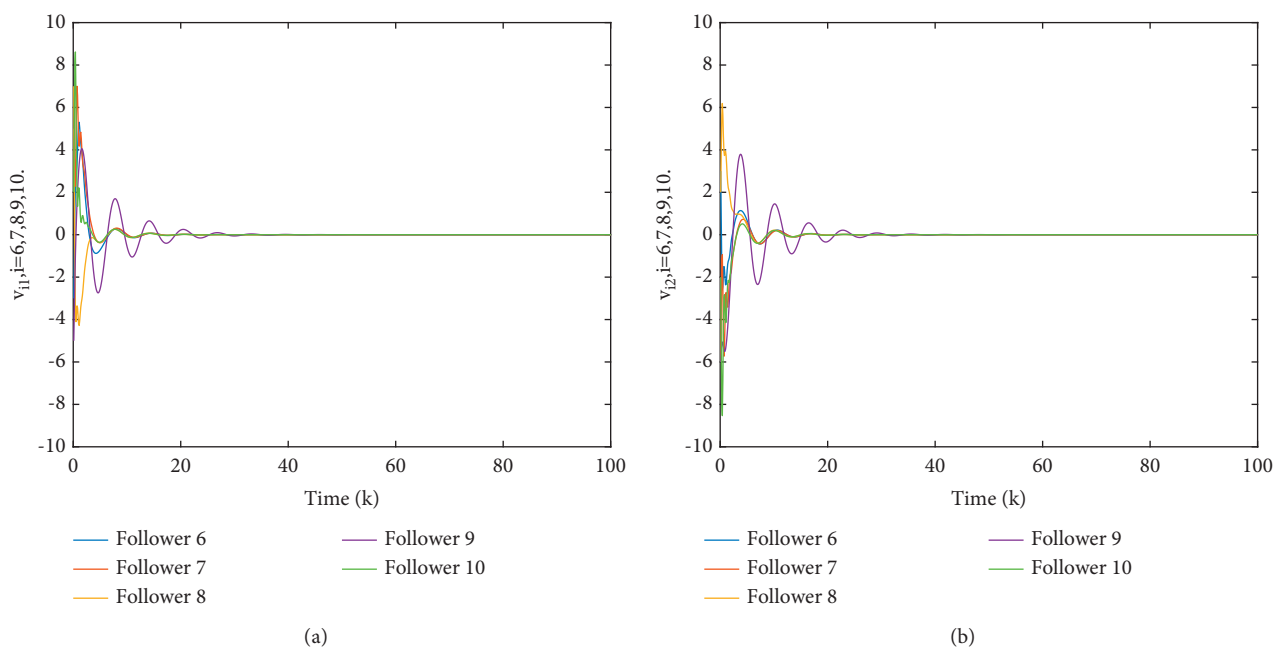

Figure 4: Velocity trajectories of all followers in Example 2. (a) Case 1. (b) Case 2.

From equation (30a), we can directly obtain that $(I_{n-m} - TL_{ff})\alpha_0 = \alpha_0$, that is, $TL_{ff}\alpha_0 = 0$. Thereon, it follows that $\alpha = 0$. It arrives to a contradiction, where $\alpha \neq 0$ is assumed in equation (29). Hence, every eigenvalue of Φ_{ff} is less than 1.

Once the leaders achieved the desired information, the states of virtual followers would become

$$\begin{aligned}\lim_{k\longrightarrow\infty} \xi_f(k+1) &= \lim_{k\longrightarrow\infty}\left[\Phi_{ff}^{k+1}\xi_f(0) + \left(\Phi_{ff}^{k}\Phi_{fl} + \Phi_{ff}^{k-1}\Phi_{fl} + \cdots + \Phi_{ff}\Phi_{fl} + \Phi_{fl}\right)\xi_l\right] \\ &= \lim_{k\longrightarrow\infty}\left[\Phi_{ff}^{k+1}\xi_f(0) + \sum_{i=0}^{k}\Phi_{ff}^{i}\Phi_{fl}\xi_l\right] \\ &= \left(I_{(n-m)\times(\lceil\overline{\tau}/T\rceil+1)} - \Phi_{ff}\right)^{-1}\Phi_{fl}\xi_l \\ &= \Gamma\xi_l,\end{aligned} \tag{31}$$

where $\Gamma = 1_{\lceil\overline{\tau}/T\rceil+1} \otimes [L_{ff}^{-1}A_{fl0}, L_{ff}^{-1}A_{fl1}, \ldots, L_{ff}^{-1}A_{fl\lceil\overline{\tau}/T\rceil}]\xi_l$.

Finally, the positions of the virtual followers can be given by

$$\begin{aligned} y_f &= \left[L_{ff}^{-1}A_{fl0}, L_{ff}^{-1}A_{fl1}, \ldots, L_{ff}^{-1}A_{fl\lceil\overline{\tau}/T\rceil}\right]\xi_l \\ &= L_{ff}^{-1}A_{fl}x_l. \end{aligned} \tag{32}$$

It is not difficult to verify that $L_{ff}^{-1}A_{fl1}1_m = 1_{n-m}$. Besides, all the entries of $L_{ff}^{-1}A_{fl1}$ are nonnegative. Considering the definition of convex hull, the result reveals that all of the followers converge to the convex hull spanned by the leaders' final states. □

5. Simulation Results

5.1. Example 1. First of all, considering a containment problem of discrete-time multiagent systems (DTMASs), its communication topology graph is shown in Figure 1(a), where $l = \{1, 2, 3\}$ and $f = \{4, 5, 6\}$. It is evident that each follower has at least one directed path to the leaders. To avoid stochastic factors, two sets of parameters are tested on this example.

In the first case of validation, take

$\gamma = 0.5, T = 0.1, \eta_1 = (2, 2)^T, \eta_2 = (-2, 2)^T, \eta_3 = (0, -3)^T$, $\tau = 0.1/T, x_1(0) = (3, -3)^T, x_2(0) = (-8, 4)^T, x_3(0) = (4, 7)^T, x_4(0) = (-4, -6)^T, x_5(0) = (7, 8)^T$, and $x_6(0) = (-5, 5)^T$.

In the second case of validation, take $\gamma = 0.5, T = 0.1, \eta_1 = (2, 2)^T, \eta_2 = (-2, 2)^T, \eta_3 = (0, -3)^T$, $\tau = 0.1/T$, $x_1(0) = (3, -3)^T, x_2(0) = (-8, 4)^T, x_3(0) = (4, 7)^T, x_4(0) = (-3, 3)^T, x_5(0) = (5, 6)^T$, and $x_6(0) = (7, 2)^T$.

No matter in which case, the state trajectories of all agents ($t \to \infty$) in the phase plane are presented in Figure 2(a), and the velocity trajectories of all followers in these two cases over time are depicted in Figures 3(a) and 3(b), respectively. It can be seen from Figures 2(a) and Figure 3 that the containment control of the systems can be achieved without the influence of initial positions.

5.2. Example 2. Now, take a more complex system into consideration, similar to example 1, but more vertices are added. Its communication topology graph is shown in Figure 1(b), where $l = \{1, 2, 3, 4, 5\}$ and $f = \{6, 7, 8, 9, 10\}$. It is noteworthy that each follower harbors at least one directed path to the leaders. Likewise, two cases are conducted for the confirmation.

In the first case, the parameters are set to be

$T = 0.1, \gamma = 0.5, \tau = 0.1/T, \eta_1 = (0, 4)^T, \eta_2 = (3, 0)^T, \eta_3 = (3, -3)^T$, $\eta_4 = (-3, -3)^T$, $\eta_5 = (-3, 0)^T$, $x_1(0) = (3, -3)^T$, $x_2(0) = (-8, 4)^T, x_3(0) = (4, 7)^T$, $x_4(0) = (-4, -6)^T$, $x_5(0) = (7, 8)^T$, $x_6(0) = (-5, 5)^T$, $x_7(0) = (-10, 9)^T$, $x_8(0) = (8.5, -7.5)^T, x_9(0) = (-5, 7)^T$, and $x_{10}(0) = (-4.5, 8.5)^T$.

In the second case, the parameters are set to be

$T = 0.1$, $\gamma = 0.5$, $\tau = 0.1/T$, $\eta_1 = (0, 4)^T$, $\eta_2 = (3, 0)^T$, $\eta_3 = (3, -3)^T$, $\eta_4 = (-3, -3)^T, \eta_5 = (-3, 0)^T$, $x_1(0) = (3, -3)^T, x_2(0) = (-8, 4)^T, x_3(0) = (4, 7)^T, x_4(0) = (-4, -6)^T$, $x_5(0) = (7, 8)^T, x_6(0) = (-3, 3)^T, x_7(0) = (5, -6)^T, x_8(0) = (7, 2)^T, x_9(0) = (-5, -6)^T$, and $x_{10}(0) = (2, -2)^T$.

In both cases, when $t \to \infty$, the state trajectories of all agents in the phase plane are illustrated in Figure 2(b), and the velocity trajectories of all followers in these two cases over time are depicted in Figures 4(a) and 4(b), respectively. From Figures 2(b) and 4, it can be seen that the containment control of the systems can be achieved with the number of agents increasing. The results unveil that the control protocol is efficient and robust for the containment problem.

6. Conclusion

This paper studies the containment control of heterogeneous discrete-time multiagent systems with time delay. In this manuscript,

(1) The double-integrator followers and single-integrator leaders are investigated.

(2) The containment control problem is of two layers. For the leaders, the information among multiple leaders is interactive and the leaders converge to the expected values. As for the followers, the states converge into the convex hull shaped by the final states of the leaders.

(3) The sufficient conditions of the sampling time, feedback gain, and delay to ensure the consensus control are given by using a reduced-order method.

(4) The maximum allowed time delay is determined by using the Z-transform.

Finally, the validity of our results is guaranteed by the simulation. In the future, our attention will be focused on the problems such as fractional-order dynamics with nonsymmetric time delays.

Data Availability

The data used to support the findings of the study are available within the article.

Conflicts of Interest

The authors declare that there are no conflicts of interest regarding the publication of this article.

Acknowledgments

This work was supported by the National Natural Science Foundation of China, under Grant 61772063, and Beijing Municipal Natural Science Foundation, under Grant Z180005.

References

[1] T. Vicsek, A. Czirók, E. Ben-Jacob, I. Cohen, and O. Shochet, "Novel type of phase transition in a system of self-driven particles," *Physical Review Letters*, vol. 75, no. 6, pp. 1226–1229, 1995.

[2] J. Ali, J. Lin, and A. Stephen Morse, "Coordination of groups of mobile autonomous agents using nearest neighbor rules," *IEEE Transactions on Automatic Control*, vol. 48, no. 6, pp. 988–1001, 2003.

[3] R. Olfati-Saber and R. M. Murray, "Consensus problems in networks of agents with switching topology and time-delays," *IEEE Transactions on Automatic Control*, vol. 49, no. 9, pp. 1520–1533, 2004.

[4] Y. Zhang and Q. Han, "Network-based synchronization of delayed neural networks," *IEEE Transactions on Circuits and Systems I: Regular Papers*, vol. 60, no. 3, pp. 676–689, 2013.

[5] Z. Qu, J. Wang, A. Richard, and Hull, "Cooperative control of dynamical systems with application to autonomous vehicles," *IEEE Transactions on Automatic Control*, vol. 53, no. 4, pp. 894–911, 2008.

[6] X. Liu, P. Guan, and C. W. Chan, "Nonlinear multivariable power plant coordinate control by constrained predictive scheme," *IEEE Transactions on Control Systems Technology*, vol. 18, no. 5, pp. 1116–1125, 2009.

[7] F.-Y. Wang, Y.-H. Ni, Z.-X. Liu, and Z.-Q. Chen, "Fully distributed containment control for second-order multi-agent systems with communication delay," *ISA Transactions*, vol. 99, pp. 123–129, 2020.

[8] W. Yu, G. Chen, and M. Cao, "Some necessary and sufficient conditions for second-order consensus in multi-agent dynamical systems," *Automatica*, vol. 46, no. 6, pp. 1089–1095, 2010.

[9] J. Qin, H. Gao, and W. X. Zheng, "Second-order consensus for multi-agent systems with switching topology and communication delay," *Systems & Control Letters*, vol. 60, no. 6, pp. 390–397, 2011.

[10] X. Yi, R. Guo, and Y. Qi, "Stabilization of chaotic systems with both uncertainty and disturbance by the ude-based control method," *IEEE Access*, vol. 8, pp. 62471–62477, 2020.

[11] L. Liu, B. Li, and R. Guo, "Consensus control for networked manipulators with switched parameters and topologies," *IEEE Access*, vol. 9, pp. 9209–9217, 2021.

[12] T. Hou, Y. Liu, and F. Deng, "Stability for discrete-time uncertain systems with infinite markov jump and time-delay," *Sciece China Information Sciences*, vol. 64, no. 5, 2021.

[13] J. Ni, L. Liu, C. Liu, and J. Liu, "Fixed-time leader-following consensus for second-order multiagent systems with input delay," *IEEE Transactions on Industrial Electronics*, vol. 64, no. 11, pp. 8635–8646, 2017.

[14] G. Wen, W. Yu, Z. Li, X. Yu, and J. Cao, "Neuro-adaptive consensus tracking of multiagent systems with a high-dimensional leader," *IEEE Transactions on Cybernetics*, vol. 47, no. 7, pp. 1730–1742, 2017.

[15] G. Wen, H. Wang, X. Yu, and W. Yu, "Bipartite tracking consensus of linear multi-agent systems with a dynamic leader," *IEEE Transactions on Circuits and Systems II: Express Briefs*, vol. 65, no. 9, pp. 1204–1208, 2018.

[16] G. Wen, Y. Zhao, Z. Duan, W. Yu, and G. Chen, "Containment of higher-order multi-leader multi-agent systems: a dynamic output approach," *IEEE Transactions on Automatic Control*, vol. 61, no. 4, pp. 1135–1140, 2016.

[17] J. Li, W. Ren, and S. Xu, "Distributed containment control with multiple dynamic leaders for double-integrator dynamics using only position measurements," *IEEE Transactions on Automatic Control*, vol. 57, no. 6, pp. 1553–1559, 2012.

[18] X. Wang, S. Li, and P. Shi, "Distributed finite-time containment control for double-integrator multiagent systems," *IEEE Transactions on Cybernetics*, vol. 44, no. 9, pp. 1518–1528, 2014.

[19] H. Liu and G. Xie, "Sampled-data based containment control of continuous-time multi-agent systems with switching topology and time-delays," *Neurocomputing*, vol. 286, pp. 19–30, 2018.

[20] L. Shi, J. Shao, M. Cao, and H. Xia, "Asynchronous group consensus for discrete-time heterogeneous multi-agent systems under dynamically changing interaction topologies," *Information Sciences*, vol. 463-464, pp. 282–293, 2018.

[21] Y. Zheng and L. Wang, "Containment control of heterogeneous multi-agent systems," *International Journal of Control*, vol. 87, no. 1, pp. 1–8, 2014.

[22] L. Shi, J. Shao, M. Cao, and H. Xia, "Distributed containment of heterogeneous multi-agent systems with switching topologies," *Neurocomputing*, vol. 312, pp. 41–48, 2018.

[23] X. Quan, P. Lin, W. Ren, C. Yang, and W. Gui, "Containment control for discrete-time multiagent systems with communication delays and switching topologies," *IEEE Transactions on Cybernetics*, vol. 49, no. 10, pp. 3827–3830, 2019.

[24] X. Dong, Q. Li, R. Zhang, and Y. Zhong, "Formation-containment analysis and design for high-order linear time-invariant swarm systems with time delays," in *Proceedings of the 2015 34th Chinese Control Conference (CCC)*, pp. 6847–6853, Hangzhou, China, July 2015.

[25] Y. Cao and W. Ren, "Containment control with multiple stationary or dynamic leaders under a directed interaction graph," in *Proceedings of the 48h IEEE Conference on Decision and Control (CDC) Held Jointly with 2009 28th Chinese*

Control Conference, pp. 3014–3019, Shanghai, China, December 2009.

[26] H. Liu, G. Xie, and L. Wang, "Necessary and sufficient conditions for containment control of networked multi-agent systems," *Automatica*, vol. 48, no. 7, pp. 1415–1422, 2012.

[27] X. Xie, "Stable polynomials with complex coefficients," in *Proceedings of the 1985 24th IEEE Conference on Decision and Control*, vol. 324–325, Fort Lauderdale, FL, USA, December 1985.

[28] M. Asgari and H. Atrianfar, "Necessary and sufficient conditions for containment control of heterogeneous linear multi-agent systems with fixed time delay," *IET Control Theory & Applications*, vol. 13, no. 13, pp. 2065–2074, 2019.

Hindawi
Mathematical Problems in Engineering
Volume 2021, Article ID 9941692, 11 pages
https://doi.org/10.1155/2021/9941692

Research Article

A Higher-Order Finite Difference Scheme for Singularly Perturbed Parabolic Problem

Shifang Tian, Xiaowei Liu, and Ran An

School of Mathematics and Statistics, Qilu University of Technology (Shandong Academy of Sciences), Jinan 250353, China

Correspondence should be addressed to Xiaowei Liu; xwliuvivi@hotmail.com

Received 3 April 2021; Accepted 22 July 2021; Published 20 August 2021

Academic Editor: Hui Wang

In this paper, we deal with a singularly perturbed parabolic convection-diffusion problem. Shishkin mesh and a hybrid third-order finite difference scheme are adopted for the spatial discretization. Uniform mesh and the backward Euler scheme are used for the temporal discretization. Furthermore, a preconditioning approach is also used to ensure uniform convergence. Numerical experiments show that the method is first-order accuracy in time and almost third-order accuracy in space.

1. Introduction

We consider the singularly perturbed parabolic problem posed on the domain $G = \Omega_x \times \Omega_t = (0,1) \times (0,T]$ as follows:

$$\begin{cases} Lu + \dfrac{\partial u}{\partial t} := -\varepsilon \dfrac{\partial^2 u}{\partial x^2} - a(x,t)\dfrac{\partial u}{\partial x} + c(x,t)u + \dfrac{\partial u}{\partial t} = f(x,t), & (x,t) \in G, \\ u(0,t) = u(1,t) = 0, & x \in \overline{\Omega}_t, \\ u(x,0) = u_0(x), & x \in \overline{\Omega}_x, \end{cases} \tag{1}$$

where $\overline{\Omega}_t = [0,T]$, $\overline{\Omega}_x = [0,1]$, and ε is a small positive perturbation parameter satisfying

$$0 < \varepsilon \le \varepsilon^* \ll 1, \tag{2}$$

with a positive constant ε^*, and $u_0(x)$ is the initial value when $t = 0$. We assume that the functions $a(x,t)$, $c(x,t)$, and $f(x,t)$ are sufficiently smooth, and that $a(x,t)$ and $c(x,t)$ satisfy

$$\begin{aligned} a(x,t) &\ge \beta > 0, \\ c(x,t) &> 0, \\ \forall (x,t) &\in \overline{G}, \end{aligned} \tag{3}$$

where β is a positive constant.

With these conditions, there exists a unique $C^{4,2}(\overline{G})$-solution u of problem (1) (see, for instance, [1]). The $C^{4,2}(\overline{G})$-solutions u of problem (1) satisfied from its original

function u to its fourth partial derivative for spatial variable u_{xxxx} are continuous, and solutions from its original function u to its second partial derivative for temporal variable u_{tt} are also continuous.

Singular perturbation problems play an important role in many areas, such as astronomy, mechanics, and fluid dynamics. It also has a broad background and important applications in control systems with different time scales [2–4]. It is especially important to find a uniform and effective approximate solution when the exact solution cannot be obtained. There are many methods for solving singular perturbation problems. Recent convergence analysis of the finite element method is referred to [5–14]. Except the finite element method, the finite difference method is the most widely used one at present. Nowadays, more and more people begin to study higher-order finite difference schemes for solving singular perturbation problems. In 1988, Vulanović in [15] proposed a third-order hybrid finite difference scheme and showed numerical results on the Shishkin mesh. Afterwards, Vulanovic and Nhan in [16] improved on what had already been done and proposed a new uniformly convergent numerical scheme. Both the methods proposed in [15, 17] have been analyzed on a piecewise-uniform Shishkin mesh and were proved to be almost third-order accuracy in space. Comparing the previous scheme, the difference is that when ε is large enough, the accuracy of the new scheme is better than the that of the previous scheme. However, when ε is small enough, there is no difference between these two methods.

In this paper, our primary aim is to propose and analyze a higher-order hybrid finite difference scheme for problem (1). This is accomplished by discretizing the domain Ω_x using the Shishkin mesh and by considering the uniform mesh in the temporal direction. In order to obtain the fully discrete scheme, we adopt the two-stage discretization process. The first stage consists of discretizing the time derivative with the backward difference scheme on the uniform mesh. In the second stage, discretize in the spatial direction by utilizing a hybrid finite difference scheme on the Shishkin mesh.

The ultimate goal of numerical methods for problem (1) is to obtain a series of discrete solutions so as to achieve a numerical approximation of the continuous solution. Such that its error converges to 0 uniformly as $N \longrightarrow +\infty$, where N is the number of discretization on the spatial mesh. Apart from this, in numerical experiments, we also need to illustrate that the proposed scheme is almost third-order accurate in space.

The rest of the paper is as follows. In Section 2, we define the meshes for temporal and spatial discretization and introduce some special difference operators. In Section 3, we define some difference operators and the final finite difference scheme. In Section 4, we give the linear equations needed to solve the problem and get the coefficient matrix and the right end term. In Section 5, we preprocess the coefficient matrix. In Section 6, we give the pseudo code to solve the problem. In Section 7, we give the results of numerical experiments. In Section 8, some final conclusions are given.

2. The Mesh

Here, in this section, we describe the uniform mesh for the temporal discretization of the domain Ω_t and the Shishkin mesh for the spatial discretization of the domain Ω_x.

We will often use the assumption that

$$\varepsilon \le C_* N^{-1}, \tag{4}$$

where C_* is a sufficiently small positive constant which is independent of both ε and N. All constants, independent of ε and N, are denoted generically by C.

2.1. The Uniform Mesh. For the time domain $[0, T]$, we use a uniform mesh with time step Δt, such that

$$\Omega_t^M = \left\{ t_n = n\Delta t \quad n = 0, \ldots, M \quad \Delta t = \frac{T}{M} \right\}, \tag{5}$$

where M is the number of mesh points in the t-direction on the interval $[0, T]$.

2.2. Shishkin Mesh. Since problem (1) has a boundary layer along the side $x = 1$, the mesh should be condensing in the neighborhood of $x = 1$. Define

$$\sigma = \min\left\{ \frac{1}{2}, \frac{\alpha\varepsilon}{\beta} \ln N \right\}, \tag{6}$$

with $\alpha \ge 4$ (the proof of range of α was given in [16]). To define the piecewise-uniform mesh, we divide the domain $[0, 1]$ into two subdomains, such that $[0, 1] = [0, 1-\sigma] \cup [1-\sigma, 1]$ and then divide each of the subdomains into $(N/2)$ equal intervals. Set

$$\begin{cases} h := h_i = \dfrac{(1-\sigma)}{N}, & \text{for } i = 0, 1, 2, \ldots, (N/2), \\ H := h_i = \dfrac{\sigma}{N}, & \text{for } i = (N/2) + 1, \ldots, N. \end{cases} \tag{7}$$

Now, we denote the spatial grids by

$$\Omega_x^N = \{0 = x_0, x_1, \ldots, x_{N/2} = 1 - \sigma, \ldots, x_N = 1\}, \tag{8}$$

where

$$x_i = \begin{cases} ih, & \text{for } i = 0, 1, 2, \ldots, (N/2), \\ 1 - \sigma + \left(i - \dfrac{N}{2}\right)H, & \text{for } i = (N/2) + 1, \ldots, N, \end{cases} \tag{9}$$

and $N \ge 4$ be a positive even integer. Here, the transition point $1 - \sigma$ separates the coarse and fine portions of the mesh.

Moreover, define

$$x_{i+z} = \begin{cases} x_i + zh_{i+1}, & \text{if } z \in [0, 1), \\ x_i + zh_i, & \text{if } z \in (-1, 0], \end{cases} \tag{10}$$

where z is some fixed constant.

3. Discretization

In this section, we will give different difference operators corresponding to different points on the Shishkin mesh and combine these difference operators to form the final numerical scheme.

Firstly, we denote by U_i^j the approximation of u at point (x_i, t_j) and set $f_{i+z}^j = f(x_{i+z}, t_j)$. Then, we use $D_{\chi,z}^{(0)}U_i^j$, $D_{\chi,z}^{(1)}U_i^j$, and $D_{\chi,z}^{(2)}U_i^j$ as the approximations of $u(x_{i+z}, t_j)$, $u_x(x_{i+z}, t_j)$, and $u_{xx}(x_{i+z}, t_j)$, respectively. They are defined by the following equation [16]:

$$\begin{cases} D_{\chi,z}^{(0)}U_i^j = \dfrac{1}{2}\left[z(z-1)U_{i-1}^j + 2\left(1-z^2\right)U_i^j + z(z+1)U_{i+1}^j\right], \\ D_{\chi,z}^{(1)}U_i^j = \dfrac{1}{6\chi}\left[\left(-3z^2+6z-2\right)U_{i-1}^j + 3\left(3z^2-4z-1\right)U_i^j + 3\left(-3z^2+2z+2\right)U_{i+1}^j + \left(3z^2-1\right)U_{i+2}^j\right], \\ D_{\chi,z}^{(2)}U_i^j = \dfrac{1}{\chi^2}\left[(1-z)U_{i-1}^j + (3z-2)U_i^j + (1-3z)U_{i+1}^j + zU_{i+2}^j\right], \end{cases} \tag{11}$$

where χ is the step size of a uniform mesh and z is a constant satisfying $z \in (-1, 1)$. We set $e_{i+z}^{(n)}$ as the truncation error between the numerical solution and the exact solution.

$$e_{i+z}^{(n)} = D_{\chi,z}^{(n)}U_i^j - u\left(x_{i+z}, t_j\right), \quad n = 0, 1, 2. \tag{12}$$

Firstly, $e_{i+z}^{(0)} = D_{\chi,z}^{(0)}U_i^j - u(x_{i+z}, t_j)$.

Lemma 1. *Suppose that*

$$\left|\frac{\partial^m}{\partial x^m}u(x,t)\right| \le C, \quad (x,t) \in \overline{\Omega}_x \times \overline{\Omega}_t,\ m \ge 0. \tag{13}$$

The truncation error associated to $e_{i+z}^{(0)}$ satisfies

$$\left\|e_{i+z}^0\right\|_\infty \le C\chi^3, \tag{14}$$

where χ is the step size.

Proof. We substitute $u(x_{i-1}, t_j)$, $u(x_i, t_j)$, and $u(x_{i+1}, t_j)$ for U_{i-1}^j, U_i^j, and U_{i+1}^j in operator $D_{\chi,z}^{(0)}U_i^j$ and apply the Taylor expansion to obtain

$$\begin{aligned} e_{i+z}^{(0)} = \frac{1}{2}\Big[&z(z-1)\left(u\left(x_i,t_j\right) - \chi u'\left(x_i,t_j\right) + \frac{1}{2}\chi^2 u''\left(x_i,t_j\right) - \frac{1}{6}\chi^3 u^3\left(x_i,t_j\right) + \cdots\right) + 2\left(1-z^2\right)u\left(x_i,t_j\right) \\ &+ z(z+1)\left(u\left(x_i,t_j\right) - \chi u'\left(x_i,t_j\right) + \frac{1}{2}\chi^2 u''\left(x_i,t_j\right) - \frac{1}{6}\chi^3 u^3\left(x_i,t_j\right) + \cdots\right)\Big] - \Big(u\left(x_i,t_j\right) - \chi u'\left(x_i,t_j\right) + \frac{1}{2}\chi^2 u''\left(x_i,t_j\right) \\ &- \frac{1}{6}\chi^3 u^3\left(x_i,t_j\right) + \cdots\Big) = \frac{1}{6}z\chi^3 u^3\left(x_i,t_j\right) - \frac{1}{6}z^3\chi^3 u^3\left(x_i,t_j\right) + O\chi^4. \end{aligned} \tag{15}$$

Thus,

$$\left\|e_{i+z}^{(0)}\right\|_\infty \le C\chi^3. \tag{16}$$

Secondly, $e_{i+z}^{(1)} = D_{\chi,z}^{(1)}U_i^j - u(x_{i+z}, t_j)$. □

Lemma 2. *Suppose that*

$$\left|\frac{\partial^m}{\partial x^m}u(x,t)\right| \le C, \quad (x,t) \in \overline{\Omega}_x \times \overline{\Omega}_t,\ m \ge 0. \tag{17}$$

The truncation error associated to $e_{i+z}^{(1)}$ satisfies

$$\left\|e_{i+z}^{(1)}\right\|_\infty \le C\chi^3, \tag{18}$$

where χ is the step size.

Proof. Similar to above, we substitute $u(x_{i-1}, t_j)$, $u(x_i, t_j)$, $u(x_{i+1}, t_j)$, and $u(x_{i+2}, t_j)$ for U_{i-1}^j, U_i^j, U_{i+1}^j, and U_{i+2}^j in operator $D_{\chi,z}^{(1)}U_i^j$ and again apply the Taylor expansion to obtain

$$
\begin{aligned}
e_{i+z}^{(1)} = {} & \frac{1}{6\chi}\Big[\left(-3z^2+6z-2\right)\Big(u\left(x_i,t_j\right)-\chi u'\left(x_i,t_j\right)+\frac{1}{2}\chi^2u''\left(x_i,t_j\right)-\frac{1}{6}\chi^3u^3\left(x_i,t_j\right)+\cdots\Big) \\
& +3\left(3z^2-4z-1\right)u\left(x_i,t_j\right)+3\left(-3z^2+2z+2\right)\Big(u\left(x_x,t_j\right)-\chi u'\left(x_i,t_j\right)+\frac{1}{2}\chi^2u''\left(x_i,t_j\right)-\frac{1}{6}\chi^3u^3\left(x_i,t_j\right)+\cdots\Big) \\
& +\left(3z^2-1\right)\Big(u\left(x_x,t_j\right)-\chi u'\left(x_i,t_j\right)+\frac{1}{2}(2\chi)^2u''\left(x_i,t_j\right)-\frac{1}{6}(2\chi)^3u^3\left(x_i,t_j\right)+\cdots\Big)\Big] \\
& -\Big(u\left(x_i,t_j\right)-\chi zu'\left(x_i,t_j\right)+\frac{1}{2}(\chi z)^2u''\left(x_i,t_j\right)-\frac{1}{6}(\chi z)^3u^3\left(x_i,t_j\right)+\cdots\Big) \\
= {} & \frac{1}{6}z\chi^3u^3\left(x_i,t_j\right)-\frac{1}{6}z^3\chi^3u^4\left(x_i,t_j\right)+O\chi^4.
\end{aligned}
\tag{19}
$$

Thus,

$$\left\|e_{i+z}^{(1)}\right\|_\infty \le C\chi^3. \tag{20}$$

In conclusion, both $D_{\chi,z}^{(0)}U_i^j$ and $D_{\chi,z}^{(1)}U_i^j$ are third-order accurate with respect to the spatial variable x for any value of z; if $z=(1/\sqrt{3})$, $D_{\chi,z}^{(1)}U_i^j$ is transformed into the classical three-point scheme. And in the same way, operator $D''U_i^j$ (27), $\overline{D}^{(0)}U_{N/2}^j$ (29), $\widehat{D}''U_{N/2}^j$ (30), and time difference operator $D_t^-U_i^j$ can all be proven.

Moreover, $e_{i+z}^{(2)} = D_{\chi,z}^{(2)}U_i^j - u(x_{i+z},t_j)$. □

Lemma 3. *Assume that*

$$\left|\frac{\partial^m}{\partial x^m}u(x,t)\right| \le C, \quad (x,t)\in\overline{\Omega}_x\times\overline{\Omega}_t,\ m\ge 0. \tag{21}$$

The truncation error associated to $e_{i+z}^{(2)}$ satisfies that if $z=((3-\sqrt{15})/6)$,

$$\left\|e_{i+z}^{(2)}\right\|_\infty \le C\chi^3, \tag{22}$$

else

$$\left\|e_{i+z}^{(2)}\right\|_\infty \le C\chi^2, \tag{23}$$

where χ is the step size.

Proof. Once more, substituting $u(x_{i-1},t_j), u(x_i,t_j)$, $u(x_{i+1},t_j)$, and $u(x_{i+2},t_j)$ for $U_{i-1}^j, U_i^j, U_{i+1}^j$, and U_{i+2}^j in operator $D_{\chi,z}^{(2)}U_i^j$ and applying the Taylor expansion results in

$$
\begin{aligned}
e_{i+z}^{(2)} = {} & \frac{1}{\chi^2}\Big[(1-z)\Big(u\left(x_i,t_j\right)-\chi u'\left(x_i,t_j\right)+\frac{1}{2}\chi^2u''\left(x_i,t_j\right)-\frac{1}{6}\chi^3u^3\left(x_i,t_j\right)+\frac{1}{24}\chi^4u^4\left(x_i,t_j\right)-\frac{1}{120}\chi^5u^5\left(x_i,t_j\right)+\cdots\Big) \\
& +(3z-2)u\left(x_i,t_j\right)+(1-3z)\Big(u\left(x_i,t_j\right)-\chi u'\left(x_i,t_j\right)+\frac{1}{2}\chi^2u''\left(x_i,t_j\right)-\frac{1}{6}\chi^3u^3\left(x_i,t_j\right) \\
& +\frac{1}{24}\chi^4u^4\left(x_i,t_j\right)-\frac{1}{120}\chi^5u^5\left(x_i,t_j\right)+\cdots\Big)+z\Big(u\left(x_i,t_j\right)-\chi u'\left(x_i,t_j\right)+\frac{1}{2}(2\chi)^2u''\left(x_i,t_j\right)-\frac{1}{6}(2\chi)^3u^3\left(x_i,t_j\right) \\
& +\frac{1}{24}(2\chi)^4u^4\left(x_i,t_j\right)-\frac{1}{120}(2\chi)^5u^5\left(x_i,t_j\right)+\cdots\Big)\Big] \\
& -\Big(u''\left(x_i,t_j\right)+z\chi u^3\left(x_i,t_j\right)+\frac{1}{2}(z\chi)^2u^4\left(x_i,t_j\right)+\frac{1}{6}(z\chi)^3u^5\left(x_i,t_j\right)+\cdots\Big) \\
= {} & \left(\frac{3}{4}-\frac{1}{12}z-\frac{z^2}{2}\right)\chi^2u^4\left(x_i,t_j\right)+\left(\frac{1}{4}+\frac{1}{30}z+\frac{z^3}{6}\right)\chi^3u^5\left(x_i,t_j\right)+O\chi^4,
\end{aligned}
\tag{24}
$$

we can found that the operator $D_{\chi,z}^{(2)}U_i^j$ in general is second-order accurate, and if $z=((3-\sqrt{15})/6)$, it is third-order accurate.

These schemes can be used to create the following difference operator $\Lambda_{\chi,z}$:

$$
\begin{aligned}
\Lambda_{\chi,z}U_i^j = {} & -\varepsilon D_{\chi,z}^{(2)}U_i^j - a\left(x_{i+z},t_j\right)D_{\chi,z}^{(1)}U_i^j \\
& + c\left(x_{i+z},t_j\right)D_{\chi,z}^{(0)}U_i^j, \quad i=1,\ldots,\frac{N}{2}-2,
\end{aligned}
\tag{25}
$$

where $z = ((3-\sqrt{15})/6)$ and $\chi = h$. The operator $\Lambda_{\chi,z}$ is only used as part of the discretization on the Shishkin grid because the Shishkin grid is not uniform in the entire computational domain. More specifically, the difference operator $\Lambda_{\chi,z}$ cannot be applied at $x_{(N/2)-1}$ and x_{N-1}. □

Remark 1. Because scheme $\Lambda_{\chi,z}$ has point (x_{i+2}, t_j) in it, the Shishkin grid used is divided into two intervals, $[0, x_{N/2}]$ and $[x_{(N/2)+1}, x_N]$. Since the step size is different and the point x_{i+2} spans two intervals, the difference operator $\Lambda_{\chi,z}$ cannot be applied at either $x_{(N/2)-1}$ or x_{N-1}.

Now, we introduce the difference operator as follows:

$$\widetilde{\Lambda}_{\chi,z}U_i^j = -\varepsilon\, D''U_i^j + a\left(x_{i+z}, t_j\right)D_{\chi,z}^{(1)}U_i^j + c\left(x_{i+z}, t_j\right)D_{\chi,z}^{(0)}U_i^j, \quad i = \frac{N}{2}+1, \ldots, N-1, \tag{26}$$

with

$$D''U_i^j = \frac{2}{h_i^j + h_{i+1}^j}\left(\frac{U_{i+1}^j - U_i^j}{h_{i+1}^j} - \frac{U_i^j - U_{i-1}^j}{h_i^j}\right), \tag{27}$$

where $z = (1/\sqrt{3})$ and $\chi = H$, and it is also third-order accurate.

Then, we give the scheme at point $x_{N/2}$ by means of one-side difference schemes as follows:

$$\widehat{\Lambda}_{H,1-z}U_{N/2}^j = -\varepsilon\widehat{D}''U_{N/2}^j + a\left(x_{(N/2)+1-z}, t_j\right)D_{H,1-z}^{(1)}U_{N/2}^j + c\left(x_{(N/2)+1-z}, t_j\right)\overline{D}^{(0)}U_{N/2}^j, \tag{28}$$

with

$$\overline{D}^{(0)}U_{N/2}^j = \left(\frac{1}{6}+\frac{z}{2}\right)U_{N/2}^j + \frac{2}{3}U_{(N/2)+1}^j + \left(\frac{1}{6}-\frac{z}{2}\right)U_{(N/2)+2}^j, \tag{29}$$

and

$$\widehat{D}''U_{N/2}^j = \frac{1}{H^2}\left(U_{N/2}^j - 2U_{(N/2)+1}^j + U_{(N/2)+2}^j\right), \tag{30}$$

where $z = 1-(1/\sqrt{3})$ and $\chi = H$, and both $\overline{D}^{(0)}U_{N/2}^j$ and $\widehat{D}''U_{N/2}^j$ have third-order accuracy in space.

In addition, about the t-direction, the discretization of $u_t(x_i, t_j)$ by the backward Euler scheme is defined by

$$D_t^- U_i^j = \frac{U_i^j - U_i^{j-1}}{\Delta t} \approx u_t\left(x_i, t_j\right), \tag{31}$$

with the time step Δt, and it is first-order accurate with respect to the temporal variable t.

Finally, we combine $D_t^- U_i^j$ with three difference operators $\Lambda_{\chi,z}U_i^j$, $\widetilde{\Lambda}_{\chi,z}U_i^j$, and $\widehat{\Lambda}_{\chi,z}U_i^j$ at different points, respectively, and finally propose the following numerical scheme:

$$\begin{cases} \Lambda_{h,z}U_i^j + D_t^- U_i^j = f_{i+z}^j\left(z = \dfrac{3-\sqrt{15}}{6}\right), & \text{for } 1 \le i \le \dfrac{N}{2}-2, \\ \widetilde{\Lambda}_{h,z}U_i^j + D_t^- U_i^j = f_{i+z}^j\left(z = \dfrac{1}{\sqrt{3}}\right), & \text{for } i = \dfrac{N}{2}-1, \\ \widehat{\Lambda}_{H,z}U_i^j + D_t^- U_i^j = f_{i+z}^j\left(z = 1-\dfrac{1}{\sqrt{3}}\right), & \text{for } i = \dfrac{N}{2}, \\ \widetilde{\Lambda}_{H,z}U_i^j + D_t^- U_i^j = f_{i+z}^j\left(z = \dfrac{1}{\sqrt{3}}\right), & \text{for } \dfrac{N}{2}+1 \le i \le N-1, \end{cases} \tag{32}$$

with $j = 1, \ldots, M$.

4. Linear Problem

The corresponding difference schemes of u_{xx}, u_x, and u at point (x_{i+z}, t_j) and u_t at point (x_i, t_j) are substituted into equation (1). When combined with scheme (32), the following linear equations (33) are obtained:

$$r_1U_{i-1}^j + r_2U_i^j + r_3U_{i+1}^j + r_4U_{i+2}^j = g^j, \tag{33}$$

where U_i^j is the approximation of $u(x_i, t_j)$ and r_1, r_2, r_3, r_4, and g^j are defined as follows: if $1 \le i \le (N/2)-2$,

$$\begin{cases} r_1 = \dfrac{-\varepsilon(1-z)\Delta t}{h^2} - \dfrac{\Delta t b\left(x_{i+z}, t_j\right)\left(-3z^2+6z-2\right)}{6h} + \dfrac{1}{2}\Delta t z(z-1) + \dfrac{1}{2}z(z-1), \\ r_2 = \dfrac{-\varepsilon\Delta t(3z-2)}{h^2} - \dfrac{\Delta t b\left(x_{i+z}, t_j\right)\left(3q^2-4z-1\right)}{2h} + \Delta t\left(1-z^2\right) + z(z+1), \\ r_3 = \dfrac{-\varepsilon\Delta t(1-3z)}{h^2} - \dfrac{\Delta t b\left(x_{i+z}, t_j\right)\left(-3z^2+2z+2\right)}{2h} + \dfrac{1}{2}\Delta t z(z+1) + \dfrac{1}{2}z(z+1), \\ r_4 = \dfrac{-\varepsilon\Delta t z}{h^2} - \dfrac{\Delta t b\left(x_{i+z}, t_j\right)\left(3z^2-1\right)}{6h}, \\ g^j = \Delta t f\left(x_{i+z}, t_j\right) + D_{h,z}^{(0)} U_i^{j-1}, \end{cases} \tag{34}$$

where Δt is the time steps, h is the space steps defined by (7), $z = ((3-\sqrt{15})/6)$, and $D_{h,z}^{(0)} U_i^{j-1}$ is defined by (11). If $i = (N/2) - 1$,

$$\begin{cases} r_1 = \dfrac{-\varepsilon\Delta t}{h^2} - \dfrac{\Delta t b\left(x_{i+z}, t_j\right)\left(-3z^2+6z-2\right)}{6h} + \dfrac{1}{2}\Delta t z(z-1) + \dfrac{1}{2}z(z-1), \\ r_2 = \dfrac{\varepsilon\Delta t}{h^2} + \dfrac{\varepsilon\Delta t}{h^2} - \dfrac{\Delta t b\left(x_{i+z}, t_j\right)\left(3z^2-4z-1\right)}{2h} + \Delta t\left(1-z^2\right) + \left(1-z^2\right), \\ r_3 = \dfrac{-\varepsilon\Delta t}{h^2} - \dfrac{\Delta t b\left(x_{i+z}, t_j\right)\left(-3z^2+2z+2\right)}{2h} + \dfrac{1}{2}\Delta t z(z+1) + \dfrac{1}{2}z(z-1), \\ r_4 = 0, \\ g^j = \Delta t f\left(x_{i+z}, t_j\right) + D_{h,z}^{(0)} U_i^{j-1}, \end{cases} \tag{35}$$

where Δt is the time steps, h is the space steps defined by (7), $z = (1/\sqrt{3})$, and $D_{h,z}^{(0)} U_i^{j-1}$ is defined by (11). If $i = (N/2)$,

$$\begin{cases} r_1 = 0, \\ r_2 = \dfrac{-\varepsilon \Delta t}{H^2} - \dfrac{\Delta t b\left(x_{i+z}, t_j\right)\left(3z^2 - 2z - 2\right)}{2H} + \dfrac{1}{2}\Delta t\left(\dfrac{1}{3} + z\right) + \dfrac{1}{2}\left(\dfrac{1}{3} + z\right), \\ r_3 = \dfrac{-\varepsilon \Delta t z}{H^2} - \dfrac{\Delta t b\left(x_{i+z}, t_j\right)\left(3z^2 - 1\right)}{6H} + \dfrac{2}{3}\Delta t + \dfrac{2}{3}, \\ r_4 = \dfrac{-\varepsilon \Delta t}{H^2} - \dfrac{\Delta t b\left(x_{i+z}, t_j\right)\left(3z^2 - 6z + 2\right)}{6H} + \dfrac{1}{2}\Delta t\left(\dfrac{1}{3} - z\right) + \dfrac{1}{2}\left(\dfrac{1}{3} - z\right), \\ g^j = \Delta t f\left(x_{i+1-z}, t_j\right) + \overline{D}^{(0)} U_{N/2}^{j-1}, \end{cases} \tag{36}$$

where Δt is the time steps, H is the space steps defined by (7), $z = 1 - (1/\sqrt{3})$, and $\overline{D}^{(0)} U_{N/2}^{j-1}$ is defined by (11). If $(N/2) + 1 \le i \le N - 1$,

$$\begin{cases} r_1 = \dfrac{-\varepsilon \Delta t}{H^2} - \dfrac{\Delta t b\left(x_{i+z}, t_j\right)\left(-3z^2 + 6z - 2\right)}{6H} + \dfrac{1}{2}\Delta t z\,(z-1) + \dfrac{1}{2} z\,(z-1), \\ r_2 = \dfrac{\varepsilon \Delta t}{H^2} + \dfrac{\varepsilon \Delta t}{H^2} - \dfrac{\Delta t b\left(x_{i+z}, t_j\right)\left(3z^2 - 4z - 1\right)}{2H} + \Delta t\left(1 - z^2\right) + \left(1 - z^2\right), \\ r_3 = \dfrac{-\varepsilon \Delta t}{H^2} - \dfrac{\Delta t b\left(x_{i+z}, t_j\right)\left(-3z^2 + 2z + 2\right)}{2H} + \dfrac{1}{2}\Delta t z\,(z+1) + \dfrac{1}{2} z\,(z+1), \\ r_4 = 0, \\ g^j = \Delta t f\left(x_{i+z}, t_j\right) + D_{H,z}^{(0)} U_i^{j-1}, \end{cases} \tag{37}$$

where Δt is the time steps, H is the space steps defined by (7), $z = (1/\sqrt{3})$, and $D_{H,z}^{(0)} U_i^{j-1}$ is defined by (11).

Finally, the linear system for numerical scheme (32) is obtained, that is,

$$\widehat{A}x = g. \tag{38}$$

Here, the coefficient matrix $\widehat{A}$ is defined by

$$\begin{array}{c} \text{row} \\ 1 \\ 2 \\ 3 \\ \vdots \\ \frac{N}{2}-2 \\ \frac{N}{2}-1 \\ \frac{N}{2} \\ \frac{N}{2}+1 \\ \frac{N}{2}+2 \\ \vdots \\ N-2 \\ N-1 \end{array} \begin{pmatrix} r_2 & r_3 & r_4 & & & & & & & & & \\ r_1 & r_2 & r_3 & r_4 & & & & & & & & \\ & r_1 & r_2 & r_3 & r_4 & & & & & & & \\ & & \ddots & \ddots & \ddots & \ddots & & & & & & \\ & & & r_1 & r_2 & r_3 & r_4 & & & & & \\ & & & & r_1 & r_2 & r_3 & & & & & \\ & & & & & & r_2 & r_3 & r_4 & & & \\ & & & & & & r_1 & r_2 & r_3 & & & \\ & & & & & & & r_1 & r_2 & r_3 & & \\ & & & & & & & & \ddots & \ddots & \ddots & \\ & & & & & & & & & r_1 & r_2 & r_3 \\ & & & & & & & & & & r_1 & r_2 \end{pmatrix}, \tag{39}$$

where each unwritten element is 0. The unknown term x is defined by $(x_0, x_1, x_2, \ldots, x_{N-1}, x_N)^T$ with $x_0 = 0$ and $x_N = 1$, and the right end term g is defined by $(g_0, g_1, g_2, \ldots, g_{N-1}, g_N)^T$.

5. Preconditioning

In this section, we analyze the $(N-1) \times (N-1)$ matrix $\widehat{A}$, which corresponds to the first scheme (32) and is acquired in Section 4. We need to assume (4) and that N is sufficiently large and

$$N \geq N_*, \tag{40}$$

where N_* is a positive integer independent of ε. There exist constants N_* and C_* such that (4) and (40) are satisfied, and the matrix $\widehat{A}$ has the following structure:

$$\begin{array}{c} \text{row} \\ 1 \\ 2 \\ 3 \\ \vdots \\ \frac{N}{2}-2 \\ \frac{N}{2}-1 \\ \frac{N}{2} \\ \frac{N}{2}+1 \\ \frac{N}{2}+2 \\ \vdots \\ N-2 \\ N-1 \end{array} \begin{pmatrix} + & - & + & & & & & & & & & \\ - & + & - & + & & & & & & & & \\ & - & + & - & + & & & & & & & \\ & & \ddots & \ddots & \ddots & \ddots & & & & & & \\ & & & - & + & - & + & & & & & \\ & & & & - & + & - & & & & & \\ & & & & & & + & - & + & & & \\ & & & & & & - & + & - & & & \\ & & & & & & & - & + & - & & \\ & & & & & & & & \ddots & \ddots & \ddots & \\ & & & & & & & & & - & + & - \\ & & & & & & & & & & - & + \end{pmatrix}, \tag{41}$$

where each unwritten element is 0.

Multiply its equations $1, 2, \ldots, (N/2) - 1$ by (h/H). We do this to achieve consistency uniform in ε, but at the same time, the coefficient matrix gets preconditioned as well (the preconditioning be described in [18, 19]).

Thus, we take the matrix of the preconditioned system as follows:

$$\widehat{B} := \operatorname{diag}(m_1, m_2, \ldots, m_{N-1})\widehat{A}, \tag{42}$$

where

$$m_i = \begin{cases} \dfrac{h}{H}, & \text{for } i = 0, 1, 2, \ldots, \dfrac{N}{2} - 1, \\[2ex] 1, & \text{for } i = \dfrac{N}{2}, \ldots, N-1. \end{cases} \tag{43}$$

6. Pseudo Code

In this section, the pseudo code needed to solve problem (1) using numerical scheme (32) in MATLAB will be presented. In general, if mathematical tools are used to solve problem like this, by scheme (32), there are six steps as follows [17]:

(1) Set the uniform mesh for temporal variable (M is the total number of points in t-direction)

(2) Set the Shishkin mesh for spatial variable (N is the total number of points in space)

(3) Write down the coefficient matrix $\widehat{A}$ and the right end term g for the linear system as follows:

$$\widehat{A} = \begin{cases} \text{for } n = 1\colon M \text{ (temporal points)}, \\ \begin{cases} \text{for } i = \dfrac{N}{2} - 2, \\ h(i,n) = x(i,n) - x(i-1,n), \\ r_1 U_{i-1}^n + r_2 U_i^n + r_3 U_{i+1}^n + r_4 U_{i+2}^n = g^n, \\ \text{end}, \end{cases} \\ \begin{cases} \text{for } i = \dfrac{N}{2} - 1, \\ h(i,n) = x(i,n) - x(i-1,n), \\ r_1 U_{i-1}^n + r_2 U_i^n + r_3 U_{i+1}^n + r_4 U_{i+2}^n = g^n, \\ \text{end}, \end{cases} \\ \begin{cases} \text{for } i = \dfrac{N}{2}, \\ h(i,n) = x(i,n) - x(i-1,n), \\ r_1 U_{i-1}^n + r_2 U_i^n + r_3 U_{i+1}^n + r_4 U_{i+2}^n = g^n, \\ \text{end}, \end{cases} \\ \begin{cases} \text{for } i = \dfrac{N}{2} + 1\colon N - 1, \\ h(i,n) = x(i,n) - x(i-1,n), \\ r_1 U_{i-1}^n + r_2 U_i^n + r_3 U_{i+1}^n + r_4 U_{i+2}^n = g^n, \\ \text{end}, \end{cases} \\ \text{end}, \end{cases} \tag{44}$$

where U_i^n is the approximation of $u(x_i, t_n)$, $h(i,n)$ is the space steps, r_1, r_2, r_3, and r_4 are the elements of the coefficient matrix, and g^n is the right end term (it is defined in Section 4)

(4) A new matrix $\widehat{B}$ (from Section 5) is obtained by preprocessing the matrix $\widehat{A}$

(5) The new matrix $\widehat{B}$ and the right end term g are used to solve problem (1)

(6) The maximum pointwise errors and the orders of convergence are calculated

7. Numerical Experiments

In this section, we shall present the numerical results obtained by the proposed numerical schemes (32) for the test problem (45) on the piecewise-uniform rectangular mesh $G = \Omega_x^N \times \Omega_t^M$. In both cases, we perform the numerical experiments by choosing the constants $\alpha = 4$ and $\beta = 1$ in (6) and the time step $\Delta t = (1.0/M)$.

For numerical tests, we consider the following singularly perturbed parabolic problem:

$$\begin{cases} -\varepsilon \dfrac{\partial^2 u}{\partial x^2} - (x+1)\dfrac{\partial u}{\partial x} + u + \dfrac{\partial u}{\partial t} = f(x,t), \quad (x,t) \in G, \\ u(0,t) = u(1,t) = 0, \quad t \in [0,1], \\ u(x,0) = 0, \quad x \in [0,1], \end{cases} \tag{45}$$

where $G := (0,1) \times (0,1]$. We choose the initial data $u(x,0) = 0$ and the exact solution for problem (45) as follows [16]:

$$u(x,t) = t\left(e^{-(x/\varepsilon)} - e^x + \left(e - e^{-(1/\varepsilon)}\right)x\right). \tag{46}$$

As the exact solution of problem (45) is known, we calculate the maximum pointwise error by

$$E_\varepsilon^{N,\Delta t} = \max\left|u_{i,j} - U_{i,j}^{N,\Delta t}\right|, \tag{47}$$

for each ε, where $u_{i,j}$ and $U_{i,j}^{N,\Delta t}$ denote the exact solution and numerical solution on (x_i, t_j), respectively. The convergence order is calculated by the following formula:

$$R_\varepsilon^{N,\Delta t} = \log_2\left[\frac{E_\varepsilon^{N,\Delta t}}{E_\varepsilon^{2N,(\Delta t/2)}}\right]. \tag{48}$$

The maximum pointwise errors $E_\varepsilon^{N,\Delta t}$ and the order of convergence $R_\varepsilon^{N,\Delta t}$ by using schemes (32) are presented in Table 1. In table, we can observe the ε-uniform convergence of the numerical scheme. The order of convergence in Table 1 is first-order due to the effect of time error. In order to justify the spatial order of convergence precisely, we take $M = N^3$ and the order of convergence is defined by

Table 1: Temporal errors and converge orders of scheme (32), E_ε, R_ε.

	$N, \Delta t$					
ε	32, (1/(32))	64, (1/(64))	128, (1/(128))	256, (1/(256))	512, (1/(512))	
10^{-2}	0.01367	0.006294	0.002864	0.001293	$5.788e-04$	E_ε
10^{-2}	1.12	1.14	1.15	1.15	—	R_ε
10^{-4}	0.02067	0.010505	0.005285	0.00265	0.001325	
10^{-4}	0.9710	0.9910	0.9966	0.9989	—	
10^{-6}	0.02075	0.01055	0.005315	0.00267	0.001335	
10^{-6}	0.9754	0.9898	0.9954	0.9977	—	
10^{-8}	0.02075	0.01055	0.005315	0.002665	0.001335	
10^{-8}	0.9754	0.9898	0.9954	0.9983	—	

Table 2: Spatial errors and converge orders of scheme (32), E_ε, R_ε.

	$N, \Delta t$					
ε	32, $(1/(32)^3)$	64, $(1/(64)^3)$	128, $(1/(128)^3)$	256, $(1/(256)^3)$	512, $(1/(512)^3)$	
10^{-2}	0.0088	0.0021	$4.538e-04$	$8.644e-05$	$1.453e-05$	E_ε
10^{-2}	2.05	2.22	2.39	2.57	—	R_ε
10^{-4}	0.0088	0.0021	$4.538e-04$	$8.644e-05$	$1.453e-05$	
10^{-4}	2.05	2.22	2.39	2.57	—	
10^{-6}	0.0089	0.0022	$4.715e-04$	$9.397e-05$	$1.739e-05$	
10^{-6}	2.03	2.22	2.31	2.44	—	
10^{-8}	0.0089	0.0022	$4.714e-04$	$9.397e-05$	$1.7393e-05$	
10^{-8}	2.04	2.20	2.33	2.43	—	

$$R_\varepsilon^{N,\Delta t} = \log_2\left[\frac{E_\varepsilon^{N,\Delta t}}{E_\varepsilon^{2N,(\Delta t/8)}}\right]. \tag{49}$$

The numerical results are presented in Table 2, where the spatial convergence order is almost third-order.

8. Conclusion

A hybrid scheme is proposed for obtaining a numerical solution to the singularly perturbed parabolic problem. The idea is based on the methods presented in the existing research study [15–19]. It can be seen from the results of numerical experiments, whether in space or in time, the scheme is robust insomuch the error of the numerical solution does not increase when $\varepsilon \longrightarrow 0$. On the contrary, the proposed schemes improve as ε diminishes, becoming almost third-order accurate with the spatial variable and first-order accurate with the temporal variable. The numerical results were compared with those from literature [15–18, 20, 21] which showed that all results reach the expected order of convergence. However, so far it is not possible to construct an arbitrary high-order difference scheme for Shishkin grids, meaning further research is needed. It should be noted that parallelization is not discussed in this article, so the reader is encouraged to refer to additional work [20, 21].

Data Availability

The data used to support the findings of this study are openly available in web of science at https://doi.org/10.1016/j.amc.2020.125495.

Conflicts of Interest

The authors declare that they have no conflicts of interest.

Acknowledgments

This research was partially supported by National Natural Science Foundation of China (11771257 and 11601251).

References

[1] J. Lorenz, "Stability and monotonicity properties of stiff quasilinear boundary value problems," *Review of Research Faculty of Science—University of Novi Sad*, vol. 12, pp. 151–175, 1982.

[2] X. Yi, R. Guo, and Y. Qi, "Stabilization of chaotic systems with both uncertainty and disturbance by the UDE-based control method," *IEEE Access*, vol. 8, no. 1, pp. 62471–62477, 2020.

[3] L. Liu, B. Li, and R. Guo, "Consensus control for networked manipulators with switched parameters and topologies," *IEEE Access*, vol. 9, pp. 9209–9217, 2021.

[4] T. Hou, Y. Liu, and F. Deng, "Stability for discrete-time uncertain systems with infinite Markov jump and time-delay," *Science China Information Sciences*, vol. 64, no. 5, pp. 1–11, 2021.

[5] X. Liu, M. Stynes, and J. Zhang, "Supercloseness of edge stabilization on Shishkin rectangular meshes for convection-diffusion problems with exponential layers," *IMA Journal of Numerical Analysis*, vol. 38, no. 4, pp. 2105–2122, 2018.

[6] J. Zhang and X. Liu, "Analysis of SDFEM on Shishkin triangular meshes and hybrid meshes for problems with characteristic layers," *Journal of Scientific Computing*, vol. 68, no. 3, pp. 1299–1316, 2016.

[7] J. Zhang and X. Liu, "Supercloseness of the SDFEM on Shishkin triangular meshes for problems with exponential

layers," *Advances in Computational Mathematics*, vol. 43, no. 4, pp. 759–775, 2017.

[8] J. Zhang and X. Liu, "Optimal order of uniform convergence for finite element method on Bakhvalov-type meshes," *Journal of Scientific Computing*, vol. 85, no. 1, p. 2, 2020.

[9] J. Zhang and X. Liu, "Supercloseness of linear finite element method on Bakhvalov-type meshes for singularly perturbed convection-diffusion equation in 1D," *Applied Mathematics Letters*, vol. 111, Article ID 106624, 2021.

[10] M. Yang, "Higher-order finite volume element methods based on Barlow points for one-dimensional elliptic and parabolic problems," *Numerical Methods for Partial Differential Equations*, vol. 31, no. 4, pp. 977–994, 2015.

[11] J. Zhang and Y. Lv, "High-order finite element method on a Bakhvalov-type mesh for a singularly perturbed convection-diffusion problem with two parameters," *Applied Mathematics and Computation*, vol. 397, Article ID 125953, 2021.

[12] J. Zhang and M. Stynes, "Supercloseness of continuous interior penalty method for convection-diffusion problems with characteristic layers," *Computer Methods in Applied Mechanics and Engineering*, vol. 319, pp. 549–566, 2017.

[13] M. Stynes and E. O'Riordan, "A uniformly convergent Galerkin method on a Shishkin mesh for a convection-diffusion problem," *Journal of Mathematical Analysis and Applications*, vol. 214, no. 1, pp. 36–54, 1997.

[14] H.-G. Roos, M. Stynes, and L. Tobiska, "Robust numerical methods for singularly perturbed differential equations," *Springer Series in Computational Mathematics*, Springer-Verlag, vol. 24, Springer-Verlag, Berlin, Germany, 2nd edition, 2008.

[15] R. Vulanović, "Higher order monotone schemes for a nonlinear singular perturbation problem," *ZAMM: Zeitschrift für Angewandte Mathematik und Mechanik*, vol. 68, no. 5, 1988.

[16] R. Vulanović and T. A. Nhan, "Robust hybrid schemes of higher order for singularly perturbed convection-diffusion problems," *Journal of Computational and Applied Mathematics*, vol. 386, Article ID 125495, 2020.

[17] S. Gowrisankar and S. Natesan, "An efficient robust numerical method for singularly perturbed Burgers' equation," *Applied Mathematics and Computation*, vol. 346, pp. 385–394, 2019.

[18] A. Das and S. Natesan, "Uniformly convergent hybrid numerical scheme for singularly perturbed delay parabolic convection-diffusion problems on Shishkin mesh," *Applied Mathematics and Computation*, vol. 271, pp. 168–186, 2015.

[19] H.-G. Roos, "A note on the conditioning of upwind schemes on Shishkin meshes," *IMA Journal of Numerical Analysis*, vol. 16, no. 4, pp. 529–538, 1996.

[20] J. Vigo-Aguiar and S. Natesan, "A parallel boundary value technique for singularly perturbed two-point boundary value problems," *The Journal of Supercomputing*, vol. 27, no. 2, pp. 195–206, 2004.

[21] S. Natesan, J. Vigo-Aguiar, and N. Ramanujam, "A numerical algorithm for singular perturbation problems exhibiting weak boundary layers," *Applied Mathematics and Computation*, vol. 45, no. 1–3, pp. 469–479, 2003.

Hindawi
Mathematical Problems in Engineering
Volume 2021, Article ID 9937008, 10 pages
https://doi.org/10.1155/2021/9937008

Research Article

Finite-Time H_∞ Control of Affine Nonlinear Singular Systems Subject to Actuator Saturation

Liying Sun,[1] **Meiqing Li**,[2] **and Renming Yang**[3]

[1]*School of Business, Shanghai Dianji University, Shanghai 201306, China*
[2]*School of Automation, Nanjing University of Science and Technology, Nanjing 210094, China*
[3]*School of Information Science and Electrical Engineering, Shandong Jiaotong University, Jinan 250357, China*

Correspondence should be addressed to Liying Sun; ss_sunly@163.com

Received 4 March 2021; Revised 29 June 2021; Accepted 19 July 2021; Published 29 July 2021

Academic Editor: Maria Patrizia Pera

This paper discusses the finite-time stable and finite-time H_∞ control problems of affine nonlinear singular systems subject to actuator saturation. Some sufficient conditions, to guarantee the system is finite-time stable, are established for the affine nonlinear singular systems subject to actuator saturation. First, the finite-time stable problem is investigated by the state undecomposed method, and then the finite-time robust H_∞ control law is presented for the system. Finally, the effectiveness of the designed controllers is shown by an example of a nonlinear singular circuit system in this paper.

1. Introduction

Singular system, also called descriptor system, is applied to many areas, such as engineering, economic, and biological systems [1]. In the past decades, the singular system has attracted interest of more and more researchers, and a lot of results are proposed for the linear singular system [1–10]. However, due to the complexity of the structure, few explore the nonlinear singular systems [11–15]. With the linear matrix inequality (LMI) method, the author in [11] has studied the robust control problem in connection with a set of stochastically nonlinear singular jump systems, while the guaranteed cost control and stabilization problems have been investigated for a set of time-delay nonlinear singular systems in [12, 13], respectively. Based on the approach of state undecomposed, scholars have considered the asymptotic stabilization of the nonlinear singular system in [14], including systems subject to actuator saturation in [15]. In [16], the control design of singular discrete-time systems has been studied based on simulation relations and behavioral theory.

It is well known that actuator saturation can compromise the functions of the closed loop system and cause instability of the system. Hence, scholars have been studying the stabilization problem of systems subject to actuator saturation for two decades [2–5, 17, 18]. Scholars have studied the stability problem in connection with the singular system with input saturation via the Lyapunov method in [2]. For the linear singular system with actuator saturation, the studies are proposed based on the stabilization conditions of the closed loop system, and the domain of attraction has been estimated by LMI technique in [3], while the authors in [4] proposed the estimate of the domain of attraction by the saturated state feedback method. In [5], the stochastic stability has been investigated for singular discrete-time Markov jump systems subject to input saturation by LMI approach. The stabilization controller has been designed based on the adaptive dynamic programming algorithm on nonlinear systems with input saturation in [17]. Fridman et al. [18] have studied local stabilization and H_∞ control for the system with time delay and input saturation via the LMI and Lyapunov–Krasovskii functional method. The robust output regulation problem has been studied for discrete-time singular systems subject to actuator saturation with an additional control term to the nonlinear feedback in [19]. Zong et al. [20] investigated the decentralized adaptive output feedback saturated control problem for interconnected nonlinear systems with strong interconnections.

For nonlinear systems with actuator fault and saturation, the authors in [21] applied the surface control technique to address the finite-time adaptive output feedback control and the authors in [22] used the sliding mode and neutral networks methods to design the adaptive fault-tolerant controller.

Unlike the asymptotical stability [23–26], the finite-time stable (FTS) is that the state (weighted) norm does not exceed a certain boundary within a fixed time T. In many practical applications, FTS plays an important role, such as analyzing the transient behavior of the controlled system within a finite interval. Due to its extensive engineering application background, the FTS problem has attracted much scholarly interest [6, 7, 27–42]. In [27, 28], the FTS problem of the linear system has been investigated. To guarantee FTS of switched linear systems subject to actuator saturation, the authors in [29] designed the FTS controllers with the time domain approach. The authors in [30, 31] gave the sufficient and necessary conditions of FTS for the impulsive linear system by using the LMI method. Ma et al. and Wang and Feng [6, 32] considered the FTS for singular discrete-time Markov jump systems subject to input saturation by using the Lyapunov–Krasovskii functional method and using the mode-dependent parameter approach, respectively. Feng et al. [7]investigated the FTS for the linear singular system with the LMI method. Based on the sliding mode control design, FTS and input-output FTS problems are, respectively, dealt with in [33–35] for a class of nonlinear systems. In [36–38], the finite-time asynchronous dissipative filtering, finite-time asynchronous L_2-gain control, and finite region asynchronous H_∞ control have been, respectively, studied for nonlinear Markov jump systems while an annular finite-time H_∞ filter has been considered for networked switched systems in [39]. The finite-time H_∞ controller has been given for the nonlinear singular discrete-time system in [40, 41] and for the nonlinear singular continuous time system in [42], respectively. It is worth pointing out that there is another definition of finite-time stability, where all states of the system reach the equilibrium point within a fixed time T and stay at the equilibrium point permanently [21, 43–47]. Based on the Hamiltonian function method, the authors in [43] studied the observer design problem of general nonlinear time-delay systems and gave the finite-time robust stabilization results; the authors in [44] investigated the finite-time stabilization problem for a class of singular systems by the constructed new Lyapunov functional while the finite-time robust simultaneous stabilization and adaptive robust simultaneous stabilization have been investigated for nonlinear systems with time delay in [45, 46], respectively. In [47], the finite-time stabilization problem has been considered for a class of high-order stochastic nonlinear systems by using the backstepping method.

Because the control input is limited by the saturation nonlinear function, it is more difficult to design a control for nonlinear singular systems with input saturation compared with the case without actuator saturation. To the best of the knowledge, the authors are only aware of few results related to the FTS of the nonlinear singular systems with input saturation. Compared with the mentioned results, the main contributions of the paper are highlighted as follows:

(1) The state feedback controllers designed in the paper have simple form, so it has low computational complexity

(2) The design method proposed in the paper has low conservative criteria, and the singular matrix E does not need to satisfy any restriction conditions

(3) The nonlinear function $\phi(x)$ does not need to satisfy Lipschitz conditions

This paper, in Section 2, introduces the definition of FTS and provides the design method of FTS controller for affine nonlinear singular systems subject to actuator saturation (ANSSAS). With the state undecomposed method, Section 3 discusses the finite-time H_∞ control problem and designs a corresponding controller for the ANSSAS with external disturbance. In Section 4, an example of a circuit system is given to illustrate the effectiveness of the proposed controllers, and the simulation curves are presented. Section 5 provides a brief conclusion.

Notations. In the paper, $\mathbb{R}^n$ denotes the n-dimensional Euclidean space. $A \in \mathbb{R}^{n\times n}$ implies that A is an $n \times n$-matrix in real number field. A^T is the transpose of matrix A. $\lambda_{\max}(Q_1)$ and $\lambda_{\min}(Q_1)$ are the maximum and minimum eigenvalues of square matrix Q_1, respectively. $Q_1 > 0$ $(Q_1 \geq 0)$ implies that square matrix Q_1 is positive definite (positive semidefinite). The Euclidean norm of vectors z is denoted by $\|z\|$.

2. FTS of ANSSAS

This section discusses the FTS problem for ANSSAS.

Consider the ANSSAS as follows:

$$\begin{aligned} E\dot{x}(t) &= \phi(x(t)) + B(x(t))\mathrm{sat}(u(t)), \\ Ex(0) &= Ex_0, \\ \phi(0) &= 0, \end{aligned} \tag{1}$$

where $x(t) \in \mathbb{R}^n$ is the state, $E \in \mathbb{R}^{n\times n}$, $0 <$ rank $E = r < n$; $B(x(t)) \in \mathbb{R}^{n\times m}$, $\phi(x(t)) \in \mathbb{R}^n$ is a sufficiently smooth vector field; $\mathrm{sat}(u(t)) \in \mathbb{R}^m$ is the saturation nonlinearity control input, and

$$\mathrm{sat}(u_i(t)) = \begin{cases} l\iota_i, & u_i(t) > \iota_i, \\ u_i(t), & -\iota_i \leq u_i(t) \leq \iota_i, i = 1, 2, \ldots, m, \\ -\iota_i, & u_i(t) < \iota_i. \end{cases} \tag{2}$$

To study system (1), we present the following definition and lemmas.

Definition 1 (see [48]). For any initial condition Ex_0, if the resulted closed loop singular system is impulsive free, then the control law $u(x(t))$ is said to be admissible, and the original system is said to be impulse controllable.

Lemma 1 (see [49]). *If a vector function $S(x(t))$ with $S(0) = 0$ ($x(t) \in \mathbb{R}^n$) has continuous n th-order partial derivatives, then $S(x(t))$ can be rewritten as*

$$S(x(t)) = a_1(x(t))x_1(t) + \cdots + a_n(x(t))x_n(t) = A(x(t))x(t), \tag{3}$$

where $A(x(t)) = [a_1(x(t))\, a_2(x(t)) \cdots a_n(x(t))] \in \mathbb{R}^{n\times n}$.

Lemma 2 (see [15]). *Denote*

$$\operatorname{sat}(u(t)) = u(t) - \delta(t). \tag{4}$$

Then, there exists a positive real number ζ such that

$$\delta^T(t)\delta(t) \le \zeta u^T(t)u(t), \tag{5}$$

where $0 < \zeta < 1$, $\delta(t) = [\delta_1(t), \delta_2(t), \ldots, \delta_m(t)]^T \in \mathbb{R}^m$, and $\delta_i(t)$ is the dead-zone nonlinearity function, $i = 1, 2, \ldots, m$.

According to [7, 27, 41], we introduce the definition as follows.

Definition 2. ANSSAS (1) is called FTS with respect to (c_1, c_2, T, R), with $0 < c_1 < c_2$ and $R > 0$ if ANSSAS (1) is impulse controllable and $x^T(0)E^TREx(0) \le c_1$ such that $x^T(t)E^TREx(t) < c_2$, $\forall t \in [0, T]$.

According to Lemma 1, system (1) can be transformed into

$$E\dot{x}(t) = A(x(t))x(t) + B(x(t))\operatorname{sat}(u(t)). \tag{6}$$

To facilitate the analysis of system (6), we provide an assumption and a lemma.

Assumption 1. $\operatorname{Rank}\begin{bmatrix} 0 & E & 0 \\ E & A(x(t)) & B(x(t)) \end{bmatrix} = n + \operatorname{rank} E$, $\forall x(t) \in \mathbb{R}^n$.

Lemma 3 (see [14]). *Assume Assumption 1 holds, then system (6) is impulse controllable.*

Under Assumption 1, the following result is given.

Theorem 1. *Consider ANSSAS (1) and its equivalent system (6). If Assumption 1 holds, there exist two positive real numbers β and ζ and three matrices $K(x(t)) \in \mathbb{R}^{m\times n}$, $Q_1 \in \mathbb{R}^{n\times n}$, and $P \in \mathbb{R}^{n\times n}$ such that*

$$(A(x(t)) - B(x(t))K(x(t)))^T PE + E^T P(A(x(t)) - B(x(t))K(x(t))) + E^T PBB^T PE + \zeta K^T K - \beta E^T PE \le 0, \tag{7}$$

$$\lambda_{\max}(Q_1)c_1 e^{\beta T} < c_2 \lambda_{\min}(Q_1), \tag{8}$$

then the FTS controller of system (1) can be given as follows:

$$u = -K(x(t))x(t), \tag{9}$$

where $c_2 > c_1 > 0$, $0 < \zeta < 1$, $R > 0$, $Q_1 > 0$, $P > 0$, and $P = R^{1/2}Q_1R^{1/2}$.

Proof. Applying (4) and (9) to system (6), it has

$$E\dot{x}(t) = (A(x(t)) - B(x(t))K(x(t)))x(t) - B(x(t))\delta(t). \tag{10}$$

According to Lemma 3, we know that system (10) has no impulsive solution under Assumption 1.

Based on system (10), we construct a proper Lyapunov function $V(x(t)) = x^T(t)E^TPEx(t) \ge 0$; according to inequality (5) and condition (7), we have

$$\begin{aligned}
&\dot{V}(x(t)) - \beta V(x(t)) \\
&\quad = (E\dot{x}(t))^T PEx(t) + x^T(t)E^T PE\dot{x}(t) - \beta x^T(t)E^T PEx(t) \\
&\quad = x^T(t)(A(x(t)) - B(x(t))K(x(t)))^T PEx(t) + x^T(t)E^T P(A(x(t)) - B(x(t))K(x(t)))x(t) \\
&\qquad - 2x^T(t)E^T PB(x(t))\delta - \beta x^T(t)E^T PEx(t) \\
&\quad \le x^T(t)\Big((A(x(t)) - B(x(t))K(x(t)))^T PE + E^T P(A(x(t)) - B(x(t))K(x(t)))\Big)x(t) \\
&\qquad + x^T(t)E^T PB(x(t))B^T(x(t))PEx(t) + \delta^T\delta(t) - \beta x^T(t)E^T PEx(t) \\
&\quad \le x^T\Big((A(x(t)) - B(x(t))K(x(t)))^T PE + E^T P(A(x(t)) - B(x(t))K(x(t))) \\
&\qquad + E^T PB(x(t))B^T(x(t))PE + \zeta K^T(x(t))K(x(t)) - \beta E^T PE\Big)x(t) \\
&\quad \le 0,
\end{aligned} \tag{11}$$

which is

$$\dot{V}(x(t)) \le \beta V(x(t)), \quad \forall t \in [0,T]. \tag{12}$$

Next, we prove that system (10) is FTS. By integrating inequality (12) between 0 and T with $t \in [0,T]$, it follows that

$$\ln \frac{V(x(t))}{V(x(0))} \le \beta t. \tag{13}$$

It is clear that

$$V(x(t)) \le e^{\beta t} V(x(0)). \tag{14}$$

Given the chain of inequalities as follows:

$$\begin{aligned} V(x(t)) &= x^T(t) E^T R^{1/2} Q_1 R^{1/2} E x(t) \\ &\ge \lambda_{\min}(Q_1) x^T(t) E^T R E x(t), \end{aligned} \tag{15}$$

$$\begin{aligned} V(x(0)) e^{\beta t} &= x^T(0) E^T R^{1/2} Q_1 R^{1/2} E x(0) e^{\beta t} \\ &\le \lambda_{\max}(Q_1) x^T(0) E^T R E x(0) e^{\beta T}. \end{aligned} \tag{16}$$

According to $x^T(0)E^T R E x(0) \le c_1$, putting together (14)–(16), we have

$$x^T(t) E^T R E x(t) \le \frac{\lambda_{\max}(Q_1) c_1 e^{\beta T}}{\lambda_{\min}(Q_1)}. \tag{17}$$

From (8) and (17), it can be obtained that $x^T(t)E^T R E x(t) < c_2$, $\forall t \in [0,T]$. So, system (1) is FTS with respect to (c_1, c_2, T, R). □

3. Finite Time H_∞ Control of ANSSAS

Based on Section 2, this section studied the finite-time H_∞ control law for the ANSSAS.

Consider ANSSAS as follows:

$$\begin{cases} E\dot{x}(t) = \phi(x(t)) + B(x(t))\mathrm{sat}(u(t)) + E\, d(x(t)) w(t), \\ Ex(0) = Ex_0, \phi(0) = 0, \\ y(t) = h_2(x(t)), \\ z(t) = h_1(x(t)), \end{cases} \tag{18}$$

where $y(t) \in \mathbb{R}^s$ is the output, $z(t) \in \mathbb{R}^q$ is the penalty signal, $w(t) \in \mathbb{R}^s$ is the external disturbance, and $d(x(t)) \in \mathbb{R}^{n\times s}$, E, $x(t)$, $\phi(x(t))$, $\mathrm{sat}(u(t))$, and $B(x(t))$ are the same as those in ANSSAS (1).

Choose $h_1(x(t)) = L(x(t))B^T(x(t))x(t)$, $h_2(x(t)) = d^T(x(t))E^T x(t)$, where $L(x(t))$ is full column rank. From Section 2, we know that we can design an admissible finite-time H_∞ control law $u(t)$ for system (18) under Assumption 1. The design steps of the finite-time H_∞ controller are as follows. First, we design an admissible control law u such that the L_2 gain of the closed loop system is not greater than γ, where $\gamma > 0$ is a given disturbance attenuation level. Next, we demonstrate that the resulted closed loop system is FTS when $w(t) = 0$. To design the finite-time H_∞ controller for the ANSSAS, we recall the following lemma:

Lemma 4 (see [50]). *Consider an affine nonlinear system:*

$$\begin{cases} \dot{x} = f(x) + g(x)w, \quad f(x_0) = 0, \\ z = h(x), \end{cases} \tag{19}$$

where $x \in \mathbb{R}^n$, $w \in \mathbb{R}^s$, and $z \in \mathbb{R}^q$ are the state, disturbance, and penalty signal of the system, respectively. If there exists a function $V(x) \ge 0$ $(V(x_0) = 0)$ such that the Hamiltonian–Jacobian inequality

$$\frac{\partial^T V}{\partial x} f(x) + \frac{1}{2\gamma^2} \frac{\partial^T V}{\partial x} g g^T \frac{\partial V}{\partial x} + \frac{1}{2} h^T h \le 0, \tag{20}$$

holds, then the L_2 gain of system (19) (from w to z) is bounded by γ, i.e.,

$$\int_0^{\mathcal{T}} \|z(t)\|^2 \mathrm{d}t \le \gamma^2 \int_0^{\mathcal{T}} \|w(t)\|^2 \mathrm{d}t, \quad \forall w \in L_2[0,\mathcal{T}], \tag{21}$$

where γ is a positive number.

Based on with, we give the following theorem.

Theorem 2. *Consider ANSSAS (18). Suppose that Assumption 1 holds. Let*

$$\begin{aligned} u(t) &= -\left(K(x(t)) + \frac{1}{2}\left(L^T(x(t)) L(x(t)) + \frac{1}{\gamma^2} I_m \right) B^T(x(t)) \right) \\ &=: -K_1(x(t)) x(t). \end{aligned} \tag{22}$$

If

$$\begin{aligned} &\left(A(x(t)) - B(x(t))K_1(x(t))\right)^T PE + E^T P\left(A(x(t)) - B(x(t))K_1(x(t))\right) + \frac{2}{\gamma^2} E^T PE\, d(x(t)) d^T(x(t)) E^T PE \\ &\quad + \frac{1}{2} B(x(t)) L^T(x(t)) L(x(t)) B^T(x(t)) + \zeta K_1^T(x(t)) K_1(x(t)) + E^T PBB^T PE \le 0, \end{aligned} \tag{23}$$

$$\lambda_{\max}(Q_1) c_1 e^{\beta T} < c_2 \lambda_{\min}(Q_1), \tag{24}$$

then controller (22) is the finite-time H_∞ control law of ANSSAS (18), where P, Q_1, β, ζ, c_1, and c_2 are the same as those in Theorem 1.

Proof. Based on Section 2 and controller (22), we can give

$$\begin{cases} E\dot{x}(t) = \big(A(x(t)) - B(x(t))K_1(x(t))\big)x(t) - B(x(t))\delta(t) + E\ d(x(t))w(t), \\ y(t) = d^T(x(t))E^T x(t), \\ z(t) = L(x(t))B^T(x(t))x(t). \end{cases} \tag{25}$$

Choose a proper Lyapunov function $V(x(t)) = x^T(t)E^T PEx(t)$; according to (23), we have

$$\begin{aligned} &\dot{V}(x(t)) - \frac{\partial^T V(x(t))}{\partial x(t)} d(x(t))w(t) + \frac{1}{2\gamma^2}\frac{\partial^T V(x(t))}{\partial x(t)} d(x(t))d^T(x(t))\frac{\partial V(x(t))}{\partial x(t)} + \frac{1}{2}h_1^T(x(t))h_1(x(t)) \\ &\quad = x^T(t)\Big(\big(A(x(t)) - B(x(t))K_1(x(t))\big)^T PE + E^T P\big(A(x(t)) - B(x(t))K_1(x(t))\big)\Big)x(t) \\ &\qquad - 2x^T(t)E^T PB(x(t))\delta(t) + w^T(t)d^T(x(t))E^T PEx(t) + x^T(t)E^T PE\ d(x(t))w(t) - 2x^T(t)E^T PE\ d(x(t))w(t) \\ &\qquad + \frac{2}{\gamma^2}x^T(t)E^T PE\ d(x(t))d^T(x(t))E^T PEx(t) + \frac{1}{2}x^T(t)B(x(t))L^T(x(t))L(x(t))B^T(x(t))x(t) \\ &\quad \le x^T(t)\Big(\big(A(x(t)) - B(x(t))K_1(x(t))\big)^T PE + E^T P\big(A(x(t)) - B(x(t))K_1(x(t))\big) \\ &\qquad + \frac{2}{\gamma^2}E^T PE\ d(x(t))d^T(x(t))E^T PE + \frac{1}{2}B(x(t))L^T(x(t))L(x(t))B^T(x(t)) \\ &\qquad + \zeta K_1^T(x(t))K_1(x(t)) + E^T PB(x(t))B^T(x(t))PE\Big)x(t) \le 0. \end{aligned} \tag{26}$$

By Lemma 4, the L_2 gain of system (25) is not more than γ.

Next, we prove that the system is FTS if $w(t) = 0$.

$$\begin{aligned} \dot{V}(x(t)) - \beta V(x(t)) &= \frac{\partial^T V(x(t))}{\partial x(t)}\dot{x}(t) - \beta x^T(t)E^T PEx(t) \\ &= x^T(t)\Big(\big(A(x(t)) - B(x(t))K_1(x(t))\big)^T PE + E^T P\big(A(x(t)) - B(x(t))K_1(x(t))\big) \\ &\quad - \beta E^T PE\Big)x(t) - 2x^T(t)E^T PB(x(t))\delta \\ &\le x^T(t)\Big(\big(A(x(t)) - B(x(t))K_1(x(t))\big)^T PE + E^T P\big(A(x(t)) - B(x(t))K_1(x(t))\big) \\ &\quad + \zeta K_1^T(x(t))K_1(x(t)) + E^T PB(x(t))B^T(x(t))PE\Big)x(t) \\ &\le x^T(t)\Big(\big(A(x(t)) - B(x(t))K_1(x(t))\big)^T PE + E^T P\big(A(x(t)) - B(x(t))K_1(x(t))\big) \\ &\quad + \frac{2}{\gamma^2}E^T PE\ d(x(t))d^T(x(t))E^T PE + \frac{1}{2}B(x(t))L^T(x(t))L(x(t))B^T(x(t)) \\ &\quad + \zeta K_1^T(x(t))K_1(x(t)) + E^T PB(x(t))B^T(x(t))PE\Big)x(t) \le 0. \end{aligned} \tag{27}$$

The following proof is the same as that in Theorem 1. So, the closed loop system (25) is FTS if $w(t) = 0$.

4. A Circuit Example

This section proposes a circuit example to show the effectiveness of the finite-time H_∞ controller designed in Theorem 2.

Example 1. Consider the circuit system as Figure 1, where i_w is a disturbance signal, $u_1 = \varphi_1(q_1), u_2 = \varphi_2(q_2)$.

From Kirchhoff's current law and voltage law, the circuit system can be expressed as

$$\begin{cases} \dot{q}_1 + \dot{q}_2 = \operatorname{sat}(I_s) - \dfrac{\varphi_1(q_1)}{R_3} - i_w, \\ 0 = \operatorname{sat}(U_s) + \varphi_1(q_1) - \varphi_2(q_2). \end{cases} \tag{28}$$

We introduce $\varphi_1(q_1) = q_1, \varphi_2(q_2) = q_2^3$, $R_3 = (1/2)\Omega$, and $|U_s| \le 8\,V, |I_s| \le 4\,A$. Let $v = [v_1, v_2]^T =: [U_s, I_s]^T$, $x(t) = [x_1(t), x_2(t)]^T =: [q_1, q_2]^T$, and $w(t) = i_w$. Then, system (28) can be rewritten as

$$\begin{bmatrix} 1 & 1 \\ 0 & 0 \end{bmatrix} \dot{x}(t) = \begin{bmatrix} -3x_1(t) - x_1(t)x_2^2(t) \\ x_1(t) - 6x_2(t) - 2x_2^3(t) \end{bmatrix} + \begin{bmatrix} 0 & 1 \\ 1 & 0 \end{bmatrix} \operatorname{sat}(v) + \begin{bmatrix} -1 \\ 0 \end{bmatrix} w(t). \tag{29}$$

Choose the penalty signal $z = (1/2)[q_2, q_1]^T$. Thus, system (29) and z can be combined to

$$\begin{cases} \begin{bmatrix} 1 & 1 \\ 0 & 0 \end{bmatrix} \dot{x}(t) = \begin{bmatrix} -3x_1(t) - x_1(t)x_2^2(t) \\ x_1(t) - 6x_2(t) - 2x_2^3(t) \end{bmatrix} + \begin{bmatrix} 0 & 1 \\ 1 & 0 \end{bmatrix} \operatorname{sat}(v) + \begin{bmatrix} -1 \\ 0 \end{bmatrix} w(t), \\ z = \dfrac{1}{2} \begin{bmatrix} c x_2(t) \\ x_1(t) \end{bmatrix}, \end{cases} \tag{30}$$

where $L(x(t)) = \begin{bmatrix} 1/2 & 0 \\ 0 & 1/2 \end{bmatrix}$.

According to $\phi(0) = 0$, we have $A(x(t)) = \begin{bmatrix} -3 - x_2^2(t) & 0 \\ 1 & -6 - 2x_2^2(t) \end{bmatrix}$. It is not difficult to verify that Assumption 1 holds.

Let

$$\begin{aligned} P &= \begin{bmatrix} 2 & 1 \\ 1 & 2 \end{bmatrix}, \\ Q_1 &= \begin{bmatrix} 2 & 1 \\ 1 & 2 \end{bmatrix}, \\ R &= \begin{bmatrix} 1 & 0 \\ 0 & 1 \end{bmatrix}, \\ K(x(t)) &= \begin{bmatrix} \dfrac{5}{2} & 0 \\ 0 & \dfrac{8}{5} \end{bmatrix}, \end{aligned} \tag{31}$$

for given disturbance attenuation $\gamma = 1$; choose some parameter values $c_1 = 0.5, c_2 = 3, T = 6, \beta = 0.1$, and $\zeta = 0.1$, then

$$\begin{aligned} &(A(x(t)) - B(x(t))K_1(x(t)))^T PE \\ &\quad + E^T P(A(x(t)) - B(x(t))K_1(x(t))) \\ &\quad + \frac{2}{\gamma^2} E^T PE\, d(x(t)) d^T(x(t)) E^T PE \\ &\quad + \frac{1}{2} B(x(t)) L^T(x(t)) L(x(t)) B^T(x(t)) \\ &\quad + \zeta K_1^T(x(t)) K_1(x(t)) + E^T PBB^T PE \\ &= \begin{bmatrix} -3.711 - 4x_2^2(t) & -5.319 - 4x_2^2(t) \\ -5.319 - 4x_2^2(t) & -6.230 - 4x_2^2(t) \end{bmatrix} \le 0, \\ &\frac{\lambda_{\max}(Q_1) c_1}{\lambda_{\min}(Q_1)} e^{\beta T} = 3c_1 e^{0.6} < c_2, \end{aligned} \tag{32}$$

hold.

Obviously, it is illustrated that all conditions of Theorem 2 can be satisfied.

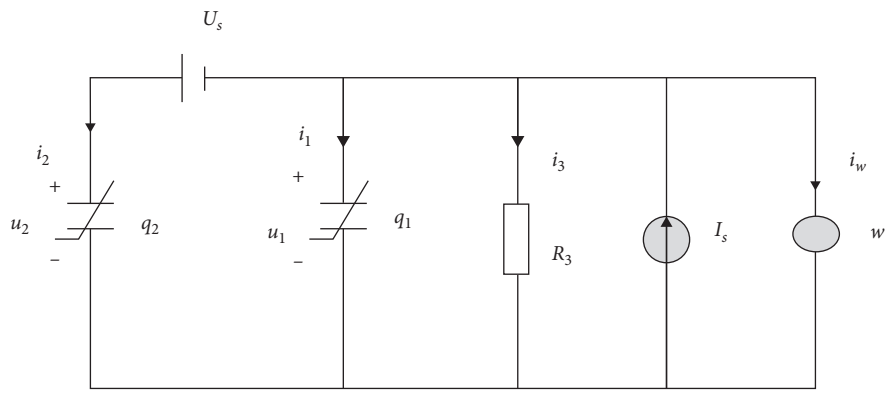

FIGURE 1: Nonlinear singular circuit system.

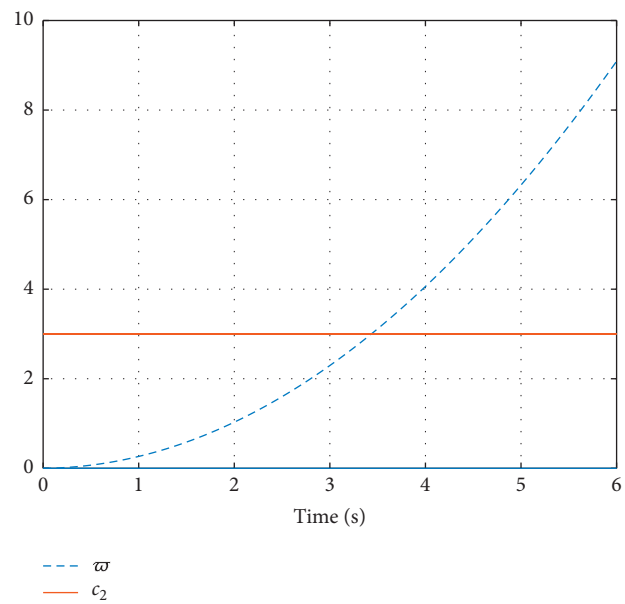

FIGURE 2: Response of $\varpi = x^T(t)E^T REx(t)$ for the open loop system.

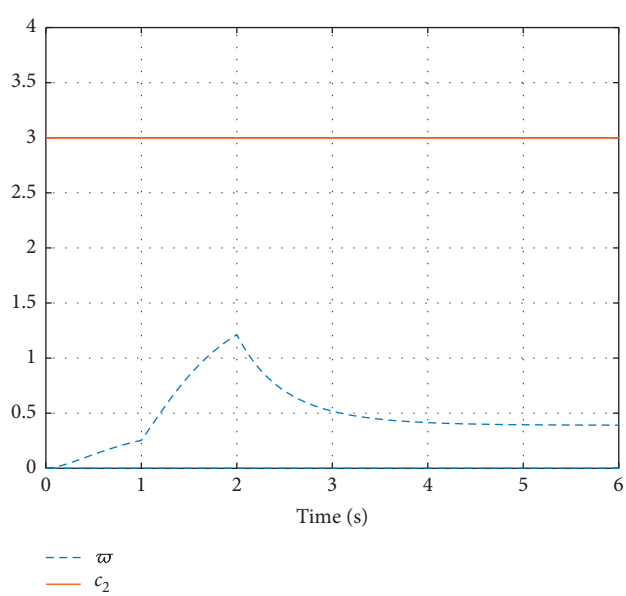

FIGURE 3: Response of $\varpi = x^T(t)E^T REx(t)$ for the closed loop system.

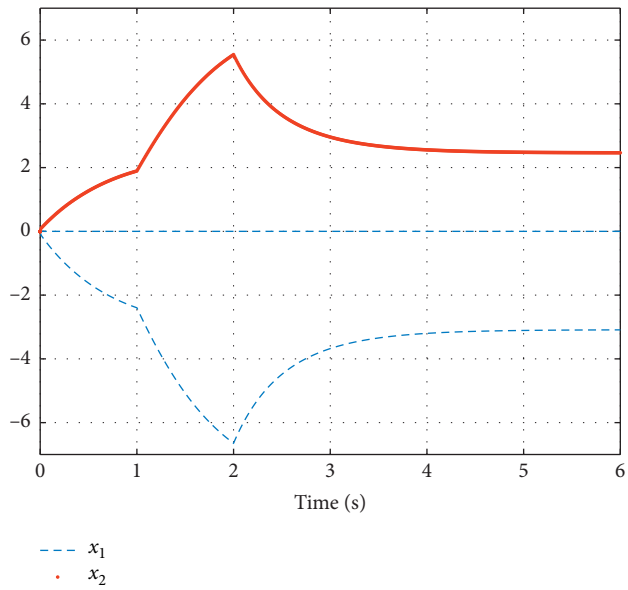

Figure 4: Response of the state $x(t)$ for the closed loop system.

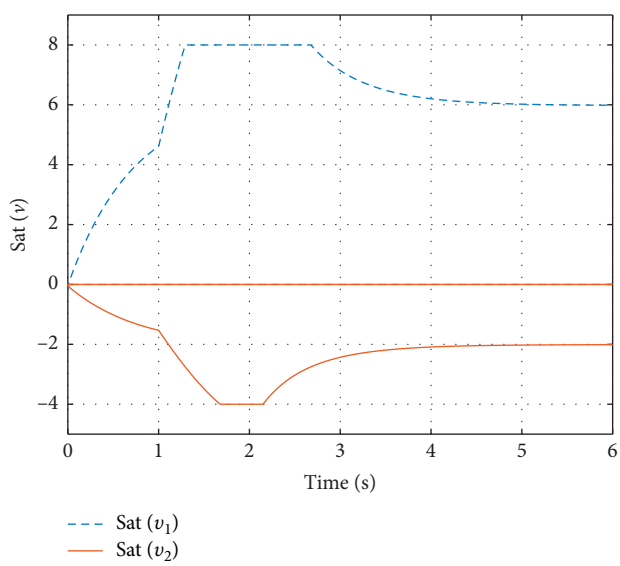

Figure 5: Saturation control signal sat (v) for the closed loop system.

Thus, we can give the following finite-time H_∞ controller of system (29):

$$v = -\begin{bmatrix} \frac{5}{2} & \frac{5}{8} \\ \frac{5}{8} & \frac{8}{5} \end{bmatrix} x(t). \tag{33}$$

To check the effectiveness of the control law (33), give $Ex(0) = [0.5,\ 0]^T$ and input a square-wave disturbance of amplitude $[0, 2]^T$ in the time duration $[1\,\mathrm{s} - 2\,\mathrm{s}]$ for the system. The response of $\varpi = x^T(t)E^T REx(t)$ is presented in Figures 2 and 3 for the open-loop system and the closed loop system, respectively. It is clear that $x^T(t)E^T REx(t) > 3$ in the open loop system $\forall t \in [3.5, 6]$, whereas $x^T(t)E^T REx(t) < 3$ in the closed loop system $\forall t \in [0, 6]$. The responses of state x and saturation input sat(v) are given in Figures 4 and 5, respectively. According to Figures 2–5, it is clear that the circuit system (29) is FTS with respect to $(0.5, 3, 6, I)$ under the admissible H_∞ control law (33).

5. Conclusion

This paper investigates the finite-time control problem for affine nonlinear singular systems subject to actuator saturation by using the state undecomposed method. First, saturation input is represented by control input and dead-zone nonlinear compensation. Then, the finite-time control law has been designed under sufficient condition of the system impulsive controllable. Based on with, the finite-time

H_∞ control problem is solved via the suitable state feedback. New results on the finite-time control and finite-time H_∞ control problems have been presented for affine nonlinear singular systems subject to actuator saturation. In the future, the input-output finite-time control problems can be studied for affine nonlinear singular systems subject to actuator saturation.

Data Availability

The data used to support the findings of this study are available from the corresponding author upon request.

Conflicts of Interest

The authors declare that they have no conflicts of interest.

Acknowledgments

This work was supported by National Nature Science Foundation of China (61877028 and 61773015), Shandong Province Nature Science Foundation (ZR2019MF032), Shandong Province Key Research and Development Project (2018GGX105003), and Shanghai Dianji University Nature Science Foundation (B102882100701020).

References

[1] L. Y. Dai, *Singular Control Systems*, Springer-Verlag, Berlin, Germany, 1989.

[2] J. R. Liang, H. L. Choi, and J. T. Lim, "On stability of singular systems with saturating actuators," *IEICE Transactions on Fundamentals of Electronics Communications and Computer Sciences*, vol. 86, no. 10, pp. 2700–2703, 2003.

[3] Z. Lin and L. Lv, "Set invariance conditions for singular linear systems subject to actuator saturation," *IEEE Transactions on Automatic Control*, vol. 52, no. 12, pp. 2351–2355, 2007.

[4] Y. L. Li and Z. L. Lin, "Improved set invariance conditions for singular linear systems subject to actuator saturation," *Control Theory and Applications*, vol. 31, no. 7, pp. 955–961, 2014.

[5] S. P. Ma, C. Zhang, and S. Q. Zhu, "Robust stability for discrete-time uncertain singular Markov jump systems with actuator saturation," *IET Control Theory and Applications*, vol. 5, no. 2, pp. 255–262, 2011.

[6] Y. Ma, X. Jia, and D. Liu, "Finite-time dissipative control for singular discrete-time Markovian jump systems with actuator saturation and partly unknown transition rates," *Applied Mathematical Modelling*, vol. 53, pp. 49–70, 2018.

[7] J. E. Feng, Z. Wu, J. B. Sun, and Z. Cheng, "Finite time control of linear singular systems subject to parametric uncertain and disturbances," in *Proceedings of the 5th World Congress on Intelligence Control and Automation*, Hangzhou, China, June 2004.

[8] J. Tian and S. Ma, "Existence of nonimpulsive unique solution and stability for discrete-time linear rectangular descriptor Markov jump systems," *IEEE Transactions on Automatic Control*, vol. 64, no. 10, pp. 4245–4251, 2019.

[9] J. Wang, Z. Huang, Z. Wu, J. Cao, and H. Shen, "Extended dissipative control for singularly perturbed PDT switched systems and its application," *IEEE Transactions on Circuits and Systems I: Regular Papers*, vol. 67, no. 12, pp. 5281–5289, 2020.

[10] J. Wang, Z. G. Huang, Z. G. Wu et al., "Extended dissipative control for singularly perturbed PDT switched systems and its application," *IEEE Transactions on Fuzzy Systems*, vol. 67, no. 12, pp. 5281–5289, 2021.

[11] Q. Zhu, "Stabilization of stochastically singular nonlinear jump systems with unknown parameters and continuously distributed delays," *International Journal of Control, Automation and Systems*, vol. 11, no. 4, pp. 683–691, 2013.

[12] R. Q. Lu, H. Y. Su, J. Z. Wang, A. Xue, and T. Shi, "Robust optimal control for a class of nonlinear uncertain singular systems with time-delay," in *Proceedings of the 2006 American Control Conference*, pp. 5020–5024, Minneapolis, MN, USA, June 2006.

[13] J. C. Wu, S. L. Wo, and G. P. Lu, "Asymptotic stability and stabilization for a class of nonlinear descriptor systems with delay," *Asian Journal of Control*, vol. 13, no. 2, pp. 361–367, 2011.

[14] L. Sun and Y. Wang, "An undecomposed approach to control design for a class of nonlinear descriptor systems," *International Journal of Robust and Nonlinear Control*, vol. 23, no. 6, pp. 695–708, 2013.

[15] L. Sun, Y. Wang, and G. Feng, "Control design for a class of affine nonlinear descriptor systems with actuator saturation," *IEEE Transactions on Automatic Control*, vol. 60, no. 8, pp. 2195–2200, 2015.

[16] S. Haesaert, F. Chen, A. Abate, and S. Weiland, "Formal control synthesis via simulation relations and behavioral theory for discrete-time descriptor systems," *IEEE Transactions on Automatic Control*, vol. 66, no. 3, pp. 1024–1039, 2021.

[17] B. Zhao, L. H. Jia, H. B. Xia, and Y. Li, "Adaptive dynamic programming-based stabilization of nonlinear systems with unknown actuator saturation," *Nonlinear Dynamics*, vol. 93, pp. 2089–2103, 2018.

[18] E. Fridman, A. Pila, and U. Shaked, "Regional stabilization and H∞ control of time-delay systems with saturating actuators," *International Journal of Robust and Nonlinear Control*, vol. 13, no. 9, pp. 885–907, 2003.

[19] E. Jafari and T. Binazadeh, "Robust output regulation in discrete-time singular systems with actuator saturation and uncertainties," *IEEE Transactions on Circuits and Systems II: Express Briefs*, vol. 67, no. 2, pp. 340–344, 2020.

[20] G. Zong, H. Sun, and S. K. Nguang, "Decentralized adaptive neuro-output feedback saturated control for INS and its application to AUV," *IEEE Transactions on Neural Networks and Learning Systems*, pp. 1–10, 2021.

[21] R. Ji, J. Ma, D. Li, and S. S. Ge, "Finite-time adaptive output feedback control for MIMO nonlinear systems with actuator faults and saturations," *IEEE Transactions on Fuzzy Systems*, pp. 1–15, 2020.

[22] M. Qian, Z. Zheng, and P. Cheng, "Adaptive NFTSM-based fault tolerant control for a class of nonlinear system with actuator fault and saturation," *IEEE Access*, vol. 7, pp. 107083–107095, 2019.

[23] X. Yi, R. Guo, and Y. Qi, "Stabilization of chaotic systems with both uncertainty and disturbance by the UDE-based control method," *IEEE Access*, vol. 8, no. 1, pp. 62471–62477, 2020.

[24] L. Liu, B. Li, and R. Guo, "Consensus control for networked manipulators with switched parameters and topologies," *IEEE Access*, vol. 9, pp. 9209–9217, 2021.

[25] T. Hou, Y. Liu, and F. Deng, "Stability for discrete-time uncertain systems with infinite Markov jump and time-delay," *Science China: Information Sciences*, vol. 64, p. 1C11, 2021.

[26] R. Peng, C. Jiang, and R. Guo, "Stabilization of a class of fractional order systems with both uncertainty and disturbance," *IEEE Access*, vol. 9, pp. 42697–42706, 2021.

[27] F. Amato, M. Ariola, and P. Dorato, "Finite-time control of linear systems subject to parametric uncertainties and disturbances," *Automatica*, vol. 37, no. 9, pp. 1459–1463, 2001.

[28] F. Amato, M. Ariola, and C. Cosentino, "Finite-time stabilization via dynamic output feedback," *Automatica*, vol. 42, no. 2, pp. 337–342, 2006.

[29] X. Lin, X. Li, Y. Zou, and S. Li, "Finite-time stabilization of switched linear systems with nonlinear saturating actuators," *Journal of the Franklin Institute*, vol. 351, no. 3, pp. 1464–1482, 2014.

[30] R. Ambrosino, F. Calabrese, C. Cosentino, and G. De Tommasi, "Sufficient conditions for finite-time stability of impulsive dynamical systems," *IEEE Transactions on Automatic Control*, vol. 54, no. 4, pp. 861–865, 2009.

[31] F. Amato, G. De Tommasi, and A. Pironti, "Input-output finite-time stabilization of impulsive linear systems: necessary and sufficient conditions," *Nonlinear Analysis: Hybrid Systems*, vol. 19, pp. 93–106, 2016.

[32] G. Wang and B. Feng, "Finite-time stabilization for discrete-time delayed Markovian jump systems with partially delayed actuator saturation," *Discrete Dynamics in Nature and Society*, vol. 2016, Article ID 1304379, 12 pages, 2016.

[33] J. Song, Y. Niu, and Y. Zou, "Finite-time stabilization via sliding mode control," *IEEE Transactions on Automatic Control*, vol. 62, no. 3, pp. 1478–1483, 2017.

[34] X. Lv, Y. Niu, and J. Song, "Finite-time boundedness of uncertain Hamiltonian systems via sliding mode control approach," *Nonlinear Dynamics*, vol. 104, no. 1, pp. 497–507, 2021.

[35] J. Song, Y. Niu, and Y. Zou, "Finite-time sliding mode control synthesis under explicit output constraint," *Automatica*, vol. 65, pp. 111–114, 2016.

[36] X. Zhang, S. P. He, V. Stojanovic et al., "Finite-time asynchronous dissipative filtering of conic-type nonlinear Markov jump systems," *Science China: Information Sciences*, vol. 64, pp. 152206:1–152206:12, 2021.

[37] C. Ren, S. He, X. Luan, F. Liu, and H. R. Karimi, "Finite-time L2-gain asynchronous control for continuous-time positive hidden Markov jump systems via T-S fuzzy model approach," *IEEE Transactions on Cybernetics*, vol. 51, no. 1, pp. 77–87, 2021.

[38] P. Cheng, S. He, X. Luan, and F. Liu, "Finite-region asynchronous H∞ control for 2D Markov jump systems," *Automatica*, vol. 129, no. 2021, Article ID 109590, 2021.

[39] G. Zong, H. Ren, and H. R. Karimi, "Event-triggered communication and annular finite-time H∞ filtering for networked switched systems," *IEEE Transactions on Cybernetics*, vol. 51, no. 1, pp. 309–317, 2021.

[40] X. Lu, X. Zhang, and L. Sun, "Finite-time H∞ control for nonlinear discrete Hamiltonian descriptor systems," *Journal of the Franklin Institute*, vol. 354, no. 14, pp. 6138–6151, 2017.

[41] M. Li, L. Sun, and R. Yang, "Finite-time H∞ control for a class of discrete-time nonlinear singular systems," *Journal of the Franklin Institute*, vol. 355, no. 13, pp. 5384–5393, 2018.

[42] M. Li and L. Sun, "Finite-time stabilisation for a class of nonlinear descriptor systems," *IET Control Theory & Applications*, vol. 12, no. 17, pp. 2399–2406, 2018.

[43] R. Yang, G. Zhang, and L. Sun, "Observer-based finite-time robust control of nonlinear time-delay systems via Hamiltonian function method," *International Journal of Control*, vol. 4, pp. 1–18, 2020.

[44] R. Yang, L. Sun, G. Zhang, and Q. Zhang, "Finite-time stability and stabilization of nonlinear singular time-delay systems via Hamiltonian method," *Journal of the Franklin Institute*, vol. 356, no. 12, pp. 5961–5992, 2019.

[45] R. Yang, G. Zhang, and L. Sun, "Finite-time robust simultaneous stabilization of a set of nonlinear time-delay systems," *International Journal of Robust and Nonlinear Control*, vol. 30, no. 5, pp. 1733–1753, 2020.

[46] R. M. Yang, W. H. Pei, Y. Z. Han, and L. Sun, "Finite-time adaptive robust simultaneous stabilization of nonlinear delay systems by the Hamiltonian function method," *Science China Information Science*, vol. 64, no. 6, pp. 169201:1–169201:3, 2020.

[47] H. Wang and Q. Zhu, "Finite-time stabilization of high-order stochastic nonlinear systems in strict-feedback form," *Automatica*, vol. 54, pp. 284–291, 2015.

[48] H. Xu and K. Mizukami, "Hamilton-Jacobi equation for descriptor systems," *Systems & Control Letters*, vol. 21, no. 4, pp. 321–327, 1993.

[49] W. Langson and A. Allcync, "Infinite horizon optimal control of a class of nonlinear systems," in *Proceedings of the 1997 American Control Conference*, Albuquerque, NM, USA, June 1997.

[50] T. Shen, S. Mei, Q. Lu, W. Hu, and K. Tamura, "Adaptive nonlinear excitation control with L2 disturbance attenuation for power systems," *Automatica*, vol. 39, no. 1, pp. 81–89, 2003.

Hindawi
Mathematical Problems in Engineering
Volume 2021, Article ID 2831064, 9 pages
https://doi.org/10.1155/2021/2831064

Research Article

Automated Detection of Arrhythmia for Hybrid Neural Network of LSTM-Residual with Multi-Information Fusion

Liang Tao,[1] **Baoning Liu**,[1] **and Wei Liang**[2]

[1]*School of Information and Electrical Engineering, Shandong Jianzhu University, Jinan 250101, China*
[2]*School of Electrical Engineering and Automation, Qilu University of Technology (Shandong Academy of Sciences), Jinan 250353, China*

Correspondence should be addressed to Wei Liang; dzhlw0918@qlu.edu.cn

Received 2 May 2021; Accepted 19 July 2021; Published 28 July 2021

Academic Editor: Giovanni Garcea

Arrhythmia is a common cardiovascular disease; the electrocardiogram (ECG) is widely used as an effective tool for detecting arrhythmia. However, real-time arrhythmia detection monitoring is difficult, so this study proposes a long short-term memory-residual model. Individual beats provide morphological features and combined with adjacent segments provide temporal features. Our proposed model captures the time-domain and morphological ECG signal information simultaneously and fuses the two information types. At the same time, the attention block is applied to the network to further strengthen the useful information, capture the hidden information in the ECG signal, and improve the model classification performance. Our model was finally trained and tested on the MIT-BIH arrhythmia database, and the entire dataset was divided into intrapatient and interpatient modes. Accuracies of 99.11% and 85.65%, respectively, were obtained under the two modes. Experimental results demonstrate that our proposed method is an efficient automated detection method.

1. Introduction

Arrhythmia is a common cardiovascular disease with an important clinical significance [1]. Common methods for detecting arrhythmias generally rely on electrocardiogram (ECG) and doctors' experience [2]. This process is complex and cumbersome and is easily influenced by the doctor's subjective inference. Therefore, research on the automatic detection of arrhythmias has become trending.

In recent years, with the development of machine learning, an increasing number of automatic detection methods for arrhythmias have been applied [3, 4]. Machine learning methods generally require the manual extraction of features. First, the data are preprocessed for refinement, and then features are extracted through a series of mathematical methods, such as wavelet transform, linear discriminant analysis, independent component analysis, and principal component analysis (PCA). The extracted features are input into a classifier to complete the classification [5–11]. Generally, classifiers include support vector machine (SVM), decision tree, and artificial neural network [12–14]. Traditional feature extraction methods of ECG signals are complex and subject to the limitations of specific knowledge fields. In addition, the nonlinear fitting ability is limited. Therefore, the extracted features do not necessarily represent the optimal features, and even the key information of the ECG signals may be omitted.

To overcome the disadvantages of machine learning, deep learning has been applied to the automatic detection of arrhythmias. Compared to machine learning, deep learning no longer requires the manual extraction of features [15]. Convolutional neural networks (CNNs) are a type of deep learning that can automatically extract advanced features of ECG signals by stacking layers and are no longer limited to specific domain knowledge [16]. Al Rahhal et al. proposed a dense convolutional network to detect arrhythmias and proposed focal loss to reduce the problems caused by data imbalance [17]. Yang et al. proposed an ECG classification method based on a lead CNN, which used fuzzy sets to reduce the order of extracted ECG image features and

optimized the network using the residual structure [18]. In addition, long short-term memory (LSTM) has been widely used in the classification of ECG signals owing to its excellent performance in processing time series data. Kim and Pyun proposed an automatic arrhythmia detection algorithm based on two-way LSTM, and the experimental results showed that it was superior to the traditional LSTM [19]. Sharma et al. used Fourier–Bessel expansion to process the RR interval and then input the processed data to the LSTM for ECG classification, obtaining good results [20].

Considering the characteristics of ECGs and the superiority of the two networks, an automatic arrhythmia detection algorithm based on multi-information LSTM combined with a residual block is proposed. The algorithm includes two parallel inputs, which are used to fully mine the temporal and morphological characteristics of the ECG. The main contributions of this study are as follows:

(1) A residual block and attention block are introduced. The residual block used for even deeper networks can maintain the integrity of the information and prevent gradient explosion. An attention block is used to generate attention weight, enhance information useful features, weaken useless characteristics, and improve model performance.

(2) The multiscale depth model is applied, and the ECG beats and segments (include RR interval) are used as inputs to the model, which can focus on both the morphological and temporal characteristics of ECG signals. This method fully excavates hidden information in ECG signals and exhibits excellent performance in arrhythmia detection.

(3) In this study, we no longer need to manually extract the features. We conducted experiments in both interpatient and intrapatient modes and achieved excellent results.

2. Materials and Methods

2.1. Data Source. The MIT-BIH arrhythmia database (MITDB) dataset was used in the experiments [21]. The database included 48 records, each containing two leads. According to the classification rules of the Association for the Advancement of Medical Instrumentation, we divided all the data into five types of arrhythmias, as presented in Table 1. Because the number of unknown beats (Q) was small and contained less useful information, it was deleted, and only the other four disease types were retained. We divided the data into two modes, interpatient and intrapatient, and the data were divided into DS1 and DS2, with each mode containing 22 records. Four of these records were not included in DS1 and DS2 owing to poor signal quality, including 102, 104, 107, and 217.

DS1: 101, 106, 108, 109, 112, 114, 115, 116, 118, 119, 122, 124, 201, 203, 205, 207, 208, 209, 215, 220, 223, and 230.

DS2: 100, 103, 105, 111, 113, 117, 121, 123, 200, 202, 210, 212, 213, 214, 219, 221, 222, 228, 231, 232, 233, and 234.

In general, trained models need to be tested for performance using untrained data. In the interpatient mode, DS1 and DS2 were used for training and testing, respectively. There was no patient data overlap between the two. In contrast, in the intrapatient model, data from the training and testing sets might have been from the same patient. In general, the interpatient model is more in line with the actual requirements. Table 2 lists the number of disease types in the ECG database.

2.2. ECG Signal Preprocessing. In our model, we generally had to specify a fixed length as the input. Since the voltage value of R wave is the largest in the ECG signal, it is easy to locate. In contrast, low amplitude waveforms, such as P and T waves, are difficult to detect. Therefore, the segmentation of ECG signal is generally based on R wave as the center. We used the classical R-peak algorithm to detect the position of the R-wave peak [22]. The ECG beat was taken as input 1. With the peak of the R wave as the center, 100 sampling points were taken forward, and 152 sampling points were taken backward; a total of 252 sampling points were taken. With segments (include RR interval) as input, 2, 252 points were taken forward, and 252 points were taken backward with the peak of the R wave as the center; a total of 504 points were taken. Waveform visualization is depicted in Figure 1, which shows the ECG beat and segment. The entire segment contained the current beat waveform and a wider range of information, which constitute the time-domain characteristics of the ECG signal, and a single beat constituted the morphological characteristics of the ECG signal.

To reduce the impact of large differences in the data value range and improve the overall operation rate of the model, Z-score normalization was used for data processing. The normalization function is defined as in

$$X^* = \frac{X - Z}{D}, \tag{1}$$

where X^* refers to the values of the ECG recording and Z and D refer to the mean and standard deviation of these values, respectively.

2.3. LSTM Block. By introducing the gate mechanism, LSTM overcomes the disadvantage of the traditional recurrent neural network (RNN), namely, gradient disappearance. The forget gate, input gate, and output gate are introduced to LSTM to allow LSTM to overcome long-term dependency and maintain information integrity, which makes LSTM more suitable than RNN for processing temporal data. Figure 2 demonstrates the structure of the LSTM. Equations (2)–(6) represent the calculation formulas for each part of the LSTM:

$$F(t) = \sigma\left(W_f\left[H_{t-1}, X_t\right] + b_f\right), \tag{2}$$

$$I(t) = \sigma\left(W_i\left[H_{t-1}, X_t\right] + b_i\right), \tag{3}$$

$$O(t) = \sigma\left(W_o\left[H_{t-1}, X_t\right] + b_o\right), \tag{4}$$

$$L(t) = \tanh\left(W_l\left[H_{t-1}, X_t\right] + b_l\right), \tag{5}$$

Table 1: Types of arrhythmias.

N (nonectopic)	Normal beat	Left bundle branch block beat	Right bundle branch block beat	Atrial escape beat	Nodal (junctional) escape beat
SVEB (Supraventricular ectopic beat)	Atrial premature beat	Aberrated atrial premature beat	Nodal (junctional) premature beat	Supraventricular premature beat	
VEB (Ventricular ectopic beat)	Premature ventricular beat	Ventricular escape beat			
F (fusion beat)	Fusion of ventricular and normal beat				
Q	Paced beat	Fusion of paced and normal beat			

Table 2: Number of disease types in the ECG database.

	N	SVEB	VEB	*F*	Total
DS1	45341	893	3700	411	50345
DS2	44172	1826	3166	382	49546
Total	89513	2719	6866	793	99891

$$c_t = F_t * c_{t-1} + I_t * L \ , \tag{6}$$

where σ and tanh refer to the sigmoid and tanh functions, respectively. W and b refer to the weights and bias values, respectively. I_t, F_t, O_t, and c_t refer to the input gate, forget gate, output gate, and cell state, respectively. L refers to the accumulated information of the present moment.

2.4. Residual Block. In deep learning, CNNs rely on the sliding of the convolutional window on the input data to extract the local features of the data, and they rely on the pooling layer to refine the features and extract important information from the input data. In general, the more the number of convolutional layers, the more advanced the extracted features will be. However, as the number of convolutional layers reaches a certain level, the model suffers from the problem of gradient explosion. Therefore, to alleviate the gradient problem, a residual block structure was introduced [23]. The skip connection is applied to the residual network to connect useful information to a deeper network for transmission. This effect is superior to the simple stacked structure in the traditional CNN. Figure 3 demonstrates the structure of the residual block; (a) represents the residual block in the attention block, (b) represents the residual block in the backbone network, and Mul denotes multiplication. The output of the first convolutional layer is connected to the subsequent convolutional layers through skip connections so that it can keep the information intact in the deeper network.

2.5. Attention Block. In the detection of arrhythmias, owing to the different activation mapping on the related characteristics of arrhythmias, the recognition degree is different, and other signals may cause interference. Therefore, certain characteristics of generation may not be related to arrhythmia diseases. Hence, this study used the attention block to enhance the information associated with arrhythmias and weaken the irrelevant information. In this study, four attention blocks were used to continuously enhance the relevant information and enhance the recognition performance of the model [24]. Figure 4 depicts the concrete structure of an attention block.

First, the input data are processed through a convolution layer, and then the processed data are introduced into a down-up sampling phase, which is used to expand the receiving domain. Maxpooling and nearest interpolation were used as the downsampling and upsampling operations, respectively. Finally, the final feature is obtained through the residual structure and the 1*1 convolution layer, which is input into the sigmoid function to obtain the attention weight. Symmetric downsampling and upsampling architectures can quickly extend the receiving domain to obtain global information. The batch normalization (BN) layer is added before the sigmoid function to prevent the gradient problem and overfitting in the training process.

2.6. Proposed Model. In this study, we proposed a novel deep learning model with parallel input. The two branches had the same structure, including one LSTM block, four residual blocks, four attention blocks, and four convolution layers, followed by a maxpooling layer (MAXP) and a global average pooling layer (GAP). Finally, the outputs of the two parallel branches were fused and sent to the full connection layer for classification. Before the full connection layer, dropout with a parameter of 0.5 was added to reduce overfitting. The step size of the largest pooling layer in the entire network was two, and the pooling window was two. The Adam algorithm was used to train the model, and the learning rate was set to 0.001. To fully train the model and achieve better results, the batch size was set to 128 and epochs were set to 100. Validation sets were also added to the intrapatient model. The ratio of the training set, validation set, and testing set was 3 : 1 : 1. Figure 5 shows the concrete structure of the proposed model, where "x4" represents that part to be repeated four times. The number of filters in each part was increased successively, namely, 32, 64, 128, and 256, the stride size was two, and the kernel size was two. The last convolution layer in the attention block had a kernel size of one.

3. Results

To more authoritatively evaluate the performance of the entire model, three recognized evaluation indexes, namely, specificity (Spe), sensitivity (Sen), and accuracy (Acc), were

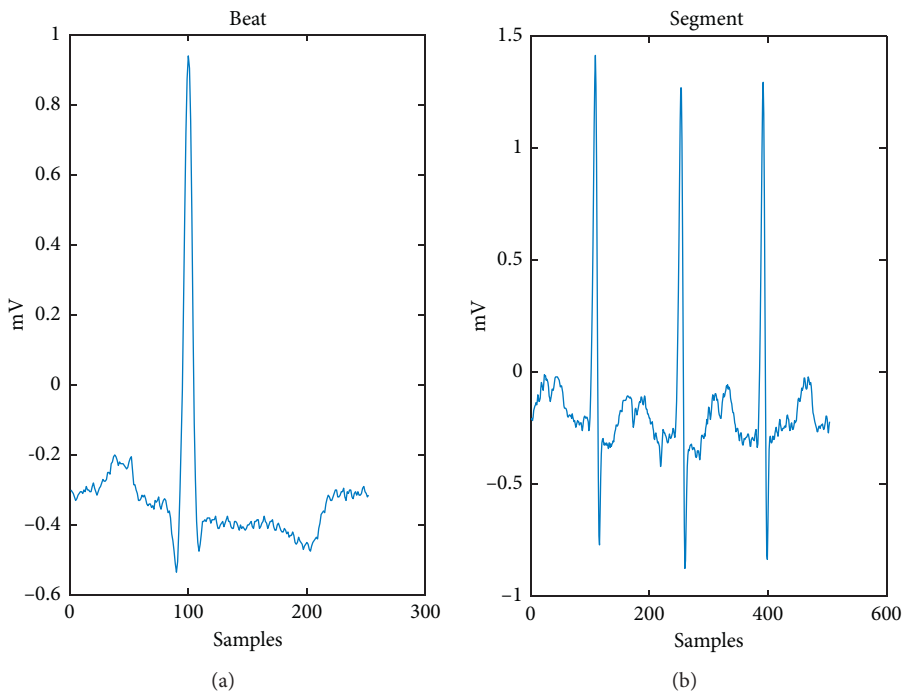

Figure 1: Waveform visualization.

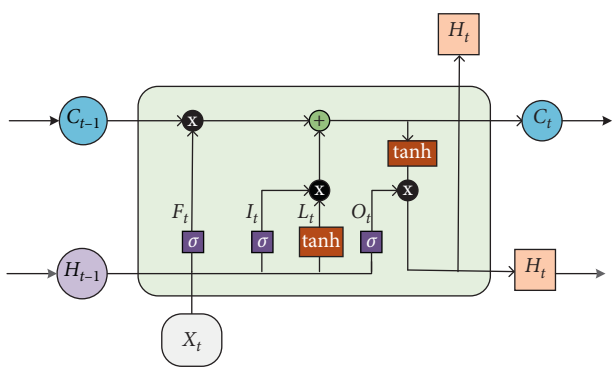

Figure 2: Structure diagram of the LSTM.

applied to evaluate the model. Equations (7)–(9) represent the calculation formulas for each evaluation standard:

$$\text{Spe} = \frac{\text{TN}}{\text{TN} + \text{FP}}, \tag{7}$$

$$\text{Sen} = \frac{\text{TP}}{\text{TP} + \text{FN}}, \tag{8}$$

$$\text{Acc} = \frac{\text{TP} + \text{TN}}{\text{TP} + \text{TN} + \text{FP} + \text{FN}}, \tag{9}$$

where TP, TN, FP, and FN represent true positive, true negative, false positive, and false negative, respectively.

Table 3 presents the final results of our model in the intrapatient model. As observed from Table 3, our method achieved a relatively good performance. The overall Acc was 99.11%, and the average Spe and Sen were 98.56% and 91.63%, respectively. We separately input segments and ECG beats into the model to verify that the performance of our double-input model is superior to that of the single-input model. Tables 4 and 5 present the confusion matrix, Spe, and Sen of the single-input model. The overall Acc of the model with ECG beat and segment was 98.58% and 98.60%, respectively.

No-LSTM network is also designed to show the advantages of LSTM network in the processing of time series data. No-LSTM is to remove the LSTM network in the proposed method and keep the rest unchanged. Table 6 presents the confusion matrix, Spe, and Sen of No-LSTM network. The overall Acc of the model with No-LSTM was 98.53%.

Figure 6 illustrates the changes in the Acc of the training and validation sets and the loss during the training process. In the initial stage, the curves of the training and validation sets changed rapidly and gradually tended to be stable with increasing epoch times and constant parameter optimization. There was no overfitting or underfitting problem in our training process.

We also designed an interpatient model. DS1 and DS2 were applied to the training and testing sets, respectively. Meanwhile, there was no validation set. Table 7 presents the confusion matrix of the interpatient model. The overall Acc was 85.65%. Figure 7 depicts the change curves of the Acc and loss in the model training process, without any fitting phenomenon.

4. Discussion

The traditional ECG signal classification is typically composed of feature extraction and classification. We propose a method based on deep learning that combines feature

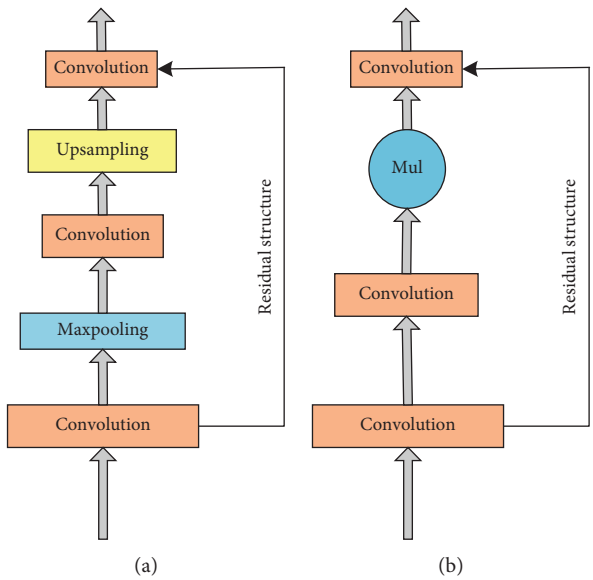

Figure 3: Details of the residual block.

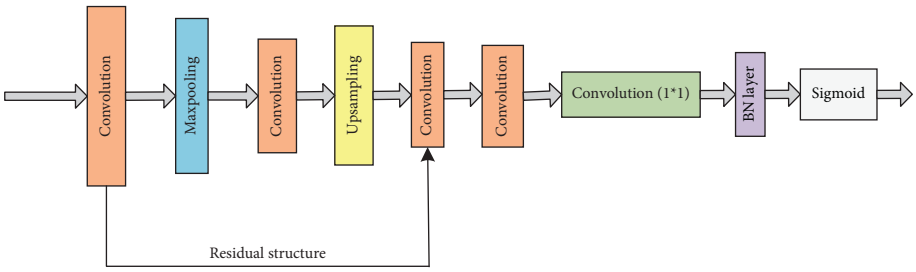

Figure 4: Concrete structure of an attention block.

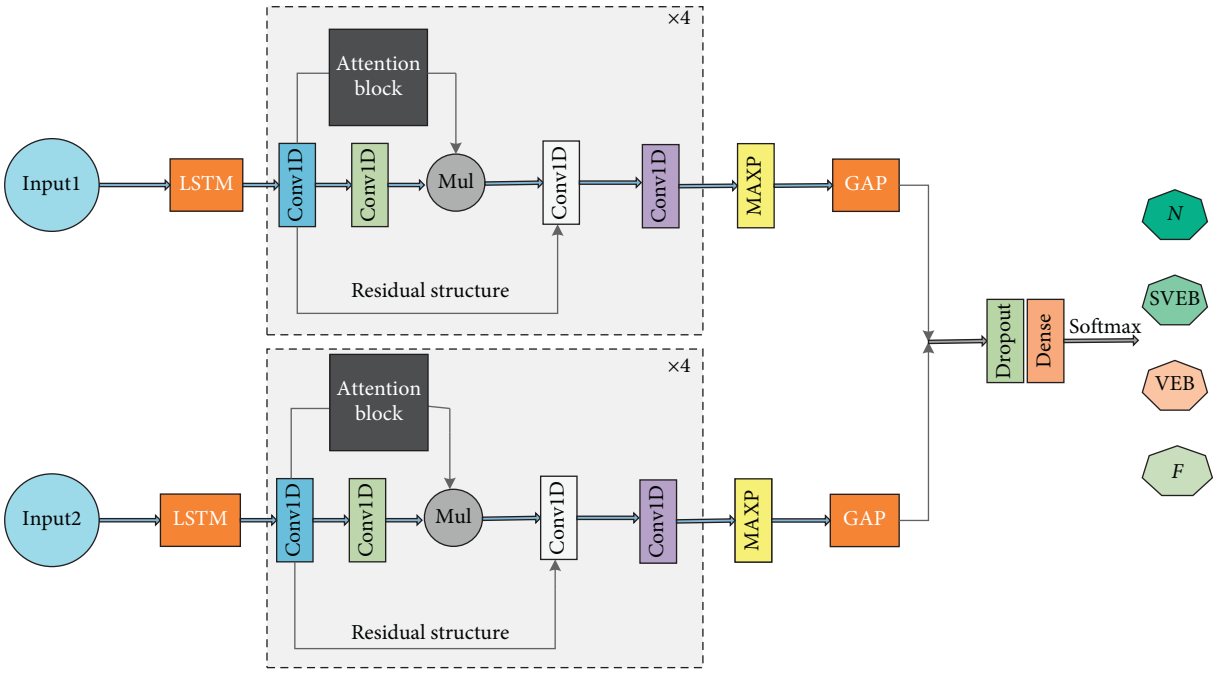

Figure 5: Concrete structure of the proposed model.

Table 3: Confusion matrix-intrapatient model (segment and beat).

		Predicated label				Spe (%)	Sen (%)
		N	SVEB	VEB	*F*		
True label	*N*	17818	22	2	9	94.56	98.13
	SVEB	60	496	4	2	99.85	88.2
	VEB	30	6	1346	16	99.95	96.28
	F	24	0	3	141	99.86	83.92

Overall Acc: 99.11%.

Table 4: Confusion matrix-intrapatient model (only beat).

		Predicated label				Spe (%)	Sen (%)
		N	SVEB	VEB	*F*		
True label	*N*	17774	49	27	1	91.26	99.56
	SVEB	92	466	4	0	99.74	82.9
	VEB	44	1	1352	1	99.74	96.71
	F	48	0	16	104	99.99	62

Overall Acc: 98.58%.

Table 5: Confusion matrix-intrapatient model (only segment).

		Predicated label				Spe (%)	Sen (%)
		N	SVEB	VEB	*F*		
True label	*N*	17808	11	31	1	90.7	99.76
	SVEB	99	450	13	0	99.94	80
	VEB	54	1	1343	0	99.62	96.01
	F	42	0	26	100	99.99	60

Overall Acc: 98.60%.

Table 6: Confusion matrix-intrapatient model (No-LSTM).

		Predicated label				Spe (%)	Sen (%)
		N	SVEB	VEB	*F*		
True label	*N*	17767	49	34	1	91.30	99.53
	SVEB	125	436	1	0	99.73	77.58
	VEB	35	1	1353	9	99.74	96.78
	F	23	2	13	130	99.44	77.38

Overall Acc: 98.53%.

extraction and classification, avoiding the complex feature extraction process and eliminating the need for a separate classifier. To verify the performance of our model, we conducted three comparative experiments. On the one hand, segments and ECG beats were input into our model as single inputs. On the other hand, No-LSTM network was designed. According to Tables 3–6, notably, the Sen of the model to SVEB and *F* was low, and it was highly possible that these two types of arrhythmias constituted a small proportion of the total data quantity. It could be noted from Table 8 that the overall Acc, Spe, and Sen of our double-input model were 99.11%, 98.56%, and 91.63%, respectively, which was better than the overall performance of two single-input models and No-LSTM network. In particular, the Sen of our double-input model was 7.68% (segments) and 6.34% (beats) higher than that of the single-input model. Meanwhile, the Sen of our double-input model was 3.81% higher than No-LSTM network. The information provided by both the segment and the ECG beat improved the Sen of our model, and LSTM has an excellent role in processing time series data.

As depicted in Figure 6, our model had no overfitting, except for slight oscillations. It can be demonstrated that an accurate detection of arrhythmias requires sufficient information from ECG beats and segments.

Existing ECG classification algorithms are summarized in Table 9. Gao et al. used PCA and the dynamic time warping (DTW) method to extract the features of selected ECG fragments and input the extracted features into an SVM [25]. The overall Acc was 97.80%, and the Spe was 88.83%. Although the model achieved good results, the process of feature extraction was complicated and required skilled techniques. Wang et al. proposed a method combining CNN with multilayer perceptron (MLP), in which CNN was used to extract features, and the extracted features were fused with the RR interval and input into MLP, with an Acc rate of 96.27% [26]. Wang et al. used

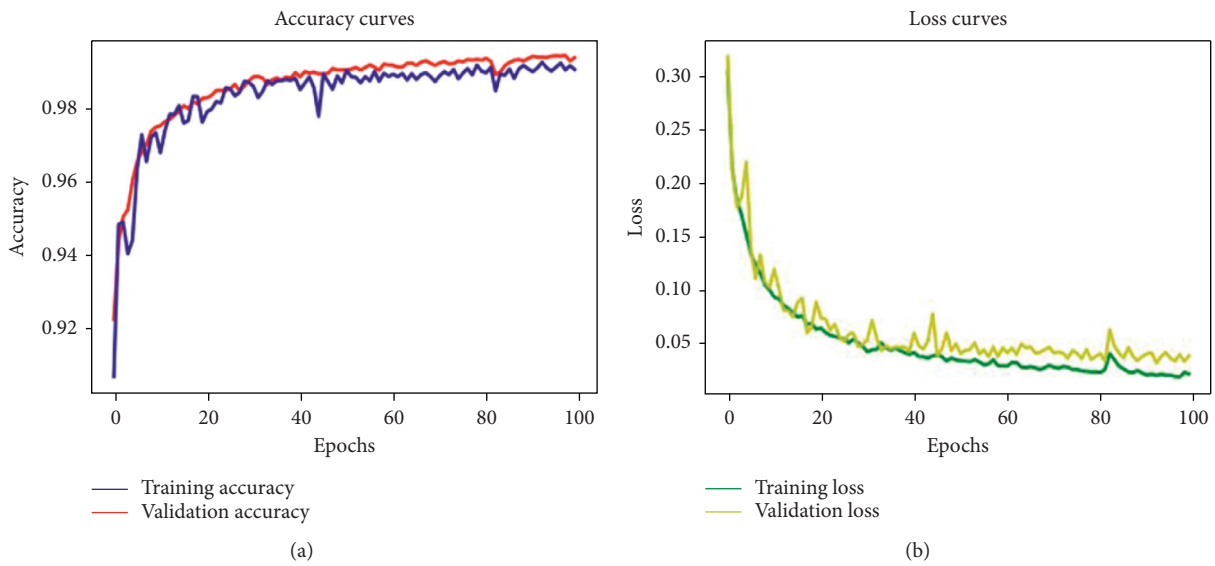

Figure 6: Accuracy and loss change curves of the training and validation sets.

Table 7: Confusion matrix-interpatient model.

		Predicated label			
		N	SVEB	VEB	*F*
True label	*N*	39719	249	1258	2946
	SVEB	1738	26	43	19
	VEB	331	11	2660	164
	F	251	0	98	33

Overall Acc: 85.65%.

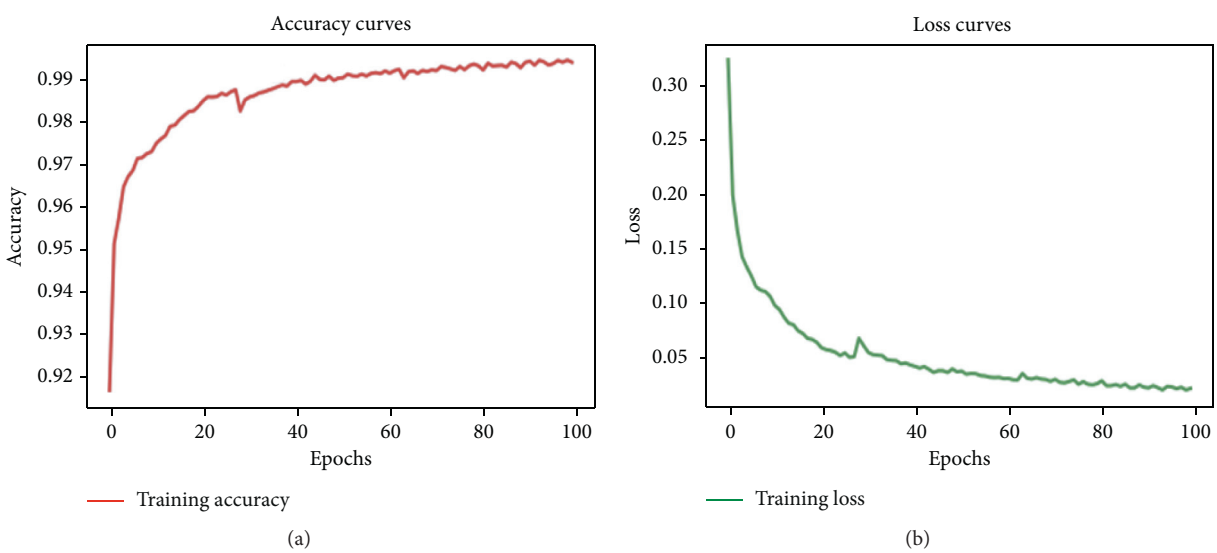

Figure 7: Accuracy and loss change curves of the training set.

continuous wavelet transform (CWT) to decompose ECG signals and used a CNN to extract features from a two-dimensional scale spectrum composed of the aforementioned time-frequency components [27]. The Acc and Sen were 98.74% and 67.47%, respectively. Niu et al. proposed a new deep learning method for ECG classification based on adversarial domain adaptation, which completed the classification of arrhythmias by constructing three modules, and the final classification result was 92.3% [28]. Our model exhibited excellent performance, particularly in terms of Sen. Our model

Table 8: Performance of each model.

Methods	Overall Acc (%)	Spe (%)	Sen (%)
Double-input	99.11	98.56	91.63
Single-input (segments)	98.60	97.56	83.95
Single-input (beats)	98.58	97.68	85.29
Double-input (No-LSTM)	98.53	97.55	87.82

Table 9: Comparison of the proposed method against existing methods.

Paper	Method	Database	Acc (%)	Sen (%)
25	PCA + DTW + SVM	MITDB	97.80	88.83
26	CNN + MLP	MITDB	96.27	68.55
27	CWT + CNN	MITDB	98.74	67.47
28	Adversarial domain adaptation	MITDB	92.30	
Proposed	LSTM + residual network	MITDB	99.11	91.63

had certain limitations: (1) the overall model had several parameters, which required a large amount of calculations. (2) The sample data were not balanced, and normal samples accounted for a large proportion. (3) In the interpatient mode, the performance of our model was poor. (4) It had a low recognition degree for a small number of samples.

5. Conclusions

In this paper, a new automatic detection method for arrhythmias is proposed. In our proposed method, both the segment and ECG beat were used as inputs. LSTM combined with a residual block model was used to extract and refine features. Furthermore, the attention block was used to enhance useful information and weaken useless information. The entire process no longer required manual feature production. However, our model simultaneously extracted important information from the time-domain characteristics and morphological characteristics of ECG signals and then integrated the extracted information to the final full connection layer to complete the classification. To effectively evaluate the performance of our model, our entire experiment was conducted on MITDB. The data were divided into interpatient and intrapatient models, and Acc was achieved at 85.65% in the interpatient model and 99.11% in the intrapatient model. The experimental results demonstrated that our model simultaneously captured temporal and morphological characteristics, which is an effective automatic detection technique.

Furthermore, the model can be applied to wearable devices to assist doctors in diagnosis. In the future, our research will be extended to other databases to achieve more disease classifications.

Data Availability

The data used to support the findings of this study have not been made available because the data also form part of an ongoing study. Original data of the study can be obtained at https://physionet.org/.

Conflicts of Interest

The authors declare no conflicts of interest.

Acknowledgments

This study was partly supported by the National Natural Science Foundation of China (Grant no. 61903226).

References

[1] A. Y. Hannun, P. Rajpurkar, M. Haghpanahi et al., "Cardiologist-level arrhythmia detection and classification in ambulatory electrocardiograms using a deep neural network," *Nature Medicine*, vol. 25, no. 1, pp. 65–69, 2019.

[2] S. S. Lobodzinski and M. M. Laks, "New devices for very long-term ECG monitoring," *Cardiology Journal*, vol. 19, no. 2, pp. 210–214, 2012.

[3] Q. U. Mastoi, M. S. Memon, A. Lakhan et al., "Machine learning-data mining integrated approach for premature ventricular contraction prediction," *Neural Computing & Applications*, Springer, Berlin, Germany, 2021.

[4] S. T. Simon, D. Mandair, P. Tiwari, and M. A. Rosenberg, "Prediction of drug-induced long QT syndrome using machine learning applied to harmonized electronic health record data," *Journal of Cardiovascular Pharmacology and Therapeutics*, vol. 26, Article ID 1074248421995348, 2021.

[5] M. Merah, T. A. Abdelmalik, and B. H. Larbi, "R-peaks detection based on stationary wavelet transform," *Computer Methods and Programs in Biomedicine*, vol. 121, no. 3, pp. 149–160, 2015.

[6] S. Velmurugan, A. Mahabub Basha, and M. Vijayakumar, "Gabor wavelet multi-linear discriminant analysis for data extraction in ECG signals," *Cluster Computing*, vol. 22, no. S6, pp. 14219–14229, 2019.

[7] X. Yi and R. Guo, "Stabilization of chaotic systems with both uncertainty and disturbance by the UDE-based control method," *IEEE Access*, vol. 8, no. 1, pp. 62471–62477, 2020.

[8] M. Jayasanthi, G. Rajendran, and R. B. Vidhyakarl, "Independent component analysis with learning algorithmfor electrocardiogram feature extraction and classification," *Signal Image and Video Processing*, vol. 15, no. 2, pp. 391–399, 2021.

[9] L. X. Liu, B. Li, and R. W. Guo, "Consensus control for networked manipulators with switched parameters and topologies," *IEEE Access*, vol. 9, pp. 9209–9217, 2021.

[10] I. Tobore, A. Kandwal, J. Z. Li et al., "Towards adequate prediction of prediabetes using spatiotemporal ECG and EEG feature analysis and weight-based multi-model approach," *Knowledge-Based Systems*, vol. 209, Article ID 106464, 2020.

[11] T. Hou, Y. Y. Liu, and F. Q. Deng, "Stability for discrete-time uncertain systems with infinite Markov jump and time-delay," *Science Chine-Information Sciences*, vol. 64, pp. 1–11, 2021.

[12] W. Y. Yang, Y. J. Si, D. Wang, and B. H. Guo, "Automatic recognition of arrhythmia based on principal component analysis network and linear support vector machine," *Computers in Biology and Medicine*, vol. 101, pp. 22–32, 2018.

[13] A. Jovic and N. Bogunovic, "Electrocardiogram analysis using a combination of statistical, geometric,and nonlinear heart rate variability features," *Artificial Intelligence in Medicine*, vol. 51, no. 3, pp. 175–186, 2011.

[14] F. Y. Ma, J. Y. Zhang, W. Liang, and J. Y. Xue, "Automated classification of atrial fibrillation using artificial neural

network for wearable devices," *Mathematical Problems in Engineering*, vol. 2020, Article ID 9159158, 6 pages, 2020.

[15] J. Q. Xu, Z. J. Hu, J. Z. Zou, and A. Q. Bi, "Intelligent emotion detection method based on deep learning in medical and health data," *IEEE Access*, vol. 8, pp. 3802–3811, 2020.

[16] A. Ullah, S. U. Rehman, S. S. Tu et al., "A hybrid deep CNN model for abnormal arrhythmia detection based on cardiac ECG signal," *Sensors*, vol. 23, no. 3, 2021.

[17] M. M. Al Rahhal, Y. Bazi, H. Almubarak, N. Alajlan, and M. Al Zuair, "Dense convolutional networks with focal loss and image generation for electrocardiogram classification," *IEEE Access*, vol. 7, pp. 182225–182237, 2019.

[18] X. F. Yang, Q. P. Hu, and S. H. Li, "Electrocardiogram classification of lead convolutional neural network based on fuzzy algorithm," *Journal of Intelligent & Fuzzy Systems*, vol. 38, no. 4, pp. 3539–3548, 2020.

[19] B. H. Kim and J. Y. Pyun, "ECG identification for personal authentication using LSTM-based deep recurrent neural networks," *Sensors*, vol. 20, no. 11, Article ID 3069, 2020.

[20] A. Sharma, N. Garg, S. Patidar, R. S. Tan, and U. R. Acharya, "Automated pre-screening of arrhythmia using hybrid combination of Fourier–Bessel expansion and LSTM," *Computers in Biology and Medicine*, vol. 120, Article ID 103753, 2020.

[21] A. L. Goldberger, L. A. N. Amaral, L. Glass et al., "Physiobank, physiotoolkit, and physionet: components of a new research resource for complex physiologic signals," *Circulation*, vol. 101, no. 23, pp. 215–220, 2000.

[22] J. Pan and W. J. Tompkins, "A real-time QRS detection algorithm," *IEEE Transactions on Biomedical Engineering*, vol. 32, no. 3, pp. 230–236, 1985.

[23] A. Y. Chen, F. Wang, W. H. Liu et al., "Multi-information fusion neural networks for arrhythmia automatic detection," *Computer Methods and Programs in Biomedicine*, vol. 193, Article ID 105479, 2020.

[24] Y. B. Gao, H. Wang, and Z. H. Liu, "An end-to-end atrial fibrillation detection by a novel residual-based temporal attention convolutional neural network with exponential nonlinearity loss," *Knowledge-Based Systems*, vol. 212, Article ID 106589, 2021.

[25] W. L. Zhu, X. H. Chen, Y. Wang, and L. R. Wang, "Arrhythmia recognition and classification using ECG morphology and segment feature analysis," *IEEE-ACM Transactions on Computational Biology and Bioinformatics*, vol. 16, no. 1, pp. 131–138, 2019.

[26] T. Wang, C. H. Lu, M. Yang, F. Hong, and C. Liu, "A hybrid method for heartbeat classification via convolutional neural networks, multilayer perceptrons and focal loss," *Peerj Computer Science*, vol. 6, Article ID e324, 2020.

[27] T. Wang, C. H. Lu, Y. N. Sun et al., "Automatic ECG classification using continuous wavelet transform and convolutional neural network," *Entropy*, vol. 23, no. 1, Article ID 119, 2021.

[28] L. S. Niu, C. Chen, H. Liu, S. W. Zhou, and M. L. Shu, "A deep-learning approach to ECG classification based on adversarial domain adaptation," *Healthcare*, vol. 8, no. 4, Article ID 437, 2020.

Hindawi
Mathematical Problems in Engineering
Volume 2021, Article ID 7282940, 11 pages
https://doi.org/10.1155/2021/7282940

Research Article

Fuzzy Observer-Based H_2/H_∞ Output-Feedback Control for Stochastic Nonlinear Systems with Multiplicative Noise

Wenxuan Yang[1] and Ting Hou[2,3]

[1]*School of Mathematics and Statistics, Qilu University of Technology (Shandong Academy of Sciences), Jinan 250353, China*
[2]*School of Mathematics and Statistics, Shandong Normal University, Jinan 250014, China*
[3]*College of Mathematics and Systems Science, Shandong University of Science and Technology, Qingdao 266590, China*

Correspondence should be addressed to Ting Hou; ht_math@sina.com

Received 7 May 2021; Accepted 30 June 2021; Published 19 July 2021

Academic Editor: Renming Yang

A design method is established for the mixed H_2/H_∞ output-feedback control of stochastic nonlinear systems with multiplicative noise. Firstly, using T-S fuzzy rules, we obtain a fuzzy model to approximate the original nonlinear system. Then, by Schur's complement, the suboptimal H_2/H_∞ output-feedback control design is transformed into a two-step convex optimization problem. A numerical example is given to show the effectiveness of the proposed method.

1. Introduction

One of the objectives of system control is to design a controller for the object model so that the closed-loop system achieves good performance while ensuring internal stability [1–4]. H_2 control and H_∞ control have been attractive subjects since they are of great practical significance in the field of engineering [5–9]. H_2 control has a high request of model accuracy and generally does not consider the influence of model error. However, in practical control systems, the system could not exclude the implication of uncertain factors. Being put forward by Zames in 1981, nowadays the H_∞ design idea has grown into an important robust control theory to eliminate external interference [10]. Accordingly, the combination of H_2 and H_∞ control design methods will ensure the robustness and optimality of the controlled system at the same time (we refer the readers to [11–14]).

It is noticeable that randomness is ubiquitous in the real world [15]. For example, there is a great deal of randomness in financial risk managements. Correspondingly, stochastic H_2/H_∞ control has been an attractive subject in recent decades. Chen et al. [16] implemented a detailed study on stochastic H_2/H_∞ control problems for linear systems with state-dependent noise. Subsequently, [17–20] reported research progress on H_2/H_∞ control of Markov jump systems.

On the other hand, nonlinearity is a universal phenomenon existing in engineering systems [21, 22]. Giving an example, a buck-boost circuit is rich in nonlinear dynamics. Generally speaking, control problems of nonlinear systems are more complicated than those of linear systems [23–25]. Linearizing the nonlinear system has become mature technology to treat the nonlinear problems. [26] introduced a suitable linear model gained by the T-S fuzzy rule to approximate a nonlinear system. [27] designed a mixed H_2/H_∞ controller for nonlinear systems based on fuzzy observer.

According to all above, robust control for stochastic nonlinear systems is definitely worthy both from the theoretical and practical application views. Compared with [27], in which the considered system model does not contain multiplicative noise, it is clear that H_2/H_∞ control for nonlinear systems with multiplicative noise has broader application prospects. The other contribution of this paper is that the suboptimal H_2/H_∞ output-feedback control design is transformed into a two-step convex optimization problem, which is convenient for solving by MATLAB efficiently.

This article is organized as follows. Section 2 builds up an approximate model of the original nonlinear system by the T-S fuzzy rule. Section 3 designs a fuzzy observer-based H_2/H_∞ output-feedback controller by solving a two-step convex optimization problem. A numerical example is given to illustrate the efficiency of the proposed design method in Section 4. Section 5 gives the summary of this paper.

For convenience, we adopt the following notations:

$\mathrm{tr}(A)$: the trace of matrix A

A^T: the transpose of matrix A

$A \geq 0$ ($A > 0$): a positive semidefinite (positive definite) matrix A

I: the identity matrix

$\|x\|$: the Euclidean 2-norm of the n-dimensional real vector x

2. Problem Description

Consider the following nonlinear random perturbation system:

$$\begin{cases} \mathrm{d}x(t) = [f(x(t)) + g(x(t))u(t)]\mathrm{d}t + C(t)x(t)\mathrm{d}w_1, \\ y(t) = h(x(t)) + v(t), \end{cases} \tag{1}$$

where $x(t) = [x_1(t), x_2(t), \ldots, x_n(t)]^T \in R^{n\times 1}$ is the state vector, $u(t)$ is the input of the system, and $y(t)$ is the measured output. We assume that w_1 is a one-dimensional standard Wiener process. $f(x(t))$, $g(x(t))$, and $h(x(t))$ are supposed to be smooth functions. System (1) is influenced by $v(t)$ which is a bounded measurement noise, that is, $E\int_0^T vv'\mathrm{d}t = R_0 \geq 0$.

Using T-S fuzzy rule, we establish a linear fuzzy model for the stochastic model (1). Specifically, by the fuzzy rule, R_i: if $m_1(t)$ is $F_{i1}, \ldots, m_g(t)$ is F_{ig}, $i = 1, 2, \ldots, L$, then we have

$$\begin{cases} \mathrm{d}x(t) = [A_i(t)x(t) + B_i(t)u(t)]\mathrm{d}t + C(t)x(t)\mathrm{d}w_1, \\ y(t) = D_i(t)x(t) + v(t), \end{cases} \tag{2}$$

where R_i represents the i th rule, L demotes the rule number, $m(t) = [m_1(t), \ldots, m_g(t)]^{\mathrm{T}}$ are the measurable prerequisite variables, F_{ij} is the fuzzy set, and A_i, B_i, D_i $(i = 1, 2, \ldots, L)$ are matrices with right dimensions.

By using the single point blur method, the product of reasoning, and the average weighted fuzzification, the following form of fuzzy model is obtained:

$$\begin{cases} \mathrm{d}x(t) = \dfrac{\sum_{i=1}^L \mu_i(m(t))[A_i(t)x(t) + B_i(t)u(t)]\mathrm{d}t}{\sum_{i=1}^L \mu_i(m(t))} + C(t)x(t)\mathrm{d}w_1 = \displaystyle\sum_{i=1}^L h_i(m(t))[A_i(t)x(t) + B_i(t)u(t)]\mathrm{d}t + C(t)x(t)\mathrm{d}w_1, \\ y(t) = \dfrac{\sum_{i=1}^L \mu_i(m(t))D_i(t)x(t)}{\sum_{i=1}^L \mu_i(m(t))} + v(t) = \displaystyle\sum_{i=1}^L h_i(m(t))D_i(t)x(t) + v(t), \end{cases} \tag{3}$$

where $\mu_i(m(t)) = \prod_{j=1}^g F_{ij}(m_j(t))$, $h_i(m(t)) = \mu_i(m(t)) / \sum_{i=1}^L \mu_i(m(t))$, $m(t) = [m_1(t), \ldots, m_g(t)]^T$, and $F_{ij}(m_j(t))$ is the grade of membership of $m_j(t)$ in F_{ij}. We suppose that $\mu_i(m(t)) \geq 0$, $i = 1, 2, \ldots, L$. It is easy to see

$$\begin{aligned} &h_i(m(t)) \geq 0, \\ &\sum_{i=1}^L h_i(m(t)) = 1. \end{aligned} \tag{4}$$

Thus, system (1) is equivalent to the following system:

$$\begin{cases} \mathrm{d}x(t) = \displaystyle\sum_{i=1}^L h_i(m(t))[A_i(t)x(t) + B_i(t)u(t)]\mathrm{d}t + C(t)x(t)\mathrm{d}w_1 + (\Delta f + \Delta g)\mathrm{d}t, \\ y(t) = \displaystyle\sum_{i=1}^L h_i(m(t))D_i(t)x(t) + v(t) + \Delta h, \end{cases} \tag{5}$$

where

$$\Delta f = \left[f(x(t)) - \sum_{i=1}^{L} h_i(m(t)) A_i x(t) \right],$$
$$\Delta g = \left[g(x(t)) - \sum_{i=1}^{L} h_i(m(t)) B_i u(t) \right], \tag{6}$$
$$\Delta h = \left[h(x(t)) - \sum_{i=1}^{L} h_i(m(t)) D_i x(t) \right]$$

represent the approximate error between system (3) and nonlinear model (1).

Select the finite-dimension compensator shown below:

$$\begin{cases} \mathrm{d}\hat{x}(t) = \sum_{i=1}^{L} h_i(m(t)) \left[A_i(t)\hat{x}(t) + B_i(t)u(t) + L_i\left(y - \sum_{i=1}^{L} h_i(m(t)) D_i(t)\hat{x}(t) \right) \right]\mathrm{d}t, \\ u(t) = \sum_{j=1}^{L} h_j(m(t)) k_j \hat{x}(t), \quad \hat{x}(0) = \hat{x}_0, \end{cases} \tag{7}$$

where $u(t) = \sum_{j=1}^{L} h_j(m(t)) k_j \hat{x}(t)$ is the fuzzy controller and $k_j\,(j = 1, 2, \ldots, L)$ is the control parameter.

Setting $\tilde{x} = x - \hat{x}$ and $\overline{x} = [\hat{x}, \tilde{x}]^T$, we get the following closed-loop system:

$$\mathrm{d}\overline{x} = \sum_{i=1}^{L} \sum_{j=1}^{L} h_i(m(t)) h_j(m(t)) \left(\overline{A}_{ij}\overline{x} + \overline{B}_i v \right)\mathrm{d}t + \overline{C}\overline{x}\mathrm{d}w_1 + (\overline{\Delta f} + \overline{\Delta g} + \overline{\Delta h})\mathrm{d}t, \tag{8}$$

where

$$\overline{A}_{ij} = \begin{bmatrix} A_i + B_i k_j & L_i D_i \\ 0 & A_i - L_i D_i \end{bmatrix},$$
$$\overline{B}_i = \begin{bmatrix} L_i \\ -L_i \end{bmatrix}, \overline{C} = \begin{bmatrix} 0 & 0 \\ C & C \end{bmatrix}, \tag{9}$$
$$\overline{\Delta f} = \begin{bmatrix} 0 \\ \Delta f \end{bmatrix}, \overline{\Delta g} = \begin{bmatrix} 0 \\ \Delta g \end{bmatrix}, \overline{\Delta h} = \left[\sum_{i=1}^{L} h_i(m(t)) L_i \Delta h - \sum_{i=1}^{L} h_i(m(t)) L_i \Delta h \right].$$

Next we consider H_∞ control performance. Given $\gamma > 0$ and weighting matrix $Q_1 > 0$, if $(\overline{x}(0) = 0)$,

$$E \int_0^T \overline{x}^T Q_1 \overline{x} \mathrm{d}t < \gamma^2 E \int_0^T v^T v \mathrm{d}t \triangleq \gamma^2 tr(R_0), \tag{10}$$

then we call the H_∞ performance is satisfied.

H_∞ control aims to eliminate the influence of external interference, but the performance of the closed-loop system may not be ideal. Therefore, a mixed H_2/H_∞ control design based on fuzzy observer will be implemented. H_2 performance is defined as follows:

$$J(\overline{x}, u) = E \int_0^T \left(\overline{x}^T Q_2 \overline{x} + u^T R_1 u \right)\mathrm{d}t, \tag{11}$$

where $Q_2 > 0$ and $R_1 > 0$.

3. Output-Feedback Control Design Based on Fuzzy Observer

In the previous work, using the T-S fuzzy rule, we got a fuzzy model (3) and the approximate error between nonlinear system (1) and the fuzzy model. This section attempts to design an output-feedback control satisfying H_∞ performance and H_2 performance for fuzzy model (3).

Let the following inequalities be true:

$$\begin{aligned} \|\Delta f\| &\le \|\Delta A x(t)\|, \\ \|\Delta g\| &\le \left\| \sum_{i=1}^{L} h_i(m(t)) \Delta B k_j \hat{x}(t) \right\|, \\ \left\| \sum_{i=1}^{L} h_i(m(t)) L_i \Delta h \right\| &\le \left\| \sum_{i=1}^{L} h_i(m(t)) L_i \Delta D x(t) \right\|. \end{aligned} \tag{12}$$

By computation and the above inequalities, we have

$$\begin{aligned} (\overline{\Delta f})^T (\overline{\Delta f}) &= (\Delta f)^T (\Delta f) \\ &= \left(f(x(t)) - \sum_{i=1}^{L} h_i(m(t)) A_i x(t) \right)^T \times \left((f x(t)) - \sum_{i=1}^{L} h_i(m(t)) A_i x(t) \right) \\ &\le (\Delta A x(t))^T (\Delta A x(t)) \\ &= (\Delta A \hat{x}(t) + \Delta A \tilde{x}(t))^T \times (\Delta A \hat{x}(t) + \Delta A \tilde{x}(t)) \\ &= ([\Delta A, \Delta A] \overline{x}(t))^T \times ([\Delta A, \Delta A] \overline{x}(t)) \\ &= (\Phi \overline{x}(t))^T (\Phi \overline{x}(t)), \\ (\overline{\Delta g})^T (\overline{\Delta g}) &= (\Delta g)^T (\Delta g) \\ &\le \left(\sum_{j=1}^{L} h_j(m(t)) \Delta B k_j \hat{x}(t) \right)^T \times \left(\sum_{j=1}^{L} h_j(m(t)) \Delta B k_j \hat{x}(t) \right) \\ &= \left(\sum_{j=1}^{L} h_j(m(t)) \left[\Delta B k_j, 0 \right] \overline{x}(t) \right)^T \times \left(\sum_{j=1}^{L} h_j(m(t)) \left[\Delta B k_j, 0 \right] \overline{x}(t) \right) \\ &= \left(\sum_{j=1}^{L} h_j(m(t)) \Omega_j \overline{x}(t) \right)^T \left(\sum_{j=1}^{L} h_j(m(t)) \Omega_j \overline{x}(t) \right) \\ &\le \sum_{j=1}^{L} h_j(m(t)) \overline{x}^T(t) \Omega_j^T \Omega_j \overline{x}(t), \\ (\overline{\Delta h})^T (\overline{\Delta h}) &= 2 \left(\sum_{i=1}^{L} h_i(m(t)) L_i \Delta h \right)^T \times \left(\sum_{i=1}^{L} h_i(m(t)) L_i \Delta h \right) \\ &\le 2 \left(\sum_{i=1}^{L} h_i(m(t)) L_i \Delta D x(t) \right)^T \times \left(\sum_{i=1}^{L} h_i(m(t)) L_i \Delta D x(t) \right) \\ &= 2 \left(\sum_{i=1}^{L} h_i(m(t)) \left[L_i \Delta D, L_i \Delta D \right] \overline{x}(t) \right)^T \times \left(\sum_{i=1}^{L} h_i(m(t)) \left[L_i \Delta D, L_i \Delta D \right] \overline{x}(t) \right) \\ &= 2 \left(\sum_{i=1}^{L} h_i(m(t)) \Xi_i \overline{x}(t) \right)^T \left(\sum_{i=1}^{L} h_i(m(t)) \Xi_i \overline{x}(t) \right) \\ &\le 2 \sum_{i=1}^{L} h_i(m(t)) \overline{x}^T(t) \Xi_i^T \Xi_i \overline{x}(t), \end{aligned} \tag{13}$$

where $\Phi = [\Delta A, \Delta A]$, $\Omega_j = [\Delta B k_j, 0]$, $\Xi_i = [L_i \Delta D, L_i \Delta D]$, $j = 1, 2, \ldots, L, i = 1, 2, \ldots, L$.

For the smooth progress of subsequent work, let us choose a Lyapunov function for system (8):

$$V(\overline{x}(t)) = \overline{x}^T(t)P\overline{x}(t), \tag{14}$$

where P is a weighted matrix with appropriate dimensions.

By integrating (14), we have

$$\begin{aligned}
E\int_0^T d(V(\overline{x}(t))) &= E\int_0^T d\left(\overline{x}^T P\overline{x}\right)\\
&= \sum_{i=1}^{L}\sum_{j=1}^{L} h(m(t))h_j(m(t))E_i\int_0^T\Big[\left(\overline{A}_{ij}\overline{x}+\overline{\Delta f}+\overline{\Delta g}+\overline{\Delta h}\right)^T P\overline{x}+\overline{x}^T P\left(\overline{A}_{ij}\overline{x}+\overline{\Delta f}+\overline{\Delta g}+\overline{\Delta h}\right)\\
&\quad + \overline{x}^T\overline{C}^T P\overline{C}\overline{x}+v^T\overline{B}_i^T P\overline{x}+\overline{x}^T P\overline{B}_i v\Big]\mathrm{d}t\\
&\le \sum_{i=1}^{L}\sum_{j=1}^{L} h_i(m(t))h_j(m(t))E\int_0^T \overline{x}^T\left(3P^2+P\overline{A}_{ij}+\overline{A}_{ij}^T P+\overline{C}^T P\overline{C}+\Phi^T\Phi+\Omega_j^T\Omega_j+2\Xi_i^T\Xi_i\right)\overline{x}\mathrm{d}t\\
&\quad + \sum_{i=1}^{L} h_i(m(t))E\int_0^T\left(v^T\overline{B}_i^T P\overline{x}+\overline{x}^T P\overline{B}_i v\right)\mathrm{d}t\\
&= \sum_{i=1}^{L}\sum_{j=1}^{L} h_i(m(t))h_j(m(t))E\int_0^T \overline{x}^T 3P^2+P\overline{A}_{ij}+\overline{A}_{ij}^T P+\overline{C}^T P\overline{C}+\Phi^T\Phi+\Omega_j^T\Omega_j+2\Xi_i^T\Xi_i\overline{x}\mathrm{d}t\\
&\quad - E\int_0^T\left(\gamma^{-1}\overline{x}^T P\left(\sum_{i=1}^{L} h_i(m(t))\overline{B}_i\right)-\gamma v^T\right)\cdot\left(\gamma^{-1}\overline{x}^T P\left(\sum_{i=1}^{L} h_i(m(t))\overline{B}_i\right)-\gamma v^T\right)^T\mathrm{d}t\\
&\quad + E\int_0^T\left[\gamma^{-2}\overline{x}^T P\left(\sum_{i=1}^{L} h_i(m(t))\overline{B}_i\right)\cdot\left(\sum_{i=1}^{L} h_i(m(t))\overline{B}_i\right)^T P\overline{x}+\gamma^2 v^T v\right]\mathrm{d}t\\
&\le \sum_{i=1}^{L}\sum_{j=1}^{L} h_i(m(t))h_j(m(t))E\int_0^T \overline{x}^T 3P^2+P\overline{A}_{ij}+\overline{A}_{ij}^T P+\overline{C}^T P\overline{C}+\Phi^T\Phi+\Omega_j^T\Omega_j+2\Xi_i^T\Xi_i\\
&\quad + \gamma^{-2}P\overline{B}_i\overline{B}_i^T\overline{x}\mathrm{d}t+E\int_0^T\gamma^2 v^T v\mathrm{d}t.
\end{aligned} \tag{15}$$

Based on (15), we can derive the following theorem.

Theorem 1. *If there exists a $P>0$ satisfying the following inequalities:*

$$3P^2+P\overline{A}_{ij}+\overline{A}_{ij}^T P+\overline{C}^T P\overline{C}+\gamma^{-2}P\overline{B}_i\overline{B}_i^T P+Q_1+\Phi^T\Phi+\Omega_j^T\Omega_j+2\Xi_i^T\Xi_i<0, \tag{16}$$

$$4P^2+P\overline{A}_{ij}+\overline{A}_{ij}^T P+\overline{C}^T P\overline{C}+\widetilde{k}_j^T R_1\widetilde{k}_j+Q_2+\Phi^T\Phi+\Omega_j^T\Omega_j+2\Xi_i^T\Xi_i<0, \tag{17}$$

where $\widetilde{k}_j=\left[k_j,0\right]$, then

(a) H_∞ control performance (10) is fulfilled.

(b) H_2 performance (11) has a upper bound, that is,

$$\begin{aligned}
J\left(\overline{x},u=k_j\widehat{x}\right) &\le \|\overline{x}(0)\|^2\mathrm{tr}(P)\\
&\quad + \mathrm{tr}\left[\left(\sum_{i=1}^{L} h_i(m(t))\overline{B}_i\right)R_0\left(\sum_{i=1}^{L} h_i(m(t))\overline{B}_i\right)^T\right].
\end{aligned} \tag{18}$$

Proof. For given $Q_1 > 0$, by Schur's complement and (15), one can see that

$$\begin{aligned}
&E\int_0^T \overline{x}^T Q_1 \overline{x}\mathrm{d}t - \gamma^2 E\int_0^T v^T v\mathrm{d}t \\
&\le E\int_0^T \left(\overline{x}^T Q_1 \overline{x} - \gamma^2 v^T v\right)\mathrm{d}t + \sum_{i=1}^{L}\sum_{j=1}^{L} h_i(m(t))h_j(m(t))E\int_0^T \Big[\overline{x}^T P\left(\overline{A}_{ij}\overline{x} + \overline{\Delta f} + \overline{\Delta g} + \overline{\Delta h}\right) \\
&\quad + \left(\overline{A}_{ij}\overline{x} + \overline{\Delta f} + \overline{\Delta g} + \overline{\Delta h}\right)^T P\overline{x} + \overline{x}^T P\overline{B}_i v + v^T \overline{B}_i^T P\overline{x} + \overline{x}^T \overline{C}^T P\overline{C}\overline{x}\Big]\mathrm{d}t \\
&\le \sum_{i=1}^{L}\sum_{j=1}^{L} h_i(m(t))h_j(m(t))E\int_0^T \Big[\overline{x}^T\left(3P^2 + \overline{A}_{ij}^T P + P\overline{A}_{ij} + \overline{C}^T P\overline{C} + Q_1 + \Phi^T\Phi + \Omega_j^T\Omega_j + 2\Xi_i^T\Xi_i\right)\overline{x} \\
&\quad + \overline{x}^T P\overline{B}_i v + v^T\overline{B}_i^T P\overline{x} - \gamma^2 v^T v\Big]\mathrm{d}t \\
&= \sum_{i=1}^{L}\sum_{j=1}^{L} h_i(m(t))h_j(m(t))E\int_0^T \begin{bmatrix}\overline{x}\\ v\end{bmatrix}^T \begin{bmatrix} X & P\overline{B}_i \\ \overline{B}_i^T P & -\gamma^2 I\end{bmatrix}\begin{bmatrix}\overline{x}\\ v\end{bmatrix}\mathrm{d}t < 0,
\end{aligned} \tag{19}$$

where $X = 3P^2 + P\overline{A}_{ij} + \overline{A}_{ij}^T P + \overline{C}^T P\overline{C} + Q_1 + \Phi^T\Phi + \Omega_j^T\Omega_j + 2\Xi_i^T\Xi_i$. Therefore, $E\int_0^T \overline{x}^T Q_1\overline{x}\mathrm{d}t < \gamma^2 E\int_0^T v^T v\mathrm{d}t$ is directly derived, i.e., conclusion (a) is valid.

Now let us prove (b). Under the constraint of (8), with the help of the method of completing square, we assert that

$$\begin{aligned}
J\left(\overline{x}, u = k_j\widehat{x}\right) &= E\int_0^T \left(\overline{x}^T Q_2\overline{x} + u^T R_1 u\right)\mathrm{d}t \\
&\le \sum_{i=1}^{L}\sum_{j=1}^{L} h_i(m(t))h_j(m(t))E\int_0^T \Big[\overline{x}^T Q_2\overline{x} + \left(k_j\widehat{x}\right)^T\widetilde{R}_2\left(k_j\widehat{x}\right) + \overline{x}^T P\left(\overline{A}_{ij}\overline{x} + \overline{\Delta f} + \overline{\Delta g} + \overline{\Delta h}\right) \\
&\quad + \left(\overline{A}_{ij}\overline{x} + \overline{\Delta f} + \overline{\Delta g} + \overline{\Delta h}\right)^T P\overline{x} + \overline{x}^T P\overline{B}_i v + v^T\overline{B}_i^T P\overline{x} + \overline{x}^T\overline{C}^T P\overline{C}\overline{x}\Big]\mathrm{d}t + \overline{x}^T(0)P\overline{x}(0) \\
&\le \sum_{i=1}^{L}\sum_{j=1}^{L} h_i(m(t))h_j(m(t))E\int_0^T \overline{x}^T\Big[\left(3P^2 + \overline{A}_{ij}^T P + P\overline{A}_{ij} + \overline{C}^T P\overline{C} + Q_2 + \widetilde{k}_j^T R_1\widetilde{k}_j + \Phi^T\Phi + \Omega_j^T\Omega_j + 2\Xi_i^T\Xi_i\right)\overline{x}dt \\
&\quad + E\int_0^T v^T\left(\sum_{i=1}^{L} h_i(m(t))\overline{B}_i\right)^T\left(\sum_{i=1}^{L} h_i(m(t))\overline{B}_i\right)v\mathrm{d}t + \overline{x}^T(0)P\overline{x}(0) \\
&\le \overline{x}^T(0)P\overline{x}(0) + E\int_0^T v^T\left(\sum_{i=1}^{L} h_i(m(t))\overline{B}_i\right)^T\left(\sum_{i=1}^{L} h_i(m(t))\overline{B}_i\right)v\mathrm{d}t \\
&\quad + \sum_{i=1}^{L}\sum_{j=1}^{L} h_i(m(t))h_j(m(t))E\int_0^T \overline{x}^T\left(4P^2 + \overline{A}_{ij}^T P + P\overline{A}_{ij} + \overline{C}^T P\overline{C} + Q_2 + \widetilde{k}_j^T R_2\widetilde{k}_j + \Phi^T\Phi + \Omega_j^T\Omega_j + 2\Xi_i^T\Xi_i\right)\overline{x}dt \\
&\le \|\overline{x}(0)\|^2\mathrm{tr}(P) + \mathrm{tr}\left[\left(\sum_{i=1}^{L} h_i(m(t))\overline{B}_i\right)R_0\left(\sum_{i=1}^{L} h_i(m(t))\overline{B}_i\right)^T\right],
\end{aligned} \tag{20}$$

which shows that (b) holds. The proof of this theorem is concluded.

According to Theorem 1, suboptimal H_2/H_∞ control design has been transformed into solving the optimization problem $\min_{P>0}\mathrm{tr}(P)$ under the constraint of (16) and (17). However, because P_{22}, L_i, and W_{11} are coupled in some components, the optimization problem is not convex. So, we need to convert it into convex optimization problems.

Express P, Q_1, and Q_2 as follows:

$$P = \begin{bmatrix} P_{11} & 0 \\ 0 & P_{22} \end{bmatrix}, Q_1 = \begin{bmatrix} Q_{11}^{(1)} & 0 \\ 0 & Q_{22}^{(1)} \end{bmatrix}, Q_2 = \begin{bmatrix} Q_{11}^{(2)} & 0 \\ 0 & Q_{22}^{(2)} \end{bmatrix}. \tag{21}$$

Plugging these representations into (16) and (17), one gets

$$\begin{bmatrix} A_{11} & A_{12} \\ A_{21} & A_{22} \end{bmatrix} < 0, \tag{22}$$

$$\begin{bmatrix} B_{11} & B_{12} \\ B_{21} & B_{22} \end{bmatrix} < 0, \tag{23}$$

where

$$\begin{aligned}
A_{11} &= 3P_{11}^2 + P_{11}\left(A_i + B_i k_j\right) + \left(A_i + B_i k_j\right)^T P_{11} + C^T P_{22} C + \gamma^{-2} P_{11} L_i L_i^T P_{11} + Q_{11}^{(1)} + \Delta A^T \Delta A + k_j^T \Delta B^T \Delta B k_j + 2\Delta D^T L_i^T L_i \Delta D, \\
A_{12} &= P_{11} L_i D_i + C^T P_{22} C - \gamma^{-2} P_{11} L_i L_i^T P_{22} + \Delta A^T \Delta A + 2\Delta D^T L_i^T L_i \Delta D, \\
A_{21} &= D_i^T L_i^T P_{11} + C^T P_{22} C - \gamma^{-2} P_{22} L_i L_i^T P_{11} + \Delta A^T \Delta A + 2\Delta D^T L_i^T L_i \Delta D, \\
A_{22} &= 3P_{22}^2 + P_{22}\left(A_i - L_i D_i\right) + \left(A_i - L_i D_i\right)^T P_{22} + C^T P_{22} C + \gamma^{-2} P_{22} L_i L_i^T P_{22} + Q_{22}^{(1)} + \Delta A^T \Delta A + 2\Delta D^T L_i^T L_i \Delta D, \\
B_{11} &= 4P_{11}^2 + P_{11}\left(A_i + B_i k_j\right) + \left(A_i + B_i k_j\right)^T P_{11} + C^T P_{22} C + Q_{11}^{(2)} + k_j^T \widetilde{R}_2 k_j + \Delta A^T \Delta A + k_j^T \Delta B^T \Delta B k_j + 2\Delta D^T L_i^T L_i \Delta D, \\
B_{12} &= P_{11} L_i D_i + C^T P_{22} C + \Delta A^T \Delta A + 2\Delta D^T L_i^T L_i \Delta D, \\
B_{21} &= D_i^T L_i^T P_{11} + C^T P_{22} C + \Delta A^T \Delta A + 2\Delta D^T L_i^T L_i \Delta D, \\
B_{22} &= 4P_{22}^2 + P_{22}\left(A_i - L_i D_i\right) + \left(A_i - L_i D_i\right)^T P_{22} + C^T P_{22} C + Q_{22}^{(2)} + \Delta A^T \Delta A + 2\Delta D^T L_i^T L_i \Delta D.
\end{aligned} \tag{24}$$

Next, let $W = \operatorname{diag}(W_{11}, I)$ with $W_{11} = P_{11}^{-1}$. Multiplying both sides of (22) and (23) by W and setting $Z_i = P_{22} L_i$, $Y_j = k_j W_{11}$, we have

$$\begin{bmatrix} C_{11} & C_{12} \\ C_{21} & C_{22} \end{bmatrix} < 0, \tag{25}$$

$$\begin{bmatrix} D_{11} & D_{12} \\ D_{21} & D_{22} \end{bmatrix} < 0, \tag{26}$$

where

$$\begin{aligned}
C_{11} &= 3I + A_i W_{11} + W_{11} A_i^T + B_i Y_j + Y_j^T B_i^T + W_{11} C^T P_{22} C W_{11} + \gamma^{-2} L_i L_i^T + W_{11} Q_{11}^{(1)} W_{11} + W_{11} \Delta A^T \Delta A W_{11} + Y_j^T \Delta B^T \Delta B Y_j \\
&\quad + 2W_{11} \Delta D^T L_i^T L_i \Delta D W_{11}, \\
C_{12} &= L_i D_i + W_{11} C^T P_{22} C - \gamma^{-2} L_i Z_i^T + W_{11} \Delta A^T \Delta A + 2W_{11} \Delta D^T L_i^T L_i \Delta D, \\
C_{21} &= D_i^T L_i^T + C^T P_{22} C W_{11} - \gamma^{-2} Z_i L_i^T + \Delta A^T \Delta A W_{11} + 2\Delta D^T L_i^T L_i \Delta D W_{11}, \\
C_{22} &= 3I + P_{22} A_i + A_i^T P_{22} - Z_i D_i - D_i^T Z_i^T + C^T P_{22} C + \gamma^{-2} Z_i Z_i^T + Q_{22}^{(1)} + \Delta A^T \Delta A + 2\Delta D^T L_i^T L_i \Delta D, \\
D_{11} &= 4I + A_i W_{11} + W_{11} A_i^T + B_i Y_j + Y_j^T B_i^T + W_{11} C^T P_{22} C W_{11} + W_{11} Q_{11}^{(2)} W_{11} + Y_j^T \widetilde{R}_2 Y_j + Y_j^T \Delta B^T \Delta B Y_j + W_{11} \Delta A^T \Delta A W_{11} \\
&\quad + 2W_{11} \Delta D^T L_i^T L_i \Delta D W_{11}, \\
D_{12} &= L_i D_i + W_{11} C^T P_{22} C + W_{11} \Delta A^T \Delta A + 2W_{11} \Delta D^T L_i^T L_i \Delta D, \\
D_{21} &= D_i^T L_i^T + C^T P_{22} C W_{11} + \Delta A^T \Delta A W_{11} + 2\Delta D^T L_i^T L_i \Delta D W_{11}, \\
D_{22} &= 4P_{22}^2 + P_{22} A_i + A_i^T P_{22} - Z_i D_i - D_i^T Z_i^T + C^T P_{22} C + Q_{22}^{(2)} + \Delta A^T \Delta A + 2\Delta D^T L_i^T L_i \Delta D.
\end{aligned} \tag{27}$$

By Schur's complement, (25) and (26) can be rewritten as

$$\begin{bmatrix} M_{11} & W_{11} & Y_j^T & M_{14} & 0 \\ W_{11} & M_{22} & 0 & 0 & 0 \\ Y_j^T & 0 & M_{33} & 0 & 0 \\ M_{14}^T & 0 & 0 & M_{44} & L_i \\ 0 & 0 & 0 & L_i^T & -\gamma^2 I \end{bmatrix} < 0, \qquad (28)$$

$$\begin{bmatrix} N_{11} & W_{11} & Y_j^T & N_{14} \\ W_{11} & N_{22} & 0 & 0 \\ Y_j & 0 & N_{33} & 0 \\ N_{14}^T & 0 & 0 & N_{44} \end{bmatrix} < 0,$$

where

$$\begin{aligned}
M_{11} &= 3I + A_i W_{11} + W_{11} A_i^T + B_i Y_j + Y_j^T B_i^T + Y_j^T \Delta B^T \Delta B Y_j, \\
M_{14} &= L_i D_i + W_{11}^T C^T P_{22} C - \gamma^{-2} L_i Z_i^T + W_{11} \Delta A^T \Delta A + 2 W_{11} \Delta D^T L_i^T L_i \Delta D, \\
M_{22} &= -\left(Q_{11}^{(1)} + \Delta A^T \Delta A + 2 \Delta D^T L_i^T L_i \Delta D\right)^{-1}, \\
M_{33} &= -\left(\Delta B^T \Delta B\right)^{-1}, \\
M_{44} &= 3P_{22}^2 + P_{22} A_i + A_i^T P_{22} - Z_i D_i - D_i^T Z_i^T + C^T P_{22} C + \gamma^{-2} Z_i Z_i^T + Q_{22}^{(1)} + \Delta A^T \Delta A + 2 \Delta D^T L_i^T L_i \Delta D, \\
N_{11} &= 4I + A_i W_{11} + W_{11} A_i^T + B_i Y_j + Y_j^T B_i^T, \\
N_{14} &= L_i D_i + W_{11} C^T P_{22} C + W_{11} \Delta A^T \Delta A + 2 W_{11} \Delta D^T L_i^T L_i \Delta D, \\
N_{22} &= -\left(Q_{11}^{(2)} + \Delta A^T \Delta A + 2 \Delta D^T L_i^T L_i \Delta D\right)^{-1}, \\
N_{33} &= -\left(R_1 + \Delta B^T \Delta B\right)^{-1}, \\
N_{44} &= 4P_{22}^2 + P_{22} A_i + A_i^T P_{22} - Z_i D_i - D_i^T Z_i^T + C^T P_{22} C + Q_{22}^{(2)} + \Delta A^T \Delta A + 2 \Delta D^T L_i^T L_i \Delta D.
\end{aligned} \qquad (29)$$

Noticing that if (16) and (17) are true, then $M_{44} < 0$ and $N_{44} < 0$, the following two inequalities hold:

$$\begin{aligned}
3P_{22}^2 + P_{22} A_i + A_i^T P_{22} - Z_i D_i - D_i^T Z_i^T + C^T P_{22} C + \gamma^{-2} Z_i Z_i^T + Q_{22}^{(1)} + \Delta A^T \Delta A + 2 \Delta D^T L_i^T L_i \Delta D < 0, \\
4P_{22}^2 + P_{22} A_i + A_i^T P_{22} - Z_i D_i - D_i^T Z_i^T + C^T P_{22} C + Q_{22}^{(2)} + \Delta A^T \Delta A + 2 \Delta D^T L_i^T L_i \Delta D < 0,
\end{aligned} \qquad (30)$$

which can be written as the following LMIs:

$$\begin{bmatrix} G_1 & P_{22} & Z_i \\ P_{22} & \dfrac{-1}{3I} & 0 \\ Z_i^T & 0 & -\gamma^2 I \end{bmatrix} < 0, \qquad (31)$$

$$\begin{bmatrix} G_2 & P_{22} \\ P_{22} & \dfrac{-1}{4I} \end{bmatrix} < 0, \qquad (32)$$

where

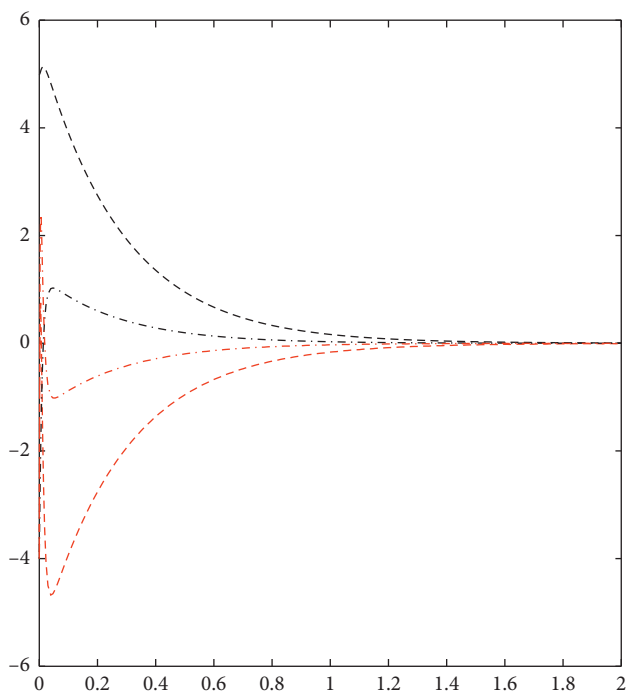

FIGURE 1: The trajectories of states x_1 and x_2.

$$\begin{aligned} G_1 &= P_{22}A_i + A_i^T P_{22} - Z_i D_i - D_i^T Z_i^T + C^T P_{22} C + Q_{22}^{(1)} + \Delta A^T \Delta A + 2\Delta D^T L_i^T L_i \Delta D, \\ G_2 &= P_{22}A_i + A_i^T P_{22} - Z_i D_i - D_i^T Z_i^T + C^T P_{22} C + Q_{22}^{(2)} + \Delta A^T \Delta A + 2\Delta D^T L_i^T L_i \Delta D. \end{aligned} \tag{33}$$

Therefore, the observer-based suboptimal stochastic H_2/H_∞ control design can be transformed into solving a two-step convex optimization problem.

The first step: under the constraint of (31) and (32), solve the convex optimization problem:

$$\min_{P_{22}>0} \operatorname{tr}(P_{22}). \tag{34}$$

It can be obtained that P_{22}, Z_i and $L_i = P_{22}^{-1} Z_i$.

The second step: under the constraint of (25) and (26), solve the following convex optimization problem:

$$\min_{W_{11}>0} \operatorname{tr}(W_{11}). \tag{35}$$

We can get $P_{11} = W_{11}^{-1}$ and the feedback gain k_j. A suboptimal solution $P = \operatorname{diag}(P_{11}, P_{22})$ and compensator (7) are achieved.

To sum up, we state the following main result. □

Theorem 2. *If the above convex optimization problems (34) and (35) have solutions, then* $L_i = P_{22}^{-1} Z_i$ *and* $k_j = Y_j W_{11}^{-1}$. *Moreover, we have* $u^*(t) = Y_j W_{11}^{-1} \hat{x}(t)$, *and* $J^*(\overline{x}, u^*) = tr(W_{11}^{-1} + P_{22})\|\overline{x}(0)\|^2 + tr[(\sum_{i=1}^{h} h_i (m(t))\overline{B}_i) R_0 (\sum_{i=1}^{L} h_i (m(t))\overline{B}_i)^T]$.

4. A Numerical Example

For system (5), we define the fuzzy number as "big and small" and assume its coefficient matrices are

$$\begin{aligned} A_1 &= \begin{bmatrix} 0.2 & 3.2 \\ 2.8 & 0.5 \end{bmatrix}, A_2 = \begin{bmatrix} 0.6 & 2.6 \\ 3.4 & 0.3 \end{bmatrix}, \\ B_1 &= \begin{bmatrix} 0 \\ -0.3 \end{bmatrix}, B_2 = \begin{bmatrix} 0 \\ -0.2 \end{bmatrix}, \\ C &= \begin{bmatrix} 2.5 & 3 \\ 2.8 & 2 \end{bmatrix}, D_1 = D_2 = \begin{bmatrix} 1 & 1 \end{bmatrix}. \end{aligned} \tag{36}$$

Give

$$\Delta A = \begin{bmatrix} 0.4 & 0.6 \\ 0.6 & 0.2 \end{bmatrix}, \Delta B = \begin{bmatrix} 0 \\ 0.1 \end{bmatrix}. \tag{37}$$

We have $\Delta l = 0$, $\Delta h = 0$ and $\Delta C = 0$, $\Delta D = 0$.

Choose $\gamma^2 = 0.9$. Using LMI toolbox in MATLAB, we get

$$P_{22} = \begin{bmatrix} 0.3140 & -0.3253 \\ -0.3253 & 0.3761 \end{bmatrix}, W_{11} = \begin{bmatrix} 4.9206 & -4.9454 \\ -4.9454 & 4.9958 \end{bmatrix},$$
$$Z_1 = \begin{bmatrix} 1.0971 \\ 1.1117 \end{bmatrix}, Z_2 = \begin{bmatrix} 1.0752 \\ 1.1196 \end{bmatrix},$$
$$Y_1 = \begin{bmatrix} 0.9422 & 34.3978 \end{bmatrix}, Y_2 = \begin{bmatrix} -1.1508 & 29.9927 \end{bmatrix}. \tag{38}$$

According to $L_i = P_{22}^{-1} Z_i$, $k_j = Y_j W_{11}^{-1}$, the parameters of observer and controller are

$$L_1 = \begin{bmatrix} 63.0966 \\ 57.5249 \end{bmatrix}, L_2 = \begin{bmatrix} 62.6370 \\ 57.1486 \end{bmatrix},$$
$$k_1 = \begin{bmatrix} 1.4025 & 1.3952 \end{bmatrix} \times 10^3, k_2 = \begin{bmatrix} 1.1374 & 1.1319 \end{bmatrix} \times 10^3. \tag{39}$$

Taking the controller $u^*(t)$ into account, the simulation results are shown in Figure 1. It is shown that the system can achieve the desired control effects under the fuzzy controller.

5. Conclusions

In this paper, the mixed H_2/H_∞ output-feedback control problem for stochastic nonlinear systems in a finite horizon has been studied. Firstly, the nonlinear system is transformed into a linear fuzzy model by T-S rules, and the error between the original system and the fuzzy one has been considered. A fuzzy observer-based two-step convex optimization method has been proposed to treat the suboptimal H_2/H_∞ problem. The method is simple and effective. The closed-loop system can guarantee the robustness and minimize the energy output. Since time delays exist widely in practical systems, how to generalize the obtained H_2/H_∞ output-feedback controller design method to stochastic nonlinear systems with delays is one of the directions of future research.

Data Availability

No data were used to support this study.

Conflicts of Interest

The authors declare that they have no conflicts of interest.

Acknowledgments

This study was supported by the National Natural Science Foundation of China under grant no. 62073204, Key Research and Development Plan of Shandong Province under grant no. 2019GGX101052, and Natural Science Foundation of Shandong Province under grant no. ZR2020MF071.

References

[1] Z. Ji, H. Lin, S. Cao, Q. Qi, and H. Ma, "The complexity in complete graphic characterizations of multiagent controllability," *IEEE Transactions on Cybernetics*, vol. 51, no. 1, pp. 64–76, 2021.

[2] J. Qu, Z. Ji, and Y. Shi, "The graphical conditions for controllability of multiagent systems under equitable partition," *IEEE Transactions on Cybernetics*, vol. 99, pp. 1–12, 2020.

[3] R. Peng, C. Jiang, and R. Guo, "Stabilization of a class of fractional order systems with both uncertainty and disturbance," *IEEE Access*, vol. 9, pp. 42697–42706, 2021.

[4] L. Liu, B. Li, and R. Guo, "Consensus control for networked manipulators with switched parameters and topologies," *IEEE Access*, vol. 9, pp. 9209–9217, 2021.

[5] H. Hua, Y. Qin, J. Geng, C. Hao, and J. Cao, "Robust mixed H_2/H_∞ controller design for energy routers in energy internet," *Energies*, vol. 12, no. 3, p. 340, 2019.

[6] Q. Zhu and Y. Ma, "H_2/H_∞antivertical controller based on particle swarm optimization (PSO) using active T-foils and trim tabs for a fast catamaran," *Mathematical Problems in Engineering*, vol. 2019, Article ID 4868473, 17 pages, 2019.

[7] W. Zhang, L. Ma, and T. Zhang, "Discrete-time mean-field stochastic H_2/H_∞ control," *Journal of Systems Science and Complexity*, vol. 30, no. 4, pp. 765–781, 2017.

[8] B. Bor-Sen Chen, C. Chung-Shi Tseng, and H. Huey-Jian Uang, "Mixed H_2/H_∞ fuzzy output-feedback control design for nonlinear dynamic systems: an LMI approach," *IEEE Transactions on Fuzzy Systems*, vol. 8, no. 3, pp. 249–265, 2000.

[9] T. Hou, W. Zhang, and H. Ma, "Finite horizon H_2/H_∞ control for discrete-time stochastic systems with Markovian jumps and multiplicative noise," *IEEE Transactions on Automatic Control*, vol. 55, no. 5, pp. 1185–1191, 2000.

[10] J. C. Doyle, K. Glover, P. P. Khargonekar, and B. A. Francis, "State-space solutions to standard H_2 and p H_∞ roblems," *IEEE Transactions on Automatic Control*, vol. 34, no. 8, pp. 831–847, 1989.

[11] D. J. N. Limebeer, B. D. O. Anderson, and B. Hendel, "A nash game approach to mixed H_2/H_∞ control," *IEEE Transactions on Automatic Control*, vol. 39, no. 1, pp. 69–82, 1994.

[12] B.-S. Chen, H.-C. Lee, and C.-F. Wu, "Pareto optimal filter design for nonlinear stochastic fuzzy systems via multi-objective H_2/H_∞ optimization," *IEEE Transactions on Fuzzy Systems*, vol. 23, no. 2, pp. 387–399, 2015.

[13] C.-S. Wu, B.-S. Chen, and Y.-W. Jan, "Unified design for H_2, H_∞ and mixed control of spacecraft," *Journal of Guidance, Control, and Dynamics*, vol. 22, no. 6, pp. 884–896, 1999.

[14] C.-S. Wu and B.-S. Chen, "Adaptive attitude control of spacecraft: mixed approach," *Journal of Guidance, Control, and Dynamics*, vol. 24, no. 4, pp. 755–766, 2001.

[15] P. Shi, X. Su, and F. Li, "Dissipativity-based filtering for fuzzy switched systems with sochastic perturbation," *IEEE Transactions on Automatic Control*, vol. 61, no. 6, pp. 1694–1699, 2016.

[16] B.-S. Chen and W. Zhang, "Stochatic H_2/H_∞ control with state-dependent noise," *IEEE Transactions on Automatic Control*, vol. 49, no. 1, pp. 45–57, 2004.

[17] M. Wang, Q. Meng, and Y. Shen, "H_2/H_∞control for stochastic jump-diffusion systems with Markovian switching," *Journal of Systems Science and Complexity*, vol. 34, no. 3, pp. 924–954, 2021.

[18] Z. Yan, Y. Song, and J. H. Park, "Finite-time H_2/H_∞ control for linear it $\hat{o}$ stochastic Markovian jump systems: mode-dependent approach," *IET Control Theory & Applications*, vol. 14, no. 20, pp. 3557–3567, 2021.

[19] D. P. de Farias, J. C. Geromel, J. B. R. do Val, and O. L. V. Costa, "Output feedback control of Markov jump

linear systems in continuous-time," *IEEE Transactions on Automatic Control*, vol. 45, no. 5, pp. 944–949, 2000.

[20] T. Hou, Y. Liu, and F. Deng, "Finite horizon H_2/H_∞ control for SDEs with infinite Markovian jumps," *Nonlinear Analysis: Hybrid Systems*, vol. 34, pp. 108–120, 2019.

[21] C.-F. Wu, B.-S. Chen, and W. Zhang, "Multiobjective investment policy for a nonlinear stochastic financial system: a fuzzy approach," *IEEE Transactions on Fuzzy Systems*, vol. 25, no. 2, pp. 460–474, 2017.

[22] X. Zhao, Y. Yin, L. Zhang, and H. Yang, "Control of switched nonlinear systems via T-S fuzzy modeling," *IEEE Transactions on Fuzzy Systems*, vol. 24, no. 1, pp. 235–241, 2016.

[23] W. Li, Z. Xie, J. Zhao, P. K. Wong, H. Wang, and X. Wang, "Static-output-feedback based robust fuzzy wheelbase preview control for uncertain active suspensions with time delay and finite frequency constraint," *IEEE/CAA Journal of Automatica Sinica*, vol. 8, no. 3, pp. 664–678, 2021.

[24] X. Cai, S. Zhong, J. Wang, and K. Shi, "Robust H_∞ control for uncertain delayed T-S fuzzy systems with stochastic packet dropouts," *Applied Mathematics and Computation*, vol. 385, 2020.

[25] B.-S. Chen and S.-J. Ho, "Multiobjective tracking control design of T-S fuzzy systems: fuzzy pareto optimal approach," *Fuzzy Sets and Systems*, vol. 290, no. 1, pp. 39–55, 2016.

[26] T. Takagi and M. Sugeno, "Fuzzy identification of systems and its applications to modeling and control," *IEEE Transactions on Systems, Man, and Cybernetics*, vol. SMC-15, no. 1, pp. 116–132, 1985.

[27] C.-F. Wu, B.-S. Chen, and W. Zhang, "Multiobjective H_2/H_∞ control design of the nonlinear mean-field stochastic jump-diffusion systems via fuzzy approach," *IEEE Transactions on Fuzzy Systems*, vol. 27, no. 4, pp. 686–700, 2019.

Hindawi
Mathematical Problems in Engineering
Volume 2021, Article ID 1835490, 26 pages
https://doi.org/10.1155/2021/1835490

Research Article

Some Properties of Numerical Solutions for Semilinear Stochastic Delay Differential Equations Driven by G-Brownian Motion

Haiyan Yuan

Department of Mathematics, Heilongjiang Institute of Technology, Harbin 150050, China

Correspondence should be addressed to Haiyan Yuan; yhy82_47@163.com

Received 10 April 2021; Accepted 21 June 2021; Published 6 July 2021

Academic Editor: Yi Qi

This paper is concerned with the numerical solutions of semilinear stochastic delay differential equations driven by G-Brownian motion (G-SLSDDEs). The existence and uniqueness of exact solutions of G-SLSDDEs are studied by using some inequalities and the Picard iteration scheme first. Then the numerical approximation of exponential Euler method for G-SLSDDEs is constructed, and the convergence and the stability of the numerical method are studied. It is proved that the exponential Euler method is convergent, and it can reproduce the stability of the analytical solution under some restrictions. Numerical experiments are presented to confirm the theoretical results.

1. Introduction

Many models in many branches of science and industry, such as economics, finance, biology, and medicine, reveal stochastic effects and are introduced as stochastic differential equations (SDEs). Some phenomena in various fields such as population dynamics [1], optimal pricing in economics [2], thermal noise [3], and spread of virus [4] show stochastic behaviors. However, since most SDEs cannot be solved explicitly, numerical approximations which are on the basis of incorporating the stochastic factor in the classical numerical approximations for DDEs have become an important tool in the study of SDEs. A lot of numerical results for the SDEs have been obtained; please see the works of Chassagneux et al. [5], Higham et al. [6, 7], Banihashemi et al. [8], Babaei et al. [9], Liu and Mao [10], and so on.

The phenomenon of stiffness appears in the process of applying a certain numerical method to ODEs and SDEs. It is known that the stiffness makes standard explicit integrators useless. Nevertheless, the implicit scheme does not perform well for the step size reduction which is forced by accuracy requirements: the method tends to resolve all the oscillations in the solutions and hence leads to its numerical inefficiency. Due to the cost of computing the Jacobian and the exponential or related function of Jacobian, many works are directed at the semilinear stochastic problems and exploring the exponential integrators to approximate the semilinear stochastic problems as they can solve exactly the linear part and maintain some qualitative behaviors (including stability) of the exact solutions. We refer the readers to the works of Higham et al. [11], Hochbruck and Ostermann [12], Bouc and Pardoux [13], Maset and Zennaro [14], Pardoux [15], Altman [16], and Yuan [17].

In the real world, we are often faced with two kinds of uncertainties, that is, probabilistic uncertainty and model uncertainty. Model uncertainty is due to incomplete information, vague data, imprecise probability, and so forth. Many researchers investigate the characteristics of model uncertainty in order to provide a framework for theory and applications. Hou et al. [18] developed the stability analysis for discrete-time uncertain time-delay systems governed by an infinite-state Markov chain. They derived some sufficient conditions for the exponential stability in mean square with conditioning via linear matrix inequalities and established the equivalence among asymptotical stability in mean square, stochastic stability, and exponential stability in mean square. Yi et al. [19] investigated the stabilization of a class of chaotic systems with both model uncertainty and external disturbance. They developed a new UDE-based control method by combining the dynamic

feedback control method and the uncertainty and disturbance estimator- (UDE-) based control method. Peng [20] gave the notions of G-expectation and G-Brownian motion on sublinear expectation space which provide the new perspective for the stochastic calculus under model uncertainty, which has aroused great interest. Based on the fundamental theory of time-consistent G-expectation, Peng [21] introduced the so-called G-Gaussian distribution and the G-Brownian motion and used them to set up the associated Itô integral. Since then, many works have been carried out on the stochastic calculus with respect to the G-Brownian motion. One can see the works of Denis et al. [22], Dolinsky et al. [23], Faizullah et al. [24–26], Ullah and Faizullah [27], Fadina and Herzberg [28], Hu and Peng [29], Li et al. [30], Ren et al. [31], Yin and Ren [32], Yang and Zhu [33], and Zhang and Chen [34]. It can be found that most researches focus on linear and nonlinear SDEs, SDDEs, and NSDDEs with G-Brownian motion; there are a few numerical analysis results for semilinear SDDEs with G-Brownian motion (G-SLSDDEs). To fill this gap, we investigate the numerical solutions of G-SLSDDEs and give some results in the present paper.

The remainder of the paper is organized as follows. In Section 2, we introduce some basic notations, assumptions, and properties which will be used in this paper. We devote Section 3 to presenting the existence and uniqueness of the exact solution for the G-SLSDDEs. In Section 4, we are in a position to establish the exponential integrators for G-SLDDEs and we derive conclusions about the convergence and the exponential mean-square stability of the exact solution for the G-SLSDDEs. We are also successful in establishing the exponential Euler method and proving that the exponential Euler method can preserve the mean-square stability of the exact solution. In Section 5, numerical simulations are presented to demonstrate the theoretical results; and a short conclusion is given in Section 6.

2. Preliminaries

We recall some basic definitions and notions from [20, 21]. Let Ω be a (nonempty) basic space and let $\mathscr{H}$ be a linear space of real-valued functions defined on Ω such that the constant $C \in \mathscr{H}$ and if $X_1, X_2, \ldots, X_n \in \mathscr{H}$, then $\varphi(X_1, X_2, \ldots, X_n) \in \mathscr{H}$ for each $\varphi \in \mathbb{C}_{l.\mathrm{Lip}}(R^n)$, where $\mathbb{C}_{l.\mathrm{Lip}}(R^n)$ is the space of linear function φ defined as follows:

$$\mathbb{C}_{l.\mathrm{Lip}}(R^n) = \{\varphi\colon R^n \longrightarrow R \mid \exists C \in R^+, m \in N, \text{s.t.}\ |\varphi(x) - \varphi(y)| \le C(1 + |x|^m + |y|^m)|x - y|\}, \tag{1}$$

for $x, y \in R^n$. We consider that $\mathscr{H}$ is the space of random variables.

Definition 1 (see [20]; sublinear expectation). A function $\widehat{E}\colon \mathscr{H} \longrightarrow R$ is called sublinear expectation if, $\forall X, Y \in \mathscr{H}, C \in R$, and $\lambda \ge 0$, it satisfies the following properties:

(1) **Monotonicity**: if $X \ge Y$, then $\widehat{E}[X] \ge \widehat{E}[Y]$

(2) **Constant preserving**: $\widehat{E}[C] = C$

(3) **Subadditivity**: $\widehat{E}[X + Y] \ge \widehat{E}[X] + \widehat{E}[Y]$ or $\widehat{E}[X] - \widehat{E}[Y] \ge \widehat{E}[X - Y]$

(4) **Positive homogeneity**: $\widehat{E}[\lambda X] = \lambda \widehat{E}[X]$

Also, if $\widehat{E}[X] = \widehat{E}[-X] = 0$, then $\widehat{E}[C + \lambda X + Y] = C + \widehat{E}[Y]$.

The triple $(\Omega, \mathscr{H}, \widehat{E})$ is called a sublinear expectation space. If (7) and (18) are satisfied, the aforementioned function $\widehat{E}\colon \mathscr{H} \longrightarrow R$ is called a nonlinear expectation and the triple $(\Omega, \mathscr{H}, \widehat{E})$ is relevantly called a nonlinear expectation space. For the details of the notions of G-normal distribution, G-expectation, G-conditional expectation, and G-Brownian motion, see Chapters 2 and 3 of Peng [21].

Definition 2 (see [21]; G-normal distribution). Let $(\Omega, \mathscr{H}, \widehat{E})$ be a sublinear expectation space, and $X \in \mathscr{H}$ with

$$\overline{\sigma}^2 = \widehat{E}\left[X^2\right], \underline{\sigma}^2 = -\widehat{E}\left[-X^2\right]. \tag{2}$$

Then, X is said to be G-distributed or $N(0; [\overline{\sigma}^2, \underline{\sigma}^2])$-distributed, if, $\forall a, b \ge 0$, we have

$$aX + bY \sim \sqrt{a^2 + b^2}X, \tag{3}$$

where each $Y \in \mathscr{H}$ is an independent copy of X; that is, $Y \sim X$, and Y is independent from X.

Definition 3 (see [21]; G-Brownian motion). The sublinear expectation $\widehat{E}\colon L_{ip}(\Omega) \longrightarrow R$ is called a G-expectation if the corresponding canonical process $\{\omega(t)\}_{t \ge 0}$ on the sublinear expectation space $(\Omega, L_{ip}(\Omega), \widehat{E})$ is a G-Brownian motion; that is, for $0 \le s < t$, it satisfies the following conditions:

(1) $\omega(0) = 0$

(2) The increment $\omega(t + s) - \omega(s)$ is independent of $\omega(t_1), \omega(t_2), \ldots, \omega(t_n)$ for each $n \in Z^+$, and $0 \le t_1 \le \cdots \le t_n \le t$

(3) The increment $\omega(t + s) - \omega(s)$ is $N(0, [s\underline{\sigma}^2, s\overline{\sigma}^2])$–distributed

For each fixed $T \ge 0$, set $\Omega_T = \{\omega_{\cdot \wedge T}\colon \omega \in \Omega\}$.

$$L_{ip}(\Omega_T) = \left\{\varphi(\omega(t_1), \omega(t_2), \ldots, \omega(t_n))\colon t_1, t_2, \ldots, t_n \in [0, T], \varphi \in \mathbb{C}_{l.Lip}(R^n), n \in N\right\}, \tag{4}$$

where $L_{ip}(\Omega_t) \subseteq L_{ip}(\Omega_T)$ for $t \le T$ and $L_{ip}(\Omega_T) = \cup_{m=1}^{\infty} L_{ip}(\Omega_m)$. The completion of $L_{ip}(\Omega)$ under the norm $|X|_p = (\widehat{E}[|X|^p])^{1/p}$ for $p \ge 1$ is denoted by $L_G^p(\Omega)$ and $L_G^p(\Omega_t) \subset L_G^p(\Omega_T) \subset L_G^p(\Omega)$ for $0 \le t \le T < \infty$. An important proposition about conditional G-expectation $\widehat{E}[\cdot|\Omega_t]$, $t \in [0,T]$ is presented as follows.

Proposition 1 (see [21]). *ie conditional expectation $\widehat{E}[\cdot|\Omega_t]$, $t \in [0,T]$ holds for each $X, Y \in L_G^1(\Omega_t)$:*

(1) If $X \ge Y$, then $\widehat{E}[X|\Omega_t] \ge \widehat{E}[Y|\Omega_t]$

(2) $\widehat{E}[\eta|\Omega_t] = \eta$, for each $t \in [0,\infty)$ and $\eta \in L_G^1(\Omega_t)$

(3) $\widehat{E}[X] - \widehat{E}[Y] \le \widehat{E}[X - Y|\Omega_t]$

(4) $\widehat{E}[\eta X|\Omega_t] = \eta^+ \widehat{E}[X|\Omega_t] + \eta^- \widehat{E}[-X|\Omega_t]$ for each bounded $\eta \in L_G^1(\Omega_t)$

(5) $\widehat{E}[\widehat{E}[X|\Omega_t]|\Omega_s] = \widehat{E}[X|\Omega_{t\wedge s}]$; in particular, $\widehat{E}[\widehat{E}[X|\Omega_t]] = \widehat{E}[X]$

For $T \in R^+$, a partition π_T of $[0,T]$ is a finite-ordered subset $\pi = \{t_1, \ldots, t_N\}$ such that $0 = t_0 < t_1 < \cdots < t_N = T$. Let $p \ge 1$ be fixed. Define

$$M_G^{p,0}(0,T) = \eta(t) = \eta(t,\omega) = \sum_{j=1}^{N} \xi_{j-1}(\omega) I_{[t_{j-1},t_j)}(t); \xi_{j-1} \in L_G^p\left(\mathscr{F}_{t_{j-1}}\right), t_{j-1} < t_j, \quad j = 1,2,\ldots,N, t_0 = 0, t_N = T, N \ge 1, \tag{5}$$

where $L_G^p(\mathscr{F}_t) = \left\{\xi \in L_G^1(\mathscr{F}_t): \widehat{E}(|\xi|^p) < \infty\right\}$. For $\eta(t) = \sum_{j=0}^{N-1} \xi_j(\omega) I_{[t_j,t_{j+1})}(t) \in M_G^{p,0}(0,T)$, set

$$\widehat{E}_T(\eta) := \frac{1}{T}\int_0^T \widehat{E}[\eta(t)]\mathrm{d}t = \frac{1}{T}\sum_{j=0}^{N-1} \widehat{E}\left(\xi_j\right)\left(t_{j+1} - t_j\right). \tag{6}$$

Then, $\widehat{E}_T$: $M_G^{p,0}(0,T) \mapsto R$ forms a sublinear expectation. For each $p \ge 1$, $M_G^p(0,T)$ denotes the completion of $M_G^{p,0}(0,T)$ under the norm

$$\|\eta\|_{M_G^{p,0}(0,T)} := \frac{1}{T}\left(\int_0^T \widehat{E}\left[|\eta(t)|^p\right]\mathrm{d}t\right)^{1/p}. \tag{7}$$

Definition 4 (see [20]; It ô integral) For each $\eta \in M_G^{p,0}(0,T)$ with the form

$$\eta(t) = \sum_{j=0}^{N-1} \xi_j(\omega) I_{[t_j,t_{j+1})}(t), \tag{8}$$

the Itô integral of G-Brownian motion is defined as

$$I(\eta) = \int_0^T \eta(s)\mathrm{d}\omega^a(s) := \sum_{j=0}^{N-1} \xi_j\left(\omega^a\left(t_{j+1}\right) - \omega^a\left(t_j\right)\right). \tag{9}$$

The mapping I: $M_G^{2,0}(0,T) \mapsto L_G^2(\mathscr{F}_T)$ can be continuously extended to I: $M_G^2(0,T) \mapsto L_G^2(\mathscr{F}_T)$. For each $\eta \in M_G^2(0,T)$, the stochastic integral is defined by

$$\int_0^T \eta(s)\mathrm{d}\omega^a(s) := I(\eta). \tag{10}$$

Definition 5 (see [20]; quadratic variation process). Let $\pi_t^N = \{t_0^N, t_1^N, \ldots, t_N^N\}$, let $N = 1,2,\ldots,$ be a sequence of partitions of $[0,t]$, and set $\mu(\pi_t^N) = \max_{1\le i\le N}|t_i^N - t_{i-1}^N|$. An increasing process $\{\langle\omega^a\rangle(t), t \ge 0\}$ with $\langle\omega^a\rangle(0) = 0$, defined by

$$\langle\omega^a\rangle(t) = \lim_{\mu(\pi_t^N)} \sum_{k=0}^{N-1} \left(\omega^a\left(t_{k+1}^N\right) - \omega^a\left(t_k^N\right)\right)^2 = \left(\omega^2(t)\right)^2 - 2\int_0^t \omega^a(s)\mathrm{d}\omega^a(s), \tag{11}$$

is called the quadratic variation process of G-Brownian motion. Furthermore, for each fixed $s \ge 0$,

$$\langle\omega^a\rangle(t+s) - \langle\omega^a\rangle(s) = \langle\left(\omega^s\right)^a\rangle(t), \tag{12}$$

where $\omega^s(t) = \omega(s+t) - \omega(s)$, $t \ge 0$, $(\omega^s)^a(t) = (a, \omega^s(t))$, and $(x,y) = \sum_{i=1}^d x_i y_i$ for $x, y \in R^d$.

Let $\{\omega\}_{t\ge0}$ be a 1-dimensional G-Brownian motion with $G(a) = 1/2\widehat{E}[a\omega_1^2] = 1/2(\overline{\sigma}^2 a^+ - \underline{\sigma}^2 a^-)$, where $\widehat{E}[\omega_1^2] = \overline{\sigma}^2, -\widehat{E}[-\omega_1^2] = \underline{\sigma}^2$, and $0 \le \underline{\sigma} \le \overline{\sigma}$. As for the definitions of Itô integral and the quadratic variation process with G-Brownian motion, we present two propositions in the following.

Proposition 2 (see [35]). *For any $0 \le t \le T < \infty$, let the quadratic variation of G-Brownian motion $\langle\omega\rangle_t = \int_0^t u_s ds$. Then, one obtains*

$$\underline{\sigma}^2(T-t) \le \langle\omega\rangle_T - \langle\omega\rangle_t \le \overline{\sigma}^2(T-t)\, q.s. \tag{13}$$

Moreover, $\underline{\sigma}^2 dt \le \langle\omega\rangle_t = u_t dt \le \overline{\sigma}^2 dt$ q.s; and $G(a) \ge 1/2au_t$ q.s.

Proposition 3 (see [21]). *For any $0 \le t \le T < \infty$,*

(1) $\widehat{E}[\int_0^T \eta_t d\omega_t] = 0$; $\widehat{E}|\int_0^T \eta_t d\langle\omega\rangle_t| \le \overline{\sigma}^2 \widehat{E}[\int_0^T |\eta_t| dt]$, $\forall \eta_t \in M_G^1(0,T)$

(2) $\widehat{E}[(\int_0^T \eta_t d\omega_t)^2] = \widehat{E}[\int_0^T \eta_t^2 d\langle\omega\rangle_t]$, $\forall \eta_t \in M_G^2(0,T)$
(3) $\widehat{E}[\int_0^T |\eta_t|^p dt] \le \int_0^T \widehat{E}[|\eta_t|^p]dt$, $\forall \eta_t \in M_G^2(0,T)$, $p \le 1$

Lemma 1 (see [36]).

(1) Let $p \ge 1$, $a, \widehat{a} \in R^d$, $\eta \in M_G^p([0,T])$, *and* $0 \le s \le t \le T$. *Then,*

$$\widehat{E}\left(\sup_{s\le u\le t}\left|\int_s^u \eta_r \mathrm{d}\langle w^a, w^{\widehat{a}}\rangle_r\right|^p\right) \le \left(\frac{\sigma_{(a+\widehat{a})(a+\widehat{a})^T} + \sigma_{(a-\widehat{a})(a-\widehat{a})^T}}{4}\right)^p \cdot |t-s|^{p-1}\int_s^t \widehat{E}\left[|\eta_t|^p\right]\mathrm{d}u. \tag{14}$$

(2) Let $p \ge 2$, $\eta \in M_G^p([0,T])$, *and* $0 \le s \le t \le T$. *Then,*

$$\widehat{E}\left(\sup_{s\le u\le t}\left|\int_s^u \eta_r \mathrm{d}w_r\right|^p\right) \le C_p \widehat{E}\left(\left|\int_s^t |\eta_u|^2 \mathrm{d}u\right|^{p/2}\right) \le C_p |t-s|^{p/2-1}\int_s^t \widehat{E}\left[|\eta_u|^p\right]\mathrm{d}u, \tag{15}$$

where C_p *is a positive constant independent of* η.

Lemma 2 (see [37]). *Doob martingale inequality). Let* $\{X(t)\}_{t\ge 0}$ *be an* R^n*-value G-martingale and let* $[a,b]$ *be a bounded interval of* R^+*; if* $p > 1$, $X(t) \in L_G^p(\Omega, R^n)$, *then*

$$\widehat{E}\left(\sup_{a\le t\le b}|X(t)|^p\right) \le \left(\frac{p}{p-1}\right)^p \widehat{E}(X(b))^p. \tag{16}$$

3. Existence and Uniqueness Theorem

Throughout this paper, unless otherwise specified, $a\wedge b$ and $a\vee b$ denote $\max\{a,b\}$ and $\min\{a,b\}$, respectively. Let $\tau > 0$ and $\mathrm{BC}([-\tau,0];R^d)$ denote the family of all bound continuous R^d-valued functions φ defined on $[-\tau,0]$ with norm $\|\varphi\| = \sup_{-\tau\le\theta\le 0}|\varphi(\theta)|$. For $p > 0$ and $t \ge 0$, let $(\Omega, \mathscr{F}, \{\mathscr{F}\}_{t\ge 0}, P)$ be a complete probability space with a filtration $\{\mathscr{F}\}_{t\ge 0}$ satisfying the usual conditions. Let ω_t be a one-dimensional G-Brownian motion with $\omega_t \sim N(0, [\underline{\sigma}^2 t, \overline{\sigma}^2 t])$.

In this paper, we focus on the G-SLSDDEs with the following form:

$$\begin{aligned} \mathrm{d}y(t) &= (Ay(t) + f(t, y(t), y(t-\tau))\mathrm{d}t + g(t, y(t), y(t-\tau))\mathrm{d}\omega_t + h(t, y(t), y(t-\tau))\mathrm{d}\langle\omega\rangle_t, \quad t \in [0,T], \\ y(t) &= y_0, \quad t \in [-\tau, 0], \end{aligned} \tag{17}$$

with initial condition

$$y_0 = \xi = \left\{\varphi\colon \varphi \text{ is } \mathscr{F}_0 - \text{measurable}, \mathrm{BC}\left([-\tau,0];R^d\right) - \text{value random variable, such that } \varphi \in M_G^2\left([-\tau,0];R^d\right)\right\}, \tag{18}$$

where $A \in R^{d\times d}$, $f, g, h\colon R \times R^d \times R^d \longrightarrow R^d$, as well as $f, g, h \in M_G^2([0,T];R^d)$, $\forall T \ge 0$, and $\{\langle\omega\rangle(t), t \ge 0\}$ is the quadratic variation process of G-Brownian motion $\{\langle\omega\rangle(t), t \ge 0\}$.

The G-SLSDDEs (7) with initial value (18) can be written in the following equivalent form:

$$y(t) = y_0 + \int_0^t [Ay(u) + f(u, y(u), y(u-\tau))]\mathrm{d}u + \int_0^t g(u, y(u), y(u-\tau))\mathrm{d}\omega(u) + \int_0^t h(u, y(u), y(u-\tau))\mathrm{d}\langle\omega\rangle(u). \tag{19}$$

To ensure the existence and uniqueness of the solutions, we assume that f, g, and h satisfy the following Lipschitz condition:

(H1) Lipschitz condition: There exists a positive constant L_1, for all $x_1, y_1, x_2, y_2 \in R^d$, $t \geq 0$, such that

$$\left|f(t,x_1,y_1)-f(t,x_2,y_2)\right|^2 \vee \left|g(t,x_1,y_1)-g(t,x_2,y_2)\right|^2 \vee \left|g(t,x_1,y_1)-g(t,x_2,y_2)\right|^2 \leq L_1\left(\left|x_1-x_2\right|^2+\left|y_1-y_2\right|^2\right). \quad (20)$$

According to (20), it is easy to obtain the following linear growth condition:

$$|f(t,x,y)|^2 \leq 2|f(t,x,y)-f(t,0,0)|^2+2|f(t,0,0)|^2 \leq L_1\left(|x|^2+|y|^2\right)+2|f(t,0,0)|^2 \leq G_1\left(1+|x|^2+|y|^2\right). \quad (21)$$

Similarly,

$$|g(t,x,y)| \leq G_1\left(1+|x|^2+|y|^2\right), |h(t,x,y)| \leq G_1\left(1+|x|^2+|y|^2\right), \quad (22)$$

where $G_1 = L_1 \vee 2|f(t,0,0)|^2 \vee 2|g(t,0,0)|^2$.

Theorem 1. *Assume that f, g, and h satisfy the Lipschitz condition (20), and there is a nonnegative constant $\lambda > 0$ such that*

$$\langle z, f(t,z,0)\rangle \leq -\lambda|z|^2, \quad (23)$$

hold for all $t \geq 0$, $z \in R^d$. Then there exists a unique solution $y = \{y(t), t \in [0,\infty)\}$ of equation (7) and the solution belongs to $M_G^2(R^+;R^d)$. Moreover, the solution $y(t)$ satisfies the condition

$$\widehat{E}\left(\sup_{0\leq s\leq T}\left|y_n(s)\right|^2\right) \leq \left[\left(4+8|A|^2+16G_1+32\overline{\sigma}^2G_1+8G_1\overline{\sigma}^4T\right)\widehat{E}\left|y_0\right|^2+8G_1T^2+16\overline{\sigma}^2G_1T+4G_1\overline{\sigma}^4T^2\right]\cdot e^{\left(8|A|^2+16G_1+32\overline{\sigma}^2G_1+8G_1\overline{\sigma}^4T\right)}. \quad (24)$$

Proof. The proof is rather technical, and we shall divide the whole proof into several steps. □

Step 1. Boundedness. For every $T > 0$ and integer $n \geq 1$, define the stopping time

$$\tau_n = T \wedge \inf\{t \in [0,T]: |y(t)| \geq n\}. \quad (25)$$

Clearly, $\tau_n \uparrow T$ almost surely. Set $y_n(t) = y(t \wedge \tau_n)$ for $t \in [0,T]$. Then $y_n(t)$ satisfies the equation

$$\begin{aligned} y_n(t) = y_0 &+ \int_0^t \left(Ay_n(s)+f(s,y_n(s),y_n(s-\tau))I_{[[0,\tau_n]]}(s)\mathrm{d}s\right. \\ &+ \int_0^t g(s,y_n(s),y_n(s-\tau))I_{[[0,\tau_n]]}(s)\mathrm{d}\omega(s)+\int_0^t h(s,y_n(s),y_n(s-\tau))I_{[[0,\tau_n]]}(s)\mathrm{d}\langle\omega\rangle(s). \end{aligned} \quad (26)$$

Using the elementary inequality $|a+b+c+d|^2 \leq 4(|a|^2+|b|^2+|c|^2+|d|^2)$, we have

$$\begin{aligned} \left|y_n(t)\right|^2 \leq 4\left|y_0\right|^2 &+ 4\left|\int_0^t\left(Ay_n(s)+f(s,y_n(s),y_n(s-\tau))I_{[[0,\tau_n]]}(s)\right)\mathrm{d}s\right|^2 \\ &+ 4\left|\int_0^t g(s,y_n(s),y_n(s-\tau))I_{[[0,\tau_n]]}(s)\mathrm{d}\omega(s)\right|^2+4\left|\int_0^t h(s,y_n(s),y_n(s-\tau))I_{[[0,\tau_n]]}(s)\mathrm{d}\langle\omega\rangle(s)\right|^2. \end{aligned} \quad (27)$$

Therefore,

$$\begin{aligned}\sup_{0\le s\le t}\left|y_n(s)\right|^2 \le 4\left|y_0\right|^2 &+ 4\sup_{0\le s\le t}\left|\int_0^t\left(Ay_n(s)+f\left(s,y_n(s),y_n(s-\tau)\right)I_{[[0,\tau_n]]}(s)\right)\mathrm{d}s\right|^2\\ &+4\sup_{0\le s\le t}\left|\int_0^t g\left(s,y_n(s),y_n(s-\tau)I_{[[0,\tau_n]]}(s)\mathrm{d}\omega(s)\right)\right|^2\\ &+4\sup_{0\le s\le t}\left|\int_0^t h\left(s,y_n(s),y_n(s-\tau)\right)I_{[[0,\tau_n]]}(s)\mathrm{d}\langle\omega\rangle(s)\right|^2.\end{aligned} \tag{28}$$

Taking the G-expectation on both sides, it gives

$$\begin{aligned}\widehat{E}\left(\sup_{0\le s\le t}\left|y_n(s)\right|^2\right) \le 4\widehat{E}&\left(\left|y_0\right|^2+\sup_{0\le s\le t}\left|\int_0^t\left(Ay_n(s)+f\left(s,y_n(s),y_n(s-\tau)\right)I_{[[0,\tau_n]]}(s)\right)\mathrm{d}s\right|^2\right)\\ &+4\widehat{E}\left(\sup_{0\le s\le t}\left|\int_0^t g\left(s,y_n(s),y_n(s-\tau)\right)I_{[[0,\tau_n]]}(s)\mathrm{d}\omega(s)\right|^2\right)\\ &+4\widehat{E}\left(\sup_{0\le s\le t}\left|\int_0^t h\left(s,y_n(s),y_n(s-\tau)\right)I_{[[0,\tau_n]]}(s)\mathrm{d}\langle\omega\rangle(s)\right|^2\right).\end{aligned} \tag{29}$$

It follows from Hö lder's inequality and the linear growth condition (21) that

$$\begin{aligned}&\widehat{E}\left(\sup_{0\le s\le t}\left|\int_0^t\left(Ay_n(s)+f\left(s,y_n(s),y_n(s-\tau)\right)I_{[[0,\tau_n]]}(s)\right)\mathrm{d}s\right|^2\right)\\ &\le T\int_0^t\left(2|A|^2\widehat{E}\left|y_n(s)\right|^2+2G_1\left(1+\widehat{E}\left|y_n(s)\right|^2+\widehat{E}\left|y_n(s-\tau)\right|^2\right)\mathrm{d}s\right)\\ &\le 2G_1T^2+\left(2|A|^2+4G_1\right)\int_0^t\widehat{E}\left(\sup_{-\tau\le v\le s}\left|y_n(v)\right|^2\right)\mathrm{d}s.\end{aligned} \tag{30}$$

Together with Proposition 3 and Doob martingale inequality, one can get

$$\begin{aligned}&\widehat{E}\left(\sup_{0\le s\le t}\left|\int_0^t g\left(s,y_n(s),y_n(s-\tau)\right)I_{[[0,\tau_n]]}(s)\mathrm{d}\omega(s)\right|^2\right)\\ &\le 4\overline{\sigma}^2\widehat{E}\left(\int_0^t\left|g\left(s,y_n(s),y_n(s-\tau)\right)\right|^2\mathrm{d}s\right)\\ &\le 4\overline{\sigma}^2G_1\widehat{E}\left(\int_0^t\left(1+\left|y_n(s)\right|^2+\left|y_n(s-\tau)\right|^2\right)\mathrm{d}s\right)\\ &\le 4\overline{\sigma}^2G_1T+8\overline{\sigma}^2G_1\int_0^t\widehat{E}\left(\sup_{-\tau\le v\le s}\left|y_n(v)\right|^2\right)\mathrm{d}s.\end{aligned} \tag{31}$$

Similarly, it follows from Proposition 2 and Hö lder's inequality that one gains

$$\begin{aligned}
&\widehat{E}\left(\sup_{0\le s\le t}\left|\int_0^t h(s,y_n(s),y_n(s-\tau))I_{[[[0,\tau_n]]]}(s)\mathrm{d}\langle\omega\rangle(s)\right|^2\right)\\
&\quad\le \widehat{E}\left(\sup_{0\le s\le t}\left|\int_0^t h(s,y_n(s),y_n(s-\tau))u_s\mathrm{d}s\right|^2\right)\\
&\quad\le \widehat{E}\left[\int_0^t u_s^2\mathrm{d}s\left(\int_0^t\left|h(s,y_n(s),y_n(s-\tau))\right|^2\mathrm{d}s\right)\right]\\
&\quad\le G_1\overline{\sigma}^4T^2+2G_1\overline{\sigma}^4T\int_0^t\widehat{E}\left(\sup_{-\tau\le v\le s}\left|y_n(v)\right|^2\right)\mathrm{d}s.
\end{aligned}\tag{32}$$

Substituting (30)–(32) into (29), one obtains

$$\begin{aligned}
\widehat{E}\left(\sup_{0\le s\le t}\left|y_n(s)\right|^2\right)&\le 4\widehat{E}\left|y_0\right|^2+8G_1T^2+\left(8|A|^2+16G_1\right)\int_0^t\widehat{E}\left(\sup_{-\tau\le v\le s}\left|y_n(v)\right|^2\right)\mathrm{d}s\\
&\quad+16\overline{\sigma}^2G_1T+32\overline{\sigma}^2G_1\int_0^t\widehat{E}\left(\sup_{-\tau\le v\le s}\left|y_n(v)\right|^2\right)\mathrm{d}s+4G_1\overline{\sigma}^4T^2+8G_1\overline{\sigma}^4T\int_0^t\widehat{E}\left(\sup_{-\tau\le v\le s}\left|y_n(v)\right|^2\right)\mathrm{d}s\\
&=4\widehat{E}\left|y_0\right|^2+8G_1T^2+16\overline{\sigma}^2G_1T+4G_1\overline{\sigma}^4T^2+\left(8|A|^2+16G_1+32\overline{\sigma}^2G_1+8G_1\overline{\sigma}^4T\right)\int_0^t\widehat{E}\left(\sup_{-\tau\le v\le s}\left|y_n(v)\right|^2\right)\mathrm{d}s\\
&\le\left(4+8|A|^2+16G_1+32\overline{\sigma}^2G_1+8G_1\overline{\sigma}^4T\right)\widehat{E}\left|y_0\right|^2+8G_1T^2+16\overline{\sigma}^2G_1T\\
&\quad+4G_1\overline{\sigma}^4T^2+\left(8|A|^2+16G_1+32\overline{\sigma}^2G_1+8G_1\overline{\sigma}^4T\right)\int_0^t\widehat{E}\left(\sup_{0\le v\le s}\left|y_n(v)\right|^2\right)\mathrm{d}s.
\end{aligned}\tag{33}$$

An application of the Gronwall inequality yields that

$$\widehat{E}\left(\sup_{0\le s\le t}\left|y_n(s)\right|^2\right)\le\left[\left(4+8|A|^2+16G_1+32\overline{\sigma}^2G_1+8G_1\overline{\sigma}^4T\right)\widehat{E}\left|y_0\right|^2+8G_1T^2+16\overline{\sigma}^2G_1T+4G_1\overline{\sigma}^4T^2\right]\cdot e^{\left(8|A|^2+16G_1+32\overline{\sigma}^2G_1+8G_1\overline{\sigma}^4T\right)}.\tag{34}$$

Thus,

$$\widehat{E}\left(\sup_{0\le s\le \tau_n}\left|y_n(s)\right|^2\right)\le\left[\left(4+8|A|^2+16G_1+32\overline{\sigma}^2G_1+8G_1\overline{\sigma}^4T\right)\widehat{E}\left|y_0\right|^2+8G_1T^2+16\overline{\sigma}^2G_1T+4G_1\overline{\sigma}^4T^2\right]\cdot e^{\left(8|A|^2+16G_1+32\overline{\sigma}^2G_1+8G_1\overline{\sigma}^4T\right)}.\tag{35}$$

Finally, the required inequality (24) follows by letting $n \longrightarrow \infty$.

Step 2. Uniqueness. Let $y(t)$ and $\overline{y}(t)$ be two solutions of Equation (7). By the proof of boundedness, we know that both belong to $M_G^2(R^+; R^d)$, and

$$\begin{aligned} y(t) - \overline{y}(t) = &\int_0^t [A(y(s) - \overline{y}(s)) + f(s, y(s), y(s-\tau)) - f(s, \overline{y}(s), \overline{y}(s-\tau))]\mathrm{d}s \\ &+ \int_0^t [g(s, y(s), y(s-\tau)) - g(s, \overline{y}(s), \overline{y}(s-\tau))]\mathrm{d}\omega(s) \\ &+ \int_0^t [h(s, y(s), y(s-\tau)) - h(s, \overline{y}(s), \overline{y}(s-\tau))]\mathrm{d}\langle\omega\rangle(s). \end{aligned} \tag{36}$$

In the same way as the proof of the boundedness, we have

$$\widehat{E}\left(\sup_{0\le s\le t} |y(s) - \overline{y}(s)|^2\right) \le \left(8|A|^2 + 16L_1 + 32\overline{\sigma}^2 L_1 + 8L_1\overline{\sigma}^4 T\right) \int_0^t \widehat{E}\left(\sup_{0\le v\le s} |y(v) - \overline{y}(v)|^2\right)\mathrm{d}s. \tag{37}$$

An application of the Gronwall inequality yields that

$$\widehat{E}\left(\sup_{0\le t\le T} |y(t) - \overline{y}(t)|^2\right) = 0. \tag{38}$$

Hence, $y(t) = \overline{y}(t)$ for all $0 \le t \le T$ almost surely. The uniqueness has been proved.

Step 3. Existence: Set $y_0(t) = y_0$, for $0 \le t \le T$. Let $y_0^n = \varphi$, $n = 1, 2, \ldots$, and for $t \in [0, T]$, define the Picard iterations

$$\begin{aligned} y_n(t) = y_0 &+ \int_0^t \left(Ay_{n-1}(s) + f\left(s, y_{n-1}(s), y_{n-1}(s-\tau)\right)\right)\mathrm{d}s \\ &+ \int_0^t g\left(s, y_{n-1}(s), y_{n-1}(s-\tau)\right)\mathrm{d}\omega(s) + \int_0^t h\left(s, y_{n-1}(s), y_{n-1}(s-\tau)\right)\mathrm{d}\langle\omega\rangle(s). \end{aligned} \tag{39}$$

Obviously, $y_0(t) \in M_G^2([0, T]; R^d)$. Moreover, it is easy to see by induction that $y_n(t) \in M_G^2([0, T]; R^d)$; in fact,

$$\begin{aligned} \left|y_n(t)\right|^2 \le 4E\left|y_0\right|^2 &+ 4\left|\int_0^t \left(Ay_{n-1}(s) + f\left(s, y_{n-1}(s), y_{n-1}(s-\tau)\right)\right)\mathrm{d}s\right|^2 \\ &+ 4\left|\int_0^t g\left(s, y_{n-1}(s), y_{n-1}(s-\tau)\right)\mathrm{d}\omega(s)\right|^2 + 4\left|\int_0^t h\left(s, y_{n-1}(s), y_{n-1}(s-\tau)\right)\mathrm{d}\langle\omega\rangle(s)\right|^2. \end{aligned} \tag{40}$$

Taking the G-expectation on both sides, it follows from Propositions 2 and 3 and Doob martingale inequality (taking $p = 2$) that

$$\begin{aligned} \widehat{E}\left(\left|y_n(t)\right|^2\right) \le 4\widehat{E}\left|y_0\right|^2 &+ 4t\widehat{E}\int_0^t \left|Ay_{n-1}(s) + f\left(s, y_{n-1}(s), y_{n-1}(s-\tau)\right)\right|^2\mathrm{d}s \\ &+ 16\overline{\sigma}^2\widehat{E}\int_0^t \left|g\left(s, y_{n-1}(s), y_{n-1}(s-\tau)\right)\right|^2\mathrm{d}s + 4\overline{\sigma}^4 t\widehat{E}\int_0^t \left|h\left(s, y_{n-1}(s), y_{n-1}(s-\tau)\right)\right|^2\mathrm{d}s. \end{aligned} \tag{41}$$

Using inequality (21) and the Cauchy inequality, we obtain

$$\begin{aligned}\widehat{E}\left(\left|y_n(t)\right|^2\right) &\le 4\widehat{E}\left|y_0\right|^2 + 8t\widehat{E}\int_0^t \left|Ay_{n-1}(s)\right|^2 + \left|f\left(s, y_{n-1}(s), y_{n-1}(s-\tau)\right)\right|^2 \mathrm{d}s + 16\overline{\sigma}^2\widehat{E}\int_0^t \left|g\left(s, y_{n-1}(s), y_{n-1}(s-\tau)\right)\right|^2 \mathrm{d}s \\ &\quad + 4\overline{\sigma}^4 t\widehat{E}\int_0^t \left|h\left(s, y_{n-1}(s), y_{n-1}(s-\tau)\right)\right|^2 \mathrm{d}s \le 4E\left|y_0\right|^2 \\ &\quad + 8T\widehat{E}\int_0^t \left(G_1 + \left(|A|^2 + G_1\right)\left|y_{n-1}(s)\right|^2 + G_1\left|y_{n-1}(s-\tau)\right|^2\right)\mathrm{d}s + 16\overline{\sigma}^2\widehat{E}\int_0^t \left(G_1 + G_1\left|y_{n-1}(s)\right|^2 + G_1\left|y_{n-1}(s-\tau)\right|^2\right)\mathrm{d}s \\ &\quad + 4\overline{\sigma}^4 T\widehat{E}\int_0^t \left(G_1 + G_1\left|y_{n-1}(s)\right|^2 + G_1\left|y_{n-1}(s-\tau)\right|^2\right)\mathrm{d}s \\ &\le C_1 + \left(8T + 16\overline{\sigma}^2 + 4\overline{\sigma}^4 T\right)\widehat{E}\int_0^t \left(\left(|A|^2 + G_1\right)\left|y_{n-1}(s)\right|^2 + G_1\left|y_{n-1}(s-\tau)\right|^2\right)\mathrm{d}s \\ &\le C_1 + \left(8T + 16\overline{\sigma}^2 + 4\overline{\sigma}^4 T\right)\int_0^t \left(\left(|A|^2 + 2G_1\right)\widehat{E}\sup_{0\le r\le s}\left|y_{n-1}(r)\right|^2 + G_1\widehat{E}\left|y_0\right|^2\right)\mathrm{d}s \\ &\le C_2 + 4\left(|A|^2 + 2G_1\right)\left(2T + 4\overline{\sigma}^2 + \overline{\sigma}^4 T\right)\int_0^t \widehat{E}\sup_{0\le r\le s}\left|y_{n-1}(r)\right|^2 \mathrm{d}s \\ &\le C_2 + 4\left(|A|^2 + 2G_1\right)\left(2T + 4\overline{\sigma}^2 + \overline{\sigma}^4 T\right)\int_0^t \widehat{E}\left|y_{n-1}(s)\right|^2 \mathrm{d}s.\end{aligned} \tag{42}$$

where $C_1 = 4\widehat{E}|y_0|^2 + (8T + 16\overline{\sigma}^2 + 4\overline{\sigma}^4 T)\mathrm{TG}_1$ and $C_2 = C_1 + (8T + 16\overline{\sigma}^2 + 4\overline{\sigma}^4 T)G_1 T\widehat{E}|y_0|^2$.

Hence, for any $k \ge 1$, we derive that

$$\max_{1\le n\le k}\widehat{E}\left|y_n(t)\right|^2\Big) \le C_2 + 4\left(|A|^2 + 2G_1\right)\left(2T + 4\overline{\sigma}^2 + \overline{\sigma}^4 T\right)\int_0^t \max_{1\le n\le k}\widehat{E}\left|y_{n-1}(s)\right|^2 \mathrm{d}s. \tag{43}$$

Note that

$$\max_{1\le n\le k}\widehat{E}\left|y_{n-1}(s)\right|^2 \le \max\left\{\widehat{E}\left|y_0\right|^2, \max_{1\le n\le k}\widehat{E}\left|y_n(s)\right|^2\right\} \le \widehat{E}\left|y_0\right|^2 + \max_{1\le n\le k}\widehat{E}\left|y_n(s)\right|^2. \tag{44}$$

We have

$$\begin{aligned}&\max_{1\le n\le k}\widehat{E}\left|y_n(t)\right|^2\Big) \\ &\quad \le C_2 + 4\left(|A|^2 + 2G_1\right)\left(2T + 4\overline{\sigma}^2 + \overline{\sigma}^4 T\right)\int_0^t \left(\widehat{E}\left|y_0\right|^2 + \max_{1\le n\le k}\widehat{E}\left|y_n(s)\right|^2\right)\mathrm{d}s \\ &\quad \le C_3 + 4\left(|A|^2 + 2G_1\right)\left(2T + 4\overline{\sigma}^2 + \overline{\sigma}^4 T\right)\int_0^t \max_{1\le n\le k}\widehat{E}\left|y_n(s)\right|^2 \mathrm{d}s,\end{aligned} \tag{45}$$

where $C_3 = C_2 + 4T(|A|^2 + 2G_1)(2T + 4\overline{\sigma}^2 + \overline{\sigma}^4 T)\widehat{E}|y_0|^2$. It follows from the Gronwall inequality that

$$\max_{1\le n\le k}\widehat{E}\left|y_n(t)\right|^2 \le C_3 e^{4\left(|A|^2+2G_1\right)\left(2T+4\overline{\sigma}^2+\overline{\sigma}^4 T\right)}. \tag{46}$$

Since k is arbitrary, we can have

$$\widehat{E}\left|y_n(t)\right|^2\Big) \le C_3 e^{4\left(|A|^2+2G_1\right)\left(2T+4\overline{\sigma}^2+\overline{\sigma}^4 T\right)}, \quad \text{for all } 0 \le t \le T, n \ge 1. \tag{47}$$

This shows that $y_n(t) \in M_G^2([0,T];R^d)$.

Using the elementary inequality, we obtain

$$\begin{aligned}\left|y_1(t)-y_0(t)\right|^2 &= \left|y_1(t)-y_0\right|^2 \\ &\le 3\left|\int_0^t \left(Ay_0(s)+f\left(s,y_0,y_0(s-\tau)\right)\right)\mathrm{d}s\right|^2 + 3\left|\int_0^t g\left(s,y_0(s),y_0(s-\tau)\right)\mathrm{d}\omega(s)\right|^2 \\ &\quad + 3\left|\int_0^t h\left(s,y_0(s),y_0(s-\tau)\right)\mathrm{d}\langle\omega\rangle(s)\right|^2.\end{aligned} \tag{48}$$

Taking the G-expectation on (48), it follows from Propositions 2 and 3 and the properties of G-Itô integral that

$$\begin{aligned}&\widehat{E}\left|y_1(t)-y_0(t)\right|^2 \\ &\quad\le 3\widehat{E}\left|\int_0^t \left(Ay_0(s)+f\left(s,y_0(s),y_0(s-\tau)\right)\right)\mathrm{d}s\right|^2 + 3\widehat{E}\left|\int_0^t g\left(s,y_0(s),y_0(s-\tau)\right)\mathrm{d}\omega(s)\right|^2 + 3\widehat{E}\left|\int_0^t h\left(s,y_0(s),y_0(s-\tau)\right)d\langle\omega\rangle(s)\right|^2 \\ &\quad\le 3t\widehat{E}\int_0^t \left|Ay_0(s)+f\left(s,y_0(s),y_0(s-\tau)\right)\right|^2\mathrm{d}s + 12\overline{\sigma}^2\int_0^t \left|g\left(s,y_0(s),y_0(s-\tau)\right)\right|^2\mathrm{d}s + 3\overline{\sigma}^4 t\int_0^t \left|h\left(s,y_0(s),y_0(s-\tau)\right)\right|^2\mathrm{d}s \\ &\quad\le \left(6t+12\overline{\sigma}^2+3\overline{\sigma}^4 t\right)\widehat{E}\int_0^t \left(G_1+\left(2G_1+|A|^2\right)\left|y_0(s)\right|^2\right)\mathrm{d}s \\ &\quad\le \left(6t+12\overline{\sigma}^2+3\overline{\sigma}^4 t\right)G_1 t + \left(6t+12\overline{\sigma}^2+3\overline{\sigma}^4 t\right)\left(2G_1+|A|^2\right)t\widehat{E}\left|y_0\right|^2,\end{aligned} \tag{49}$$

that is,

$$\max_{0\le s\le t}\widehat{E}\left|y_1(s)-y_0(s)\right|^2 \le \left(6t+12\overline{\sigma}^2+3\overline{\sigma}^4 t\right)G_1 t + \left(6t+12\overline{\sigma}^2+3\overline{\sigma}^4 t\right)\left(2G_1+|A|^2\right)t\widehat{E}\left|y_0\right|^2. \tag{50}$$

Taking $t = T$,

$$\max_{0\le s\le t}\widehat{E}\left|y_1(s)-y_0(s)\right|^2 \le \left(6t+12\overline{\sigma}^2+3\overline{\sigma}^4 t\right)G_1 T + \left(6t+12\overline{\sigma}^2+3\overline{\sigma}^4 t\right)\left(2G_1+|A|^2\right)T\widehat{E}\left|y_0\right|^2 := \overline{C}. \tag{51}$$

By the same ways as earlier, we compute

$$\begin{aligned}\widehat{E}\left|y_2(t)-y_1(t)\right|^2 &\le 6t\widehat{E}\int_0^t \left(\left|Ay_1(s)-Ay_0(s)\right|^2+\left|f\left(s,y_1,y_1(s-\tau)\right)-f\left(s,y_0(s),y_0(s-\tau)\right)\right|^2\right)\mathrm{d}s \\ &\quad + 12\overline{\sigma}^2\int_0^t \left|g\left(s,y_1(s),y_1(s-\tau)\right)-g\left(s,y_0(s),y_0(s-\tau)\right)\right|^2\mathrm{d}s \\ &\quad + 3\overline{\sigma}^4 t\int_0^t \left|h\left(s,y_1(s),y_1(s-\tau)\right)-h\left(s,y_0(s),y_0(s-\tau)\right)\right|^2\mathrm{d}s,\end{aligned} \tag{52}$$

and thus, we derive that

$$\begin{aligned}
&\widehat{E}\left(\sup_{0\le s\le t}\left|y_2(s)-y_1(s)\right|^2\right)\\
&\quad\le 6t\widehat{E}\int_0^t\left(|A|^2|y_1(s)-y_0(s)|^2+L_1\left(\left|y_1(s)-y_0(s)\right|^2+\left|y_1(s-\tau)-y_0(s-\tau)\right|^2\right)\right)\mathrm{d}s\\
&\qquad+12\overline{\sigma}^2\int_0^t L_1\left(|y_1(s)-y_0(s)|^2+\left|y_1(s-\tau)-y_0(s-\tau)\right|^2\right)\mathrm{d}s+3\overline{\sigma}^4t\int_0^t L_1\left(\left|y_1(s)-y_0(s)\right|^2+\left|y_1(s-\tau)-y_0(s-\tau)\right|^2\right)\mathrm{d}s\\
&\quad\le 3\left(2T+4\overline{\sigma}^2+\overline{\sigma}^4T\right)\widehat{E}\int_0^t\left(|A|^2+2L_1\right)\left(\sup_{0\le r\le s}\left|y_1(r)-y_0(r)\right|^2\right)\mathrm{d}s\\
&\quad\le 3\left(2T+4\overline{\sigma}^2+\overline{\sigma}^4T\right)\left(|A|^2+2L_1\right)t\overline{C}.
\end{aligned}\tag{53}$$

Similarly,

$$\begin{aligned}
&\widehat{E}\left(\sup_{0\le s\le t}\left|y_3(s)-y_2(s)\right|^2\right)\\
&\quad\le 3\left(2T+4\overline{\sigma}^2+\overline{\sigma}^4T\right)\widehat{E}\int_0^t\left(|A|^2+2L_1\right)\left(\sup_{0\le r\le s}\left|y_2(r)-y_1(r)\right|^2\right)\mathrm{d}s\\
&\quad\le 3\left(2T+4\overline{\sigma}^2+\overline{\sigma}^4T\right)\left(|A|^2+2L_1\right)\widehat{E}\int_0^t 3\left(2T+4\overline{\sigma}^2+\overline{\sigma}^4T\right)\left(|A|^2+2L_1\right)s\overline{C}\mathrm{d}s\\
&\quad\le\frac{3^2\left(2T+4\overline{\sigma}^2+\overline{\sigma}^4T\right)^2\left(|A|^2+2L_1\right)^2t^2\overline{C}}{2!},
\end{aligned}\tag{54}$$

continuing this process to find that

$$\begin{aligned}
&\widehat{E}\left(\sup_{0\le s\le t}\left|y_4(s)-y_3(s)\right|^2\right)\\
&\quad\le 3\left(2T+4\overline{\sigma}^2+\overline{\sigma}^4T\right)\widehat{E}\int_0^t\left(|A|^2+2L_1\right)\left(\sup_{0\le s\le t}\left|y_3(r)-y_2(r)\right|^2\right)\mathrm{d}s\\
&\quad\le 3\left(2T+4\overline{\sigma}^2+\overline{\sigma}^4T\right)\left(|A|^2+2L_1\right)\widehat{E}\int_0^t 3^2\left(2T+4\overline{\sigma}^2+\overline{\sigma}^4T\right)^2\left(|A|^2+2L_1\right)^2s^2\overline{C}\mathrm{d}s\\
&\quad\le\frac{3^3\left(2T+4\overline{\sigma}^2+\overline{\sigma}^4T\right)^3\left(|A|^2+2L_1\right)^3t^3\overline{C}}{3!}.
\end{aligned}\tag{55}$$

Now, we claim that, for all $n\ge 0$,

$$\widehat{E}\left(\sup_{0\le s\le t}\left|y_{n+1}(s)-y_n(s)\right|^2\right)\le\frac{\overline{C}(Mt)^n}{n!},\quad 0\le t\le T,\tag{56}$$

where $M=3\left(2T+4\overline{\sigma}^2+\overline{\sigma}^4T\right)\left(|A|^2+2L_1\right)$.

When $n=0,1,2,3,$ inequality (56) holds. We suppose that (56) holds for some n, now to check (56) for $(n+1)$. In fact,

$$\begin{aligned}
&\widehat{E}\left(\sup_{0\le s\le t}\left|y_{n+2}(s)-y_{n+1}(s)\right|^2\right)\\
&\quad\le 3\left(2T+4\overline{\sigma}^2+\overline{\sigma}^4T\right)\widehat{E}\int_0^t\left(|A|^2+2L_1\right)\left(\sup_{0\le r\le s}\left|y_{n+1}(r)-y_n(r)\right|^2\right)\mathrm{d}s\\
&\quad= M\int_0^t\widehat{E}\left(|A|^2+2L_1\right)\left(\sup_{0\le r\le s}\left|y_{n+1}(r)-y_n(r)\right|^2\right)\mathrm{d}s.
\end{aligned}\tag{57}$$

By induction and (56),

$$\begin{aligned}
\widehat{E}\left(\sup_{0\le s\le t}\left|y_{n+2}(s)-y_{n+1}(s)\right|^2\right)&\le M\int_0^t\frac{\overline{C}[M(s)]^n}{n!}\mathrm{d}s\\
&=\frac{\overline{C}(Mt)^{n+1}}{(n+1)!}.
\end{aligned}\tag{58}$$

It is easy to see that (56) holds for $n+1$. Therefore, by induction, (56) holds for all $n\ge 0$.

Next, to verify that $\{y_n(t), n\ge 0\}$ converge to $y(t)$ at the sense of L_G^2 and probability 1 on $M_G^2((0,T];R^d)$, moreover, $y(t)$ is the solution of (7). For (56), taking $t=T$,

$$\widehat{E}\left(\sup_{0\le t\le T}\left|y_{n+1}(t)-y_n(t)\right|^2\right)\le\frac{\overline{C}(\mathrm{MT})^n}{n!}.\tag{59}$$

By Chebyshev's inequality,

$$\widehat{E}\left\{\sup_{0\le t\le T}\left|y_{n+1}(t)-y_n(t)\right|>\frac{1}{2^n}\right\}\le\frac{\overline{C}(2\mathrm{MT})^n}{n!}.\tag{60}$$

Since $\sum_{n=0}^{\infty}\overline{C}(2\mathrm{MT})^n/n!<\infty$, the Borel-Cantelli lemma yields that there exists a positive integer n_0 such that

$$\sup_{0\le t\le T}\left|y_{n+1}(t)-y_n(t)\right|\le\frac{1}{2^n}\text{ whenever }n\ge n_0.\tag{61}$$

It follows that, with probability 1, the partial sums,

$$y_0(t)+\sum_{i=0}^{n-1}\left[y_{i+1}(t)-y_i(t)\right]=y_n(t),\tag{62}$$

are convergent uniformly in $t\in[0,T]$. Denote the limit by $y(t)$. Clearly, $y(t)$ is continuous and $\mathscr{F}_t$-adapted. On the other hand, one sees from (56) that, for every t, $\{y_n(t)\}_{n\ge1}$ is a Cauchy sequence in L_G^2 as well. Hence, we also have $y_n(t)\longrightarrow y(t)$ in L_G^2; that is,

$$\widehat{E}\left|y_n(t)-y(t)\right|^2\longrightarrow 0,\quad n\longrightarrow\infty.\tag{63}$$

Letting $n\longrightarrow\infty$ in (47) then yields that

$$\widehat{E}\left|y(t)\right|^2\big)\le C_3e^{4\left(|A|^2+2G_1\right)\left(2T+4\overline{\sigma}^2+\overline{\sigma}^4T\right)},\quad\text{for all }0\le t\le T.\tag{64}$$

Therefore, $y(\cdot)\in M^2([0,T];R^d)$. It remains to show that $y(t)$ satisfies the G-SLSDDE in integral form. Note that

$$\begin{aligned}
&\widehat{E}\left|\int_0^t\left(Ay_n(s)+f\left(s,y_n(s),y_n(s-\tau)\right)\right)\mathrm{d}s-\int_0^t\left(Ay(s)+f\left(s,y(s),y(s-\tau)\right)\right)\mathrm{d}s\right|^2\\
&\quad+\widehat{E}\left|\int_0^t g\left(s,y_n(s),y_n(s-\tau)\right)\mathrm{d}\omega(s)-\int_0^t g\left(s,y(s),y(s-\tau)\right)\mathrm{d}\omega(s)\right|^2\\
&\quad+\widehat{E}\left|\int_0^t h\left(s,y_n(s),y_n(s-\tau)\right)\mathrm{d}\langle\omega\rangle(s)-\int_0^t h\left(s,y(s),y(s-\tau)\right)\mathrm{d}\langle\omega\rangle(s)\right|^2\\
&\le t\widehat{E}\int_0^t\left|Ay_n(s)+f\left(s,y_n(s),y_n(s-\tau)\right)-Ay(s)-f\left(s,y(s),y(s-\tau)\right)\right|^2\mathrm{d}s\\
&\quad+4\overline{\sigma}^2\widehat{E}\int_0^t\left|g\left(s,y_n(s),y_n(s-\tau)\right)-g\left(s,y(s),y(s-\tau)\right)\right|^2\mathrm{d}s+\overline{\sigma}^4t\widehat{E}\int_0^t\left|h\left(s,y_n(s),y_n(s-\tau)\right)-h\left(s,y(s),y(s-\tau)\right)\right|^2\mathrm{d}s\\
&\le L_1\left[\left(1+\overline{\sigma}^4\right)T+4\overline{\sigma}^2\right]\left(\frac{|A|^2}{L_1}+2\right)\int_0^t\widehat{E}\sup_{0\le r\le s}\left|y_n(r)-y(r)\right|^2\mathrm{d}s\\
&\le L_1\left[\left(1+\overline{\sigma}^4\right)T+4\overline{\sigma}^2\right]\left(\frac{|A|^2}{L_1}+2\right)\int_0^t\widehat{E}\left|y_n(s)-y(s)\right|^2\mathrm{d}s.
\end{aligned}\tag{65}$$

Noting that sequence $\{y_n(t), n \geq 0\}$ uniformly converges on $(0, T]$, it means that, for any given $\varepsilon > 0$, there exists a positive integer n_0 such that as $n \geq n_0$, for any $(0, T]$, one then deduces that $\widehat{E}|y_n(t) - y(t)|^2 < \varepsilon$. Furthermore, we obtain

$$\begin{aligned}
&\widehat{E}\left|\int_0^t \left(Ay_n(s) + f\left(s, y_n(s), y_n(s-\tau)\right)\right)\mathrm{d}s - \int_0^t \left(Ay(s) + f\left(s, y(s), y(s-\tau)\right)\right)\mathrm{d}s\right|^2 \\
&\quad + \widehat{E}\left|\int_0^t g\left(s, y_n(s), y_n(s-\tau)\right)\mathrm{d}\omega(s) - \int_0^t g\left(s, y(s), y(s-\tau)\right)\mathrm{d}\omega(s)\right|^2 \\
&\quad + \widehat{E}\left|\int_0^t h\left(s, y_n(s), y_n(s-\tau)\right)\mathrm{d}\langle\omega\rangle(s) - \int_0^t h\left(s, y(s), y(s-\tau)\right)\mathrm{d}\langle\omega\rangle(s)\right|^2 \\
&\leq L_1\left[\left(1+\overline{\sigma}^4\right)T + 4\overline{\sigma}^2\right]\left(\frac{|A|^2}{L_1} + 2\right)\int_0^t \widehat{E}\left|y_n(s) - y(s)\right|^2\mathrm{d}s \leq L_1\left[\left(1+\overline{\sigma}^4\right)T + 4\overline{\sigma}^2\right]\left(\frac{|A|^2}{L_1} + 2\right)T\varepsilon.
\end{aligned} \tag{66}$$

In other words, for $t \in [0, T]$, we have

$$\begin{aligned}
\int_0^t \left(Ay_n(s) + f\left(s, y_n(s), y_n(s-\tau)\right)\right)\mathrm{d}s &\longrightarrow \int_0^t \left(Ay(s) + f\left(s, y(s), y(s-\tau)\right)\right)\mathrm{d}s \text{ in } L_G^2, \\
\int_0^t g\left(s, y_n(s), y_n(s-\tau)\right)\mathrm{d}s &\longrightarrow \int_0^t g\left(s, y(s), y(s-\tau)\right)\mathrm{d}\omega(s) \text{ in } L_G^2, \\
\int_0^t h\left(s, y_n(s), y_n(s-\tau)\right)\mathrm{d}s &\longrightarrow \int_0^t h\left(s, y(s), y(s-\tau)\right)\mathrm{d}\langle\omega\rangle(s) \text{ in } L_G^2.
\end{aligned} \tag{67}$$

For $0 \leq t \leq T$, taking limits on both sides of (47), we obtain

$$\begin{aligned}
\lim_{n\longrightarrow\infty} y_n(t) = y(0) &+ \lim_{n\longrightarrow\infty}\int_0^t \left(Ay_n(s) + f\left(s, y_n(s), y_n(s-\tau)\right)\right)\mathrm{d}s + \lim_{n\longrightarrow\infty}\int_0^t g\left(s, y_n(s), y_n(s-\tau)\right)\mathrm{d}\omega(s) \\
&+ \lim_{n\longrightarrow\infty}\int_0^t h\left(s, y_n(s), y_n(s-\tau)\right)\mathrm{d}\langle\omega\rangle(s),
\end{aligned} \tag{68}$$

that is,

$$y(t) = y(0) + \int_0^t \left(Ay(s) + f\left(s, y(s), y(s-\tau)\right)\right)\mathrm{d}s + \int_0^t g\left(s, y(s), y(s-\tau)\right)\mathrm{d}\omega(s) + \int_0^t h\left(s, y(s), y(s-\tau)\right)\mathrm{d}\langle\omega\rangle(s), \quad 0 \leq t \leq T. \tag{69}$$

The aformentioned expression demonstrates that $y(t)$ is the solution of (7). So far, the existence of Theorem 1 is completed.

4. Exponential Euler Method and the Numerical Analysis

We can now give the numerical solution for the G-SLSDDE (7). In order to avoid the storage problem and improve the convergence order, we introduce the exponential Euler scheme.

To formulate the grid, let t_0 be an arbitrary but fixed positive number, define $t_n = t_0 + nh$, $n = 0, 1, 2, \ldots$, $h > 0$ is the step size which satisfies $h = \tau/m$, m is a positive integer, and the solution of (19) at $t_{n+1} = t_n + h$ has the form

$$\begin{aligned} y(t_{n+1}) = e^{Ah_n} y(t_n) &+ \int_{t_n}^{t_{n+1}} e^{As} f(t_n, y(s), y(s-\tau)) \mathrm{d}s + \int_{t_n}^{t_{n+1}} e^{As} g(t_n, y(s), y(s-\tau)) \mathrm{d}\omega(s) \\ &+ \int_{t_n}^{t_{n+1}} e^{As} h(t_n, y(s), y(s-\tau)) \mathrm{d}\langle\omega\rangle(s). \end{aligned} \tag{70}$$

Approximating the functions f, g, and h with the integral by left rectangle formula at the known values $f(t_n, y(t_n), y(t_n-\tau))$, $g(t_n, y(t_n), y(t_n-\tau))$, and $h(t_n, y(t_n), y(t_n-\tau))$ only leads to the exponential Euler method:

$$y_{n+1} = e^{Ah_n} y_n + e^{Ah_n} f(t_n, y_n, y_{n-m}) h_n + e^{Ah_n} g(t_n, y_n, y_{n-m}) \Delta\omega_n + e^{Ah_n} h(t_n, y_n, y_{n-m}) \Delta\langle\omega\rangle_n. \tag{71}$$

where y_n is an approximation to $y(t_n)$ and y_{n-m} is an approximation to $y(t_n - \tau)$. The increments $\Delta\omega_n = \omega(t_n) - \omega(t_{n-1})$ and $\Delta\langle\omega\rangle_n = \langle\omega\rangle(t_n) - \langle\omega\rangle(t_{n-1})$. We assume that y_n is $\mathscr{F}_{t_n}$–measurable at the mesh point t_n.

Let $\underline{u} = \lfloor u/h \rfloor h$ with $\lfloor y \rfloor$ denoting the largest integer which is smaller than y, and $z(t) = \sum_{k=0}^{\infty} y_k I_{[t_k, t_{k+1})}(t)$ with $I_{[t_k, t_{k+1})}(t)$ denoting the indicator function on $[t_k, t_{k+1})$; namely, $I_{[t_k, t_{k+1})} = 1$ if $t \in [t_k, t_{k+1}]$ or 0 otherwise. Then, we can extend the discrete exponential Euler method (71) to the continuous one as follows:

$$\begin{aligned} \widehat{y(t)} = e^{At} y_0 &+ \int_0^t e^{A(t-\underline{u})} f(\underline{u}, z(u), (u-\tau)) \mathrm{d}u + \int_0^t e^{A(t-\underline{u})} g(\underline{u}, z(u), z(u-\tau)) \mathrm{d}\omega(u) \\ &+ \int_0^t e^{A(t-\underline{u})} h(\underline{u}, z(u), z(u-\tau)) \mathrm{d}\langle\omega\rangle(u). \end{aligned} \tag{72}$$

It is not difficult to see that $\widehat{y(t_n)} = y_n$ for $n = 0, 1, 2, \cdots$, that is, the continuous extension $\widehat{y(t)}$ coincides with the discrete numerical solutions at the mesh points.

4.1. Convergence of the Exponential Euler Method. Now, we show the convergence of the exponential Euler approximate solution to the exact solution for system (7). To obtain this result, we first need to show the following several definitions.

Definition 6.

(1) The global error for exponential Euler method is defined as follows:

$$\varepsilon_n = y(t_n) - y_n. \tag{73}$$

(2) For fixed $T < \infty$, the approximation y_n is convergent in the mean-square sense on mesh points, with strong order p if

$$\max_{1 \le n \le N} \left(\widehat{E} |\varepsilon_n|^2 \right)^{1/2} \le C h^p, \text{ as } h \longrightarrow 0, \tag{74}$$

where C is a positive constant.

We will use the following lemma to analyze the convergence of the exponential Euler method.

Lemma 3. *Under the Lipschitz condition (20), there exists a constant $\widetilde{C}_1 > 0$, such that the analytic solution $y(t)$ of*

Equation (7) and the numerical solution $\widehat{y(t)}$ of continuous exponential Euler approximate (72) satisfy the following inequality:

$$\widehat{E}\sup_{0\le t\le T}|y(t)|^2 \vee \widehat{E}\sup_{0\le t\le T}|\widehat{y(t)}|^2 \le \widetilde{C}_1, \tag{75}$$

where $\widetilde{C}_1$ is independent of h, and

$$\widetilde{C}_1 = \max\left\{4e^{2|A|T}\left(\widehat{E}\left|y_0\right|^2 + \left(T + 4\overline{\sigma}^2 + \overline{\sigma}T\right)\mathrm{TG}_1\right)e^{8e^{2|A|T}\left(T+4\overline{\sigma}^2+\overline{\sigma}T\right)\mathrm{TG}_1}, C_3 e^{4\left(|A|^2+2G_1\right)\left(2T+4\overline{\sigma}^2+\overline{\sigma}T\right)}\right\}. \tag{76}$$

Proof. The detailed proofs are similar to the proofs in [17] which are omitted here. □

Theorem 2. *Under the Lipschitz condition (20), there exists a nonnegative constant G_2, such that, for any $s, t \in [0, T]$ and $t > s$,*

$$|f(t,x,y) - f(s,x,y)|^2 \vee |g(t,x,y) - g(s,x,y)|^2 \vee |h(t,x,y) - g(s,x,y)|^2 \le G_2\left(1 + |x|^2 + |y|^2\right)|s - t|. \tag{77}$$

The numerical solution produced by the continuous exponential Euler method (72) converges to the analytical solution of equation (7) in MS sense with the strong order 1/2; that is, there exists a positive constant C, such that

$$E\sup_{0\le t\le T}|y(t) - \widehat{y(t)}|^2 \le Ch, \text{ as } h \longrightarrow 0. \tag{78}$$

Proof. Taking the difference between (19) and (72) and squaring its both sides, we can get

$$\begin{aligned}
&|y(t) - \widehat{y(t)}|^2 \\
&= \left|\int_0^t e^{A(t-u)} f(u, y(u), y(u-\tau))\mathrm{d}u - \int_0^t e^{A(t-\underline{u})} f\left(\underline{u}, z(u), z(u-\tau)\right)\mathrm{d}u + \int_0^t e^{A(t-u)} g(u, y(u), y(u-\tau))\mathrm{d}\omega(u)\right. \\
&\quad \left. - \int_0^t e^{A(t-\underline{u})} g\left(\underline{u}, z(u), z(u-\tau)\right)\mathrm{d}\omega(u-\tau)\right|^2 \\
&\quad + \int_0^t e^{A(t-u)} h(u, y(u), y(u-\tau))\mathrm{d}\omega(u) - \int_0^t e^{A(t-\underline{u})} h\left(\underline{u}, z(u), z(u-\tau)\right)\mathrm{d}\langle\omega\rangle(u-\tau)|^2.
\end{aligned} \tag{79}$$

With the help of the elementary inequality and Propositions 2 and 3, we can get

$$
\begin{aligned}
&|y(t)-\widehat{y(t)}|^2 \\
&\quad\le 3\left|\int_0^t e^{A(t-u)} f(u,y(u),y(u-\tau))\mathrm{d}u-\int_0^t e^{A(t-\underline{u})} f(\underline{u},z(u),z(u-\tau))\mathrm{d}u\right|^2 \\
&\qquad+3\left|\int_0^t e^{A(t-u)} g(u,y(u),y(u-\tau))\mathrm{d}\omega(u)-\int_0^t e^{A(t-\underline{u})} g(\underline{u},z(u),z(u-\tau))\mathrm{d}\omega(u)\right|^2 \\
&\qquad+3\left|\int_0^t e^{A(t-u)} h(u,y(u),y(u-\tau))\mathrm{d}\langle\omega\rangle(u)-\int_0^t e^{A(t-\underline{u})} h(\underline{u},z(u),z(u-\tau))\mathrm{d}\langle\omega\rangle(u)\right|^2 \\
&\quad\le 9T\int_0^t |e^{A(t-u)} f(u,y(u),y(u-\tau))-e^{A(t-\underline{u})} f(u,y(u),y(u-\tau))|^2\mathrm{d}u \\
&\qquad+9T\int_0^t \left|e^{A(t-\underline{u})} f(u,y(u),y(u-\tau))-e^{A(t-\underline{u})} f(\underline{u},y(u),y(u-\tau))\right|^2\mathrm{d}u \\
&\qquad+9T\int_0^t \left|e^{A(t-\underline{u})} f(\underline{u},y(u),y(u-\tau))-e^{A(t-\underline{u})} f(\underline{u},z(u),z(u-\tau))\right|^2\mathrm{d}u \\
&\qquad+36\overline{\sigma}^2\int_0^t \left|e^{A(t-u)} g(u,y(u),y(u-\tau))-e^{A(t-\underline{u})} g(u,y(u),y(u-\tau))\right|^2\mathrm{d}u \\
&\qquad+36\overline{\sigma}^2\int_0^t \left|e^{A(t-\underline{u})} g(u,y(u),y(u-\tau))-e^{A(t-\underline{u})} g(\underline{u},y(u),y(u-\tau))\right|^2\mathrm{d}u \\
&\qquad+36\overline{\sigma}^2\int_0^t \left|e^{A(t-\underline{u})} g(\underline{u},y(u),y(u-\tau))-e^{A(t-\underline{u})} g(\underline{u},z(u),z(u-\tau))\right|^2\mathrm{d}u \\
&\qquad+9\overline{\sigma}^4T\int_0^t \left|e^{A(t-u)} h(u,y(u),y(u-\tau))-e^{A(t-\underline{u})} h(u,y(u),y(u-\tau))\right|^2\mathrm{d}u \\
&\qquad+9\overline{\sigma}^4T\int_0^t \left|e^{A(t-\underline{u})} h(u,y(u),y(u-\tau))-e^{A(t-\underline{u})} h(\underline{u},y(u),y(u-\tau))\right|^2\mathrm{d}u \\
&\qquad+9\overline{\sigma}^4T\int_0^t \left|e^{A(t-\underline{u})} h(\underline{u},y(u),y(u-\tau))-e^{A(t-\underline{u})} h(\underline{u},z(u),z(u-\tau))\right|^2\mathrm{d}u.
\end{aligned}
\tag{80}
$$

Taking G-expectation on both sides of (80), for arbitrary $0 \le t_1 \le T$, we arrive at

$$
\begin{aligned}
&\widehat{E}\left(\sup_{0\le t\le t_1} |y(t)-\widehat{y(t)}|^2\right)\\
&\quad\le 9T\widehat{E}\left(\sup_{0\le t\le t_1}\int_0^t \left|e^{A(t-u)}f(u,y(u),y(u-\tau))-e^{A(t-\underline{u})}f(u,y(u),y(u-\tau))\right|^2 \mathrm{d}u\right)\\
&\qquad+9T\widehat{E}\left(\sup_{0\le t\le t_1}\int_0^t \left|e^{A(t-\underline{u})}f(u,y(u),y(u-\tau))-e^{A(t-\underline{u})}f(\underline{u},y(u),y(u-\tau))\right|^2 \mathrm{d}u\right)\\
&\qquad+9T\widehat{E}\left(\sup_{0\le t\le t_1}\int_0^t \left|e^{A(t-\underline{u})}f(\underline{u},y(u),y(u-\tau))-e^{A(t-\underline{u})}f(\underline{u},z(u),z(u-\tau))\right|^2 \mathrm{d}u\right)\\
&\qquad+36\overline{\sigma}^2\widehat{E}\left(\sup_{0\le t\le t_1}\int_0^t \left|e^{A(t-u)}g(u,y(u),y(u-\tau))-e^{A(t-\underline{u})}g(u,y(u),y(u-\tau))\right|^2 \mathrm{d}u\right)\\
&\qquad+36\overline{\sigma}^2\widehat{E}\left(\sup_{0\le t\le t_1}\int_0^t \left|e^{A(t-\underline{u})}g(u,y(u),y(u-\tau))-e^{A(t-\underline{u})}g(\underline{u},y(u),y(u-\tau))\right|^2 \mathrm{d}u\right)\\
&\qquad+36\overline{\sigma}^2\widehat{E}\left(\sup_{0\le t\le t_1}\int_0^t \left|e^{A(t-\underline{u})}g(\underline{u},y(u),y(u-\tau))-e^{A(t-\underline{u})}g(\underline{u},z(u),z(u-\tau))\right|^2 \mathrm{d}u\right)\\
&\qquad+9\overline{\sigma}^4T\widehat{E}\left(\sup_{0\le t\le t_1}\int_0^t \left|e^{A(t-u)}h(u,y(u),y(u-\tau))-e^{A(t-\underline{u})}h(u,y(u),y(u-\tau))\right|^2 \mathrm{d}u\right)\\
&\qquad+9\overline{\sigma}^4T\widehat{E}\left(\sup_{0\le t\le t_1}\int_0^t \left|e^{A(t-\underline{u})}h(u,y(u),y(u-\tau))-e^{A(t-\underline{u})}h(\underline{u},y(u),y(u-\tau))\right|^2 \mathrm{d}u\right)\\
&\qquad+9\overline{\sigma}^4T\widehat{E}\left(\sup_{0\le t\le t_1}\int_0^t \left|e^{A(t-\underline{u})}h(\underline{u},y(u),y(u-\tau))-e^{A(t-\underline{u})}h(\underline{u},z(u),z(u-\tau))\right|^2 \mathrm{d}u\right)\\
&\quad\le 9TJ_1(t)+9TJ_2(t)+9TJ_3(t)+36\overline{\sigma}^2J_4(t)+36\overline{\sigma}^2J_5(t)\\
&\qquad+36\overline{\sigma}^2J_6(t)+9\overline{\sigma}^4TJ_7(t)+9\overline{\sigma}^4TJ_8(t)+9\overline{\sigma}^4TJ_9(t),
\end{aligned}
\tag{81}
$$

where

$$
\begin{aligned}
J_1(t)&=\widehat{E}\left(\sup_{0\le t\le t_1}\int_0^t \left|e^{A(t-u)}f(u,y(u),y(u-\tau))-e^{A(t-\underline{u})}f(u,y(u),y(u-\tau))\right|^2 \mathrm{d}u\right),\\
J_2(t)&=\widehat{E}\left(\sup_{0\le t\le t_1}\int_0^t \left|e^{A(t-\underline{u})}f(u,y(u),y(u-\tau))-e^{A(t-\underline{u})}f(\underline{u},y(u),y(u-\tau))\right|^2 \mathrm{d}u\right),\\
J_3(t)&=\widehat{E}\left(\sup_{0\le t\le t_1}\int_0^t \left|e^{A(t-\underline{u})}f(\underline{u},y(u),y(u-\tau))-e^{A(t-\underline{u})}f(\underline{u},z(u),z(u-\tau))\right|^2 \mathrm{d}u\right),\\
J_4(t)&=\widehat{E}\left(\sup_{0\le t\le t_1}\int_0^t \left|e^{A(t-u)}g(u,y(u),y(u-\tau))-e^{A(t-\underline{u})}g(u,y(u),y(u-\tau))\right|^2 \mathrm{d}u\right),\\
J_5(t)&=\widehat{E}\left(\sup_{0\le t\le t_1}\int_0^t \left|e^{A(t-\underline{u})}g(u,y(u),y(u-\tau))-e^{A(t-\underline{u})}g(\underline{u},y(u),y(u-\tau))\right|^2 \mathrm{d}u\right),\\
J_6(t)&=\widehat{E}\left(\sup_{0\le t\le t_1}\int_0^t \left|e^{A(t-\underline{u})}g(\underline{u},y(u),y(u-\tau))-e^{A(t-\underline{u})}g(\underline{u},z(u),z(u-\tau))\right|^2 \mathrm{d}u\right),\\
J_7(t)&=\widehat{E}\left(\sup_{0\le t\le t_1}\int_0^t \left|e^{A(t-u)}h(u,y(u),y(u-\tau))-e^{A(t-\underline{u})}h(u,y(u),y(u-\tau))\right|^2 \mathrm{d}u\right),\\
J_8(t)&=\widehat{E}\left(\sup_{0\le t\le t_1}\int_0^t \left|e^{A(t-\underline{u})}h(u,y(u),y(u-\tau))-e^{A(t-\underline{u})}h(\underline{u},y(u),y(u-\tau))\right|^2 \mathrm{d}u\right),\\
J_9(t)&=\widehat{E}\left(\sup_{0\le t\le t_1}\int_0^t \left|e^{A(t-\underline{u})}h(\underline{u},y(u),y(u-\tau))-e^{A(t-\underline{u})}h(\underline{u},z(u),z(u-\tau))\right|^2 \mathrm{d}u\right).
\end{aligned}
\tag{82}
$$

To estimate (81), we need to estimate $J_i(t)$ $(i = 1, 2, 3, 4, 5, 7, 8, 9)$.

For $J_1(t)$, we have that

$$\begin{aligned} J_1(t) &\le \widehat{E}\left(\sup_{0\le t\le t_1}\int_0^t \left|e^{A(t-u)} - e^{A(t-\underline{u})}\right|^2 |f(u, y(u), y(u-\tau))|^2 \mathrm{d}u\right) \\ &= \widehat{E}\left(\sup_{0\le t\le t_1}\int_0^t \left|e^{A(t-u)}\right|^2 \left|I - e^{A(u-\underline{u})}\right|^2 |f(u, y(u), y(u-\tau))|^2 \mathrm{d}u\right). \end{aligned} \tag{83}$$

Due to the linear growth condition (21) and $|e^{Ah} - I| \le |A| h e^{|A|T}$, inequality (83) gives

$$\begin{aligned} &\widehat{E}\left(\sup_{0\le t\le t_1}\int_0^t \left|e^{A(t-u)} - e^{A(t-\underline{u})}\right|^2 |f(u, y(u), y(u-\tau))|^2 \mathrm{d}u\right) \\ &\quad \le G_1 \widehat{E}\left(\sup_{0\le t\le t_1}\int_0^t \left|e^{2A(t-u)}\right| \left|I - e^{A(u-\underline{u})}\right|^2 \left(1 + |y(u)|^2 + |y(u-\tau)|^2\right) \mathrm{d}u\right) \\ &\quad \le G_1 e^{2|A|T} T |A|^2 h^2 e^{2|A|T} \left(1 + 2\widetilde{C}_1\right). \end{aligned} \tag{84}$$

Using (78) and Lipschitz condition (20), it follows from $J_2(t)$ and $J_3(t)$ that

$$\begin{aligned} J_2(t) &\le G_2 e^{2|A|T} \widehat{E}\left(\sup_{0\le t\le t_1}\int_0^t \left(1 + |y(u)|^2 + |y(u-\tau)|^2\right) |u - \underline{u}| \mathrm{d}u\right) \\ &\le G_2 e^{2|A|T} T h \left(1 + 2\widetilde{C}_1\right), \end{aligned} \tag{85}$$

$$\begin{aligned} J_3(t) &\le L_1 e^{2|A|T} \widehat{E}\left(\sup_{0\le t\le t_1}\int_0^t \left(|y(u) - z(u)|^2 + |y(u-\tau) - z(u-\tau)|^2\right) \mathrm{d}u\right) \\ &\le 2L_1 e^{2|A|T} T \int_0^{t_1} \widehat{E}\left(\sup_{0\le u\le t} |y(u) - \widehat{y(u)}|^2\right) \mathrm{d}t. \end{aligned} \tag{86}$$

Similar to estimates $J_1(t)$, $J_2(t)$, and $J_3(t)$, one obtains

$$J_4(t) \le G_1 e^{2|A|T} T |A|^2 h^2 e^{2|A|T} \left(1 + 2\widetilde{C}_1\right), \tag{87}$$

$$J_5(t) \le G_2 e^{2|A|T} T h \left(1 + 2\widetilde{C}_1\right), \tag{88}$$

$$J_6(t) \le 2L_1 e^{2|A|T} T \int_0^{t_1} \widehat{E} \sup_{0\le u\le t} y(u) - \widehat{y(u)}|^2 \mathrm{d}t, \tag{89}$$

$$J_7(t) \le G_1 e^{2|A|T} T |A|^2 h^2 e^{2|A|T} \left(1 + 2\widetilde{C}_1\right), \tag{90}$$

$$J_8(t) \le G_2 e^{2|A|T} T h \left(1 + 2\widetilde{C}_1\right), \tag{91}$$

$$J_9(t) \le 2L_1 e^{2|A|T} T \int_0^{t_1} \widehat{E} \sup_{0\le u\le t} |y(u) - \widehat{y(u)}|^2 \mathrm{d}t. \tag{92}$$

Substituting (84)–(92) into (81) and rearranging (81), we obtain

$$\begin{aligned}
&\widehat{E}\left(\sup_{0\le t\le t_1}|y(t)-\widehat{y(t)}|^2\right)\\
&\quad\le\left(9T+36\overline{\sigma}^2+9T\overline{\sigma}^4\right)G_1e^{2|A|T}T|A|^2h^2e^{2|A|T}\left(1+2\widetilde{C}_1\right),
\end{aligned}\tag{93}$$

$$\begin{aligned}
&\quad+\left(9T+36\overline{\sigma}^2+9T\overline{\sigma}^4\right)G_2e^{2|A|T}Th\left(1+2\widetilde{C}_1\right)\\
&\quad+2\left(9T+36\overline{\sigma}^2+9T\overline{\sigma}^4\right)L_1e^{2|A|T}T\int_0^{t_1}\widehat{E}\left(\sup_{0\le u\le t}y(u)-\widehat{y(u)}|^2\right)\mathrm{d}t\\
&\le\left(9T+36\overline{\sigma}^2+9T\overline{\sigma}^4\right)e^{2|A|T}Th\left(G_1|A|^2he^{2|A|T}+G_2\right)\left(1+2\widetilde{C}_1\right)\\
&\quad+2\left(9T+36\overline{\sigma}^2+9T\overline{\sigma}^4\right)L_1e^{2|A|T}T\int_0^{t_1}\widehat{E}\left(\sup_{0\le u\le t}|y(u)-\widehat{y(u)}|^2\right)\mathrm{d}t.
\end{aligned}\tag{94}$$

By Gronwall's inequality, it gives

$$\begin{aligned}
&\widehat{E}\left(\sup_{0\le t\le T}|y(t)-\widehat{y(t)}|^2\right)\\
&\quad\le\left(9T+36\overline{\sigma}^2+9T\overline{\sigma}^4\right)e^{2|A|T}h(T+4)\left(G_1|A|^2he^{2|A|T}+G_2\right)\left(1+2\widetilde{C}_1\right)\cdot e^{2\left(9T+36\overline{\sigma}^2+9T\overline{\sigma}^4\right)L_1e^{2|A|T}T},
\end{aligned}\tag{95}$$

and then, letting $h\longrightarrow 0$, one can draw the conclusion. The proof is completed.

Theorem 2 shows that if the coefficients of f, g, and h obey the Lipschitz condition, in addition to the conditions imposed in Lemma 3, then the exponential Euler approximate solution converges to the exact solution for system (7). □

4.2. The Mean-Square Stability. In this section, we are in a position to explore the exponential stability of the exact solution and the numerical approximation. For this purpose, we further assume that $f(t,0,0)=0$, $g(t,0,0)=0$, and $h(t,0,0)=0$. Therefore, system (7) admits a trivial solution. Moreover, from condition (20), it is easy to get

$$|f(t,x,y)|^2\vee|g(t,x,y)|^2\vee|h(t,x,y)|^2\le L_1\left(|x|^2+|y|^2\right),\quad\forall x,y\in R^d.\tag{96}$$

In the following, we first give some necessary assumptions and definitions for the mean-square exponential stability.

Definition 7. Equation (7) is said to be mean-square exponentially stable if there exist positive constants v and C, which is dependent on the initial data $y_0(t)\in C^b_{\mathcal{F}_0}([0,T];R^d)$ and independent of t, such that

$$\widehat{E}|y(t)|^2\le Ce^{-vt},\quad t\ge 0.\tag{97}$$

For convenience, we introduce the logarithmic norm $\mu[A]$ proposed in [38].

Definition 8. The logarithmic norm $\mu[A]$ of A is defined by

$$\mu[A]=\lim_{\Delta\longrightarrow 0^+}\frac{|I+\Delta A|-1}{\Delta}.\tag{98}$$

In particular, if $|\cdot|$ is an inner product norm, $\mu[A]$ can also be written as

$$\mu[A]=\max_{y\ne 0}\frac{\langle Ay,y\rangle}{|y|^2}.\tag{99}$$

Theorem 3. *Assume that f, g, and h satisfy the Lipschitz condition (20). If there exist positive constants λ_1 and λ_2, such that*

$$2x^Tf(t,x,y)\le-\lambda_1|x|^2+\lambda_2|y|^2,\quad x,y\in R^d,\tag{100}$$

holds, then the analytical solution of equation (7) is mean-square exponentially stable under the condition

$$\lambda_1-2\mu[A]-\lambda_2-6\overline{\sigma}^4L_1-4\overline{\sigma}^4\sqrt{L_1}>0.\tag{101}$$

Proof. Let $V(t,y(t))=1+|y(t)|^2=1+y^T(t)y(t)$. By the matrix derivative rule and the Itô formula, we can derive that

$$\begin{aligned}\mathrm{d}V(t,y(t)) = &\left[V_t(t,y(t)) + V_y(t,y(t))f(t,y(t),y(t-\tau))\right]\mathrm{d}t \\ &+ V_y(t,y(t))g(t,y(t),y(t-\tau))\mathrm{d}\omega(t) + \left[V_y(t,y(t))h(t,y(t),y(t-\tau))\right] \\ &+\frac{1}{2}\mathrm{trace}g^T V_{yy}(t,y(t),y(t-\tau))g\Big]\mathrm{d}\langle\omega\rangle(t).\end{aligned} \tag{102}$$

The aforementioned equation is equivalent to the following stochastic integral equation:

$$\begin{aligned}V(t,y(t)) = V(0,y(0)) &+ \int_0^t \left[V_s(s,y(s)) + V_y(s,y(s))f(s,y(s),y(s-\tau))\right]\mathrm{d}s + \int_0^t V_y(s,y(s))g(s,y(s),y(s-\tau))\mathrm{d}\omega(s) \\ &+ \int_0^t \Big[V_y(s,y(s))h(s,y(s),y(s-\tau)) + \frac{1}{2}\mathrm{trace}\, g^T V_{yy}(s,y(s),y(s-\tau))g\Big]\mathrm{d}\langle\omega\rangle(s),\end{aligned} \tag{103}$$

that is,

$$\begin{aligned}1+|y(t)|^2 = 1+|y(0)|^2 &+ 2\int_0^t \langle y(s), Ay(s) + f(s,y(s),y(s-\tau))\rangle\mathrm{d}s + 2\int_0^t \langle y(s), g(s,y(s),y(s-\tau))\rangle\mathrm{d}\omega(s) \\ &+ 2\int_0^t \langle y(s), h(s,y(s),y(s-\tau))\rangle\mathrm{d}\langle\omega\rangle(s) + \int_0^t |g(s,y(s),y(s-\tau))|^2 d\langle\omega\rangle(s).\end{aligned} \tag{104}$$

Taking G-expectation on both sides of (101), we get

$$\begin{aligned}\widehat{E}\left(1+|y(t)|^2\right) = 1+|y(0)|^2 &+ 2\widehat{E}\left(\int_0^t \langle y(s), Ay(s) + f(s,y(s),y(s-\tau))\rangle\mathrm{d}s\right) \\ &+ 2\widehat{E}\left(\int_0^t \langle y(s), g(s,y(s),y(s-\tau))\rangle\mathrm{d}\omega(s)\right) \\ &+ 2\widehat{E}\left(\int_0^t \langle y(s), h(s,y(s),y(s-\tau))\rangle\mathrm{d}\langle\omega\rangle(s)\right) + \widehat{E}\left(\int_0^t |g(s,y(s),y(s-\tau))|^2\mathrm{d}\langle\omega\rangle(s)\right).\end{aligned} \tag{105}$$

With the condition in (100), the inequality in (105) obtains

$$\begin{aligned}\widehat{E}\left(\sup_{0\le s\le t}\left(1+|y(s)|^2\right)\right) \le 1+|y(0)|^2 &+ \widehat{E}\left(\int_0^t \left((2\mu[A]-\lambda_1)|y(s)|^2 + \lambda_2|y(s-\tau)|^2\right)\mathrm{d}s\right) \\ &+ 2\widehat{E}\left(\sup_{0\le s\le t}\int_0^s \langle y(u), g(u,y(u),y(u-\tau))\rangle\mathrm{d}\omega(u)\right) \\ &+ 2\widehat{E}\left(\sup_{0\le s\le t}\int_0^s \langle y(u), h(u,y(u),y(u-\tau))\rangle\mathrm{d}\langle\omega\rangle(u)\right) + \widehat{E}\left(\sup_{0\le s\le t}\int_0^s |g(u,y(u),y(u-\tau))|^2\mathrm{d}\langle\omega\rangle(u)\right).\end{aligned} \tag{106}$$

Combining Proposition 3 with Lemma 1, we have

$$\begin{aligned}
&2\widehat{E}\left(\sup_{0\le s\le t}\int_0^s \langle y(u), g(u, y(u), y(u-\tau))\rangle \mathrm{d}\omega(u)\right)\\
&\le 2\overline{\sigma}^2\widehat{E}\left(\int_0^t |y(s)|^2|g(s, y(s), y(s-\tau))|^2\mathrm{d}s\right)^{1/2}\\
&\le 2\overline{\sigma}^2\widehat{E}\left\{\left(\sup_{0\le s\le t}|y(s)|^2\right)\int_0^t |g(s, y(s), y(s-\tau))|^2\mathrm{d}s\right\}^{1/2}\\
&\le \frac{1}{2}\widehat{E}\left(\sup_{0\le s\le t}\left(1+|y(s)|^2\right)\right)+2\overline{\sigma}^4L_1\widehat{E}\left(\int_0^t\left(|y(s)|^2+|y(s-\tau)|^2\right)\mathrm{d}s\right).
\end{aligned}\tag{107}$$

Similarly, we have

$$\begin{aligned}
&2\widehat{E}\left(\sup_{0\le s\le t}\int_0^s \langle y(u), h(u, y(u), y(u-\tau))\rangle \mathrm{d}\langle\omega\rangle(u)\right)\\
&\le 2\overline{\sigma}^4\widehat{E}\left(\int_0^{st}|y(s)||h(s, y(s), y(s-\tau))|\mathrm{d}s\right)\\
&\le \overline{\sigma}^4\widehat{E}\left(\int_0^t 2\sqrt[4]{L_1}|y(s)|\frac{|h(s, y(s), y(s-\tau))|}{\sqrt[4]{L_1}}\mathrm{d}s\right)\\
&\le \overline{\sigma}^4\widehat{E}\left(\int_0^t\left(\sqrt{L_1}\,|y(s)|^2+\frac{|h(s, y(s), y(s-\tau))|^2}{\sqrt{L_1}}\right)\mathrm{d}s\right)\\
&\le \overline{\sigma}^4\sqrt{L_1}\widehat{E}\left(\int_0^t\left(|y(s)|^2+|y(s)|^2+|y(s-\tau)|^2\right)\mathrm{d}s\right)\\
&\le 2\overline{\sigma}^4\sqrt{L_1}\widehat{E}\left(\int_0^t\left(|y(s)|^2+|y(s-\tau)|^2\right)\mathrm{d}s\right).
\end{aligned}\tag{108}$$

and

$$\begin{aligned}
&\widehat{E}\left(\sup_{0\le s\le t}\int_0^s |g(u, y(u), y(u-\tau))|^2\mathrm{d}\langle\omega\rangle(u)\right)\\
&\le \overline{\sigma}^4L_1\widehat{E}\left(\int_0^t\left(|y(s)|^2+|y(s-\tau)|^2\right)\mathrm{d}s\right).
\end{aligned}\tag{109}$$

Substituting (107)–(109) into (106), we obtain

$$\begin{aligned}
&\widehat{E}\left(\sup_{0\le s\le t}\left(1+|y(s)|^2\right)\right)\\
&\le 1+|y(0)|^2+\widehat{E}\left(\int_0^t\left((2\mu[A]-\lambda_1)|y(u)|^2+\lambda_2|y(u-\tau))|^2\right)\mathrm{d}u\right)\\
&\quad+\frac{1}{2}\widehat{E}\left(\sup_{0\le s\le t}\left(1+|y(s)|^2\right)\right)+2\overline{\sigma}^4L_1\widehat{E}\left(\int_0^t\left(|y(s)|^2+|y(s-\tau)|^2\right)\mathrm{d}s\right)\\
&\quad+2\overline{\sigma}^4\sqrt{L_1}\widehat{E}\left(\int_0^t\left(|y(s)|^2+|y(s-\tau)|^2\right)\mathrm{d}s\right)+\overline{\sigma}^4L_1\widehat{E}\left(\int_0^t\left(|y(s)|^2+|y(s-\tau)|^2\right)\mathrm{d}s\right),
\end{aligned}\tag{110}$$

that is,

$$\begin{aligned}&\widehat{E}\left(\sup_{0\le s\le t}\left(1+|y(s)|^2\right)\right)\\&\le 2\left(1+|y(0)|^2\right)+2\left(2\mu[A]-\lambda_1+\lambda_2+6\overline{\sigma}^4L_1+4\overline{\sigma}^4\sqrt{L_1}\right)\widehat{E}\left(\int_0^t\sup_{0\le s\le t}|y(s)|^2\mathrm{d}s\right).\end{aligned}\tag{111}$$

From the Gronwall inequality, we have

$$\widehat{E}\left(\sup_{0\le s\le t}\left(|y(s)|^2\right)\right)\le 2\left(1+|y(0)|^2\right)e^{2\left(2\mu[A]-\lambda_1+\lambda_2+6\overline{\sigma}^4L_1+4\overline{\sigma}^4\sqrt{L_1}\right)t}\le Ce^{-\nu t}.\tag{112}$$

where $C=2(1+|y(0)|^2)$ and $\nu=2(\lambda_1-2\mu[A]-\lambda_2-6\overline{\sigma}^4L_1-4\overline{\sigma}^4\sqrt{L_1})$. The proof is completed. □

Then the question is, will the exponential Euler method reproduce the stability of analytical solutions of equation (7) under the Lipschitz condition? In order to answer this question, we introduce the following definition of mean-square stability from [39] at first and present the stability theorem of the exponential Euler approximation.

Definition 9. A numerical method is said to be asymptotically mean-square stable (with respect to a given G-SLSDDE) if

$$\lim_{n\longrightarrow\infty}\widehat{E}\left|y_n\right|^2=0.\tag{113}$$

Theorem 4. *Let (H1) hold. Assume that there exist positive constants λ_3 and λ_4, such that*

$$2\overline{\sigma}^2x^Th(t,x,y)\le-\lambda_3|x|^2+\lambda_4|y|^2,\quad x,y\in R^d.\tag{114}$$

If the inequalities $L_1\overline{\sigma}^2-\lambda_1-\lambda_3<0$ and $2\mu[A]+\lambda_2+\lambda_4+\lambda_1+\lambda_3<0$ hold, then the exponential Euler method is asymptotically mean-square stable for all

$$h_n<h_0=\frac{1/2\lambda_1+1/2\lambda_3-1/2L_1\overline{\sigma}^2}{L_1+L_1\overline{\sigma}^4+L_1\overline{\sigma}^2}.\tag{115}$$

Proof. Squaring both sides of (71), we have

$$\begin{aligned}y_{n+1}^2=&\,e^{2\mu[A]h_n}\left(y_n^2+f^2(t_n,y_n,y_{n-m})h_n^2+g^2(t_n,y_n,y_{n-m})\left|\Delta\omega_n\right|^2+h^2(t_n,y_n,y_{n-m})\left|\Delta\langle\omega\rangle_n\right|^2\right)+2e^{2\mu[A]h_n}y_n^Tf(t_n,y_n,y_{n-m})h_n\\&+2e^{2\mu[A]h_n}y_n^Tg(t_n,y_n,y_{n-m})\Delta\omega_n+2e^{2\mu[A]h_n}y_n^Th(t_n,y_n,y_{n-m})\Delta\langle\omega\rangle_n+2e^{2\mu[A]h_n}f(t_n,y_n,y_{n-m})^Tg(t_n,y_n,y_{n-m})h_n\Delta\omega_n\\&+2e^{2\mu[A]h_n}f(t_n,y_n,y_{n-m})^Th(t_n,y_n,y_{n-m})h_n\Delta\langle\omega\rangle_n+2e^{2\mu[A]h_n}g(t_n,y_n,y_{n-m})^Th(t_n,y_n,y_{n-m})\Delta\omega_n\Delta\langle\omega\rangle_n.\end{aligned}\tag{116}$$

Taking G-expectation on both sides of (116) and considering that y_k and y_{k-m} are $\mathscr{F}_{t_k}$-measurable, by Proposition 3, one can get

$$\begin{aligned}\widehat{E}\left[g^2(t_k,y_k,y_{k-m})\left(\left|\Delta\omega_k\right|^2-\overline{\sigma}^2h_k\right)\right]&=\widehat{E}\left[\widehat{E}\left(g^2(t_k,y_k,y_{k-m})\left(\left|\Delta\omega_k\right|^2-\overline{\sigma}^2h_k\right)|\mathscr{F}_{t_k}\right)\right]\\&=\widehat{E}\left[g^2(t_k,y_k,y_{k-m})\widehat{E}\left((\Delta\omega_k)^2-\overline{\sigma}^2h_k|\mathscr{F}_{t_k}\right)\right]=0,\\\widehat{E}\left[y_k^Tg(t_k,y_k,y_{k-m})\Delta\omega_k\right]&=\widehat{E}\left[\widehat{E}\left(y_k^Tg(t_k,y_k,y_{k-m})\Delta\omega_k|\mathscr{F}_{t_k}\right)\right]\\&=\widehat{E}\left[y_k^Tg(t_k,y_k,y_{k-m})\widehat{E}\left(\Delta\omega_k|\mathscr{F}_{t_k}\right)\right]=0.\end{aligned}\tag{117}$$

By Proposition 2, one obtains

$$\begin{aligned}
\widehat{E}\left[h^2(t_k, y_k, y_{k-m})\left(\left|\Delta\langle\omega\rangle_k\right|^2 - \overline{\sigma}^4 h_k^2\right)\right] &= \widehat{E}\left[\widehat{E}\left(h^2(t_k, y_k, y_{k-m})\left(\left|\Delta\langle\omega\rangle_k\right|^2 - \overline{\sigma}^4 h_k^2\right)|\mathscr{F}_{t_k}\right)\right] \\
&= \widehat{E}\left[g^2(t_k, y_k, y_{k-m})\widehat{E}\left(\left(\Delta\langle\omega\rangle_k\right)^2 - \overline{\sigma}^4 h_k^2|\mathscr{F}_{t_k}\right)\right] \le 0, \\
\widehat{E}\left[y_k^T h(t_k, y_k, y_{k-m})\Delta\langle\omega\rangle_k\right] &= \widehat{E}\left[\widehat{E}\left(y_k^T g(t_k, y_k, y_{k-m})\Delta\langle\omega\rangle_k|\mathscr{F}_{t_k}\right)\right] \\
&= \widehat{E}\left[y_k^T h(t_k, y_k, y_{k-m})\widehat{E}\left(\Delta\langle\omega\rangle_k|\mathscr{F}_{t_k}\right)\right] \le \overline{\sigma}^2 h_k \widehat{E}\left[y_k^T h(t_k, y_k, y_{k-m})\right], \\
\widehat{E}\left[g^T(t_k, y_k, y_{k-m})h(t_k, y_k, y_{k-m})\Delta\omega_k\Delta\langle\omega\rangle_k\right] &= \widehat{E}\left[\widehat{E}\left(g^T(t_k, y_k, y_{k-m})h(t_k, y_k, y_{k-m})\Delta\omega_k\Delta\langle\omega\rangle_k|\mathscr{F}_{t_k}\right)\right] \\
&= \widehat{E}\left[g^T(t_k, y_k, y_{k-m})h(t_k, y_k, y_{k-m})\widehat{E}\left(\Delta\omega_k\Delta\langle\omega\rangle_k|\mathscr{F}_{t_k}\right)\right] \\
&\le \overline{\sigma}^2 h_k \widehat{E}\left[g^T(t_k, y_k, y_{k-m})h(t_k, y_k, y_{k-m})\widehat{E}\left(\Delta\omega_k|\mathscr{F}_{t_k}\right)\right] = 0, \\
\widehat{E}\left[f^T(t_k, y_k, y_{k-m})h(t_k, y_k, y_{k-m})h_k\Delta\langle\omega\rangle_k\right] &= \widehat{E}\left[\widehat{E}\left(f^T(t_k, y_k, y_{k-m})h(t_k, y_k, y_{k-m})h_k\Delta\langle\omega\rangle_k|\mathscr{F}_{t_k}\right)\right] \\
&= h_k\widehat{E}\left[f^T(t_k, y_k, y_{k-m})h(t_k, y_k, y_{k-m})\widehat{E}\left(\Delta\langle\omega\rangle_k|\mathscr{F}_{t_k}\right)\right] \\
&\le \overline{\sigma}^2 h_k^2 \widehat{E}\left[f^T(t_k, y_k, y_{k-m})h(t_k, y_k, y_{k-m})\right].
\end{aligned} \tag{118}$$

Then, it follows from (100), (114), and (99) that

$$\begin{aligned}
\widehat{E}\left|y_{n+1}\right|^2 &= e^{2\mu[A]h_n}|\widehat{E}\left|y_n\right|^2 + \widehat{E}\left[f^2(t_n, y_n, y_{n-m})\right]h_n^2 + \widehat{E}\left[g^2(t_n, y_n, y_{n-m})\right]\overline{\sigma}^2 h_n + \widehat{E}\left[h^2(t_n, y_n, y_{n-m})\right]\overline{\sigma}^4 h_n^2 \\
&\quad + 2y_n^T f(t_n, y_n, y_{n-m})h_n + 2\overline{\sigma}^2 h_n \widehat{E}\left[y_n^T h(t_n, y_n, y_{n-m})\right] \\
&\quad + 2\overline{\sigma}^2 h_n^2 \widehat{E}\left[f(t_n, y_n, y_{n-m})^T h(t_n, y_n, y_{n-m})\right]| \le e^{2\mu[A]h_n}|\widehat{E}\left|y_n\right|^2 + \widehat{E}\left(L_1\left|y_n\right|^2 + L_1\left|y_{n-m}\right|^2\right)h_n^2 \\
&\quad + \widehat{E}\left(L_1\left|y_n\right|^2 + L_1\left|y_{n-m}\right|^2\right)\overline{\sigma}^2 h_n \\
&\quad + \widehat{E}\left(L_1\left|y_n\right|^2 + L_1\left|y_{n-m}\right|^2\right)\overline{\sigma}^4 h_n^2 + \left(-\lambda_1\widehat{E}\left|y_n\right|^2 + \lambda_2\widehat{E}\left|y_{n-m}\right|^2\right)h_n + h_n\widehat{E}\left(-\lambda_3\left|y_n\right|^2 + \lambda_4\left|y_{n-m}\right|^2\right) \\
&\quad + 2\overline{\sigma}^2 h_n^2 \widehat{E}\left(L_1\left|y_n\right|^2 + L_1\left|y_{n-m}\right|^2\right)| \\
&= e^{2\mu[A]h_n}|\left(1 + L_1 h_n^2 + L_1\overline{\sigma}^2 h_n + L_1\overline{\sigma}^4 h_n^2 - \lambda_1 h_n - \lambda_3 h_n + L_1\overline{\sigma}^2 h_n^2\right)\widehat{E}\left|y_n\right|^2 \\
&\quad + \left(L_1 h_n^2 + L_1\overline{\sigma}^2 h_n + L_1\overline{\sigma}^4 h_n^2 + \lambda_2 h_n + \lambda_4 h_n + L_1\overline{\sigma}^2 h_n^2\right)\widehat{E}\left|y_{n-m}\right|^2 = \left|A_1\widehat{E}\left|y_n\right|^2 + A_2\widehat{E}\left|y_{n-m}\right|^2\right|,
\end{aligned} \tag{119}$$

where $A_1 = e^{2\mu[A]h_n}(1 + (L_1\overline{\sigma}^2 - \lambda_1 - \lambda_3)h_n + (L_1 + L_1\overline{\sigma}^4 + L_1\overline{\sigma}^2)h_n^2)$ and $A_2 = e^{2\mu[A]h_n}((L_1\overline{\sigma}^2 + \lambda_2 + \lambda_4)h_n + (L_1 + L_1\overline{\sigma}^4 + L_1\overline{\sigma}^2)h_n^2)$.

Considering $L_1\overline{\sigma}^2 - \lambda_1 - \lambda_3 < 0$, for any $h_n < h_0 = 1/2\lambda_1 + 1/2\lambda_3 - 1/2L_1\overline{\sigma}^2/L_1 + L_1\overline{\sigma}^4 + L_1\overline{\sigma}^2$, the following inequalities hold:

$$A_1 \le e^{2\mu[A]h_n}\left(1 + \left(\frac{1}{2}L_1\overline{\sigma}^2 - \frac{1}{2}\lambda_1 - \frac{1}{2}\lambda_3\right)h_n\right), \tag{120}$$

$$\begin{aligned}
\left|A_1 + A_2\right| \le \left|A_1\right| + \left|A_2\right| &= \left|e^{2\mu[A]h_n}\left(1 + \left(\frac{1}{2}L_1\overline{\sigma}^2 - \frac{1}{2}\lambda_1 - \frac{1}{2}\lambda_3\right)h_n\right)\right| + \left|e^{2\mu[A]h_n}\left(\left(L_1\overline{\sigma}^2 + \lambda_2 + \lambda_4\right)h_n + \left(L_1 + L_1\overline{\sigma}^4 + L_1\overline{\sigma}^2\right)h_n^2\right)\right| \\
&\le e^{2\mu[A]h_n}\left(1 + \left(\frac{1}{2}\lambda_1 + \frac{1}{2}\lambda_3 - \frac{1}{2}L_1\overline{\sigma}^2\right)h_n\right) + e^{2\mu[A]h_n}\left(L_1\overline{\sigma}^2 + \lambda_2 + \lambda_4 + \frac{1}{2}\lambda_1 + \frac{1}{2}\lambda_3 - \frac{1}{2}L_1\overline{\sigma}^2\right)h_n \\
&\le e^{2\mu[A]h_n}(1 + (\lambda_2 + \lambda_4 + \lambda_1 + \lambda_3)h_n).
\end{aligned} \tag{121}$$

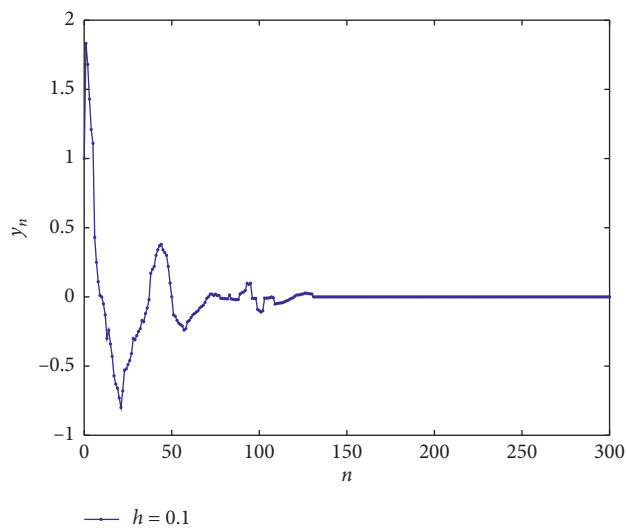

Figure 1: The numerical solution with $h = 0.1$ of the exponential Euler method.

Therefore,

$$\begin{aligned}\widehat{E}\left|y_{n+1}\right|^2 &\le e^{2\mu[A]h_n}\left(1+(\lambda_2+\lambda_4+\lambda_1+\lambda_3)h_n\right)\max\left\{\widehat{E}\left|y_n\right|^2, \widehat{E}\left|y_{n-m}\right|^2\right\}\\ &\le e^{(2\mu[A]+\lambda_2+\lambda_4+\lambda_1+\lambda_3)h_n}\max\left\{\widehat{E}\left|y_n\right|^2, \widehat{E}\left|y_{n-m}\right|^2\right\}.\end{aligned} \tag{122}$$

The condition $2\mu[A]+\lambda_2+\lambda_4+\lambda_1+\lambda_3<0$ gives that $e^{(2\mu[A]+\lambda_2+\lambda_4+\lambda_1+\lambda_3)h_n}<1$; it is not difficult to see that $\widehat{E}|y_n|^2 \le \widehat{E}|y_{n-m}|^2$; therefore,

$$\begin{aligned}\widehat{E}\left|y_{n+1}\right|^2 &\le e^{(2\mu[A]+\lambda_2+\lambda_4+\lambda_1+\lambda_3)h_n}\widehat{E}\left|y_{n-m}\right|^2\\ &\le e^{2(2\mu[A]+\lambda_2+\lambda_4+\lambda_1+\lambda_3)h_n}\widehat{E}\left|y_{n-2m}\right|^2\\ &\vdots\\ &\le e^{\lfloor n-2/m\rfloor(2\mu[A]+\lambda_2+\lambda_4+\lambda_1+\lambda_3)h_n}\widehat{E}\left|y_0\right|^2\end{aligned}, \tag{123}$$

and hence

$$\lim_{n\longrightarrow\infty}\widehat{E}\left|y_n\right|^2 = 0. \tag{124}$$

The above theorem gives the sufficient conditions for keeping mean-square stability by exponential Euler method for equation (7). On the premise of its stability, it is found that the stability and step size of exponential Euler method depend on the norm of A. □

5. Numerical Examples

In this section, we discuss a numerical example to illustrate the effectiveness of the obtained results.

Example 1. Let $\omega(t)$ be a scalar G-Brownian motion with $\omega(t) \sim N(0, [1/8, 1/4])$. Consider the scalar nonlinear G-SLSDDE with the form

$$\begin{aligned}\mathrm{d}y(t) &= \left(-\frac{1}{2}y(t)-\frac{1}{8}\left[y(t)-\sin y(t-1)\right]\right)\mathrm{d}t+\frac{1}{2}y(t-1)\mathrm{d}\omega(t)-\frac{1}{4}y(t)\mathrm{d}\langle\omega\rangle(t), \quad t\ge 0,\\ y(t) &= t+1, \quad t\in[-1,0].\end{aligned} \tag{125}$$

Then, the numerical solution of this system is convergent and asymptotically mean-square stable.

Obviously, from system (125), one can obtain $\mu[A] = -1/2$ and $f(t,0,0) = g(t,0,0) = h(t,0,0) = 0$. It is easy to see that f, g, h satisfy the condition in (H1). Moreover, $|f(t,x,y)|^2 \le 1/32(|x|^2+|y|^2)$, $|g(t,x,y)|^2 = 1/4|y|^2$, and $|h(t,x,y)|^2 = 1/16|x|^2$. Therefore, $|f(t,x,y)|^2 \vee |g(t,x,y)|^2 \vee |h(t,x,y)|^2 \le 1/4(|x|^2+|y|^2)$; that is, $L_1 = 1/4$.

Further, by Young's inequality, one can obtain

$$\begin{aligned}2x^T f(t,x,y) &= 2x^T\left(-\frac{1}{8}\left[x-\sin y\right]\right) \le -\frac{3}{16}|x|^2+\frac{1}{4}|y|^2,\\ 2\overline{\sigma}^2 x^T h(t,x,y) &= 2\frac{1}{4}x^T\left(-\frac{1}{4}x\right) \le -\frac{1}{8}|x|^2+\frac{1}{8}|y|^2.\end{aligned} \tag{126}$$

Therefore, $\lambda_1 = 3/16$, $\lambda_2 = 1/4$, $\lambda_3 = 1/8$, and $\lambda_4 = 1/8$ satisfy $L_1\overline{\sigma}^2-\lambda_1-\lambda_3<0$, $2\mu[A]+\lambda_2+\lambda_4+\lambda_1+\lambda_3<0$, and $\lambda_1-2\mu[A]-\lambda_2-6\overline{\sigma}^4L_1-4\overline{\sigma}^4\sqrt{L_1}>0$. Then, it follows from

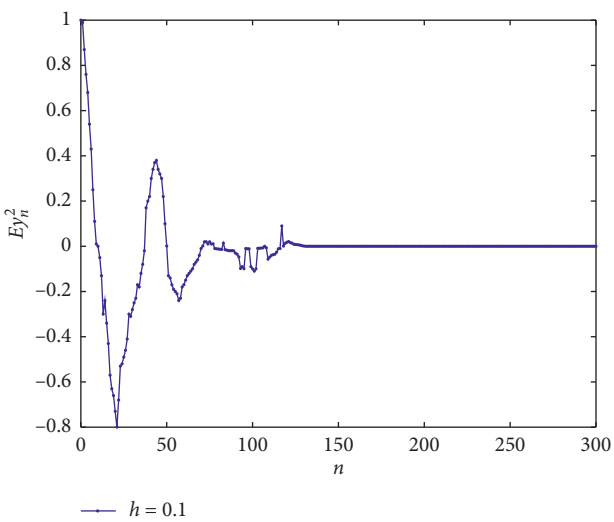

Figure 2: The G-expectation of numerical solution with $h = 0.1$ of the exponential Euler method.

Theorem 3 that the trivial solution of the example is mean-square exponentially stable.

Noticing that

$$h_0 = \frac{1/2\lambda_1 + 1/2\lambda_3 - 1/2L_1\overline{\sigma}^2}{L_1 + L_1\overline{\sigma}^4 + L_1\overline{\sigma}^2} = \frac{8}{21}, \tag{127}$$

by Theorem 2 and Theorem 4, we see that the exponential Euler method is convergent and asymptotically mean-square stable.

On the other hand, by the exponential Euler method, choose the step size $h < 8/21$ and the initial value $y(0) = 1$ to simulate the numerical solution y_n and $\widehat{E}y_n^2$ for system (125), which are shown in Figures 1 and 2 , respectively. It follows from Figure 1 that the numerical solution of system (125) converges to zero. Moreover, it follows from Figure 2 that numerical solution of system (125) is asymptotically mean-square stable. In brief, the numerical simulation results are consistent with our theoretical results.

6. Conclusions

This paper is devoted to applying the exponential integrators to the semilinear stochastic delay differential equations driven by G-Brownian motion (G-SLSDDEs) and dealing with the convergence and stability properties of exponential integrators for G-SLSDDEs. It first investigates some suitable conditions for the mean-square stability of the analytic solution and then shows that the exponential integrators numerical solution converges to the analytic solution for the G-SLSDDEs with the strong order 1/2. Furthermore, it proves that the exponential Euler method can keep the mean-square exponential stability of the analytic solution under some restrictions on the step size.

G-framework is a new study area which many scholars begin to pay attention to. Recently, some results related to G-framework have been obtained; however, it is a pity that there are few numerical conclusions. In the future, we will further discover more efficient numerical methods, such as the transferred Legendre pseudospectral method in [40], to solve semilinear stochastic delay differential equations with time-variable delay driven by G-Brownian motion. Influenced by experience gained from solving stochastic fractional differential equations driven by fractional Brownian motion, we will further study stochastic fractional differential equations driven by G-Brownian motion with "dy (t)" as fractional order in future research [41].

Data Availability

The data used to support the findings of this study are included within the article.

Conflicts of Interest

The author declares no conflicts of interest.

Acknowledgments

This research was supported by the National Natural Science Foundation of China (project no. 11901173), by the Heilongjiang Province Natural Science Foundation (no. LH2019A030), by Provincial Echelon Training Program of Heilongjiang Institute of Technology (no. 2020LJ01), and by the Innovation Talent Foundation of Heilongjiang Institute of Technology (no. 2018CX17).

References

[1] S. Singh and S. Ray, "Numerical solutions of stochastic Fisher equation to study migration and population behavior in biological invasion," *International Journal of Biomathematics*, vol. 10, pp. 1–14, 2017.

[2] X. Chen, P. Hu, S. Shum, and Y. Zhang, "Dynamic stochastic inventory management with reference price effects," *Operations Research*, vol. 64, no. 6, pp. 1529–1536, 2016.

[3] N. Gillard, E. Belin, and F. Chapeau-Blondeau, "Stochastic antiresonance in qubit phase estimation with quantum thermal noise," *Physics Letters A*, vol. 381, no. 32, pp. 2621–2628, 2017.

[4] A. Babaei, H. Jafari, S. Banihashemi, and M. Ahmadi, "Mathematical analysis of a stochastic model for spread of Coronavirus," *Chaos, Solitons, and Fractals*, vol. 145, Article ID 110788, 2021.

[5] J.-F. Chassagneux, A. Jacquier, and I. Mihaylov, "An explicit Euler scheme with strong rate of convergence for financial SDEs with non-Lipschitz coefficients," *SIAM Journal on Financial Mathematics*, vol. 7, no. 1, pp. 993–1021, 2016.

[6] D. J. Higham, X. Mao, and A. M. Stuart, "Strong convergence of Euler-type methods for nonlinear stochastic differential equations," *SIAM Journal on Numerical Analysis*, vol. 40, no. 3, pp. 1041–1063, 2002.

[7] D. J. Higham, X. Mao, and C. Yuan, "Almost sure and moment exponential stability in the numerical simulation of stochastic differential equations," *SIAM Journal on Numerical Analysis*, vol. 45, no. 2, pp. 592–609, 2007.

[8] S. Banihashemi, H. Jafaria, and A. Babaei, "A novel collocation approach to solve a nonlinear stochastic differential equation of fractional order involving a constant delay," *Discrete & Continuous Dynamical Systems-S*, 2021.

[9] A. Babaei, H. Jafari, and S. Banihashemi, "A collocation approach for solving time-fractional stochastic heat equation driven by an additive noise," *Symmetry*, vol. 12, 2020.

[10] W. Liu and X. Mao, "Almost sure stability of the Euler-Maruyama method with random variable stepsize for stochastic differential equations," *Numerical Algorithms*, vol. 74, no. 2, pp. 573–592, 2017.

[11] D. J. Higham, X. Mao, and A. M. Stuart, "Exponential mean-square stability of numerical solutions to stochastic differential equations," *LMS Journal of Computation and Mathematics*, vol. 6, pp. 297–313, 2003.

[12] M. Hochbruck and A. Ostermann, "Explicit exponential runge-kutta methods for semilinear parabolic problems," *SIAM Journal on Numerical Analysis*, vol. 43, no. 3, pp. 1069–1090, 2005.

[13] R. Bouc and E. Pardoux, "Moments of semilinear random evolutions," *SIAM Journal on Applied Mathematics*, vol. 41, no. 2, pp. 370–399, 1981.

[14] S. Maset and M. Zennaro, "Stability properties of explicit exponential Runge-Kutta methods," *IMA Journal of Numerical Analysis*, vol. 33, no. 1, pp. 111–135, 2013.

[15] E. Pardoux, "Semi-linear stochastic models: computation of moments and conditional moments," *Bulletin of Mathematical Biology*, vol. 45, no. 4, pp. 591–597, 1983.

[16] E. Altman, "Semi-linear stochastic difference equations," *Discrete Event Dynamic Systems*, vol. 19, no. 1, pp. 115–136, 2009.

[17] H. Y. Yuan, "Convergence and stability of exponential integrators for semi-linear stochastic variable delay integro-differential equations," *International Journal of Computer Mathematics*, vol. 98, no. 2, pp. 1–32, 2020.

[18] T. Hou, Y. Liu, and F. Deng, "Stability for discrete-time uncertain systems with infinite Markov jump and time-delay," *Science China Information Sciences*, vol. 64, no. 5, pp. 1–11, 2021.

[19] X. Yi, R. Guo, and Y. Qi, "Stabilization of chaotic systems with both uncertainty and disturbance by the UDE-based control method," *IEEE Access*, vol. 8, pp. 62471–62477, 2020.

[20] S. Peng, "G-expectation, G-brownian motion and related stochastic calculus of itô type," *Stochastic Analysis and Applications*, vol. 3, pp. 541–567, 2007.

[21] S. Peng, "Nonlinear expectations and stochastic calculus under uncertainty," 2010, http://arxiv.org/abs/1002.4546.

[22] L. Denis, M. Hu, and S. Peng, "Function spaces and capacity related to a sublinear expectation: application to G-Brownian motion paths," *Potential Analysis*, vol. 34, no. 2, pp. 139–161, 2011.

[23] Y. Dolinsky, M. Nutz, and H. M. Soner, "Weak approximation of G-expectations," *Stochastic Processes and Their Applications*, vol. 122, no. 2, pp. 664–675, 2012.

[24] F. Faizullah, "A note on pth moment estimates for stochastic functional differential equations in the framework of G-Brownian motion," *Iranian Journal of Science and Technology, Transactions A: Science*, vol. 41, no. 4, pp. 1131–1138, 2017.

[25] F. Faizullah, M. Bux, M. A. Rana, and G. Rahman, "Existence and stability of solutions to non-linear neutral stochastic functional differential equations in the framework of G-Brownian motion," *Iranian Journal of Science and Technology. Transaction A, Science*, vol. 41, no. 4, 2017.

[26] F. Faizullah, M. Shahzad, and M. I. Chohan, "On existence and comparison results for solutions to stochastic functional differential equations in the G-framework," *Journal of Computational Analysis and Applications*, vol. 23, pp. 693–702, 2017.

[27] R. Ullah and F. Faizullah, "On existence and approximate solutions for stochastic differential equations in the framework of G-Brownian motion," *The European Physical Journal Plus*, vol. 132, no. 10, pp. 435–443, 2017.

[28] T. Fadina and F. Herzberg, "Weak approximation of g-expectation with discrete state space," 2015.

[29] M.-S. Hu and S.-G. Peng, "On representation theorem of G-expectations and paths of G-Brownian motion," *Acta Mathematicae Applicatae Sinica, English Series*, vol. 25, no. 3, pp. 539–546, 2009.

[30] X. Li, X. Lin, and Y. Lin, "Lyapunov-type conditions and stochastic differential equations driven by G-Brownian motion," *Journal of Mathematical Analysis and Applications*, vol. 439, no. 1, pp. 235–255, 2016.

[31] Y. Ren, Q. Bi, and R. Sakthivel, "Stochastic functional differential equations with infinite delay driven by G -Brownian motion," *Mathematical Methods in the Applied Sciences*, vol. 36, no. 13, pp. 1746–1759, 2013.

[32] W. Yin and Y. Ren, "Asymptotical boundedness and stability for stochastic differential equations with delay driven byG-Brownian motion," *Applied Mathematics Letters*, vol. 74, pp. 121–126, 2017.

[33] Q. Yang and P. Zhu, "Stepanov-like doubly weighted pseudo almost automorphic processes and its application to Sobolev-type stochastic differential equations driven byG-Brownian motion," *Mathematical Methods in the Applied Sciences*, vol. 40, no. 18, pp. 6602–6622, 2017.

[34] D. Zhang and Z. Chen, "Exponential stability for stochastic differential equation driven by G-Brownian motion," *Applied Mathematics Letters*, vol. 25, no. 11, pp. 1906–1910, 2012.

[35] W. Fei and C. Fei, "On exponential stability for stochastic differential equations disturbed by G-Brownian motion," 2013, http://arxiv.org/abs/1311.7311v1.

[36] Y. Ren, X. Jia, X. Jia, and L. Hu, "Exponential stability of solutions to impulsive stochastic differential equations driven by G-Brownian motion," *Discrete & Continuous Dynamical Systems-B*, vol. 20, no. 7, pp. 2157–2169, 2015.

[37] X. Mao, *Stochastic Differential Equations and Applications*, Horwood Publishing Limited, Chichester, England, 2nd edition, 2008.

[38] C. T. H. Baker and E. Buckwar, "Exponential stability in p-th mean of solutions, and of convergent Euler-type solutions, of stochastic delay differential equations," *Journal of Computational and Applied Mathematics*, vol. 184, no. 2, pp. 404–427, 2005.

[39] L. Xu, "Some notes on linear growth condition," *Journal of Hubei Normal University (Natural Science)*, vol. 28, pp. 13–16, 2008.

[40] H. Jafari, M. Mahmoudi, and M. H. Noori Skandari, "A new numerical method to solve pantograph delay differential equations with convergence analysis," *Advances in Difference Equations*, vol. 2021, no. 1, pp. 129–141, 2021.

[41] L. Liu, B. Li, and R. Guo, "Consensus control for networked manipulators with switched parameters and topologies," *IEEE Access*, vol. 9, pp. 9209–9217, 2021.

Hindawi
Mathematical Problems in Engineering
Volume 2021, Article ID 1468979, 5 pages
https://doi.org/10.1155/2021/1468979

Research Article

The Efficient Proportional Myerson Values for Hypergraph Games

Guangming Wang,[1,2] **Lei Cai**,[1] **and Erfang Shan**[1]

[1]*School of Management, Shanghai University, Shanghai 200444, China*
[2]*School of Mathematical Sciences, University of Jinan, Jinan 250022, China*

Correspondence should be addressed to Erfang Shan; efshan@shu.edu.cn

Received 6 May 2021; Accepted 15 June 2021; Published 29 June 2021

Academic Editor: Cuimei Jiang

This study deals with a class of efficient extensions of Myerson value for games with hypergraph communication situations in which the surplus is allocated proportionally. We introduce w-fairness of surplus and provide axiomatic characterizations of the new allocation rule. Furthermore, we give an example of research fund distribution amongst researchers, compare the numerical results with several values, and realize other efficient extensions of Myerson value can be obtained depending on the different measure function w on the hypergraph.

1. Introduction

Cooperative games with transferable utility (TU-game) [1] usually describe situations in which a viable alliance can be formed and earn the corresponding worth by cooperating. However, in many situations, viable alliance is restricted by some hierarchical, cultural, or communicational technology constraints. For this reason, Myerson [2] introduced the Myerson value which is a kind of Shapley value [3] depended on graph and characterized by component efficiency and fairness. Later, Myerson [4] and Slikker and van den Nouweland [5] studied other axiomatic characterizations of the Myerson value. In recent years, several works have devoted to the study of Myerson value. Li and Shan [6–8] studied the Myerson value on structures of coalitions or for directed graph games. van den Nouweland [9] and Shan and Zhang [10] extended the idea initiated by Myerson to hypergraph games.

The Myerson value satisfying component efficiency, i.e., the worth of every component, is distributed among its members. However, in many situations, every player obtains distribution of the worth generated by the grand coalition such as research fund distribution amongst researchers. Motivated by this idea, van den Brink [11] introduced the efficient egalitarian Myerson value (EEMy) for graph games which is the first efficient extension of the Myerson value. Beal [12] proved that EEMy is the unique efficient and fair extension of Myerson value. Casajus [13–16] introduced the efficient two-step egalitarian surplus Myerson value (ESMy) on graph communication situations which is the first nonfair efficient extension of the Myerson value. However, an axiomatic characterization of the efficient extension of the Myerson value for hypergraph games remains an open problem. Motivated by the above discussion, we investigate a class of efficient extensions of the Myerson value for games with hypergraph communication situations in which the surplus is allocated proportionally.

The rest of this paper is organized as follows. In Section 2, we provide some preliminaries on TU-games, the graph, and the hypergraph games' allocation rule. In Section 3, we propose a class of efficient extensions of the Myerson value, provide a characterization of E^wMy, and give an example of research fund distribution amongst researchers. Section 4 concludes with some remarks.

2. Preliminaries

A transferable utility game (TU-game) represented by a pair (N, v), where $N = \{1, 2, \ldots, n\}$, is a set of players and v: $2^N \longrightarrow \mathbb{R}$ is a characteristic function with $v(\varnothing) = 0$. An

allocation rule (A value) is a function about the payoff of player in a TU-game. A very famous value is the Shapley value: $\mathrm{Sh}_i(v) = \sum_{S\subseteq N} (|N| - |S|)!\,(|S| - 1)!/|N|!\,(v(S) - v(S\setminus\{i\}))$, $i \in N$.

The triple (N, v, H) represents a hypergraph games, which is composed of two parts: the TU-game (N, v) and the hypergraph structure (N, H) on N, where $H \subseteq H^N := \{e \subseteq N \mid |e| \geq 2\}$; i.e., H is a family of nonsingleton subsets of N, called hyperlinks. In particular, a hypergraph (N, H) is a graph if $|e| = 2$.

For each player $i \in N$, $H_i := \{e \in H \mid i \in e\}$ is the set of hyperlinks containing i in (N, H). A node $i \in N$ is *incident* to a hyperlink $e \in H$ if $i \in e$. Two nodes $i, j \in N$ are adjacent if there is a hyperlink e in H satisfying $i, j \in e$. We say that nodes i and j are connected *in* (N, H) if there exists is a sequence $i = i_1, e_1, i_2, e_2, \ldots, i_k, e_k, i_{k+1} = j$ such that $i_l, i_{l+1} \in e_l$, for $l = 1, 2, \ldots, k$. A hypergraph is connected if every pair of nodes is connected. Connectedness in (N, H) induces a partition of N into components. A component is a maximal set of nodes of N in which every pair of nodes are connected. Let N/H be the set of components of (N, H) and $(N/H)_i$ be the component containing $i \in N$. We denote by HG the set of all hypergraph games and G the set of all graph games. Hypergraph (graph) games are called connected if the associated hypergraph (graph) is connected. We denote, by HG_C, the class of all connected hypergraph games and, G_C, the class of all connected graph games.

An allocation rule or value $f(N, v, H)$ on hypergraph communication situations is a n-dimensional vector function defined on hypergraph games. The Myerson value for hypergraph communication situations is defined as follows:

$$\mathrm{My}_i(N, v, H) = \mathrm{Sh}_i\left(N, v^H\right), \quad \text{for any } i \in N, \tag{1}$$

where $v^H(S) = \sum_{T \in S/H} v(T)$ for any $S \subseteq N$. The game (N, v^H) is called the point game.

The Myerson value is the unique hypergraph games' allocation rule which satisfies component efficiency (**CE**) and fairness (**F**).

Component efficiency (**CE**): For any $(N, v, H) \in \mathrm{HG}$ and $C \in N/H$,

$$\sum_{i \in C} f_i(N, v, H) = v(C). \tag{2}$$

Fairness (**F**): For any $(N, v, H) \in \mathrm{HG}$ and $ij \in H$,

$$\begin{aligned} f_i(N, v, H) - f_i(N, v, H\setminus\{ij\}) &= f_j(N, v, H) \\ &\quad - f_j(N, v, H\setminus\{ij\}). \end{aligned} \tag{3}$$

More axioms for efficiency extensions of the Myerson value are as follows.

Efficiency (**E**): For any $(N, v, H) \in \mathrm{HG}$,

$$\sum_{i \in N} f_i(N, v, H) = v(N). \tag{4}$$

Coherence with the Myerson value for connected hypergraphs (**CMC**): For any $(N, v, H) \in \mathrm{HG}_C$,

$$f(N, v, H) = \mathrm{My}(N, v, H). \tag{5}$$

3. A Class of Efficient Extensions of Myerson Value for Hypergraph Games

In this section, we propose a class of efficient extensions of the Myerson value which distributes the surplus of the Myerson value by defining some measure function w on hypergraph. Let (N, v, H) be any hypergraph games and let us define a function w: $(N, H) \longrightarrow R$ which assigns to every player $i \in N$, a real number $w_i(N, H)$. We define the efficient $w-$proportional Myerson value $E^w\mathrm{My}$:

$$\begin{aligned} E^w\mathrm{My}_i(N, v, H) &= \mathrm{My}_i(N, v, H) \\ &\quad + \frac{w_i(N, H)}{\sum_{k \in N} w_k(N, H)}\left[v(N) - v^H(N)\right]. \end{aligned} \tag{6}$$

In order to characterize efficient $w-$proportional Myerson value *Myerson value* $E^w\mathrm{My}$, we propose the following property.

w-fairness of surplus (**FS**^{w}): a value on HG satisfies **FS**^{w} if, for any $(N, v, H) \in \mathrm{HG}$ and any $i, j \in N$,

$$\begin{aligned} &\frac{1}{w_i(N, H)}\left[\xi_i(N, v, H) - \xi_i\left(C_i, v_{C_i}, H_{C_i}\right)\right] \\ &\quad = \frac{1}{w_j(N, H)}\left[\xi_j(N, v, H) - \xi_j\left(C_j, v_{C_j}, H_{C_j}\right)\right]. \end{aligned} \tag{7}$$

Then, we provide a characterization of $E^w\mathrm{My}$.

Theorem 1. *The efficient extension Myerson value E^wMy on hypergraph communication situations is the unique allocation which satisfies efficiency(E), w-fairness of surplus (**FS**^{w}), and coherence with the Myerson value for connected hypergraphs (CMC).*

Proof. (existence). Let (N, v, H) is any hypergraph games. It is easy to see that $E^w\mathrm{My}(N, v, H)$ satisfies **E** and **CMC**.

Next, we prove that $E^w\mathrm{My}(N, v, H)$ satisfies w-fairness of surplus (**FS**^{w}). By the definition of $E^w\mathrm{My}(N, v, H)$, we have

$$\begin{aligned}
&\frac{1}{w_i(N,H)}\left[E^w\mathrm{My}_i(N,v,H)-E^w\mathrm{My}_i\left(C_i,v_{C_i},H_{C_i}\right)\right]\\
&=\frac{1}{w_i(N,H)}\left[\mathrm{My}_i(N,v,H)+\frac{w_i(N,H)}{\sum_{k\in N}w_k(N,H)}\left(v(N)-v^H(N)\right)-\mathrm{My}_i\left(C_i,v_{C_i},H_{C_i}\right)\right]\\
&=\frac{1}{w_i(N,H)}\left[My_i\left(C_i,v_{C_i},H_{C_i}\right)+\frac{w_i(N,H)}{\sum_{k\in N}w_k(N,H)}\left(v(N)-v^H(N)\right)-\mathrm{My}_i\left(C_i,v_{C_i},H_{C_i}\right)\right]\\
&=\frac{1}{\sum_{k\in N}w_k(N,H)}\left(v(N)-v^H(N)\right),
\end{aligned}\tag{8}$$

where the second equality follows from the component decomposability of the Myerson value. Similarly, we have

$$\begin{aligned}
&\frac{1}{w_j(N,H)}\left[E^w\mathrm{My}_j(N,v,H)-E^w\mathrm{My}_j\left(C_j,v_{C_j},H_{C_j}\right)\right]\\
&=\frac{1}{w_j(N,H)}\left[\mathrm{My}_j(N,v,H)+\frac{w_j(N,H)}{\sum_{k\in N}w_k(N,H)}\left(v(N)-v^H(N)\right)-\mathrm{My}_j\left(C_j,v_{C_j},H_{C_j}\right)\right]\\
&=\frac{1}{w_i(N,H)}\left[My_j\left(C_j,v_{C_j},H_{C_j}\right)+\frac{w_j(N,H)}{\sum_{k\in N}w_k(N,H)}\left(v(N)-v^H(N)\right)-\mathrm{My}_j\left(C_j,v_{C_j},H_{C_j}\right)\right]\\
&=\frac{1}{\sum_{k\in N}w_k(N,H)}\left(v(N)-v^H(N)\right).
\end{aligned}\tag{9}$$

Therefore, we obtain

$$\begin{aligned}
&\frac{1}{w_i(N,H)}\left[E^w\mathrm{My}_i(N,v,H)-E^w\mathrm{My}_i\left(C_i,v_{C_i},H_{C_i}\right)\right]\\
&=\frac{1}{w_j(N,H)}\left[E^w\mathrm{My}_j(N,v,H)-E^w\mathrm{My}_j\left(C_j,v_{C_j},H_{C_j}\right)\right].
\end{aligned}\tag{10}$$

Hence, $E^w\mathrm{My}_i(N,v,H)$ satisfies $\mathbf{FS}^w$. To show uniqueness and recall $\mathbf{FS}^w$,

$$\begin{aligned}
&\frac{1}{w_i(N,H)}\left[\xi_i(N,v,H)-\xi_i\left(C_i,v_{C_i},H_{C_i}\right)\right]\\
&=\frac{1}{w_j(N,H)}\left[\xi_j(N,v,H)-\xi_j\left(C_j,v_{C_j},H_{C_j}\right)\right]=t.
\end{aligned}\tag{11}$$

There exists a constant t, such that

$$\xi_i(N,v,H)-\xi_i\left(C_i,v_{C_i},H_{C_i}\right)=tw_i(N,H),\quad \text{for all } i\in N.\tag{12}$$

We have

$$\xi_i(N,v,H)=\xi_i\left(C_i,v_{C_i},H_{C_i}\right)+tw_i(N,H).\tag{13}$$

By summing up over all $i\in N$, we obtain

$$\sum_{i\in N}\xi_i(N,v,H)=\sum_{i\in N}\xi_i\left(C_i,v_{C_i},H_{C_i}\right)+t\sum_{i\in N}w_i(N,H),\tag{14}$$

By efficiency, $\sum_{i\in N}\xi_i(N,v,H)=v(N)$ and $\sum_{i\in N}\xi_i(C_i,v_{C_i},H_{C_i})=v^H(N)$. Thus,

$$v(N)=v^H(N)+t\sum_{i\in N}w_i(N,H).\tag{15}$$

Then, $t=1/\sum_{i\in N}w_i(N,H)[v(N)-v^H(N)]$. By equation (13), we obtain

$$\begin{aligned}
\xi_i(N,v,H)&=\xi_i\left(C_i,v_{C_i},H_{C_i}\right)\\
&\quad+\frac{w_i(N,H)}{\sum_{i\in N}w_i(N,H)}\left[v(N)-v^H(N)\right].
\end{aligned}\tag{16}$$

Since ξ satisfies **CMC**, then $\xi_i(C_i,v_{C_i},H_{C_i})=\mathrm{My}_i(C_i,v_{C_i},H_{C_i})$. Furthermore, $\mathrm{My}_i(C_i,v_{C_i},H_{C_i})=\mathrm{My}_i(N,v,H)$ because of component decomposability of the Myerson value. Hence,

$$\begin{aligned}
\xi_i(N,v,H)&=\mathrm{My}_i(N,v,H)\\
&\quad+\frac{w_i(N,H)}{\sum_{i\in N}w_i(N,H)}\left[v(N)-v^H(N)\right].
\end{aligned}\tag{17}$$

Obviously, $\xi_i(N,v,H)=E^w\mathrm{My}_i(N,v,H)$, as desired. □

In particular, when $w_i(N,H) = c$(c is nonzero constant), $w-$ fairness of surplus is reduced to fairness of surplus:

$$f_i(N,v,H) - f_i\left(C_i, v_{C_i}, H_{C_i}\right) = f_j(N,v,H) - f_j\left(C_j, v_{C_j}, H_{C_j}\right). \tag{18}$$

and

$$\begin{aligned} E^w\mathrm{My}_i\ (N,v,H):& \\ &= \mathrm{My}_i\ (N,v,H) + \frac{w_i(N,H)}{\sum_{k\in N} w_k(N,H)}\left[v(N) - v^H(N)\right] \\ &= \mathrm{My}_i\ (N,v,H) + \frac{c}{|N|c}\left[v(N) - v^H(N)\right] \\ &= \mathrm{My}_i\ (N,v,H) + \frac{v(N) - v^H(N)}{|N|} \\ &= \mathrm{EEMy}_i\ (N,v,H). \end{aligned} \tag{19}$$

Theorem 2. *The efficient egalitarian Myerson value EEMy on hypergraph communication situations is the unique allocation satisfy efficiency (E), fairness of surplus (***FS***), and coherence with the Myerson value for connected hypergraphs (CMC).*

Furthermore, when restrict hypergraph communication situations (N,v,H) to graph communication situations (N,v,L) and $w_i(N,H) = c$, we obtain the conclusion of van den Brink et al. [11] as an immediate consequence of Theorem 1:

$$\mathrm{EEMy}_i\ (N,v,L) \coloneqq \mathrm{My}_i\ (N,v,L) + \frac{v(N) - v^L(N)}{|N|}, \tag{20}$$

Theorem 3. *The efficient egalitarian Myerson value EEMy on graph communication situations is the unique allocation satisfy efficiency (E), fairness of surplus (***FS***), and coherence with the Myerson value for connected graphs (CMC).*

When $w_i(N,H) = 1/|C_i|$, $w-$ fairness of surplus is reduced to per capita fairness of surplus:

$$\begin{aligned} &|C_i|\left(f_i(N,v,H) - f_i\left(C_i, v_{C_i}, H_{C_i}\right)\right) \\ &\quad = |C_j|\left(f_j(N,v,H) - f_j\left(C_j, v_{C_j}, H_{C_j}\right)\right) \end{aligned} \tag{21}$$

and

$$\begin{aligned} E^w\mathrm{My}_i\ (N,v,H):& \\ &= \mathrm{My}_i\ (N,v,H) + \frac{1/|C_i|}{\sum_{k\in N} 1/|C_k|}\left[v(N) - v^H(N)\right] \\ &= \mathrm{My}_i\ (N,v,H) + \frac{v(N) - v^H(N)}{|N/H||C_i|} \\ &= \mathrm{ESMy}_i\ (N,v,H). \end{aligned} \tag{22}$$

Theorem 4. *The efficient two-step egalitarian surplus Myerson value ESMy on hypergraph communication situations is the unique allocation satisfy per capita fairness of surplus fairness of surplus (***PRFS***), efficiency (E), and coherence with the Myerson value for connected hypergraphs (CMC).*

Furthermore, when restricting hypergraph communication situations (N,v,H) to graph communication situations (N,v,L) and $w_i(N,H) = 1/|C_i|$, we obtain the conclusion of Casajus which introduced the efficient two-step egalitarian surplus Myerson value(ESMy) on graph communication situations [13] as another immediate consequence of Theorem 1:

$$\mathrm{ESMy}_i\ (N,v,L) \coloneqq \mathrm{My}_i\ (N,v,L) + \frac{v(N) - v^L(N)}{|N/L||T|}. \tag{23}$$

Theorem 5. *The efficient two-step egalitarian surplus Myerson value ESMy on graph communication situations is the unique allocation which satisfies per capita fairness of surplus of surplus (***PRFS***), efficiency (E), and coherence with the Myerson value for connected graphs (CMC).*

Example 1. Consider a problem of research fund distribute amongst researchers. Suppose fund total amounts is 4, A is a researcher of subject one, D is a researcher of subject two, B, C are the researchers of subject one and subject two, E is a researcher of subject there, and hypergraph communication situations is (N,v,H) with Figure 1, where $N = \{A, B, C, D, E\}$, $H = \{\{A,B,C\},\{B,C,D\}$, and $v(S) = |S| - 1$, $|S| = 1, 2, 3, 4, 5$.

The Shapley value of v is efficient and $\mathrm{Sh}(v) = (4/5, 4/5, 4/5, 4/5, 4/5)$. The Myerson value is component efficient and $\mathrm{My}(v,H) = (2/3, 5/6, 5/6, 2/3, 0)$. Although fund amounts is 4, by component efficient, the total amount of the Myerson value is 3. Fund surplus is $v(N) - v^H(N) = 4 - 3 = 1$.

On the one hand, $v(N) - v^H(N)/|N| = 1/5$, efficient $w-$ proportional Myerson value $E^w\mathrm{My}\ \ (w_i(N,H) = c)$ reduces to efficient egalitarian Myerson value EEMy, i.e., $E^w\mathrm{My}\ (v,H) = \mathrm{EEMy}\ \ (v,H) = (13/15, 31/30,\ 31/30, 13/15,\ 1/5)$, the allocation satisfy **FS**: $f_i(N,v,H) - f_i(c_i, v_{c_i}, H_{c_i}) = f_j(N,v,H) - f_j(c_j, v_{c_j}, H_{c_j}) = 1/5$.

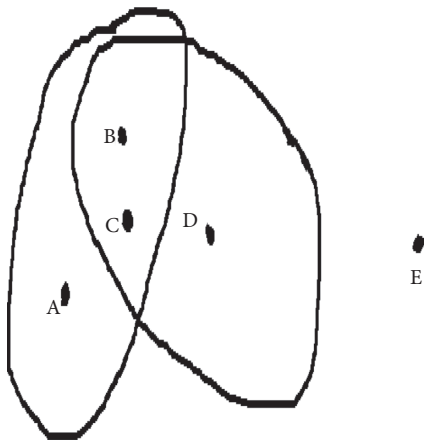

Figure 1: Fund distribution amongst researchers.

On the other hand, $v(N) - v^H(N)/|N/H||C_i| = 1/2 * 4$, $i = A, B, C, D$, $v(N) - v^H(N)/|N/H||C_i| = 1/2 * 1$, $i = E$, and efficient w − proportional Myerson value $E^w\mathrm{My}(w_i(N, H) = 1/|C_i|)$ reduce to efficient two-step egalitarian surplus Myerson value ESMy, i.e., $E^w\mathrm{My}(v, H) = \mathrm{ESMy}(v, H) = (19/24, 23/24, 23/24, 19/24, 1/2)$, and the allocation satisfies **PRFS**: $|C_i|(f_i(N, v, H) - f_i(c_i, v_{c_i}, H_{c_i})) = |C_j|(f_j(N, v, H) - f_j(c_j, v_{c_j}, H_{c_j}))$, $4 * 1/8 = 1 * 1/2 = 1/2$.

4. Conclusion

In this paper, we investigate a class of efficient extensions of the Myerson value for hypergraph games and provide a characterization of $E^w\mathrm{My}$. When restricting hypergraph games to graph games, we obtain the conclusion of van den Brink et al. and Casajus as an immediate consequence. Further research can consider degree and probabilistic hypergraph efficient extensions of the Myerson value.

Data Availability

The data used to support the findings of the study are available from the corresponding author upon request.

Conflicts of Interest

The authors declare that they have no conflicts of interest.

References

[1] R. Branzei, D. Dimitrov, S. Tijs et al., *Models in Cooperative Game Theory*, Springer, Berlin, Germany, 2008.

[2] R. B. Myerson, "Graphs and cooperation in games," *Mathematics of Operations Research*, vol. 2, pp. 225–229, 1977.

[3] L. S. Shapley, "A value for n-person games," *Contributions to the Theory of Games (AM-28)*, Princeton University Press, Princeton, NJ, USA, pp. 307–318, 1953.

[4] R. B. Myerson, "Conference structures and fair allocation rules," *International Journal of Game Theory*, vol. 9, pp. 169–182, 1980.

[5] M. Slikker and A. van den Nouweland, *Social and Economic Networks in Cooperative Game Theory*, Kluwer Academic Publishers, Boston, MA, USA, 2001.

[6] D. Li and E. Shan, "The Myerson value on local structures of coalitions," *Journal of the Operations Research Society of China*, vol. 7, Article ID 461C473, 2019.

[7] D. Li Li and E. Shan, "The Myerson value for directed graph games," *Operations Research Letters*, vol. 48, pp. 42–46, 2020.

[8] E. Shan, J. Han, and J. Shi, "The efficient proportional Myerson values," *Operations Research Letters*, vol. 47, pp. 574–578, 2019.

[9] A. van den Nouweland, P. Borm, and S. Tijs, "Allocation rules for hypergraph communication situations," *International Journal of Game Theory*, vol. 20, pp. 255–268, 1992.

[10] E. Shan and G. Zhang, "The position value and the Myerson value for hypergraph communication situations," *Frontiers of Dynamic Games Theory*, vol. 19, pp. 237–250, 2018.

[11] R. van den Brink, A. B. Khmelnitskaya, and G. van der Laan, "An efficient and fair solution for communication graph games," *Economics Letters*, vol. 117, pp. 786–789, 2012.

[12] S. Béal, A. Casajus, and F. Huettner, "Efficient extensions of communication values," *Annals of Operations Research*, vol. 264, no. 1-2, pp. 41–56, 2018.

[13] A. Casajus, "An efficient value for TU games with a cooperation structure," Universitat Leipzig, Leipzig, Germany, Working paper, 2007.

[14] X. Yi, R. Guo, and Yi Qi, "Stabilization of chaotic systems with both uncertainty and disturbance by the UDE-based control method," *IEEE Access*, vol. 8, no. 1, pp. 62471–62477, 2020.

[15] L. Liu, B. Li, and R. Guo, "Consensus control for networked manipulators with switched parameters and topologies," *IEEE Access*, vol. 9, pp. 9209–9217, 2021.

[16] T. Hou, Y. Liu, and F. Deng, "Stability for discrete-time uncertain systems with infinite Markov jump and time-delay," *Science China-Information Sciences*, vol. 64, pp. 1–11, 2021.

Hindawi
Mathematical Problems in Engineering
Volume 2021, Article ID 7497720, 10 pages
https://doi.org/10.1155/2021/7497720

Research Article

Finite-Time Simultaneous Stabilization of a Set of Nonlinear Singular Systems

Liying Sun [1] **and Meiqing Li** [2]

[1] *School of Business, Shanghai Dianji University, Shanghai 201306, China*
[2] *School of Automation, Nanjing University of Science and Technology, Nanjing 210094, China*

Correspondence should be addressed to Liying Sun; ss_sunly@163.com

Received 19 April 2021; Accepted 11 June 2021; Published 19 June 2021

Academic Editor: Cuimei Jiang

This study addresses the problems of finite-time simultaneous stabilization for two nonlinear singular systems and more than two nonlinear singular systems. First, we design a suitable output feedback controller and combine the two nonlinear singular systems to generate an augmented system by using an augmented technique. Based on a sufficient condition of the augmented system impulse-free, an important result, that is, the augmented system is finite-time stabilization is presented. Then, the finite-time stabilization problem of more than two singular systems is investigated by dividing the N systems into two sets. Finally, a numerical example is provided to demonstrate the effectiveness of the proposed finite-time stabilization controller for two nonlinear singular systems.

1. Introduction

In recent years, the singular system has attracted extensive attention of researchers, which is also called the descriptor system, generalized state-space system, differential-algebraic system, and so on. Due to its unique properties and structure, the singular system is more complex than the normal state-space system. It needs to consider impulse-free (continue-time system) or causality (discrete-time system), regularity, and stable [1].

It is worth pointing out that the simultaneous stabilization problem of the normal state-space system is introduced in 1982. Abundant results of simultaneous stabilization have been obtained in recent years [2–6]. In [2], several simultaneous external and internal stabilization problems have been considered under appropriate adaptive low-and-high gain feedback controllers. Simultaneous stabilization of linear systems has been solved by the static output feedback in [3]. In [4], the simultaneous stabilization of the multiinput-multioutput system has been investigated to develop a stabilizing controller. A necessary and sufficient condition for the existence of simultaneously quadratically stabilizing state feedback laws is derived for a collection of single-input discrete-time nonlinear systems in [5]. In [6], simultaneous stabilization of a set of nonlinear port-controlled Hamiltonian systems is investigated by using the dissipative Hamiltonian structural properties. Subsequently, some results of simultaneous stabilization are obtained for singular systems [7, 8]. Simultaneous stabilization problems are investigated for nonlinear singular systems with actuator saturation by using a suitable output feedback in [7] and an uncertain singular system with input saturation via using linear matrix inequalities in [8], respectively.

By the virtue of the method of simultaneous stabilization, the finite-time simultaneous stabilization problem is considered for the nonlinear singular system. Definition of finite-time stabilization is proposed for the linear system [9, 10] and then extended to the linear singular system [11]. Furthermore, the finite-time stabilization is investigated for the nonlinear discrete-time Hamiltonian singular system [12]. Finite-time stabilization, which is different from asymptotic stability [13–17], is used to describe that the state does not exceed a certain bound during a fixed finite-time interval. The finite-time stabilization of the nonlinear continue-time singular system and nonlinear discrete-time singular system is investigated via

the state-undecomposed method in [18, 19], respectively. In [20], the stochastic finite-time H_∞ filtering issue for a class of nonlinear continuous-time singular semi-Markov jump systems is discussed in the forms of strict LMIs. While, stability of the robust finite-time for linear singular Markovian jump systems with impulsive effects and time-varying norm-bounded disturbance is considered under the designed state feedback controller and estimation of domain of attraction in [21]. To our best knowledge, a few results are presented for finite-time simultaneous stabilization of the singular system. In [22], finite-time control and fault detection are studied simultaneously for the singular system via the average dwell time approach and using some novel integral inequalities. When it comes to the nonlinear singular system, the finite-time simultaneous stabilization of two nonlinear singular systems and more than two nonlinear singular systems is considered in this study. It is worth noticing that it is also called finite-time stability, i.e., states of the system reach the equilibrium point within a fixed time T and stay at the equilibrium point when $t > T$ [23–29]. The finite-time robust stabilization problem of general nonlinear time-delay systems is studied based on the Hamiltonian function method and observer design in [26]. In [27], the finite-time stabilization is investigated for a class of singular systems by the constructed new Lyapunov functional, while the finite-time robust simultaneous stabilization and adaptive robust simultaneous stabilization have been investigated for nonlinear systems with time delay in [28, 29], respectively.

In this study, our goal is to discuss the simultaneous stabilization problem of two nonlinear singular systems or more than two nonlinear singular systems and propose the designed method of the output feedback controller. The study is divided into three parts. (i) Two nonlinear singular systems discussed about state bound in finite-time interval under the nonlinear function need not to satisfy the Lipschitz condition, and the suitable output feedback law is constructed. (ii) Based on the above method, finite-time simultaneous stabilization of more than two nonlinear singular systems is studied by dividing the N systems into two sets. (iii) The numerical example of two nonlinear singular systems is used to illustrate the validity of the proposed finite-time stable controller.

2. Finite-Time Simultaneous Stabilization of Two Nonlinear Singular Systems

Consider the following two nonlinear singular systems:

$$\begin{cases} E_1\dot{x} = f_1(x) + g_1(x)u, \\ E_1x(0) = E_1x_0, \\ f_1(0) = 0, \\ y = b_1(x)x, \end{cases} \tag{1}$$

$$\begin{cases} E_2\dot{\xi} = f_2(\xi) + g_2(\xi)u, \\ E_2\xi(0) = E_2\xi_0, \\ f_2(0) = 0, \\ \eta = b_2(\xi)\xi, \end{cases} \tag{2}$$

where $x \in \mathbb{R}^{n_1}$ and $\xi \in \mathbb{R}^{n_2}$ are the states of the two systems, $u \in \mathbb{R}^q$ is the control input, $y, \eta \in \mathbb{R}^m$ are the outputs, $E_i \in \mathbb{R}^{n_i \times n_i}$ is the singular matrix, and $0 <$ rank $(E_i) = r_i < n$; $b_i(x) \in \mathbb{R}^{m \times n_i}$, $g_i(.) \in \mathbb{R}^{n_i \times q}$, $f_i(.)$ is a sufficiently smooth vector field with proper dimensions, $i = 1, 2$.

To facilitate the analysis of the two systems (1) and (2), we show the following definition and lemma.

Definition 1 (see [30]). A control law $u(x)$ is called an admissible control law, if for any initial condition Ex_0, the resulted closed-loop descriptor system has no impulsive solution, and accordingly, the original system is called impulse controllable.

Lemma 1 (see [31]). *If a scalar function $h(x)$ with $h(0) = 0$ ($x \in \mathbb{R}^n$) has continuous n^{th} order partial derivatives, then $h(x)$ can be expressed as*

$$h(x) = a_1(x)x_1 + \cdots + a_n(x)x_n = A(x)x, \tag{3}$$

where $a_i(x), i = 1, 2, \ldots, n$ are the scalar functions.

As mentioned above, the two systems can be described as follows:

$$\begin{cases} E_1\dot{x} = A_1(x)x + g_1(x)u, \\ E_1x(0) = E_1x_0, \\ f_1(0) = 0, \\ y = b_1(x)x, \end{cases} \tag{4}$$

$$\begin{cases} E_2\dot{\xi} = A_2(\xi)\xi + g_2(\xi)u, \\ E_2\xi(0) = E_2\xi_0, \\ f_2(0) = 0, \\ \eta = b_2(\xi)\xi. \end{cases} \tag{5}$$

We can design an output feedback controller:

$$u = -K(y - \eta), \tag{6}$$

where $K \in \mathbb{R}^{m \times m}$ is a symmetric matrix. Substituting (6) into systems (4) and (5), the systems can be given as follows:

$$\begin{cases} E_1\dot{x} = (A_1(x) - g_1(x)Kb_1(x))x + g_1(x)Kb_2(\xi)\xi, \\ y = b_1(x)x, \end{cases} \tag{7}$$

$$\begin{cases} E_2\dot{\xi} = (A_2(\xi) + g_2(\xi)Kb_2(\xi))\xi - g_2(\xi)Kb_1(x)x, \\ \eta = b_2(\xi)\xi. \end{cases} \tag{8}$$

Combine the two closed-loop singular systems (7) and (8) into an augmented system:

$$\begin{cases} E\dot{X} = A(X)X, \\ Y = B(X)X, \end{cases} \tag{9}$$

where

$$X = \begin{bmatrix} x \\ \xi \end{bmatrix},$$
$$Y = \begin{bmatrix} y \\ \eta \end{bmatrix},$$
$$E = \begin{bmatrix} E_1 & 0 \\ 0 & E_2 \end{bmatrix},$$
$$B(X) = \begin{bmatrix} b_1(x) & 0 \\ 0 & b_2(\xi) \end{bmatrix},$$
$$A(X) = \begin{bmatrix} A_1(x) - g_1(x)Kb_1(x) & g_1(x)Kb_2(\xi) \\ -g_2(\xi)Kb_1(x) & A_2(\xi) + g_2(\xi)Kb_2(x) \end{bmatrix}. \tag{10}$$

Lemma 2. *If* $\operatorname{rank}\begin{bmatrix} 0 & E \\ E & A(X) \end{bmatrix} = n_1 + n_2 + r_1 + r_2$, *then system (9) is impulse-free.*

Proof. From $E = \operatorname{diag}[E_1, E_2]$, we know $\operatorname{rank}(E) = r_1 + r_2$. So, there exist two nonsingular matrices M, $N \in \mathbb{R}^{(n_1+n_2)\times(n_1+n_2)}$, such that

$$\mathrm{MEN} = \begin{bmatrix} I_{r_1+r_2} & 0 \\ 0 & 0 \end{bmatrix}. \tag{11}$$

Denote

$$\overline{X} = N^{-1}X = \begin{bmatrix} X_1 \\ X_2 \end{bmatrix},$$
$$MA(X)N = \begin{bmatrix} \widetilde{A}_{11}(X) & \widetilde{A}_{12}(X) \\ \widetilde{A}_{21}(X) & \widetilde{A}_{22}(X) \end{bmatrix} = \begin{bmatrix} A_{11}(X) & A_{12}(X) \\ A_{21}(X) & A_{22}(X) \end{bmatrix},$$
$$MB(X) = \begin{bmatrix} \widetilde{B}_1(X) \\ \widetilde{B}_2(X) \end{bmatrix} = \begin{bmatrix} B_1(\overline{X}) \\ B_2(\overline{X}) \end{bmatrix}, \tag{12}$$

where $\overline{X} \in \mathbb{R}^{n_1+n_2}$, $X_1 \in \mathbb{R}^{r_1+r_2}$, and $X_2 \in \mathbb{R}^{n_1+n_2-r_1-r_2}$. Then, system (9) can be expressed as follows:

$$\begin{cases} \dot{X}_1 = A_{11}(\overline{X})X_1 + A_{12}(\overline{X})X_2, \\ 0 = A_{21}(\overline{X})X_1 + A_{22}(\overline{X})X_2, \\ Y = B_1(\overline{X})X_1 + B_2(\overline{X})X_2. \end{cases} \tag{13}$$

Noticing that

$$\begin{aligned} n_1 + n_2 + r_1 + r_2 &= \operatorname{rank}\begin{bmatrix} 0 & E \\ E & A(X) \end{bmatrix} = \operatorname{rank}\begin{bmatrix} M & \\ & M \end{bmatrix}\begin{bmatrix} 0 & E \\ E & A(X) \end{bmatrix}\begin{bmatrix} N & \\ & N \end{bmatrix} \\ &= \operatorname{rank} A_{22}(\overline{X}) + 2r_1 + 2r_2, \end{aligned} \tag{14}$$

we can obtain that $\operatorname{rank} A_{22}(\overline{X}) = n_1 + n_2 - r_1 - r_2$, which implies that the index of equivalent closed-loop singular system (9) is one at the equilibrium point 0, that is, system (9) is impulse-free.

Next, we present the definition of the finite-time simultaneous stable. □

Definition 2. The two nonlinear singular systems (4) and (5) are said to be the finite-time simultaneous stable (FTSS) with respect to (c_1, c_2, T, R), with $0 < c_1 < c_2$ and $R = \operatorname{diag}\{R_1, R_2\} > 0$, if $X^T(0)E^TREX(0) \le c_1$, such that $X^T(t)E^TREX(t) < c_2, \forall t \in [0, T]$, where $x^T(0)E_1^TR_1E_1x(0) \le c_{11}$, $\xi^T(0)E_2^TR_2E_2\xi(0) \le c_{21}$, and $c_1 \ge c_{11} + c_{21}$, $c_{11}, c_{12} > 0$.

Based on augmented system (9), we give the following result of the finite-time simultaneous stable of systems (4) and (5).

Theorem 1. *If there exist symmetric positive definite matrices* $Q \in \mathbb{R}^{(n_1+n_2)\times(n_1+n_2)}$, $P_1 \in \mathbb{R}^{n_1\times n_1}$, *and* $P_2 \in \mathbb{R}^{n_2\times n_2}$, *such that*

$$\begin{bmatrix} \Omega_1 & \Omega_2 \\ \Omega_2^T & \Omega_3 \end{bmatrix} \le 0, \tag{15}$$

$$\lambda_{\max}(Q)c_1e^{\alpha T} < \lambda_{\min}(Q)c_2, \tag{16}$$

$$\operatorname{rank}\begin{bmatrix} 0 & E \\ E & A(X) \end{bmatrix} = n_1 + n_2 + r_1 + r_2. \tag{17}$$

Then, under the output feedback control law (6), the nonlinear singular systems (4) and (5) are finite-time simultaneous stable with respect to (c_1, c_2, T, R), where

$$\begin{aligned} \Omega_1 &= (A_1(x) - g_1(x)Kb_1(x))^TP_1E_1 + E_1^TP_1(A_1(x) - g_1(x)Kb_1(x)) - \alpha E_1^TP_1E_1, \\ \Omega_2 &= (g_1(x)Kb_2(\xi))^TP_1E_1 - E_2^TP_2(g_2(\xi)Kb_1(x)), \\ \Omega_3 &= (A_2(\xi) + g_2(\xi)Kb_2(\xi))^TP_2E_2 + E_2^TP_2(A_2(\xi) + g_2(\xi)Kb_2(\xi)) - \alpha E_2^TP_2E_2, \end{aligned} \tag{18}$$

$R = \begin{bmatrix} R_1 & 0 \\ 0 & R_2 \end{bmatrix} > 0$, $Q = \begin{bmatrix} Q_1 & 0 \\ 0 & Q_2 \end{bmatrix} > 0$, $P_1 = R_1^{(1/2)} Q_1 R_1^{(1/2)}$, $P_2 = R_2^{(1/2)} Q_2 R_2^{(1/2)}$, $\alpha > 0$, *and* $\lambda_{\max}(.)$ *and* $\lambda_{\min}(.)$ *indicate the maximum and minimum eigenvalues of the argument, respectively.*

Proof. According to Lemma 2 and condition (17), it is clear that augmented system (9) is impulse-free. Choose the Lyapunov function

$$V(X(t)) = X^T(t) E^T P E X(t) \geq 0, \forall t \in [0, T], \tag{19}$$

i.e., $V(X(t)) = V_1(x(t)) + V_2(\xi(t)) = x^T(t) E_1^T P_1 \; E_1 x(t) + \xi^T(t) E_2^T P_2 E_2 \xi(t) \geq 0$, where $P = \begin{bmatrix} P_1 & 0 \\ 0 & P_2 \end{bmatrix} = R^{(1/2)} Q R^{(1/2)}$.

Based on system (9),

$$\begin{aligned} \dot{V}(X(t)) - \alpha V(X(t)) &= X^T \left(A^T(X) P E + E^T P A(X) - \alpha E^T P E \right) X \\ &= \begin{bmatrix} x \\ \xi \end{bmatrix}^T \begin{bmatrix} \left(A_1(x) - g_1(x) K b_1(x)\right)^T P_1 E_1 + E_1^T P_1 \left(A_1(x) - g_1(x) K b_1(x)\right) - \alpha E_1^T P_1 E_1 & \left(g_1(x) K b_2(\xi)\right)^T P_1 E_1 - E_2^T P_2 \left(g_2(\xi) K b_1(x)\right) \\ -\left(g_2(\xi) K b_1(x)\right)^T P_2 E_2 + E_1^T P_1 \left(g_1(x) K b_2(\xi)\right) & \left(A_2(\xi) + g_2(\xi) K b_2(\xi)\right)^T P_2 E_2 + E_2^T P_2 \left(A_2(\xi) + g_2(\xi) K b_2(\xi)\right) - \alpha E_2^T P_2 E_2 \end{bmatrix} \begin{bmatrix} x \\ \xi \end{bmatrix} \\ &= \begin{bmatrix} x \\ \xi \end{bmatrix}^T \begin{bmatrix} \Omega_1 & \Omega_2 \\ \Omega_2^T & \Omega_3 \end{bmatrix} \begin{bmatrix} x \\ \xi \end{bmatrix}. \end{aligned} \tag{20}$$

Under condition (15), there is

$$\dot{V}(X(t)) \leq \alpha V(X(t)), \quad \forall t \in [0, T]. \tag{21}$$

Furthermore, by integrating the inequality (21) between 0 and t, it is clear that

$$V(X(t)) \leq e^{\alpha t} V(X(0)), \quad \forall t \in [0, T]. \tag{22}$$

Consider the following chain of inequalities:

$$V(X(t)) = X^T(t) E^T P E X(t) = X^T(t) E^T R^{(1/2)} Q R^{(1/2)} E X(t) \geq \lambda_{\min}(Q) X^T(t) E^T R E X(t), \tag{23}$$

$$V(X(0)) e^{\alpha t} = X^T(0) E^T P E X(0) = X^T(0) E^T R^{(1/2)} Q R^{(1/2)} E X(0) e^{\alpha t} \leq \lambda_{\max}(Q) X^T(0) E^T R E X(0) e^{\alpha T}, \tag{24}$$

where $\lambda_{\min}(Q) = \min\{\lambda_{\min}(Q_1), \lambda_{\min}(Q_2)\}$, and $\lambda_{\max}(Q) = \max\{\lambda_{\max}(Q_1), \lambda_{\max}(Q_2)\}$.

If $X^T(0) E^T R E X(0) \leq c_1$, taking account of (16), (22)–(24), it can be deduced that

$$\begin{aligned} X^T(t) E^T R E X(t) &\leq \frac{\lambda_{\max}(Q) X^T(0) E^T R E X(0)}{\lambda_{\min}(Q)} e^{\alpha T} \\ &\leq \frac{\lambda_{\max}(Q)(c_1)}{\lambda_{\min}(Q)} e^{\alpha T} \\ &< c_2. \end{aligned} \tag{25}$$

Hence, system (9) is finite-time stable with respect to (c_1, c_2, T, R).

To proceed further, systems (4) and (5) can be finite-time simultaneous stabilization with respect to (c_1, c_2, T, R). □

3. Finite-Time Simultaneous Stabilization of More than Two Nonlinear Singular Systems

Consider N nonlinear singular systems:

$$\begin{cases} E_i \dot{x}^i = f_i\left(x^i\right) + g_i\left(x^i\right) u, \\ E_i x^i(0) = E_i x_0^i, \\ f_i(0) = 0, \\ y_i = b_i\left(x^i\right) x^i, \quad i = 1, 2, \ldots, N, \end{cases} \tag{26}$$

where $x^i \in \mathbb{R}^{n_i}$, $y_i \in \mathbb{R}^m$, and $u \in \mathbb{R}^q$ are the states, the outputs, and the inputs of the N systems, respectively; $g_i(x^i) \in \mathbb{R}^{n_i \times q}$, $E_i \in \mathbb{R}^{n_i \times n_i}$, $0 < \operatorname{rank}(E_i) = r_i < n_i$, and $b_i(x) \in \mathbb{R}^{m \times n_i}$, $i = 1, 2, \ldots, N$.

Based on the method given in Section 2, we can represent system (26) into the following forms:

$$\begin{cases} E_i\dot{x}^i = A_i(x^i)x^i + g_i(x^i)u, \\ y_i = b_i(x^i)x^i, \quad i = 1, 2, \ldots, N. \end{cases} \tag{27}$$

Suppose that $(i_1, i_2, \ldots, i_N)$ is an arbitrary permutation of $1, 2, \ldots, N$ and that L is a position integer satisfying $1 \le L \le N-1$. Denote $T_1 = n_{i_1} + \cdots + n_{i_L}$ and $T_2 = n_{i_{L+1}} + \cdots + n_{i_N}$. We divide the N systems into two sets:

$$\begin{cases} E_a\dot{X}^a = A_a(X^a)X^a + G_a(X^a)u, \\ Y_a = B_a(X^a)X^a, \end{cases} \tag{28}$$

$$\begin{cases} E_b\dot{X}^b = A_b(X^b)X^b + G_b(X^b)u, \\ Y_b = B_b(X^b)X^b, \end{cases} \tag{29}$$

where

$$\begin{aligned} X^a &= \left[\left(x^{i_1}\right)^T, \ldots, \left(x^{i_L}\right)^T\right]^T \in \mathbb{R}^{T_1}, \\ X^b &= \left[\left(x^{i_{L+1}}\right)^T, \ldots, \left(x^{i_N}\right)^T\right]^T \in \mathbb{R}^{T_2}, \\ E_a &= \operatorname{diag}\left\{E_{i_1}, \ldots, E_{i_L}\right\}, \\ E_b &= \operatorname{diag}\left\{E_{i_{L+1}}, \ldots, E_{i_N}\right\}, \\ A_a(X^a) &= \operatorname{diag}\left\{A_{i_1}\left(x^{i_1}\right), \ldots, A_{i_L}\left(x^{i_L}\right)\right\}, \\ A_b(X^b) &= \operatorname{diag}\left\{A_{i_{L+1}}\left(x^{i_{L+1}}\right), \ldots, A_{i_L}\left(x^{i_N}\right)\right\}, \\ Y_a &= y_{i_1} + \cdots + y_{i_L}, \\ Y_b &= y_{i_{L+1}} + \cdots + y_{i_N}, \\ G_a(X^a) &= \left[g_{i_1}^T\left(x^{i_1}\right), \ldots, g_{i_L}^T\left(x^{i_L}\right)\right]^T, \\ G_b(X)^b &= \left[g_{i_{L+1}}^T\left(x^{i_{L+1}}\right), \ldots, g_{i_N}^T\left(x^{i_N}\right)\right]^T, \\ B_a(X^a) &= \left[b_{i_1}\left(x^{i_1}\right), \ldots, b_{i_L}\left(x^{i_L}\right)\right], \\ B_b(X^b) &= \left[b_{i_{L+1}}\left(x^{i_{L+1}}\right), \ldots, b_{i_N}\left(x^{i_N}\right)\right]. \end{aligned} \tag{30}$$

Design an output feedback controller:

$$u = -K(Y_a - Y_b) := -K\left(B_a(X^a)X^a - B_b(X^b)X^b\right), \tag{31}$$

where matrix $K \in \mathbb{R}^{m\times m}$ is the symmetric. Substitute (31) into systems (28) and (29), respectively. Then, the closed-loop systems can be given as follows:

$$\begin{cases} E_a\dot{X}^a = (A_a(X^a) - G_a(X^a)KB_a(X_a))X^a + G_a(X^a)KB_b(X^b)X^b, \\ Y_a = B_a(X^a)X^a, \end{cases} \tag{32}$$

$$\begin{cases} E_b\dot{X}^b = \left(A_b(X^b) + G_b(X^b)KB_b(X_b)\right)X^b - G_b(X^b)KB_a(X^a)X^a, \\ Y_b = B_b(X^b)X^b. \end{cases} \tag{33}$$

By the system-augmentation technique, systems (32) and (33) can be transformed as

$$\begin{cases} \overline{E}\,\dot{\overline{X}} = \overline{A}(\overline{X})\overline{X}, \\ \overline{Y} = \overline{B}(\overline{X})\overline{X}, \end{cases} \tag{34}$$

where

$$\begin{aligned} \overline{X} &= \begin{bmatrix} X^a \\ X^b \end{bmatrix}, \\ \overline{E} &= \begin{bmatrix} E_a & 0 \\ 0 & E_b \end{bmatrix}, \\ \overline{A} &= \begin{bmatrix} A_a - G_aKB_a & G_aKB_b \\ -G_bKB_a & A_b + G_bKB_b \end{bmatrix}, \\ \overline{Y} &= \begin{bmatrix} Y^a \\ Y^b \end{bmatrix}, \\ \overline{B} &= \begin{bmatrix} B_a & 0 \\ 0 & B_b \end{bmatrix}. \end{aligned} \tag{35}$$

Based on Theorem 1, we can obtain the following result.

Theorem 2. *If there exists a positive scalar α and symmetric positive definite matrices $\overline{Q} \in \mathbb{R}^{(T_1+T_2)\times(T_1+T_2)}$, $P_a \in \mathbb{R}^{T_1\times T_1}$, and $P_b \in \mathbb{R}^{T_2\times T_2}$, such that*

$$\begin{bmatrix} \Xi_1 & \Xi_2 \\ \Xi_2^T & \Xi_3 \end{bmatrix} \le 0, \tag{36}$$

$$\lambda_{\max}(\overline{Q})\overline{c}_1 e^{\alpha T} < \lambda_{\min}(\overline{Q})\overline{c}_2, \tag{37}$$

$$\operatorname{Rank}\begin{bmatrix} 0 & \overline{E} \\ \overline{E} & \overline{A}(\overline{X}) \end{bmatrix} = \sum_{i=1}^{N}(n_i + r_i), \tag{38}$$

then, under the output feedback control law (31), system (26) is finite-time simultaneous stabilization with respect to $(\overline{c}_1, \overline{c}_2, \overline{T}, \overline{R})$, where $\overline{c}_2 > \overline{c}_1 > 0$, $\overline{R} > 0$, K, $\lambda_{\max}(.)$, and $\lambda_{\min}(.)$ are the same as those in Theorem 1. Noted that,

$$\begin{aligned} \Xi_1 &= (A_a(X^a) - G_a(X^a)KB_a(X^a))^T P_aE_a + E_a^T P_a(A_a(X^a) - G_a(X^a)KB_a(X^a)) - \alpha E_a^T P_aE_a, \\ \Xi_2 &= \left(G_a(X^a)KB_b(X^b)\right)^T P_aE_a - E_b^T P_b\left(G_b(X^b)KB_a(X^a)\right), \\ \Xi_3 &= \left(A_b(X^b) + G_b(X^b)KB_b(X^b)\right)^T P_bE_b + E_b^T P_b\left(A_b(X^b) + G_b(X^b)KB_b(X^b)\right) - \alpha E_b^T P_bE_b. \end{aligned} \tag{39}$$

Proof. Taking the same as Theorem 1, system (34) is impulse-free depending on Lemma 2 and condition (38). We choose a Lyapunov function $V(\overline{X}(t)) = \overline{X}^T(t)\overline{E}^T\overline{P}\,\overline{E}\,\overline{X}(t) \geq 0, \forall t \in [0,T]$, where $\overline{P} = \begin{bmatrix} P_a & 0 \\ 0 & P_b \end{bmatrix} = \begin{bmatrix} R_a^{(1/2)} & 0 \\ 0 & R_b^{(1/2)} \end{bmatrix}\begin{bmatrix} Q_a & 0 \\ 0 & Q_b \end{bmatrix}\begin{bmatrix} R_a^{(1/2)} & 0 \\ 0 & R_b^{(1/2)} \end{bmatrix} = \overline{R}^{(1/2)}\ \overline{QR}^{(1/2)}$, and $\overline{Q}, \overline{P}, \overline{R}$ are the symmetric positive definite matrices.

Based on conditions (36) and (37), we have

$$\begin{aligned}
\dot{V}(\overline{X}) - \alpha V(\overline{X}) &= \overline{X}^T\left(\overline{E}^T\overline{P}\,\overline{A} + \overline{A}^T\overline{P}\,\overline{E} - \alpha\overline{E}\,\overline{P}\,\overline{E}\right)\overline{X} \\
&= \begin{bmatrix} X^a \\ X^b \end{bmatrix}^T \begin{bmatrix} (A_a(X^a) - G_a(X^a)KB_a(X^a))^T P_a E_a + E_a^T P_a (A_a(X^a) - G_a(X^a)KB_a(X^a)) - \alpha E_a^T P_a E_a & E_a^T P_a G_a(X^a)KB_b(X^b) - (G_b(X^b)KB_a(X^a))^T P_b E_b \\ (G_a(X^a)KB_b(X^b))^T P_a E_a - E_b^T P_b (G_b(X^b)KB_a(X^a)) & (A_b(X^b) + G_b(X^b)KB_b(X^b))^T P_b E_b + E_b^T P_b (A_b(X^b) + G_b(X^b)KB_b(X^b)) - \alpha E_b^T P_b E_b \end{bmatrix} \begin{bmatrix} X^a \\ X^b \end{bmatrix} \\
&= \begin{bmatrix} X^a \\ X^b \end{bmatrix}^T \begin{bmatrix} \Xi_1 & \Xi_2 \\ \Xi_2^T & \Xi_3 \end{bmatrix} \begin{bmatrix} X^a \\ X^b \end{bmatrix} \leq 0.
\end{aligned} \tag{40}$$

To sum up,

$$\dot{V}(\overline{X}(t)) \leq \alpha V(\overline{X}(t)). \tag{41}$$

By integrating inequality (41) between 0 and T with $t \in [0,T]$, the following result can be presented:

$$V(\overline{X}(t)) \leq e^{\alpha t} V(\overline{X}(0)). \tag{42}$$

Next, we will prove the finite-time simultaneous stabilization for more than two nonlinear singular systems.

It is straightforward to see

$$\begin{aligned}
V(\overline{X}(t)) &= \overline{X}^T(t)\overline{E}^T\overline{P}\,\overline{E}\,\overline{X}(t) = \overline{X}^T(t)\overline{E}^T\overline{R}^{(1/2)}\overline{QR}^{(1/2)}\overline{E}\,\overline{X}(t) \geq \lambda_{\min}(\overline{Q})\overline{X}^T(t)\overline{E}^T\overline{R}\,\overline{E}\,\overline{X}(t), \\
V(\overline{X}(0))e^{\alpha t} &= \overline{X}^T(0)\overline{E}^T\overline{P}\,\overline{E}\,\overline{X}(0)e^{\alpha t} = \overline{X}^T(0)\overline{E}^T\overline{R}^{(1/2)}\overline{QR}^{(1/2)}\overline{E}\,\overline{X}(0)e^{\alpha t} \leq \lambda_{\max}(\overline{Q})\overline{X}^T(0)\overline{E}^T\overline{R}\,\overline{E}\,\overline{X}(0)e^{\alpha T},
\end{aligned} \tag{43}$$

where $\lambda_{\max}(\overline{Q}) = \max\{\lambda_{\max}(Q_a), \lambda_{\max}(Q_b)\}$, and $\lambda_{\min}(\overline{Q}) = \min\{\lambda_{\min}(Q_a), \lambda_{\min}(Q_b)\}$. According to the concept of finite-time simultaneous stable, from $\overline{X}^T(0)\overline{E}^T\overline{R}\,\overline{E}\,\overline{X}(0) \leq \overline{c}_1$ and (37), we can obtain

$$\begin{aligned}
\overline{X}^T(t)\overline{E}^T\overline{R}\,\overline{E}\,\overline{X}(t) &\leq \frac{\lambda_{\max}(\overline{Q})\overline{X}^T(0)\overline{E}^T\overline{R}\,\overline{E}\,\overline{X}(0)}{\lambda_{\min}(\overline{Q})}e^{\alpha T} \\
&\leq \frac{\lambda_{\max}(\overline{Q})\overline{c}_1}{\lambda_{\min}(\overline{Q})}e^{\alpha T} < \overline{c}_2.
\end{aligned} \tag{44}$$

By using the similar method as that in Theorem 1, system (34) is finite-time stable with respect to $(\overline{c}_1, \overline{c}_2, \overline{T}, \overline{R})$, and it can be shown that system (26) is finite-time simultaneous stabilization with respect to $(\overline{c}_1, \overline{c}_2, \overline{T}, \overline{R})$. □

4. Illustrative Example

In this section, we present an example to illustrate the effectiveness of the proposed method which addresses the finite-time simultaneous stabilization problem of the two nonlinear singular systems.

Example 1. Consider the two nonlinear singular systems:

$$\begin{cases} E_1\dot{x} = f_1(x) + g_1(x)u, \\ E_1x(0) = E_1x_0, \\ f_1(0) = 0, \\ y = b_1(x)x, \end{cases} \tag{45}$$

$$\begin{cases} E_2\dot{\xi} = f_2(\xi) + g_2(\xi)u, \\ E_2\xi(0) = E_2\xi_0, \\ f_2(0) = 0, \\ \eta = b_2(\xi)\xi, \end{cases} \tag{46}$$

where $x = [x_1, x_2]^T \in \mathbb{R}^2, \xi = [\xi_1, \xi_2]^T \in \mathbb{R}^2, u \in \mathbb{R}^2$, we give the following parameters:

$$
\begin{aligned}
E_1 &= \begin{bmatrix} 1 & 2 \\ 1 & 2 \end{bmatrix}, \\
E_2 &= \begin{bmatrix} 1 & 1 \\ 0 & 0 \end{bmatrix}, \\
f_1(x) &= \begin{bmatrix} -2x_1x_2^2 - 4x_1 - 5x_2 \\ -5x_1 - 2x_2^3 - 1.5x_2 \end{bmatrix}, \\
f_2(\xi) &= \begin{bmatrix} -0.55\xi_1\xi_2^2 - 2.3\xi_1 + 5\xi_2 \\ 5\xi_1 - 2.2\xi_2^3 - 2\xi_2 \end{bmatrix}, \\
g_1(x) &= \begin{bmatrix} -1 & 0 \\ 0 & -1 \end{bmatrix}, \\
g_2(\xi) &= \begin{bmatrix} -1 & 0 \\ 0 & -1 \end{bmatrix}, \\
b_1(x) &= \begin{bmatrix} 1 & 0 \\ 0 & 1 \end{bmatrix}, \\
b_2(\xi) &= \begin{bmatrix} 1 & 0 \\ 0 & 1 \end{bmatrix}.
\end{aligned} \tag{47}
$$

Based on Lemma 1, it can deduce that

$$
\begin{aligned}
A_1(x) &= \begin{bmatrix} -2x_2^2 - 4 & -5 \\ -5 & -2x_2^2 - 1.5 \end{bmatrix}, \\
A_2(\xi) &= \begin{bmatrix} -0.55\xi_2^2 - 2.3 & 5 \\ 5 & -2.2\xi_2^2 - 2 \end{bmatrix}.
\end{aligned} \tag{48}
$$

Design an output feedback controller

$$
\begin{aligned}
u &= -K(y - \eta) = -\begin{bmatrix} 3 & 5 \\ 5 & 0.5 \end{bmatrix} \begin{bmatrix} x_1 - \xi_1 \\ x_2 - \xi_2 \end{bmatrix} \\
&= \begin{bmatrix} -3x_1 - 5x_2 + 3\xi_1 + 5\xi_2 \\ -5x_1 - 0.5x_2 + 5\xi_1 + 0.5\xi_2 \end{bmatrix}.
\end{aligned} \tag{49}
$$

Substituting (49) into systems (45) and (46), respectively, we obtain

$$
\begin{cases} E_1\dot{x} = \left(A_1(x) - g_1(x)Kb_1(x)\right)x + g_1(x)Kb_2(\xi), \\ y = b_1(x)x, \end{cases} \tag{50}
$$

$$
\begin{cases} E_2\dot{\xi} = \left(A_2(\xi) + g_2(\xi)Kb_2(\xi)\right)\xi - g_2(\xi)Kb_1(x), \\ \eta = b_2(\xi)\xi. \end{cases} \tag{51}
$$

Based on form (9), we have

$$
\begin{cases} E\dot{X} = A(X)X, \\ Y = B(X)X, \end{cases} \tag{52}
$$

where

$$
\begin{aligned}
X &= [x\ \xi]^T = \begin{bmatrix} x_1 \\ x_2 \\ \xi_1 \\ \xi_2 \end{bmatrix}, \\
E &= \begin{bmatrix} 1 & 2 & 0 & 0 \\ 1 & 2 & 0 & 0 \\ 0 & 0 & 1 & 1 \\ 0 & 0 & 0 & 0 \end{bmatrix}, \\
B &= \begin{bmatrix} 1 & 0 & 0 & 0 \\ 0 & 1 & 0 & 0 \\ 0 & 0 & 1 & 0 \\ 0 & 0 & 0 & 1 \end{bmatrix}, \\
A(X) &= \begin{bmatrix} -2x_2^2 - 1 & 0 & -3 & -5 \\ 0 & -2x_2^2 - 1 & -5 & -0.5 \\ 3 & 5 & -0.55\xi_2^2 - 5.3 & 0 \\ 5 & 0.5 & 0 & -2.2\xi_2^2 - 2.5 \end{bmatrix}.
\end{aligned} \tag{53}
$$

Choose

$$
\begin{aligned}
M &= \begin{bmatrix} 1 & 0 & 0 & 0 \\ 0 & 0 & 1 & 0 \\ -1 & 1 & 0 & 0 \\ 0 & 0 & 0 & 1 \end{bmatrix}, \\
N &= \begin{bmatrix} 1 & 0 & 0 & -2 \\ 0 & 0 & 0 & 1 \\ 0 & 0 & 1 & 0 \\ 0 & 1 & -1 & 0 \end{bmatrix}.
\end{aligned} \tag{54}
$$

According to Lemma 2, we can easy check that the augmented system is impulse-free.

Next, we give Lyapunov function $V(X(t)) = X^T(t)E^TPEX(t)$, where $P = \begin{bmatrix} 1 & 0 & 0 & 0 \\ 0 & 2 & 0 & 0 \\ 0 & 0 & 2 & 0 \\ 0 & 0 & 0 & 4 \end{bmatrix}$. Let

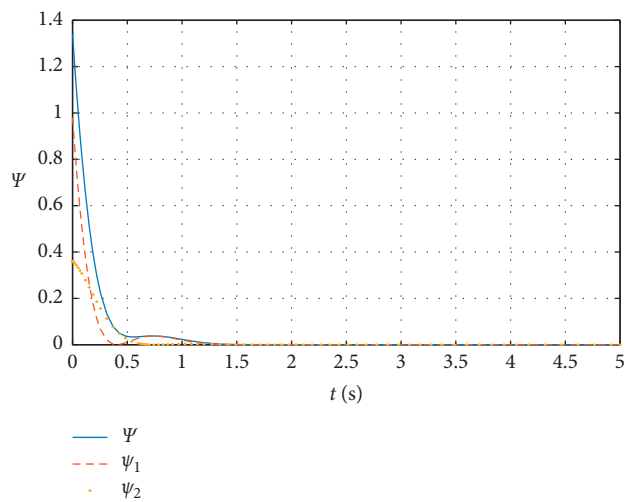

Figure 1: Responses of the values ψ, ψ_1, and ψ_2.

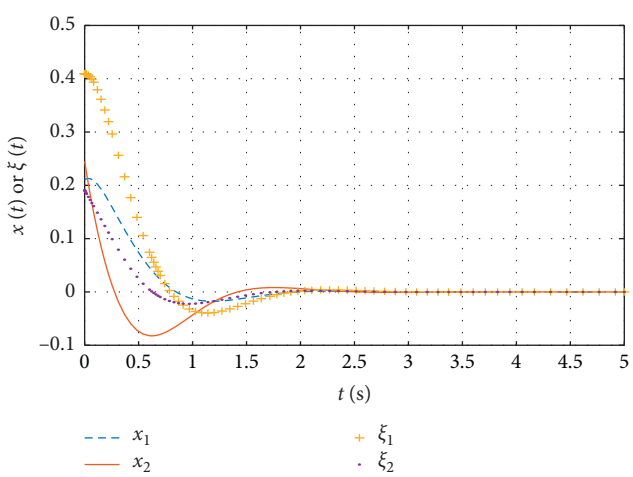

Figure 2: Responses of the state x and ξ.

$\alpha = 0.2, Q = P, R = I, c_1 = 1.34, c_2 = 8.75$, and $T = 2$. By the virtue of conditions (15) and (16) in Theorem 1, we have

$$\begin{bmatrix} \Omega_1 & \Omega_2 \\ \Omega_2^T & \Omega_3 \end{bmatrix} = \begin{bmatrix} -4x_2^2 - 2.6 & -8x_2^2 - 5.2 & -7 & -16 \\ -8x_2^2 - 5.2 & -16x_2^2 - 10.4 & 0 & -2 \\ -7 & 0 & -2.2\xi_2^2 - 21.2 & -1.1\xi_2^2 - 10.6 \\ -16 & -2 & -1.1\xi_2^2 - 10.6 & -0.4 \end{bmatrix} \leq 0, \tag{55}$$

$$\frac{\lambda_{\max}(Q) c_1 e^{\alpha T}}{\lambda_{\min}(Q)} = \frac{4c_1}{1} e^{0.2T} < c_2.$$

Choose the initial state $E_1 x(0) = [0.7, 0.7]^T$ and $E_2 \xi(0) = [0.6, 0]^T$, then $X(0)^T E^T R E X(0) \leq c_1$, the trajectory of $\Psi = X(t)^T E^T R E X(t) < c_2, \forall t \in [0, 2]$. Denote $\psi_1 = x(t)^T E_1^T R_1 E_1 x(t)$ and $\psi_2 = \xi(t)^T E_2^T R_2 E_2 \xi(t)$. The trajectories of Ψ, ψ_1 and ψ_2, state response, and control signal are shown in Figures 1–3, respectively. Obviously, the

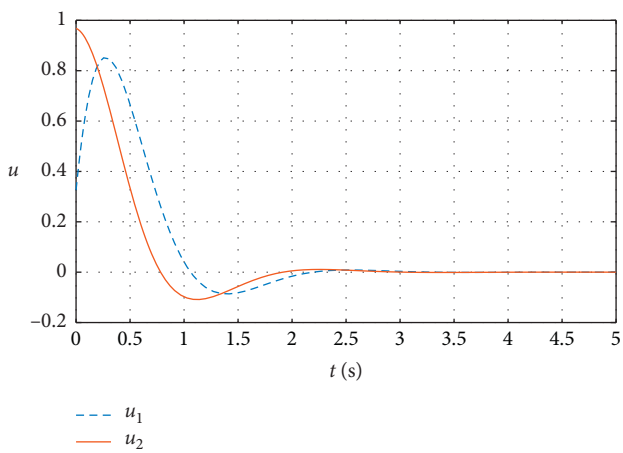

Figure 3: Responses of the control signal u.

augmented nonlinear singular system (52) is finite-time stable with respect to $(1.34, 8.75, 2, I)$. Hence, under the output feedback controller (49), systems (45) and (46) are finite-time simultaneous stabilization.

5. Conclusion

The finite-time simultaneous stabilization problem is considered for the two nonlinear singular systems or more than two nonlinear singular systems in this study. Under a suitable output feedback controller, the augmented singular system is first proved to be impulse-free and then is proved to be finite-time simultaneous stable by using the system-augmented technique. Finally, the finite-time simultaneous stabilization problem of more than two nonlinear singular systems is investigated with the same method. Moreover, the proposed method in this study can be extended to handle finite-time H_∞ simultaneous stabilization of the two or more than two nonlinear singular systems.

Data Availability

The data used to support the findings of this study are available from the corresponding author upon request.

Conflicts of Interest

The authors declare that they have no conflicts of interest.

References

[1] L. Dai, *Singular Control Systems*, Springer-Verlag, Berlin, Germany, 1989.

[2] X. Wang, A. Saberi, A. A. Stoorvogel, and P. Sannuti, "Simultaneous global external and internal stabilization of linear time-invariant discrete-time systems subject to actuator saturation," *Automatica*, vol. 48, no. 5, pp. 699–711, 2012.

[3] S. Kim, Y. Moon, and S. Kwon, "Simultaneous stabilization by static output feedback: a rank-constrained LMI approach," in *Proceedings of the IEEE Conference on Decision and Control*, pp. 5162–5167, San Diego, CA, USA, December 2006.

[4] H.-B. Chen, J. H. Chow, M. A. Kale, and K. D. Minto, "Simultaneous stabilization using stable system inversion," *Automatica*, vol. 31, no. 4, pp. 531–542, 1995.

[5] J. Jenq-Lang Wu, "Simultaneous quadratic stabilization for discrete-time nonlinear systems," *IEEE Transactions on Automatic Control*, vol. 55, no. 6, pp. 1443–1448, 2010.

[6] Y. Wang, G. Feng, and D. Cheng, "Simultaneous stabilization of a set of nonlinear port-controlled Hamiltonian systems," *Automatica*, vol. 43, no. 3, pp. 403–415, 2007.

[7] L. Sun, "Parallel simultaneous stabilization of a class of nonlinear descriptor systems with actuator saturation," in *Proceedings of the 34th Chinese Control Conference*, pp. 856–860, Hangzhou, China, July 2015.

[8] Y. Chen, T. Xu, C. Zeng, Z. Zhou, and Q. Zhang, "Simultaneous stabilization for uncertain descriptor systems with input saturation," *International Journal of Robust and Nonlinear Control*, vol. 22, no. 17, pp. 1938–1951, 2012.

[9] F. Amato, M. Ariola, and P. Dorato, "Finite-time control of linear systems subject to parametric uncertainties and disturbances," *Automatica*, vol. 37, no. 9, pp. 1459–1463, 2001.

[10] F. Amato, M. Ariola, and C. Cosentino, "Finite-time stabilization via dynamic output feedback," *Automatica*, vol. 42, no. 2, pp. 337–342, 2006.

[11] J. Feng, Z. Wu, J. Sun et al., "5^{th}Finite time control of linear singular systems subject to parametric uncertain and disturbances," in *Proceedings of the World Congress on Intelligence Control and Automation*, vol. 2, no. 2, pp. 1002–1006, Hangzhou, China, October 2004.

[12] X. Lu, X. Zhang, and L. Sun, "Finite-time H ∞ control for nonlinear discrete Hamiltonian descriptor systems," *Journal of the Franklin Institute*, vol. 354, no. 14, pp. 6138–6151, 2017.

[13] R. Yang and Y. Wang, "Stability for a class of nonlinear time-delay systems via Hamiltonian functional method," *Science China Information Sciences*, vol. 55, no. 5, pp. 1218–1228, 2012.

[14] X. Yi, R. Guo, and Y. Qi, "Stabilization of chaotic systems with both uncertainty and disturbance by the UDE-based control method," *IEEE Access*, vol. 8, no. 1, pp. 62471–62477, 2020.

[15] L. Liu, B. Li, and R. Guo, "Consensus control for networked manipulators with switched parameters and topologies," *IEEE Access*, vol. 9, pp. 9209–9217, 2021.

[16] T. Hou, Y. Liu, and F. Deng, "Stability for discrete-time uncertain systems with infinite Markov jump and time-delay," *Science China: Information Sciences*, vol. 64, p. 1C11, 2021.

[17] R. Peng, C. Jiang, and R. Guo, "Stabilization of a class of fractional order systems with both uncertainty and disturbance," *IEEE Access*, vol. 9, pp. 42697–42706, 2021.

[18] M. Li, L. Sun, and R. Yang, "Finite-time H∞ control for a class of discrete-time nonlinear singular systems," *Journal of the Franklin Institute*, vol. 355, no. 13, pp. 5384–5393, 2018.

[19] M. Li and L. Sun, "Finite-time stabilisation for a class of nonlinear descriptor systems," *IET Control Theory and Applications*, vol. 12, no. 17, pp. 2399–2406, 2018.

[20] J. Wang, S. Ma, and C. Zhang, "Finite-time H ∞ filtering for nonlinear continuous-time singular semi-markov jump systems," *Asian Journal of Control*, vol. 21, no. 2, pp. 1017–1027, 2019.

[21] X. Su and X. Zhao, "Robust finite-time control of descriptor Markovian jump systems with impulsive," *Advances in Difference Equations*, vol. 2019, no. 1, Article ID 196, 2019.

[22] M. Luo, S. Zhong, and J. Cheng, "Simultaneous finite-time control and fault detection for singular markovian jump delay systems with average dwell time constraint," *Circuits, Systems, and Signal Processing*, vol. 37, no. 12, pp. 5279–5310, 2018.

[23] R. Yang and R. Guo, "Adaptive finite-time robust control of nonlinear delay Hamiltonian systems via Lyapunov-Krasovskii method," *Asian Journal of Control*, vol. 20, no. 1, pp. 332–342, 2018.

[24] R. Yang and L. Sun, "Finite-time robust control of a class of nonlinear time-delay systems via Lyapunov functional method," *Journal of the Franklin Institute*, vol. 356, no. 3, pp. 1155–1176, 2019.

[25] R. Yang, F. Zang, L. Sun, P. Zhou, and B. Zhang, "Finite-time adaptive robust control of nonlinear time-delay uncertain systems with disturbance," *International Journal of Robust and Nonlinear Control*, vol. 29, no. 4, pp. 919–934, 2019.

[26] R. Yang, G. Zhang, and L. Sun, "Observer-based finite-time robust control of nonlinear time-delay systems via Hamiltonian function method," *International Journal of Control*, vol. 4, pp. 1–18, 2020.

[27] R. Yang, L. Sun, G. Zhang, and Q. Zhang, "Finite-time stability and stabilization of nonlinear singular time-delay systems via Hamiltonian method," *Journal of the Franklin Institute*, vol. 356, no. 12, pp. 5961–5992, 2019.

[28] R. Yang, G. Zhang, and L. Sun, "Finite-time robust simultaneous stabilization of a set of nonlinear time-delay systems," *International Journal of Robust and Nonlinear Control*, vol. 30, no. 5, pp. 1733–1753, 2020.

[29] R. Yang, W. Pei, Y. Han, and L. Sun, "Finite-time adaptive robust simultaneous stabilization of nonlinear delay systems by the Hamiltonian function method," *Science China Information Sciences*, vol. 64, no. 6, Article ID 169201, 2021.

[30] H. Xu and K. Mizukami, "Hamilton-Jacobi equation for descriptor systems," *Systems and Control Letters*, vol. 21, no. 4, pp. 321–327, 1993.

[31] W. Langson and A. Allcync, "Infinite horizon optimal control of a class of nonlinear systems," in *Proceedings of the 1997 American Control Conference*, vol. 5, no. 1, pp. 3017–3022, Albuquerque, New Mexico, June 1997.

Hindawi
Mathematical Problems in Engineering
Volume 2021, Article ID 4152160, 10 pages
https://doi.org/10.1155/2021/4152160

Research Article

Synchronization Problem of a Novel Fractal-Fractional Orders' Hyperchaotic Finance System

Yaru Zhang[1] and Yingxue Du[2]

[1]*School of Mathematics and Statistics, Qilu University of Technology (Shandong Academy of Sciences), Jinan 250353, China*
[2]*School of Automation and Electrical Engineering, Linyi University, Linyi 276005, China*

Correspondence should be addressed to Yingxue Du; duyingxue@yeah.net

Received 7 May 2021; Accepted 3 June 2021; Published 19 June 2021

Academic Editor: Yi Qi

This paper investigates the synchronization problem of a novel fractal-fractional (FF) orders' hyperchaotic finance system with model uncertainty and external disturbance. Firstly, a controller is designed to realize the synchronization of the nominal FF-orders' hyperchaotic finance system. Secondly, a suitable filer is designed to estimate uncertainty and disturbance, and then, the uncertainty and disturbance estimator- (UDE-) based control method is proposed to realize the synchronization problem of such system. Finally, numerical simulations are carried out to verify the correctness and the effectiveness of the obtained results.

1. Introduction

The fractional calculus was introduced in 1695, and it is the generalization of integer-order calculus. Fractional calculus is a research hotspot in many scientific fields, especially in mathematics and engineering. Different to the integer-order calculus, fractional derivatives can describe long-term memory, as detailed in [1–6]. Chaotic motion is an advanced form of complex motion. Its most important characteristic is its high sensitivity to initial values, that is, small differences in initial values will lead to huge differences in system states. Since Lorenz proposed the first chaotic system in 1963, many researchers have begun to study this chaotic phenomenon. Over the past few decades, chaos and fractals have been treated differently for different purposes. Chaotic theory was introduced to capture multifaceted systems that exhibit impulsive randomness and are very sensitive to small changes in conditions. Fractals are created to replicate infinitely complex patterns that are self-similar at different scales. In recent years, the FF-orders' problem has been expressed in [7–18]. The results show that the FF-order model is more suitable for practical problems than the integer-order model. In recent years, the synchronization of fractional-order chaotic systems has attracted great attention, and various control methods have been proposed, such as adaptive control [19, 20], active control [21], passive control [22], and sliding model control [23]. Although scholars have made great efforts in the control of fractional-order chaotic systems, there are still many challenges and problems to be solved. For example, the uncertainty of the system has not taken into account the control channels and control technologies designed in many controllers and control combinations [24–26]. It is well known that chaotic systems are very sensitive to parametric and external perturbations. Therefore, it is difficult to synchronize chaotic systems with parametric perturbations and external perturbations. Fortunately, some work has been done on the synchronization problem of integer-order chaotic systems with parametric and external perturbations. But, the results of synchronization research for chaotic systems with model uncertainty and external disturbance have some limitations, such as model uncertainties and external perturbations are assumed to be bounded, and these bounds are usually small. Moreover, the obtained method is based on linear matrix inequality (LMI) tools, thus the obtained results are conservative in some sense. Recently, the UDE-based control method has shown some advantages over the aforementioned results, see [27–34]. Therefore, we shall apply the

existing UDE-based control method to study the synchronization problem of the FF hyperchaotic finance system.

Inspired by the above discussion, we consider the newly defined FF-operators of fractional calculus, which are defined in the Caputo sense. In this paper, we investigate the synchronization of the FF hyperchaotic finance system with model uncertainty and external disturbance and propose a new UDE-based control method to realize the synchronization of the FF hyperchaotic finance system. Numerical simulations are carried out to verify the effectiveness and validity of the obtained theoretical results.

2. Preliminaries and Problem Formation

2.1. Preliminaries. Firstly, we introduce the definition of the FF-order differential equation in the Caputo sense and some preliminaries of fractional-order chaotic systems.

Consider the following FF-order differential equation in the Caputo sense:

$$ {}^{C}D_t^{\alpha,\beta} f(x) = \xi f(x), \quad n-1 < \alpha \text{ and } \beta \le n. \tag{1} $$

Definition 1 (see [13]). Let $f(x)$ be differentiable in opened interval (a,b); if $f(x)$ is fractal differentiable on (a,b) with order β, then the FF-derivative of $f(x)$ of order α in the Caputo sense with the power law is given as

$$ {}^{C}D_t^{\alpha,\beta} f(x) = \frac{1}{\Gamma(n-\alpha)} \int_a^t (t-\tau)^{n-\alpha-1} \frac{\mathrm{d}^n f(\tau)}{\mathrm{d}t^\beta} |d|\tau. \tag{2} $$

Then, some properties of fractional calculus are introduced.

Property 1 (see [35]). The fractional-order calculus defined by Caputo is a linear operator and satisfies

$$ D_t^{\alpha}(\lambda f(t) + \mu g(t)) = \lambda D_t^{\alpha,\beta} f(t) + \mu D_t^{\alpha,\beta} g(t). \tag{3} $$

Proof. where λ and μ are real constants. □

Property 2 (see [36]). For fractional-order nonlinear system (1), $f(x)$ meets the following Lipschitz condition:

$$ \|f(y) - f(x)\| \le L\|y - x\|. \tag{4} $$

Proof. where $\|\cdot\|$ is an ∞-norm and L is a positive real number. □

Property 3 (see [36]). Let $x \in R$ be a continuous differentiable function, and for any continuous time $t \ge t_0$, i.e.,

$$ \frac{1}{2} D_t^{\alpha} x^2 \le x D_t^{\alpha} x, \quad 0 < \alpha < 1. \tag{5} $$

2.2. Problem Formation. The FF hyperchaotic finance system is given in the following form:

$$ {}^{C}D_t^{\alpha,\beta} x = f(x) + u_d + Bu, \tag{6} $$

where $x \in R^4$ is the state and $u_d = \Delta f(x) + d(t)$ is the uncertainty and disturbance, i.e.,

$$ \begin{aligned} f(x) &= \begin{pmatrix} f_1(x) \\ f_2(x) \\ f_3(x) \\ f_4(x) \end{pmatrix} = \begin{pmatrix} x_3 + (x_2 - 0.9)x_1 + x_4 \\ 1 - 0.1x_2 - x_1^2 \\ -x_1 - x_3 \\ -0.05x_1x_3 - 0.6x_4 \end{pmatrix}, \\ B &= \begin{pmatrix} 1 & 0 \\ 0 & 0 \\ 0 & 0 \\ 0 & 1 \end{pmatrix}, \\ \Delta f(x) &= \begin{pmatrix} 0.03x_1x_3 \\ 0 \\ 0 \\ 0.2x_1x_3 \end{pmatrix}, \\ d(t) &= \begin{pmatrix} 1000 \\ 0 \\ 0 \\ 500 \end{pmatrix}, \end{aligned} \tag{7} $$

or

$$ d(t) = \begin{pmatrix} \sin(t) \\ 0 \\ 0 \\ 3\sin(t) \end{pmatrix}, \tag{8} $$

where u is the controller to be designed.

Let system (6) be the master system; then, the corresponding slave system is

$$ {}^{C}D_t^{\alpha,\beta} y = f(y), \tag{9} $$

where

$$y = \begin{pmatrix} y_1 \\ y_2 \\ y_3 \\ y_4 \end{pmatrix},$$
$$f(y) = \begin{pmatrix} f_1(y) \\ f_2(y) \\ f_3(y) \\ f_4(y) \end{pmatrix} = \begin{pmatrix} y_3 + (y_2 - 0.9)y_1 + y_4 \\ 1 - 0.1y_2 - y_1^2 \\ -y_1 - y_3 \\ -0.05y_1y_3 - 0.6y_4 \end{pmatrix}. \tag{10}$$

The error system $(e = x - y)$ is presented as

$$^{C}D_t^{\alpha,\beta} e = f(x) - f(y) + u_d + Bu, \tag{11}$$

where $e \in R^4$ is the state, u_d and B are given in equation (6), and

$$f(x) - f(y) = \begin{pmatrix} e_3 - 0.9e_1 + e_4 - e_1e_2 + x_2e_1 + x_1e_2 \\ -0.1e_2 - 2x_1e_1 + e_1^2 \\ -e_1 - e_3 \\ 0.05e_1e_3 - 0.05x_3e_1 - 0.05x_1e_3 - 0.6e_4 \end{pmatrix}. \tag{12}$$

The main goal of this paper is to design a controller u to meet the following performance:

$$\lim_{t \longrightarrow +\infty} \|e(t)\| = 0. \tag{13}$$

3. Main Results

The stabilization of error system (11) with $u_d = 0$ is firstly stabilized by the controller u_s, and a conclusion is obtained as follows.

Theorem 1. *Conside error system (11) with $u_d = 0$. If $(f(x) - f(y), B)$ can be stabilized, then the controller u_s is designed as*

$$u_s = \begin{pmatrix} u_1 \\ u_2 \\ u_3 \\ u_4 \end{pmatrix} = \begin{pmatrix} -e_4 - x_2e_1 + x_1e_2 \\ 0 \\ 0 \\ -0.05e_1e_3 + 0.05x_3e_1 + 0.05x_1e_3 \end{pmatrix}. \tag{14}$$

Proof. Define the following nonnegative function:

$$V = \frac{1}{2}\left(e_1^2 + e_2^2 + e_3^2 + e_4^2\right). \tag{15}$$

From Property 1, we get

$$^{C}D_t^{\alpha,\beta} V = \frac{1}{2}{}^{C}D_t^{\alpha,\beta} e_1^2 + \frac{1}{2}{}^{C}D_t^{\alpha,\beta} e_2^2 + \frac{1}{2}{}^{C}D_t^{\alpha,\beta} e_3^2 + \frac{1}{2}{}^{C}D_t^{\alpha,\beta} e_4^2. \tag{16}$$

From Property 3, it results in

$$\begin{cases} \frac{1}{2}{}^{C}D_t^{\alpha,\beta} e_1^2 \le e_1{}^{C}D_t^{\alpha,\beta} e_1 = e_1\left(e_3 - 0.9e_1 + e_4 - e_1e_2 + x_2e_1 + x_1e_2 + u_1\right), \\ \frac{1}{2}{}^{C}D_t^{\alpha,\beta} e_2^2 \le e_2{}^{C}D_t^{\alpha,\beta} e_2 = e_2\left(-0.1e_2 - 2x_1e_1 + e_1^2\right), \\ \frac{1}{2}{}^{C}D_t^{\alpha,\beta} e_3^2 \le e_3{}^{C}D_t^{\alpha,\beta} e_3 = e_3\left(-e_1 - e_3\right), \\ \frac{1}{2}{}^{C}D_t^{\alpha,\beta} e_4^2 \le e_4{}^{C}D_t^{\alpha,\beta} e_4 = e_4\left(0.05e_1e_3 - 0.05x_3e_1 - 0.05x_1e_3 - 0.6e_4 + u_4\right). \end{cases} \tag{17}$$

Calculating the Caputo derivative of V along the system in equation (15):

$$\begin{aligned}
{}^{C}D_t^{\alpha,\beta}V &= \frac{1}{2}{}^{C}D_t^{\alpha,\beta}\left(e_1^2+e_2^2+e_3^2+e_4^2\right)\\
&= \frac{1}{2}{}^{C}D_t^{\alpha,\beta}e_1^2+\frac{1}{2}{}^{C}D_t^{\alpha,\beta}e_2^2+\frac{1}{2}{}^{C}D_t^{\alpha,\beta}e_3^2+\frac{1}{2}{}^{C}D_t^{\alpha,\beta}e_4^2\\
&\le e_1{}^{C}D_t^{\alpha,\beta}e_1+e_2{}^{C}D_t^{\alpha,\beta}e_2+e_3{}^{C}D_t^{\alpha,\beta}e_3+e_4{}^{C}D_t^{\alpha,\beta}e_4\\
&= e_1\left(e_3-0.9e_1+e_4-e_1e_2+x_2e_1+x_1e_2+u_1\right)+e_2\left(-0.1e_2-2x_1e_1+e_1^2\right)\\
&\quad+e_3\left(-e_1-e_3\right)+e_4\left(0.05e_1e_3-0.05x_3e_1-0.05x_1e_3-0.6e_4+u_4\right)\\
&= e_1\left(e_3-0.9e_1+e_4-e_1e_2+x_2e_1+x_1e_2\right)+e_1\left(-e_4-x_2e_1+x_1e_2\right)\\
&\quad+e_2\left(-0.1e_2-2x_1e_1+e_1^2\right)+e_3\left(-e_1-e_3\right)\\
&\quad+e_4\left(0.05e_1e_3-0.05x_3e_1-0.05x_1e_3-0.6e_4+e_4\left(-0.05e_1e_3+0.05x_3e_1+0.05x_1e_3\right)\right.=-ae_1^2-be_2^2-ce_3^2-de_4^2\le 0.
\end{aligned} \tag{18}$$

Therefore, master system (6) with $u_d = 0$ synchronizes slave system (9) by the controller u_s.

Then, error system (11) is stabilized, and a result is presented as follows. □

Theorem 2. *Consider error system (11). If $(f(x)-f(y), B)$ can be stabilized and there exists a suitable filter $g_f(t)$ such that*

$$\tilde{u}_d = u_d - \hat{u}_d \longrightarrow 0, \quad t \longrightarrow \infty, \tag{19}$$

where

$$\hat{u}_d = u_d * g_f(t) = \left(D_t^{\alpha}e - F(x,e) - Bu_{ude}\right) * g_f(t), \tag{20}$$

and u_d satisfies the following structural constraints:

$$\left[I_n - BB^{+}\right]u_d \equiv 0, \tag{21}$$

where I_n is the identity matrix of order n; then, the UDE-based controller u is designed as

$$u = u_s + u_{ude}, \tag{22}$$

where u_s is given in equation (15), and

$$u_{ude} = \begin{cases} u_{ude\,1} = B^{+}\left\{\ell^{-1}\left[\dfrac{G_f(s)}{1-G_f(s)}\right] * F(e_1) - \ell^{-1}\left[\dfrac{s^{\alpha}G_f(s)}{1-G_f(s)}\right] * e_1(t)\right\},\\[2ex] u_{ude\,2} = B^{+}\left\{\ell^{-1}\left[\dfrac{G_f(s)}{1-G_f(s)}\right] * F(e_4) - \ell^{-1}\left[\dfrac{s^{\alpha}G_f(s)}{1-G_f(s)}\right] * e_4(t)\right\},\end{cases} \tag{23}$$

$0<\alpha\le 1$, $F(x,e) = f(x)-f(y)+Bu_s$, $B^{+} = (B^TB)^{-1}B^T$, $G_f(s) = \ell[g_f(t)]$, ℓ represents Laplace transform, ℓ^{-1} represents Laplace inverse transform, and $*$ represents convolution.

Proof. Substituting the controller u given in equation (22) into error system (11), we obtain

$$D_t^{\alpha}e(t) = F(x,e) + u_d + Bu_{ude}, \tag{24}$$

where $F(x,e) = f(x)-f(y)+Bu_s$. Note that

$$u_d = D_t^{\alpha}e(t) - F(x,e) - B_{ude}, \tag{25}$$

and the system $D_t^{\alpha}e(t) = F(x,e)$ is asymptotically stable according to Theorem 1.

According to condition given in equation (19), if the controller u_{ude} meets the following equation

$$\begin{aligned} Bu_{ude} &= -\hat{u}_d = -u_d * g_f(t)\\ &= -\left(D_t^{\alpha}e(t) - F(x,e) - Bu_{ude}\right) * g_f(t), \end{aligned} \tag{26}$$

then this controller is proposed.

Taking the Laplace transform of both sides of equation (26), it yields that

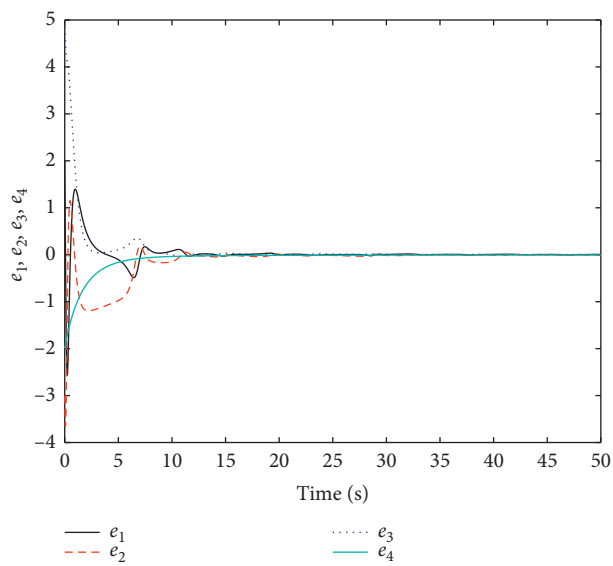

Figure 1: Error system (11) is also asymptotically stable.

$$Bu_{ude}(s) = -s^{\alpha}e(s)G_f(s) + F(s)G_f(s) + Bu_{ude}(s)G_f(s), \tag{27}$$

i.e.,

$$Bu_{ude}(s) - Bu_{ude}(s)G_f(s) = -s^{\alpha}e(s)G_f(s) + F(s)G_f(s). \tag{28}$$

Furthermore, we obtain

$$u_{ude}(s) = B^{+}\left\{\left[\frac{G_f(s)}{1-G_f(s)}\right]F(s) - \left[\frac{s^{\alpha}G_f(s)}{1-G_f(s)}\right]e(s)\right\}, \tag{29}$$

that is,

$$u_{ude}(t) = B^{+}\left\{\ell^{-1}\left[\frac{G_f(s)}{1-G_f(s)}\right] * F(x,e)\right\} - B^{+}\left\{\ell^{-1}\left[\frac{s^{\alpha}G_f(s)}{1-G_f(s)}\right] * e(t)\right\}, \tag{30}$$

$0 < \alpha \leq 1$, which completes the proof. □

4. Numerical Simulations

In this section, we use MATLAB to do the numerical simulation of the FF hyperchaotic finance system in the sense of Caputo. Firstly, the numerical simulation of the nominal FF hyperchaotic finance system is carried out. Then, the numerical simulation of the FF hyperchaotic finance system with model uncertainty and external disturbance is carried out.

4.1. Numerical Simulation of the Nominal FF Hyperchaotic Finance System. Numerical simulation is carried out by choosing the initial conditions of master system (6): $x(0) = [5, 2, 4, -1]^T$, the initial conditions of slave system (9): $y(0) = [3, 5, -1, 1]^T$, and $\alpha = 0.95$ and $\beta = 1$. Figure 1 shows that error system (11) is asymptotically stable, that is to say, master system (6) and slave system (9) realize complete synchronization. The states of master system (6) and slave system (9) are displayed in Figure 2, respectively.

4.2. Numerical Simulation of the FF Hyperchaotic Finance System with Model Uncertainty and External Disturbance. Numerical simulation of the FF hyperchaotic finance system with model uncertainty and external disturbance is carried out. Noted that external disturbance is $d(t)$ two cases are presented as follows.

When the external disturbance $d(t)$ is constant, i.e.,

$$d(t) = \begin{pmatrix} 1000 \\ 0 \\ 0 \\ 500 \end{pmatrix}. \tag{31}$$

Numerical simulation is carried out with the initial conditions of master system (6) and slave system (9): $x(0) = [5, 2, 4, -1]^T$ and $y(0) = [3, 5, -1, 1]^T$, respectively, and $\alpha = 0.95$, and $\beta = 1$. Figure 3 displays that error system (11) is also asymptotically stable, which implies that master system (6) and slave system (9) reach complete synchronization. The states of master system (6) and slave system (9) are shown in Figure 4, respectively. Figure 5 demonstrates

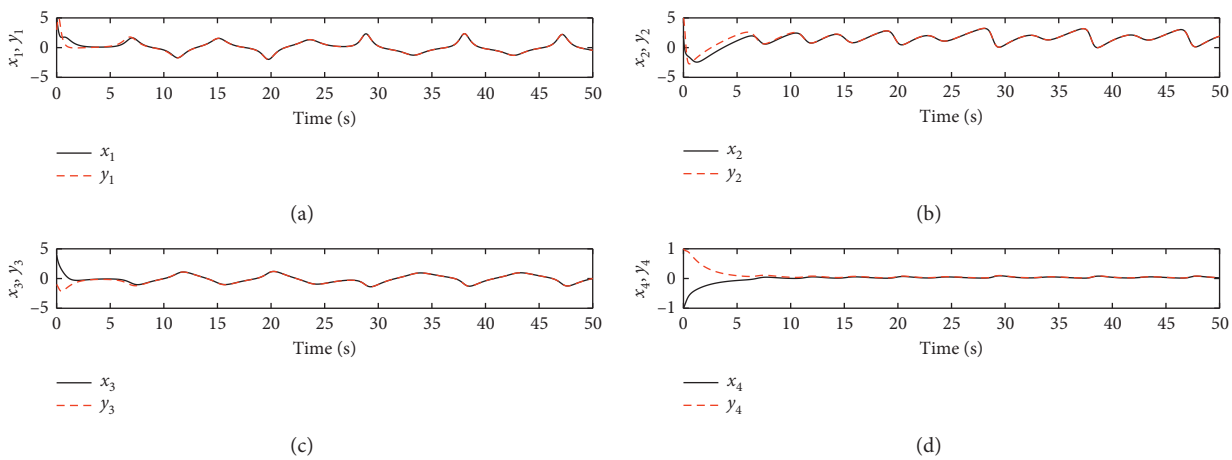

Figure 2: The states of master system (6) and slave system (9).

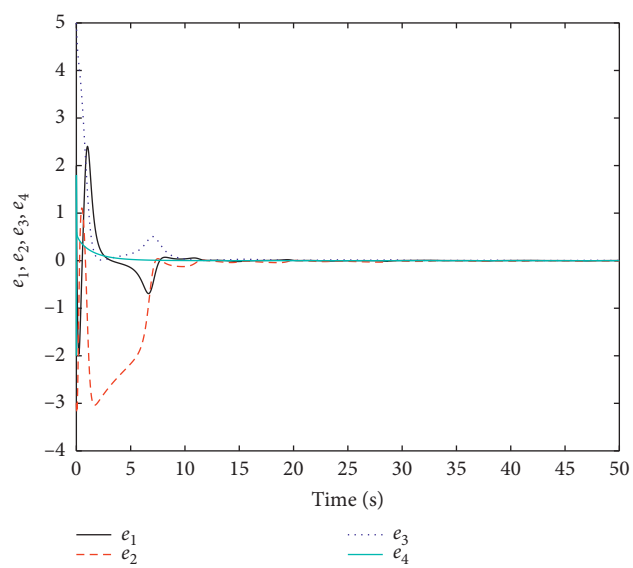

Figure 3: Error system (11) is also asymptotically stable.

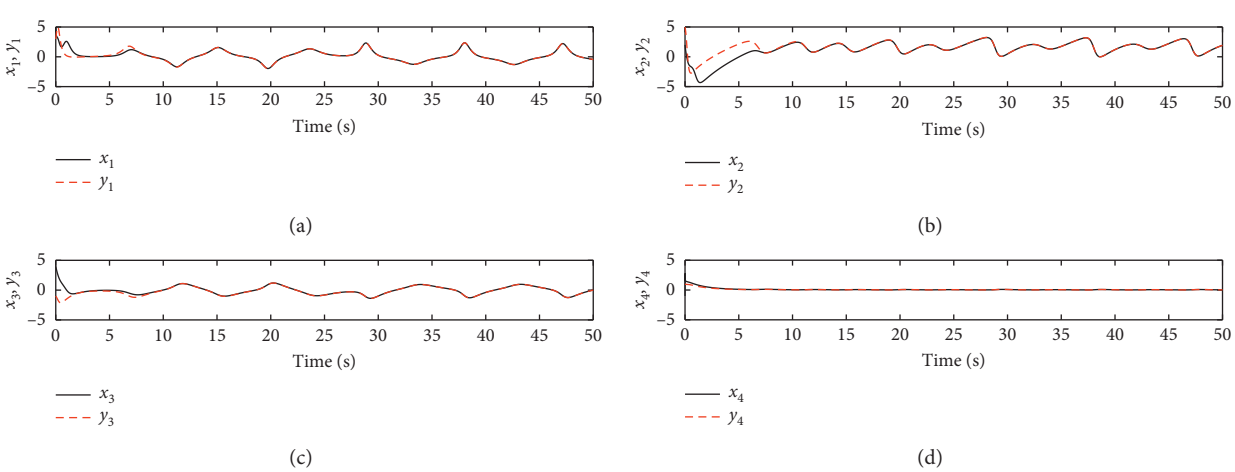

Figure 4: The states of master system (6) and slave system (9).

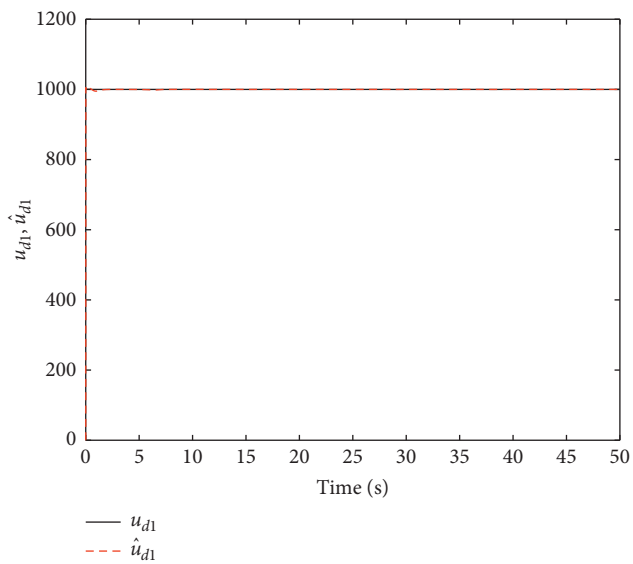

Figure 5: $\hat{u}_{d1}$ asymptotically tends to u_{d1}.

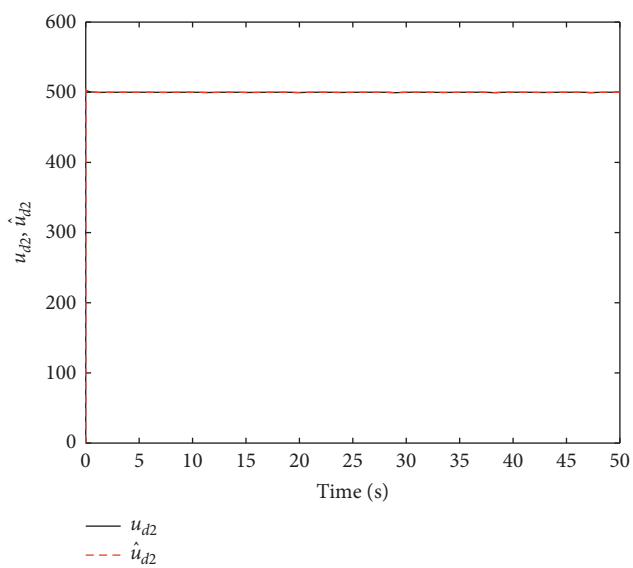

Figure 6: $\hat{u}_{d2}$ asymptotically tends to u_{d2}.

that $\hat{u}_{d1}$ asymptotically tends to u_{d1}. Figure 6 demonstrates that $\hat{u}_{d2}$ asymptotically tends to u_{d2}.

The other case $d(t)$ is given as follows:

$$d(t) = \begin{pmatrix} \sin t \\ 0 \\ 0 \\ 3 \sin t \end{pmatrix}. \tag{32}$$

Numerical simulation is carried out with the initial conditions of master system (6) and slave system (9): $x(0) = [5, 2, 4, -1]^T$ and $y(0) = [3, 5, -1, 1]^T$, respectively, and $\alpha = 0.95$, and $\beta = 1$. Figure 7 displays that error system (11) is also asymptotically stable, which implies that master system (6) and slave system (9) reach complete synchronization. The states of master system (6) and slave system (9) are shown in Figure 8, respectively. Figure 9 demonstrates

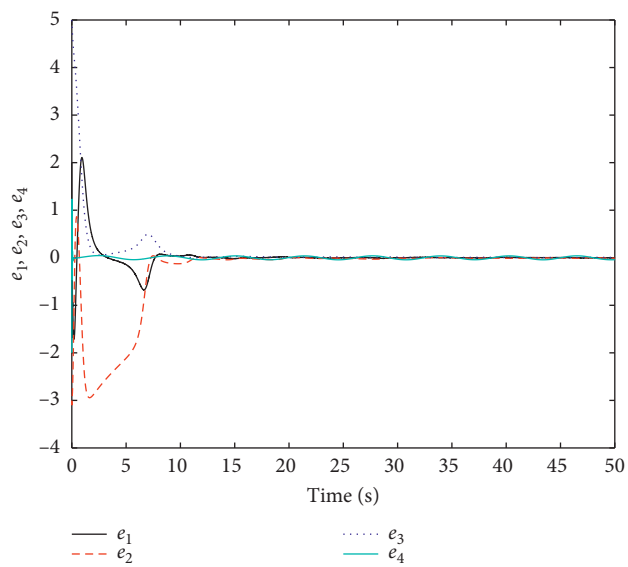

FIGURE 7: Error system (11) is also asymptotically stable.

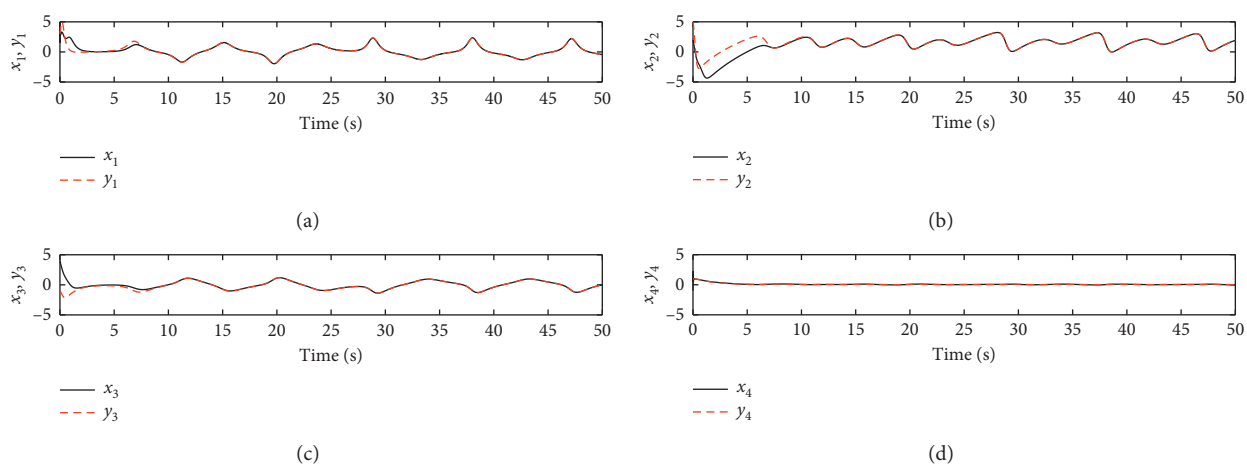

FIGURE 8: The states of master system (6) and slave system (9).

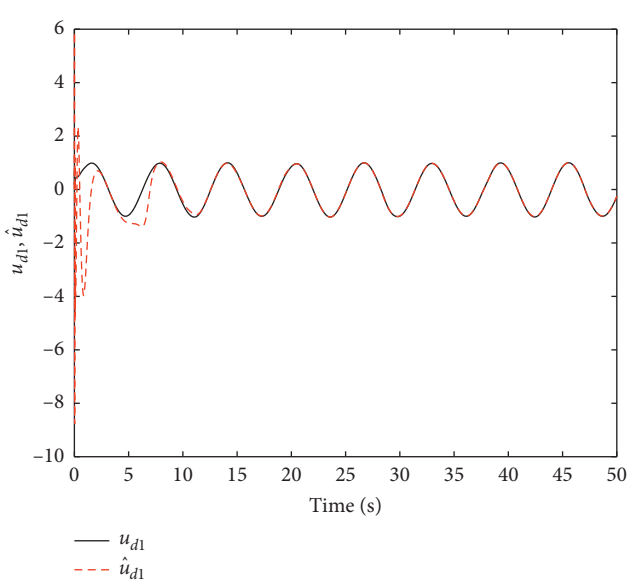

FIGURE 9: $\hat{u}_{d1}$ asymptotically tends to u_{d1}.

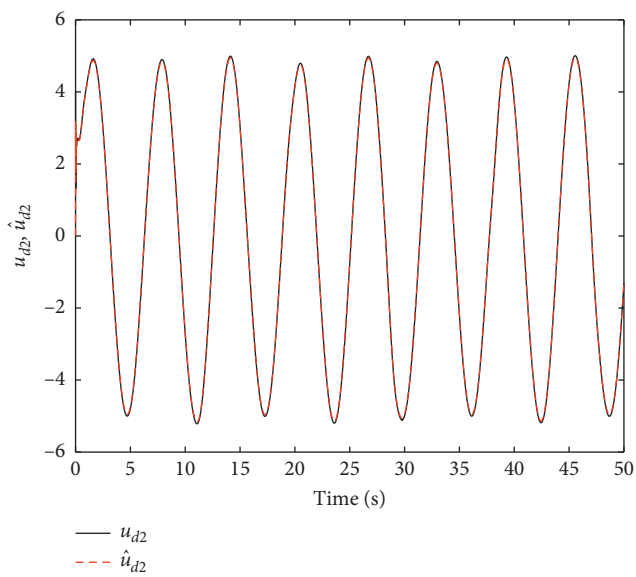

FIGURE 10: $\hat{u}_{d2}$ asymptotically tends to u_{d2}.

that $\hat{u}_{d1}$ asymptotically tends to u_{d1}. Figure 10 demonstrates that $\hat{u}_{d2}$ asymptotically tends to u_{d2}.

5. Conclusions

In conclusion, the synchronization of the FF hyperchaotic finance system with model uncertainty and external disturbances has been investigated. Firstly, a controller has been proposed for the nominal FF hyperchaotic finance system. Then, the UDE-based controller has been designed for the FF hyperchaotic finance system. The correctness and validity of the obtained results have been verified by numerical simulation. It is noted that the simulation results show that the aforementioned control method has good performance.

In the future, the obtained control method and the synchronization result are maybe extended to some potential applications, such as the nonlinear digital communication.

Data Availability

No data were used in this paper.

Conflicts of Interest

The authors declare that there are no conflicts of interest regarding the publication of this paper.

References

[1] W. G. Yu, "Stabilization of three-dimensional chaotic systems via single state feedback controller," *Physics Letters A*, vol. 374, no. 13-14, pp. 1488–1492, 2010.

[2] W. Yu, "Finite-time stabilization of three-dimensional chaotic systems based on CLF," *Physics Letters A*, vol. 374, no. 30, pp. 3021–3024, 2010.

[3] W. Yu, "Synchronization of three dimensional chaotic systems via a single state feedback," *Communications in Nonlinear Science and Numerical Simulation*, vol. 16, no. 7, pp. 2880–2886, 2011.

[4] T. Hou, Y. Liu, and F. Deng, "Finite horizon H2/H∞ control for SDEs with infinite Markovian jumps," *Nonlinear Analysis: Hybrid Systems*, vol. 34, pp. 108–120, 2019.

[5] R. M. Xu and F. Zhang, "ε-Nash mean-field games for general linear-quadratic systems with applications," *Automatica*, vol. 114, no. 1–6, 2020.

[6] R. Guo, "Projective synchronization of a class of chaotic systems by dynamic feedback control method," *Nonlinear Dynamics*, vol. 90, no. 1, pp. 53–64, 2017.

[7] A. Atangana and J. F. Gómez-Aguilar, "Fractional derivatives with no-index law property: application to chaos and statistics," *Chaos, Solitons & Fractals*, vol. 114, pp. 516–535, 2018.

[8] J. F. Gómez-Aguilar, "Multiple attractors and periodicity on the Vallis model for El Nio/La Nia-Southern oscillation model," *Journal of Atmospheric and Solar-Terrestrial Physics*, vol. 197, pp. 1–22, 2020.

[9] C. Xu, M. Liao, and P. Li, "Bifurcation control of a fractional-order delayed competition and cooperation model of two enterprises," *Science China Technological Sciences*, vol. 62, no. 12, pp. 2130–2143, 2019.

[10] C. Xu, C. Aouiti, and Z. Liu, "A further study on bifurcation for fractional order BAM neural networks with multiple delays," *Neurocomputing*, vol. 417, pp. 501–515, 2020.

[11] C. Xu, M. Liao, and P. Li, "Bifurcation control for a fractional-order competition model of Internet with delays," *Nonlinear Dynamics*, vol. 95, no. 4, pp. 3335–3356, 2019.

[12] J. F. Gómez-Aguilar, "Chaos and multiple attractors in a fractal-fractional Shinriki's oscillator model," *Physica A: Statistical Mechanics and its Applications*, vol. 539, pp. 1–34, 2020.

[13] A. Atangana and S. Qureshi, "Modeling attractors of chaotic dynamical systems with fractal-fractional operators," *Chaos, Solitons & Fractals*, vol. 123, pp. 320–337, 2019.

[14] E. O. Alzahrani and M. A. Khan, "Comparison of numerical techniques for the solution of a fractional epidemic model," *The European Physical Journal Plus*, vol. 135, no. 1, pp. 1–28, 2020.

[15] H. Liu, Y. Chen, G. J. Li, W. Xiang, and G. K. Xu, "Adaptive fuzzy synchronization of fractional-order chaotic (hyperchaotic) systems with input saturation and unknown parameters," *Complexity*, vol. 2017, Article ID 6853826, 16 pages, 2017.

[16] B. Yan, S. B. He, and S. J. Wang, "Multistability in a fractional-order centrifugal flywheel governor system and its adaptive control," *Complexity*, vol. 2020, Article ID 8844657, 11 pages, 2020.

[17] C. Yin, S. Dadras, S.-M. Zhong, and Y. Chen, "Control of a novel class of fractional-order chaotic systems via adaptive sliding mode control approach," *Applied Mathematical Modelling*, vol. 37, no. 4, pp. 2469–2483, 2013.

[18] R. Zhang and S. Yang, "Adaptive synchronization of fractional-order chaotic systems via a single driving variable," *Nonlinear Dynamics*, vol. 66, no. 4, pp. 831–837, 2011.

[19] J. H. Park, "Adaptive synchronization of Rossler system with uncertain parameters," *Chaos, Solitons & Fractals*, vol. 25, no. 2, pp. 333–338, 2005.

[20] S. Kuntanapreeda, "Adaptive control of fractional-order unified chaotic systems using a passivity-based control approach," *Nonlinear Dynamics*, vol. 84, no. 4, pp. 2505–2515, 2016.

[21] S. Bhalekar and V. Daftardar-Gejji, "Synchronization of different fractional order chaotic systems using active

control," *Communications in Nonlinear Science and Numerical Simulation*, vol. 15, no. 11, pp. 3536–3546, 2010.

[22] C. Li and W. Deng, "Chaos synchronization of fractional-order differential systems," *International Journal of Modern Physics B*, vol. 20, no. 7, pp. 791–803, 2006.

[23] Y. Xu and H. Wang, "Synchronization of fractional-order chaotic systems with Gaussian fluctuation by sliding mode control," *Abstract and Applied Analysis*, vol. 2013, Article ID 948782, 228 pages, 2013.

[24] Q. Wang and D.-L. Qi, "Synchronization for fractional order chaotic systems with uncertain parameters," *International Journal of Control, Automation and Systems*, vol. 14, no. 1, pp. 211–216, 2016.

[25] Y. P. Wu and G. D. Wang, "Synchronization between fractional-order and integer-order hyperchaotic systems via sliding mode controller," *Journal of Applied Mathematics*, vol. 2013, no. 1, 63 pages, Article ID 151025, 2013.

[26] T. Hou, Y. Liu, and F. Deng, "Stability for discrete-time uncertain systems with infinite Markov jump and time-delay," *Science China Information Sciences*, vol. 64, no. 5, p. 152202, 2021.

[27] B. Ren, Q.-C. Zhong, and J. Chen, "Robust control for a class of nonaffine nonlinear systems based on the uncertainty and disturbance estimator," *IEEE Transactions on Industrial Electronics*, vol. 62, no. 9, pp. 5881–5888, 2015.

[28] X. Yi, R. Guo, and Y. Qi, "Stabilization of chaotic systems with both uncertainty and disturbance by the UDE-based control method," *IEEE Access*, vol. 8, pp. 62471–62477, 2020.

[29] L. Liu, B. Li, and R. Guo, "Consensus control for networked manipulators with switched parameters and topologies," *IEEE Access*, vol. 9, pp. 9209–9217, 2021.

[30] R. Peng, C. Jiang, and R. Guo, "Stabilization of a class of fractional order systems with both uncertainty and disturbance," *IEEE Access*, vol. 9, pp. 42697–42706, 2021.

[31] R. Guo and Y. Qi, "Partial anti-synchronization in a class of chaotic and hyper-chaotic systems," *IEEE Access*, vol. 9, pp. 46303–46312, 2021.

[32] R. Peng, C. Jiang, and R. Guo, "Partial anti-synchronization of the fractional-order chaotic systems through dynamic feedback control," *Mathematics*, vol. 9, no. 7, p. 718, 2021.

[33] R. Guo, Y. R. Zhang, and C. Jiang, "Synchronization of fractional-order chaotic systems with model uncertainty and external disturbance," *Mathematics*, vol. 9, no. 8, p. 877, 2021.

[34] C. M. Jiang, A. Zada, M. T. Senel, and T. X. Li, "Synchronization of bidirectional N-coupled fractional-order chaotic systems with ring connection based on antisymmetric structure," *Advances in Difference Equations*, vol. 456, p. 16, 2019.

[35] R. Gorenflo and F. Mainardi, "Fractional calculus: integral and differential equations of fractional order," *Mathematics*, vol. 49, no. 2, pp. 277–290, 2008.

[36] N. Aguila-Camacho, M. A. Duarte-Mermoud, and J. A. Gallegos, "Lyapunov functions for fractional order systems," *Communications in Nonlinear Science and Numerical Simulation*, vol. 19, no. 9, pp. 2951–2957, 2014.

Hindawi
Mathematical Problems in Engineering
Volume 2021, Article ID 1126757, 6 pages
https://doi.org/10.1155/2021/1126757

Research Article

Algebraic Relations among Four Types of Right Semi-Tensor Product

Nating Chen,[1,2] **Menglei Lin**,[1,2] **and Yiliang Li**[3]

[1]*School of Mathematics and Statistics, Minnan Normal University, Zhangzhou, Fujian 363400, China*
[2]*Institute of Meteorological Big Data-Digital, Minnan Normal University, Zhangzhou, Fujian 363400, China*
[3]*School of Mathematics, Shandong University, Jinan, Shandong 250100, China*

Correspondence should be addressed to Menglei Lin; menglei36@126.com

Received 6 May 2021; Accepted 7 June 2021; Published 14 June 2021

Academic Editor: Renming Yang

In this paper, algebraic relations among four kinds of right semi-tensor product (STP) are discussed. Firstly, this paper provides definitions of right STPs, consisting of the first right matrix-matrix STP, the second right matrix-matrix STP, the first right matrix-vector STP, and the second right matrix-vector STP. Secondly, relations among these right STPs are proposed. Finally, the main results show the convertibility of these right STPs.

1. Introduction

Cheng product, also called semi-tensor product (STP), was first introduced by Prof. Cheng [1]. A significant breakthrough of STP is that it overcomes the dimension barrier, which limits the development of conventional matrix product. The first type of STP is called left matrix-matrix (MM) STP, which expends the dimension of each matrix by right multiplying the identity matrix. Here, the matrix product refers to the Kronecker product. Thanks to the left MM STP, a Boolean network can be converted into a linear discrete-time form, which stimulates the development of Boolean networks [2–4]. In addition, the left MM STP also plays an important role in finite game [5–7], fuzzy systems [8, 9], and graph theory [10, 11].

However, the left MM STP loses its ability in discussing dimension-varying linear systems because the result of left MM STP of a matrix and a vector is a matrix instead of a vector. Thus, the second type of STP, called left matrix-vector (MV) STP, was proposed in [12]. Compared with the left MM STP, the left MV STP expends the dimension of vector by right multiplying a column vector whose elements are 1. Based on the left MV STP, dimension-varying linear systems were modeled [13]. Besides, the solution and stability of continuous-time dimension-varying linear systems were studied in [14]. References [15, 16] considered state dimensions of dimension-varying discrete linear systems.

Due to the importance of left MM STP and left MV STP, the authors in [17] explored more general STPs, which help to expand the possible applications of STP. In the following, the left MM STP and left MV STP are denoted by left MM-1 STP and left MV-1 STP. By right multiplying $J_n = (1/n)1_{n\times n}$, the left MM-2 STP and left MV-2 STP are defined in [18]. Here, $1_{n\times n}$ is an $n \times n$ dimensional matrix, whose elements are 1. Relations among these four kinds of left STP are discussed in [19].

By changing the way of dimension expansion, the authors in [17] defined four corresponding right STPs, including right MM-1 STP, right MM-2 STP, right MV-1 STP, and right MV-2 STP. However, relations between these right STPs are not studied. Hence, this paper reviews definitions of right STP and discusses relations among these right STPs. The main results show the convertibility of these right STPs.

The rest of this paper is organised as follows. Section 2 introduced definitions of four kinds of right STP. Relations among these right STPs are investigated in Section 3. Section 4 gives some concluding remarks.

Before ending this section, we provided a list of notations, most of which can be found in [20, 21].

(i) $\mathscr{M}_{m\times n}$ contains all $m\times n$ dimensional matrices. The i-th column (row) of matrix M is denoted by $\mathrm{Col}_i(M)$ ($\mathrm{Row}_i(M)$). Particularly, $M_{ij}=\mathrm{Row}_i(\mathrm{Col}_j(M))$.

(ii) $\mathscr{V}_p$ includes all p dimensional column vectors.

(iii) I_n is the n dimensional identity matrix.

(iv) $1_{n\times n}=(1_n,1_n,\ldots,1_n)$, where $1_n=\sum_{i=1}^{n}\mathrm{Col}_i(I_n)$.

(v) $0_{m\times n}$ is an $m\times n$ dimensional zero matrix.

(vi) A^T is the transpose of matrix A.

(vii) $\otimes$ is the Kronecker product

2. Definitions of Right STP

In this section, definitions of right STP are introduced. To begin with, the right STP of two matrices is proposed. In this paper, STP refers to right STP.

Definition 1 (see [12, 17]). Let $A\in\mathscr{M}_{m\times n}$ and $B\in\mathscr{M}_{p\times q}$. Suppose $t=[n,p]$ is the least common multiple of n and p.

(1) The first right MM STP (MM-1 STP) of A and B, denoted by $A\rtimes_1 B$, is defined as

$$A\rtimes_1 B=\left(I_{t/n}\otimes A\right)\left(I_{t/p}\otimes B\right). \tag{1}$$

(2) The second right MM STP (MM-2 STP) of A and B, denoted by $A\rtimes_2 B$, is defined as

$$A\rtimes_2 B=\left(J_{t/n}\otimes A\right)\left(J_{t/p}\otimes B\right), \tag{2}$$

where $J_k=(1/k)1_{k\times k}$ and $k=(t/n)$ or $k=(t/p)$.

Remark 1. If $n=p$, then $A\rtimes_1 B=A\rtimes_2 B=AB$. It means that MM-1 STP and MM-2 STP are generalizations of the conventional matrix product. In addition, MM-1 STP and MM-2 STP not only keep main properties of conventional matrix product available but add some new properties such as certain commutativity [12].

Given a matrix $A\in\mathscr{M}_{m\times n}$ and a vector $x\in\mathscr{V}_n$. Then, the conventional matrix product of A and x can be viewed as a linear mapping on $\mathscr{V}_n$. However, MM-1 STP and MM-2 STP cannot be regarded as linear mappings because results of MM-1 STP and MM-2 STP are matrices instead of vectors. Thus, other definitions of right STP, as extensions of linear mappings, are provided.

Definition 2 (see [12, 17]). Let $A\in\mathscr{M}_{m\times n}$ and $x\in\mathscr{V}_r$. Suppose $s=[n,r]$ is the least common multiple of n and r.

(1) The first right MV STP (MV-1 STP) of A and x, denoted by $A\overrightarrow{\rtimes}_1 x$, is defined as

$$A\overrightarrow{\rtimes}_1 x=\left(I_{s/n}\otimes A\right)\left(1_{s/r}\otimes x\right). \tag{3}$$

(2) The second right MV STP (MV-2 STP) of A and x, denoted by $A\overrightarrow{\rtimes}_2 x$, is defined as

$$A\overrightarrow{\rtimes}_2 x=\left(J_{s/n}\otimes A\right)\left(1_{s/r}\otimes x\right). \tag{4}$$

Definition 3. Given $A\in\mathscr{M}_{m\times n}$ and $B\in\mathscr{M}_{p\times q}$. Suppose $t=[n,p]$ is the least common multiple of n and p. Then,

$$A\overrightarrow{\rtimes}_1 B=\left(I_{t/n}\otimes A\right)\left(1_{t/p}\otimes B\right), \tag{5}$$

$$A\overrightarrow{\rtimes}_2 B=\left(J_{t/n}\otimes A\right)\left(1_{t/p}\otimes B\right). \tag{6}$$

3. Algebraic Relation among Four Types of STP

In this section, algebraic relations among four types of STP are discussed. The following three cases are considered: (1) STP of two vectors, (2) STP of matrices and vectors, and (3) STP of two matrices.

3.1. TP of Two Vectors. Firstly, algebraic relations among STPs of two column vectors are concerned.

Theorem 1. *Let $x\in\mathscr{V}_n$ and $y\in\mathscr{V}_p$ be two column vectors. Then, the following results hold:*

(1) $x\overrightarrow{\rtimes}_1 y=x\rtimes_1 y=y\otimes x$

(2) $x\overrightarrow{\rtimes}_2 y=x\rtimes_2 y=(1/p)\sum_{i=1}^{p}y_i(1_p\otimes x)$, *where* $y=(y_1,y_2,\ldots,y_p)^T$

Proof. (1) The correctness of the first item is obvious, so the proof is omitted. (2) In the light of the definition of MM-2 STP, one calculates

$$x\rtimes_2 y=\left(J_p\otimes x\right)y=\frac{1}{p}\left(1_{p\times p}\otimes x\right)y=\frac{1}{p}\left(1_p^T\otimes 1_p\otimes x\right)y=\frac{1}{p}\sum_{i=1}^{p}y_i\left(1_p\otimes x\right). \tag{7}$$

In addition, it is easy to see that $x\overrightarrow{\rtimes}_2 y=x\rtimes_2 y$ holds for any column vectors x and y. □

The following results are about algebraic relation among STPs of two row vectors.

Theorem 2. *Let $x^T\in\mathscr{V}_n$ and $y^T\in\mathscr{V}_p$ be two column vectors. Then, the following results hold:*

(1) $x\rtimes_1 y=x\otimes y$

(2) $x\overrightarrow{\rtimes}_2 y=x\overrightarrow{\rtimes}_1 y=\sum_{i=1}^{n}x_i y$, *where* $x=(x_1,x_2,\ldots,x_n)$

(3) $x \rtimes_2 y = (1/n)1_n^T \otimes (x \overrightarrow{\rtimes}_2 y) = (1/n)\ 1_n^T \otimes (x \overrightarrow{\rtimes}_1 y) = (1/n)\sum_{i=1}^n x_i (1_n^T \otimes y)$, *where* $x = (x_1, x_2, \ldots, x_n)$

Proof

(1) The correctness of the first item is obvious, so the proof is omitted.

(2) By computing directly, one can see that $x \overrightarrow{\rtimes}_1 y = x(1_n \otimes y) = \sum_{i=1}^n x_i y$ holds

(3) From the definition of MM-2 STP, we get

$$x \rtimes_2 y = x(J_n \otimes y) = \frac{1}{n} x(1_{n\times n} \otimes y) = \frac{1}{n} x\left(1_n^T \otimes 1_n \otimes y\right) = \frac{1}{n} 1_n^T \otimes (x(1_n \otimes y)) = \frac{1}{n} 1_n^T \otimes \left(x \overrightarrow{\rtimes}_2 y\right). \tag{8}$$

Combined with the first two items, one obtains $x \rtimes_2 y = (1/n)1^T \otimes (x \overrightarrow{\rtimes}_1 y) = (1/n)1_n^T \otimes (\sum_{i=1}^n x_i y) = (1/n)\sum_{i=1}^n x_i (1_n^T \otimes y)$. □

3.2. STP of Matrices and Vectors. In this subsection, algebraic relations among four types of STP of matrices and vectors are studied. To begin with, we focus on STP of matrices and column vectors.

Theorem 3. *Given* $A \in \mathscr{M}_{m\times n}$ *and* $x \in \mathscr{V}_p$. *Suppose* $t = [n, p]$ *is the least common multiple of n and p. Then, the following results hold:*

(1) $A \overrightarrow{\rtimes}_1 x = \sum_{i=1}^{t/p} Col_i(A \rtimes_1 x)$

(2) $A \overrightarrow{\rtimes}_2 x = (n/t)1_{t/n} \otimes (\sum_{i=1}^{t/n} Blk_i(A \overrightarrow{\rtimes}_1 x))$, *where* $Blk_i(A \overrightarrow{\rtimes}_1 x)$ *is the i-th block of* $A \overrightarrow{\rtimes}_1 x$ *via dividing* $A \overrightarrow{\rtimes}_1 x$ *into* (t/n) *equal blocks by rows*

(3) $A \rtimes_2 x = (p/t)1_{t/p}^T \otimes (A \overrightarrow{\rtimes}_2 x)$

Proof

(1) Since $1_n = \sum_{i=1}^n \mathrm{Col}_i(I_n)$, we have $1_n \otimes x = \sum_{i=1}^n \mathrm{Col}_i(I_n) \otimes x = \sum_{i=1}^n (\mathrm{Col}_i(I_n \otimes x))$ for each $x \in \mathscr{V}_p$. According to definitions of MM-1 STP and MV-1 STP, one derives

$$\begin{aligned} &A \overrightarrow{\rtimes}_1 x \\ &= (I_{t/n} \otimes A)\left(1_{t/p} \otimes x\right) = (I_{t/n} \otimes A)\left(\sum_{i=1}^{t/p} \mathrm{Col}_i\left(I_{t/p} \otimes x\right)\right) \\ &= \sum_{i=1}^{t/p} \mathrm{Col}_i\left(\left(I_{t/p} \otimes A\right)\left(I_{t/p} \otimes x\right)\right) = \sum_{i=1}^{t/p} \mathrm{Col}_i(A \rtimes_1 x). \end{aligned} \tag{9}$$

(2) Divide $I_{t/n} \otimes A$ into t/n equal blocks by rows. The i-th block of $I_{t/n} \otimes A$ is denoted by $Blk_i(I_{t/n} \otimes A) = (0_{m\times n}, \ldots, A, \ldots, 0_{m\times n})$. It is easy to see that $1_{t/n}^T \otimes A = \sum_{i=1}^{t/n} Blk_i(I_{t/n} \otimes A)$ holds. Thus, one gets

$$\begin{aligned} &\left(1_{t/n\times t/n} \otimes A\right)\left(1_{t/p} \otimes x\right) \\ &= \left(1_{t/n} \otimes 1_{t/n}^T \otimes A\right)\left(1_{t/p} \otimes x\right) = 1_{t/n} \otimes \left(\left(1_{t/n}^T \otimes A\right)\left(1_{t/p} \otimes x\right)\right) = 1_{t/n} \otimes \left(\left(\sum_{i=1}^{t/n} Blk_i(I_{t/n} \otimes A)\right)\left(1_{t/p} \otimes x\right)\right) \\ &= 1_{t/n} \otimes \sum_{i=1}^{t/n} Blk_i\left(\left(I_{t/n} \otimes A\right)\left(1_{t/p} \otimes x\right)\right) = 1_{t/n} \otimes \sum_{i=1}^{t/n} Blk_i\left(A \overrightarrow{\rtimes}_1 x\right). \end{aligned} \tag{10}$$

Combined with the definition of MV-2 STP, we can draw the following conclusion:

$$A \overrightarrow{\rtimes}_2 x = (J_{t/n} \otimes A)\left(1_{t/p} \otimes x\right) = \frac{n}{t}(1_{t/n\times t/n} \otimes A)\left(1_{t/p} \otimes x\right) = \frac{n}{t} 1_{t/n} \otimes \sum_{i=1}^{t/n} Blk_i\left(A \overrightarrow{\rtimes}_1 x\right). \tag{11}$$

(3) From the definition of MM-2 STP, it is not hard to compute

$$A \rtimes_2 x$$
$$= (J_{t/n} \otimes A)(J_{t/p} \otimes x) = \frac{p}{t}(J_{t/n} \otimes A)(1_{t/p}^T \otimes 1_{t/p} \otimes x) \quad (12)$$
$$= \frac{p}{t} 1_{t/p}^T \otimes ((J_{t/n} \otimes A)(1_{t/p} \otimes x)) = \frac{p}{t} 1_{t/p}^T \otimes (A \overrightarrow{\rtimes}_2 x).$$

□

Based on Theorem 3, another relations among four types of STP of matrices and column vectors can be introduced.

Corollary 1. *Given $A \in \mathscr{M}_{m\times n}$ and $x \in \mathscr{V}_p$. Suppose $t = [n, p]$ is the least common multiple of n and p. Relations among all types of STP of A and x are shown as follows:*

(1) $A \overrightarrow{\rtimes}_2 x = (n/t) 1_{t/n} \otimes (\sum_{i=1}^{t/n} \sum_{j=1}^{t/p} Blk_i(Col_j(A \rtimes_1 x)))$, where $Blk_i(M)$ is the i-th block of M via dividing M into t/n equal blocks by rows, $M = Col_j(A \rtimes_1 x)$.

(2) $A \rtimes_2 x = (np/t^2) 1_{t/n\times t/p} \otimes (\sum_{i=1}^{t/n} Blk_i(A \overrightarrow{\rtimes}_1 x))$, where $Blk_i(A \overrightarrow{\rtimes}_1 x)$ is the i-th block of $A \overrightarrow{\rtimes}_1 x$ via dividing $A \overrightarrow{\rtimes}_1 x$ into t/n equal blocks by rows.

(3) $A \rtimes_2 x = (np/t^2) 1_{t/n\times t/p} \otimes (\sum_{i=1}^{t/n} \sum_{j=1}^{t/p} Blk_i(Col_j(A \rtimes_1 x)))$, where $Blk_i(M)$ is the i-th block of M via dividing M into t/n equal blocks by rows, $M = Col_j(A \rtimes_1 x)$.

The following theorem shows different results between STP of column vectors and matrices and STP of matrices and column vectors.

Theorem 4. *Given $A \in \mathscr{M}_{m\times n}$. Let $x \in \mathscr{V}_p$ be a column vector. Then, the following results hold:*

(1) $x \overrightarrow{\rtimes}_1 A = x \rtimes_1 A = A \otimes x$

(2) $x \overrightarrow{\rtimes}_2 A = x \rtimes_2 A = (1/m) 1_m \otimes (\sum_{i=1}^{m} Row_i(A) \otimes x)$

Proof

(1) Since $x \overrightarrow{\rtimes}_1 A = (I_m \otimes x)A = ((I_m \otimes x)\ \mathrm{Col}_1(A) \cdots (I_m \otimes x)\mathrm{Col}_n(A))$, one can see easily that $x \overrightarrow{\rtimes}_1 A = A \otimes x$ holds according to the first item of Theorem 1. Moreover, we can conclude that $x \rtimes_1 A = A \otimes x$ is true.

(2) Similarly, $x \rtimes_2 A = (J_m \otimes x)A = ((J_m \otimes x)\ \mathrm{Col}_1(A) \cdots (J_m \otimes x)\mathrm{Col}_n(A))$ holds. From the second item of Theorem 1, we derive $(J_m \otimes x)\mathrm{Col}_i(A) = (1/m) \sum_{j=1}^{m} A_{ji}(1_m \otimes x)$. Thus, one computes

$$\begin{aligned} & x \rtimes_2 A \\ & = ((J_m \otimes x)\mathrm{Col}_1(A) \cdots (J_m \otimes x)\mathrm{Col}_n(A)) \\ & = \frac{1}{m}\left(\sum_{j=1}^{m} A_{1i}(1_m \otimes x) \cdots \sum_{j=1}^{m} A_{ni}(1_m \otimes x)\right) = \frac{1}{m} 1_m \otimes \left(\sum_{i=1}^{m} \mathrm{Row}_i(A) \otimes x\right). \end{aligned} \quad (13)$$

Based on the definition of MV-2 STP, we also get

$$x \overrightarrow{\rtimes}_2 A = \frac{1}{m} 1_m \otimes \left(\sum_{i=1}^{m} \mathrm{Row}_i(A) \otimes x\right). \quad (14)$$

Next, we investigate algebraic relations among four types of STP of matrices and row vectors. □

Theorem 5. *Given $A \in \mathscr{M}_{m\times n}$. Let $x^T \in \mathscr{V}_p$ be a column vector. Then, the following results hold:*

(1) $A \rtimes_1 x = A \otimes x$

(2) $A \overrightarrow{\rtimes}_2 x = A \overrightarrow{\rtimes}_1 x = x \rtimes_1 (\sum_{i=1}^{n} Col_i(A) \otimes I_p)$

(3) $A \rtimes_2 x = (1/n) 1_n^T \otimes (A \overrightarrow{\rtimes}_2 x) = (1/n) 1_n^T \otimes (x \rtimes_1 (\sum_{i=1}^{n} Col_i(A) \otimes I_p))$

Proof. (1) It is not hard to find $A \rtimes_1 x = A(I_n \otimes x) = ((\mathrm{Row}_1(A) I_n \otimes x)^T \cdots (\mathrm{Row}_m(A)(I_n \otimes x))^T)^T$. The first item of Theorem 2 shows that $\mathrm{Row}_i(A)(I_n \otimes x) = \mathrm{Row}_i(A) \rtimes_1 x = \mathrm{Row}_i(A) \otimes x$ is true. Hence, $A \rtimes_1 x = ((\mathrm{Row}_1(A) \otimes x)^T \cdots (\mathrm{Row}_m(A) \otimes x)^T)^T = A \otimes x$ holds.

(2) By computation direct, we draw the following conclusion:

$$\begin{aligned} & A \overrightarrow{\rtimes}_1 x \\ & = A \overrightarrow{\rtimes}_2 x = A(1_n \otimes x) = \sum_{i=1}^{n} \mathrm{Col}_i(A) \otimes x \\ & = (I_m \otimes x)\left(\sum_{i=1}^{n} \mathrm{Col}_i(A) \otimes I_p\right) = x \rtimes_1 \left(\sum_{i=1}^{n} \mathrm{Col}_i(A) \otimes I_p\right). \end{aligned} \quad (15)$$

(3) Combining (15) with definitions of STP, one derives the following results:

$$
\begin{aligned}
&A \rtimes_2 x \\
&= A\left(J_n \otimes x\right) = \frac{1}{n} A\left(1_{n\times n} \otimes x\right) = \frac{1}{n} A\left(1_n^T \otimes 1_n \otimes x\right) = \frac{1}{n} 1_n^T \otimes \left(A\left(1_n \otimes x\right)\right) \\
&= \frac{1}{n} 1_n^T \otimes \left(A \overrightarrow{\rtimes}_2 x\right) = \frac{1}{n} 1_n^T \otimes \left(A \overrightarrow{\rtimes}_1 x\right) \\
&= \frac{1}{n} 1_n^T \otimes \left(x \rtimes_1 \left(\sum_{i=1}^{n} \mathrm{Col}_i(A) \otimes I_p \right) \right).
\end{aligned} \tag{16}
$$

□

3.3. STP of Two Matrices. Combined with the analysis above, algebraic relations among four types of STP of two matrices are derived easily.

Theorem 6. *Given $A \in \mathscr{M}_{m\times n}$ and $B \in \mathscr{M}_{p\times q}$. Suppose $t = [n, p]$ is the least common multiple of n and p. Then, the following results hold:*

(1) $A \overrightarrow{\rtimes}_1 B = (\sum_{i=1}^{t/p} Col_i(A \rtimes_1 B) \cdots \sum_{i=(q-1)t/p+1}^{tq/p} Col_i(A \rtimes_1 B))$

(2) $A \overrightarrow{\rtimes}_2 B = (n/t) 1_{t/n} \otimes (\sum_{i=1}^{t/n} Blk_i(A \overrightarrow{\rtimes}_1 B))$, *where* $Blk_i(A \overrightarrow{\rtimes}_1 B)$ *is the i-th block of* $A \overrightarrow{\rtimes}_1 B$ *via dividing* $A \overrightarrow{\rtimes}_1 x$ *into t/n equal blocks by rows*

(3) $A \rtimes_2 B = (p/t) 1_{t/p}^T \otimes (A \overrightarrow{\rtimes}_2 B)$

Proof. Since proofs of these tree items are similar, we only prove (1).

(1) From equation (5), one finds $A \overrightarrow{\rtimes}_1 B = (A \overrightarrow{\rtimes}_1 \mathrm{Col}_1(B) \cdots A \overrightarrow{\rtimes}_1 \mathrm{Col}_q(B))$. Because $A \overrightarrow{\rtimes}_1 \mathrm{Col}_i(B) = \sum_{j=1}^{t/p} \mathrm{Col}_j(A \rtimes_1 \mathrm{Col}_i(B))$ holds according to Theorem 3, it is not difficult to see $A \overrightarrow{\rtimes}_1 B = (\sum_{j=1}^{t/p} \mathrm{Col}_j(A \rtimes_1 \mathrm{Col}_1(B)) \cdots \sum_{j=1}^{t/p} \mathrm{Col}_j(A \rtimes_1 \mathrm{Col}_q(B)))$. By calculation, we conclude that

$$
A \overrightarrow{\rtimes}_1 B = \left(\sum_{i=1}^{t/p} \mathrm{Col}_i(A \rtimes_1 B) \cdots \sum_{i=(q-1)t/p+1}^{tq/p} \mathrm{Col}_i(A \rtimes_1 B) \right), \tag{17}
$$

which is true. □

Similarly, another relation among of four types of STP of two matrices is presented.

Corollary 2. *Given $A \in \mathscr{M}_{m\times n}$ and $B \in \mathscr{M}_{p\times q}$. Suppose $t = [n, p]$ is the least common multiple of n and p. Relations among all types of STP of A and B are shown as follows:*

(1) $A \overrightarrow{\rtimes}_2 B = (n/t) 1_{t/n} \otimes \sum_{i=1}^{t/n} Blk_i(\sum_{j=1}^{t/} pCol_j(A \rtimes_1 B) \cdots \sum_{j=(q-1)t/p+1}^{tq/p} Col_j(A \rtimes_1 B))$, *where* $Blk_i(M)$ *is the i-th block of M via dividing M into t/n equal blocks by rows,* $M = (\sum_{j=1}^{t/p} Col_j(A \rtimes_1 B) \cdots \sum_{j=(q-1)t/p+1}^{tq/p} Col_j(A \rtimes_1 B))$

(2) $A \rtimes_2 B = (np/t^2) 1_{t/n\times t/p} \otimes (\sum_{i=1}^{t/n} Blk_i(A \overrightarrow{\rtimes}_1 B))$, *where* $Blk_i(A \overrightarrow{\rtimes}_1 B)$ *is the i-th block of* $A \overrightarrow{\rtimes}_1 B$ *via dividing* $A \overrightarrow{\rtimes}_1 x$ *into t/n equal blocks by rows*

(3) $A \rtimes_2 B = (np/t^2) 1_{t/n\times}\ t/p \otimes \sum_{i=1}^{t/n} Blk_i(\sum_{j=1}^{t/} pCol_j(A \rtimes_1 B) \cdots \sum_{j=(q-1)t/p+1}^{tq/p} Col_j(A \rtimes_1 B))$, *where* $Blk_i(M)$ *is the i-th block of M via dividing M into t/n equal blocks by rows,* $M = (\sum_{j=1}^{t/p} Col_j(A \rtimes_1 B) \cdots \sum_{j=(q-1)t/p+1}^{tq/p} Col_j(A \rtimes_1 B))$

4. Conclusion

This paper has studied relations among four kinds of right STPs under three cases, containing STP of two vectors, STP of matrices and vectors, and STP of two matrices. The results obtained in this paper have shown the convertibility of these right STPs.

Data Availability

No data were used to support this study.

Conflicts of Interest

The authors declare that they have no conflicts of interest.

Acknowledgments

This work was supported by the grants from the Natural Science Foundation Project of Fujian, China (no. 2020J01795).

References

[1] D. Cheng, "Semi-tensor product of matrices and its application to morgen's problem," *Science China Information Sciences*, vol. 44, no. 3, pp. 195–212, 2001.

[2] Y. Zheng, H. Li, and J.-E. Feng, "State-feedback set stabilization of logical control networks with state-dependent delay," *Science China Information Sciences*, vol. 64, no. 6, p. 169203, 2021 1–169203:3.

[3] Y. Li, J. Li, and J.-e. Feng, "Set controllability of Boolean control networks with impulsive effects," *Neurocomputing*, vol. 418, pp. 263–269, 2020.

[4] Y. Li, J. Li, and J.-E. Feng, "Output tracking of Boolean control networks with impulsive effects," *IEEE Access*, vol. 8, pp. 157793–157799, 2020.

[5] D. Cheng, "On finite potential games," *Automatica*, vol. 50, no. 7, pp. 1793–1801, 2014.
[6] D. Cheng and T. Liu, "From Boolean game to potential game," *Automatica*, vol. 96, pp. 51–60, 2018.
[7] C. Li, Y. Xing, F. He, and D. Cheng, "A strategic learning algorithm for state-based games," *Automatica*, vol. 113, pp. 1–9, 2020.
[8] D. Cheng, J.-e. Feng, and H. Lv, "Solving fuzzy relational equations via semitensor product," *IEEE Transactions on Fuzzy Systems*, vol. 20, no. 2, pp. 390–396, 2012.
[9] J. Feng, H. Lv, and D. Cheng, "Multiple fuzzy relation and its application to coupled fuzzy control," *Asian Journal of Control*, vol. 15, no. 5, pp. 1313–1324, 2013.
[10] Y. Wang, C. Zhang, and Z. Liu, "A matrix approach to graph maximum stable set and coloring problems with application to multi-agent systems," *Automatica*, vol. 48, no. 7, pp. 1227–1236, 2012.
[11] M. Meng and J. Feng, "A matrix approach to hypergraph stable set and coloring problems with its application to storing problem," *Journal of Applied Mathematics*, pp. 1–10, 2014.
[12] D. Cheng, "On equivalence of matrices," *Asian Journal of Mathematics*, vol. 23, no. 2, pp. 257–348, 2019.
[13] D. Cheng, Z. Liu, and H. Qi, "Cross-dimensional linear systems," 2017, https://arxiv.org/abs/1710.03530.
[14] Q.-l. Zhang, B. Wang, and J.-e. Feng, "Solution and stability of continuous-time cross-dimensional linear systems," *Frontiers of Information Technology and Electronic Engineering*, vol. 22, no. 2, pp. 210–221, 2021.
[15] J.-e. Feng, B. Wang, and Y. Yu, "On dimensions of linear discrete dimension-unbounded systems," *International Journal of Control, Automation and Systems*, vol. 19, no. 1, pp. 471–477, 2021.
[16] P. Zhao, H. Guo, Y. Yu, and J. Feng, "On dimensions of dimension-bounded linear systems," *Science China Information Sciences*, vol. 64, no. 5, pp. 1–3, 2021.
[17] D. Cheng, Z. Liu, Z. Xu, and T. Shen, "Generalised semi-tensor product of matrices," *IET Control Theory and Applications*, vol. 14, no. 1, pp. 85–95, 2020.
[18] D. Cheng, Z. Xu, and T. Shen, "Equivalence-based model of dimension-varying linear systems," *IEEE Transactions on Automatic Control*, vol. 65, no. 12, pp. 5444–5449, 2020.
[19] J. Feng, Y. Li, and J. Zhao, "Four kinds of semi-tensor products and their relationships," *Journal of Liaocheng University (Nat. Sci.)*, vol. 33, no. 4, pp. 1–7, 2020, in Chinese.
[20] D. Cheng, H. Qi, and Z. Li, *Analysis and Control of Boolean Networks: A Semi-tensor Product Approach*, Springer, London, UK, 2011.
[21] D. Cheng, H. Qi, and Y. Zhao, *An Introduction to Semi-tensor Product of Matrices and its Application*, World Scientific, Singapore, 2011.

Hindawi
Mathematical Problems in Engineering
Volume 2021, Article ID 9930142, 17 pages
https://doi.org/10.1155/2021/9930142

Research Article

A BSDE Approach to Stochastic Differential Games with Regime Switching

J. Y. Li[1] and M. N. Tang[2]

[1]*College of Science, University of Shanghai for Science and Technology, Shanghai 200433, China*
[2]*Department of Mathematics, Huzhou University, Huzhou, Zhejiang 313000, China*

Correspondence should be addressed to M. N. Tang; tmorning@zjhu.edu.cn

Received 19 March 2021; Revised 6 April 2021; Accepted 17 April 2021; Published 10 June 2021

Academic Editor: Rongwei Guo

In this paper, we study a two-player zero-sum stochastic differential game with regime switching in the framework of forward-backward stochastic differential equations on a finite time horizon. By means of backward stochastic differential equation methods, in particular that of the notion from stochastic backward semigroups, we prove a dynamic programming principle for both the upper and the lower value functions of the game. Based on the dynamic programming principle, the upper and the lower value functions are shown to be the unique viscosity solutions of the associated upper and lower Hamilton–Jacobi–Bellman–Isaacs equations.

1. Introduction

The differential game is concerned with the problem that multiple players make decisions, according to their own advantages and trade-off with other partners in a dynamic system. Stochastic differential games (SDGs) have been well studied. Recently, Lv [1] studied the two-player zero-sum SDGs in a regime switching model with an infinite horizon. Compared with the traditional diffusion model, the regime switching model has two obvious advantages. First, the underlying Markov chain can be used to model discrete events with larger long-term system impact. For instance, in financial markets, it is easy to capture market trend by using finite state Markov chain. However, it is difficult to incorporate this dynamic into pure diffusion model. Second, when conducting numerical experiments, regime switching models require very limited data input. In recent years, due to the capacity for characterizing all kinds of random events and the tractability, regime switching models have attracted extensive attention [1–3]. In this paper, we introduce a new method, which is different from the method in [1]. We investigate two-player zero-sum SDGs with regime switching on a finite time horizon by using the backward stochastic differential equation (BSDE) methods.

Pardoux and Peng [4] first introduced the nonlinear BSDEs in 1990. The theory of BSDE was originally developed by Peng [5] for stochastic control theory. And later Hamadène and Lepeltier [6] and Hamadène et al. [7] introduced this theory to SDGs. Buckdahn and Li [8] studied a recursive SDG problem and interpreted the relationship between the controlled system and the Hamilton–Jacobi–Bellman–Isaacs (HJBI) equation. The theory of BSDEs has been well studied and applied to many fields, such as stochastic control, SDGs, mathematical finance, and partial differential equation theory (see [5–7, 9–11] for details). The readers interested in other topics about game theory are referred to [12–15].

In this paper, let $(\Omega, \mathcal{F}, \mathbb{P})$ be a fixed probability space on which a d-dimensional Brownian motion $\{B_s\}_{s\in[0,T]}$ and a Markov chain $\{\theta_s\}_{s\in[0,T]}$ are defined on some sample space Ω, $\mathcal{F}$ is the completed Borel σ-algebra over Ω, and P is the Wiener measure. Here, we assume that $\mathcal{F} = (\mathcal{F}_s)_{s\in[0,T]}$, where $\mathcal{F}_s \triangleq \mathcal{F}_s^{\theta} \vee \mathcal{F}_s^{B}$. Let $(\mathcal{F}_s^{B})_{s\in[0,T]}$ denote the filtration

generated by Brownian motion $\{B_s\}_{s\in[0,T]}$. And $(\mathscr{F}_s^{\theta})_{s\in[0,T]}$ denote the filtration generated by the Markov chain $\{\theta_s\}_{s\in[0,T]}$. Assume that $B_\cdot$ and $\theta_\cdot$ are independent. The Markov chain $\{\theta_s\}_{s\in[0,T]}$ takes values in a finite state space $\mathscr{M} = \{1,\ldots,m\}$ and is observable. And the generator $Q = (q_{ik})_{i,k\in\mathscr{M}} \in R^{m\times m}$ of the Markov chain $\{\theta_s\}_{s\in[0,T]}$ is given by

$$P(\theta_{s+\delta} = k \mid \theta_s = i, s\in[0,T]) = \begin{cases} q_{ik}\delta + o(\delta), & \text{if } k\neq i,\\ 1 + q_{ii}\delta + o(\delta), & \text{if } k = i,\end{cases} \tag{1}$$

where q_{ik} is the transition rate from market regime i to k, $q_{ii} = -\sum_{k\neq i} q_{ik} < 0$, and $q_{ik}\geq 0$, for every $(i,k)\in\mathscr{M}\times\mathscr{M}$.

We will investigate a two-player zero-sum SDG with regime switching in the framework of BSDE on a finite time horizon. The dynamics of the SDG are described by the following functional stochastic differential equation (SDE): for $t\in[0,T]$,

$$\begin{cases} \mathrm{d}X_s^{t,x,i;u,v} = b\left(s, X_s^{t,x,i;u,v}, \theta_s^{t,i}, u_s, v_s\right)\mathrm{d}s + \sigma\left(s, X_s^{t,x,i;u,v}, \theta_s^{t,i}, u_s, v_s\right)\mathrm{d}B_s, & s\in[t,T],\\ X_t^{t,x,i;u,v} = x, & \theta_t^{t,i} = i,\end{cases} \tag{2}$$

where $T>0$ is a fixed finite time horizon, $(t,x,i)\in[0,T]\times R^n\times\mathscr{M}$ is regarded as the initial state, and $P\left\{\theta_t^{t,i} = i\right\} = 1$. X_t is the value of X at time t, and $(u,v) = (u_s,v_s)_{s\in[t,T]}$ are the pair of $\mathscr{F}_t$-adapted processes, take their values in some compact metric spaces U and V, and are called admissible controls of the two players I and II, respectively. Precise assumptions on the coefficients b and σ are given in the next section.

The cost functional is introduced by BSDE:

$$\begin{aligned} Y_s^{t,x,i;u,v} &= \Phi\left(X_T^{t,x,i;u,v}, \theta_T^{t,i}\right)\\ &\quad + \int_s^T f\left(r, X_r^{t,x,i;u,v}, Y_r^{t,x,i;u,v}, Z_r^{t,x,i;u,v}, \theta_r^{t,i}, u_r, v_r\right)\mathrm{d}r - \int_s^T Z_r^{t,x,i,u,v}\mathrm{d}B_r,\\ &\quad s\in[t,T],\end{aligned} \tag{3}$$

where $X^{t,x,i;u,v}$ and $\theta^{t,i}$ are introduced in (2). The above BSDE has a unique solution $(Y_s^{t,x,i;u,v}, Z_s^{t,x,i;u,v})_{s\in[t,T]}$. And for given control processes $u\in U_{t,T}$ and $v\in V_{t,T}$, we introduce the associated cost functional:

$$J(t,x,i;u,v) := E\left[Y_t^{t,x,i;u,v} \mid \mathscr{F}_t\right], \quad (t,x,i)\in[0,T]\times R^n\times\mathscr{M}, \tag{4}$$

where $Y^{t,x,i;u,v}$ is defined by BSDE (3). In the game, player I aims to maximize (4) and contrarily player II aims to minimize (4). We define the lower and the upper value functions W and U, respectively:

$$W(t,x,i) := \operatorname*{essinf}_{\beta\in\mathscr{B}_{t,T}} \operatorname*{esssup}_{u\in U_{t,T}} J(t,x,i;u,\beta(u)), \tag{5}$$

$$U(t,x,i) := \operatorname*{esssup}_{\alpha\in\mathscr{A}_{t,T}} \operatorname*{essinf}_{v\in V_{t,T}} J(t,x,i;\alpha(v),v). \tag{6}$$

Precise definitions of α and β are given in the next section. In the case $W = U$ we say that the game admits a value. The main objective of this paper is to show that W and U are, respectively, the unique viscosity solutions of the following lower and upper HJBI equations, and both are systems consisting of m coupled equations:

$$\begin{cases} \dfrac{\partial}{\partial t}W(t,x,i) + H^-\left(t,x,i,W,DW,D^2W\right) + \displaystyle\sum_{k\neq i} q_{ik}\left[W(t,x,k) - W(t,x,i)\right] = 0,\\ W(T,x,i) = \Phi(x,i),\end{cases} \tag{7}$$

$$\begin{cases} \dfrac{\partial}{\partial t}U(t,x,i) + H^+\left(t,x,i,U,DU,D^2U\right) + \displaystyle\sum_{k\neq i} q_{ik}\left[U(t,x,k) - U(t,x,i)\right] = 0\\ U(T,x,i) = \Phi(x,i),\end{cases} \tag{8}$$

associated with

$$H^{-}(t,x,i,r,p,A,u,v)=\sup_{u\in U}\inf_{v\in V}H(t,x,i,r,p,A,u,v),$$
$$H^{+}(t,x,i,r,p,A,u,v)=\inf_{v\in V}\sup_{u\in U}H(t,x,i,r,p,A,u,v), \tag{9}$$

where H is defined as

$$H(t,x,i,p,A,u,v)=\frac{1}{2}\mathrm{Tr}\left(\sigma\sigma^{T}(t,x,i,u,v)\cdot A\right)+\langle b(t,x,i,u,v),p\rangle + f\left(t,x,i,r,\sigma^{T}(t,x,i,u,v)p,u,v\right), \tag{10}$$

for $(t,x,i,r,p,A,u,v)\in[0,T]\times R^{n}\times\mathscr{M}\times R\times R^{n}\times R^{n\times n}\times U\times V\longrightarrow R$. If Isaacs' condition holds, i.e., $H^{-}=H^{+}$, then (5) and (6) coincide, and the uniqueness of viscosity solution implies $W=U$, that is, the game admits a value.

The paper is organized as follows. In Section 2, we introduce some notations and preliminaries, which will be needed in what follows. In Section 3, we introduce the dynamic programming principle. In Section 4, based on the dynamic programming principle, we investigate that the upper and the lower value functions are the unique viscosity solutions of the associated upper and lower HJBI equations.

2. Preliminaries

Let us introduce the following spaces, which will be needed in what follows.

$$\begin{aligned}
&L^{2}(\Omega,\mathscr{F}_{T},P;R^{n});=\left\{\xi\colon\Omega\longrightarrow R^{n}\text{ is }\mathscr{F}_{T}-\text{measurable variable such that }E\left[|\xi|^{2}\right]<+\infty\right\},\\
&\mathscr{S}^{2}(0,T;\mathrm{R}^{n}):=\left\{(\psi(t))_{t\in[0,T]}\mathrm{R}^{n}-\text{valued }\mathscr{F}_{T}^{\theta}\vee\mathscr{F}^{B}-\text{adapted continous process: }E\left[\sup_{t\in[0,T]}|\psi(t)|^{2}\right]<+\infty\right\},\\
&\mathscr{H}^{2}(0,T;\mathrm{R}^{n}):=\left\{(\psi(t))_{t\in[0,T]}\mathrm{R}^{n}-\text{valued }\mathscr{F}_{T}^{\theta}\vee\mathscr{F}^{B}-\text{adapted process: }E\left[\int_{0}^{T}|\psi(t)|^{2}\mathrm{d}t\right]<+\infty\right\}.
\end{aligned} \tag{11}$$

We consider the BSDE with data (f,ξ):

$$Y_{t}=\xi+\int_{t}^{T}f(s,Y_{s},Z_{s})\mathrm{d}s-\int_{t}^{T}Z_{s}\mathrm{d}B_{s},\quad t\in[0,T]. \tag{12}$$

Here $f\colon\Omega\times[0,T]\times R\times R^{d}\longrightarrow R$ is such that, for any $(y,z)\in R\times R^{d}$, $f(\cdot,y,z)$ is $\mathscr{F}_{T}^{\theta}\vee\mathscr{F}^{B}$-progressively measurable. We make the following assumptions:

(A1) There exists a positive constant C such that for all $(t,y_{i},z_{i})\in[0,T]\times R\times R^{d}, i=1,2,$

$$\left|f(t,y_{1},z_{1})-f(t,y_{2},z_{2})\right|\le C\left(\left|y_{1}-y_{2}\right|+\left|z_{1}-z_{2}\right|\right),\text{ a.s.} \tag{13}$$

(A2) $f(\cdot,0,0)\in\mathscr{H}^{2}(0,T;R)$.

Lemma 1. *Let assumptions (A1) and (A2) hold; then, for any random variable $\xi\in L^{2}(\Omega,\mathscr{F}_{T},P)$, BSDE (12) has a unique solution:*

$$(Y,Z)\in\mathscr{S}^{2}(0,T;R)\times\mathscr{H}^{2}\left(0,T;R^{d}\right). \tag{14}$$

We give the comparison theorem for solutions of BSDEs.

Lemma 2 (comparison theorem). *Let $\xi^{1},\xi^{2}\in L^{2}(\Omega,\mathscr{F}_{T},P;R)$ and f^{1} and f^{2} satisfy (A1) and (A2). We denote by (Y^{1},Z^{1}) and (Y^{2},Z^{2}) the solutions of BSDEs with data (f^{1},ξ^{1}) and (f^{2},ξ^{2}), respectively, and we suppose that*

(i) $\xi^{1}\le\xi^{2}, P-a.s.$

(ii) $f^{1}(t,Y_{t}^{2},Z_{t}^{2})\le f^{2}(t,Y_{t}^{2},Z_{t}^{2}), dtdP-a.e.$

Then, we have $Y_{t}^{1}\le Y_{t}^{2}$, a.s., for all $t\in[0,T]$. Moreover, if $P(\xi^{1}<\xi^{2})>0$, then $P(Y_{t}^{1}<Y_{t}^{2})>0, t\in[0,T]$, and in particular, $Y_{0}^{1}<Y_{0}^{2}$.

With the notations in the above lemma, we assume that, for some $f\colon[0,T]\times R\times R^{d}\longrightarrow R$ satisfying (A1) and (A2), the drivers $f_{i}, i=1,2$ have the following form:

$$\begin{aligned}
f^{1}(s,y,z)&=f(s,y,z)+\varphi_{1}(s),\\
f^{2}(s,y,z)&=f(s,y,z)+\varphi_{2}(s).
\end{aligned} \tag{15}$$

Then, we have the following lemma.

Lemma 3. *The difference of the solutions (Y^{1},Z^{1}) and (Y^{2},Z^{2}) of BSDE (12) with the data (ξ^{1},f^{1}) and (ξ^{2},f^{2}), respectively, satisfies the following estimate:*

$$\begin{aligned}
&\left|Y_{t}^{1}-Y_{t}^{2}\right|+\frac{1}{2}E\left\{\int_{t}^{T}e^{\beta(t-s)}\left[\left|Y_{s}^{1}-Y_{s}^{2}\right|^{2}+\left|Z_{s}^{1}-Z_{s}^{2}\right|^{2}\right]\mathrm{d}s|\mathscr{F}_{t}\right\}\\
&\quad\le E\left\{e^{\beta(T-t)}\left|\xi^{1}-\xi^{2}\right|^{2}|\mathscr{F}_{t}\right\}\\
&\qquad+E\left\{\int_{t}^{T}e^{\beta(t-s)}\left|\varphi_{1}(s)-\varphi_{2}(s)\right|^{2}\mathrm{d}s|\mathscr{F}_{t}\right\},
\end{aligned} \tag{16}$$

where $\beta=16(1+C^{2})$ and C is the Lipschitz constant in (A1).

For the proof of the above two lemmas, the readers can refer to [11, 16].

We now consider the assumptions on the coefficients b and σ. The coefficients b: $[0,T]\times R^n\times\mathscr{M}\times U\times V\longrightarrow R^n$ and σ: $[0,T]\times R^n\times\mathscr{M}\times U\times V\longrightarrow R^{n\times d}$ are two given functions. The mappings b and σ satisfy the following conditions:

(A3)

(i) For every fixed $x\in R^n, i\in\mathscr{M}$, $b(\cdot,x,i,\cdot,\cdot)$ and $\sigma(\cdot,x,i,\cdot,\cdot)$ are continuous with respect to (t,u,v).

(ii) For any $x,x'\in R^n, i\in\mathscr{M}$, $u\in U$ and $v\in V$, there exists a positive constant C such that

$$\left|b(t,x,i,u,v)-b(t,x',i,u,v)\right|+\left|\sigma(t,x,i,u,v)-\sigma(t,x',i,u,v)\right|\le C\left|x-x'\right|. \tag{17}$$

From (A3), we can get the global linear growth conditions of b and σ, i.e., the existence of some $C>0$ such that, for all $t\in[0,T]$, $u\in U$, $v\in V$, $x\in R^n$, $i\in\mathscr{M}$,

$$|b(t,x,i,u,v)|+|\sigma(t,x,i,u,v)|\le C(1+|x|). \tag{18}$$

Suppose the above assumptions hold; for any $u\in U$ and $v\in V$, control system (2) has a unique solution $\{X_s^{t,x,i;u,v}, s\in[t,T]\}$. And we have the following estimates.

Lemma 4. *Under the assumptions of the mappings b and σ, there exists a positive constant C such that, for any $x,x'\in R^n$, $i\in\mathscr{M}$, and $u\in U, v\in V$,*

$$\begin{gathered}E\left\{\sup_{s\in[t,T]}\left|X_s^{t,x,i;u,v}\right|^2|\mathscr{F}_t\right\}\le C\left(1+|x|^2\right),\quad P-\text{a.s.},\\ E\left\{\sup_{s\in[t,T]}\left|X_s^{t,x,i;u,v}-X_s^{t,x',i;u,v}\right|^2|\mathscr{F}_t\right\}\le C\left|x-x'\right|^2,\quad P-\text{a.s.}\end{gathered} \tag{19}$$

Suppose that the two functions f: $[0,T]\times R^n\times R\times R^d\times R^{m\times m}\times U\times V\longrightarrow R$ and the terminal cost Φ: $R^n\longrightarrow R$ satisfy the following conditions:

(A4)

(i) For any fixed $(x,y,z,i)\in R^n\times R\times R^d\times\mathscr{M}$, $f(\cdot,x,y,z,i,\cdot,\cdot)$ is continuous with respect to (t,u,v).

(ii) There exists $C>0$ such that, for all $t\in[0,T]$, $x,x'\in R^n$, $y,y'\in R$, $z,z'\in R^d$, $i\in\mathscr{M}$, $u\in U$ and $v\in V$,

$$\begin{aligned}&\left|f(t,x,y,z,i,u,v)-f(t,x',y',z',i,u,v)\right|\\ &\quad\le C\left(\left|x-x'\right|+(y-y')+\left|z-z'\right|\right).\end{aligned} \tag{20}$$

(iii) There is a constant $C>0$ such that, for all $x,x'\in R^n$, $i\in\mathscr{M}$,

$$\left|\Phi(x,i)-\Phi(x',i)\right|\le C\left|x-x'\right|. \tag{21}$$

Under the above conditions, (3) has a unique solution $(Y_s^{t,x,i;u,v}, Z_s^{t,x,i;u,v})_{s\in[t,T]}$. And we have the following estimates.

Lemma 5. *For all $t\in[0,T]$, $i\in\mathscr{M}$, $u\in U$, and $v\in V$, there exists a constant $C>0$ such that,*

$$\begin{gathered}\left|Y_t^{t,x,i;u,v}\right|\le C(1+|x|),\quad P-\text{a.s.},\\ \left|Y_t^{t,x,i;u,v}-Y_t^{t,x',i;u,v}\right|\le C\left|x-x'\right|,\quad P-\text{a.s.}\end{gathered} \tag{22}$$

For the proof of this lemma, the readers can refer to [17].

Now, we introduce the admissible controls and admissible strategies. Let t_1, t_2 be two deterministic times, and $0\le t\le t_1\le t_2\le T$.

Definition 1. An admissible control process $u=\{u_r, r\in[t_1,t_2]\}$ (resp., $v=\{v_r, r\in[t_1,t_2]\}$) for player I (resp., player II) on $[t_1,t_2]$ is a process taking values in U (resp., V), progressively measurable with respect to the filtration $\mathscr{F}$, where $\mathscr{F}=\{\mathscr{F}_r, r\in[t_1,t_2]\}$ is the filtration generated by B and θ.

The set of all admissible controls for player I (resp., player II) on time $[t,T]$ is denoted by $U_{t,T}$ (resp., $V_{t,T}$).

Definition 2. A nonanticipative strategy for player I on $[t,T]$ is a mapping α: $V\longrightarrow U$ such that, for any $\mathscr{F}_t$-stopping time S and any $v,v'\in V_{t,T}$, if $v\equiv v'$ on t,S (with the notation $t,S=\{(s,\omega)\in[0,T]\times\Omega, t\le s\le S(\omega)\}$). In the same way, we define a nonanticipative strategy β: $U_{t,T}\longrightarrow V_{t,T}$ for player II on $[t,T]$.

The set of all nonanticipative strategies for player I (resp., player II) on $[t,T]$ is denoted by $\mathscr{A}_{t,T}$ (resp., $\mathscr{B}_{t,T}$).

Now we give some properties about the lower and the upper value functions W and U. The following lemma was established in [8], and the situation was slightly different. For the proof of this lemma, the readers can refer to [8].

Lemma 6. *Under the assumptions (A3) and (A4), for all $(t,x,i)\in[0,T]\times R^n\times\mathscr{M}$, the value functions $W(t,x,i)$ and $U(t,x,i)$ are deterministic functions.*

From (4), (5), and (22), we get the properties of the lower value function W in the following.

Lemma 7. *Under the assumptions (A3) and (A4), for all $(t,x,i)\in[0,T]\times R^n\times\mathscr{M}$ and $x,x'\in R^n$, we have*

(i)

$$|W(t,x,i)| \le C(1+|x|). \tag{23}$$

(ii) $W(\cdot,x,i)$ *is* $(1/2)$*-Hölder continuous with respect to* t*:*

$$\left|W(t,x,i)-W(t',x,i)\right| \le C(1+|x|)\left|t-t'\right|^{(1/2)}. \tag{24}$$

(iii)

$$\left|W(t,x,i)-W(t,x',i)\right| \le C\left|x-x'\right|. \tag{25}$$

The same properties hold true for the function U.

3. Dynamic Programming Principles

The dynamic programming principle is one of the principal and most commonly used methods to solve the optimal control problem. In this section, we present the dynamic programming principle for a two-player zero-sum SDG with regime switching in the framework of BSDE on a finite time horizon. It will be used in the next section.

We first introduce the backward stochastic semigroup. For given initial state (t,x,i), a positive number $\delta \le T-t$, for admissible control processes $u_\cdot \in U_{t,t+\delta}$ and $v_\cdot \in V_{t,t+\delta}$, and a real value random variable $\eta \in (\Omega, \mathscr{F}_{t+\delta}, P; R)$, we define

$$G_{t,t+\delta}^{t,x,i;u,v}[\eta] := \overline{Y}_t^{t,x,i;u,v}, \tag{26}$$

where $(\overline{Y}_s^{t,x,i;u,v}, \overline{Z}_s^{t,x,i;u,v})_{s\in[t,t+\delta]}$ is the solution of the following BSDE with terminal time $t+\delta$:

$$\begin{aligned}\overline{Y}_s^{t,x,i;u,v} &= \eta + \int_s^{t+\delta} f\left(r, X_r^{t,x,i;u,v}, \overline{Y}_r^{t,x,i;u,v}, \overline{Z}_r^{t,x,i;u,v}, \theta_r^{t,i}, u_r, v_r\right)\mathrm{d}r \\ &\quad - \int_s^{t+\delta} \overline{Z}_r^{t,x,i;u,v}\mathrm{d}B_r, \quad P-\text{a.s.}, s\in[t,t+\delta],\end{aligned} \tag{27}$$

and $X^{t,x,i;u,v}$ is the solution of SDE (2). According to the uniqueness of the solution of the BSDE, we observe that for the solution $Y^{t,x,i;u,v}$ of BSDE (3), we have

$$\begin{aligned}J(t,x,i;u,v) &= E\left[Y_t^{t,x,i;u,v}|\mathscr{F}_t\right] = E\left[G_{t,T}^{t,x,i;u,v}\left[\Phi\left(X_T^{t,x,i;u,v},\theta_T^{t,i}\right)\right]|\mathscr{F}_t\right] \\ &= E\left[G_{t,t+\delta}^{t,x,i;u,v}\left[Y_{t+\delta}^{t,x,i;u,v}\right]|\mathscr{F}_t\right] \\ &= E\left[G_{t,t+\delta}^{t,x,i;u,v}\left[E\left[Y_{t+\delta}^{t,x,i;u,v}|\mathscr{F}_{t+\delta}\right]\right]|\mathscr{F}_t\right] \\ &= E\left[G_{t,t+\delta}^{t,x,i;u,v}\left[J\left(t+\delta, X_{t+\delta}^{t,x,i;u,v}, \theta_{t+\delta}^{t,i}; u,v\right)\right]|\mathscr{F}_t\right].\end{aligned} \tag{28}$$

We now introduce the dynamic programming principle for the value functions of SDGs with regime switching.

Proposition 1. *Under the assumptions (A3) and (A4), the following dynamic programming principle holds: for all* $0<\delta\le T-t$, $x\in R^n$, $i\in\mathscr{M}$,

$$\begin{aligned}U(t,x,i) &= \operatorname*{esssup}_{\alpha\in\mathscr{A}_{t,t+\delta}} \operatorname*{essinf}_{v\in V_{t,t+\delta}} E\left[G_{t,t+\delta}^{t,x,i;\alpha(v),v}\left[U\left(t+\delta, X_{t+\delta}^{t,x,i;\alpha(v),v}, \theta_{t+\delta}^{t,i}\right)\right]|\mathscr{F}_t\right], \\ W(t,x,i) &= \operatorname*{essinf}_{\beta\in\mathscr{B}_{t,t+\delta}} \operatorname*{esssup}_{u\in U_{t,t+\delta}} E\left[G_{t,t+\delta}^{t,x,i;u,\beta(u)}\left[W\left(t+\delta, X_{t+\delta}^{t,x,i;u,\beta(u)}, \theta_{t+\delta}^{t,i}\right)\right]|\mathscr{F}_t\right].\end{aligned} \tag{29}$$

Put

$$W_\delta(t,x,i) = \operatorname*{essinf}_{\beta\in\mathscr{B}_{t,t+\delta}} \operatorname*{esssup}_{u\in U_{t,t+\delta}} E\left[G_{t,t+\delta}^{t,x,i;u,\beta(u)}\left[W\left(t+\delta, X_{t+\delta}^{t,x,i;u,\beta(u)}, \theta_{t+\delta}^{t,i}\right)\right]|\mathscr{F}_t\right]. \tag{30}$$

We proceed with the proof that $W_\delta(t,x,i)$ coincides with $W(t,x,i)$ into the following steps.

Step 1. Let $\beta\in\mathscr{B}_{t,T}$ be arbitrarily fixed. Then, given a $u_2\in U_{t+\delta,T}$, we define as follows the restriction β_1 of β to $U_{t,t+\delta}$:

$$\beta_1(u_1) := \beta(u_1\oplus u_2)|_{[t,t+\delta]}, \quad u_1\in U_{t,t+\delta}, \tag{31}$$

where $u_1\oplus u_2 := u_1\chi_{[t,t+\delta]} + u_2\chi_{(t+\delta,T]}$ extends u_1 to an element of $U_{t,T}$. Obviously, $\beta_1\in\mathscr{B}_{t,t+\delta}$. And, from the nonanticipative property of β we deduce that β_1 is independent of the special choice of $u_2\in U_{t+\delta,T}$. Thus, from the definition of $W_\delta(t,x,i)$,

$$W_\delta(t,x,i) \le \operatorname*{esssup}_{u_1\in U_{t,t+\delta}} E\left[G_{t,t+\delta}^{t,x,i;u_1,\beta_1(u_1)}\left[W\left(t+\delta, X_{t+\delta}^{t,x,i;u_1,\beta_1(u_1)}, \theta_{t+\delta}^{t,i}\right)\right]|\mathscr{F}_t\right], \tag{32}$$

and we use the notation $\mathscr{I}_\delta(t,x,i;u,v) := E[G_{t,t+\delta}^{t,x,i;u,v}[W(t+\delta, X_{t+\delta}^{t,x,i;u,v}, \theta_{t+\delta}^{t,i})]|\mathscr{F}_t]$ for some sequences $\{u_l^1, l \geq 1\} \subset U_{t,t+\delta}$ such that,

$$\mathscr{I}_\delta(t,x,i;\beta_1) := \operatorname*{esssup}_{u_1 \in U_{t,t+\delta}} \mathscr{I}_\delta(t,x,i;u_1,\beta_1(u_1)) = \sup_{l\geq 1} \mathscr{I}_\delta\left(t,x,i;u_l^1,\beta_1\left(u_l^1\right)\right), \quad P-\text{a.s.} \tag{33}$$

Let $\varepsilon > 0$ and set $\widetilde{\Gamma}_l := \{\mathscr{I}_\delta(t,x,i;\beta_1) \leq \mathscr{I}_\delta(t, x, i; u_l^1, \beta_1(u_l^1)) + \varepsilon\} \in \mathscr{F}_t, l \geq 1$. Construct $\Gamma_1 := \widetilde{\Gamma}_1$, $\Gamma_l := \widetilde{\Gamma}_l, (\cup_{k=1}^{l-1}\widetilde{\Gamma}_k) \in \mathscr{F}_t, l \geq 2$. Certainly, $\{\Gamma_l\}_{l\geq 1}$ forms an $(\Omega, \mathscr{F}_t)$-partition, and $u_1^\varepsilon := \sum_{l\geq 1}\chi_{\Gamma_l}u_l^1 \in U_{t,t+\delta}$. Moreover, from the nonanticipativity of β_1, we have $\beta_1(u_1^\varepsilon) = \sum_{l\geq 1}\chi_{\Gamma_l}\beta_1(u_l^1)$. According to the existence and uniqueness of the BSDEs, it follows that

$$\mathscr{I}_\delta(t,x,i;u_1^\varepsilon,\beta_1(u_1^\varepsilon)) = \sum_{l\geq 1}\chi_{\Gamma_l}\mathscr{I}_\delta\left(t,x,i;u_l^1,\beta_1\left(u_l^1\right)\right), \quad P-\text{a.s.}, \tag{34}$$

for $\beta_1 \in \mathscr{B}_{t,t+\delta}$. Hence,

$$\begin{aligned} W_\delta(t,x,i) &\leq \mathscr{I}_\delta(t,x,i;\beta_1) \\ &\leq \sum_{l\geq 1}\chi_{\Gamma_l}\mathscr{I}_\delta\left(t,x,i;u_l^1,\beta_1\left(u_l^1\right)\right) + \varepsilon \\ &= \mathscr{I}_\delta(t,x,i;u_1^\varepsilon,\beta_1(u_1^\varepsilon)) + \varepsilon \\ &= E\left[G_{t,t+\delta}^{t,x,i;u_1^\varepsilon,\beta_1(u_1^\varepsilon)}\left[W\left(t+\delta, X_{t+\delta}^{t,x,i;u_1^\varepsilon,\beta_1(u_1^\varepsilon)}, \theta_{t+\delta}^{t,i}\right)\right]|\mathscr{F}_t\right] + \varepsilon, \quad P-\text{a.s.} \end{aligned} \tag{35}$$

We now focus on the interval $[t+\delta, T]$. Because $\beta_1(\cdot) := \beta(\cdot \oplus u_2) \in \mathscr{B}_{t,t+\delta}$ does not depend on $u_2 \in U_{t+\delta,T}$, we can define $\beta_2(u_2) := \beta(u_1^\varepsilon \oplus u_2)|_{[t+\delta,T]}$, for any $u_2 \in U_{t+\delta,T}$. From $\beta \in \mathscr{B}_{t,T}$, we know that $\beta_2 \colon U_{t+\delta,T} \longrightarrow V_{t+\delta,T}$ belongs to $\mathscr{B}_{t+\delta,T}$. Thus, from the definition of $W(t+\delta, y, j)$, for any $(y,j) \in R^n \times \mathscr{M}$,

$$W(t+\delta,y,j) \leq \operatorname*{esssup}_{u_2\in U_{t+\delta,T}} J(t+\delta,y,j;u_2,\beta_2(u_2)), \quad P-\text{a.s.} \tag{36}$$

From Lemmas 5 and 7, there exists a constant $C \in R$ such that, for any $u_2 \in U_{t+\delta,T}$, $y, y' \in R^n$,

$$\begin{aligned} &(i)\ \left|W(t+\delta,y,j) - W(t+\delta,y',j)\right| \leq C\left|y-y'\right|, \\ &(ii)\ \left|J(t+\delta,y,j;u_2,\beta_2(u_2)) - J(t+\delta,y',j;u_2,\beta_2(u_2))\right| \leq C\left|y-y'\right|, \quad P-\text{a.s.} \end{aligned} \tag{37}$$

We can show by approximating $X_{t+\delta}^{t,x,i;u_1^\varepsilon,\beta_1(u_1^\varepsilon)}$ that

$$\begin{aligned} &W\left(t+\delta, X_{t+\delta}^{t,x,i;u_1^\varepsilon,\beta_1(u_1^\varepsilon)}, \theta_{t+\delta}^{t,i}\right) \\ &\quad \leq \operatorname*{esssup}_{u_2\in U_{t+\delta,T}} J\left(t+\delta, X_{t+\delta}^{t,x,i;u_1^\varepsilon,\beta_1(u_1^\varepsilon)}, \theta_{t+\delta}^{t,i}; u_2, \beta_2(u_2)\right), \quad P-\text{a.s.} \end{aligned} \tag{38}$$

To estimate the right side of the latter inequality, we note that there exists some sequence $\{u_k^2, k \geq 1\} \subset U_{t+\delta,T}$ such that

$$\begin{aligned} &\operatorname*{esssup}_{u_2\in U_{t+\delta,T}} J\left(t+\delta, X_{t+\delta}^{t,x,i;u_1^\varepsilon,\beta_1(u_1^\varepsilon)}, \theta_{t+\delta}^{t,i}; u_2, \beta_2(u_2)\right) \\ &\quad = \sup_{k\geq 1} J\left(t+\delta, X_{t+\delta}^{t,x,i;u_1^\varepsilon,\beta_1(u_1^\varepsilon)}, \theta_{t+\delta}^{t,i}, u_k^2, \beta_2\left(u_k^2\right)\right), \quad P-\text{a.s.} \end{aligned} \tag{39}$$

Let $\varepsilon > 0$ and set $\widetilde{\triangle}_k := \{\operatorname{esssup}_{u_2\in U_{t+\delta,T}} J(t+\delta, X_{t+\delta}^{t,x,i;u_1^\varepsilon,\beta_1(u_1^\varepsilon)}, \theta_{t+\delta}^{t,i}; u_2, \beta_2(u_2)) \leq J(t+\delta, X_{t+\delta}^{t,x,i;u_1^\varepsilon,\beta_1(u_1^\varepsilon)}, \theta_{t+\delta}^{t,i}; u_k^2, \beta_2(u_k^2)) + \varepsilon\} \in \mathscr{F}_{t+\delta}, k \geq 1$. Construct $\Delta_1 := \widetilde{\Delta}_1$, $\Delta_k := \widetilde{\Delta}_k, (\cup_{j=1}^{k-1}\widetilde{\Delta}_j) \in \mathscr{F}_{t+\delta}, k \geq 2$. Certainly, $\{\Delta_k\}_{k\geq 1}$

forms an $(\Omega, \mathscr{F}_{t+\delta})$-partition; moreover, $u_2^\varepsilon := \sum_{k\geq 1}\chi_{\triangle_k} u_k^2 \in U_{t+\delta,T}$. Therefore, from the non-anticipativity of β_2, we have $\beta_2(u_2^\varepsilon) = \sum_{k\geq 1}\chi_{\triangle_k}\beta_2(u_k^2)$, and from the definition of β_1, β_2, we know that $\beta(u_1^\varepsilon \oplus u_2^\varepsilon) = \beta_1(u_1^\varepsilon) \oplus \beta_2(u_2^\varepsilon)$. According the existence and uniqueness of our BSDE, it follows that

$$\begin{aligned} J\left(t+\delta, X_{t+\delta}^{t,x,i;u_1^\varepsilon,\beta_1(u_1^\varepsilon)}, \theta_{t+\delta}^{t,i}; u_2^\varepsilon, \beta_2(u_2^\varepsilon)\right) &= E\left[Y_{t+\delta}^{t+\delta, X_{t+\delta}^{t,x,i;u_1^\varepsilon,\beta_1(u_1^\varepsilon)}, \theta_{t+\delta}^{t,i}; u_2^\varepsilon, \beta_2(u_2^\varepsilon)} \middle| \mathscr{F}_{t+\delta}\right] \\ &= E\left[\sum_{k\geq 1}\chi_{\Delta_k} Y_{t+\delta}^{t+\delta, X_{t+\delta}^{t,x,i;u_1^\varepsilon,\beta_1(u_1^\varepsilon)}, \theta_{t+\delta}^{t,i}; u_k^\varepsilon, \beta_2(u_k^\varepsilon)} \middle| \mathscr{F}_{t+\delta}\right] \\ &= \sum_{k\geq 1}\chi_{\Delta_k} J\left(t+\delta, X_{t+\delta}^{t,x,i;u_1^\varepsilon,\beta_1(u_1^\varepsilon)}, \theta_{t+\delta}^{t,i}; u_k^\varepsilon, \beta_2(u_k^\varepsilon)\right), \quad P-\text{a.s.} \end{aligned} \tag{40}$$

Therefore,

$$\begin{aligned} &W\left(t+\delta, X_{t+\delta}^{t,x,i;u_1^\varepsilon,\beta_1(u_1^\varepsilon)}, \theta_{t+\delta}^{t,i}\right) \\ &\leq \operatorname*{esssup}_{u_2\in U_{t+\delta,T}} J\left(t+\delta, X_{t+\delta}^{t,x,i;u_1^\varepsilon,\beta_1(u_1^\varepsilon)}, \theta_{t+\delta}^{t,i}; u_2, \beta_2(u_2)\right) \\ &\leq E\left[\sum_{k\geq 1}\chi_{\Delta_k} Y_{t+\delta}^{t,x,i;u_1^\varepsilon\oplus u_k^2,\beta(u_1^\varepsilon\oplus u_k^2)} \middle| \mathscr{F}_{t+\delta}\right] + \varepsilon \\ &= E\left[Y_{t+\delta}^{t,x,i;u_1^\varepsilon\oplus u_2^\varepsilon,\beta(u_1^\varepsilon\oplus u_2^\varepsilon)} \middle| \mathscr{F}_{t+\delta}\right] + \varepsilon \\ &= E\left[Y_{t+\delta}^{t,x,i;u^\varepsilon,\beta(u^\varepsilon)} \middle| \mathscr{F}_{t+\delta}\right] + \varepsilon, \quad P-\text{a.s.}, \end{aligned} \tag{41}$$

where $u^\varepsilon := u_1^\varepsilon \oplus u_2^\varepsilon \in U_{t,T}$. From (35) and (41),

$$\begin{aligned} W_\delta(t,x,i) &\leq E\left[G_{t,t+\delta}^{t,x,i;u_1^\varepsilon,\beta_1(u_1^\varepsilon)}\left[E\left[Y_{t+\delta}^{t,x,i;u^\varepsilon,\beta(u^\varepsilon)} \middle| \mathscr{F}_{t+\delta}\right] + \varepsilon\right] \middle| \mathscr{F}_t\right] \\ &\leq E\left[G_{t,t+\delta}^{t,x,i;u_1^\varepsilon,\beta_1(u_1^\varepsilon)}\left[E\left[Y_{t+\delta}^{t,x,i;u^\varepsilon,\beta(u^\varepsilon)} \middle| \mathscr{F}_{t+\delta}\right]\right] \middle| \mathscr{F}_t\right] + (C+1)\varepsilon \\ &= E\left[G_{t,t+\delta}^{t,x,i;u^\varepsilon,\beta(u^\varepsilon)}\left[E\left[Y_{t+\delta}^{t,x,i;u^\varepsilon,\beta(u^\varepsilon)} \middle| \mathscr{F}_{t+\delta}\right]\right] \middle| \mathscr{F}_t\right] + (C+1)\varepsilon \\ &= E\left[G_{t,t+\delta}^{t,x,i;u^\varepsilon,\beta(u^\varepsilon)}\left[Y_{t+\delta}^{t,x,i;u^\varepsilon,\beta(u^\varepsilon)}\right] \middle| \mathscr{F}_t\right] + (C+1)\varepsilon \\ &= E\left[Y_t^{t,x,i;u^\varepsilon,\beta(u^\varepsilon)} \middle| \mathscr{F}_t\right] + (C+1)\varepsilon \\ &\leq \operatorname*{esssup}_{u\in U_{t,T}} E\left[Y_t^{t,x,i;u,\beta(u)} \middle| \mathscr{F}_t\right] + (C+1)\varepsilon, \quad P-\text{a.s.} \end{aligned} \tag{42}$$

Since $\beta \in \mathscr{B}_{t,T}$ has been arbitrarily chosen, we have (42) for all $\beta \in \mathscr{B}_{t,T}$. Thus,

$$\begin{aligned} W_\delta(t,x,i) &\leq \operatorname*{essinf}_{\beta\in\mathscr{B}_{t,T}} \operatorname*{esssup}_{u\in U_{t,T}} E\left[Y_t^{t,x,i;u,\beta(u)} \middle| \mathscr{F}_t\right] + (C+1)\varepsilon \\ &= W(t,x,i) + (C+1)\varepsilon. \end{aligned} \tag{43}$$

Then, letting $\varepsilon \longrightarrow 0$, we get $W_\delta(t,x,i) \leq W(t,x,i)$.

Step 2. We now deal with the other case: $W(t,x,i) \leq W_\delta(t,x,i)$. From the definition of $W_\delta(t,x,i)$, we have

$$\begin{aligned} W_\delta(t,x,i) &= \operatorname*{essinf}_{\beta_1\in\mathscr{B}_{t,t+\delta}} \operatorname*{esssup}_{u_1\in U_{t,t+\delta}} E\left[G_{t,t+\delta}^{t,x,i;u_1,\beta_1(u_1)}\left[W\left(t+\delta, X_{t+\delta}^{t,x,i;u_1,\beta_1(u_1)}, \theta_{t+\delta}^{t,i}\right)\right] \middle| \mathscr{F}_t\right] \\ &= \operatorname*{essinf}_{\beta_1\in\mathscr{B}_{t,t+\delta}} \mathscr{I}_\delta(t,x,i;\beta_1), \end{aligned} \tag{44}$$

for some $\{\beta_l^1, l \geq 1\} \subset \mathscr{B}_{t,t+\delta}$ such that,

$$W_\delta(t,x,i) = \inf_{l\geq 1} \mathscr{I}_\delta\left(t,x,i;\beta_l^1\right), \quad P-\text{a.s.} \tag{45}$$

For any $\varepsilon > 0$, we put $\widetilde{\Lambda}_l := \{\mathscr{I}_\delta(t,x,i;\beta_l^1) - \varepsilon \leq W_\delta(t,x,i)\} \in \mathscr{F}_t, l \geq 1$, $\Lambda := \widetilde{\Lambda}_1$, and $\Lambda_l := \widetilde{\Lambda}_l, (\cup_{k=1}^{l-1}\widetilde{\Lambda}_k) \in \mathscr{F}_t, l \geq 2$. Certainly, $\{\Lambda_l\}_{l\geq 1}$ forms an $(\Omega, \mathscr{F}_t)$-partition; moreover, $\beta_1^\varepsilon := \sum_{l\geq 1}\chi_{\Lambda_l}\beta_l^1 \in \mathscr{B}_{t,t+\delta}$. According the existence and uniqueness of our BSDE, we conclude that

$$\mathscr{I}_\delta(t,x,i;u_1,\beta_1^\varepsilon(u_1)) = \sum_{l\geq 1}\chi_{\Lambda_l}\mathscr{I}_\delta\left(t,x,i;u_1,\beta_l^1(u_1)\right), \quad P-\text{a.s}, \tag{46}$$

for all $u_1 \in U_{t,t+\delta}$. Next,

$$\begin{aligned}
&W_\delta(t,x,i)\\
&\quad\geq \sum_{l\geq 1}\chi_{\Lambda_l}\mathscr{I}_\delta\left(t,x,i;\beta_l^1\right) - \varepsilon\\
&\quad\geq \sum_{l\geq 1}\chi_{\Lambda_l}\mathscr{I}_\delta\left(t,x,i;u_1,\beta_l^1(u_1)\right) - \varepsilon\\
&\quad= \mathscr{I}_\delta(t,x,i;u_1,\beta_1^\varepsilon(u_1)) - \varepsilon\\
&\quad= E\left[G_{t,t+\delta}^{t,x,i;u_1,\beta_1^\varepsilon(u_1)}\left[W\left(t+\delta, X_{t+\delta}^{t,x,i;u_1,\beta_1^\varepsilon(u_1)}, \theta_{t+\delta}^{t,i}\right)\right]|\mathscr{F}_t\right] - \varepsilon, \quad P-\text{a.s},
\end{aligned} \tag{47}$$

for all $u_1 \in U_{t,t+\delta}$.

We now focus on the interval $[t+\delta, T]$. From the definition of $W(t+\delta, y, j)$, we deduce that, for any $(y,j) \in R^n \times \mathscr{M}$, there exists $\beta_{y,j}^\varepsilon \in \mathscr{B}_{t+\delta,T}$ such that

$$W(t+\delta,y,j) \geq \operatorname*{esssup}_{u_2\in U_{t+\delta,T}} J\left(t+\delta,y,j;u_2,\beta_{y,j}^\varepsilon(u_2)\right) - \varepsilon, \quad P-\text{a.s.} \tag{48}$$

Now consider a decomposition of R^n, namely, $\sum_{l\geq 1}O_l = R^n$ such that $\operatorname{diam}(O_l) \leq \varepsilon$, for each $l \geq 1$. Take any $(y_l, j) \in O_l \times \mathscr{M}, l \geq 1$ fixed and define $\overline{X_{t+\delta}^{t,x,i;u_1,\beta_1^\varepsilon(u_1)}} := \sum_{l\geq 1, j\in\mathscr{M}} y_l \chi_{\left\{X_{t+\delta}^{t,x,i;u_1,\beta_1^\varepsilon(u_1)}\in O_l, \theta_{t+\delta}^{t,i}=j\right\}}$. Clearly, we always have

$$\left|X_{t+\delta}^{t,x,i;u_1,\beta_1^\varepsilon(u_1)} - \overline{X_{t+\delta}^{t,x,i;u_1,\beta_1^\varepsilon(u_1)}}\right| \leq \varepsilon, \tag{49}$$

everywhere on Ω, for each $u_1 \in U_{t,t+\delta}$. Moreover, for every y_l and j, there exists some $\beta_{y_l,j}^\varepsilon \in \mathscr{B}_{t+\delta,T}$ such that (48) holds, and clearly,

$$\beta_{u_1}^\varepsilon := \sum_{l\geq 1, j\in\mathscr{M}} \chi_{\left\{X_{t+\delta}^{t,x,i;u_1,\beta_1^\varepsilon(u_1)}\in O_l, \theta_{t+\delta}^{t,i}=j\right\}}\beta_{y_l,j}^\varepsilon \in \mathscr{B}_{t+\delta,T}. \tag{50}$$

Now we can define the new strategy $\beta^\varepsilon(u) := \beta_1^\varepsilon(u_1) \oplus \beta_{u_1}^\varepsilon(u_2), u \in U_{t,T}$, where $u_1 = u|_{[t,t+\delta]}$, $u_2 = u|_{(t+\delta,T]}$. Obviously, β^ε: $U_{t,T} \longrightarrow V_{t,T}$.

Next we shall show that β^ε is nonanticipating: indeed, let $\mathscr{S}$: $\Omega \longrightarrow [t,T]$ be an $\mathscr{F}$-stopping time and $u, u' \in U_{t,T}$ be such that $u \equiv u'$ on $t, \mathscr{S}$. Decomposing u, u' into $u_1, u_1' \in U_{t,t+\delta}$, $u_2, u_2' \in U_{t+\delta,T}$ such that $u = u_1 \oplus u_2$ and $u' = u_1' \oplus u_2'$. We have $u_1 \equiv u_1'$ on $t, \mathscr{S}\wedge(t+\delta)$ since $\beta_1^\varepsilon(u_1) \equiv \beta_1^\varepsilon(u_1')$ on $t, \mathscr{S}\wedge(t+\delta)$. On the other hand, $u_2 \equiv u_2'$ on $]\!]t+\delta, \mathscr{S}\wedge(t+\delta)]\!]$ $(\subset (t+\delta, T] \times \{\mathscr{S} > t+\delta\})$, and on $\mathscr{S} > t+\delta$, we have $X_{t+\delta}^{t,x,i;u_1,\beta_1^\varepsilon(u_1)} = X_{t+\delta}^{t,x,i;u_1',\beta_1^\varepsilon(u_1')}$. Thus, from the definition, $\beta_{u_1}^\varepsilon = \beta_{u_1'}^\varepsilon$ on $\{\mathscr{S} > t+\delta\}$ and $\beta_{u_1}^\varepsilon(u_2) \equiv \beta_{u_1'}^\varepsilon(u_2')$ on $]\!]t+\delta, \mathscr{S}\vee(t+\delta)]\!]$. This yields $\beta^\varepsilon(u) = \beta_1^\varepsilon(u_1) \oplus \beta_{u_1}^\varepsilon(u_2) \equiv \beta_1^\varepsilon(u_1') \oplus \beta_{u_1'}^\varepsilon(u_2') = \beta^\varepsilon(u')$ on $t, \mathscr{S}$, from which it follows that $\beta^\varepsilon \in \mathscr{B}_{t,T}$.

Fix $u \in U_{t,T}$ arbitrarily and decompose into $u_1 = u|_{[t,t+\delta]} \in U_{t,t+\delta}$, $u_2 = u|_{(t+\delta,}\, T] \in U_{t+\delta,T}$. Then, from (37), (47), (i), and (49), we have

$$\begin{aligned}
&W_\delta(t,x,i)\\
&\quad\geq E\left[G_{t,t+\delta}^{t,x,i;u_1,\beta_1^\varepsilon(u_1)}\left[W\left(t+\delta, X_{t+\delta}^{t,x,i;u_1,\beta_1^\varepsilon(u_1)}, \theta_{t+\delta}^{t,i}\right)\right]|\mathscr{F}_t\right] - \varepsilon\\
&\quad\geq E\left[G_{t,t+\delta}^{t,x,i;u_1,\beta_1^\varepsilon(u_1)}\left[W\left(t+\delta, \overline{X_{t+\delta}^{t,x,i;u_1,\beta_1^\varepsilon(u_1)}}, \theta_{t+\delta}^{t,i}\right) - C\varepsilon\right]|\mathscr{F}_t\right] - \varepsilon\\
&\quad\geq E\left[G_{t,t+\delta}^{t,x,i;u_1,\beta_1^\varepsilon(u_1)}\left[W\left(t+\delta, \overline{X_{t+\delta}^{t,x,i;u_1,\beta_1^\varepsilon(u_1)}}, \theta_{t+\delta}^{t,i}\right)\right]|\mathscr{F}_t\right] - C\varepsilon\\
&\quad= E\left[G_{t,t+\delta}^{t,x,i;u_1,\beta_1^\varepsilon(u_1)}\left[\sum_{l\geq 1, j\in\mathscr{M}} \chi_{\left\{X_{t+\delta}^{t,x,i;u_1,\beta_1^\varepsilon(u_1)}\in O_l, \theta_{t+\delta}^{t,i}=j\right\}} W(t+\delta, y_l, j)\right]|\mathscr{F}_t\right] - C\varepsilon.
\end{aligned} \tag{51}$$

From (37), (48), (ii), and (49), it follows that

$$
\begin{aligned}
&W_\delta(t,x,i)\\
&\geq E\left[G_{t,t+\delta}^{t,x,i;u_1,\beta_1^\varepsilon(u_1)}\left[\sum_{l\geq 1, j\in\mathscr{M}}\chi_{\left\{X_{t+\delta}^{t,x,i;u_1,\beta_1^\varepsilon(u_1)}\in O_l,\theta_{t+\delta}^{t,i}=j\right\}}J\left(t+\delta,y_l,j;u_2,\beta_{y_l}^\varepsilon(u_2)\right)-\varepsilon\right]|\mathscr{F}_t\right]-C\varepsilon\\
&\geq E\left[G_{t,t+\delta}^{t,x,i;u_1,\beta_1^\varepsilon(u_1)}\left[\sum_{l\geq 1, j\in\mathscr{M}}\chi_{\left\{X_{t+\delta}^{t,x,i;u_1,\beta_1^\varepsilon(u_1)}\in O_l,\theta_{t+\delta}^{t,i}=j\right\}}\right.\right.\\
&\left.\left.J\left(t+\delta,y_l,j;u_2,\beta_{y_l}^\varepsilon(u_2)\right)\right]|\mathscr{F}_t\right]-C\varepsilon\\
&=E\left[G_{t,t+\delta}^{t,x,i;u_1,\beta_1^\varepsilon(u_1)}\left[J\left(t+\delta,\overline{X_{t+\delta}^{t,x,i;u_1,\beta_1^\varepsilon(u_1)}},\theta_{t+\delta}^{t,i};u_2,\beta_{u_1}^\varepsilon(u_2)\right)\right]|\mathscr{F}_t\right]-C\varepsilon\\
&\geq E\left[G_{t,t+\delta}^{t,x,i;u_1,\beta_1^\varepsilon(u_1)}\left[J\left(t+\delta,X_{t+\delta}^{t,x,i;u_1,\beta_1^\varepsilon(u_1)},\theta_{t+\delta}^{t,i};u_2,\beta_{u_1}^\varepsilon(u_2)\right)-C\varepsilon\right]|\mathscr{F}_t\right]-C\varepsilon\\
&\geq E\left[G_{t,t+\delta}^{t,x,i;u_1,\beta_1^\varepsilon(u_1)}\left[J\left(t+\delta,X_{t+\delta}^{t,x,i;u_1,\beta_1^\varepsilon(u_1)},\theta_{t+\delta}^{t,i};u_2,\beta_{u_1}^\varepsilon(u_2)\right)\right]|\mathscr{F}_t\right]-C\varepsilon\\
&=E\left[G_{t,t+\delta}^{t,x,i;u,\beta^\varepsilon(u)}\left[E\left[Y_{t+\delta}^{t,x,i;u,\beta^\varepsilon(u)}|\mathscr{F}_{t+\delta}\right]\right]|\mathscr{F}_t\right]-C\varepsilon\\
&=E\left[G_{t,t+\delta}^{t,x,i;u,\beta^\varepsilon(u)}\left[Y_{t+\delta}^{t,x,i;u,\beta^\varepsilon(u)}\right]|\mathscr{F}_t\right]-C\varepsilon\\
&=E\left[Y_t^{t,x,i;u,\beta^\varepsilon(u)}|\mathscr{F}_t\right]-C\varepsilon,\quad P-\text{a.s.},
\end{aligned}
\tag{52}
$$

for any $u\in U_{t,T}$. Therefore, we obtain

$$
\begin{aligned}
W_\delta(t,x,i)&\geq \operatorname*{esssup}_{u\in U_{t,T}} J(t,x,i;u,\beta^\varepsilon(u))-C\varepsilon\\
&\geq \operatorname*{essinf}_{\beta\in\mathscr{B}_{t,T}}\operatorname*{esssup}_{u\in U_{t,T}} J(t,x,i;u,\beta(u))-C\varepsilon\\
&=W(t,x,i)-C\varepsilon,\quad P-\text{a.s.}
\end{aligned}
\tag{53}
$$

Let $\varepsilon\longrightarrow 0$, and we have $W_\delta(t,x,i)\geq W(t,x,i)$. The proof is complete.

4. Viscosity Solution of Isaacs' Equation: Existence and Uniqueness Theorem

In this section, based on the dynamic programming principle, we want to prove that the lower value function $W(t,x,i)$ introduced by (5) is the viscosity solution of (7), while the upper value function $U(t,x,i)$ defined by (6) is the viscosity solution of (8). Moreover, if Isaacs' condition holds, i.e., $H^-=H^+$, then (7) and (8) coincide, and the uniqueness of viscosity solution implies that $W=U$, that is, the game admits a value.

We first recall the definition of a viscosity solution of (7). The one for (8) can be defined in a similar way

Definition 3. A continuous $W\in(C([0,T]\times R^n))^m$ is said to be a viscosity subsolution (resp., supersolution) of (7), if $W(T,x,i)\leq\Phi(x,i)$ (resp., $W(T,x,i)\geq\Phi(x,i)$), for all $(x,i)\in R^n\times\mathscr{M}$ and if for all functions $\phi\in C_{l,b}^3([0,T]\times R^n)$ and $(t,x,i)\in[0,T)\times R^n\times\mathscr{M}$ such that $W(\cdot,\cdot)-\phi(\cdot)$ attains its local maximum (resp., minimum) value zero at (t,x), it has

$$
\begin{aligned}
&\frac{\partial\phi}{\partial t}(t,x)+H^-\left(t,x,i,\phi,D\phi,D^2\phi\right)+\sum_{k\neq i}q_{ik}\left[W(t,x,k)-W(t,x,i)\right]\leq 0,\\
&\qquad\qquad\qquad\qquad\qquad\qquad\qquad\qquad\qquad\qquad\qquad\qquad(\text{resp.},\geq 0),
\end{aligned}
\tag{54}
$$

where W is called a viscosity solution if it is both a viscosity subsolution and a viscosity supersolution.

Remark 1. $C^3_{l,b}([0,T]\times R^n)$ denotes the set of the real-valued functions that are continuously differentiable up to the third order and whose derivatives of order from 1 to 3 are bounded.

In the following, we prove that the lower value function W is a viscosity solution of (7). We only focus on the lower value function W, and the results hold for the upper value function U in a similar procedure.

Theorem 1. *Under the assumptions (A3) and (A4), the lower value function $W(t,x,i)$ is a viscosity solution of (7).*

First we prove some auxiliary lemmas. To abbreviate notations, for some arbitrarily chosen but fixed $\varphi(\cdot,\cdot)\in C^3_{l,b}([0,T]\times R^n)$,

$$\begin{aligned} F(s,x,y,z,i,u,v) &= \frac{\partial\varphi}{\partial s}(s,x)+\frac{1}{2}Tr\left(\sigma\sigma^T(s,x,i,u,v)D^2\varphi\right)+D\varphi\cdot b(s,x,i,u,v)\\ &\quad + f(s,x,y+\varphi(s,x),z+\varphi(s,x)\cdot\sigma(s,x,i,u,v),i,u,v)\\ &\quad +\sum_{k\neq i}q_{ik}[W(s,x,k)-W(s,x,i)], \end{aligned} \tag{55}$$

where $(s,x,y,z,i,u,v)\in[0,T]\times R^n\times R\times R^d\times\mathscr{M}\times U\times V$ and $\sum_{k\neq i}q_{ik}<1$, and we consider the following BSDE defined on the interval $[t,t+\delta]\,(0<\delta\le T-t)$:

$$\begin{cases} -\mathrm{d}Y^{1,u,v}_s = F\left(s,X^{t,x,i;u,v}_s,Y^{1,u,v}_s,Z^{1,u,v}_s,i,u_s,v_s\right)\mathrm{d}s - Z^{1,u,v}_s\mathrm{d}B_s,\\ Y^{1,u,v}_{t+\delta}=0, \end{cases} \tag{56}$$

where the process $X^{t,x,i;u,v}_s$ has been introduced by (2), $(t,x,i)\in[0,T]\times R^n\times\mathscr{M}$ is regarded as the initial state, X_s is the value of X at time s, and $u\in U_{t,t+\delta}, v\in V_{t,t+\delta}$.

We can characterize the solution process $Y^{1,u,v}$ as follows.

Lemma 8. *For any $s\in[t,t+\delta]$, $(t,x)\in[0,T]\times R^n$, $\phi\in C^3_{l,b}([0,T]\times R^n)$, we define $\varphi\in(C([0,T]\times R^n))^m$ by $\varphi(\cdot,\cdot,i)=\phi(\cdot)$, and $\varphi(\cdot,\cdot,k)=W(\cdot,\cdot,k)$, and for $k\neq i$, we have the following relationship:*

$$E\left[Y^{1,u,v}_s|\mathscr{F}_t\right]=E\left[G^{t,x,i;u,v}_{s,t+\delta}\left[\varphi\left(t+\delta,X^{t,x,i;u,v}_{t+\delta},\theta^{t,i}_{t+\delta}\right)\right]-\varphi\left(s,X^{t,x,i;u,v}_s,\theta^{t,i}_s\right)|\mathscr{F}_t\right],\quad P-\text{a.s.} \tag{57}$$

Proof. $G^{t,x,i;u,v}_{s,t+\delta}[\varphi(t+\delta,X^{t,x,i;u,v}_{t+\delta},\theta^{t,i}_{t+\delta})]$ is defined with the help of the solution of the BSDE:

$$\begin{cases} -\mathrm{d}Y^{u,v}_s = f\left(s,X^{t,x,i;u,v}_s,Y^{u,v}_s,Z^{u,v}_s,i,u_s,v_s\right)\mathrm{d}s - Z^{u,v}_s\mathrm{d}B_s,\\ Y^{u,v}_{t+\delta}=\varphi\left(t+\delta,X^{t,x,i;u,v}_{t+\delta},\theta^{t,i}_{t+\delta}\right),\quad s\in[t,t+\delta], \end{cases} \tag{58}$$

by the following formula:

$$G^{t,x,i;u,v}_{s,t+\delta}\left[\varphi\left(t+\delta,X^{t,x,i;u,v}_{t+\delta},\theta^{t,i}_{t+\delta}\right)\right]=Y^{u,v}_s. \tag{59}$$

Thus, we only need to prove $Y^{u,v}_s-\varphi(s,X^{t,x,i;u,v}_s,\theta^{t,i}_s)=Y^{1,u,v}_s$. We have

$$E\left[Y^{u,v}_s-\varphi\left(s,X^{t,x,i;u,v}_s,\theta^{t,i}_s\right)|\mathscr{F}_t\right]=E\left[Y^{1,u,v}_s\mid\mathscr{F}_t\right], \tag{60}$$

by applying Dynkin's formula to $\varphi(s,X^{t,x,i;u,v}_s,\theta^{t,i}_s)$. And for $s=t+\delta$,

$$E\left[Y^{u,v}_{t+\delta}-\varphi\left(t+\delta,X^{t,x,i;u,v}_{t+\delta},\theta^{t,i}_{t+\delta}\right)|\mathscr{F}_t\right]=E\left[Y^{1,u,v}_{t+\delta}\mid\mathscr{F}_t\right]=0. \tag{61}$$

Therefore, for any $s\in[t,t+\delta]$, we get the desired result. □

We consider the following simple BSDE in which $X^{t,x,i;u,v}_s$ is replaced by its deterministic initial value x:

$$\begin{cases} -\mathrm{d}Y^{2,u,v}_s = F\left(s,x,Y^{2,u,v}_s,Z^{2,u,v}_s,i,u_s,v_s\right)\mathrm{d}s - Z^{2,u,v}_s\mathrm{d}B_s,\\ Y^{2,u,v}_{t+\delta}=0,\quad s\in[t,t+\delta]. \end{cases} \tag{62}$$

Then, we have the following lemma.

Lemma 9. *There is a constant $C>0$ independent of the control processes u, v and of $\delta>0$, such that for every $u\in U_{t,t+\delta}$, $v\in V_{t,t+\delta}$,*

$$E\left[\left|Y^{1,u,v}_t-Y^{2,u,v}_t\right||\mathscr{F}_t\right]\le C\delta^{(3/2)},\quad P-\text{a.s.} \tag{63}$$

Proof. From Lemma 4, we have the existence of some constant $C>0$ such that

$$E\left[\sup_{s\in[t,T]}\left|X^{t,x,i;u,v}_s\right|^2|\mathscr{F}_t\right]\le C\left(1+|x|^2\right), \tag{64}$$

combined with

$$E\left[\sup_{s\in[t,t+\delta]}\left|X_s^{t,x,i;u,v}-x\right|^2|\mathscr{F}_t\right]\le 2E\left[\sup_{s\in[t,t+\delta]}\left|\int_t^s b\left(r,X_r^{t,x,i;u,v},i,u_r,v_r\right)\mathrm{d}r\right|^2|\mathscr{F}_t\right]$$
$$+2E\left[\sup_{s\in[t,t+\delta]}\left|\int_t^s \sigma\left(r,X_r^{t,x,i;u,v},i,u_r,v_r\right)\mathrm{d}B_r\right|^2|\mathscr{F}_t\right], \tag{65}$$

and we have

$$E\left[\sup_{s\in[t,t+\delta]}\left|X_s^{t,x,i;u,v}-x\right|^2|\mathscr{F}_t\right]\le C\delta. \tag{66}$$

From (56) and (62), using Lemma 2, set

$$\begin{aligned}\eta_1&=\eta_2=0,\\ f(s,y,z)&=F\left(s,X_s^{t,x,i;u,v},y,z,i,u_s,v_s\right),\\ \varphi_1(s)&=0,\\ \varphi_2(s)&=F\left(s,x,Y_s^{2,u,v},Z_s^{2,u,v},i,u_s,v_s\right)-F\left(s,X_s^{t,x,i;u,v},Y_s^{2,u,v},Z_s^{2,u,v},i,u_s,v_s\right).\end{aligned} \tag{67}$$

It is easy to know that g is Lipschitz with respect to (y,z), and $|\varphi_2(s)|\le C(1+|x|^2)(|X_s^{t,x,i;u,v}-x|+|X_s^{t,x,i;u,v}-x|^3)$ for $s\in[t,t+\delta]$, $(t,x,i)\in[0,T)\times R^n\times\mathscr{M}$, $u\in U_{t,t+\delta}$, $v\in V_{t,t+\delta}$. Thus,

$$\begin{aligned}&E\left[\int_t^{t+\delta}\left(\left|Y_s^{1,u,v}-Y_s^{2,u,v}\right|^2+\left|Z_s^{1,u,v}-Z_s^{2,u,v}\right|^2\right)\mathrm{d}s\,|\,\mathscr{F}_t\right]\\ &\le CE\left[\int_t^{t+\delta}\rho_0^2\left(\left|X_s^{t,x,i;u,v}-x\right|\right)\mathrm{d}s\,|\,\mathscr{F}_t\right]\\ &\le C\delta E\left[\sup_{s\in[t,t+\delta]}\rho_0^2\left(\left|X_s^{t,x,i;u,v}-x\right|\right)|\,\mathscr{F}_t\right]\le C\delta^2,\end{aligned} \tag{68}$$

where $\rho_0(r)=(1+|x|^2)(r+r^3), r\ge 0$. Therefore,

$$\begin{aligned}E\left[\left|Y_t^{1,u,v}-Y_t^{2,u,v}\right||\mathscr{F}_t\right]&=E\left[\left|E\left(Y_t^{1,u,v}-Y_t^{2,u,v}\right)|\,\mathscr{F}_t\right||\mathscr{F}_t\right]\\ &=E\left[|E\left[\int_t^{t+\delta}\left(F\left(s,X_s^{t,x,i;u,v},Y_s^{1,u,v},Z_s^{1,u,v},i,u_s,v_s\right)\right.\right.\right.\\ &\quad\left.\left.\left.-F\left(s,x,Y_s^{2,u,v},Z_s^{2,u,v},i,u_s,v_s\right)\mathrm{d}s|\mathscr{F}_t\right)\right]||\mathscr{F}_t\right]\\ &\le CE\left[\int_t^{t+\delta}\left[\rho_0\left(\left|X_s^{t,x,i;u,v}-x\right|\right)+\left|Y_s^{1,u,v}-Y_s^{2,u,v}\right|+\left|Z_s^{1,u,v}-Z_s^{2,u,v}\right|\mathrm{d}s\right]|\mathscr{F}_t\right]\\ &\le CE\left[\int_t^{t+\delta}\rho_0\left(\left|X_s^{t,x,i;u,v}-x\right|\right)\mathrm{d}s|\mathscr{F}_t\right]+C\delta^{(1/2)}E\left[\int_t^{t+\delta}\left|Y_s^{1,u,v}-Y_s^{2,u,v}\right|^2\mathrm{d}s\,|\,\mathscr{F}_t\right]^{(1/2)}\\ &\quad+C\delta^{(1/2)}E\left[\int_t^{t+\delta}\left|Z_s^{1,u,v}-Z_s^{2,u,v}\right|^2|\,\mathscr{F}_t\right]^{(1/2)}\\ &\le C\delta^{(3/2)}.\end{aligned} \tag{69}$$

The proof is complete. □

Lemma 10. *Let $Y_0(\cdot)$ be the solution of the following ordinary differential equation:*

$$\begin{cases} -\mathrm{d}Y_0(s) = F_0(s, x, Y_0(s), 0, i), & s \in [t, t+\delta], \\ Y_0(t+\delta) = 0, \end{cases} \tag{70}$$

where

$$F_0(s, x, y, z, i) = \sup_{u \in U} \inf_{v \in V} F(s, x, y, z, i; u, v). \tag{71}$$

Then, $P-$ a.s.,

$$\operatorname*{esssup}_{u \in U_{t,t+\delta}} \operatorname*{essinf}_{v \in V_{t,t+\delta}} E\left[Y_t^{2,u,v} | \mathcal{F}_t\right] = E\left[Y_0(t) \mid \mathcal{F}_t\right]. \tag{72}$$

Proof. We first introduce the function

$$F_1(s, x, y, z, i, u) = \inf_{v \in V} F(s, x, y, z, i, u, v), \tag{73}$$

where $(s, x, y, z, i, u) \in [0, T] \times R^n \times R \times R^d \times \mathcal{M} \times U$. And we consider the following equation: for $u \in U_{t,t+\delta}$,

$$\begin{cases} -\mathrm{d}Y_s^{3,u} = F_1\left(s, x, Y_s^{3,u}, Z_s^{3,u}, i, u_s\right)\mathrm{d}s - Z_s^{3,u}\mathrm{d}B_s, \\ Y_{t+\delta}^{3,u} = 0, \quad s \in t, t+\delta]. \end{cases} \tag{74}$$

Since $F_1(s, x, y, z, i, u_s)$ is Lipschitz in (y, z), for every $u \in U_{t,t+\delta}$, there exists a unique solution $(Y^{3,u}, Z^{3,u})$ to (74). Then, for every $u \in U_{t,t+\delta}$,

$$E\left[Y_t^{3,u} | \mathcal{F}_t\right] = \operatorname*{essinf}_{v \in V_{t,t+\delta}} E\left[Y_t^{2,u,v} | \mathcal{F}_t\right], \quad P-\text{a.s.} \tag{75}$$

In fact, from Lemma 2 and the definition of F_1, for every $u \in U_{t,t+\delta}$, we have

$$E\left[Y_t^{3,u} | \mathcal{F}_t\right] \le \operatorname*{essinf}_{v \in V_{t,t+\delta}} E\left[Y_t^{2,u,v} | \mathcal{F}_t\right], \quad P-\text{a.s.} \tag{76}$$

Moreover, there exists a measurable function v^4: $[t, T] \times R^n \times R \times R^d \times \mathcal{M} \times U \longrightarrow V$ such that

$$F_1(s, x, y, z, i, u) = F\left(s, x, y, z, i, u, v^4(s, x, y, z, i, u)\right) \text{for any } s, x, y, z, u. \tag{77}$$

Let $\tilde{v}_s^4 := v^4(s, x, Y_s^{3,u}, Z_s^{3,u}, i, u_s), s \in [t, t+\delta]$, and we observe that $\tilde{v}^4 \in V_{t,t+\delta}$, and

$$F_1\left(s, x, Y_s^{3,u}, Z_s^{3,u}, i, u_s\right) = F\left(s, x, Y_s^{3,u}, Z_s^{3,u}, i, u_s, \tilde{v}_s^4\right), \quad s \in [t, t+\delta]. \tag{78}$$

Thus, from the uniqueness of the solution of the BSDE, it follows that $(Y^{3,u}, Z^{3,u}) = (Y^{2,u,\tilde{v}^4}, Z^{2,u,\tilde{v}^4})$ and $E[Y_t^{3,u} | \mathcal{F}_t] = E[Y_t^{2,u,\tilde{v}^4} | \mathcal{F}_t], P-$ a.s., for every $u \in U_{t,t+\delta}$. Then, for all $u \in U_{t,t+\delta}$,

$$E\left[Y_t^{3,u} | \mathcal{F}_t\right] = \operatorname*{essinf}_{v \in V_{t,t+\delta}} E\left[Y_t^{2,u,v} | \mathcal{F}_t\right], \quad P-\text{a.s.} \tag{79}$$

Then, since $F_0(s, x, y, z, i) = \sup_{u \in U_{t,t+\delta}} F_1(s, x, y, z, i, u)$, by a similar proof, we have

$$\begin{aligned} E\left[Y_0(t) | \mathcal{F}_t\right] &= \operatorname*{esssup}_{u \in U_{t,t+\delta}} E\left[Y_t^{3,u} | \mathcal{F}_t\right] \\ &= \operatorname*{esssup}_{u \in U_{t,t+\delta}} \operatorname*{essinf}_{v \in V_{t,t+\delta}} E\left[Y_t^{2,u,v} | \mathcal{F}_t\right], \quad P-\text{a.s.} \end{aligned} \tag{80}$$

It uses the fact that (70) can be considered as a BSDE with the solution $(Y_s, Z_s) = (Y_0(s), 0)$. So, the proof is complete. □

Lemma 11. *For all $u \in U_{t,t+\delta}$, $v \in V_{t,t+\delta}$, we have*

$$E\left[\int_t^{t+\delta} \left|Y_s^{2,u,v}\right| \mathrm{d}s | \mathcal{F}_t\right] + E\left[\int_t^{t+\delta} \left|Z_s^{2,u,v}\right| \mathrm{d}s \mid \mathcal{F}_t\right] \le C\delta^{(3/2)}, \quad P-\text{a.s.}, \tag{81}$$

where the constant C is independent of the control processes u, v and of $\delta > 0$.

Proof. Since $F(s, x, \cdot, \cdot, i, u, v)$ has a linear growth in (y, z), uniformly in (u, v), we get from Lemma 2 for some constant C independent of δ and the controls u, v,

$$\left|Y_s^{2,u,v}\right|^2 \le C\delta, E\left[\int_s^{t+\delta} \left|Z_r^{2,u,v}\right| \mathrm{d}r | \mathcal{F}_s\right] \le C\delta, \quad s \in [t, t+\delta]. \tag{82}$$

Moreover, from equation (62),

$$\begin{aligned} \left|Y_s^{2,u,v}\right| &\le E\left[\int_s^{t+\delta} F\left(r, x, Y_r^{2,u,v}, Z_r^{2,u,v}, i, u_r, v_r\right)| \mathrm{d}r \mid \mathcal{F}_s\right] \\ &\le CE\left[\int_s^{t+\delta} \left(1 + |x|^2 + \left|Y_r^{2,u,v}\right| + \left|Z_r^{2,u,v}\right|\right) \mathrm{d}r \mid \mathcal{F}_s\right] \\ &\le C\delta + C\delta^{(1/2)}\left(E\left[\int_s^{t+\delta} \left|Z_r^{2,u,v}\right|^2 \mathrm{d}r \mid \mathcal{F}_s\right]\right)^{(1/2)} \\ &\le C\delta, \quad P-\text{a.s.}, s \in [t, t+\delta], \end{aligned} \tag{83}$$

and since

$$\int_t^{t+\delta} Z_s^{2,u,v} \mathrm{d}B_s = \int_t^{t+\delta} F\left(s, x, Y_s^{2,u,v}, Z_s^{2,u,v}, i, u_s, v_s\right)\mathrm{d}s - Y_t^{2,u,v}, \tag{84}$$

we get

$$E\left[\int_t^{t+\delta} \left|Z_s^{2,u,v}\right|^2 \mathrm{d}s \mid \mathcal{F}_t\right] \le C\delta^2. \tag{85}$$

Therefore,

$$E\left[\int_t^{t+\delta}\left|Y_s^{2,u,v}\right|\mathrm{d}s \mid \mathscr{F}_t\right] + E\left[\int_t^{t+\delta}\left|Z_s^{2,u,v}\right|\mathrm{d}s \mid \mathscr{F}_t\right]$$
$$\leq C\delta^2 + C\delta^{(1/2)}\left(E\left[\int_t^{t+\delta}\left|Z_s^{2,u,v}\right|^2\mathrm{d}r \mid \mathscr{F}_t\right]\right)^{(1/2)} \tag{86}$$
$$\leq C\delta^{(3/2)}, \quad P-\text{a.s.}$$

□

Proof of Theorem 1

(i) It is easy to know that $W(T,x,i) = \Phi(x,i)$, $(x,i) \in R^n \times \mathscr{M}$. We first will prove W is a viscosity supersolution. For fixed $i \in \mathscr{M}$, without loss of generality, we suppose that $\varphi(t,x,i) = W(t,x,i)$. According to Proposition 1,

$$\varphi(t,x,i) = W(t,x,i)$$
$$= \operatorname*{essinf}_{\beta\in\mathscr{B}_{t,t+\delta}} \operatorname*{esssup}_{u\in U_{t,t+\delta}} E\left[G_{t,t+\delta}^{t,x,i;u,\beta(u)}\left[W\left(t+\delta, X_{t+\delta}^{t,x,i;u,\beta(u)}, \theta_{t+\delta}^{t,i}\right)\right] \mid \mathscr{F}_t\right], \tag{87}$$

where $0 \leq \delta \leq T-t$ and from $W \geq \varphi$ and the monotonicity property of $G_{t,t+\delta}^{t,x,i;u,\beta(u)}[\cdot]$, we have

$$\operatorname*{essinf}_{\beta\in\mathscr{B}_{t,t+\delta}} \operatorname*{esssup}_{u\in U_{t,t+\delta}} E\left[\left(G_{t,t+\delta}^{t,x,i;u,\beta(u)}\left[\varphi\left(t+\delta, X_{t+\delta}^{t,x,i;u,\beta(u)}, \theta_{t+\delta}^{t,i}\right) - \varphi(t,x,i)\right]\right) \mid \mathscr{F}_t\right] \leq 0, \quad P-\text{a.s.} \tag{88}$$

From Lemma 8,

$$\operatorname*{essinf}_{\beta\in\mathscr{B}_{t,t+\delta}} \operatorname*{esssup}_{u\in U_{t,t+\delta}} E\left[Y_t^{1,u,\beta(u)} \mid \mathscr{F}_t\right] \leq 0, \quad P-\text{a.s.} \tag{89}$$

Thus, from Lemma 9, we obtain

$$\operatorname*{essinf}_{\beta\in\mathscr{B}_{t,t+\delta}} \operatorname*{esssup}_{u\in U_{t,t+\delta}} E\left[Y_t^{2,u,\beta(u)} \mid \mathscr{F}_t\right] \leq C\delta^{(3/2)}, \quad P-\text{a.s.} \tag{90}$$

Then, since

$$\operatorname*{essinf}_{v\in V_{t,t+\delta}} E\left[Y_t^{2,u,v} \mid \mathscr{F}_t\right] \leq E\left[Y_t^{2,u,\beta(u)} \mid \mathscr{F}_t\right], \quad \beta \in \mathscr{B}_{t,t+\delta}, \tag{91}$$

we have

$$\operatorname*{esssup}_{u\in U_{t,t+\delta}} \operatorname*{essinf}_{v\in V_{t,t+\delta}} E\left[Y_t^{2,u,v} \mid \mathscr{F}_t\right] \leq \operatorname*{essinf}_{\beta\in\mathscr{B}_{t,t+\delta}} \operatorname*{esssup}_{u\in U_{t,t+\delta}} E\left[Y_t^{2,u,\beta(u)} \mid \mathscr{F}_t\right] \leq C\delta^{(3/2)}, \quad P-\text{a.s,} \tag{92}$$

and Lemma 10 implies $Y_0(t) \leq C\delta^{(3/2)}, P-$a.s., where Y_0 is the unique solution of (70). Thus,

$$C\delta^{(1/2)} \geq \frac{1}{\delta}Y_0(t) = \frac{1}{\delta}\int_t^{t+\delta} F_0(s,x,Y_0(s),0,i)\mathrm{d}s, \quad \delta > 0,$$
$$\sup_{u\in U}\inf_{v\in V} F(t,x,0,0,i,u,v) = F_0(t,x,0,0,i) \leq 0, \tag{93}$$

and from the definition of F, we see that W is a viscosity supersolution of (7).

(ii) Now we prove W is a viscosity subsolution. For fixed $i \in \mathscr{M}$, without loss of generality, we suppose that $\varphi(t,x,i) = W(t,x,i)$. We must prove that

$$\sup_{u\in U}\inf_{v\in V} F(t,x,0,0,i,u,v) = F_0(t,x,0,0,i) \geq 0. \tag{94}$$

We suppose that this is not true. Then, there exists some $R > 0$ such that

$$F_0(t,x,0,0,i) = \sup_{u\in U}\inf_{v\in V} F(t,x,0,0,i,u,v) \leq -R < 0, \tag{95}$$

and we can find a measurable function ψ: $U \longrightarrow V$ such that

$$F(t,x,0,0,i,u,\psi(u)) \leq -\frac{3}{4}R \text{ for all } u \in U. \tag{96}$$

And since $F(\cdot,x,0,0,i,\cdot,\cdot)$ is uniformly continuous on $[0,T]\times U\times V$, there exists some $0 < Q \leq T-t$ such that for all $u \in U$ and $|s-t| \leq Q$,

$$F(s,x,0,0,i,u,\psi(u)) \le -\frac{1}{2}R. \tag{97}$$

Moreover, due to Proposition 1, for all $0 \le \delta \le Q$,

$$\begin{aligned}\varphi(t,x,i) &= W(t,x,i)\\ &= \operatorname*{essinf}_{\beta\in\mathscr{B}_{t,t+\delta}} \operatorname*{essinf}_{u\in U_{t,t+\delta}} E\left[G_{t,t+\delta}^{t,x,i;u,\beta(u)}\left[W\left(t+\delta, X_{t+\delta}^{t,x,i;u,\beta(u)}, \theta_{t+\delta}^{t,i}\right)\right] \mid \mathscr{F}_t\right],\end{aligned} \tag{98}$$

and similar to (i), from $W \le \varphi$ and the monotonicity property of $G_{t,t+\delta}^{t,x,i;u,\beta(u)}[\cdot]$, we have

$$\operatorname*{essinf}_{\beta\in\mathscr{B}_{t,t+\delta}} \operatorname*{esssup}_{u\in U_{t,t+\delta}} E\left[\left(G_{t,t+\delta}^{t,x,i;u,\beta(u)}\left[\varphi\left(t+\delta, X_{t+\delta}^{t,x,i;u,\beta(u)}, \theta_{t+\delta}^{t,i}\right)\right] - \varphi(t,x,i)\right) \mid \mathscr{F}_t\right] \ge 0, \quad P-\text{a.s.} \tag{99}$$

Therefore, from Lemma 8,

$$\operatorname*{essinf}_{\beta\in\mathscr{B}_{t,t+\delta}} \operatorname*{esssup}_{u\in U_{t,t+\delta}} E\left[Y_t^{1,u,\beta(u)} \mid \mathscr{F}_t\right] \ge 0, \quad P-\text{a.s.} \tag{100}$$

Thus,

$$\operatorname*{esssup}_{u\in U_{t,t+\delta}} E\left[Y_t^{1,u,\psi(u)} \mid \mathscr{F}_t\right] \ge 0, \quad P-\text{a.s.} \tag{101}$$

Here, by setting $\psi_s(u)(\omega) = \psi(u_s(\omega))$, $(s,\omega) \in [t, T] \times \Omega$, we identify ψ as an element of $\mathscr{B}_{t,t+\delta}$. Given any ε¿0, we can choose $u^\varepsilon \in U_{t,t+\delta}$ such that $E[Y_t^{1,u^\varepsilon,\psi(u^\varepsilon)} | \mathscr{F}_t] \ge -\varepsilon\delta$. From Lemma 9, we get

$$E\left[Y_t^{2,u^\varepsilon,\psi(u^\varepsilon)} \mid \mathscr{F}_t\right] \ge -C\delta^{(3/2)} - \varepsilon\delta, \quad P-\text{a.s.} \tag{102}$$

Moreover, from (62),

$$E\left[Y_t^{2,u^\varepsilon,\psi(u^\varepsilon)} | \mathscr{F}_t\right] = E\left[\int_t^{t+\delta} F\left(s,x,Y_s^{2,u^\varepsilon,\psi(u^\varepsilon)}, Z_s^{2,u^\varepsilon,\psi(u^\varepsilon)}, i, u_s^\varepsilon, \psi\left(u_s^\varepsilon\right)\right)\mathrm{d}s \mid \mathscr{F}_t\right]. \tag{103}$$

We get from the Lipschitz property of F in (y,z), (99), and Lemma 11 that

$$\begin{aligned}&E\left[Y_t^{2,u^\varepsilon,\psi(u^\varepsilon)} \mid \mathscr{F}_t\right]\\ &\le E\left[\int_t^{t+\delta}\left(C\left|Y_s^{2,u^\varepsilon,\psi(u^\varepsilon)}\right| + C\left|Z_s^{2,u^\varepsilon,\psi(u^\varepsilon)}\right| + F\left(s,x,0,0,i,u_s^\varepsilon,\psi_s\left(u^\varepsilon\right)\right)\right)\mathrm{d}s \mid \mathscr{F}_t\right]\\ &\le C\delta^{(3/2)} - \frac{1}{2}R, \quad P-\text{a.s.}\end{aligned} \tag{104}$$

Letting $\delta\downarrow 0$ and then $\varepsilon\downarrow 0$, we get that $R\leq 0$, which induces a contradiction. Then,

$$F_0(t,x,0,0,i)=\sup_{u\in U}\inf_{v\in V}F(t,x,0,0,i,u,v)\geq 0, \tag{105}$$

and from the definition of F, we see that W is a viscosity supersolution of (7). Therefore, from the above two steps, we derive that W is a viscosity solution of (7). □

Remark 2. We can also prove that U is a viscosity solution of (8) similarly by the method of Theorem 1.

We now study the uniqueness of the viscosity solution of Isaacs' equation (7):

$$\begin{cases}\dfrac{\partial}{\partial t}h(t,x,i)+H^{-}\left(t,x,i,h,Dh,D^2h\right)+\displaystyle\sum_{k\neq i}q_{ik}\left[W(t,x,k)-W(t,x,i)\right]=0,\\ \\ h(T,x,i)=\Phi(x,i),\end{cases} \tag{106}$$

where

$$\begin{aligned}H^{-}(t,x,i,p,A,u,v)=\sup_{u\in U}\inf_{v\in V}\Big\{&\frac{1}{2}\mathrm{Tr}\left(\sigma\sigma^{T}(t,x,i,u,v)\cdot A\right)+\langle b(t,x,i,u,v),p\rangle\\ &+f\left(t,x,i,r,\sigma^{T}(t,x,i,u,v)p,u,v\right)\Big\},\end{aligned} \tag{107}$$

for $(t,x,i,r,p,A,u,v)\in[0,T]\times R^n\times\mathscr{M}\times R\times R^n\times R^{n\times n}\times U\times V\longrightarrow R$. The functions b,σ,f, and Φ are still supposed to satisfy (A3) and (A4), respectively.

We will prove the uniqueness for (108) in the following space of continuous functions:

$$\begin{aligned}\Theta=\Big\{&\phi\in C\left([0,T]\times R^n\right):\ \exists\widetilde{A}>0\text{ such that}\\ &\lim_{|x|\longrightarrow\infty}\phi(t,x)\exp\left\{-\widetilde{A}\left[\log\left(\left(|x|^2+1\right)^{(1/2)}\right)\right]^2\right\}=0\text{ uniformly in }t\in[0,T]\Big\}.\end{aligned} \tag{108}$$

This growth condition was introduced in [18]. And it was shown in [18] that this kind of growth condition is optimal for the uniqueness and can, in general, not be weakened. We adapt the idea developed in [18] to Isaacs' equation (108) to prove the uniqueness of the viscosity solution in Θ. We only focus on equation (7) in Θ, and results hold for equation (8) in a similar procedure. For the proof of the uniqueness theorem, we need some auxiliary lemmas. Denoting by K a Lipschitz constant of $f(t,x,\cdot,\cdot,i,\cdot,\cdot)$, we have the following.

Lemma 12. *Let $W^1\in\Theta$ be a viscosity subsolution and $W^2\in\Theta$ be a viscosity supersolution of (108). Then, the function $h:=W^1-W^2$ is a viscosity subsolution of the equation*

$$\begin{cases}\dfrac{\partial}{\partial t}h(t,x)+\sup\limits_{u,v}\Big\{\dfrac{1}{2}\mathrm{Tr}\left(\sigma\sigma^{T}(t,x,i,u,v)D^2h\right)+Dh\cdot b(t,x,i,u,v)+K|w|+\\ \\ K|Dh\cdot\sigma(t,x,i,u,v)|\Big\}+\displaystyle\sum_{k\neq i}q_{ik}\left[h(t,x,k)-h(t,x,i)\right]=0,\\ \\ h(T,x,i)=0,\qquad(t,x,i)\in[0,T)\times R^n\times\mathscr{M}.\end{cases} \tag{109}$$

The proof of this lemma follows directly from Lemma 3.7 in [18]; it is only slightly different.

Lemma 13. *Let $W^1 \in \Theta$ be a viscosity subsolution and $W^2 \in \Theta$ be a viscosity supersolution of (108). Then, the function $\widetilde{h} := \max_{i\in\mathscr{M}}(W^1(t,x,i) - W^2(t,x,i))$ is a viscosity subsolution of the equation*

$$\begin{cases} \dfrac{\partial}{\partial t}\widetilde{h}(t,x) + \sup\limits_{u,v,i}\left\{\dfrac{1}{2}\mathrm{Tr}\left(\sigma\sigma^T(t,x,i,u,v)D^2\widetilde{h}\right) + D\widetilde{h}\cdot b(t,x,i,u,v) + K|\widetilde{h}| + \right. \\ \left. K|D\widetilde{h}\cdot\sigma(t,x,i,u,v)|\right\} = 0, \\ \widetilde{h}(T,x) = 0, \quad (t,x) \in [0,T)\times R^n. \end{cases} \tag{110}$$

Proof. For $(t_0,x_0) \in [0,T)\times R^n$, without loss of generality, we suppose that $\widetilde{h}(t_0,x_0) = W^1(t_0,x_0,i) - W^2(t_0,x_0,i)$, i.e.,

$$h(t_0,x_0,i) \geq h(t_0,x_0,k), \quad \forall k \neq i, \tag{111}$$

where $h := W^1 - W^2$. Hence,

$$\sum_{k\neq i} q_{ik}\left[\left(h(t_0,x_0,k) - h(t_0,x_0,i)\right)\right] \leq 0. \tag{112}$$

Obviously, $\widetilde{h}(T,x) \leq 0$, for all $x \in R^n$. Moreover, from (114), for all functions $\phi \in C^3_{l,b}([0,T]\times R^n)$,

$$\begin{aligned} &\frac{\partial}{\partial t}\phi(t_0,x_0) + \sup_{u,v,i}\left\{\frac{1}{2}\mathrm{Tr}\left(\sigma\sigma^T(t_0,x_0,i,u,v)D^2\phi\right) + D\phi\cdot b(t_0,x_0,i,u,v)\right. \\ &\quad \left. + K|\phi| + K\left|D\phi\cdot\sigma(t_0,x_0,i,u,v)\right|\right\} \\ &\geq \frac{\partial}{\partial t}\phi(t_0,x_0) + \sup_{u,v}\left\{\frac{1}{2}\mathrm{Tr}\left(\sigma\sigma^T(t_0,x_0,i,u,v)D^2\phi\right) + D\phi\cdot b(t_0,x_0,i,u,v)\right. \\ &\quad \left. + K|\phi| + K\left|D\phi\cdot\sigma(t_0,x_0,i,u,v)\right|\right\} \\ &\geq \frac{\partial}{\partial t}\phi(t_0,x_0) + \sup_{u,v}\left\{\frac{1}{2}\mathrm{Tr}\left(\sigma\sigma^T(t_0,x_0,i,u,v)D^2\phi\right) + D\phi\cdot b(t_0,x_0,i,u,v)\right. \\ &\quad \left. + K|\phi| + K\left|D\phi\cdot\sigma(t_0,x_0,i,u,v)\right|\right\} \\ &\quad + \sum_{k\neq i} q_{ik}\left[\left(\phi(t_0,x_0,k) - \phi(t_0,x_0,i)\right)\right]. \end{aligned} \tag{113}$$

On the other hand, for any $\phi \in C^3_{l,b}([0,T]\times R^n)$ such that $\widetilde{h} - \phi$ attains its local maximum value zero at (t_0,x_0), we have that $h(\cdot,\cdot,i) - \phi(\cdot,i)$ attains its local maximum value zero at (t_0,x_0). Since h is a viscosity subsolution of (111), we have

$$\begin{aligned} &\frac{\partial}{\partial t}\phi(t_0,x_0) + \sup_{u,v}\left\{\frac{1}{2}\mathrm{Tr}\left(\sigma\sigma^T(t_0,x_0,i,u,v)D^2\phi\right) + D\phi\cdot b(t_0,x_0,i,u,v)\right. \\ &\quad \left. + K|\phi| + K\left|D\phi\cdot\sigma(t_0,x_0,i,u,v)\right|\right\} \\ &\quad + \sum_{k\neq i} q_{ik}\left[\left(\phi(t_0,x_0,k) - \phi(t_0,x_0,i)\right)\right] \geq 0. \end{aligned} \tag{114}$$

Consequently,

$$\frac{\partial}{\partial t}\phi(t_0,x_0)+\sup_{u,v,i}\left\{\frac{1}{2}\mathrm{Tr}\left(\sigma\sigma^T(t_0,x_0,i,u,v)D^2\phi\right)+D\phi\cdot b(t_0,x_0,i,u,v)\right.$$
$$\left.+K|\phi|+K\left|D\phi\cdot\sigma(t_0,x_0,i,u,v)\right|\right\}\geq 0. \tag{115}$$

It means that $\widetilde{h}$ is a viscosity subsolution of equation (112). □

Similar to the proof of Theorem 6.1 in [8], we can prove that $\widetilde{h}\leq 0$, i.e., $W^1(t,x,i)\leq W^2(t,x,i)$. Then, we have the uniqueness theorem.

Theorem 2. *Under the assumptions (A3) and (A4), the viscosity solution of (108) is unique in* Θ.

Remark 3. Since the lower value function W is of at most linear growth, it belongs to Θ, and it is easy to know that W is the unique viscosity solution in Θ of (108). And we can prove that the upper value function U is the unique viscosity solution in Θ of (8).

Remark 4. If Isaacs' condition holds, that is, if for any $(t,x,i,r,p)\in[0,T]\times R^n\times\mathscr{M}\times R\times R^n$, $H^+(t,x,i,r,\ p,A,u,v)=H^-(t,x,i,r,p,A,u,v)$, then (8) and (108) coincide, i.e., (7) and (8) coincide, and from the uniqueness in Θ of viscosity solution, it follows that $W=U$ which means the associated SDG has a value.

Data Availability

No data were used in this study.

Conflicts of Interest

The authors declare that they have no conflicts of interest.

Acknowledgments

This study was supported by the National Natural Science Foundation of China (nos. 12071292 and 11871121) and the Natural Science Foundation of Zhejiang Province (no. LY21A010001).

References

[1] S. Lv, "Two-player zero-sum stochastic differential games with regime switching," *Automatica*, vol. 114, p. 108819, 2020.

[2] Q. Zhang, "Stock trading: an optimal selling rule," *SIAM Journal on Control and Optimization*, vol. 40, no. 1, pp. 64–87, 2001.

[3] Q. Zhang and X. Y. Zhou, "Valuation of stock loans with regime switching," *SIAM Journal on Control and Optimization*, vol. 48, no. 3, pp. 1229–1250, 2009.

[4] E. Pardoux and S. G. Peng, "Adapted solution of a backward stochastic differential equation," *Systems & Control Letters*, vol. 14, no. 1, pp. 55–61, 1990.

[5] S. Peng, "A generalized dynamic programming principle and Hamilton-Jacobi-Bellman equation," *Stochastics and Stochastic Reports*, vol. 38, no. 2, pp. 119–134, 1992.

[6] S. Hamadène and J. P. Lepeltier, "Zero-sum stochastic differential games and backward equations," *Systems & Control Letters*, vol. 24, no. 4, pp. 259–263, 1995.

[7] S. Hamadène, J.-P. Lepeltier, and S. G. Peng, "BSDEs with continuous coefficients and stochastic differential games," in *Backward Stochastic Differential Equations*, pp. 115–128, Longman, Harlow, UK, 1997.

[8] R. Buckdahn and J. Li, "Stochastic differential games and viscosity solutions of Hamilton-Jacobi-Bellman-Isaacs equations," *SIAM Journal on Control and Optimization*, vol. 47, no. 1, pp. 444–475, 2008.

[9] S. Peng, "A general stochastic maximum principle for optimal control problems," *SIAM Journal on Control and Optimization*, vol. 28, no. 4, pp. 966–979, 1990.

[10] S. G. Peng, "Probabilistic interpretation for systems of quasilinear parabolic partial difierential equations," *Stochastics and Stochastics Reports*, vol. 37, p. 10, 1991.

[11] N. El. Karoui, S. G. Peng, and M. C. Quenez, "Backward stochastic differential equations in finance," *Mathematical Finance*, vol. 7, no. 1, pp. 1–71, 1997.

[12] R. M. Xu and F. Zhang, "ϵ-nash mean-field games for general linear-quadratic systems with applications," *Automatica*, vol. 114, Article ID 108835, 2020.

[13] X. F. Yi, R. W. Guo, and Y. Qi, "Stabilization of chaotic systems with both uncertainty and disturbance by the ude-based control method," *IEEE Access*, vol. 8, pp. 62471–62477, 2020.

[14] Y. Y. Liu, T. Hou, and F. Q. Deng, "Stability for discrete-time uncertain systems with infinite markov jump and time-delay," *Science China Information Sciences*, vol. 64, Article ID 152202, 2021.

[15] R. W. Guo and Y. Qi, "Partial anti-synchronization in a class of chaotic and hyper-chaotic systems," *IEEE Access*, vol. 9, pp. 46303–46312, 2021.

[16] W. Fleming and P. Souganidis, "On the existence of value functions of two-player, zero-sum stochastic differential games," *Indiana University Mathematics Journal*, vol. 38, no. 2, pp. 293–314, 1989.

[17] S. G. Peng, "Backward stochastic differential equations-stochatic optimization theory and viscosity solutions of HJB equations," in *Stochastic Analysis,* Science Press, Beijing, China, 1997.

[18] G. Barles, R. Buckdahn, and E. Pardoux, "Backward stochastic differential equations and integral-partial differential equations," *Stochastics and Stochastic Reports*, vol. 60, no. 1-2, pp. 57–83, 1997.

Hindawi
Mathematical Problems in Engineering
Volume 2021, Article ID 5482421, 12 pages
https://doi.org/10.1155/2021/5482421

Research Article

HOSM Controller Using PI Sliding Manifold for an Integrated Active Control for Wheeled Vehicles

Antonio Navarrete Guzmán,[1,2] **Claudia Carolina Vaca García**,[3] **Stefano Di Gennaro**,[4,5] **and Cuauhtémoc Acosta Lúa**[3,5]

[1]*Department of Electrical and Electronic Engineering at the National Technological Institute of Mexico Campus Tepic, Av. Tecnológico 2595, Tepic 63175, Nayarit, Mexico*
[2]*Academic Unit of Basic Sciences and Engineering of the Autonomous University of Nayarit, City of Culture "Amado Nervo", Tepic, Nayarit, Mexico*
[3]*Departamento De Ciencias Tecnológicas, Universidad De Guadalajara, Centro Universitario De La Ciénega, Av. Universidad 1115, Ocotlán 47820, Jalisco, Mexico*
[4]*Department of Information Engineering, Computer Science and Mathematics, Via Vetoio, Loc. Coppito, L'Aquila 67100, Italy*
[5]*Center of Excellence DEWS, University of L'Aquila, Via Vetoio, Loc. Coppito, L'Aquila 67100, Italy*

Correspondence should be addressed to Cuauhtémoc Acosta Lúa; cuauhtemoc.acosta@cuci.udg.mx

Received 6 April 2021; Revised 6 May 2021; Accepted 8 May 2021; Published 3 June 2021

Academic Editor: Rongwei Guo

This study considers the design of a modified high-order sliding mode (HOSM) controller using a PI sliding surface to the attitude control of a ground vehicle. A robust-modified HOSM controller is derived, so that the lateral velocity and yaw rate tracks the desired trajectory despite the environment actions acting on the ground vehicle and parameter variations. The stability is guaranteed with Lyapunov's stability theorem function. The performance of the dynamic controllers is evaluated using the CarSim simulator considering a challenging double steer maneuver.

1. Introduction

The integrated active control for wheeled vehicles is an important topic due to improving the drivability and safety of the vehicle in a critical situation. This active control employs electronic actuators in the vehicles. The new actuators offer great flexibility when a design control architecture allows the controller to be designed as a separate block. This decoupling helps to design the controller as an active front steering (AFS) or rear torque vectoring (RTV). The AFS controller imposes a steering angle to correct the action of the driver. The RTV controller imposes an active action in the yaw momentum of the vehicle. All these control actions render more safety to the ground vehicle and passengers.

The control action is usually determined using approximation models because they capture the main aspect of the physics of the problem. But these mathematical models can be extended due to the presence of parameter uncertainties/variations and the presence of disturbances acting on the vehicle, among which are the change of parameters due to the road condition and the environmental disturbance acting on the vehicle (front and lateral wind). On this subject, the reader can find in [1–4]. However, many other mathematical models that include uncertainty in the parameters and external disturbances are available in the literature and could be considered, for instance, those in [5, 6].

The article presents the combination of the modified HOSM with a PI sliding surface. The principal idea is to design a particular sliding surface on which the system dynamics are constrained to evolve by the modified HOSM. It is noted that the controller presented here maintains the inherent properties of the HOSM, such as robustness. For the above reasons, this article deals with designing a modified high-order sliding mode (HOSM) controller using a PI sliding surface to track the desired trajectory for lateral

velocity and angular references despite variations in some parameters and external disturbances such as wind gusts. For this purpose, the active front steering (AFS) and rear torque vectoring (RTV) are considered as the integrated active control, and the aim is to improve the performance of the control system applied in automobiles. The proposed controller uses all the information from sensors that are currently available in modern vehicles. The closed-loop system stability has been proven in the sense of Lyapunov through the development of the candidate function. It was considered that the CarSim simulator to validate the controller is proposed. CarSim is a software that predicts dynamic vehicle behavior. In fact, CarSim delivers the most accurate, detailed, and efficient methods for simulating the performance of passenger vehicles and is supported by automotive enterprises, such as the Ford Motor Company and Chrysler.

Earlier research on the integrated active controller is based on the nonlinear techniques as [7–9], and for more recent results, [10–14]. In [15], a nonlinear decoupling control approach is presented for a three-degree of freedom model. In [16], a yaw-stabilizing algorithm is presented, combining AFS with a low-level control of the longitudinal wheel slip, with adaptive yaw estimating the maximum tire-road friction parameter for each wheel. In [17], AFS and RTV are combined in an integrated controller to guarantee vehicle stability, making use of adaptive feedback.

The HOSM was introduced in [18], and the main advantage of the high-order sliding mode is to overcome the chattering problem. A further notable advantage of HOSM is the possibility of considering sliding mode surfaces with a relative degree greater than one [19] and has great advantages compared to the sliding mode [20]. However, to add the integral action in discontinuous controllers as in the case of first-order sliding modes to improve the chattering phenomenon and smoothness of the controller action; the chattering is caused by reaching the sliding surface in finite time asymptotically fast, and this behavior generates the actuator commute quickly [21]. In the case of HOSM, adding a discontinuous integral action eliminates the effect of the disturbance; considering this action as an estimator of the disturbance [22], it has been shown that to continue adding integrators helps to decrease the chattering effect. Nonetheless, there are studies in which the integral action is added on the surface, improving the behavior of the controller in the transient time.

Nevertheless, the reader can find works in which HOSM uses a PI controller as the sliding surface. In [23], the PID sliding mode control scheme is designed for a high-speed train (HST) subjected to actuator faults, asymmetric nonlinear actuator saturation. A combination of SMC with PID sliding surface is used to control a 2-degree of freedom (2-DOF) planar manipulator [24]. The study by Gu et al. [25] presents an SMC-PI sliding surface for robust tracking control of a nanopositioning stage composed of piezoceramic stack actuators (PSAs) and compliant flexure mechanisms. A second-order sliding mode using PI sliding surface applied in the control of DC motor drive is used in [26]. In [27], a sliding mode control with PID sliding surface is used to activate vibration damping of pneumatically actuated soft robots. In [28], the supertwisting algorithm combined with the proportional integral derivative sliding mode control modified is designed to solve trajectory tracking and stabilize the quadrotor attitude.

The study is organized as follows. In Section 2, the mathematical model of a vehicle is recalled, and the control problem is formulated. In Section 3, a modified HOSM with the PI sliding surface controller is presented. In Section 4, the resulting controller is tested with CarSim simulations. Some comments conclude the study.

2. Mathematical Model of the Vehicle Dynamics

In this article, to obtain the mathematical model of the ground vehicle, it is considered as a rigid body connected to the ground through the tires. This model is the so-called bicycle model or single-track model [29, 30] and is widely used by scientists to design nonlinear control due to preserving the essence of basic vehicle dynamics because it uses only longitudinal/lateral and yaw dynamics. The effectiveness of the bicycle model will be validated into a virtual automobile software (CarSim simulator) where it is testing the controller performance. In [31, 32], the active front steering (AFS) is considered as an input control; this actuator will impose an incremental steer angle δ_c. On the other hand, it also considered the yaw momentum as a control input M_z, which imposes negative longitudinal forces using the active brakes. Hence, the mathematical model of the ground vehicle is

$$\begin{aligned} m\left(\dot{v}_x - v_y\omega_z\right) &= \mu_x\left(F_{x,f} + F_{x,r}\right) + F_{d,x}, \\ m\left(\dot{v}_y + v_x\omega_z\right) &= \mu_y\left(F_{y,f} + F_{y,r}\right) + F_{d,y}, \\ J_z\dot{\omega}_z &= \mu_y\left(l_f F_{y,f} - l_r F_{y,r}\right) + M_z + M_{d,z}, \end{aligned} \tag{1}$$

where v_x and v_y are the longitudinal and lateral velocities of the vehicle center of mass, and α_z and ω_z are the yaw angle and yaw rate of the vehicle, m is the vehicle mass, J_z is the inertia momentum, l_f is the distance between the center mass to the front wheels, and l_r is the distance between the center mass to the rear wheels. Also, μ_x and μ_y are the longitudinal/lateral tire-road friction coefficients. Moreover, $F_{x,f}$ and $F_{x,r}$ are the front/rear longitudinal forces and $F_{y,f}$ and $F_{y,r}$ are the rear longitudinal/lateral forces, and M_z is the yaw moment. The external disturbance forces, due to environment actions as the wind blast, acting on the vehicle dynamics are $F_{d,x}$ and $F_{d,y}$ and $M_{d,z}$ is the torque generated by the external disturbance.

The tire front lateral force $F_{y,f}$ depends directly the front tire slip angle $\alpha_f = \delta_d + \delta_c - ((v_y + l_f\omega_z)/v_x)$, where δ_d is the road wheel angle imposed to the drive and the δ_c is the active front steering imposed by the designed control. Model (1) presents nonlinearities due to the characteristics of the tires. In this article, is used the compact Pacejka magic formula:

$$F_{y,j}\left(\alpha_j\right) = D_j \sin\left[C_j \arctan\left(B_j\alpha_j\right)\right], \quad j = f, r, \tag{2}$$

where B_j, C_j, and D_j are the values obtained experimentally [33].

The tire slip angle α_j, which depends all the forces acting in the vehicle dynamics, has some properties such as the angle has a minimum/maximum value, i.e., $\alpha_j = \pm\alpha_{j,\max}$, and it is considered invertible in function to α_j: $\alpha_j \in [-\alpha_{j,\max}, \alpha_{j,\max}]$.

The tire front lateral force, $F_{y,f}(\delta_d + \delta_c, v_y, \omega_z)$, is considered an invertible function with respect to the AFS control input δ_c; therefore, for a fixed value $F_{y,f,0}$, the solution of $F_{y,f}(\delta_d + \delta_c, v_y, \omega_z) = F_{y,f,0}$ is unique and given by

$$\delta_c = \begin{cases} -\delta_d + \dfrac{v_y + l_f\omega_z}{v_x} + F_{y,f}^{-1}\left(F_{y,f,0}\right), & \text{if } \alpha_f \in \left[-\alpha_{f,\max}, \alpha_{f,\max}\right], \\ -\delta_d + \dfrac{v_y + l_f\omega_z}{v_x} \pm F_{y,f,\max}, & \text{otherwise.} \end{cases} \tag{3}$$

The lateral force $F_{y,f}(\delta_d + \delta_c, v_y, \omega_z)$ is considered an invertible function; for this reason, it is possible to consider the following control input:

$$\Delta_f = F_{y,f}\left(\delta_d + \delta_c, v_y, \omega_z\right) - F_{y,f}\left(\delta_d, v_y, \omega_z\right). \tag{4}$$

Substituting Δ_f controller into the lateral velocity and the yaw rate velocity in the mathematical model of the ground vehicle (1), besides $F_{x,f} + F_{x,r} = 0$, the vehicle dynamics is rewritten as

$$\begin{aligned} \dot{v}_x &= v_y\omega_z + \frac{1}{m}F_{d,x}, \\ \dot{v}_y &= -v_x\omega_z + \frac{\mu_y}{m}\left(F_{y,f}(\delta_d) + F_{y,r}\right) + \frac{\mu_y}{m}\Delta_f + \frac{1}{m}F_{d,y}, \\ \dot{\omega}_z &= \frac{\mu_y}{J_z}\left(l_f F_{y,f}(\delta_d) - l_r F_{y,r}\right) + \frac{\mu_y l_f}{J_z}\Delta_f + \frac{1}{J_z}M_z + \frac{1}{J_z}M_{d,z}. \end{aligned} \tag{5}$$

The control aim is to design a modified HOSM controller using PI sliding surface, such as the lateral velocity v_y that globally tracks a reference $v_{y,\text{ref}}$, and ω_z tends a reference yaw rate $\omega_{z,\text{ref}}$ in finite time, despite the presence of the external disturbances and parameter uncertainties.

In this article, it is considered that the longitudinal velocity v_x, the lateral velocity v_y and the yaw rate ω_z are measurable variables. To solve the control problem, the following assumptions will be used.

Assumption 1. The steer angle δ_d is considered a smooth function, i.e., function C^2.

Assumption 2. The variables of the reference $v_{y,\text{ref}}$ and $\omega_{z,\text{ref}}$ and their derivatives $\dot{v}_{y,\text{ref}}$ and $\dot{\omega}_{z,\text{ref}}$ are considered bounded (physically obvious).

3. Design a Modified HOSM Controller for Trajectory Tracking

In this section, a modified HOSM controller using PI sliding surface will be designed when the parameter uncertainties and external disturbances are known.

Consider the tracking error as

$$\begin{aligned} e_{v,y} &= v_y - v_{y,\text{ref}}, \\ e_{\omega,z} &= \omega_z - \omega_{z,\text{ref}}. \end{aligned} \tag{6}$$

and the dynamics of the error system is

$$\begin{aligned} \dot{e}_{v,y} &= -v_x\omega_z + \frac{\mu_y}{m}\left(F_{y,f}(\delta_d) + F_{y,r}\right) + \frac{\mu_y}{m}\Delta_f + \frac{1}{m}F_{d,y} - \dot{v}_{y,\text{ref}}, \\ \dot{e}_{\omega,z} &= \frac{\mu_y}{J_z}\left(l_f F_{y,f}(\delta_d) - l_r F_{y,r}\right) + \frac{\mu_y l_f}{J_z}\Delta_f + \frac{1}{J_z}M_z + \frac{1}{J_z}M_{d,z} - \dot{\omega}_{z,\text{ref}}. \end{aligned} \tag{7}$$

Using the tracking error (6), the PI sliding function is defined as

$$\begin{aligned} s_y &= k_{p,y}e_{v,y}(t) + k_{i,y}\int e_{v,y}(t)\mathrm{d}t, \\ s_z &= k_{p,z}e_{\omega,z}(t) + k_{i,z}\int e_{\omega,z}(t)\mathrm{d}t, \end{aligned} \tag{8}$$

where $k_{p,y}, k_{i,y}, k_{p,z}, k_{i,z} > 0$. The gains in (8) provide flexibility for the construction of the PI sliding surface.

Then, it is possible to obtain the derivative with respect to time of the PI sliding function (8) as

$$\begin{aligned} \dot{s}_y &= k_{p,y}\left(-v_x\omega_z + \frac{\mu_y}{m}\left(F_{y,f}(\delta_d) + F_{y,r}\right) + \frac{\mu_y}{m}\Delta_f + \frac{1}{m}F_{d,y} - \dot{v}_{y,\text{ref}}\right) + k_{i,y}e_{v,y}, \\ \dot{s}_z &= k_{p,z}\left(\frac{\mu_y}{J_z}\left(l_f F_{y,f}(\delta_d) - l_r F_{y,r}\right) + \frac{\mu_y l_f}{J_z}\Delta_f + \frac{1}{J_z}M_z + \frac{1}{J_z}M_{d,z} - \dot{\omega}_{z,\text{ref}}\right) + k_{i,z}e_{\omega_z}. \end{aligned} \tag{9}$$

Hence, taking into account the PI surface $\dot{s}_y$ (9), the following input control Δ_f is proposed:

$$\begin{aligned} \Delta_f = {} & -\frac{m}{\mu_y}\left(-v_x\omega_z + \frac{\mu_y}{m}\left(F_{y,f}(\delta_d) + F_{y,r}\right) + \frac{1}{m}F_{d,y} - \dot{v}_{y,\text{ref}}\right) \\ & - \frac{m}{\mu_y}\frac{k_{i,y}}{k_{p,y}}e_{v,y} + \frac{m}{\mu_y k_{p,y}}\left(-\lambda_{1,y}\left|s_y\right|^{(1/2)}\operatorname{sign}\left(s_y\right) - \lambda_{2,y}s_y + \int_0^t\left(-\lambda_{3,y}\right)\operatorname{sign}\left(s_y(\tau)\right)\mathrm{d}\tau + \int_0^t\left(-\lambda_{4,y}\right)s_y(\tau)\mathrm{d}\tau\right), \end{aligned} \tag{10}$$

where $\lambda_{1,y}, \lambda_{2,y}, \lambda_{3,y}, \lambda_{4,y} > 0$.

Similarly, the RTV controller takes into account $\dot{s}_z$ (9), and proposing the controller M_z as

$$\begin{aligned} M_z = &-J_z\left(\frac{\mu_y}{J_z}\left(l_f F_{y,f}(\delta_d) - l_r F_{y,r}\right) + \frac{\mu_y l_f}{J_z}\Delta_f + \frac{1}{J_z}M_{d,z} - \dot{\omega}_{z,\mathrm{ref}}\right) \\ &-J_z\frac{k_{i,z}}{k_{p,z}}e_{\omega_z} + \frac{J_z}{k_{p,z}}\left(-\lambda_{1,z}|s_z|^{(1/2)}\mathrm{sign}(s_z) - \lambda_{2,z}s_z + \int_0^t\left(-\lambda_{3,z}\right)\mathrm{sign}(s_z(\tau))\mathrm{d}\tau + \int_0^t\left(-\lambda_{4,z}\right)s_z(\tau)\mathrm{d}\tau\right), \end{aligned} \tag{11}$$

where $\lambda_{1,z}, \lambda_{2,z}, \lambda_{3,z}, \lambda_{4,z} > 0$.

Substituting the input control (10) into the PI sliding surface $\dot{s}_y$ in (9), one obtains

$$\begin{aligned} \dot{s}_y &= -\lambda_{1,y}|s_y|^{(1/2)}\mathrm{sign}(s_y) - \lambda_{2,y}s_y + \chi_y, \\ \dot{\chi}_y &= -\lambda_{3,y}\mathrm{sign}(s_y) - \lambda_{4,y}s_y, \end{aligned} \tag{12}$$

and the input control M_z (11) into the PI sliding surface $\dot{s}_z$, one obtains

$$\begin{aligned} \dot{s}_z &= -\lambda_{1,z}|s_z|^{(1/2)}\mathrm{sign}(s_z) - \lambda_{2,z}s_z + \chi_z, \\ \dot{\chi}_z &= -\lambda_{3,z}\mathrm{sign}(s_z) - \lambda_{4,z}s_z. \end{aligned} \tag{13}$$

In fact, from (12) and (13), one gets the following differential inclusion:

$$\begin{aligned} \dot{s}_j &= -\lambda_{1,j}s_j^{(1/2)} - \lambda_{2,j}s_j + \chi_j, \\ \dot{\chi}_j &= -\lambda_{3,j}s_j^{0} - \lambda_{4,j}s_j, \end{aligned} \tag{14}$$

where $j = s, z$, and $s_j^{(1/2)} = |s_j|^{(1/2)}\mathrm{sign}(s_j)$ and $s_j^0 = \mathrm{sign}(s_j)$.

The proof of the stability of the origin to the PI sliding surface s_j can be considered as the following Lyapunov function:

$$\begin{aligned} \mathscr{V} &= \frac{1}{2}\xi^T P\xi, \\ \lambda_{\min}^P\|\xi\|_2^2 &\le \mathscr{V}(\xi) \le \lambda_{\max}^P\|\xi\|_2^2, \end{aligned} \tag{15}$$

where $\mathscr{V}$ is continuous and differentiable when $s_j \neq 0$, and

$$\begin{aligned} \xi &= \begin{pmatrix} s_j^{(1/2)} \\ s_j \\ \chi_j \end{pmatrix}, \\ P &= \begin{pmatrix} \lambda_{1,j}^2 + 4\lambda_{3,j} & \lambda_{1,j}\lambda_{2,j} & -\lambda_{1,j} \\ \lambda_{1,j}\lambda_{2,j} & 2\lambda_{4,j} + \lambda_{2,j}^2 & -\lambda_{2,j} \\ -\lambda_{1,j} & -\lambda_{2,j} & 2 \end{pmatrix}. \end{aligned} \tag{16}$$

Let $s_j = |s_j|^{(1/2)}s_j^{(1/2)}$ and $s_j^0 = (1/2|s_j|^{(1/2)})2s_j^{(1/2)}$, the derivative of ξ with respect to time will be

$$\begin{aligned} \frac{\mathrm{d}}{\mathrm{d}t}s_j^{(1/2)} &= \frac{1}{2|s_j|^{(1/2)}}\left(-\lambda_{1,j}s_j^{(1/2)} - \lambda_{2,j}s_j + \chi_j\right) = -\frac{1}{2|s_j|^{(1/2)}}\left(\lambda_{1,j}s_j^{(1/2)} - \chi_j\right) - \frac{1}{2}\lambda_{2,j}s_j^{(1/2)}, \\ \dot{s}_j &= -\lambda_{1,j}s_j^{(1/2)} - \lambda_{2,j}s_j + \chi_j, \\ \dot{\chi}_j &= -\lambda_{3,j}s_j^{0} - \lambda_{4,j}s_j = -\frac{1}{2|s_j|^{(1/2)}}2\lambda_{3,j}s_j^{(1/2)} - \lambda_{4,j}s_j. \end{aligned} \tag{17}$$

The derivative of (15) is

$$\begin{aligned} \dot{\mathscr{V}} &= \xi^T P\dot{\xi}, \\ \dot{\xi} &= \begin{pmatrix} \dot{s}_j^{(1/2)} \\ \dot{s}_j \\ \dot{\chi}_j \end{pmatrix} = -\frac{1}{2|\dot{s}_j|^{(1/2)}}\Lambda_1\xi + \frac{1}{2}\Lambda_2\xi, \end{aligned} \tag{18}$$

with

$$\begin{aligned} \Lambda_1 &= \begin{pmatrix} \lambda_{1,j} & 0 & -1 \\ 0 & 0 & 0 \\ 2\lambda_{3,j} & 0 & 0 \end{pmatrix}, \\ \Lambda_2 &= \begin{pmatrix} \lambda_{2,j} & 0 & 0 \\ 2\lambda_{1,j} & 2\lambda_{2,j} & -2 \\ 0 & 2\lambda_{4,j} & 0 \end{pmatrix}, \end{aligned} \tag{19}$$

so that

$$\dot{\mathscr{V}} = -\frac{1}{2\left|s_j\right|^{(1/2)}}\xi^T P\Lambda_1\xi + \frac{1}{2}\xi^T P\Lambda_2\xi,$$

$$P\Lambda_1 = \begin{pmatrix} \lambda_{1,j}\left(\lambda_{1,j}^2 + 2\lambda_{3,j}\right) & 0 & -\lambda_{1,j}^2 \\ \lambda_{2,j}\left(\lambda_{1,j}^2 - 2\lambda_{3,j}\right) & 0 & -\lambda_{1,j}\lambda_{2,j} \\ -\lambda_{1,j}^2 & 0 & \lambda_{1,j} \end{pmatrix},$$

$$P\Lambda_2 = -\begin{pmatrix} -\lambda_{2,j}\left(-3\lambda_{1,j}^2 + 4\lambda_{3,j}\right) & -2\lambda_{1,j}\left(\lambda_{2,j}^2 - \lambda_{4,j}\right) & 2\lambda_{1,j}\lambda_{2,j} \\ -\lambda_{1,j}\left(3\lambda_{2,j}^2 + 4\lambda_{4,j}\right) & -2\lambda_{2,j}\left(\lambda_{2,j}^2 + \lambda_{4,j}\right) & \left(2\lambda_{2,j}^2 + 4\lambda_{4,j}\right) \\ 3\lambda_{1,j}\lambda_{2,j} & \left(2\lambda_{2,j}^2 - 4\lambda_{4,j}\right) & -2\lambda_{2,j} \end{pmatrix}. \tag{20}$$

The first term of (20), i.e., $-(1/2|s_j|^{(1/2)})\xi^T P\Lambda_1\xi$ can be rewritten as

$$-\frac{1}{2|s_j|^{1/2}}\xi^T P\Lambda_1\xi = -\frac{1}{2\left|s_j\right|^{(1/2)}}\left(\lambda_{1,j}\left(2\lambda_{3,j} + \lambda_{1,j}^2\right)\left(s_j{}^{(1/2)}\right)^2 - 2\lambda_{1,j}^2 s_j{}^{(1/2)}x_j + \lambda_{2,j}\left(\lambda_{1,j}^2 - 2\lambda_{3,j}\right)s_j{}^{(1/2)}s_j - \lambda_{1,j}\lambda_{2,j}s_jx_j + \lambda_{1,j}x_j^2\right), \tag{21}$$

if $-(1/2|s_j|^{(1/2)})\lambda_{2,j}(\lambda_{1,j}^2 - 2\lambda_{3,j})s_j{}^{(1/2)}s_j = -(1/2)\lambda_{2,j}(\lambda_{1,j}^2 - 2\lambda_{3,j})(s_j{}^{(1/2)})^2$, the first term in matrix form is written as

$$-\frac{1}{2\left|s_j\right|^{(1/2)}}\xi^T P\Lambda_1\xi = -\frac{1}{2}\xi^T\begin{pmatrix} \lambda_{2,j}\left(\lambda_{1,j}^2 - 2\lambda_{3,j}\right) & 0 & 0 \\ 0 & 0 & 0 \\ 0 & 0 & 0 \end{pmatrix}\xi - \frac{1}{2\left|s_j\right|^{(1/2)}}\xi^T\begin{pmatrix} \lambda_{1,j}\left(\lambda_{1,j}^2 + 2\lambda_{3,j}\right) & 0 & -\lambda_{1,j}^2 \\ 0 & 0 & -\frac{1}{2}\lambda_{1,j}\lambda_{2,j} \\ -\lambda_{1,j}^2 & -\frac{1}{2}\lambda_{1,j}\lambda_{2,j} & \lambda_{1,j} \end{pmatrix}\xi. \tag{22}$$

Similarly, the second term of (20) is $(1/2)\xi^T P\Lambda_2\xi$, and it is written as

$$\frac{1}{2}\xi^T P\Lambda_2\xi = \frac{1}{2}\left(-\lambda_{2,j}\left(3\lambda_{1,j} + 4\lambda_{3,j}\right)\left(s_j{}^{(1/2)}\right)^2 - 2\lambda_{2,j}\left(\lambda_{2,j} + \lambda_{4,j}\right)s_j^2 - 2\lambda_{2,j}x_j^2 - \lambda_{1,j}\left(5\lambda_{2,j}^2 + 2\lambda_{4,j}\right)s_j{}^{(1/2)}s_j + 5\lambda_{1,j}\lambda_{2,j}s_j{}^{(1/2)}x_j + 4\lambda_{2,j}^2 s_jx_j\right), \tag{23}$$

since $s_j{}^{(1/2)}s_j = (1/2|s_j|^{(1/2)})2s_j^2$ and $s_j{}^{(1/2)}x_j = (1/|s_j|^{(1/2)})s_jx_j$, the second term in matrix form is

$$\frac{1}{2}\xi^T P\Lambda_2\xi = -\frac{1}{2}\lambda_{2,j}\xi^T\begin{pmatrix} 3\lambda_{1,j}^2+4\lambda_{3,j} & 0 & 0 \\ 0 & 2\left(\lambda_{2,j}^2+\lambda_{4,j}\right) & -2\lambda_{2,j} \\ 0 & -2\lambda_{2,j} & 2 \end{pmatrix}\xi - \frac{1}{2\left|s_j\right|^{(1/2)}}\lambda_{1,j}\xi^T\begin{pmatrix} 0 & 0 & 0 \\ 0 & 5\lambda_{2,j}^2+2\lambda_{4,j} & -\frac{5}{2}\lambda_{2,j} \\ 0 & -\frac{5}{2}\lambda_{2,j} & 0 \end{pmatrix}\xi. \tag{24}$$

Finally, using (22) and (24), one rewrites (20) as

$$\dot{\mathscr{V}} = -\frac{1}{\left|s_j\right|^{(1/2)}}\xi^T Q_1\xi - \xi^T Q_2\xi, \tag{25}$$

with

$$Q_1 = \frac{\lambda_{1,j}}{2}\begin{pmatrix} \left(\lambda_{1,j}^2+2\lambda_{3,j}\right) & 0 & -\lambda_{1,j} \\ 0 & 2\lambda_{4,j}+5\lambda_{2,j}^2 & -3\lambda_{2,j} \\ -\lambda_{1,j} & -3\lambda_{2,j} & 1 \end{pmatrix},$$
$$Q_2 = \frac{\lambda_{2,j}}{2}\begin{pmatrix} 2\lambda_{1,j}^2+\lambda_{3,j} & 0 & 0 \\ 0 & \lambda_{2,j}^2+\lambda_{4,j} & -\lambda_{2,j} \\ 0 & -\lambda_{2,j} & 1 \end{pmatrix}, \tag{26}$$

where $\dot{\mathscr{V}}$ is the negative definitive if and only if the matrix $Q_1, Q_2 > 0$, namely, $\lambda_{1,j}, \lambda_{2,j}, \lambda_{3,j}, \lambda_{4,j} > 0$. Denoting by $\lambda_{\min}^{Q_1}, \lambda_{\min}^{Q_2}$ the minimum eigenvalues of the matrix Q_1, Q_2, one finally works out

$$\dot{\mathscr{V}} \le \frac{1}{\left|s_j\right|^{(1/2)}}\lambda_{\min}^{Q_1}\|\xi\|_2^2 - \lambda_{\min}^{Q_2}\|\xi\|_2^2, \tag{27}$$

and using the fact $|e_v|^{(1/2)} \le \|\xi\|_2 \le \sqrt{(2\mathscr{V}/\lambda_{\min}^P)}$, one obtains

$$\dot{\mathscr{V}} \le -\left(c_1\mathscr{V}^{(1/2)} + c_2\mathscr{V}\right), \tag{28}$$

where $c_1 = \sqrt{2\lambda_{\min}^P}\,(\lambda_{\min}^{Q_1}/\lambda_{\max}^P)$ and $c_2 = 2\,(\lambda_{\min}^{Q_2}/\lambda_{\max}^P)$.

4. Sliding Modes Dynamics Stability

To determinate the stability of the sliding surface in (8), we focus when the sliding surface occurs, $s_i = 0; i = y, z$, then

$$s_i = k_{p,i}e_{v,\kappa}(t) + k_{i,\kappa}\int e_{v,\kappa}(t)\mathrm{d}t, \quad \kappa = y, z,$$
$$e_{v,\kappa}(t) = -\frac{k_{i,\kappa}}{k_{p,\kappa}}\int e_{v,\kappa}(t)\mathrm{d}t. \tag{29}$$

For the analysis of stability of error (29), the Lyapunov candidate function is proposed as

$$V_{v,\kappa} = \frac{1}{2}e_{v,\kappa}(t)^2. \tag{30}$$

The dynamic of the Lyapunov function yields

$$\dot{V}_{v,\kappa} = -\frac{k_{i,\kappa}}{k_{p,\kappa}}e_{v,\kappa}^2(t)\mathrm{d}t, \tag{31}$$

Therefore, the error $e_{v,\kappa}(t)$ is asymptotically stable when the gains $k_{i,\kappa} > 0$ and $k_{p,\kappa} > 0$.

5. Simulation Results

In this section, the simulation results taking into account the mathematical model of the vehicle (1) and the controllers (10) and (11) are presented using the CarSim simulator. CarSim delivers the most accurate, detailed, and efficient methods for simulating the performance of passenger vehicles. The test maneuver considered in this simulation is a so-called double-step steer (Figure 1). The maneuver consists of a rapid turn on the left of 100° at $t = 1s$, followed by a turn on the right of −100° at $t = 3$ s, and finally, at $t = 5s$, the steering wheel is set to zero. The parameters considered in (1) are given in Table 1.

The reference variables $v_{y,\mathrm{ref}}(t)$ and $\omega_{z,\mathrm{ref}}(t)$ will be considered as the behavior of an "ideal" or "reference" vehicle.

$$\dot{v}_{y,r} = -v_x\omega_{z,\mathrm{ref}} + \frac{\mu_{y,r}}{m_r}\left(F_{y,f,r}\left(\alpha_{f,r}\right) + F_{y,r,r}\left(\alpha_{r,r}\right)\right),$$
$$\dot{\omega}_{z,r} = \frac{\mu_{y,r}}{J_{z,r}}\left(F_{y,f,r}\left(\alpha_{f,r}\right)l_{f,r} - F_{y,r,r}\left(\alpha_{r,r}\right)l_{r,r}\right), \tag{32}$$

where $\alpha_{f,r} = \delta_d - ((v_{y,\mathrm{ref}} + l_{f,r}\omega_{z,\mathrm{ref}})/v_x)$, $\alpha_{r,r} = (-(v_{y,\mathrm{ref}} - l_{r,r}\omega_{z,\mathrm{ref}})/v_x)$, and the tire-road friction coefficient reference $\mu_{y,r}$, which is assumed as the road, is dry. The reference forces $F_{y,f,r}$ and $F_{y,r,r}$ are obtained using the compact Pacejka magic formula (2). The parameters considered in (32) are given in Table 2.

Finally, a disturbance due to the wind is considered, which has been implemented in [2, 4]. The wind induces longitudinal/lateral forces $F_{d,x}, F_{d,y}$, and a yaw moment $M_{d,z}$ [34]. In terms of the front/lateral surfaces $A_{s,f}$, $A_{s,l}$ of the vehicle, the air density ρ, and the (dimensionless) front/lateral aerodynamic coefficients $c_{a,x}$, $c_{a,y}$, the expression of the forces, and yaw torque due to the wind are $F_{d,x} = -(A_{s,f}\rho c_{a,x}v_{aw,x}^2/2)$, $F_{d,y} = -(A_{s,l}\rho c_{a,y}v_{aw,y}^2/2)$, $M_{d,z} = l_c F_{d,y}$, where $l_c = l_{c0} + 0.025\mathscr{N}$ is the distance between the center of mass and the center of pressure, with l_{c0} the nominal value and $\mathscr{N}$ a white noise. The parameters considered are given in Table 3.

5.1. CarSim Simulations. The simulations consider the performance of the controllers (10) and (11). The model of the vehicle considered in the CarSim simulator is a C-class hatchback automobile. The tires selected are 245/40–R17.

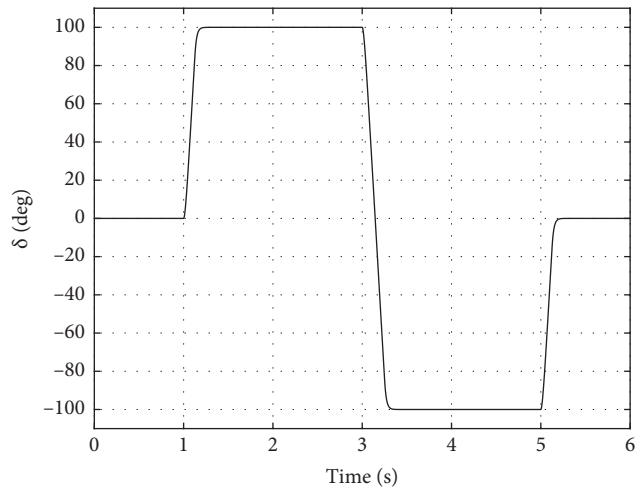

Figure 1: Steering wheel angle δ_d.

Table 1: Nominal parameter values.

$m_0 = 1565\,\text{kg}$	$B_{f,0} = 16$	$C_{f,0} = 1.41$
$J_{z,0} = 2075\,\text{kgm}^2$	$B_{r,0} = 16$	$C_{r,0} = 1.51$
Steer ratio: 16.01	$D_{f,0} = 8854\,\text{N}$	$E_{f,0} = 0$
$l_f = 1.38\,\text{m}$	$D_{r,0} = 8394\,\text{N}$	$E_{r,0} = 0$
$l_r = 1.53\,\text{m}$	—	

Table 2: Constants of the reference system (32).

$m_r = 1862\,\text{kg}$	$B_{y,f,r} = B_{y,f}$	$D_{y,f,r} = 10000\,\text{N}$
$l_{f,r} = l_f$	$B_{y,r,r} = 14.7$	$D_{y,r,r} = 10000\,\text{N}$
$l_{r,r} = l_r$	$C_{y,f,r} = C_{y,f}$	$J_{z,r} = 2488\,\text{kgm}^2$
$\mu_{y,r} = 0.9$	$C_{y,r,r} = 1.2$	—

Table 3: Parameters of the external disturbance.

$\mu_{yd} = 0.9$	$A_{s,f} = 2.59\text{m}^2$	$c_{a,x} = 0.3$
$\mu_{yw} = 0.6$	$A_{s,l} = 5.1\text{m}^2$	$c_{a,y} = 0.6$
$\mu_x = \mu_y$	$l_{c0} = -0.20\,\text{m}$	$\rho = 1.2\,\text{kg/m}^3$

The vehicle concerned has independent suspensions on both axles. The nominal values m_0, $J_{z,0}$, $D_{f,0}$, $D_{r,0}$, and l_{c0} have been used in the controller (Table 1), while the real automobile parameters are $m = 1.15m_0$, $J = 1.15J_{z,0}$, $D_f = 0.85D_{f,0}$, and $D_r = 0.85D_{r,0}$. The variables considered measurables in the CarSim are the longitudinal/lateral velocities v_x and v_y and the yaw angle and rate α_z and ω_z. The inputs to the CarSim simulator are the steering angle $\delta = \delta_d + \delta_c$, with δ_c calculated using (3), and the yaw moment M_z, and other inputs are the wind (wind-heading and wind-speed) and longitudinal/lateral tire-road.

The initial conditions used to show the performance of the controllers (10) and (11) are $v_x(0) = 100$ km/h, $v_y(0) = 0$ km/h, $\omega_z(0) = 0$ deg/s, and $\alpha_z(0) = 0$ deg, and the simulation results are shown in Figures 1–7.

The longitudinal/lateral tire-road friction coefficients mu_x and mu_y are given in Figure 2(a), and the side-slip angle behavior $\beta = (v_y/v_x)$ is given in Figure 2(b). The control input Δ_f, the corresponding incremental steering angle (AFS) δ_c, and the yaw torque M_z are shown in Figure 3. In Figures 4 and 5 are given the controlled outputs v_y and ω_z and its references $v_{y,\text{ref}}$ and $\omega_{z,\text{ref}}$ to track, and the tracking errors $v_y - v_{y,\text{ref}}$ and $\omega_z - \omega_{z,\text{ref}}$. The longitudinal velocity v_x

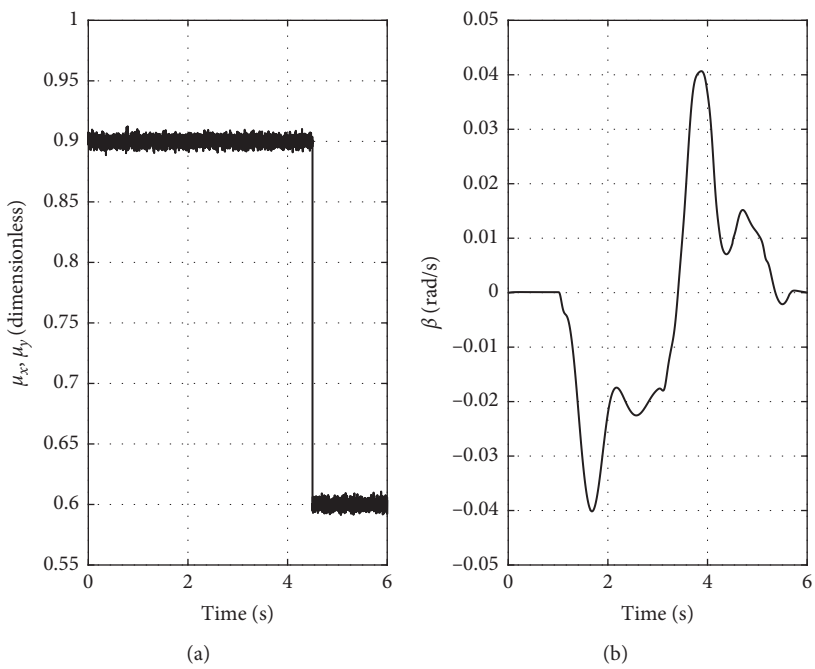

Figure 2: (a) Longitudinal/lateral tire-road friction coefficients μ_x and μ_y; and (b) sideslip angle $\beta = (v_y/v_x)$.

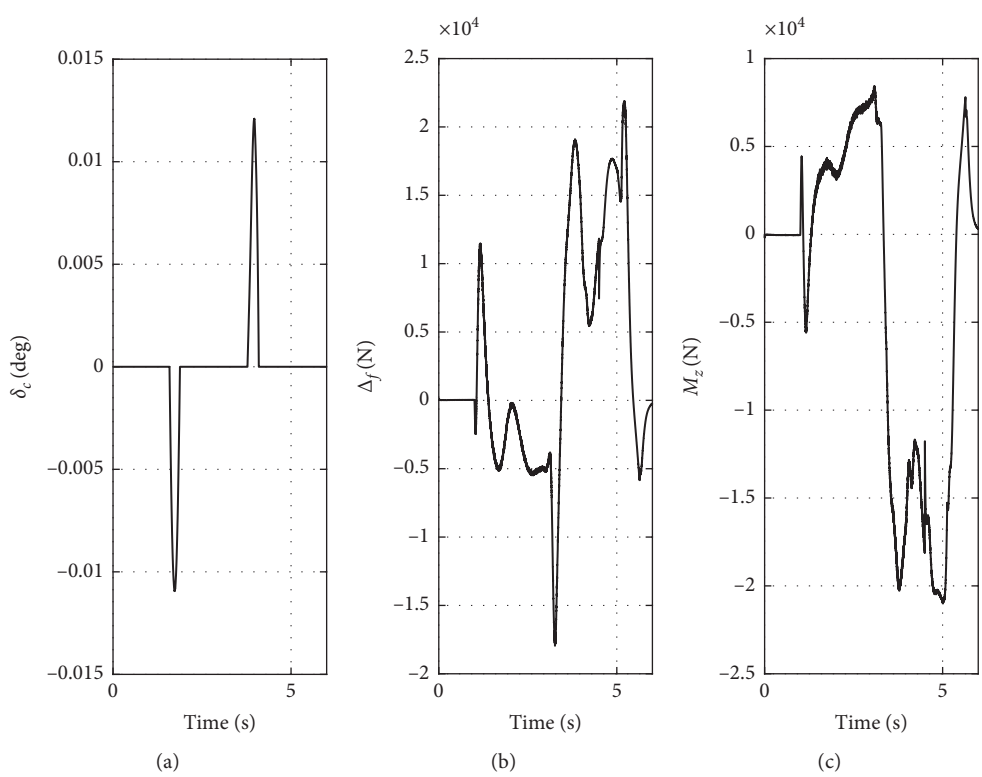

Figure 3: (a) Incremental steer angle δ_c; (b) Δ_f controller; and (c) yaw momentum M_z.

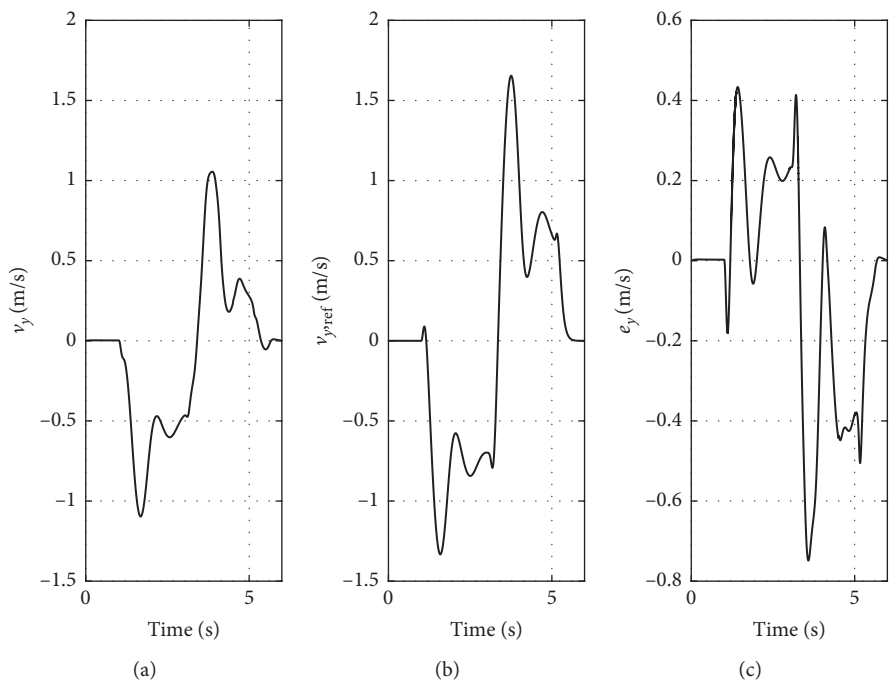

FIGURE 4: (a) Lateral velocity v_y; (b) lateral velocity reference $v_{y,\mathrm{ref}}$; and (c) $e_y = v_y - v_{y,\mathrm{ref}}$.

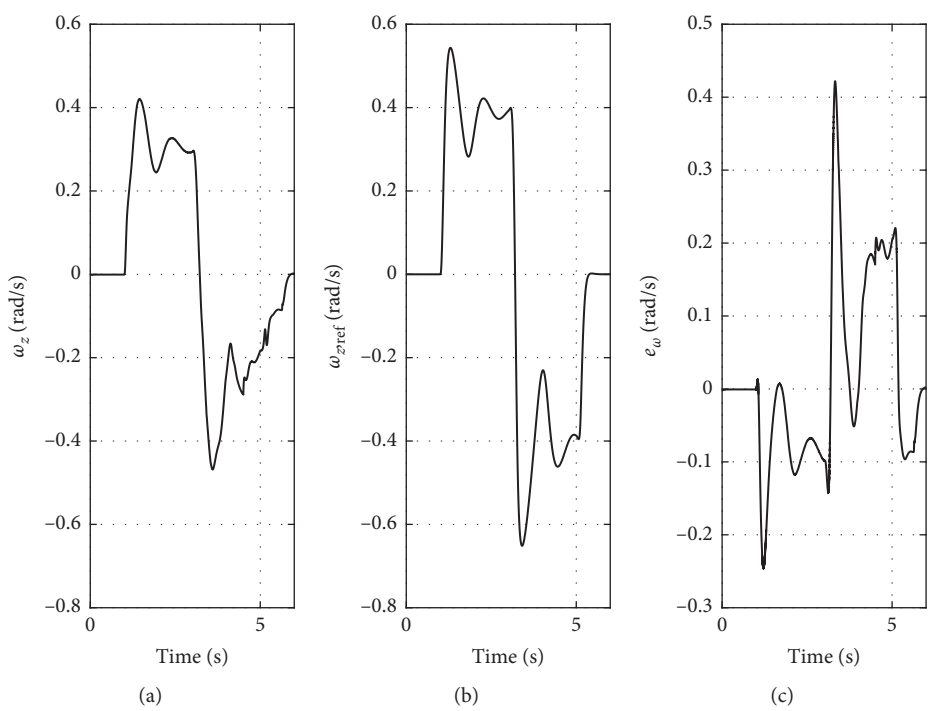

FIGURE 5: (a) Yaw rate ω_z; (b) yaw rate reference $\omega_{z,\mathrm{ref}}$; and (c) $e_\omega = \omega_z - \omega_{z,\mathrm{ref}}$.

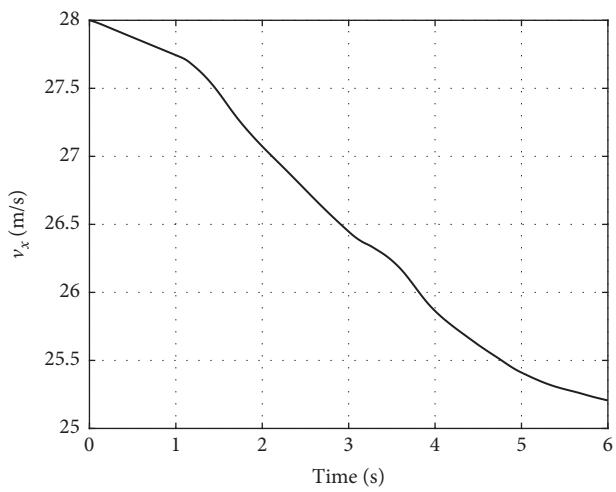

Figure 6: Longitudinal velocity v_x.

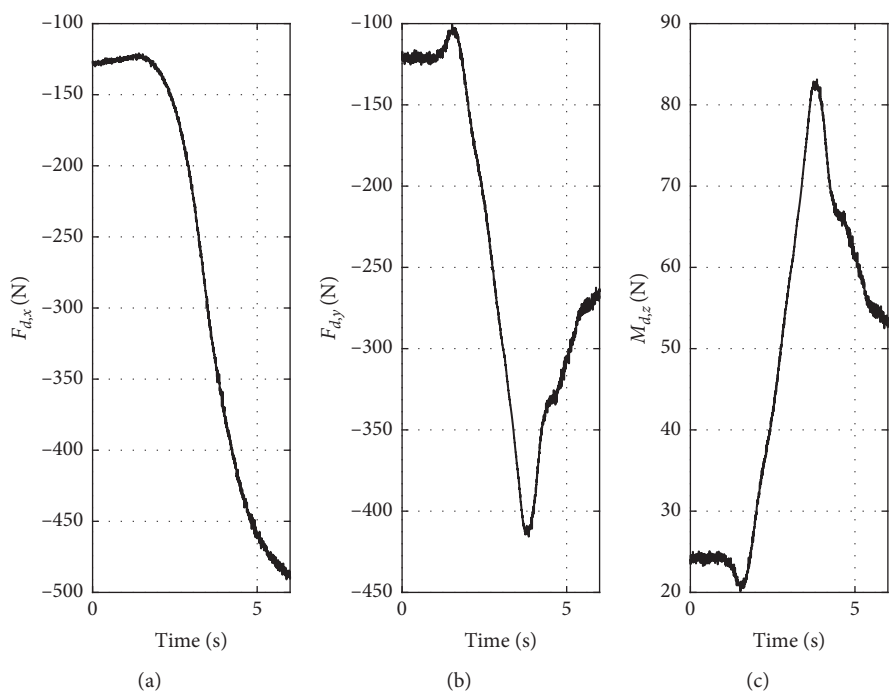

Figure 7: External disturbance: (a) $F_{d,x}$; (b) $F_{d,y}$; and (c) $M_{d,z}$.

is shown in Figure 6, and finally, the forces and moments $F_{d,x}$, $F_{d,y}$, $M_{d,z}$ are given in Figure 7.

6. Conclusions

In this study, an active front steering control and yaw moment was designed for the lateral and yaw dynamics of a vehicle. The active control of a robust nonlinear controller design uses the modified high-order sliding mode (HOSM) with the PI sliding surface. The stability performance of the PI sliding manifold was proved by the Lyapunov function. The simulation results highlight the performance of the proposed approach. The CarSim simulations show a good behavior of the HOSM-PI sliding surface even in the presence of external disturbances and parameter variations.

Data Availability

The data used to support the findings of this study are included within the article.

Conflicts of Interest

The authors declare that there are no conflicts of interest.

Acknowledgments

This study was partially supported by the European Project ECSEL–JURIA–2018 "Comp4Drones" and by the Project "Coordination of autonomous unmanned vehicles for highly complex performances" and Executive Program of Scientific and Technological Agreement between Italy (Ministry of Foreign Affairs and International Cooperation) and Mexico (Mexican International Cooperation Agency for the Development), SAAP3.

References

[1] C. Acosta Lúa, B. Castillo–Toledo, R. Cespi, and S. Di Gennaro, "Tyre–road friction coefficient estimation based on tyre lateral deflection," in *Proceedings of the 16th Congreso Latinoamericano de Control Automático – CLCA*, pp. 1089–1094, Lima, Perú, October 2014.

[2] C. Acosta Lúa, B. Castillo Toledo, R. Cespi, and S. Di Gennaro, "An integrated active nonlinear controller for wheeled vehicles," *Journal of the Franklin Institute*, vol. 352, no. 11, pp. 4890–4910, 2015.

[3] C. A. Lua, B. Castillo-Toledo, R. Cespi, and S. Di Gennaro, "Nonlinear observer-based active control of ground vehicles with non negligible roll dynamics," *International Journal of Control, Automation and Systems*, vol. 14, no. 3, pp. 743–752, 2016.

[4] C. Acosta Lúa and S. Di Gennaro, "Nonlinear adaptive tracking for ground vehicles in the presence of lateral wind disturbance and parameter variations," *Journal of the Franklin Institute*, vol. 354, no. 7, pp. 2742–2768, 2017.

[5] X. Yi, R. Guo, and Y. Qi, "Stabilization of chaotic systems with both uncertainty and disturbance by the UDE-based control method," *IEEE Access*, vol. 8, no. 1, pp. 62471–62477, 2020.

[6] L. Liu, B. Li, and R. Guo, "Consensus control for networked manipulators with switched parameters and topologies," *IEEE Access*, vol. 9, pp. 9209–9217, 2021.

[7] G. Burgio, B. Castillo–Toledo, and S. Di Gennaro, "Nonlinear adaptive tracking for ground vehicles," in *Proceedings of the 48th IEEE Conference on Decision and Control*, pp. 7645–7650, Las Vegas, NV, USA, March 2009.

[8] A. Borri, D. Bianchi, M. D. Di Benedetto, and S. Di Gennaro, "Optimal workload actuator balancing and dynamic reference generation in active vehicle control," *Journal of the Franklin Institute*, vol. 354, no. 4, pp. 1722–1740, 2017.

[9] M. Mirzaei and H. Mirzaeinejad, "Fuzzy scheduled optimal control of integrated vehicle braking and steering systems," *IEEE/ASME Transactions on Mechatronics*, vol. 22, no. 5, pp. 2369–2379, 2017.

[10] A. N. Guzman, S. D. Gennaro, J. R. Dominguez, C. A. Lua, A. G. Loukianov, and B. Castillo-Toledo, "Enhanced discrete-time modeling via variational integrators and digital controller design for ground vehicles," *IEEE Transactions on Industrial Electronics*, vol. 63, no. 10, pp. 6375–6385, 2016.

[11] Z. Sun, J. Zheng, Z. Man, H. Wang, and R. Lu, "Sliding mode-based active disturbance rejection control for vehicle steer-by-wire systems," *IET Cyber-Physical Systems: Theory & Applications*, vol. 3, no. 1, pp. 1–10, 2018.

[12] H. Guo, F. Liu, F. Xu, H. Chen, D. Cao, and Y. Ji, "Nonlinear model predictive lateral stability control of active chassis for intelligent vehicles and its FPGA implementation," *IEEE Transactions on Systems, Man, and Cybernetics: Systems*, vol. 49, no. 1, pp. 2–13, 2019.

[13] Acosta Lúa C., Di Gennaro S., Navarrete Guzman A., Ortega Cisneros S., Rivera Domínguez J.. IEEE Transactions on Industrial Informatics 2019.

[14] L. Etienne, C. Acosta Lúa, S. Di Gennaro, and J. . –P. Barbot, "A Super–twisting controller for active control of ground vehicles with lateral tire–road friction estimation and carsim validation," *International Journal of Control, Automation, and Systems*, vol. 8, no. 5, pp. 1177–1189, 2020.

[15] C. Chen, J. Zhang, J. Du, and Y. Jia, "Non-linear decoupling control of vehicle plane motion," *IET Control Theory & Applications*, vol. 6, no. 13, pp. 2083–2094, 2012.

[16] J. Tjonnas and T. A. Johansen, "Stabilization of automotive vehicles using active steering and adaptive brake control allocation," *IEEE Transactions on Control Systems Technology*, vol. 18, no. 3, pp. 545–558, 2010.

[17] D. Bianchi, A. Borri, M. D. D. Benedetto, S. D. Gennaro, and G. Burgio, "Adaptive integrated vehicle control using active front steering and rear torque vectoring," *International Journal of Vehicle Autonomous Systems*, vol. 8, pp. 85–105, 2010.

[18] S. V. Emelyanov, S. K. Korovin, and L. V. Levantovsky, "Higher order sliding regimes in the binary control systems," *Soviet Physics*, vol. 31, no. 4, pp. 291–293, 1986.

[19] L. Fridman, J. Moreno, and R. Iriarte, "Sliding modes after the first decade of the 21st century: state of the art," *Lecture Notes in Control and Information Sciences*, Springer–Verlag Berlin, vol. 412, 2011.

[20] V. Utkin, A. Poznyak, Y. Orlov, and A. Polyakov, "Conventional and high order sliding mode control," *Journal of the Franklin Institute*, vol. 357, no. 15, pp. 10244–10261, 2020.

[21] V. Utkin, "Discussion aspects of high–order sliding mode control," *IEEE Transactions on Automatic Control*, vol. 61, pp. 829–833, 2015.

[22] J. Á. Mercado-Uribe and J. A. Moreno, "Discontinuous integral action for arbitrary relative degree in sliding-mode control," *Automatica*, vol. 118, Article ID 109018, 2020.

[23] X.-G. Guo and C. K. Ahn, "Adaptive fault-tolerant pseudo-PID sliding-mode control for high-speed train with integral quadratic constraints and actuator saturation," *IEEE Transactions on Intelligent Transportation Systems*, vol. 24, pp. 1–11, 2020.

[24] U. Zakia, M. Moallem, and C. Menon, "PID-SMC controller for a 2-DOF planar robot," in *Proceedings of the International Conference on Electrical, Computer and Communication Engineering*, pp. 1–5, Kuala Lumpur, Malaysia, June 2019.

[25] G. Y. Gu, C.-X. Li, L.-M. Zhu, and S. Fatikow, "Robust tracking of nanopositioning stages using sliding mode control with a PID sliding surface," in *Proceedings of the IEEE/ASME International Conference on Advanced Intelligent Mechatronics (AIM)*, pp. 973–977, Delft, The Netherlands, July 2014.

[26] I. Eker, "Second–order sliding mode control with PI sliding surface and experimental application to an electromechanical plant," *Arabian Journal for Science and Engineering*, vol. 37, 2012.

[27] A. H. Khan and S. Li, "Sliding mode control with PID sliding surface for active vibration damping of pneumatically actuated soft robots," *IEEE Access*, vol. 8, pp. 88793–88800, 2020.

[28] M. Labbadi and M. Cherkaoui, "Novel robust super twisting integral sliding mode controller for a quadrotor under external disturbances," *International Journal of Dynamics and Control*, vol. 8, no. 3, pp. 805–815, 2020.

[29] G. J. Heydinger, W. R. Garrott, J. P. Chirstos, and D. A. Guenther, *A Methodology for Validating Vehicle*

Dynamics Simulations, Society of Automotive Engineers, Warrendale, PA, USA, Paper 900128, 1990.

[30] J. Wong, *Theory of Ground Vehicles 1978*, Wiley, New York, NY, USA.

[31] P. Setlur, J. R. Wagner, D. M. Dawson, and D. Braganza, "A trajectory tracking steer-by-wire control system for ground vehicles," *IEEE Transactions on Vehicular Technology*, vol. 55, no. 1, pp. 76–85, 2006.

[32] G. Burgio and P. Zeglaar, "Integrated vehicle control using steering and brakes," *International Journal of Control*, vol. 79, no. 2, pp. 162–169, 2006.

[33] H. Pacejka, *Tyre and Vehicle Dynamics*, Elsevier Butterworth–Heinemann, Oxford, UK, 2005.

[34] O. Hanke, T. Bertram, and M. Hiller, "Analysis and control of vehicle dynamics under crosswind conditions," in *Proceedings of the 2001 IEEE/ASME International Conference on Advanced Intelligent Mechatronics*, pp. 331–336, Como, Italy, July 2001.

Hindawi
Mathematical Problems in Engineering
Volume 2021, Article ID 2577264, 9 pages
https://doi.org/10.1155/2021/2577264

Research Article

A Portfolio Selection Model Based on the Interval Number

Jiangshan Hu,[1] Yunyun Sui ,[1] and Fang Ma[2]

[1]*School of Mathematics and Information Science, Weifang University, Weifang 261061, China*
[2]*School of Science, Shenyang University of Technology, Shenyang 110023, China*

Correspondence should be addressed to Yunyun Sui; suiyunyun1231@163.com

Received 25 April 2021; Accepted 25 May 2021; Published 2 June 2021

Academic Editor: Rongwei Guo

Traditional portfolio theory uses probability theory to analyze the uncertainty of financial market. The assets' return in a portfolio is regarded as a random variable which follows a certain probability distribution. However, it is difficult to estimate the assets return in the real financial market, so the interval distribution of asset return can be estimated according to the relevant suggestions of experts and decision makers, that is, the interval number is used to describe the distribution of asset return. Therefore, this paper establishes a portfolio selection model based on the interval number. In this model, the semiabsolute deviation risk function is used to measure the portfolio's risk, and the solution of the model is obtained by using the order relation of the interval number. At the same time, a satisfactory solution of the model is obtained by using the concept of acceptability of the interval number. Finally, an example is given to illustrate the practicability of the model.

1. Introduction

Portfolio selection refers to the way in which investors allocate a certain proportion of their wealth to a number of different assets so as to spread risks among multiple assets and obtain some stable returns. Markowitz [1] created the classic portfolio theory in 1952, which laid the foundation of modern finance. In this theory, the covariance of all the securities in the portfolio was required, which was a considerable amount of calculation at that time, but difficult to achieve in practical application. Therefore, later, scholars constantly proposed improved optimization methods and thus put forward new portfolio models (e.g., [2–5]). In 1963, the capital asset pricing model (abbreviated as CAPM) proposed by Sharp [2] divided risks into systematic risks and nonsystematic risks on the basis of the model proposed by Markowitz. Markowitz [3] proposed a semivariance model. Mao [4] and Swalm [5] used the risk that the uncertain return is lower than the expected return to measure the investment risk and established the mean-semivariance portfolio selection model. In 1991, Konno and Yamazaki [6] proposed the absolute deviation risk function and constructed a mean-absolute deviation portfolio optimization model. Since then, scholars have also proposed many portfolio optimization models based on different risk measures, such as semiabsolute deviation model [7], value-at-risk (VaR) model [8–11], and conditional value-at-risk (CVaR) model [12]. Since each measure of risk performs best in its own area and not necessarily in others, it is still up in the air whether there is a single measure of risk that is best for all portfolios [13, 14]. In this paper, we will use the semiabsolute deviation absolute risk function to measure the risk of the portfolio.

Uncertainty exists everywhere, and scholars use various methods to study it [15–21]. Traditional portfolio theory uses probability theory to analyze the uncertainty in the financial market. However, due to the nonrandom factors such as social, economic, political, psychological, and other factors existing in the real financial market, other technologies are needed to deal with the uncertainty, such as possibility theory and fuzzy set theory. Possibility theory is an important theory of fuzzy sets that was first proposed by Zadeh [22] and developed by Dubois and Prade [23] (see [24–27], for more details). Portfolio models based on theory of possibility have been fruitful (see [28–35]). In these possibilistic portfolio selection models, it is assumed that the possibility distribution of asset return in the portfolio is known, but in reality, it is often not so. The interval number

is a relatively simple fuzzy number, which is easy for experts and decision makers to estimate the interval number of fuzzy parameters in a certain precision range on the basis of comprehensive analysis of the influence of various factors. So far, there have been many reports using interval number theory to study portfolio selection, such as literature [36–42].

Lai *et al.* [37] gave the noninferior solutions of linear programming problems with interval coefficients. In [38], Ida regarded the portfolio problem with interval and fuzzy objective function coefficients as a kind of multiobjective problem containing uncertainty and gave its optimistic and pessimistic solutions. Giove *et al.* [39] established a portfolio model by taking securities' price as the interval variable and solved the model by using the minimax regret method. Bhattacharyya *et al.* [40] constructed a mean-variance-skewness portfolio model using interval numbers and used a hybrid intelligent algorithm (HIA) to solve the model. Liu [41] used an interval number to represent the expected return of an asset. According to the concept of mean-absolute deviation function, a pair of two-level portfolio model was constructed, and the upper and lower bounds of investment returns in the portfolio selection problem were calculated. Based on the semiabsolute deviation risk function proposed by Mansini and Speranza [43], a mean-semiabsolute deviation portfolio selection model with respect to the interval number will be established. The order relation of the interval number is very important for obtaining the solution of the model, so the order relation of the interval in [44] will be used to obtain the solution of the constructed model. At the same time, the satisfactory solution of the model is given according to the acceptability [45].

The rest of this paper is organized as follows. In Section 2, we will do some preliminary work and give the basic concepts and some notations that will be used later. In Section 3, the portfolio selection model construction and the solution of the model will be introduced in detail. To obtain the solution for the interval-valued programming model, the order relation and the acceptability of interval numbers are used to transform the model into a general programming model. Section 4 provides a numerical example to illustrate the proposed approach. Section 5 provides the conclusion.

2. Preliminaries

In this paper, concepts and operations related to interval numbers will be used. This section will briefly review the relevant concepts.

Definition 1 (see [46]). Given two interval numbers $a = [a_-, a_+]$ and $b = [b_-, b_+]$ and a real number λ, then

(i) $a \pm b = [a_- \pm b_-, a_+ \pm b_+]$.

(ii) $\lambda a = \begin{cases} [\lambda a_-, \lambda a_+], & \text{for } \lambda \geq 0, \\ [\lambda a_+, \lambda a_-], & \text{for } \lambda < 0. \end{cases}$

The interval number is a special fuzzy number whose membership function takes value 1 over the interval and 0 anywhere else, as discussed in detail by Hansen [47] and Alefeld and Herzberger [46]. The operations related to interval numbers are as follows.

Definition 2 (see [48–50]). Let $a = [a_-, a_+]$ and $b = [b_-, b_+]$ be two interval numbers. We define the order relation $\leq$ between a and b as

$$\begin{aligned} &(1)\ a \leq b \text{ if and only if } m(a) \leq m(b), \\ &(2)\ a < b \text{ if and only if } a \leq b \text{ and } a \neq b, \end{aligned} \tag{1}$$

where $m(a) = (1/2)(a_- + a_+)$ is the midpoints of the interval number$a$.

Specifically, if $a_+ \leq b_-$, then the inequality relationship $a \leq b$ is optimistic and satisfactory. On the contrary, if $a_+ > b_-$, the inequality relationship $a \leq b$ is pessimistic and satisfactory.

Definition 3 (see [51]). Given $a = [a_-, a_+]$ and $b = [b_-, b_+]$, then $\lambda(a \leq b) = (m(b) - m(a))/(\omega(b) + \omega(a))$ is the acceptability of $a \leq b$, where $m(a)$ and $\omega(a)$ are the midpoints and radius of the interval number a, respectively.

The notations used in this article are given below:

p_{kt0}: the opening price of the k thsecurity at period t

p_{ktc}: the closing price of the kth security at period t

r_{kt}: $(p_{ktc} - p_{kt0})/p_{kt0}$ = the return of asset k at period t

T: the total periods

r_k: $(1/T)\sum_{t=1}^{T} r_{kt}$ = the return of asset k

r_f: the return of the risk-free asset

x_k: the percentage of assets that are invested in k

$w_t(x)$: the portfolio's risk at period t

$W(x)$: the portfolio's risk

R: the portfolio's return

3. Model Foundation

Let us consider a market consisting of a riskless assets and n stocks. As usual, we assume that there are no costs or taxes on trading, all assets are infinitely divisible, and short sales is not allowed.

Thus, the portfolio's return R can be written as

$$R = \sum_{k=1}^{n} x_k r_k + r_f \left(1 - \sum_{k=1}^{n} x_k\right). \tag{2}$$

To set up a portfolio selection model, the following values need to be given.

First is the expected return of the portfolio's return $\widetilde{R}$.

The expected return on security k is $\widetilde{r}_k = [\underline{r_k}, \bar{r_k}]$. Thus, $\widetilde{R}$ is given by

$$\widetilde{R} = \sum_{k=1}^{n} \left[\underline{r_k}, \bar{r_k}\right] x_k + r_f \left(1 - \sum_{k=1}^{n} x_k\right). \tag{3}$$

Secondly, the risk of the portfolio is as follows.

As mentioned in Section 1, there is no single risk measure that is best for all portfolios, so the risk in this paper will be measured by the semiabsolute deviation function. The semiabsolute deviation of the portfolio in period t can be calculated as follows:

$$w_t(x) = \left|\min\left\{0, \sum_{k=1}^{n}(r_{kt} - r_k)x_k\right\}\right| = \max\left\{0, \sum_{k=1}^{n}(r_k - r_{kt})x_k\right\}, \quad t = 1, 2, \ldots, T. \tag{4}$$

The risk of the portfolio is given by $(1/T)\sum_{t=1}^{T} w_t(x)$. So,

$$\begin{aligned} W(x) &= \frac{1}{T}\sum_{t=1}^{T}\left|\min\left\{0, \sum_{k=1}^{n}(r_{kt} - r_k)x_k\right\}\right| \\ &= \frac{1}{T}\sum_{t=1}^{T}\left[\max\left\{0, \sum_{k=1}^{n}\left(\underline{r_k} - r_{kt}\right)x_k\right\}, \max\left\{0, \sum_{k=1}^{n}\left(\bar{r_k} - r_{kt}\right)x_k\right\}\right] \\ &= \frac{1}{T}\sum_{t=1}^{T}\left[\frac{\sum_{k=1}^{n}\left(\underline{r_k} - r_{kt}\right)x_k + \left|\sum_{k=1}^{n}\left(\underline{r_k} - r_{kt}\right)x_k\right|}{2}, \frac{\sum_{k=1}^{n}(\bar{r_k} - r_{kt})x_k + \left|\sum_{k=1}^{n}(\bar{r_k} - r_{kt})x_k\right|}{2}\right] \\ &= \frac{1}{T}\sum_{t=1}^{T}\left[\underline{w}_t(x), \bar{w}_t(x)\right], \end{aligned} \tag{5}$$

where

$$\begin{aligned} \underline{w}_t(x) &= \frac{\left(\sum_{k=1}^{n}\left(\underline{r_k} - r_{kt}\right)x_k + \left|\sum_{k=1}^{n}\left(\underline{r_k} - r_{kt}\right)x_k\right|\right)}{2}, \\ \bar{w}_t(x) &= \frac{\left(\sum_{k=1}^{n}(\bar{r_k} - r_{kt})x_k + \left|\sum_{k=1}^{n}(\bar{r_k} - r_{kt})x_k\right|\right)}{2}. \end{aligned} \tag{6}$$

Therefore, a portfolio selection model based on risk-return trade-off can be established:

$$\begin{cases} \min W(x), \\ \text{s.t. } \widetilde{R} \geq \mu, \sum_{k=1}^{n} x_k \leq 1, 0 \leq l_k \leq x_k \leq h_k, \quad k = 1, 2, \ldots, n, \end{cases} \tag{7}$$

where μ is a minimum threshold at which investors can tolerate the expected rate of return on their portfolio and set $\mu = [\mu^-, \mu^+]$ and l_k and h_k represent, respectively, the lower and the upper bounds on investment in asset k, $k = 1, 2, \ldots, n$.

As can be seen from equations (3) and (5), equation (7) can be transformed into

$$\begin{cases} \min W(x) = \frac{1}{T}\sum_{t=1}^{T}\left[\underline{w}_t(x), \bar{w}_t(x)\right], \\ \text{s.t. } \sum_{k=1}^{n}\left[\underline{r_k}, \bar{r_k}\right]x_k + r_f\left(1 - \sum_{k=1}^{n} x_k\right) \geq [\mu^-, \mu^+], \\ \sum_{k=1}^{n} x_k \leq 1, \\ 0 \leq l_k \leq x_k \leq h_k, \quad k = 1, 2, \ldots, n. \end{cases} \tag{8}$$

The solution of model (8) is equivalent to the following equation:

$$\begin{cases} \max \bar{W}(x) = -W(x) = -\frac{1}{T}\sum_{t=1}^{T}\left[\underline{w}_t(x), \bar{w}_t(x)\right], \\ \text{s.t. } \sum_{k=1}^{n}\left[\underline{r_k}, \bar{r_k}\right]x_k + r_f\left(1 - \sum_{k=1}^{n} x_k\right) \geq [\mu^-, \mu^+], \\ \sum_{k=1}^{n} x_k \leq 1, \\ 0 \leq l_k \leq x_k \leq h_k, \quad k = 1, 2, \ldots, n. \end{cases} \tag{9}$$

From Definition 1, we can have

$$\begin{cases} \max \bar{W}(x) = \frac{1}{T}\sum_{t=1}^{T}\left[-\bar{w}_t(x), -\underline{w}_t(x)\right], \\ \text{s.t. } \sum_{k=1}^{n}\left[\underline{r_k}, \bar{r_k}\right]x_k + r_f\left(1 - \sum_{k=1}^{n} x_k\right) \geq [\mu^-, \mu^+], \\ \sum_{k=1}^{n} x_k \leq 1, \\ 0 \leq l_k \leq x_k \leq h_k, \quad k = 1, 2, \ldots, n. \end{cases} \tag{10}$$

This is an interval-valued linear programming problem. For the solution method of interval-valued linear programming, scholars have carried out a lot of research and put forward some solutions. For example, Yoon [52] proposed

the error analysis method. Bryson and Mobolurin [53] proposed the linear programming method. Romelfangerf et al. [54] studied the solution method of linear programming with the interval number as the coefficient of objective function. Liu and Iwamura [55] transformed interval number linear programming into a two-objective programming problem:

$$\begin{cases} \max \bar{W}(x) = -\dfrac{1}{T}\displaystyle\sum_{t=1}^{T} \bar{w}_t(x), \\ \max \bar{W}(x) = -\dfrac{1}{T}\displaystyle\sum_{t=1}^{T} \underline{w}_t(x), \\ \text{s.t.} \displaystyle\sum_{k=1}^{n}\left[\underline{r_k}, \bar{r_k}\right]x_k + r_f\left(1 - \sum_{k=1}^{n} x_k\right) \geq [\mu^-, \mu^+], \\ \displaystyle\sum_{k=1}^{n} x_k \leq 1, \\ 0 \leq l_k \leq x_k \leq h_k, \quad k = 1, 2, \ldots, n. \end{cases} \tag{11}$$

Chankong and Haimes [56] transformed the above-mentioned two-objective programming problem (13) into the following parameter programming problem:

$$\begin{cases} \max \bar{W}(x) = \dfrac{1}{T}\displaystyle\sum_{t=1}^{T}\left[-(1-b)\bar{w}_t(x) - b\underline{w}_t(x)\right], \\ \text{s.t.} \ \widetilde{R} \geq [\mu^-, \mu^+], \displaystyle\sum_{k=1}^{n} x_k \leq 1, 0 \leq l_k \leq x_k \leq h_k, \quad k = 1, 2, \ldots, n. \end{cases} \tag{12}$$

The solution of model (12) is also the solution of the following model:

$$\begin{cases} \min H(x) = \dfrac{1}{T}\displaystyle\sum_{t=1}^{T}\left[(1-b)\bar{w}_t(x) + b\underline{w}_t(x)\right], \\ \text{s.t.} \ \widetilde{R} \geq [\mu^-, \mu^+], \displaystyle\sum_{k=1}^{n} x_k \leq 1, 0 \leq l_k \leq x_k \leq h_k, \quad k = 1, 2, \ldots, n. \end{cases} \tag{13}$$

Because

$$\begin{aligned} H(x) &= \frac{1}{T}\sum_{t=1}^{T}\left[(1-b)\bar{w}_t(x) + b\underline{w}_t(x)\right] \\ &= \frac{1}{T}\sum_{t=1}^{T}\left[(1-b)\frac{\left(\sum_{k=1}^{n}(\bar{r_k} - r_{kt})x_k + \left|\sum_{k=1}^{n}(\bar{r_k} - r_{kt})x_k\right|\right)}{2} + b\frac{\left(\sum_{k=1}^{n}\left(\underline{r_k} - r_{kt}\right)x_k + \left|\sum_{k=1}^{n}\left(\underline{r_k} - r_{kt}\right)x_k\right|\right)}{2}\right] \\ &= \sum_{k=1}^{n}\frac{(1-b)\xi_k + b\eta_k}{2T}x_k + \frac{1}{2}\sum_{t=1}^{T}\left[(1-b)\frac{\left|\sum_{k=1}^{n}(\bar{r_k} - r_{kt})x_k\right|}{T} + b\frac{\left|\sum_{k=1}^{n}\left(\underline{r_k} - r_{kt}\right)x_k\right|}{T}\right] \\ &= \sum_{k=1}^{n}\frac{(1-b)\xi_k + b\eta_k}{2T}x_k + \frac{1}{2}\sum_{t=1}^{T}\left[(1-b)\frac{u_t}{T} + b\frac{v_t}{T}\right], \end{aligned} \tag{14}$$

where

$$\begin{aligned} \xi_k &= \sum_{t=1}^{T}\left(\bar{r_k} - r_{kt}\right), \\ \eta_k &= \sum_{t=1}^{T}\left(\underline{r_k} - r_{kt}\right), \\ u_t &= \left|\sum_{k=1}^{n}\left(\bar{r_k} - r_{kt}\right)x_k\right|, \\ v_t &= \left|\sum_{k=1}^{n}\left(\underline{r_k} - r_{kt}\right)x_k\right|, \end{aligned} \tag{15}$$

then we have

$$\begin{cases} \min H(x) = \dfrac{1}{T}\displaystyle\sum_{t=1}^{T}\left[(1-b)\bar{w}_t(x) + b\underline{w}_t(x)\right], \\ \text{s.t.} \displaystyle\sum_{k=1}^{n}\left[\underline{r_k}, \bar{r_k}\right]x_k + r_f\left(1 - \sum_{k=1}^{n} x_k\right) \geq [\mu^-, \mu^+], \\ \displaystyle\sum_{k=1}^{n} x_k \leq 1, \\ 0 \leq l_k \leq x_k \leq h_k, \quad k = 1, 2, \ldots, n. \end{cases} \tag{16}$$

According to Definition 1, (16) can be transformed into

$$\begin{cases} \min H(x) = \dfrac{1}{T}\displaystyle\sum_{t=1}^{T}\left[(1-b)\bar{w}_t(x) + b\underline{w}_t(x)\right], \\ \text{s.t.} \left[\displaystyle\sum_{k=1}^{n}\underline{r_k}x_k + r_f\left(1-\sum_{k=1}^{n}x_k\right), \sum_{k=1}^{n}\bar{r}_k x_k + r_f\left(1-\sum_{k=1}^{n}x_k\right)\right] \geq [\mu^-, \mu^+], \\ \displaystyle\sum_{k=1}^{n}x_k \leq 1, \\ 0 \leq l_k \leq x_k \leq h_k, \quad k = 1, 2, \ldots, n. \end{cases} \tag{17}$$

In order to obtain the solution of (17), the order relation of the interval number in Definition 2 and (14) can be used to convert (17) into

$$\begin{cases} \min H(x) = \displaystyle\sum_{k=1}^{n}\frac{(1-b)\xi_k + b\eta_k}{2T}x_k + \frac{1}{2}\sum_{t=1}^{T}\left[(1-b)\frac{u_t}{T} + b\frac{v_t}{T}\right], \\ \text{s.t.} \ \dfrac{1}{2}\left(\displaystyle\sum_{k=1}^{n}\underline{r_k}x_k + \sum_{k=1}^{n}\bar{r}_k x_k\right) + r_f\left(1-\sum_{k=1}^{n}x_k\right) \geq \frac{1}{2}(\mu^- + \mu^+), \\ u_t + \displaystyle\sum_{k=1}^{n}\left(\bar{r}_k - r_{kt}\right)x_k \geq 0, \quad t = 1, 2, \ldots, T, \\ u_t - \displaystyle\sum_{k=1}^{n}\left(\bar{r}_k - r_{kt}\right)x_k \geq 0, \quad t = 1, 2, \ldots, T, \\ v_t + \displaystyle\sum_{k=1}^{n}\left(\underline{r_k} - r_{kt}\right)x_k \geq 0, \quad t = 1, 2, \ldots, T, \\ v_t - \displaystyle\sum_{k=1}^{n}\left(\underline{r_k} - r_{kt}\right)x_k \geq 0, \quad t = 1, 2, \ldots, T, \\ \displaystyle\sum_{k=1}^{n}x_k \leq 1, \\ 0 \leq l_k \leq x_k \leq h_k, \quad k = 1, 2, \ldots, n. \end{cases} \tag{18}$$

Then, (18) is a parameter-planning problem, which can be solved by Matlab, Lingo, and other software.

Definition 4. The optimal solution to (18) is called an interval-valued efficient portfolio.

The lower bounds of all the interval-valued efficient portfolios construct the interval-valued lower efficient frontier. The upper bounds of all the interval-valued efficient portfolios construct the interval-valued upper efficient frontier.

Meanwhile, based on the acceptability, (17) can also be transformed into

$$\begin{cases} \min H(x) = \dfrac{1}{T}\displaystyle\sum_{t=1}^{T}\left[(1-b)\bar{w}_t(x) + b\underline{w}_t(x)\right], \\ \text{s.t. } \lambda\left(\left[\displaystyle\sum_{k=1}^{n}\underline{r_k}x_k + r_f\left(1-\sum_{k=1}^{n}x_k\right), \sum_{k=1}^{n}\bar{r_k}x_k + r_f\left(1-\sum_{k=1}^{n}x_k\right)\right] \geq \left[\mu^-, \mu^+\right]\right) \geq \alpha, \\ \displaystyle\sum_{k=1}^{n}x_k \leq 1, \\ 0 \leq l_k \leq x_k \leq h_k, \quad k = 1, 2, \ldots, n, \end{cases} \tag{19}$$

where α is the minimum value of acceptability.

According to Definition 3, we can obtain

$$\begin{cases} \min H(x) = \dfrac{1}{T}\displaystyle\sum_{t=1}^{T}\left[(1-b)\bar{w}_t(x) + b\underline{w}_t(x)\right], \\ \text{s.t. } \dfrac{\sum_{k=1}^{n}\underline{r_k}x_k + \sum_{k=1}^{n}\bar{r_k}x_k + 2r_f\left(1-\sum_{k=1}^{n}x_k\right) - \left(\mu^- + \mu^+\right)}{\left(\sum_{k=1}^{n}\bar{r_k}x_k - \sum_{k=1}^{n}\underline{r_k}x_k\right) - \left(\mu^+ - \mu^-\right)} \geq \alpha, \\ \displaystyle\sum_{k=1}^{n}x_k \leq 1, \\ 0 \leq l_k \leq x_k \leq h_k, \quad k = 1, 2, \ldots, n. \end{cases} \tag{20}$$

Thus, a satisfactory solution of the model is obtained, and an acceptable efficient portfolio is obtained.

4. Numerical Example

In order to illustrate the practicality of this model, we select five securities and one risk-free asset from the Chinese stock market for investment. Annual data from 2016 to 2020 were selected. Table 1 shows the expected return.

Let the risk-free asset be a treasury bond. We use the one-year treasury bond rate as the return rate of the riskless asset. So, we get the return on risk-free asset $r = 2.8\%$ if the lower bound of the investment ratio x_k must be $l = \{0.01, 0.03, 0.01, 0.01, 0\}$ and the upper bound $h = \{0.3, 0.4, 0.1, 0.5, 0.3\}$.

Table 1: The expected return of the five securities.

Code	$\tilde{r}_k = [\underline{r_k}, \bar{r_k}]$
$S1$	[−0.557, 0.341]
$S2$	[−0.170, 0.306]
$S3$	[−0.381, 0.953]
$S4$	[−0.316, 0.258]
$S5$	[−0.503, 0.156]

Table 2 shows the effective portfolios of model (18) with different μs when $b = 0.1$. Figure 1 gives some efficient portfolios for model (18).

As can be seen from Table 2,

(1) The lower limit of the minimum expected return rate remains unchanged. With the increase of the upper limit, the investment proportion of $S5$ will increase first. When the investment proportion of $S5$ reaches its upper limit, the investment proportion of $S1$ will be increased again.

(2) As the minimum expected return rate increases, so does portfolio risk.

(3) When the minimum expected return rate increases to a certain value, the model will have no feasible solution.

Parameter b is the risk preference coefficient. The larger b is, the more investors are inclined to avoid risk; the smaller b is, the more investors are inclined to risk. As can be seen from Table 3, b reflects investors' risk preference. The bigger b is, the less risk the portfolio is and the more cautious the investor is. Figure 2 also reflects the relationship between portfolio risk and the risk preference coefficient b.

Model (19) presents the acceptable solution of the portfolio model based on the acceptability. The upper and lower limits of the portfolio are given as $h = \{0.3, 0.4, 0.2, 0.5, 0.3\}$ and $l = \{0.01, 0,03, 0.01, 0.01, 0\}$, respectively, and Tables 4 and 5, respectively, show the acceptable solution of model (20) and the risk of the portfolio for different μswhen $\alpha = 0.1$ and $\alpha = 0.2$.

As can be seen from Table 4,

(1) With the increase of μ, the investment proportion of $S3$ increases first. When μ increases to a certain

Table 2: The investment proportion and risk for different μs in (18) when $b = 0.1$

μ	$S1$	$S2$	$S3$	$S4$	$S5$	Risk	$\sum_{k=1}^{5} x_k$
[0.04, 0.04]	0.010	0.030	0.010	0.010	0.118	0.036	0.178
[0.04, 0.05]	0.010	0.030	0.010	0.010	0.153	0.042	0.213
[0.04, 0.06]	0.010	0.030	0.010	0.010	0.187	0.048	0.247
[0.04, 0.07]	0.010	0.030	0.010	0.010	0.221	0.054	0.281
[0.04, 0.08]	0.010	0.030	0.010	0.010	0.256	0.060	0.316
[0.04, 0.09]	0.010	0.030	0.010	0.010	0.290	0.066	0.350
[0.04, 0.10]	0.054	0.030	0.010	0.010	0.300	0.080	0.404
[0.04, 0.11]	0.116	0.030	0.010	0.010	0.300	0.097	0.466
[0.04, 0.12]	0.178	0.030	0.010	0.010	0.300	0.114	0.528
[0.04, 0.14]	0.300	0.030	0.010	0.220	0.300	0.182	0.860

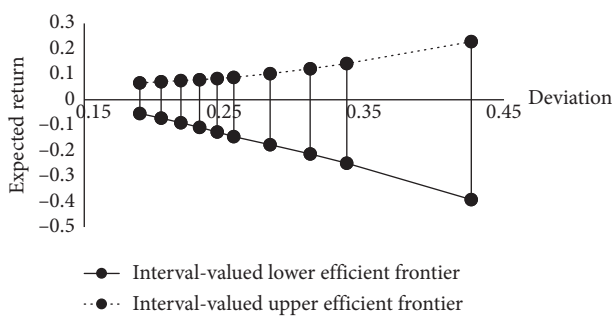

Figure 1: Some efficient portfolios for model (18).

Table 3: The investment risk for different bs in (18).

b	Risk	b	Risk
0	0.190	0.55	0.107
0.1	0.182	0.6	0.097
0.2	0.134	0.7	0.086
0.3	0.128	0.8	0.078
0.4	0.115	0.9	0.056
0.5	0.109	1.0	0.045

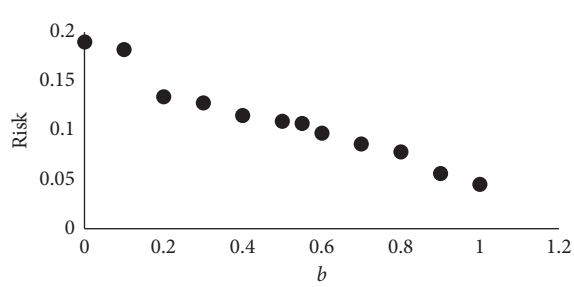

Figure 2: The scatter diagram of portfolio risk and the risk preference coefficient b.

extent, the investment proportion of $S3$ reaches the upper limit of investment, and then, the investment proportion of $S2$ increases.

Table 4: The investment proportion and risk for different μs with $\alpha = 0.1$ in (20).

μ	$S1$	$S2$	$S3$	$S4$	$S5$	Risk	$\sum_{k=1}^{5} x_k$
[0.03, 0.03]	0.010	0.030	0.034	0.010	0.010	0.028	0.094
[0.03, 0.04]	0.010	0.030	0.058	0.010	0.010	0.040	0.118
[0.03, 0.05]	0.010	0.030	0.081	0.010	0.010	0.052	0.141
[0.03, 0.06]	0.010	0.030	0.105	0.010	0.010	0.063	0.165
[0.03, 0.07]	0.010	0.030	0.128	0.010	0.010	0.075	0.188
[0.03, 0.08]	0.010	0.030	0.152	0.010	0.010	0.087	0.212
[0.03, 0.09]	0.010	0.030	0.175	0.010	0.010	0.098	0.235
[0.03, 0.10]	0.010	0.030	0.199	0.010	0.010	0.110	0.259
[0.03, 0.11]	0.010	0.293	0.200	0.010	0.010	0.157	0.523

Table 5: The investment proportion and risk for different μs with $\alpha = 0.2$ in (20).

μ	$S1$	$S2$	$S3$	$S4$	$S5$	Risk	$\sum_{k=1}^{5} x_k$
[0.03, 0.03]	0.010	0.030	0.067	0.010	0.010	0.044	0.127
[0.03, 0.04]	0.010	0.030	0.099	0.010	0.010	0.052	0.159
[0.03, 0.05]	0.010	0.030	0.131	0.010	0.010	0.076	0.191
[0.03, 0.06]	0.010	0.030	0.163	0.010	0.010	0.092	0.223
[0.03, 0.07]	0.010	0.030	0.195	0.010	0.010	0.108	0.255

(2) When μ increases to a certain extent, the model will have no feasible solution. When the acceptability of the expected return rate of the portfolio is not less than μ is 0.1, the proportion of risky assets invested will continue to increase as μ increases, and so will the risk of the portfolio. Since $\alpha = 0.1$, when μ reaches a certain level, the risk of the portfolio will no longer increase, and the investment proportion of risky assets will not change, that is, a part of the capital must be invested in the risk-free assets.

It can be seen from Table 5 that the law is similar to that in Table 4.

By comparing Tables 4 and 5, it can be found that when μ is set to the same value, α is larger, the objective function value is larger, and the investment proportion of risky assets is also higher. That is to say, the greater the acceptability of the expected return rate of the portfolio is less thanμ, the greater the risk of the portfolio and the higher the proportion of risky assets' investment.

5. Conclusions

This paper takes the assets return as the interval number and uses the semiabsolute deviation function of the interval number to measure the portfolio's risk. Therefore, a portfolio selection model with mean-semiabsolute deviation based on the interval number is constructed. In this model, firstly, the lower bound of the investors' expected rate of return is also regarded as an interval number, which can better grasp investors' psychology and measure investors' expected return rate. Secondly, when solving the semiabsolute deviation portfolio selection model, a parameter which can reflect investors' risk preference is introduced, and this

parameter can reflect investors' risk preference more intuitively. Finally, an application of the portfolio diversification problem is given by using a portfolio consisting of 5 risky assets and 1 risk-free asset. The results show that the introduced risk preference parameter can well reflect the investors' attitude to risk, and the lower bound of the expected return rate of this method is more elastic. The model can be used more widely and can describe the expected return rate of investment portfolio and the investors' attitude to risk more flexibly [56].

Data Availability

The data used to support the findings of this study are available from the corresponding author upon request.

Conflicts of Interest

The authors declare that there are no conflicts of interest regarding the publication of this paper.

Acknowledgments

This research was funded by the National Natural Science Foundation of China (11401438), the National Social Science Foundation Project of China (13CRK027), and the social science planning project of Shandong Province (21CTJJ04).

References

[1] H. Markowitz, "Portfolio selection," *The Journal of Finance*, vol. 7, no. 1, pp. 77–91, 1952.

[2] W. F. Sharpe, *Portfolio Theory and Capital Markets*, McGraw-Hill, New York, NY, USA, 1970.

[3] H. Markowitz, *Portfolio Selection: Efficient Diversification of Investments*, Yale University Press, New York, NY, USA, 1959.

[4] J. C. T. Mao, "Models of capital budgeting, E-V vs E-S," *The Journal of Financial and Quantitative Analysis*, vol. 4, no. 5, pp. 657–675, 1970.

[5] R. O. Swalm, "Utility theory--insights into risk taking," *Harvard Business Review*, vol. 44, pp. 123–136, 1966.

[6] H. Konno and H. Yamazaki, "Mean-absolute deviation portfolio optimization model and its applications to tokyo stock market," *Management Science*, vol. 37, no. 5, pp. 519–531, 1991.

[7] M. G. Speranza, "Linear programming model for portfolio optimization," *Finance*, vol. 14, pp. 107–123, 1993.

[8] P. Jorion, "Risk2: measuring the risk in value at risk," *Financial Analysts Journal*, vol. 52, no. 6, pp. 47–56, 1996.

[9] S. Basak and A. Shapiro, "Value-at-Risk-Based risk management: optimal policies and asset prices," *Review of Financial Studies*, vol. 14, no. 2, pp. 371–405, 2001.

[10] S. X. Chen and C. Y. Tang, "Nonparametric inference of value-at-risk for dependent financial returns," *Journal of Financial Econometrics*, vol. 3, no. 2, pp. 227–255, 2005.

[11] F.-Y. Chen, "Analytical VaR for international portfolios with common jumps," *Computers & Mathematics with Applications*, vol. 62, no. 8, pp. 3066–3076, 2011.

[12] R. Mansini, W. Ogryczak, and M. G. Speranza, "Conditional value at risk and related linear programming models for portfolio optimization," *Annals of Operations Research*, vol. 152, no. 1, pp. 227–256, 2007.

[13] P. Byrne and S. Lee, "Different risk measures: different portfolio compositions?" *Journal of Property Investment & Finance*, vol. 22, no. 6, pp. 501–511, 2004.

[14] H. Kandasamy, *Portfolio Selection under Various Risk Measures*, Clemson University, Clemson, South Carolina, 2008.

[15] X. Yi, R. Guo, and Y. Qi, "Stabilization of chaotic systems with both uncertainty and disturbance by the UDE-based control method," *IEEE Access*, vol. 8, pp. 62471–62477, 2020.

[16] D. Zhao, Y. Liu, Y. Liu, and X. Li, "Controllability for a class of semilinear fractional evolution systems via resolvent operators," *Communications on Pure & Applied Analysis*, vol. 18, no. 1, pp. 455–478, 2019.

[17] C. Jiang, Akbar Zada, M. Tamer Senel, and T. Li, "Synchronization of bidirectional N-coupled fractional-order chaotic systems with ring connection based on antisymmetric structure," *Advances in Difference Equations*, vol. 16, Article ID 456, 2019.

[18] L. Liu, B. Li, and R. Guo, "Consensus control for networked manipulators with switched parameters and topologies," *IEEE Access*, vol. 9, pp. 9209–9217, 2021.

[19] C. Jiang, F. Zhang, and T. Li, "Synchronization and anti-synchronization ofN-coupled fractional-order complex chaotic systems with ring connection," *Mathematical Methods in the Applied Sciences*, vol. 41, no. 7, pp. 2625–2638, 2018.

[20] D. Zhao and J. Mao, "New controllability results of fractional nonlocal semilinear evolution systems with finite delay," *Complexity*, vol. 2020, Article ID 7652648, 13 pages, 2020.

[21] T. Hou, Y. Liu, and F. Deng, "Stability for discrete-time uncertain systems with infinite Markov jump and time-delay," *Science China Information Sciences*, vol. 64, no. 5, pp. 1–11, 2021.

[22] L. A. Zadeh, "Fuzzy sets as a basis for a theory of possibility," *Fuzzy Sets and Systems*, vol. 1, no. 1, pp. 3–28, 1978.

[23] D. Dubois and H. Prade, "The mean value of a fuzzy number," *Fuzzy Sets and Systems*, vol. 24, pp. 279–300, 1978.

[24] C. Carlsson and R. Fullér, "On possibilistic mean value and variance of fuzzy numbers," *Fuzzy Sets and Systems*, vol. 122, no. 2, pp. 315–326, 2001.

[25] W. G. Zhang and Z. K. Nie, "On possibilistic variance of fuzzy numbers," *Rough Sets, Fuzzy Sets, Data Mining, and Granular Computing*, vol. 2639, pp. 398–402, 2003.

[26] C. Carlsson and R. Fullér, *Possibility for Decision: A Possibilistic Approach to Real Life Decisions*, Springer, Berlin, Germany, 2011.

[27] I. Georgescu, *Possibility Theory and the Risk*, Springer, Berlin, Germany, 2012.

[28] H. Tanaka, H. Nakayama, and A. Yanagimoto, "Possibility portfolio selection," in *Proceedings of the 1995 IEEE International Conference on Fuzzy Systems*, pp. 77–91, Yokohama, Japan, 1995.

[29] C. Carlsson, R. Fullér, and P. Majlender, "A possibilistic approach to selecting portfolios with highest utility score," *Fuzzy Sets and Systems*, vol. 131, no. 1, pp. 13–21, 2002.

[30] R. Fullér and P. Majlender, "On weighted possibilistic mean and variance of fuzzy numbers," *Fuzzy Sets and Systems*, vol. 136, no. 3, pp. 363–374, 2003.

[31] W.-G. Zhang, Y.-L. Wang, Z.-P. Chen, and Z.-K. Nie, "Possibilistic mean-variance models and efficient frontiers for portfolio selection problem," *Information Sciences*, vol. 177, no. 13, pp. 2787–2801, 2007.

[32] W. G. Zhang and Y. L. Wang, "Using fuzzy possibilistic mean and variance in portfolio selection model," *Computational Intelligence and Security*, vol. 3801, pp. 291–296, 2003.

[33] W.-G. Zhang, "Possibilistic mean-standard deviation models to portfolio selection for bounded assets," *Applied Mathematics and Computation*, vol. 189, no. 2, pp. 1614–1623, 2007.
[34] W.-G. Zhang, W.-L. Xiao, and Y.-L. Wang, "A fuzzy portfolio selection method based on possibilistic mean and variance," *Soft Computing*, vol. 13, no. 6, pp. 627–633, 2009.
[35] Y. Sui, J. Hu, and F. Ma, "A possibilistic portfolio model with fuzzy liquidity constraint," *Complexity*, vol. 2020, Article ID 3703017, 10 pages, 2020.
[36] M. A. Parra, A. B. Terol, and M. V. R. Uria, "A fuzzy goal programming approach to portfolio selection," *European Journal of Operational Research*, vol. 133, pp. 287–297, 2001.
[37] K. K. Lai, S. Y. Wang, J. P. Xu, S. S. Zhu, and Y. Fang, "A class of linear interval programming problems and its application to portfolio selection," *IEEE Transactions on Fuzzy Systems*, vol. 10, no. 6, pp. 698–704, 2002.
[38] M. Ida, "Solutions for the portfolio selection problem with interval and fuzzy coefficients," *Reliable Computing*, vol. 10, no. 5, pp. 389–400, 2004.
[39] S. Giove, S. Funari, and C. Nardelli, "An interval portfolio selection problem based on regret function," *European Journal of Operational Research*, vol. 170, pp. 253–264, 2005.
[40] R. Bhattacharyya, S. Kar, S. Kar, and D. D. Majumder, "Fuzzy mean-variance-skewness portfolio selection models by interval analysis," *Computers & Mathematics with Applications*, vol. 61, no. 1, pp. 126–137, 2011.
[41] S.-T. Liu, "The mean-absolute deviation portfolio selection problem with interval-valued returns," *Journal of Computational and Applied Mathematics*, vol. 235, no. 14, pp. 4149–4157, 2011.
[42] Y. Sui, J. Hu, and F. Ma, "A mean-variance portfolio selection model with interval-valued possibility measures," *Mathematical Problems in Engineering*, vol. 2020, pp. 1–12, 2020.
[43] R. Mansini and M. G. Speranza, "Heuristic algorithms for the portfolio selection problem with minimum transaction lots," *European Journal of Operational Research*, vol. 114, no. 2, pp. 219–233, 1999.
[44] H. Ishibuchi and H. Tanaka, "Multiobjective programming in optimization of the interval objective function," *European Journal of Operational Research*, vol. 48, no. 2, pp. 219–225, 1990.
[45] A. Sengupta, T. K. Pal, and D. Chakraborty, "Interpretation of inequality constraints involving interval coefficients and a solution to interval linear programming," *Fuzzy Sets and Systems*, vol. 119, no. 1, pp. 129–138, 2001.
[46] G. Alefeld and J. Herzberger, *Introduction to Interval Computations*, Academic Press, New York, NY, USA, 1983.
[47] E. Hansen, *Global Optimization Using Interval Analysis*, Marcel Dekker, New York, NY, USA, 1992.
[48] R. C. Young, "The algebra of many-valued quantities," *Mathematische Annalen*, vol. 104, no. 1, pp. 260–290, 1931.
[49] E. R. Moore, *Methods and Applications of Interval Analysis*, Prentice-Hall, London, UK, 1979.
[50] R. Moore and W. Lodwick, "Interval analysis and fuzzy set theory," *Fuzzy Sets and Systems*, vol. 135, no. 1, pp. 5–9, 2003.
[51] A. Sengupta and T. K. Pal, "On comparing interval numbers," *European Journal of Operational Research*, vol. 127, no. 1, pp. 28–43, 2000.
[52] K. Yoon, "The propagation of errors in multiple-attribute decision analysis: a practical approach," *Journal of the Operational Research Society*, vol. 40, no. 7, pp. 681–686, 1989.
[53] N. Bryson and A. Mobolurin, "An action learning evaluation procedure for multiple criteria decision making problems," *European Journal of Operational Research*, vol. 96, no. 2, pp. 379–386, 1997.
[54] H. Rommelfanger, R. Hanuscheck, and J. Wolf, "Linear programming with fuzzy objectives," *Fuzzy Sets and Systems*, vol. 29, no. 1, pp. 31–48, 1989.
[55] B. Baoding Liu and K. Kakuzo Iwamura, "A note on chance constrained programming with fuzzy coefficients," *Fuzzy Sets and Systems*, vol. 100, no. 1-3, pp. 229–233, 1998.
[56] V. Chankong and Y. Y. Haimes, *Multiobjective Decision Making: Theory and Methodology*, North Holland: Amsterdam, Netherlands, 1983.

Hindawi
Mathematical Problems in Engineering
Volume 2021, Article ID 7457220, 16 pages
https://doi.org/10.1155/2021/7457220

Research Article

A Novel Memristor Chaotic System with a Hidden Attractor and Multistability and Its Implementation in a Circuit

Lili Huang,[1] Yanling Wang,[1] Yicheng Jiang,[2] and Tengfei Lei[1]

[1]*Collaborative Innovation Center of Memristive Computing Application, Qilu Institute of Technology, Shandong, Jinan 250200, China*
[2]*School of Electronic Information, Nanjing University of Information Technology, Nanjing 210000, China*

Correspondence should be addressed to Tengfei Lei; leitengfei2017@qlit.edu.cn

Received 30 April 2021; Accepted 26 May 2021; Published 2 June 2021

Academic Editor: Yi Qi

By introducing an ideal and active flux-controlled memristor and tangent function into an existing chaotic system, an interesting memristor-based self-replication chaotic system is proposed. The most striking feature is that this system has infinite line equilibria and exhibits the extreme multistability phenomenon of coexisting infinitely many attractors. In this paper, bifurcation diagrams and Lyapunov exponential spectrum are used to analyze in detail the influence of various parameter changes on the dynamic behavior of the system; it shows that the newly proposed chaotic system has the phenomenon of alternating chaos and limit cycle. Especially, transition behavior of the transient period with steady chaos can be also found for some initial conditions. Moreover, a hardware circuit is designed by PSpice and fabricated, and its experimental results effectively verify the truth of extreme multistability.

1. Introduction

In 1963, the first chaotic system was discovered by Lorenz. Since then, many scientists have constructed many new chaotic systems, such as Chen system, Lu system, and Jerk system [1, 2]. Then, in 1971, Chua proposed the memristor, the fourth element after resistor [3, 4], capacitor, and inductor. People have studied chaotic systems based on memristor design. Compared with other classical chaotic systems [5], memristive nonlinear systems have more complex chaotic characteristics [6–10]. Some articles reported the phenomenon of memristive multistable state.

In addition to the sensitivity of the system to the parameters, it also depends on the initial value of the memristor. Due to the introduction of the ideal memristor [11–16], the dynamic system based on the memristor produces infinite equilibria, such as line equilibria and surface equilibria. These equilibria are related to the initial state variables of the memristor. These memristor models not only exhibit complex chaotic behaviors but also produce multistability phenomena [17, 18]. As we all know, multistability is the coexistence behavior of two or more attractors under the same parameters and different initial conditions [19–21]. Bao et al. [22] introduced an ideal and active flux-controlled memristor into an existing hypogenetic chaotic jerk system, an interesting memristor-based chaotic system with a hypogenetic jerk equation, and proposed circuit forms. The most striking feature is that this system has four line equilibria and exhibits the extreme multistability phenomenon of coexisting infinitely many attractors. Jafari et al [23] propose a newly parameter estimation method on both an ordinary chaotic system and a chaotic system with extreme multistability. It proves the importance of that difference better by comparing the efficiency of the chaotic system. Recently, the introduction of trigonometric functions, such as the tangent function, sine function, hyperbolic tangent function [24, 25], and hyperbolic sine function, has made the system produce multiscroll attractors, multiwing attractors, infinite coexistence attractors, and attractor duplication phenomena [26, 27]. This nonlinear performance is caused by the periodicity of trigonometric functions [28, 29]. This special feature has been reported in some chaotic article recently. However, there are relatively few studies on homogeneous multistability in the memristor chaotic systems of trigonometric functions [30–34].

Inspired by the abovementioned ideas, an interesting memristor-based chaotic system is constructed in this paper, which is achieved by introducing a tangent function $(\tan(z))$ and an ideal and active flux-controlled memristor with absolute value nonlinearity into an existing chaotic system boostable VB18 [31]. The newly proposed memristive system has infinite line equilibria and can exhibit the initial-condition-dependent extreme multistablity phenomenon of coexisting infinitely many attractors, which has seldom been reported in the academic literature.

The rest of this paper is organized as follows. In Section 2, a novel memristive system with infinite line equilibria is presented, upon which the stability for the infinite line equilibria are explored. In Section 3, parameter-dependent change is investigated by bifurcation diagrams and Lyapunov exponent spectra and coexisting intermittent chaos behavior revealed by phase portraits. In Section 4, initial-condition-dependent extreme multistability is investigated by coexisting bifurcation diagrams and Lyapunov exponent spectra, and coexisting infinitely many attractors' behavior and symmetric behavior are revealed by phase portraits. In Section 5, an implementation circuit is designed and PSpice circuit simulations are performed to verify the initial-condition-dependent dynamical behaviors of coexisting infinitely many attractors. In Section 6, the conclusions are summarized.

2. Model Description

According to the chaotic system VB18 reported in [31], a new memristive system can be easily constructed by the tangent function to substitute a z status variable and by introducing utilizing memristor in the chaotic system with an existing nonlinear dynamical system boostable VB18.

A VB18 chaotic system is described as

$$\begin{cases} \dot{x} = az + y^2 - 1, \\ \dot{y} = byz, \\ \dot{z} = -x - z. \end{cases} \tag{1}$$

The memductance function of the desired flux-controlled memristor is expressed as

$$W(\phi) = -m + n|\phi|, \tag{2}$$

where m and n are two memristor parameters with positive values. The abovementioned model (2) is used to describe an ideal and active flux-controlled memristor with an absolute value nonlinearity.

Through introducing the newly proposed memristor featured by (2) and trigonometric function $(\tan(z))$ into the chaotic system in [1], a new kind of memristor chaotic system is established, which can be mathematically modeled as

$$\begin{cases} \dot{x} = a\tan(z) + y^2 - 1, \\ \dot{y} = by\tan(z), \\ \dot{z} = -xW(u) - \tan(z), \\ \dot{u} = x, \end{cases} \tag{3}$$

where x, y, z, and u are the state variables of system (3), a, b, and c are the control parameters of system (3), and $W(u) = -m + n|u|$ is the normalized memductance function. u in formula (3) is φ in formula (2).

The voltage-current curves of the memristor with different values of the frequency f are plotted in Figure 1. It can be seen that the pinched hysteresis loop gradually shrinks with f increasing from 1.07 to 2.07, then to 3.07 in Figure 1(a), and keeps pinched at the original point with the origin, which is a typical 8-like hysteresis loop. It can be seen that $W(u)$ stands for the memductance related to the magnetic flux u in Figure 1(b) implying that system (2) satisfies the definition of the memristor.

When $a = 5.8$, $b = 7.9$, $m = 0.02$, and $n = 0.06$, the initial conditions (x_0, y_0, z_0, u_0) are assigned as (1, 1, 0, 5). Matlab numerical simulations are performed and several useful results are obtained, as shown in Figure 2, from which the chaotic behavior characterized by a strange attractor is revealed. System (3) displays two phase portraits in two different planes with a single-scroll attractor and double-vortex attractor. Correspondingly, the finite-time Lyapunov exponents are calculated by Wolf s method [33] as $L1 = 0.041139$, $L2 = -0.002245$, $L3 = -0.733286$, $L4 = -1.475227$, and Kaplan–York dimension $\mathrm{DKY} = 3 + (L1 + L2 + L3)/L4 = 3.4707$. Consequently, the numerical results in Figure 2 indicate that system (3) is a chaotic system.

3. Basic Dynamical Analysis

3.1. Stability Analysis of the Equilibrium Point. When $a = 5.8$, $b = 7.9$, $m = 0.02$, and $n = 0.06$, x, y, z, and w are state variables of system (3).The equilibrium points of system (3) can be easily calculated by setting the left-hand side to zero, which are not associated with the memductance function.

$$\begin{cases} a\tan(z) + y^2 - 1 = 0, \\ by\tan(z) = 0, \\ -x(-m + n|u|) - \tan(z) = 0, \\ x = 0. \end{cases} \tag{4}$$

According to the fourth dimension $x = 0$ of equation (4), it can be that the third dimension is $\tan(z) = 0$, and the solution $z\,(z = k\pi)\,(k \in N)$; then, $y^2 - 1 = 0$ in the first dimension can get $y = \pm 1$, and then, system (3) has an infinite equilibrium point $(0, \pm 1, k\pi, u)$, $(k \in N)$, where k is any real constant.

The Jacobian matrix of system (3) at the equilibrium point $E = (1, 1, 0, u)$ is yielded as

$$Jec = \begin{bmatrix} 0 & 2y & a(\sec(z))^2 & 0 \\ 0 & b\tan(z) & by(\sec(z))^2 & 0 \\ -W(u) & 0 & -(\sec(z))^2 & -xn\mathrm{sign}(u) \\ 1 & 0 & 0 & 0 \end{bmatrix}, \tag{5}$$

where $W(u) = -m + n|u|$. In consideration of $z = 0, u = h$, the characteristic polynomial equation is derived as

$$\lambda\left(a_0\lambda^3 + a_1\lambda^2 + a_2\lambda^1 + a_3\right) = 0, \tag{6}$$

where $a_1 = a_0 = 1$, $a_2 = 0.348|h| - 0.116$, and $a_3 = 0.948|h| - 0.316$, and the abovementioned characteristic

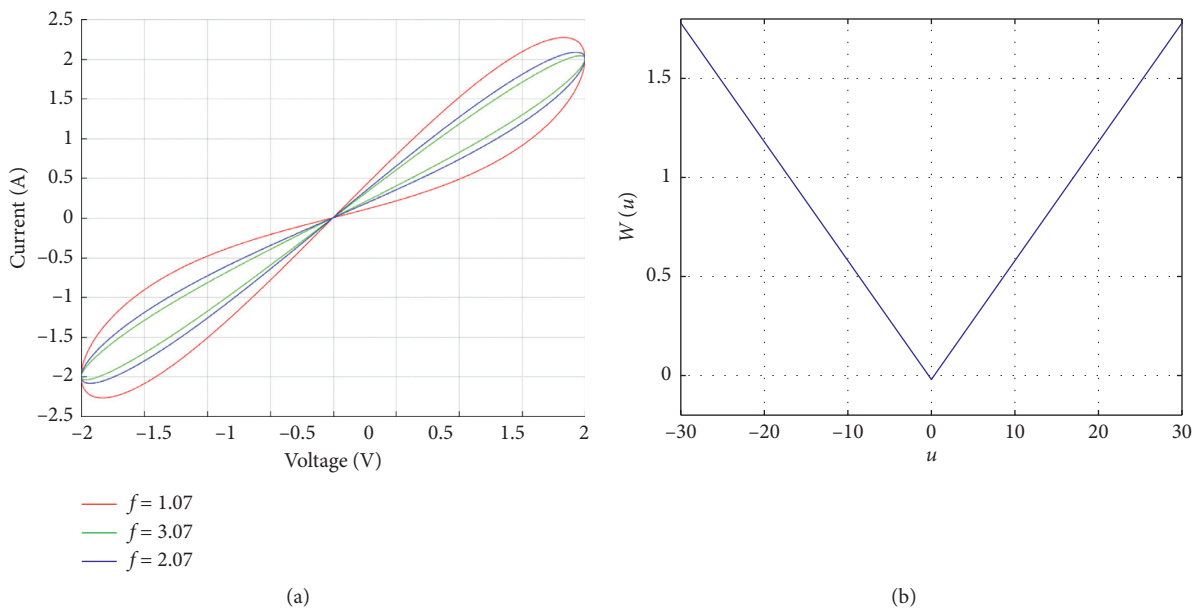

Figure 1: The memductance and pinched hysteresis loop. (a) The pinched hysteresis loop; (b) the memductance loop.

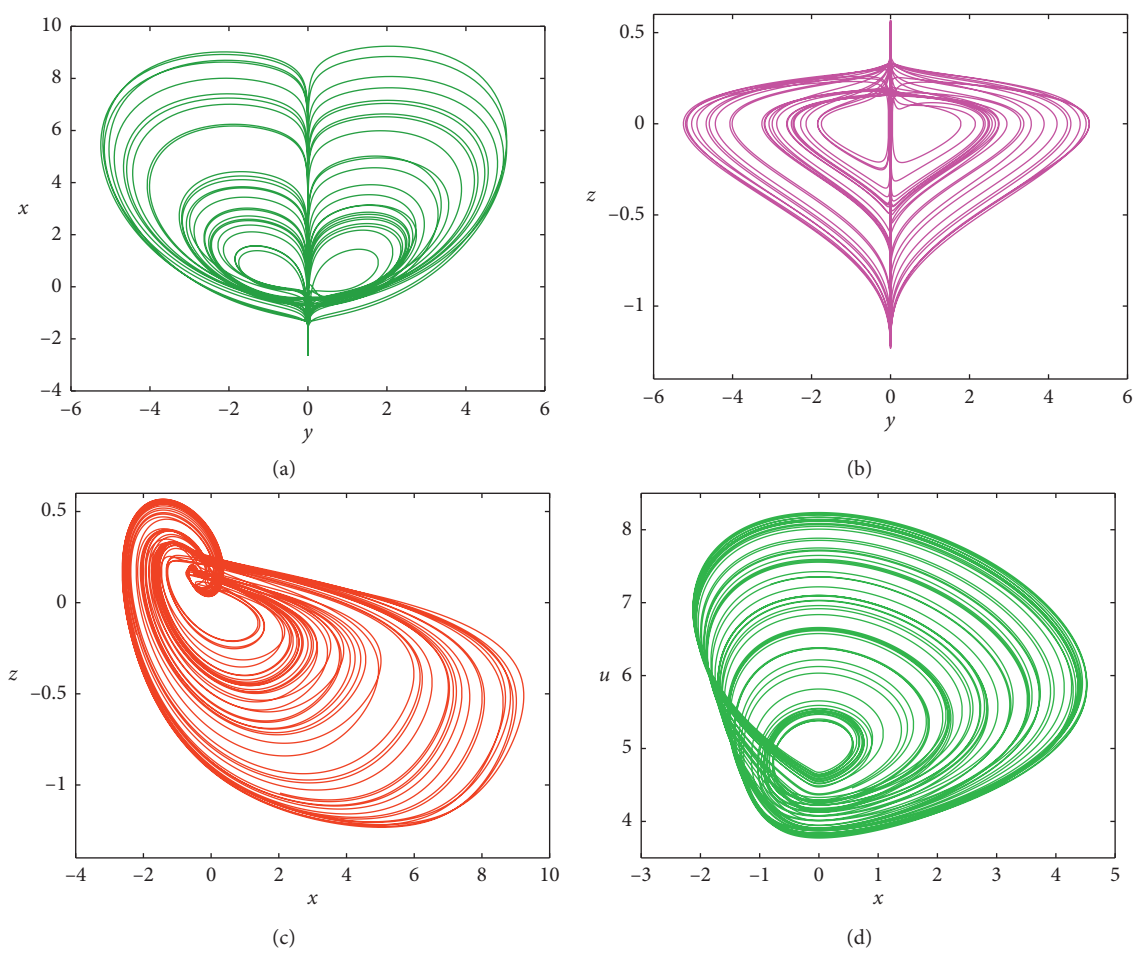

Figure 2: Chaotic behavior characterized by an symmetric chaotic attractor of system (2) with $a = 5.8$ and $b = 7.9$ under initial condition [1, 1, 0, 5]: (a) phase portrait in the x-y plane, (b) phase portrait in the y-z plane, (c) phase portrait in the z-x plane, and (d) phase portrait in the x-u plane.

polynomial implies that Jacobian matrix (5) has three nonzero roots and one zero root. For these roots, Routh–Hurwitz conditions are given as

$$H_k = \begin{vmatrix} a_1 & a_3 & a_5 \\ a_0 & a_2 & a_4 \\ 0 & a_1 & a_3 \end{vmatrix} > 0, \tag{7}$$

where $k = 1, 2, 3$, and

$$\begin{aligned} H_1 &= a_1 > 0, \\ H_2 &= a_1 a_2 - a_3 > 0, \\ H_3 &= a_3 (a_1 a_2 - a_3) > 0, \\ \text{i.e.,}\, 0.348|h| &- 0.116 + 0.316 - 0.948|h| < 0. \end{aligned} \tag{8}$$

If the conditions in (8) are satisfied, i.e.,$-(1/3) < h < (1/3)$, E is stable. Obviously, the eigenvalues of (6) are relevant to the algebraic symbols u. When $h \geq (1/3)$ or $h \leq -(1/3)$, system (3) has one positive real root and two complex conjugate roots with negative real parts. The results imply that the infinite line equilibiria of system (3) only consist of unstable saddle points and unstable saddle-foci.

3.2. Bifurcation Analysis. The dynamic properties of the system will be changed by the changing parameters, which will make the system show the phenomena of chaotic periodic divergence.

For system (3), the parameters a and b effectively determine the dynamic behavior, as shown in Figure 3. When the initial value [1, 1, 0, 5] is fixed, the parameter $b = 7.9$. When the parameter a varies in [2, 11], chaos and periodic oscillation appear alternately as shown in Figure 3. The largest finite-time Lyapunov exponents are calculated and plotted with varying parameter a, as shown in Figure 3. As we can be seen from Figure 3, when a is in the interval [6.23, 6.355] and [4.256, 4.455], the largest finite-time Lyapunov exponents are equal to 0, and the system produces cycle-4 attractors. When a is in the interval [4.85, 4.95] and [6.25, 7.25], the system produces cycle-2 attractors. When a is in the interval [7.35, 11], the system produces cycle-1 attractors. The change of parameter a makes system (3) show inverted period bifurcation behavior. When $a > 7.2$, the antiperiod bifurcation of the system has chaos and reaches a steady state. Then, the same initial value [1, 1, 0, 5] is fixed, when the parameter $a = 5.8$, and the parameter b changes in [4, 13]; the Lyapunov exponent spectrum and bifurcation diagram of system (3) are shown in Figures 4(a) and 4(b). The change of parameter b makes system (3) show period-doubling bifurcation behavior. It can be seen from Figure 4 that when the value of b is in the interval [7.566, 8.26] and [11.533, 12.155] and [12.566, 13.215], the system is in a chaotic state. Obviously, when parameter b is set to different values, the system shows periodic, chaotic, single scroll, double scroll, and other dynamic behaviors as shown in Figure 5.

4. Multistable State Analysis

When the same parameter takes different initial values, two or more attractors are called coexistent attractors or multiple attractors, which is called the multistable state. The four-dimensional initial value of system (3) has different attractors when it takes different values. It can generate various types of coexisting attractors.

4.1. Dynamics with Respect to Memristor Initial Condition (u_0). In most memristor systems, the value of a memristor has some relations with the initial condition, so we have different oscillating dynamics depending on whether the initial data of the internal variable causes different oscillations. This phenomenon is widely studied and is known as extreme polystability. In system (3), the control parameters are set as $a = 5.8$, $b = 7.9$, $m = 0.02$, and $n = 0.06$, the initial conditions are assigned $x\ (0) = 0$, $y\ (0) = 1$, and $z\ (0) = 0$, and the memristor initial condition $u\ (0)$ is taken as the bifurcation parameter. When the memristor initial condition u_0 varies in (−30, 30), system (3) has a different stable state, in which the Lyapunov exponent and bifurcation evolution are shown in Figures 6(a) and 6(b) and 7(a) and 7(b). When the memristor initial condition $u\ (0)$ is gradually changed, system (3) shows multiple period-doubling bifurcations and the chaotic state intermittent existence phenomenon. Consequently, the results of Figures 6 and 7 demonstrate that, under different memristor initial conditions, there are completely different dynamical behaviors in system (3), leading to the coexisting phenomenon of many attractors. As can be seen from Figure 6(a), with the change of initial value u_0, system (3) shows extremely complex dynamic behavior, including single period, double period, chaotic behavior, and period doubling. In particular, it can be found that the dynamic behavior of system (3) is extremely sensitive to the disturbance from small changes in initial conditions, and the initial value u_0 has a completely different dynamic behavior in the region around parameter 0. It is remarked that when the initial conditions of $x\ (0)$, $y\ (0)$, and $z\ (0)$ are assigned to different values as shown in Figure 7, system (3) has different bifurcation behaviors as the memristor initial condition $u\ (0)$ is varied, which further indicates that there exists coexisting infinitely many attractors' behavior in system (3).

To better represent extreme multisteadiness, the typical phase portraits of attractors under different u_0 are shown in Figure 8. When the initial value u_0 is different, the state of system (3) is shown in Table 1.

4.2. Dynamics with Respect to Memristor Initial Condition (Y_0). The control parameters of system (3) are kept unchanged, the initial conditions are assigned as (1 Y_0 0 5), and the initial condition Y_0 is taken as the bifurcation parameter. When Y_0 is varied in the region [−10, 10], the bifurcation diagram of the state variable Y_0 and its Lyapunov exponent spectra are plotted in Figures 9(a) and 9(b). When the initial condition Y_0 is increased from 0, system (3) goes from the normal chaotic state into the quasiperiodic state, breaks into the weak chaotic state, and then, turns into the normal chaotic state.

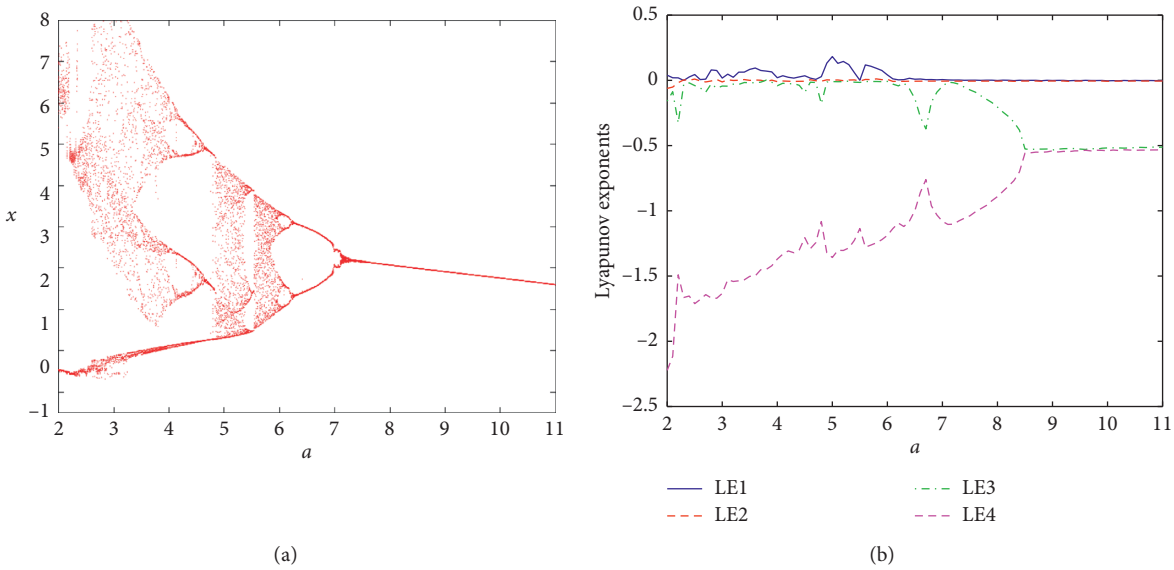

Figure 3: Lyapunov exponents and bifurcation diagram of system (3) with $b = 7.9$, when a varies in [2, 11]. (a) Bifurcation diagram; (b) Lyapunov exponents.

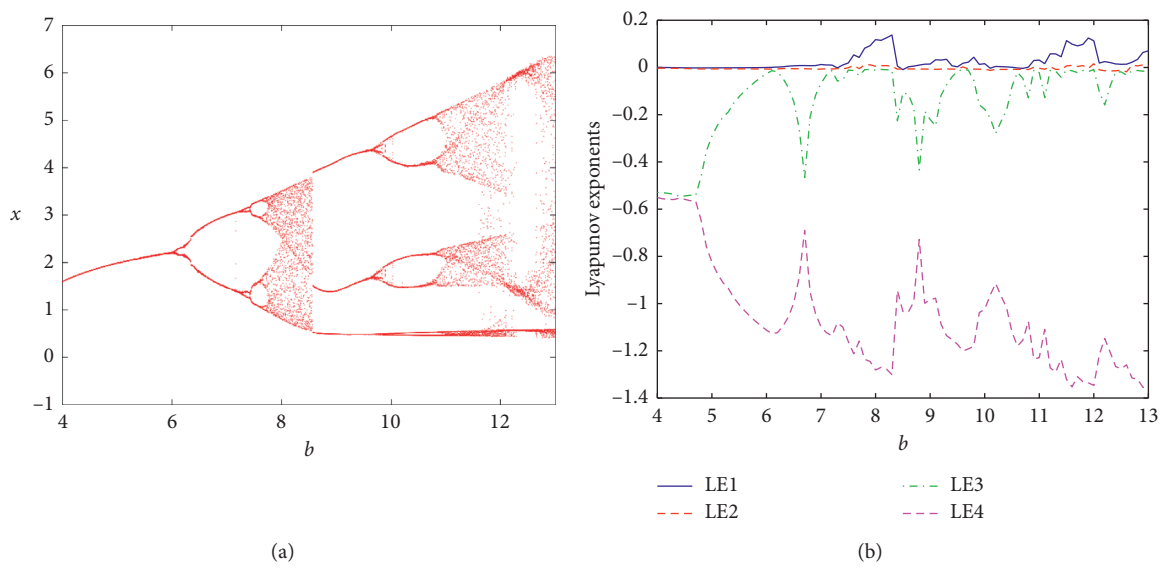

Figure 4: Lyapunov exponents and bifurcation diagram of system (3) with $a = 5.8$, when b varies in [4, 13]. (a) Bifurcation diagram; (b) Lyapunov exponents.

Near $Y_0 = 1.85$, system (3) degrades into the periodic state via chaos, but near $Y_0 = 2.09$, system (3) abruptly changes into the chaotic state with periodic stats bifurcation. When Y_0 is further increased, system (3) jumps into the periodic state again at $Y_0 = 2.5$. In the parameter region [1.85, 2.09] of Y_0, system (3) mainly operates in the periodic state. In the parameter region [2.13, 8.45] of Y_0, system (3) mainly operates in the exhibits weak chaotic behaviors but exhibits weak chaotic behaviors near $Y_0 = 2.24$, 3.22. Therefore, system (3) displays periodic state alternate with chaos. An example is taken to analyze the influence of the change of the initial value of Y_0 on the system. It can be seen that the initial value Y_0 is positive and negative, and system (3) has symmetry. When fixing $a = 5.8$ and $b = 7.9$ and initial value Y_0 changes in the interval [−10, 10], the phase diagram of the system is symmetrically distributed in the x-y plane, as shown in Figure 10. When the value of Y_0 is 1.85, the system is in the cycle-3 stats, when the value of Y_0 is 2.215, the system is in the cycle-4 stats, and when the value of Y_0 is 3.214, the system is in the cycle-6 stats. When the value of Y_0 is 1, the system is in a chaotic state. Thus, the results of Figure 10 imply that there is coexisting many attractors' behavior in system (3).

4.3. Dynamics with Respect to Memristor Initial Condition (z_0). Furthermore, for the periodic tangent function, all the infinite countless attractors can be self-reproduced in the

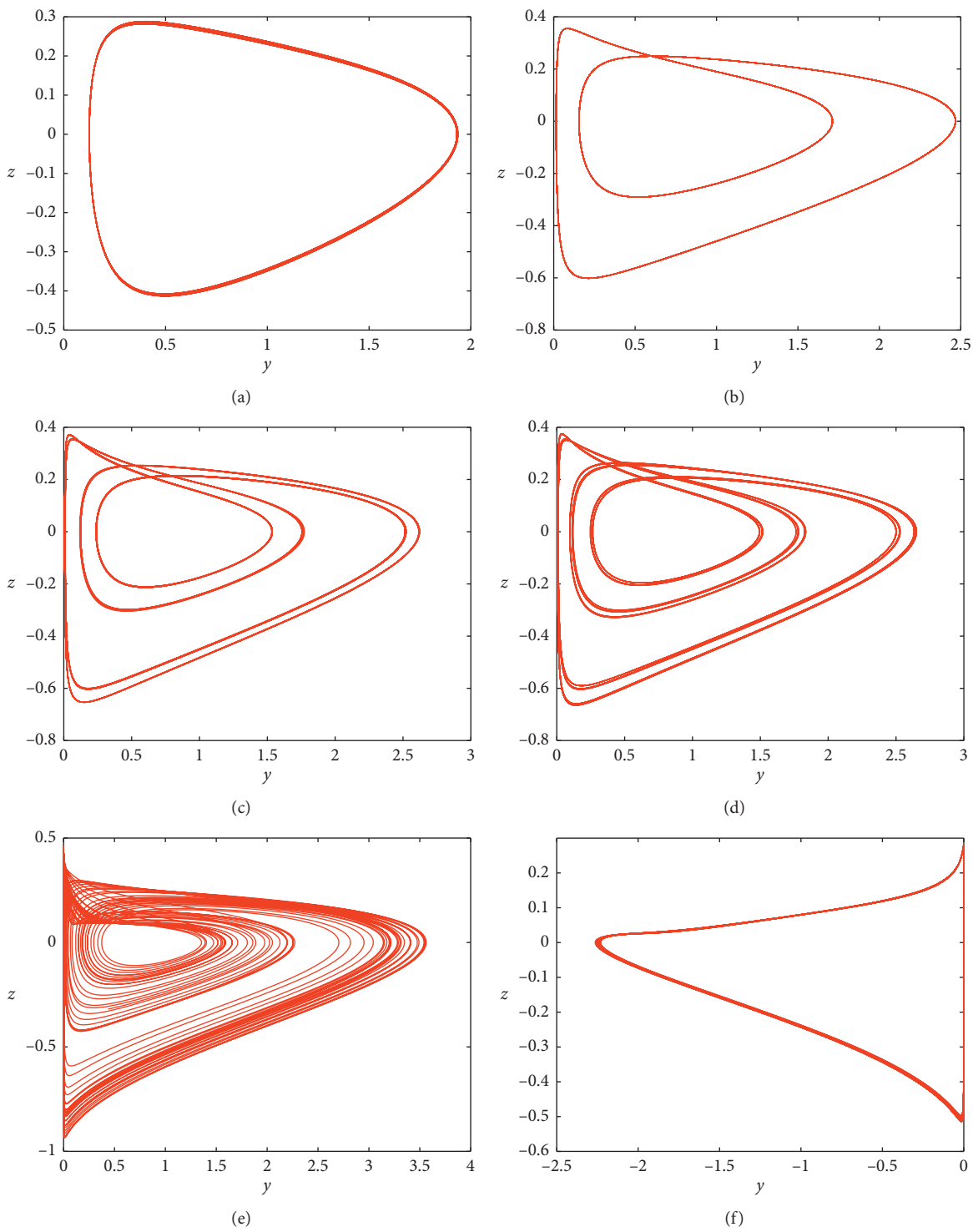

Figure 5: Continued.

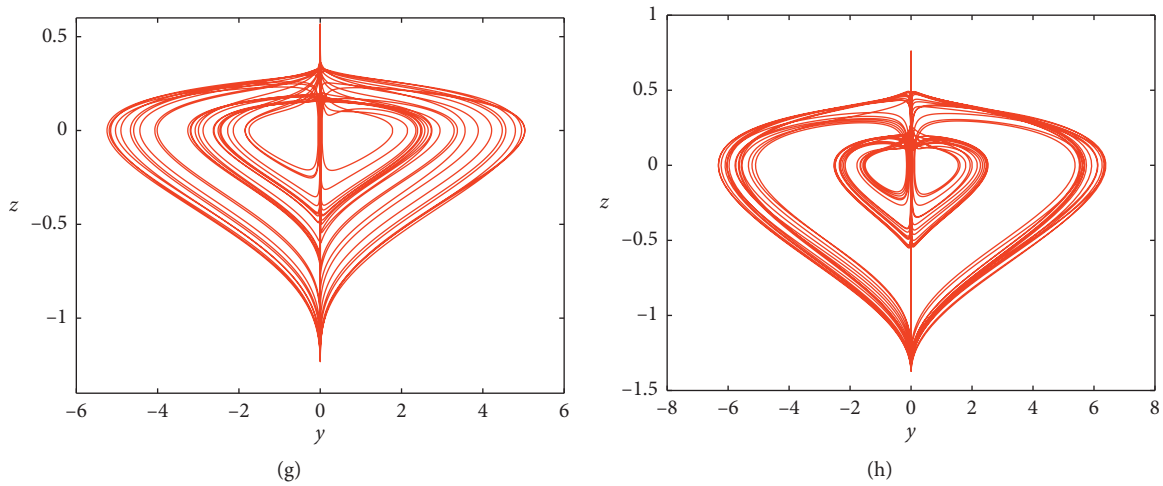

Figure 5: Phase portraits of attractors of system (3) with $a = 5.8$ and IC = (1, 1, 0, 5) on the z-y plane: (a) $b = 5$, (b) $b = 6.5$, (c) $b = 7$, (d) $b = 7.1$, (e) $b = 10$, (f) $b = 12.9833$, (g) $b = 15$, and (h) $b = 18$.

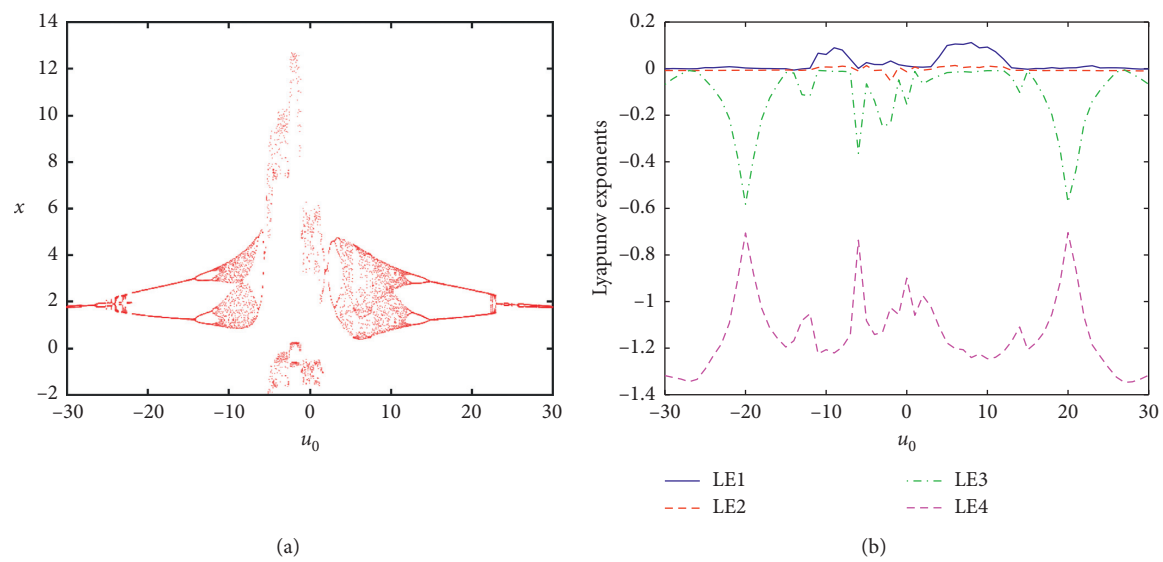

Figure 6: Dynamics with respect to $u(0)$, where $a = 5.8$ and $b = 7.9$ under the initial condition $[1, 1, 0, u_0]$. (a) Bifurcation diagram of the state variable $u(_0)$; (b) Lyapunov exponent spectra.

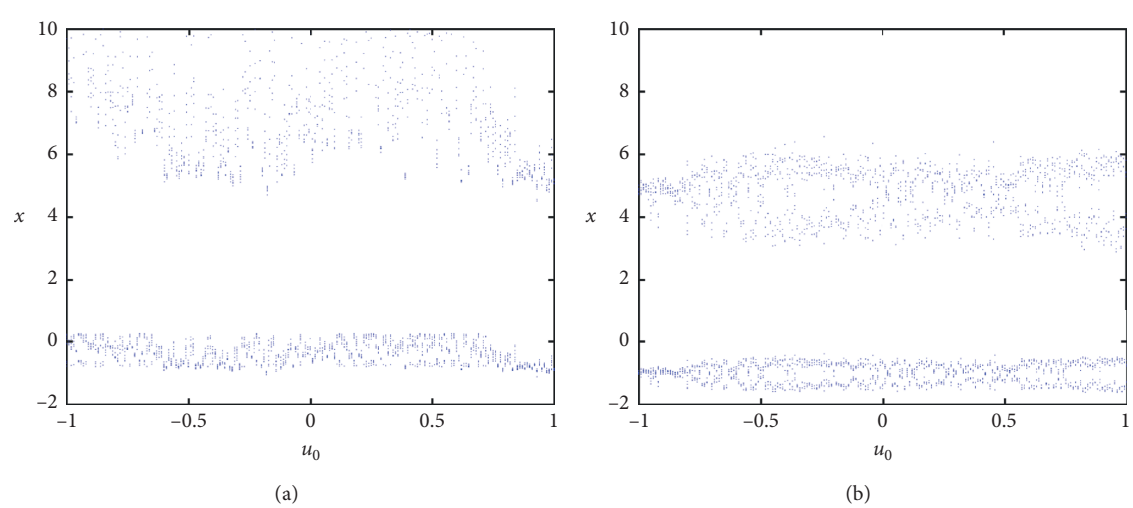

Figure 7: Bifurcation diagram of the state variable $u_0 \in (-1, 1)$. (a) The initial condition (10 1 −pi u_0); (b) the initial condition (1 1 0 u_0).

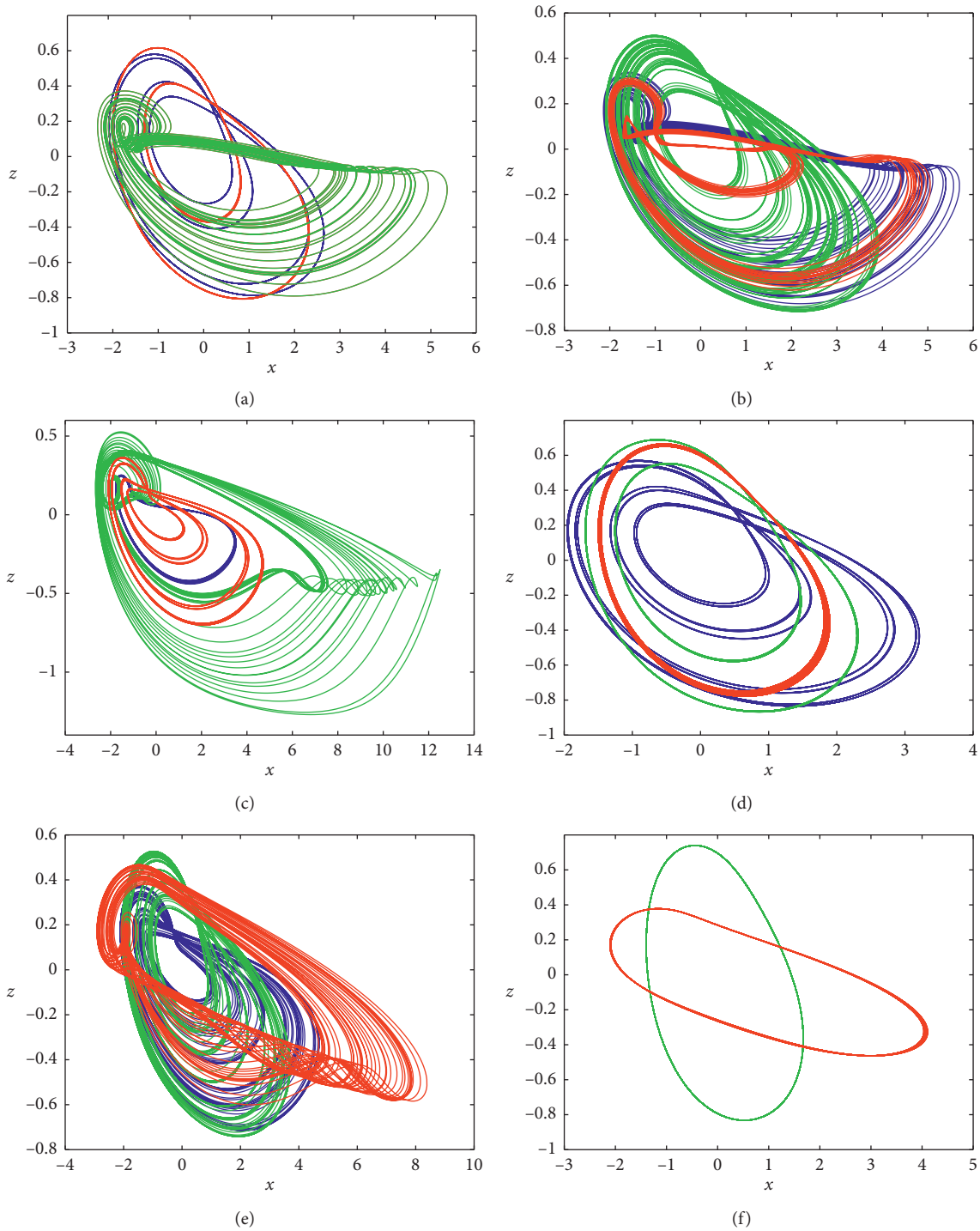

Figure 8: Coexisting attractor of system (2) with $a = 5.8$ and $b = 7.9$ under the initial condition IC1 $[1, 1, 0, u_0]$. (a) $u_0 = 0.1$ (green), $u_0 = -12.5$ (blue), and $u_0 = -15$ (red); (b) $u_0 = 1.42$ (red), $u_0 = -1$ (blue), and $u_0 = -9$ (green); (c) $u_0 = -2$ (green), $u_0 = 3.69$ (red), and $u_0 = 12.35$ (blue); (d) $u_0 = 25$ (red), $u_0 = 3.69$ (red), and $u_0 = 22.5$ (blue); (e) $u_0 = -5$ (red), $u_0 = -10$ (green), and $u_0 = 4$ (blue); and (f) $u_0 = 3.5$ (blue) and $u_0 = -5.5$ (red).

dimension of z_0. System (3) parameters are chosen as $a = 5.8$ and $b = 7.9$, the value of z_0 is representatively 0, ±pi, and ±2 ∗ pi, and five attractors appear in different positions, as shown in Figure 11. Thus, the results of Figure 11 imply that there is coexisting infinitely many attractors' behavior in system (3).

The bifurcation diagram and Lyapunov exponent spectrum under the change of the initial value z_0 are shown in Figure 12; it can be seen that when the initial value z_0 takes different values, system (3) changes from single-period, double-period, three-period and four-period, quasiperiodic, and chaotic attractors; here, four typical attractors including

Table 1: Attractors in system (2) with $a = 5.8$ and $b = 7.9$ under initial conditions of [1, 1, 0, u_0].

Initial condition (u_0)	Colour	Attractor	Figure number
$u_0 = 0.1, -9, -2, -10$	g	Chaotic	(*a*)–(*c*), (*e*)
$u_0 = -12.5$	b	Cycle-4	(*a*)
$u_0 = -15$	r	Cycle-2	(*a*)
$u_0 = 1.42, -3.68$	r	Quasiperiodicity	(*b*)-(*c*)
$u_0 = -1$	b	Chaotic	(*b*)
$u_0 = 2.25$	b	Cycle-1	(*c*)
$u_0 = 22.5$	g	Cycle-2	(*d*)
$u_0 = 12.35$	b	Quasiperiodicity	(*d*)
$u_0 = 25$	r	Cycle-1	(*d*)
$u_0 = -5$	r	Chaotic	(*e*)
$u_0 = 4$	b	Chaotic	(*e*)
$u_0 = 35, -5.5$	b, r	Cycle-1	(*f*)

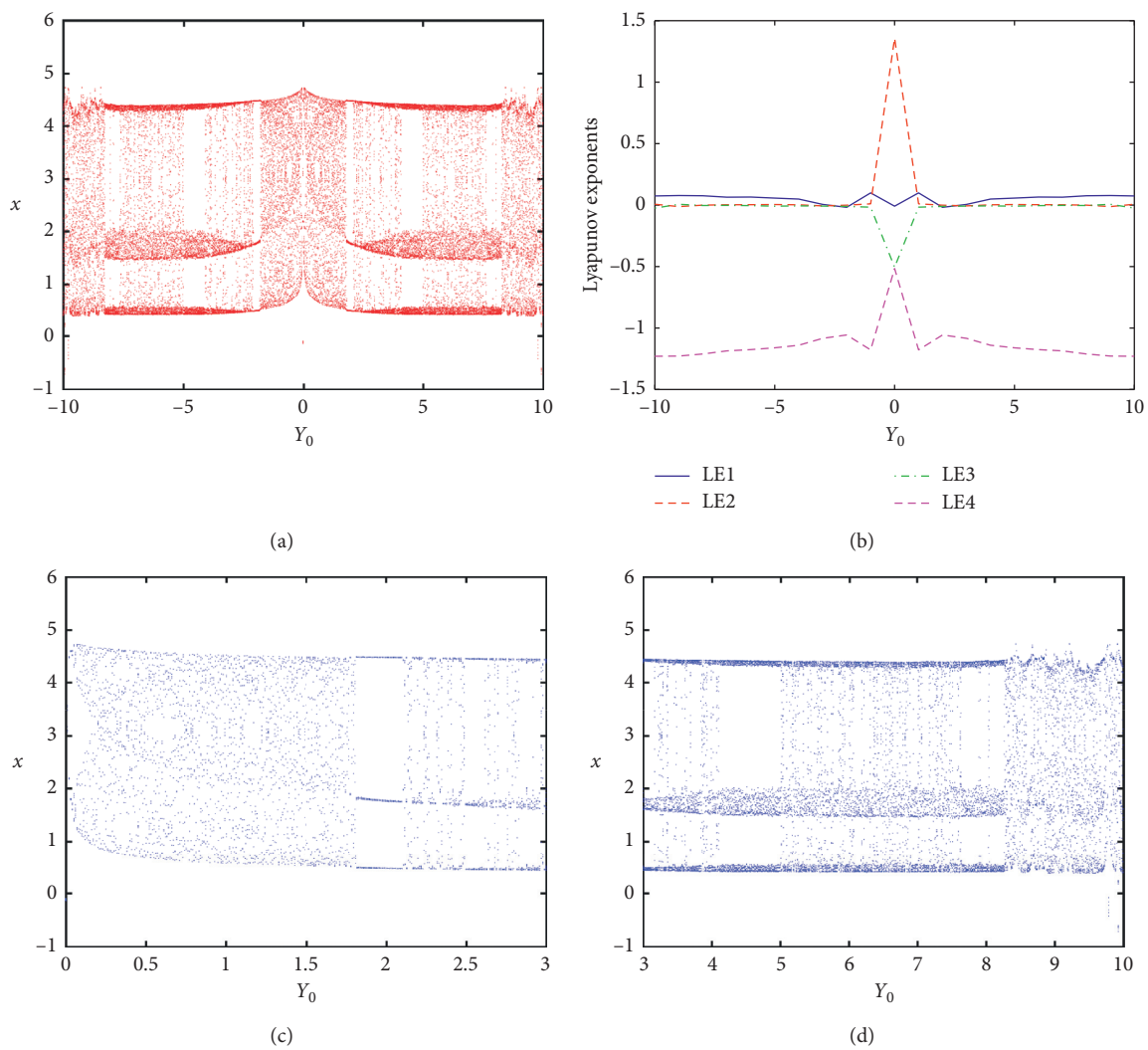

Figure 9: Lyapunov exponents and bifurcation diagram of system (2) with $a = 5.8$ and $b = 7.9$ under the initial condition [1, Y_0, 0, 5]. (a) Bifurcation diagram with $Y_0 \in (0, 10)$; (b) Lyapunov exponents; (c) bifurcation diagram with $Y_0 \in (0, 3)$; and (d) bifurcation diagram with $Y_0 \in (3, 10)$.

chaos and limit cycles are reproduced in phase space for clear demonstration. Simultaneously, the bifurcation diagram and the Lyapunov exponential spectrum are consistent. When z_0 is in the interval [−0.55, 0.8], the system is in a state of chaos and periodic state. Typical phase portraits of attractors of system (3) under different parameters are shown in Figure 13. When the value of z_0 is −0.55, the system is in the cycle-1 state, when the value of z_0 is −0.49, the

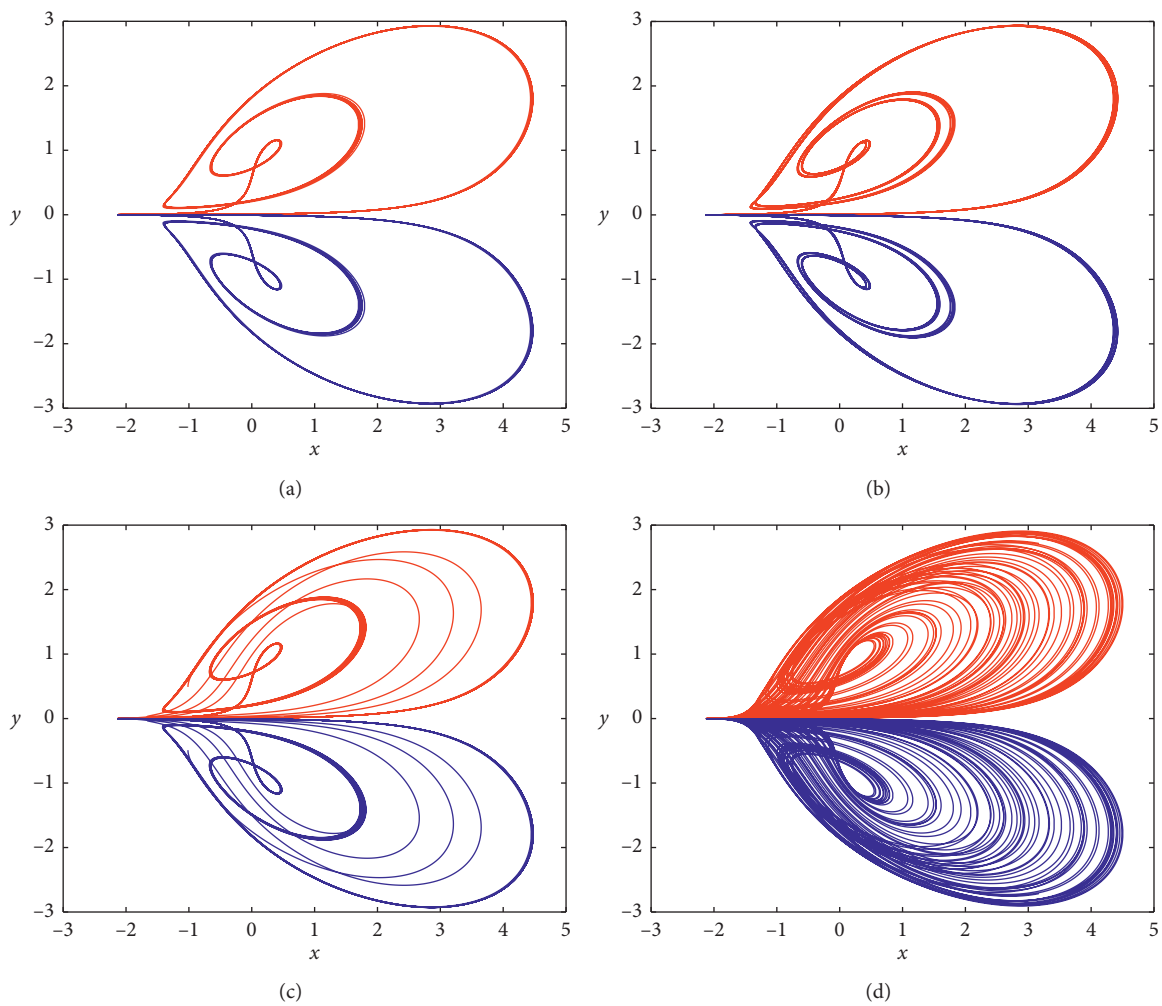

Figure 10: Coexisting and symmetry attractor of system (2) with $a = 5.8$ and $b = 7.9$ under the initial condition [1, Y_0, 0,5]. (a) Cycle-1 symmetry; (b) cycle-2 symmetry; (c) cycle-4 symmetry; and (d) chaotic symmetry.

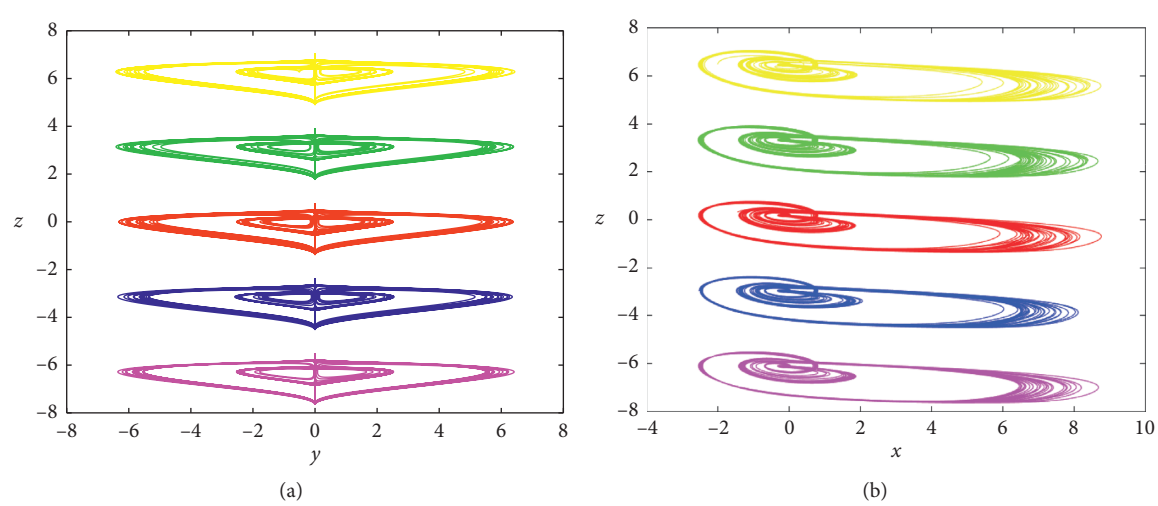

Figure 11: The self-replicating attractor of system (2), blue (1, 1, −pi, 0); red (1, 1, 0, 5); green (1, 1, pi, 5); yellow (1, 1, 2 * pi, 0); and kermes (1, 1, −2 * pi, 5). (a) y-z plane; (b) x-z plane.

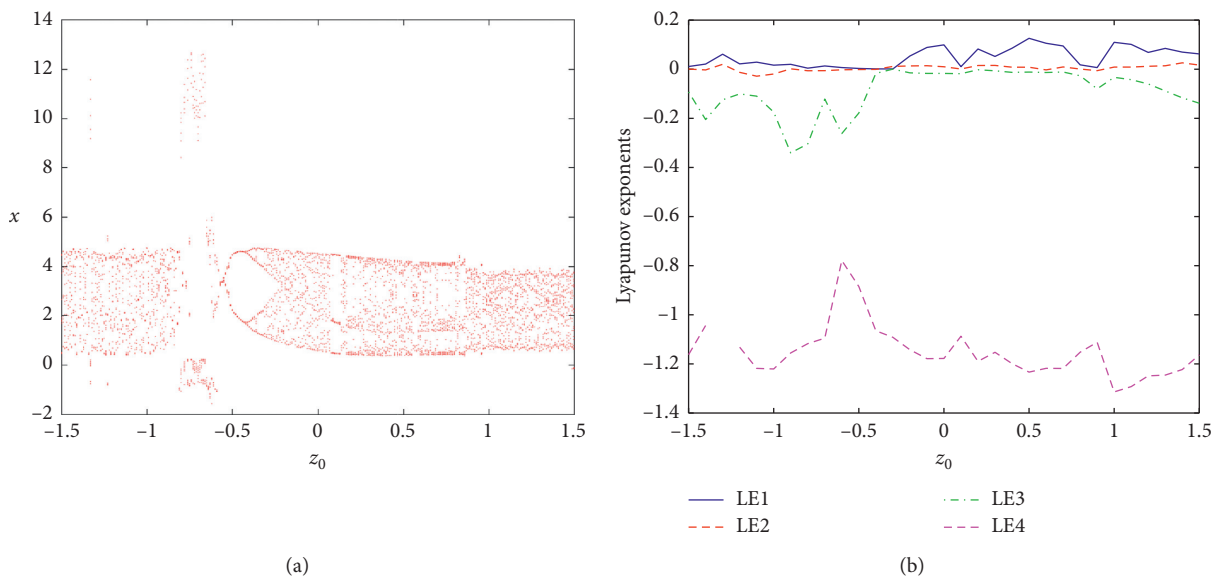

Figure 12: Lyapunov exponents and bifurcation diagram of system (2) with $a = 5.8$ and $b = 7.9$ under the initial condition [1, 1, z_0, 5]. (a) Bifurcation diagram; (b) Lyapunov exponents.

system is in the cycle-2 state, when the value of z_0 is 0.12, the system is in the cycle-3 state, when the value of z_0 is −0.32, the system is in the cycle-4 state, and when the value of z_0 is 0.24, the system is in the quasiperiodic attractor state. When the value of z_0 is 0.8, the system is in a chaotic state. Thus, the results of Figure 12 imply that there is coexisting many attractors' behavior in system (3).

5. Circuit Implementation

The analog circuit of system (3) is designed as shown in Figure 14 with the following circuit equation:

$$\begin{cases} \dot{x} = \dfrac{1}{R_1C_1}\tan(z) + \dfrac{1}{R_2C_1}y^2 - \dfrac{1}{R_{32}C_1}, \\ \dot{y} = \dfrac{1}{R_{16}C_2}\, y\, \tan(z), \\ \dot{z} = \dfrac{1}{R_{11}C_3}W(u)x - \dfrac{1}{R_{10}C_3}\tan(z), \\ \dot{u} = \dfrac{1}{R_{20}C_4}x. \end{cases} \tag{9}$$

The circuit consists of four channels to realize the integration, addition, subtraction, and nonlinear operations including absolute value function and quadratic nonlinearity, as shown in Figure 14. The main circuit with the circuit form is plotted in Figure 14(a), where x, y, and z represent three state variables of capacitor voltages, respectively, and RC stands for the time constant of the integrators. The equivalent realization unit circuit of the flux-controlled memristor $W(u)$ is depicted in Figure 14(b), where u is the inner state variable of capacitor voltage in the memristor. The operational amplifier 741 performs the addition and integration, and the analog multiplier AD633 performs the nonlinear product operation. The circuit is powered by ±15 V. When the system parameters $a = 5.8.2$ and $b = 7.9$, the corresponding circuit element parameters can be selected as R1 = 17 K, R2 = R32 = R10 = R11 = R20 = 100 KΩ, R3 = R4 = R12 = R13 = R17 = R18 = R22 = R23 = 10 KΩ, C1 = C2 = C3 = C4 = 1 nF, and R16 = 12.6 KΩ. The circuit simulation is shown in Figure 14. The corresponding memristor circuit element parameters can be selected as R40 = R36 = 470 Ω, R37 = 50 KΩ, R39 = 16.6 KΩ, and R38 = 1 KΩ. The circuit simulation diagram and a plot of pinched hysteresis loop of the memristor are shown in Figure 15. The initial voltage of the capacitor is selected as $V_1 = V_2 = 1$ V and $V_2 = -1$ V, $V_3 = 0$ V, and $V_4 = 5$ V, and the circuit simulation is shown in Figure 16(a). It can be seen that the attractors in the x-y phase diagram are symmetrically distributed. The initial voltage of the capacitor is selected as $V_1 = V_2 = 1$ V, $V_3 = \pi$ V and $V_3 = -\pi$ V, and $V_4 = 5$ V, and the circuit simulation is shown in Figure 16(b). It can be seen that the y-z phase diagram shows the growth distribution of attractors. Corresponding to various preset initial conditions given in Figure 8, the PSpice-simulated results are yielded and shown in Figures 17(a) and 17(b). The results in Figures 16 and 17 just verify the complex phenomenon revealed in the Matlab numerical simulations. Additionally, in consideration of different time scales between the mathematical model (3) and the circuit model (9), there exist some differences between the results in Figure 17 and those in Figure 8, but both show the initial-condition-dependent dynamical behavior of period with steady chaos.

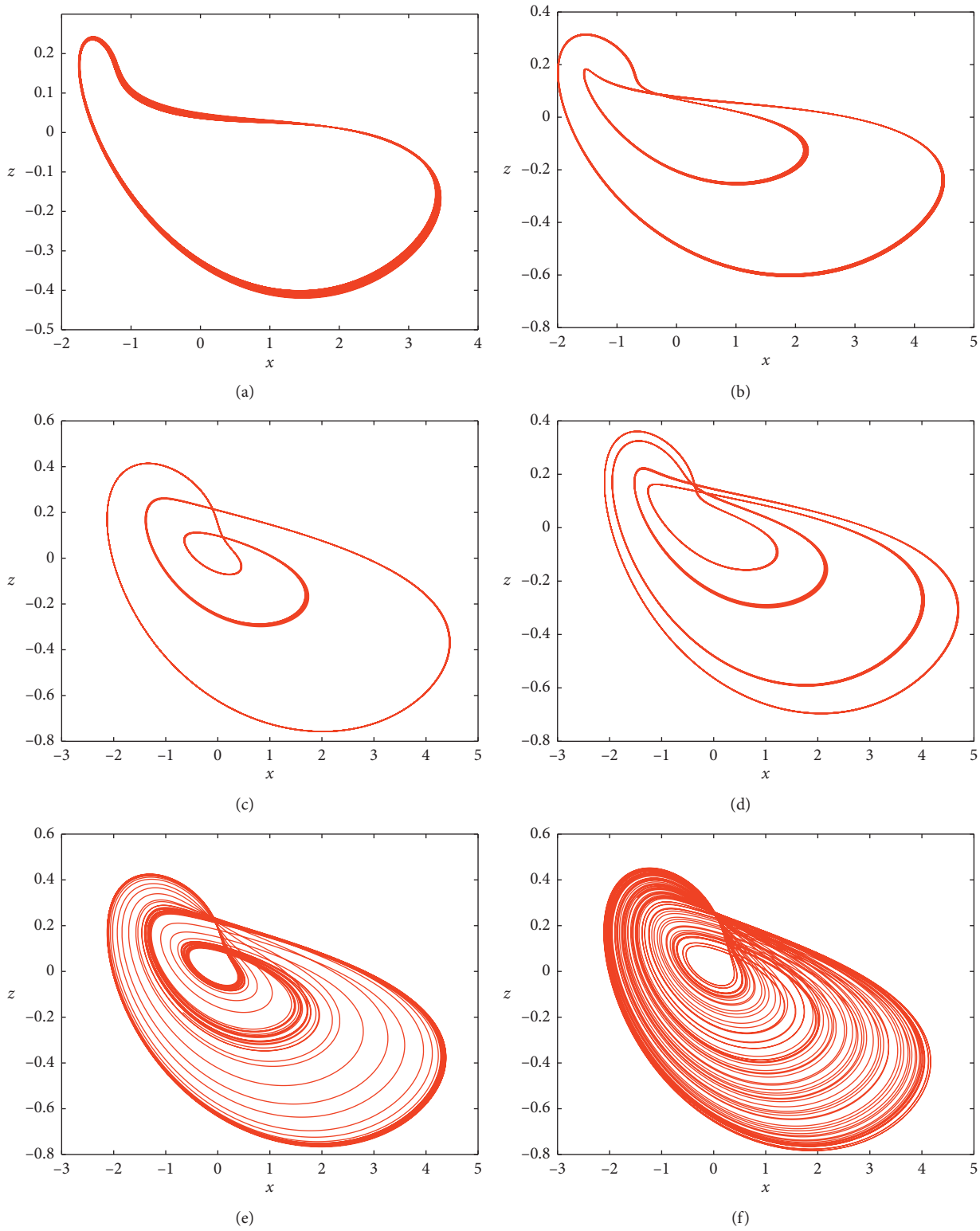

Figure 13: Coexisting attractor of system (2) with $a = 5.8$ and $b = 7.9$ under the initial condition $[1, 1, z_0, 5]$. (a) $z_0 = -0.55$; (b) $z_0 = -0.49$; (c) $z_0 = 0.12$; (d) $z_0 = -0.32$; (e) $z_0 = 0.24$; and (f) $z_0 = 0.8$.

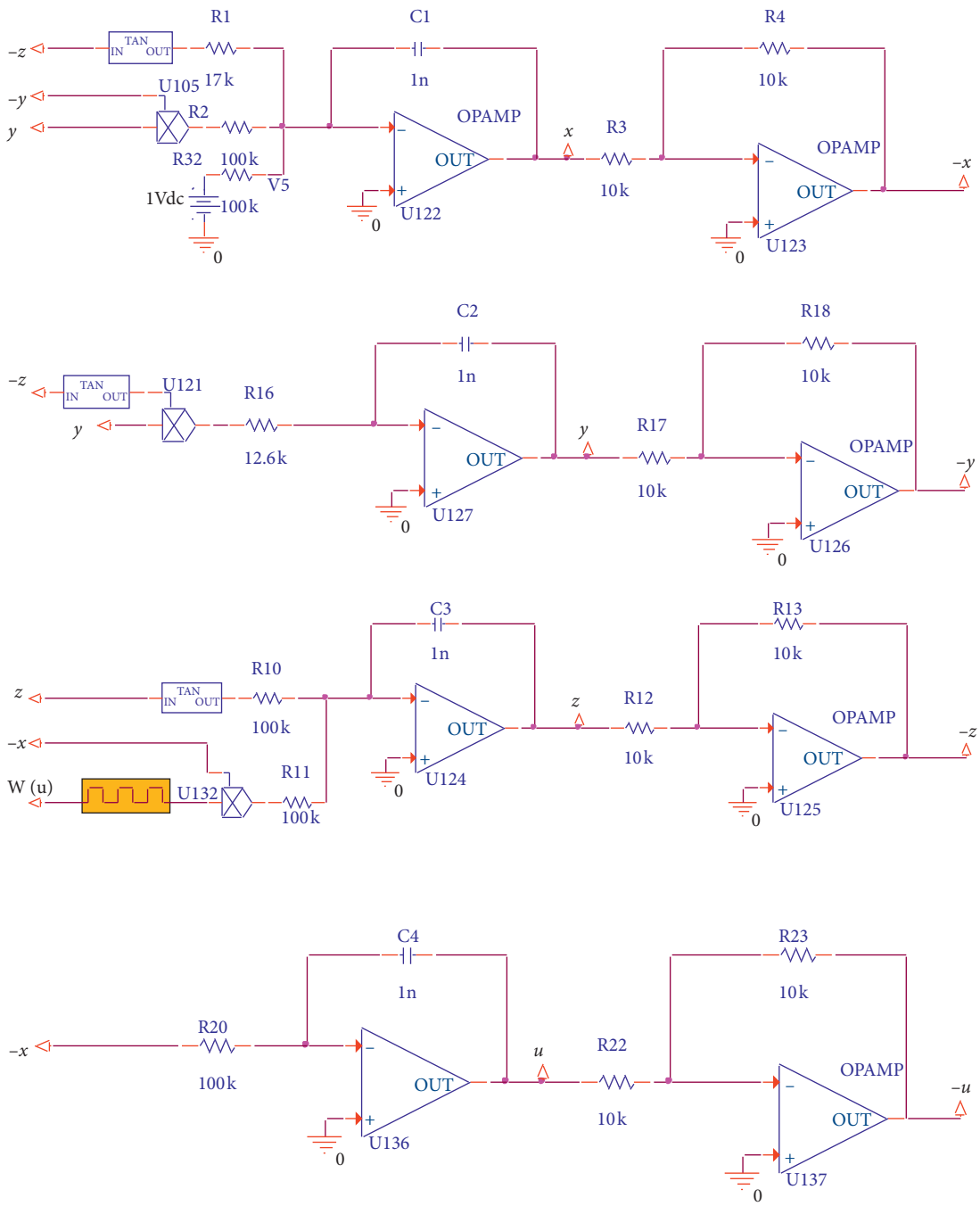

(a)

Figure 14: Continued.

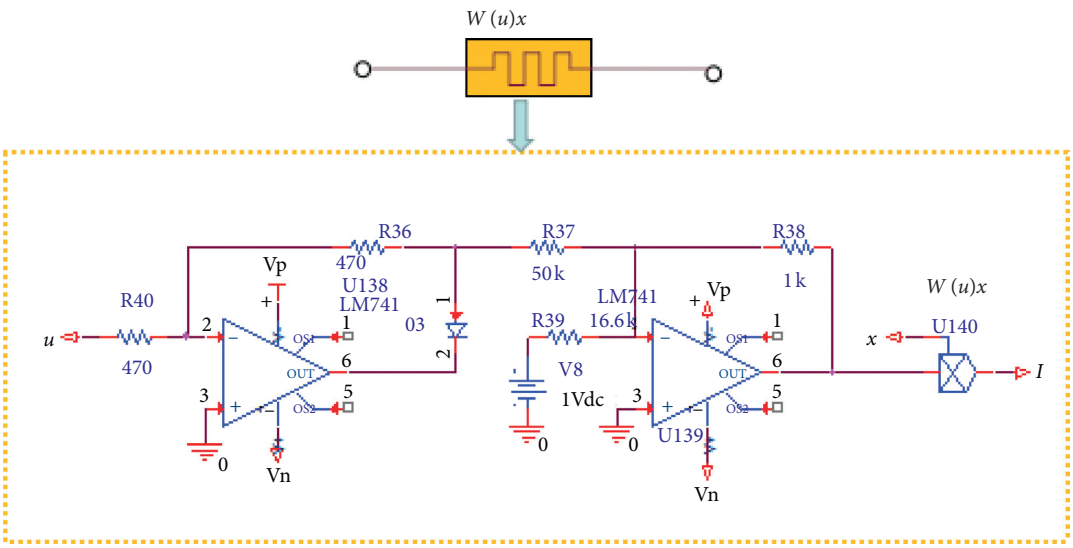

(b)

Figure 14: Hardware circuit implementation of memristive system (2): (a) main circuit; (b) memristor equivalent realization unit circuit.

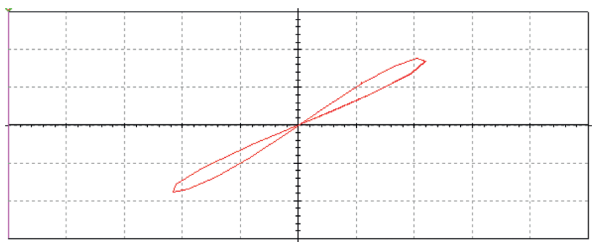

Figure 15: Pinched hysteresis loop of the memristor described by equation (3).

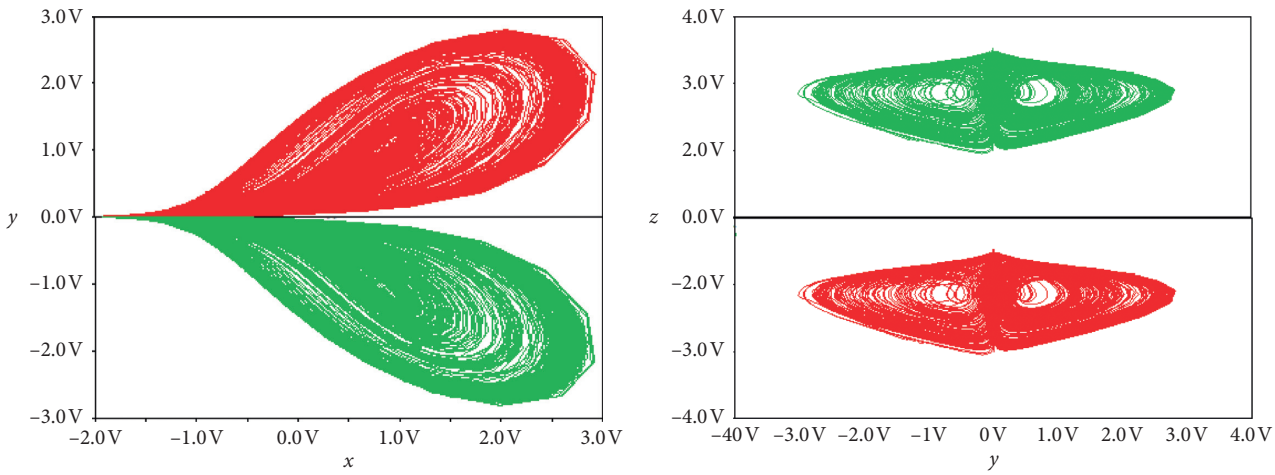

(a) (b)

Figure 16: When $a = 5.8$ and $b = 7.9$, system (3) takes chaotic attractors with different initial values. [1, 1, 0, 5], [1, −1, 0, 5], [1, 1, $-\pi$, 0], and [1, 1, π, 0] are red (a), green (a), red (b), and green (b) correspondingly: (a) x-y plane; (b) y-z plane.

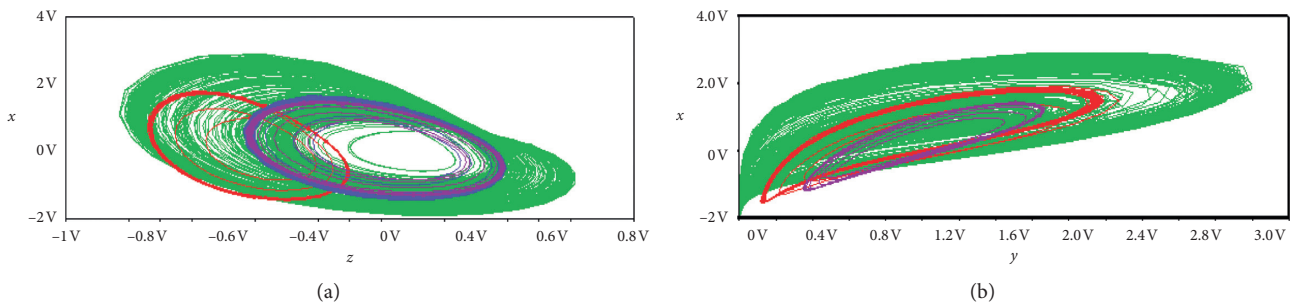

(a) (b)

Figure 17: For different initial conditions, phase portraits in the different plane by PSpice: (a) x-z plane; (b) x-y plane.

6. Conclusions

A new memristive self-replicating attractor system was obtained by introducing a tangent function and memristor into the classical system. In this case, an infinite line of equilibrium is produced, causing the phenomenon of alternating chaos and period. We analyzed the change of the initial value of each variable in the four-dimensional system, a dynamic behavior in which the transient period and steady state chaos alternately appear depending on the initial value change is newly discovered, and the super multistable state was discussed. The phenomenon of attractor self-replication appears due to the introduction of the tangent function. The results of the new system imply that there is coexisting infinitely many attractors' behavior. The initial-condition-dependent dynamical behaviors of coexisting infinitely many attractors and transient period are finally validated by hardware experiments and PSpice circuit simulations, which could enhance security for possible secure communication.

Data Availability

The data used to support the findings of this study are available from the corresponding author upon request.

Conflicts of Interest

The authors declare that there are no conflicts of interest regarding the publication of this paper.

Acknowledgments

This work was supported in part by the Natural Science Foundation of Shandong Province under Grant ZR2020KA007.

References

[1] E. N. Lorenz, "Deterministic nonperiodic flow," *Journal of the Atmospheric Sciences*, vol. 20, no. 2, pp. 130–141, 1963.

[2] X. Wang and G. Chen, "A chaotic system with only one stable equilibrium," *Communications in Nonlinear Science and Numerical Simulation*, vol. 17, no. 3, pp. 1264–1272, 2012.

[3] Z. G. Shi, S. J. Bi, H. T. Zhang, R. X. Lu, and X. M. Shen, "Improved auxiliary particle filter-based synchronization of chaotic colpitts circuit and its application to secure communication," *Wireless Communications and Mobile Computing*, vol. 15, no. 10, pp. 1456–1470, 2015.

[4] F. Min, C. Li, L. Zhang, and C. Li, "Initial value-related dynamical analysis of the memristor-based system with reduced dimensions and its chaotic synchronization via adaptive sliding mode control method," *Chinese Journal of Physics*, vol. 58, pp. 117–131, 2019.

[5] B. C. Bao, Q. Xu, H. Bao, and M. Che, "Extreme multistability in a memristive circuit," *Electronics Letters*, vol. 53, no. 12, pp. 1008–1010, 2016.

[6] J. Mou, K. Sun, J. Ruan, and S. He, "A nonlinear circuit with two memcapacitors," *Nonlinear Dynamics*, vol. 86, no. 3, pp. 1735–1744, 2016.

[7] B. C. Bao, H. Bao, N. Wang, M. Chen, and Q. Xu, "Hidden extreme multistability in memristive hyperchaotic system," *Chaos, Solitons & Fractals*, vol. 94, pp. 102–111, 2017.

[8] J. Sun, X. Zhao, J. Fang, and Y. Wang, "Autonomous memristor chaotic systems of infinite chaotic attractors and circuitry realization," *Nonlinear Dynamics*, vol. 94, no. 4, pp. 2879–2887, 2018.

[9] F. Yuan, G. Wang, and X. Wang, "Extreme multistability in a memristor-based multi-scroll hyper-chaotic system," *Chaos (Woodbury, NY.)*, vol. 26, no. 7, p. 073107, 2016.

[10] A. Akgul, C. Arslan, and B. Aricioglu, "Design of an interface for random number generators based on integer and fractional order chaotic systems," *Chaos Theory Applications*, vol. 1, no. 1, pp. 1–18, 2019.

[11] X. Y. Hu, C. X. Liu, L. Liu, Y. P. Yao, and G. C. Zheng, "Multi-scroll hidden attractors and multi-wing hidden attractors in a 5-dimensional memristive system," *Chinese Physics B*, vol. 11, pp. 124–130, 2017.

[12] H. Wu, Y. Ye, M. Chen, Q. Xu, and B. Bao, "Periodically switched memristor initial boosting behaviors in memristive hypogenetic Jerk system," *IEEE Access*, vol. 7, pp. 145022–145029, 2019.

[13] M. Mantovani, A. D. Armour, W. Belzig, and G. Rastelli, "Dynamical multistability in a quantum-dot laser," *Physics B*, vol. 99, no. 4, Article ID 045442, 2019.

[14] L. J. Ontañón-García and E. Campos-Cantón, "Widening of the basins of attraction of a multistable switching dynamical system with the location of symmetric equilibria," *Nonlinear Analysis: Hybrid Systems*, vol. 26, pp. 38–47, 2017.

[15] F. Yuan, Y. Deng, Y. Li, and G. Wang, "The amplitude, frequency and parameter space boosting in a memristor-meminductor-based circuit," *Nonlinear Dynamics*, vol. 96, no. 1, pp. 389–405, 2019.

[16] Y. N. Joglekar and S. J. Wolf, "The elusive memristor: properties of basic electrical circuits," *European Journal of Physics*, vol. 30, no. 4, pp. 661–675, 2009.

[17] Z. L. Wang, F. H. Min, and E. R. Wang, "A new hyperchaotic circuit with two memristors and its application in image encryption," *AIP Advances*, vol. 6, no. 9, pp. 80–83, 2016.

[18] D. W. Yan, L. D. Wang, and S. K. Duan, "Memristor-based multi-scroll chaotic system and its pulse synchronization control," *Acta Physica Sinica*, vol. 67, no. 11, p. 110502, 2018.

[19] M. E. Sahin, Z. G. Cam Taskiran, H. Guler, and S. E. Hamamci, "Simulation and implementation of memristive chaotic system and its application for communication systems," *Sensors and Actuators A: Physical*, vol. 290, pp. 107–118, 2019.

[20] L. Wang, T. Dong, and M.-F. Ge, "Finite-time synchronization of memristor chaotic systems and its application in image encryption," *Applied Mathematics and Computation*, vol. 347, pp. 293–305, 2019.

[21] C. Li, W. Joo-Chen Thio, H. Ho-Ching Iu, and T. Lu, "A memristive chaotic oscillator with increasing amplitude and frequency," *IEEE Access*, vol. 6, pp. 12945–12950, 2018.

[22] H. Bao, N. Wang, B. Bao, M. Chen, P. Jin, and G. Wang, "Initial condition-dependent dynamics and transient period in memristor-based hypogenetic Jerk system with four line equilibria," *Communications in Nonlinear Science and Numerical Simulation*, vol. 57, pp. 264–275, 2018.

[23] J. Sajad, A. Atefeh, A. J. M. Khalaf et al., "A new hidden chaotic attractor with extreme multi-stability," *AEU-International Journal of Electronics and Communications*, vol. 89, pp. 131–135, 2018.

[24] W. Wang, Y. C. Zeng, Z. Chen et al., "Coexisting attractors and Hopf bifuracation in floating memristors based chaotic ciruit," *Chinese Journal of Computtaional Physics*, vol. 34, no. 6, pp. 747–756, 2017.

[25] J. Huang and Y. M. Chen, "Stability and co-dimension one bifuracation analysis of a class of Lorenz chaotic systems with memristor," *Advances in Applied Mathematics*, vol. 8, no. 4, pp. 858–867, 2019.

[26] Y. M. Chen, "Research on complex dynamics of four dimensional hyper-chaotic systems based on Lorenz-type systems," Ph.D thesis, South China University of Technology, Guangzhou, China, 2014.

[27] G. Peng and F. Min, "Multistability analysis, circuit implementations and application in image encryption of a novel memristive chaotic circuit," *Nonlinear Dynamics*, vol. 90, no. 3, pp. 1607–1625, 2017.

[28] J. Liu, S. Liu, and C. Yuan, "Adaptive complex modified projective synchronization of complex chaotic (hyperchaotic) systems with uncertain complex parameters," *Nonlinear Dynamics*, vol. 79, no. 2, pp. 1035–1047, 2015.

[29] Q. Xu, Y. Lin, B. Bao, and M. Chen, "Multiple attractors in a non-ideal active voltage-controlled memristor based Chua's circuit," *Chaos, Solitons & Fractals*, vol. 83, pp. 186–200, 2016.

[30] L Zhou and C. Wang, "Generating four-wing hyperchaotic attractor and two-wing, three-wing, and four-wing chaotic attractors in 4D memristive system," *International Journal of Bifurcation and Chaos*, vol. 27, no. 2, p. 1750027, 2017.

[31] C. Li and J. C. Sprott, "Variable-boostable chaotic flows," *Optik*, vol. 127, no. 22, pp. 10389–10398, 2016.

[32] X. Yi, R. Guo, and Y. Qi, "Stabilization of chaotic systems with both uncertainty and disturbance by the UDE-based control method," *IEEE Access*, vol. 8, no. 1, pp. 62471–62477, 2020.

[33] L. Liu, B. Li, and R. Guo, "Consensus control for networked manipulators with switched parameters and topologies," *IEEE Access*, vol. 9, pp. 9209–9217, 2021.

[34] T. Hou, Y. Y. Liu, and F. Q. Deng, "Stability for discrete-time uncertain systems with infinite Markov jump and time-delay," *Science China-Information Sciences*, vol. 64, pp. 1–11, 2021.

Hindawi
Mathematical Problems in Engineering
Volume 2021, Article ID 8402334, 7 pages
https://doi.org/10.1155/2021/8402334

Research Article

Research on Efficiency of Animation Enterprises Based on Two-Stage DEA Network System Model of Sharing Input Resources

Shuo Zhang,[1,2] Xuemei Yang,[1,3] Jian Zhang,[1] Mengjie Liao,[1,3] and Lin Qi[1,2]

[1]*Beijing Information Science and Technology University, Beijing 100192, China*
[2]*Beijing World Urban Circular Economy System (Industry) Collaborative Innovation Center, Beijing 100192, China*
[3]*Beijing Knowledge Management Research Center, Beijing 100192, China*

Correspondence should be addressed to Lin Qi; qilin@bistu.edu.cn

Received 20 April 2021; Accepted 3 May 2021; Published 8 May 2021

Academic Editor: Yi Qi

This research constructs a two-stage DEA network system model of shared input resources to evaluate the efficiency of animation companies: the first-stage efficiency to reflect the production quantity and the second-stage efficiency to reflect the production quality of animation products, where the quality of animation products is judged based on the market recognition of the animation products. The overall efficiency in the research model is used to describe the development of animation enterprises. According to the result, it is concluded that the overall efficiency of the surveyed animation companies and the efficiency of each sub-stage have shown an upward trend, which is in line with the growth of the company's development.

1. Introduction

1.1. The Development Status of the Animation Industry. In the context of economic globalization, the world economy is developing rapidly, material wealth has been accumulated, traditional economic growth has encountered bottlenecks, and the spiritual and cultural needs of people who have solved the problem of food and clothing are increasing day by day [1]. More countries and governments pay more attention to the development and layout of cultural industries and propose to develop cultural industries into pillar industries of the national economy [2]. Cultural products contain aesthetics and symbolic symbols, which can cater to the needs of consumers to satisfy their self-awareness and spiritual pursuits [3–5]. The ability to innovate is endowed with cultural products that can reflect the crystallization of people's wisdom and demonstrate the level of national science and technology and cultural development. As a subdivision of cultural products, the animation industry is a new type of industry, with the characteristics of general cultural creativity, and is a sunrise industry vigorously developed by countries all over the world. There are many factors that affect the development of the animation industry [6]. Among them, cultural differences, cost expansion, and local protectionism are common factors that hinder the development of the animation industry in all countries in the world [7–9]. The improvement of the production efficiency of animation products can save the expenditure costs of animation companies and can play a positive role in promoting the development of the animation industry and even the cultural industry.

1.2. The Production Mechanism and Production Characteristics of Animation Products. The production process of animation products is the guarantee of the value of animation products. After the animation product design is completed, it is the animation production process. The production process of animation products is a step that transforms the creativity in the value chain from concept to reality. In this step, different technical environments have a greater impact on the production efficiency of animation

works, mainly because the technical participation in the production process can save a lot of production. These production costs include personnel input and time consumption. In the animation product value chain, the production process of animation products affects the quality of animation products [10]. The animation production process is the process of transforming conceptual creativity into animation works. The production process of animation products must be strictly based on creativity and design concepts. The quality of animation products will be displayed through the details of the production process [11].

The production characteristics of animation products are determined by the production process. The production process of animation products includes plot outline arrangement, drawing of human design, script creation, storyboard drawing, line draft drawing, special effects, and so on. These production processes have resulted in the production of animation products with the following three characteristics: (1) the production process is highly dependent on production technology and requires more material resources to support; (2) the process-oriented paradigm of production is relatively strong, with a certain degree of regularity and systemicity; and (3) the entire production process requires a lot of human participation, and human investment is the main input item for product manufacturing. It can be seen from the production characteristics of animation products that different heterogeneous technology integration environments will have a great impact on the production of animation products, which will result in different production efficiency of animation products.

1.3. Comprehensive Efficiency Evaluation Research. Comprehensive evaluation methods can be divided into subjective weighting method and objective weighting method [12]. Among them, subjective weighting method refers to analytic hierarchy process and entropy weighting method; objective weighting method includes principal component analysis and factor analysis. In addition, in recent years, some scholars have studied several new evaluation methods, including gray correlation analysis and fuzzy neural network evaluation [13, 14]. Among them, the field of mathematics, which is commonly used in grey relational analysis, is an analysis method to analyze the level of correlation and influence between various indicators in a specific environment [15]. The grey relational analysis method is to quantitatively analyze the data of various indicators and use the order, size, and strength of each influencing factor to carry out dynamic quantitative analysis of the indicators, which has objectivity and reference value [16].

The efficiency measurement methods can be divided into four categories. The first type is the ratio method, that is, output/input. This type of efficiency measurement considers fewer factors and the process is relatively simple; the second type is the parameter method, which is mainly random as represented by the stochastic frontier analysis (SFA); some scholars have used the stochastic frontier analysis (SFA) model to analyze the level of technical efficiency; the third category is the nonparametric method, and the nonparametric law is based on the data envelopment analysis method (as represented by data envelopment analysis, DEA); the DEA method has the advantages of freely handling the complex problems of multiple input and multiple output indicators without knowing the specific form of the production function [17–19]. Some scholars use DEA or an improved DEA model to measure efficiency because of the production of animation products [20]. The process is a complex activity with multiple inputs and multiple outputs, and it is difficult to determine the relationship of the production function, so it is more appropriate to use the DEA method to measure the efficiency [21, 22]; the fourth category, the combined measurement algorithm, combines the rolling window evaluation method and the Shannon entropy method to measure market information efficiency, using the DEA-Tobit two-step method; this type of method can be used to measure the efficiency of talent development. As a typical efficiency measurement method, DEA can be used not only for efficiency evaluation among clusters, industries, and industries but also for efficiency measurement and comparative analysis within enterprises, universities, and banks. Some scholars used the three-stage DEA to measure the internal management efficiency of various commercial banks [23].

2. Research Model Construction

2.1. DEA Method and Two-Stage DEA Model. DEA, also known as data envelopment analysis (DEA), was first used to calculate the efficiency of enterprises. It was to determine the efficiency of production by analyzing the data of production input and output. In 1953, Malmquist proposed the Malmquist index to analyze and study changes in consumption; in 1957, Fareel developed the Malmquist index and established the DEA-Malmquist index to examine changes in production efficiency. DEA-Malmquist index is based on DEA and combines the advantages of DEA. Through the DEA-Malmquist index, the efficiency of panel data can be analyzed [24]. The calculated efficiency can be further decomposed into technical level and technical efficiency, and technical efficiency can be decomposed into pure technical efficiency and scale efficiency. The expression of the DEA-Malmquist index model is as follows.

Taking time as the base period, the DEA-Malmquist index from the perspective of output is expressed as

$$M_i^t = \left[\frac{d_i^t\left(x^{t+1}, y^{t+1}\right)}{d_i^t\left(x^t, y^t\right)}\right]. \tag{1}$$

Taking time $t + 1$ as the base period, the DEA-Malmquist index from the perspective of output is expressed as

$$M_i^{t+1} = \left[\frac{d_0^{t+1}\left(x^{t+1}, y^{t+1}\right)}{d_0^{t+1}\left(x^t, y^t\right)}\right]. \quad (2)$$

The above two formulas can be used to calculate the change value of the TFPCH from the period t to the period $t+1$ of the geometric mean measurement time:

$$M_i^{t+1} = \left[\frac{d_i^t\left(x^{t+1}, y^{t+1}\right)}{d_i^t\left(x^t, y^t\right)} \times \frac{d_i^{t+1}\left(x^{t+1}, y^{t+1}\right)}{d_i^{t+1}\left(x^t, y^t\right)}\right]^{(1/2)}. \quad (3)$$

Under the premise of constant return to scale, TFPCH can be decomposed into the product of technical efficiency index (FFFCH) and technological progress index (TECHCH):

$$M_i = \frac{d_i^t\left(x^{t+1}, y^{t+1}\right)}{d_i^t\left(x^t, y^t\right)} \times \left[\frac{d_i^t\left(x^{t+1}, y^{t+1}\right)}{d_i^{t+1}\left(x^t, y^t\right)} \times \frac{d_i^t\left(x^t, y^t\right)}{d_i^{t+1}\left(x^t, y^t\right)}\right]^{(1/2)}. \quad (4)$$

Among them:

$$\begin{aligned} \text{EFFCH} &= \left[\frac{d_i^{t+1}\left(x^{t+1}, y^{t+1}\right)}{d_i^t\left(x^t, y^t\right)}\right], \\ \text{TECHCH} &= \left[\frac{d_i^t\left(x^{t+1}, y^{t+1}\right)}{d_i^{t+1}\left(x^t, y^t\right)} \times \frac{d_i^{t+1}\left(x^{t+1}, y^{t+1}\right)}{d_i^{t+1}\left(x^t, y^t\right)}\right]^{(1/2)}, \\ \text{TFPCH} &= \text{EFFCH} \times \text{TECHCH}. \end{aligned} \quad (5)$$

Traditional data envelopment analysis methods mainly include five models:C^2R, BC^2, C^2GS^2, C^2W, C^2WH.

Many scholars at home and abroad generally believe that the production efficiency of enterprises should be studied in two stages. The first stage is the development stage of technology [25]. Among them, the technology development stage is mainly resource input, including R&D funds, R&D personnel, and equipment input; the investment at this stage can promote the output of technological innovation results of the enterprise, such as patents, copyrights, and new processes. The second stage is the technology application stage, and it is also the stage where the results of the first stage are transformed into market effects. The principle of the two-stage DEA model is shown in Figure 1.

It can be seen from Figure 1 that, unlike the traditional DEA model, it is assumed in the model that there is no output outflow in the first stage, but the whole input is input into the second stage together with additional input, and the final result is output as $Y_r, r = 1, \ldots, s$.

The specific model is constructed as follows. Suppose there are n decision-making units, each decision-making unit has m types of inputs, s types of outputs, and k types of intermediate outputs, and X_i is the input of the first stage of the i decision-making unit (DMU),$X_i = (x_{i1}, x_{i2}, \ldots, x_{im})^T$; Z_g is the output of the first stage, and at the same time as the input of the second stage, $Z_g = (z_{g1}, z_{g2}, \ldots, z_{gh})^T$; Y_r is the system output of the second stage, $Y_r = (y_{r1}, y_{r2}, \ldots, y_{rs})^T$.$V = (v_1, v_2, \ldots, v_m)$, $W = (w_1, w_2, \ldots, w_k)$,

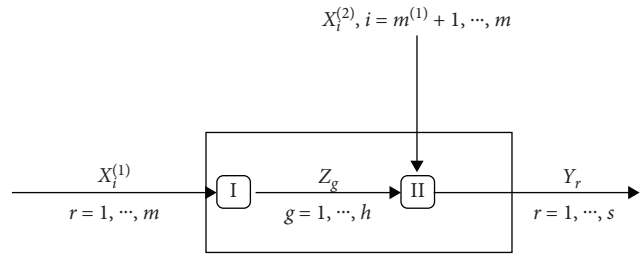

Figure 1: Two-stage network DEA model.

and $U = (u_1, u_2, \ldots, u_s)$, respectively, represent the weights of input and intermediate output changes, and the two-stage chain DEA model is $E_0 - \max U^Y Y_0$.

$$\begin{cases} V^T x_0 = 1, \\ U_T Y_i - V^T X_i \le 0, \\ \text{s.t. } W_T Z_i - V^T X_i \le 0, \\ U_T Y_i - W^T Z_i \le 0, \\ U \ge \varepsilon e_s, \\ V \ge \varepsilon e_m, \\ W \ge \varepsilon e_k, \end{cases} \quad (6)$$

where ε is the non-Archimedes infinitesimal, $e^T = (1, 1, \ldots, 1)$. If U^*, V^*, W^* are the optimal solutions of the model, the efficiency of the overall DMU and the sub-processes is $E_0 = (U^{*T} Y_0 / V^{*T} X_0)$, $E_1 = (U^{*T} Z_0 / V^{*T} X_0)$, $E_2 = (U^{*T} Y_0 / V^{*T} Z_0)$, respectively, where E_0 is the overall efficiency and E_1 and E_2 are the partial efficiencies of the two sub-stages.

2.2. Building a Two-Stage DEA Network System Model That Shares Input Resources. The two-stage DEA network system model that shares input resources also incorporates the "process between input and output" into the efficiency evaluation, so that the results can explain the overall situation more completely and prevent deviations. The specific model is shown in Figure 2.

Suppose there are n decision-making units, $\text{DMU}_j\,(j = 1, 2, \ldots, n)$; the input of the first stage is $X_{ij}\,(i = 1, 2, \ldots, m)$, and the output of the first stage is $Z_{pj}\,(p = 1, 2, \ldots, p)$; in the second stage, the reinput is $H_{pj}\,(h = 1, 2, \ldots, g)$, and the output is $Y_{rj}\,(r = 1, 2, \ldots, s)$. Furthermore, the shared input considers that the initial input has an impact on the output of the two stages. Assuming that the initial input X_{ij} has an effect ratio of $\alpha_i\,(0 \le \alpha_i \le 1)$ to the first stage, the input of the first stage is$\alpha_i X_{ij}$, and the initial input of the second stage is $(1 - \alpha_i) X_{ij}$.

Use decision variables v_i^1 and v_i^2 to represent the weight of the initial input in the two stages, respectively; w_p^1 and w_p^2represent the weight of the intermediate output in the two stages, respectively [26]; $f_h$is the weight of the reinvestment; $u_r$is the weight of the output in the second stage. Then, the overall efficiency E_k of the decision-making unit and the

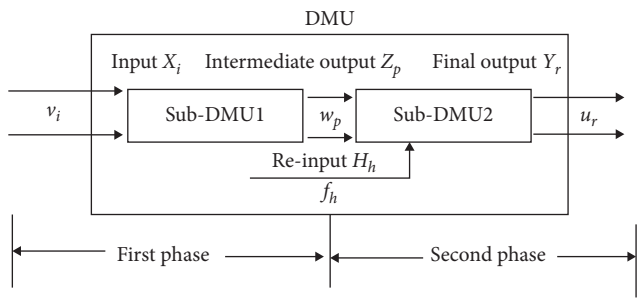

Figure 2: Two-stage DEA network system model that shares input resources.

efficiencies E_k^1 and E_k^2 of the sub-processes are shown in the following three formulas:

$$E_k^1 = \frac{\sum_{p=1}^{q} w_p^1 \times Z_{pj}}{\sum_{i=1}^{m} v_i^1 \times \alpha_i \times X_{ij}},$$
$$E_k^2 = \frac{\sum_{r=1}^{s} u_r \times Y_{rj}}{\sum_{i=1}^{m} v_i^2 \times (1-\alpha_i) \times X_{ij} + \sum_{p=1}^{q} w_p^2 \times Z_{pj} + \sum_{h=1}^{g} f_h \times H_{hj}}, \tag{7}$$
$$E_k = \frac{\sum_{p=1}^{q} w_p^1 \times Z_{pj} + \sum_{r=1}^{s} u_r \times Y_{rj}}{\sum_{i=1}^{m} v_i^1 \times \alpha_i \times X_{ij} + \sum_{i=1}^{m} v_i^2 \times (1-\alpha_i) \times X_{ij} + \sum_{p=1}^{q} w_p^2 \times Z_{pj} + \sum_{h=1}^{g} f_h \times H_{hj}}.$$

Using mathematical programming ideas, a fractional mathematical programming of a two-stage DEA model with shared input correlation is constructed to obtain the maximum efficiency. At the same time, in order to prevent the optimal solution of the requested variable from being zero, set its lower limit to Archimedes infinitesimal (ε), thereby converting the fractional mathematical programming into an equivalent linear programming, as shown in the following formula:

$$E_k = \max\left(\sum_{p=1}^{q} w_p^1 \times Z_{pk} + \sum_{r=1}^{s} U_r \times Y_{rk}\right)$$
$$\text{s.t.}\begin{cases} \sum_{i=1}^{m} \pi_i^1 \times X_{ij} - \sum_{p=1}^{q} W_p^1 Z_{pj} \geq 0, \\ \sum_{i=1}^{m} V_i^2 \times X_{ij} - \sum_{i=1}^{m} \pi_i^2 \times X_{ij} + \sum_{p=1}^{q} W_p^2 \times Z_{pj} + \sum_{h=1}^{g} F_h \times H_{hj} - \sum_{r=1}^{s} U_r \times Y_{rj} \geq 0, \\ \sum_{i=1}^{m} \pi_i^1 \times X_{ik} + \sum_{i=1}^{m} V_i^2 \times X_{ik} - \sum_{i=1}^{m} \pi_i^2 \times X_{ik} + \sum_{p=1}^{q} W_P^2 \times Z_{pk} + \sum_{h=1}^{g} F_h \times H_{hk} = 1, \\ V_i^2 \geq \pi_i^2 \geq \varepsilon, \pi_i^1, W_p^1, W_p^2, F_h, U_r \geq \varepsilon, i = 1, 2, \ldots, m; j = 1, 2, \ldots, n, \end{cases} \tag{8}$$

where $V_i^1 = t \times v_i^1, V_i^2 = t \times v_i^2$, $W_p^1 = t \times w_p^1$, $W_p^2 = t \times w_p^2$, $F_h = t \times f_h$, $U_r = t \times u_r$.

$$t = \frac{1}{\sum_i^m v_i^1 \times \alpha_i \times X_{ik} + \sum_{i=1}^m v_i^2 \times (1-\alpha_i) \times X_{ik} + \sum_{p=1}^q u_r \times Z_{pk} + \sum_{h=1}^g f_h \times H_{hk}}. \tag{9}$$

From the above calculation, the following can be obtained: animation enterprise production efficiencyE_k andπ_i^1, π_i^2, V_i^1, V_i^2, W_i^1, W_i^2, F_h, U_r, α_i.

Finally, the first-stage efficiency E_k^1 and the second-stage efficiency E_k^2 are calculated by the following two formulas:

$$E_k^1 = \frac{\sum_{p=1}^q w_p^1 \times Z_{pk}}{\sum_i^m v_i^1 \times \alpha_i \times X_{ik}} = \frac{\sum_{p=1}^q W_p^1 \times Z_{pk}}{\sum_i^m V_i^1 \times X_{ik}},$$
$$E_k^2 = \frac{\sum_{r=1}^s U_r \times Y_{rk}}{\sum_{i=1}^m V_i^2 \times (1-\alpha_i) \times X_{ik} + \sum_{p=1}^q W_P^2 \times Z_{pk} + \sum_{h=1}^g F_h \times H_{hk}}. \tag{10}$$

As far as the efficiency of animation companies is concerned, there is no significant difference between the initial input and intermediate output of the animation production process. Referring to the research of some scholars, we set the first stage of resource input to the second stage with the same amount, so $V_i^1 = V_i^2 (i = 1, 2, \ldots, m)$, $W_p^1 = W_p^2 (p = 1, 2, \ldots, q)$.

3. Index System Construction and Data Sources

3.1. Index System Construction. The basis for the two-stage division of the two-stage DEA network system model for the construction of shared input resources is to evaluate the production effects of animation products from two dimensions. The first dimension refers to the production efficiency of animation products, corresponding to the first stage in the model; the second dimension refers to the quality of the animation products produced, and the efficiency is measured by the market performance after the release of the animation products, corresponding to the model in the second stage. Since the output of the first stage is animation products, it will be used as the input of the second stage. In summary, this research is a study on the value transfer of animation products from design and production to market feedback and production quality. The efficiency measured in the first phase is the production efficiency of animation products (based on the number of animation products produced), and the second phase is used to measure the quality of the animation products produced in the first phase; the final value output of the animation company efficiency is the comprehensive feedback of the production efficiency of animation products and the quality and efficiency of animation products. The indicator system of this study will be constructed according to the specific meaning of the established two-stage DEA network system model of shared input resources. The production efficiency indicator system of animation enterprises is shown in Table 1.

3.2. Sample Selection and Data Sources. All data selected in this study come from a typical enterprise in China's animation industry. Through investigation, the researcher obtained the data of the company from June 2016 to June 2019, a total of 36 months in three years, and a total of 36 sets of observation variables. Among them, the data corresponding to the output indicators of the second stage refer to the output of the products produced by the surveyed company in the next six months in the statistical month, namely, the cumulative collection of the next six months, the cumulative number of clicks of the next six months, and the total amount of cumulative payments in the next six months.

4. Model Result Analysis

Based on the above-established model and selected indicator system, the two-stage DEA network system model of shared input resources is used to comprehensively calculate the production efficiency of a Chinese animation production company for a total of 36 months in 3 years (total decision-making units: 36). The calculation results are shown in Table 2. In Table 2, DMU represents the decision-making unit, $E_k$represents the overall efficiency, E_k^1represents the efficiency of the first stage, and E_k^2represents the efficiency of the second stage.

According to Table 2, it can be analyzed that the maximum value of overall efficiencyE_k, first-stage efficiencyE_k^1, and second-stage efficiencyE_k^2 are all 1. Among them, the minimum value of the overall efficiencyE_k is 0.34087 and the average value is 0.72843; the minimum value of the first-stage efficiencyE_k^1 is 0.42766, and the average value is

Table 1: Product production efficiency index system of animation enterprises.

First-stage investment	First-stage output	Second-stage investment	Second-stage output
Total staff salary expenditure	Number of works produced	Total staff salary expenditure	Total the amount of collection
Office rent	Number of copyright applications	Office rent	Accumulated clicks
Equipment and software purchase or use expenses	—	Equipment and software purchase or use expenses	—
Management funding	—	Management funding	Total accumulated payment
—	—	Advertising costs	—

Table 2: Two-stage DEA network system model calculation results of shared input resources.

DMU	E_k	E_k^1	E_k^2	DMU	E_k	E_k^1	E_k^2
1	0.43177	0.71575	0.30904	19	0.78261	0.94257	0.73767
2	0.42766	0.79706	0.34087	20	0.80670	0.99263	0.80076
3	0.47895	0.76324	0.36555	21	0.84476	1.00000	0.84476
4	0.51308	0.75214	0.38591	22	1.00000	1.00000	1.00000
5	0.51365	0.80483	0.41340	23	0.89492	0.94359	0.84443
6	0.56234	0.84083	0.47284	24	0.94697	0.91021	0.86194
7	0.58746	0.92773	0.54500	25	1.00000	0.92006	0.92006
8	0.56194	0.93293	0.52425	26	0.95848	0.93501	0.89619
9	0.72744	0.88199	0.64159	27	0.99653	0.97494	0.97156
10	0.69748	0.96982	0.67643	28	0.95819	0.96293	0.92267
11	0.68514	1.00000	0.68514	29	0.93465	1.00000	0.93465
12	0.59351	0.89792	0.53292	30	0.96296	1.00000	0.96296
13	0.65217	0.82416	0.53750	31	0.94327	1.00000	0.94327
14	0.74739	0.78955	0.59010	32	0.96485	0.98819	0.95346
15	0.86429	0.77253	0.66769	33	0.95621	1.00000	0.95621
16	0.83068	0.80247	0.66659	34	0.98273	0.98542	0.96840
17	0.73913	0.90671	0.67018	35	1.00000	0.98718	0.98718
18	0.73913	0.93687	0.69247	36	1.00000	1.00000	1.00000

0.78575; the minimum value of the second-stage efficiencyE_k^2 is 0.79706, and the average value is 0.91275. Therefore, this research can conclude that the production efficiency of animation products of the company has been significantly improved within three years; among them, the overall efficiencyE_k has increased the most significantly, followed by the first-stage efficiencyE_k^1, and the second-stage efficiencyE_k^2 has increased relatively slowly.

5. Conclusions

In the context of the continuous deepening of the market economy, the importance of efficiency improvement by animation companies is beyond doubt. Therefore, an effective evaluation and analysis of the efficiency of animation companies can enable animation companies to more objectively recognize their own development trends and operating conditions. This study uses a two-stage DEA network system model of shared input resources to evaluate and analyze the production efficiency of animation companies, the market performance of animation products produced, and the overall efficiency of animation companies.

Research shows that the production phase rate, market effect, and overall efficiency of animation products produced by animation companies in the growth period are showing a trend of rising volatility. In order to improve efficiency, animation companies should optimize their resource allocation capabilities, formulate reasonable and effective development plans and operating models, drive industrial development with technological innovation, and continuously enhance their brand value.

Data Availability

The data presented in this study are available on request from the corresponding author.

Conflicts of Interest

The authors declare that they have no conflicts of interest regarding the publication of this paper.

Acknowledgments

This research was funded by the National Key R&D Program of China (2017YFB1400400), Youth Talent Promotion Program of Beijing Association for Science and Technology (2020-2022-16), and Program for Promoting the Connotative Development of Beijing Information Science and Technology University (521201090A and 5026010961).

References

[1] P. Francois and T. van Ypersele, "On the protection of cultural goods," *Journal of International Economics*, vol. 56, no. 2, pp. 359–369, 2002.

[2] Y. Lee, S. Kim, Y.-K. Seock, and Y. Cho, "Tourists' attitudes towards textiles and apparel-related cultural products: a cross-cultural marketing study," *Tourism Management*, vol. 30, no. 5, pp. 724–732, 2008.

[3] T. Hou, Y. Liu, and D. Deng, "Stability for discrete-time uncertain systems with infinite Markov jump and time-delay," *Science China-Information Sciences*, vol. 64, no. 5, pp. 1–11, 2021.

[4] L. Qi, "Research on knowledge gap identification method in innovative organizations under the "internet+" environment," *Information*, vol. 11, no. 12, pp. 1–14, 2020.

[5] H. Bernard, "New knowledge as cultural production: design as research," *Australian Art Education*, vol. 30, no. 2, pp. 13–25, 2007.

[6] R. Gonzalez, J. Llopis, and J. Gasco, "Social networks in cultural industries," *Journal of Business Research*, vol. 68, no. 4, pp. 823–828, 2015.

[7] S.-l. Shan, "Chinese cultural policy and the cultural industries," *City, Culture and Society*, vol. 5, no. 3, pp. 115–121, 2014.

[8] R. Peng, C. Jiang, and R. Guo, "Stabilization of a class of fractional order systems with both uncertainty and disturbance," *IEEE Access*, vol. 9, pp. 42697–42706, 2021.

[9] M. Banks, A. Lovatt, J. O'Connor, and C. Raffo, "Risk and trust in the cultural industries," *Geoforum*, vol. 31, no. 4, pp. 103–113, 2000.

[10] Y. Aoyama, "The role of consumption and globalization in a cultural industry: the case of flamenco," *Economics and Business Letters*, vol. 32, no. 1, pp. 103–113, 2006.

[11] V. Blanco and J. Rodríguez, "Introduction to the special issue: the economics of cultural industries," *Economics and Business Letters*, vol. 3, no. 2, pp. 77-78, 2014.

[12] Y. Sohn and Y. Kim, "DEA based multi-period evaluation system for research in academia," *Expert Systems with Applications*, vol. 39, no. 9, pp. 8274–8278, 2012.

[13] G. R. Jahanshahloo, M. Soleimani-damaneh, and A. Mostafaee, "A simplified version of the DEA cost efficiency model," *European Journal of Operational Research*, vol. 184, no. 2, pp. 814-815, 2006.

[14] X. Yi, R. Guo, and Y. Qi, "Stabilization of chaotic systems with both uncertainty and disturbance by the UDE-based control method," *IEEE Access*, vol. 8, no. 1, pp. 62471–62477, 2020.

[15] Y. Chen, W. D. Cook, L. Ning, and J. Zhu, "Additive efficiency decomposition in two-stage DEA," *European Journal of Operational Research*, vol. 196, no. 3, pp. 1170–1176, 2008.

[16] X. Shi and A. Tsourdos, "Environmental efficiency evaluation of Chinese industry systems by using non-cooperative two-stage DEA model," *Mathematical Problems in Engineering*, vol. 2019, Article ID 9208367, 10 pages, 2019.

[17] J. S. Liu and W.-M. Lu, "Network-based method for ranking of efficient units in two-stage DEA models," *Journal of the Operational Research Society*, vol. 63, no. 8, pp. 1153–1164, 2012.

[18] L. Liu, B. Li, and R. Guo, "Consensus control for networked manipulators with switched parameters and topologies," *IEEE Access*, vol. 9, no. 1, pp. 9209–9217, 2020.

[19] X. Si, L. Liang, G. Jia, L. Yang, H. Wu, and Y. Li, "Proportional sharing and DEA in allocating the fixed cost," *Applied Mathematics and Computation*, vol. 219, no. 12, pp. 6580–6590, 2013.

[20] G. R. Jahanshahloo, F. Hosseinzadeh Lotfi, and M. Zohrehbandian, "Finding the efficiency score and RTS characteristic of DMUs by means of identifying the efficient frontier in DEA," *Applied Mathematics and Computation*, vol. 170, no. 2, pp. 985–993, 2004.

[21] W. Liu, Z. Zhou, C. Ma, D. Liu, and W. Shen, "Two-stage DEA models with undesirable input-intermediate-outputs," *Omega*, vol. 56, pp. 74–87, 2015.

[22] E. Gutiérrez, E. Aguilera, S. Lozano, and G. I. Guzmán, "A two-stage DEA approach for quantifying and analysing the inefficiency of conventional and organic rain-fed cereals in Spain," *Journal of Cleaner Production*, vol. 149, pp. 335–348, 2017.

[23] S. Mousavi-Nasab and A. Sotoudeh-Anvari, "A comprehensive MCDM-based approach using TOPSIS, COPRAS and DEA as an auxiliary tool for material selection problems," *Materials & Design*, vol. 121, pp. 237–253, 2017.

[24] W. Peter and C. Pestana Barros, "Efficiency drivers in Brazilian insurance: a two-stage DEA meta frontier-data mining approach," *Economic Modelling*, vol. 53, pp. 8–22, 2016.

[25] D. Khezrimotlagh, S. Salleh, and Z. Mohsenpour, "A note on integer-valued radial model in DEA," *Computers & Industrial Engineering*, vol. 66, no. 1, pp. 199-200, 2013.

[26] M. Maghbouli, A. Amirteimoori, and S. Kordrostami, "Two-stage network structures with undesirable outputs: a DEA based approach," *Measurement*, vol. 48, pp. 109–118, 2014.

Hindawi
Mathematical Problems in Engineering
Volume 2021, Article ID 5517289, 10 pages
https://doi.org/10.1155/2021/5517289

Research Article

A Novel Input Variable Selection and Structure Optimization Algorithm for Multilayer Perceptron-Based Soft Sensors

Hongxun Wang, Lin Sui, Mengyan Zhang, Fangfang Zhang, Fengying Ma, and Kai Sun

School of Electrical Engineering and Automation, Qilu University of Technology (Shandong Academy of Sciences), Jinan 250353, China

Correspondence should be addressed to Kai Sun; sunkai79@qlu.edu.cn

Received 6 January 2021; Revised 6 March 2021; Accepted 15 April 2021; Published 3 May 2021

Academic Editor: Adrian Neagu

A novel optimization algorithm for multilayer perceptron- (MLP-) based soft sensors is proposed in this paper. The proposed approach integrates input variable selection and hidden layer optimization on MLP into a constrained optimization problem. The nonnegative garrote (NNG) is implemented to perform the shrinkage of input variables and optimization of hidden layer simultaneously. The optimal garrote parameter of NNG is determined by combining cross-validation with Hannan-Quinn information criterion. The performance of the algorithm is demonstrated by an artificial dataset and the practical application of the desulfurization process in a thermal power plant. Comparative results demonstrated that the developed algorithm could build simpler and more accurate models than other state-of-the-art soft sensor algorithms.

1. Introduction

In complex industrial processes, important process parameters that influence product quality or energy consumption need to be monitored and controlled in real time and with high accuracy. However, some of them are difficult to be directly measured with hardware sensors due to the limitations of existing field conditions [1–3]. Soft sensors achieve the mathematical modeling of these hard-to-measure parameters through auxiliary variables that are easy to be measured [4, 5]. Basically, there are two categories of soft sensor techniques: mechanism analysis-based approaches and data-driven approaches. The mechanism analysis-based approaches require accurate understanding of the inherent mechanism of complex industrial processes, which is very difficult for the researchers. Data-driven algorithms provide advanced alternatives with statistical inference and machine learning techniques [6, 7]. In recent years, data-driven soft sensors including principal component regression (PCR), partial least squares (PLS) regression, support vector machine (SVM), extreme learning machine (ELM), and artificial neural networks (ANNs) have been widely studied [8–12].

Due to their powerful nonlinear modeling competence, ANNs have become the most popular nonlinear modeling techniques. There are a variety of ANNs such as convolutional neural networks (CNN) [13], generative adversarial networks (GAN) [14], radial basis networks, and recurrent neural network (RNN) [15], each of which has its own characteristics and advantages. Among them, multilayer perceptron (MLP) is the most widely used technique for nonlinear soft sensing owing to its outstanding nonlinear mapping capability and convenience of application. Heidari et al. [16] built an accurate predictive model of nanofluid viscosity with MLP. Shen et al. [17] presented an MLP-based recursive sliding mode dynamic surface control scheme for a fully actuated surface vessel with uncertain dynamics and external disturbances. In [18], MLP was applied to predict the water content of biodiesel and diesel blend in terms of temperature and composition.

With the rapid development of process automation, more and more variables are involved in the modern process industry. Redundant input variables increase the model complexity, delay the training time, and decrease the predictive accuracy of the model [19, 20]. Variable selection

technology provides a good solution to this problem and therefore is extensively studied [1, 21, 22]. Guo et al. [23] proposed an input variable selection method for a feed-forward neural network (FNN) by using partial auto-correlation function and successfully forecasted the wind speed. Fock [24] proposed a new algorithm for the selection of input variables, in which the global sensitivity analysis technique was used to select the optimal input variables. Adil et al. [25] presented a new variable selection algorithm that used the heuristic method and minimum redundancy maximum relevance, and the experimental results showed better accuracy than other algorithms. In [26], a neural network-based soft sensor was developed to predict effluent concentrations in a biological wastewater treatment plant, in which principal component analysis (PCA) was implemented to select optimal input variables.

Nonnegative garrote (NNG) is a linear coefficient shrinkage approach based on penalty likelihood function. In recent years, it has been widely used in the variable selection of ANNs [27]. Sun et al. [28] utilized the NNG to compress the input weights of the MLP to achieve nonlinear variable selection, and the superiority of the proposed algorithm was proved through two artificial dataset examples and a real industrial application. In [29], a local search strategy was incorporated into the NNG-MLP to improve its performance. However, these algorithms only consider the selection of input variables and ignore the optimization of the internal structure of the MLP network. Actually, the redundant nodes of hidden layers worsen the performance of MLP as the redundant input variables do and even lead to overfitting of the model. Pan et al. [30] proposed a novel approach of simplifying the structure of deep neural network through regularization of network architecture. Anbananthen et al. [31] presented a pruning procedure, by which redundant links were deleted from the trained network. Monika and Venkatesan [32] designed a divisive ANN clustering algorithm to prune the neurons of the hidden layer of MLP, which promoted model accuracy. Fan et al. proposed an algorithm that utilized the least absolute shrinkage and selection operator (LASSO) to perform the selection of input variables and the optimization of the hidden layer of MLP, named dLASSO [33]. However, the variable selection and hidden layer optimization of dLASSO are independent of each other, which may cause the omission of the optimal solution.

According to our investigation, few existing methods deal with the redundancy of input variables and hidden layers of ANN models synchronously. In this paper, a novel algorithm that performs global dimension reduction and structure simplification for MLP-based soft sensors is proposed by elaborately combining NNG and MLP. The MLP is implemented to cope with the nonlinear dynamics of the industrial processes, and NNG is devised to conduct the selection of the input variables and simplification of the hidden layers. To the best of our knowledge, this algorithm is a quite innovative design of a penalty function-based strategy for global optimizing the structure of ANNs. The effectiveness of the developed algorithm is validated by an artificial dataset and application to a practical industrial process to provide informative analysis.

The remainder of this paper is organized as follows. The background theories of the approach are reviewed in Section 2. Section 3 describes the detailed principles and development of the proposed algorithm. The simulation results and analysis of artificial datasets and practical industrial process are presented in Section 4. Finally, some concluding remarks are given in Section 5.

2. Theoretical Background

The architecture of a three-layer MLP discussed in the paper is demonstrated in Figure 1, which is composed of an output layer, a hidden layer, and an input layer. The number of neurons of input layer is dependent on the variables or columns of the input dataset, while that of the hidden layer is usually chosen by trial and error. The mathematical expression of the studied MLP is shown as

$$y = f\left(g\left(xw_I + b_I\right)w_O + b_O\right), \tag{1}$$

where $g(\cdot)$ and $f(\cdot)$ denote the activation functions of the hidden and output layer, respectively, $x = [x_1, x_2, \ldots, x_p]$ is the vector of input variables, and y is the output variable. The weight $w_I = \begin{bmatrix} w_{11} & \cdots & w_{1q} \\ \vdots & \ddots & \vdots \\ w_{p1} & \cdots & w_{pq} \end{bmatrix}$ is a $p \times q$ matrix that links nodes of the input and hidden layer. $b_I = [b_1, b_2, \ldots, b_q]$ is the bias vector of the hidden nodes. $w_O = [w_1^o, w_2^o, \ldots, w_q^o]^T$ represents the matrix of output weights linking the hidden and the output layer. The output bias is denoted as b_O.

For the linear regression problem,

$$y = x\beta + \varepsilon, \tag{2}$$

where $\beta = [\beta_1, \beta_2, \ldots, \beta_p]^T$ is the vector of magnitude coefficients and ε is the random error. Breiman proposed a constraint consisting of the summation of shrinkage coefficients $c = [c_1, c_2, \ldots, c_p]$ and imposed it on the ordinary least squares (OLS) regression model [34]:

$$\begin{aligned} c^*(s) &= \operatorname{argmin}\left\{\sum\left(y - (c \cdot x)\widehat{\beta}\right)^2\right\}, \quad \forall (x, y) \in \{X, Y\} \\ &\text{subject to} \quad c_i \geq 0, \quad \sum_{i=1}^{p} c_i \leq s, \end{aligned} \tag{3}$$

in which $\widehat{\beta}$ represents the coefficient vector of OLS estimation and s is the garrote parameter. X is the input dataset, in which each column corresponds to a candidate input variable, and $Y \in R^n$ is the dataset of output variable.

In [28], the NNG algorithm was devised to select the input variable of MLP by imposing c on the input layer:

$$\widehat{y} = f\left(g\left(c \cdot xw_I + b_I\right)w_O + b_O\right), \tag{4}$$

and equation (3) is consequently reformulated as

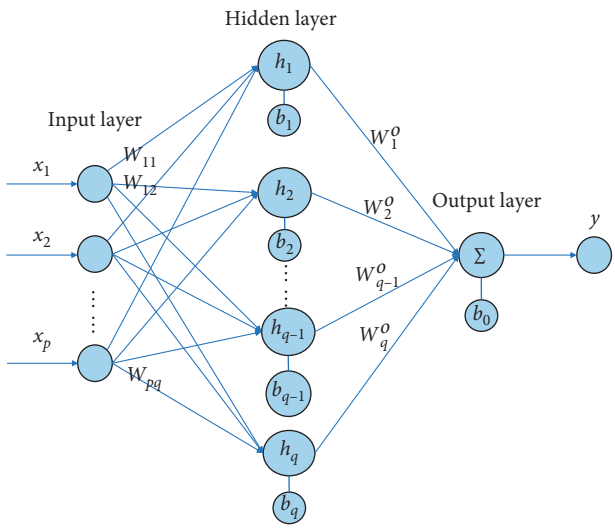

Figure 1: Architecture of a three-layer MLP.

$$c^*(s) = \operatorname{argmin}\left\{\sum (y - f(g((c \cdot x)w_I + b_I)w_O + b_O))^2\right\}, \quad \cdot\forall (x, y) \in \{X, Y\}$$

subject to

$$c_i \geq 0, \quad \sum_{i=1}^{p} c_i \leq s. \tag{5}$$

3. Development of GNNG-MLP Algorithm

3.1. Design of Global Optimization for MLP. In the study, a global optimization algorithm for MLP-based soft sensor, called GNNG-MLP, is proposed to reduce the redundancy of input and hidden layer simultaneously. The primary strategy of the proposed algorithm is to design a nonlinear quadratic optimization expression with NNG constraint that imposes the shrinkage coefficients on the input and hidden layers of MLP. The GNNG-MLP is implemented with the continuous adjustment of the garrote parameter. The schematic diagram of the proposed algorithm is illustrated in Figure 2, in which the nodes x_2 and h_2 have null impacts on the model and will be removed from the MLP. Meanwhile, the weight lines connected to them will also be invalid.

The proposed algorithm is divided into two phases. In the first phase, a well-trained MLP network is presented with the conventional MLP training algorithm. At the second phase, a set of shrinkage coefficients are imposed on input and hidden layer of the obtained MLP. Consequently, the expression of MLP is reformulated as follows:

$$y = f(g((c_I \cdot x)w_I + b_I)c_H \cdot w_O + b_O), \tag{6}$$

where $c_I = [c_1, c_2, \ldots, c_p]$ and $c_H = [c_1, c_2, \ldots, c_q]$ denote the shrinkage coefficients of the nodes of input and hidden layer, respectively. c_I^* and c_H^* are obtained by solving the following formula:

$$[c_I^*; c_H^*](s) = \operatorname{argmin}\left\{\sum (y - f(g((c_I \cdot x)w_I + b_I)c_H \cdot w_O + b_O))^2\right\}$$
$$\text{subject to} \quad c_i \geq 0, c_h \geq 0, \sum_{i=1}^{p} c_i + \sum_{j=1}^{q} c_h \leq s, \tag{7}$$

where $c_i^* = 0$ indicates that the input variable x_i is removed from the MLP and $c_h^* = 0$ means that the hidden node h_i is excluded from the model. Equation (7) is a nonlinear quadratic optimization problem with constraints that can be solved with trust-region reflective optimization algorithm [35]. After that, the optimal predictive model of MLP is presented by

$$\hat{y} = f(g((c_I^* \cdot x)w_I + b_I)c_H^* \cdot w_O + b_O). \tag{8}$$

3.2. Determination of Parameter s. The choice of parameter s is very important for the developed algorithm because it can directly affect the extent of shrinkage on the MLP structure. $s = 0$ implies that all input variables and hidden nodes will be eliminated. When $s \geq p + q$, all the input variables and the hidden nodes will be completely preserved. Therefore, the value of s directly determines the number of neurons and influences the performance of MLP. This paper adopts the enumeration approach to select the optimal s from the vector $S = [s_1, s_2, \ldots, s_u]$. Herein, s_1 is set to a constant close to zero, and s_u is set to $p + q$. The other values of S are equably distributed between s_1 and s_u.

In this paper, Hannan–Quinn information criterion (HQ) [36] that can balance the accuracy and complexity of a model is adopted as the model evaluation criterion that is formulated as

$$HQ = -2 \cdot ln \sum (\hat{y} - y)^2 + k \cdot ln(\ln n), \tag{9}$$

where n denotes the number of data samples, k represents the number of input variables, and y and $\hat{y}$ are the actual and predictive value of the output variable, respectively. Considering the randomness of ANNs, the V-fold cross-validation (CV) method is taken to validate the model. The execution is described as follows. Firstly, the group of all datasets is evenly separated into V subdatasets. Secondly, a single subdataset is taken as the validation dataset, and the other V-1 subdatasets are used as the training dataset to acquire the trained MLP. The procedure is repeated V times, and these V results are averaged to present the ultimate estimate. In this work, s is chosen by V-fold CV with HQ, whose pseudocode is shown in Algorithm 1.

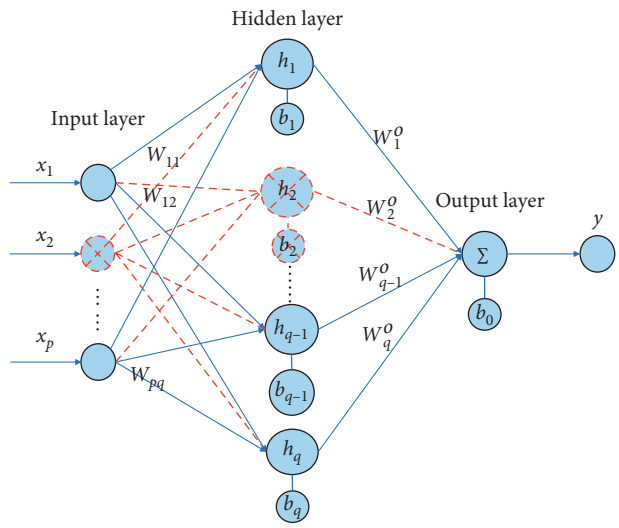

Figure 2: Schematic diagram of GNNG-MLP.

Input: dataset $\{X, Y\}$
Output: the optimal s^*
Begin Algorithm
Initialize $S = [s_1, s_2, \ldots, s_u]$;
Separate $\{X, Y\}$ into V disjoint subdatasets $\{X_1, Y_1\}, \{X_2, Y_2\}, \ldots, \{X_V, Y_V\}$;
For $i = 1$: u
$s = s_i$;
For $v = 1$: V
Train a new MLP network with dataset $\{X, Y\} = \{X, Y\} \backslash \{X_v, Y_v\}$;
Solve equation (7) with s to get c_I^*, c_H^*;
Get the new MLP by equation (8);
Compute the HQ(v) with validation dataset $\{X_v, Y_v\}$;
End for
CV_HQ(i) = mean (HQ);
End for
Output the optimal s^* with the minimum CV_HQ;
End Algorithm

Algorithm 1: Pseudocode of choice of s.

3.3. The Computational Procedure of Proposed Algorithm. In this paper, a global optimization algorithm for MLP is developed. The advancement of the proposed algorithm is that it not only deals with the redundancy of input variables but also simplifies the internal structure of MLP. The overall computation flow of the algorithm is described as follows:

Step 1. Initialization: get a trained MLP with the training dataset $\{X, Y\}$.

Step 2. Impose the NNG coefficients on the input and hidden nodes of the MLP.

Step 3. Perform Algorithm 1 to obtain the optimal s as s^*.

Step 4. Acquire the shrinkage coefficient c_I^* and c_H^* by solving equation (7) with parameter s^*.

Step 5. Updated weights of input and hidden nodes by substituting c_I^* and c_H^* into equation (8).

Step 6. Remove the columns whose corresponding coefficient $c_i^* = 0$ from $\{X, Y\}$, and delete the hidden nodes whose corresponding coefficient $c_h^* = 0$.

Step 7. Output the optimized MLP.

4. Simulation Results

4.1. Experimental Setting. In the paper, comprehensive simulations are implemented to verify the performance of the proposed algorithm, in which comparisons with other state-of-the-art variable selection algorithms such as SBS-MLP [37], NNGEO-MLP [29], and dLASSO-MLP [38] are performed. All algorithms are simulated under the same settings. The MLP structure in the case is a typical three-layer configuration, in which the activation function of hidden and output layer is hyperbolic tangent and linear, respectively. The initial number of hidden nodes is determined by

Table 1: The statistical results of artificial dataset.

	MLP	SBS-MLP	NNGEO-MLP	dLASSO-MLP	GNNG-MLP
MSE	0.1752	0.1653	0.1503	0.1223	0.1015
A_R^2	0.8979	0.9033	0.9105	0.9335	0.9437
Neurons	62	29.15	24.55	20.10	12
FS+	40	7.1500	2.9000	3.1000	0.4500
FS−	0	0	0.3500	0	0.1000

some trial runs. Training and testing data take up 80% and 20% of the overall dataset, respectively. 5-fold CV is employed in the algorithm. The performance of the involved algorithms is assessed with the following five measures.

(1) MSE: the mean square error between the predicted and the actual value with the testing dataset, $\mathrm{MSE} = 1/n \sum_{i=1}^{n} (y_i - \hat{y}_i)^2$.

(2) Adjusted R_Square (A_R^2): $\mathrm{A\_R}^2 = 1 - ((n-1) * \sum_{i=1}^{n} (y_i - \hat{y}_i)^2 / (n-p-1) * \sum_{i=1}^{n} (y_i - \overline{y_i})^2)$, where $\overline{y_i}$ is the mean value of output variable.

(3) Neurons: the total number of the input and hidden nodes in the optimized MLP.

(4) False-positive selection (FS+): the number of irrelevant variables included in the optimized MLP.

(5) False-negative selection (FS−): the number of relevant variables excluded from the optimized MLP.

4.2. Simulation Results of Artificial Dataset. In this subsection, a nonlinear model that was proposed in [28] is applied to generate artificial datasets. The input dataset X was produced from a multivariate normal distribution with covariance matrix Σ, in which covariance between two different variables (columns) $\sum_{i,j} = \rho^{|i-j|}$, $\forall i \neq j$. The mathematical expression of the model is

$$Y = \begin{cases} \sqrt{X_1\beta - 0.5} + \varepsilon, & X_1\beta \geq 0.5, \\ e^{X_1\beta + 0.5} + \varepsilon, & X_1\beta \leq 0.5, \end{cases} \tag{10}$$

where $X_1 \in \mathbb{R}^{1000\times 10}$ are relevant variables, ε is white Gaussian noise, and $\beta = [3.0, 1.5, 2.0, 4.0, 0.5, 1.3, -2.6, -3.5, -5.1, 2.0]^T$. Besides the relevant variables, irrelevant dataset $X_2 \in \mathbb{R}^{1000\times 40}$ is produced to make this case a problem of selecting 10 relevant variables out of 50 variables.

Table 1 presents the statistical results of artificial dataset with different algorithms after 20 runs. In this case, ρ of the covariance matrix is set to 0.8, which generates a dataset with a high correlation between different variables. According to the numerical comparison of MSE and A_R^2, the GNNG-MLP has the highest prediction accuracy among all algorithms. Furthermore, FS+ is the smallest, which indicates that the GNNG-MLP selects fewer irrelevant variables than other approaches. By comprehensively comparisons of FS+ and FS−, it is can be concluded that our algorithm could select relevant variables with more precision. Besides, statistical results of neurons show that GNNG-MLP can effectively remove the redundant nodes and then improve the performance of the model. It can be found from the results that our algorithm solves the problems of input variables and model redundancy simultaneously.

In addition, the capability of different algorithms is further compared by changing the value of collinearity ρ. Figure 3 shows the comparison of the five indicators with different ρs. It can be seen that the GNNG-MLP consistently yields the lowest MSE, meaning that our algorithm always has the best accuracy. The number of hidden layer nodes with GNNG-MLP is always the lowest, which proves the efficiency of reducing the redundancy with our approach. Moreover, our algorithm also performs the best on other indicators in most cases, which demonstrates that our algorithm has the best stability.

4.3. Application to an Actual Desulfurization Process of Power Plant. In this section, the developed algorithm was applied to forecast the SO_2 emissions from a desulfurization process of a thermal power plant in China. The structural diagram of the process is shown in Figure 4. This power plant adopts limestone-gypsum wet flue gas desulfurization technology, which includes SO_2 absorption system, flue gas system, and compressed air system. The technology mainly uses lime and limestone to absorb SO_2 by chemical reactions that are shown as follows:

$$SO_2 + CaO + \frac{1}{2}H_2O \longrightarrow CaSO_3 \cdot \frac{1}{2}H_2O \tag{11}$$

$$SO_2 + CaCO_3 + \frac{1}{2}H_2O \longrightarrow CaSO_3 \cdot \frac{1}{2}H_2O + CO_2 \tag{12}$$

The limestone slurry entering the primary absorption tower is dissolved in the absorption tower slurry pool. By adjusting the amount of limestone slurry entering the absorption tower or the concentration of the slurry discharged from the absorption tower, the pH value of the absorption tower slurry pool is maintained between 5.5 and 6.5 to ensure the limestone dissolution and SO_2 absorption. After the original flue gas first enters the primary absorption tower, it passes through the spray zone in countercurrent, is fully contacted with the slurry to absorb SO_2, and then enters the secondary absorption tower. The remaining SO_2 and other harmful components in the flue gas are absorbed in the spray zone. Finally, the dust is removed by a wet dust collector and discharged to the chimney. The two absorption towers adopt almost the same structure that is demonstrated in Figure 5.

Table 2 presents the statistical results of 20 runs with different soft sensor algorithms. It can be found that GNNG-MLP has better prediction accuracy with a smaller number

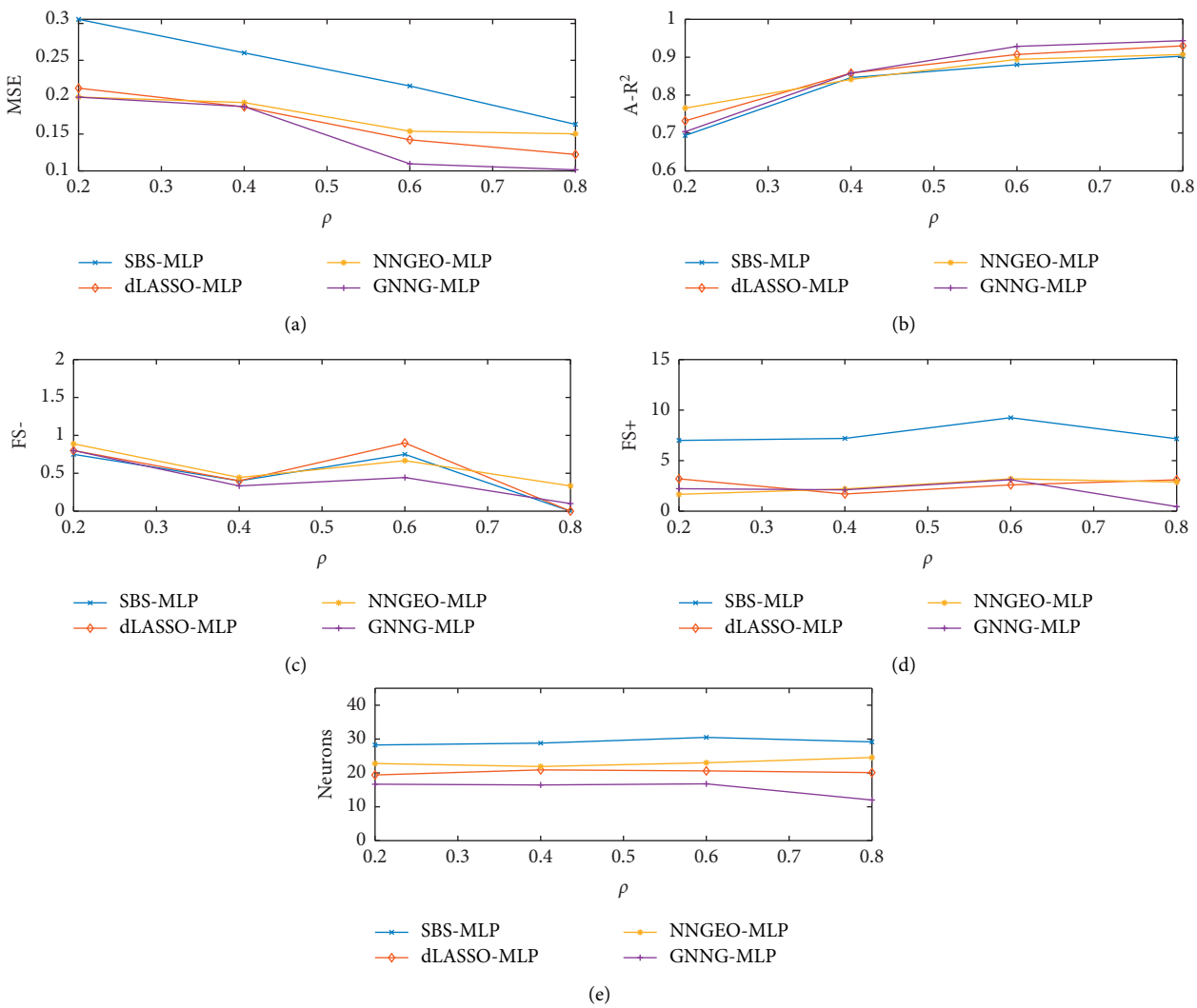

Figure 3: Comparison of performance with different ρs. (a) Comparison of MSE. (b) Comparison of FS. (c) Comparison of neurons. (d) Comparison of A-R^2. (e) Comparison of F5+.

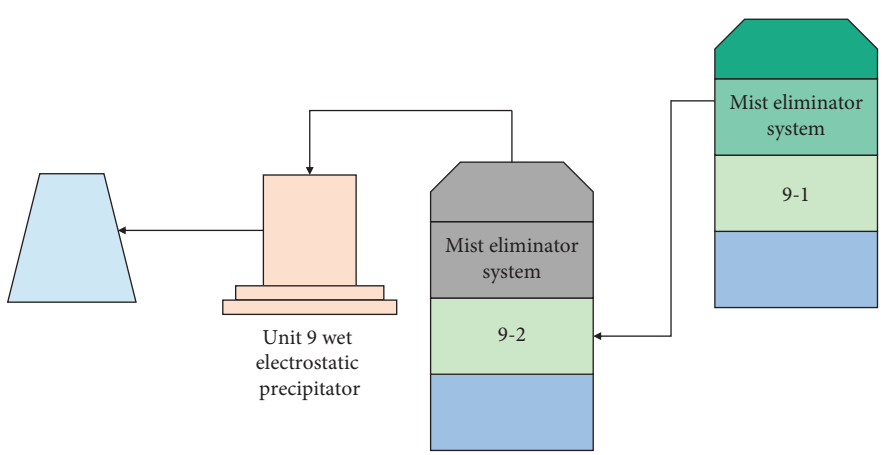

Figure 4: The framework of absorption system.

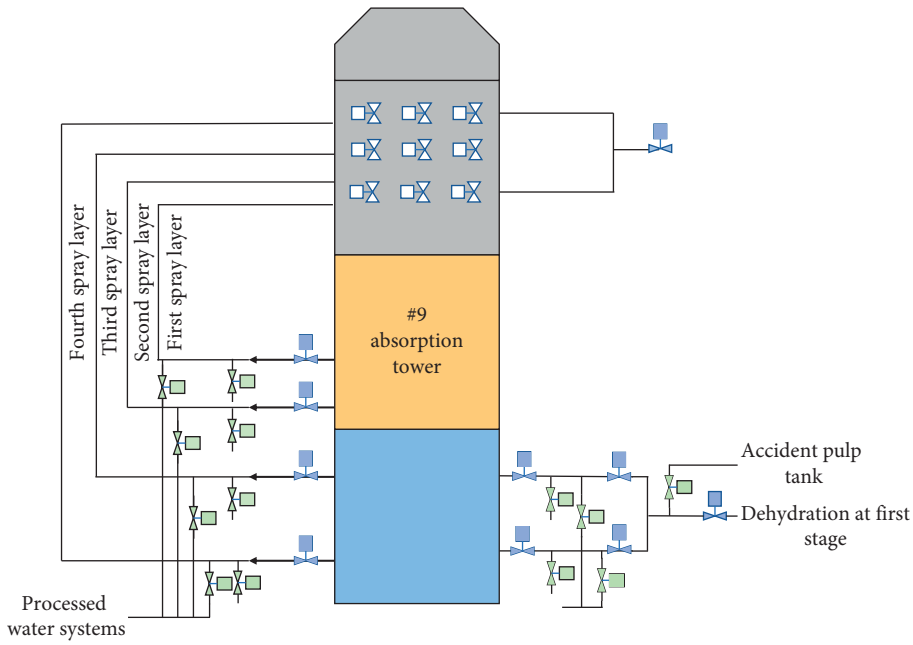

Figure 5: Schematic diagram of primary absorption tower.

Table 2: Statistical results for SO_2 concentration prediction.

	MLP	SBS-MLP	NNGEO-MLP	dLASSO-MLP	GNNG-MLP
Neurons	36	24	15	15	10
MSE	32.5388	7.2795	4.5729	3.3518	2.4640
A_R^2	0.1155	0.7105	0.8283	0.8895	0.9004

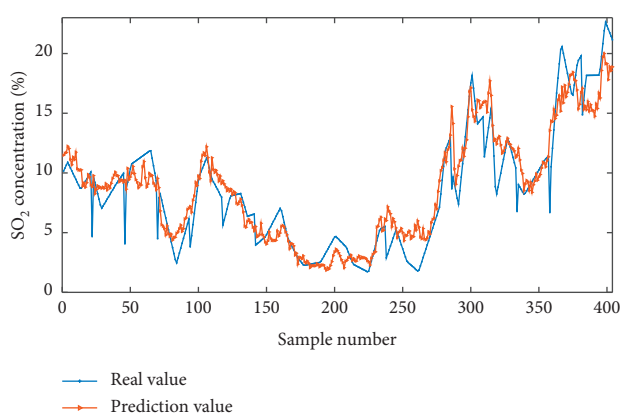

Figure 6: Measured and the predicted SO_2 concentration.

of neurons than other approaches. This result shows that GNNG-MLP can improve the accuracy of the model by simplifying the internal structure of the MLP.

Figure 6 shows the comparison of predictive and actual value of the target variable with our algorithm. Obviously, the proposed algorithm can effectively track the dynamic change of the target variable.

In order to further prove the accuracy of the proposed algorithm, error comparisons between the measured and the predicted SO_2 concentration with different algorithms are presented in Figure 7. The results show that the error of GNNG-MLP is the lowest and within the range [−4.2, 4.2] in most instances, which can meet the requirements of the field operating. The performance of the developed soft sensor is fully compliant with the standards of industry demand.

Besides, comparative analyses based on the statistical results of variable selection and the actual industrial operating experience are given. Figure 8 presents the frequency of input variable selection over 100 runs. It can be found from Figure 8 that variable 13 is included in all solutions, and variables 17 and 30 are selected more than 80 times.

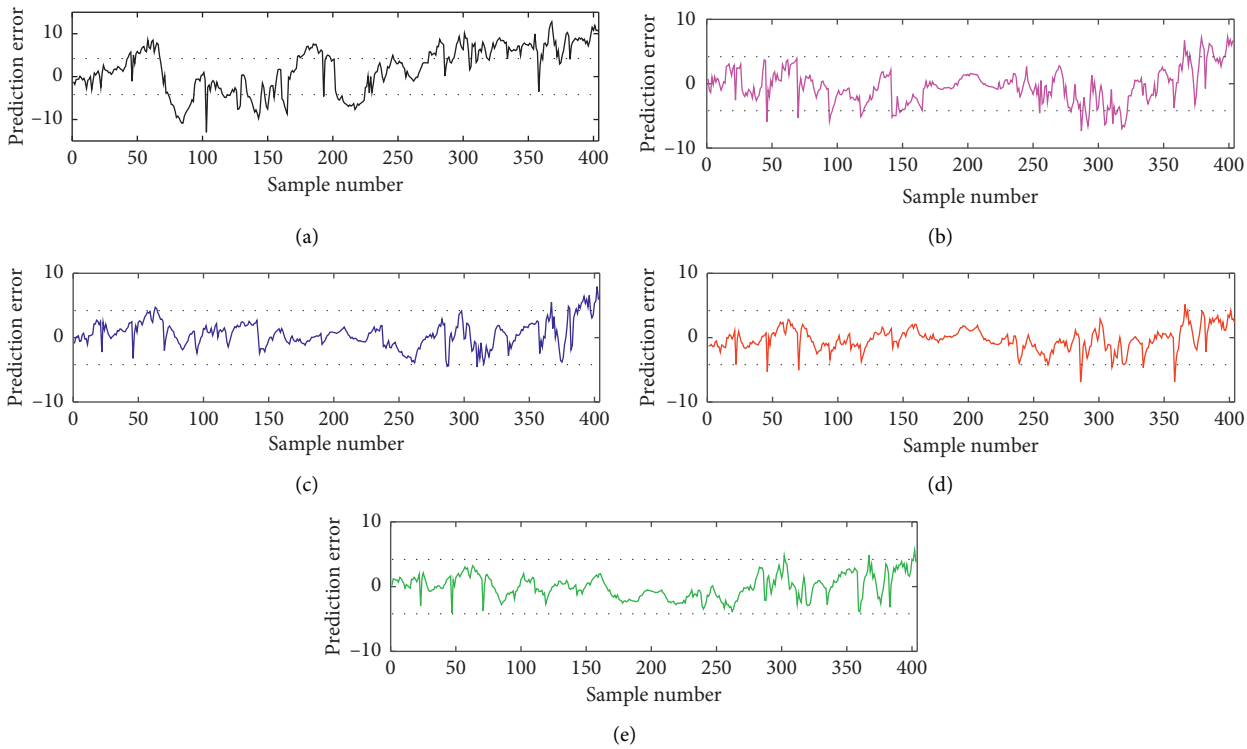

Figure 7: Comparison of prediction error with different algorithms. (a) MLP prediction error. (b) NNGEO-MLP prediction error. (c) GNNG-MLP prediction error. (d) SBS-MLP prediction error. (e) dLASSO-MLP prediction error.

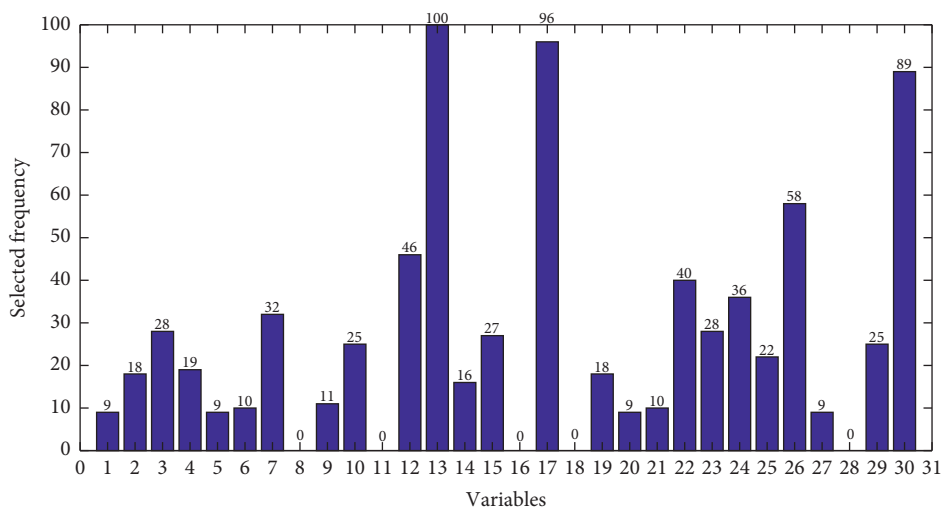

Figure 8: Variable selection frequency 100 runs by GNNG-MLP.

According to the statistics, the most relevant input variable to the output variable is variable 13. In terms of the manual book of the system, variable 13 is the SO_2 concentration of #9-1AT outlet's flue gas and the SO_2 concentration of #9-2AT inlet's flue gas. Obviously, this variable is highly related to the SO_2 concentration of final emission. Variable 17, that is, the limestone slurry to #9 AT flow, has 90% of selection frequency. It can be seen from formulas (11) and (12) that the CaO and $CaCO_3$ in limestone slurry can absorb the released SO_2. Therefore, variable 17 is included in the optimal solution. The variable 30 is the pH value of the slurry in the tower 9-2. The slurry absorbs more SO_2 when the SO_2 concentration in the flue gas is relatively high. As a result of this, a large amount of hydrogen ions will be generated, and the pH value will decrease.

5. Conclusions

This paper proposed a new optimization algorithm for MLP-based soft sensors with NNG. The advantage of this algorithm is that it can simultaneously perform the selection

of the input layer and the optimization of the hidden layer for MLP and therefore has more tendency to get the global optimal model. The simulation results on the artificial datasets demonstrate that GNNG-MLP has obvious advantages in both the number of neurons and the generalization performance of the model. In addition, the algorithm is applied to forecast the SO_2 emission in a desulfurization process to verify the reading of the online analyzer. Comprehensive results and comparisons prove that the developed soft sensor has remarkable model simplicity and accuracy. The proposed soft sensor can be further implemented for the optimization and control design of the desulfurization process.

Data Availability

The data used to support the findings of this study are currently under embargo, while the research findings are commercialized. Requests for data 24 months after publication of this article will be considered by the corresponding author.

Conflicts of Interest

The authors declare no conflicts of interest.

Acknowledgments

The work was supported by the Key Research and Development Program of Shandong Province (Grant no. 2019GGX104037).

References

[1] C. A. C. Belchior, R. A. M. Araújo, F. A. A. Souza, and J. A. C. Landeck, "Sensor-fault tolerance in a wastewater treatment plant by means of ANFIS-based soft sensor and control reconfiguration," *Neural Computing and Applications*, vol. 30, no. 5, pp. 3265–3276, 2018.

[2] X. Yuan, Z. Ge, Z. Song, Y. Wang, C. Yang, and H. Zhang, "Soft sensor modeling of nonlinear industrial processes based on weighted probabilistic projection regression," *IEEE Transactions on Instrumentation and Measurement*, vol. 66, no. 4, pp. 837–845, 2017.

[3] X. Yi, R. Guo, and Y. Qi, "Stabilization of chaotic systems with both uncertainty and disturbance by the UDE-based control method," *IEEE Access*, vol. 8, no. 1, pp. 62471–62477, 2020.

[4] Y. Calcada, "Development of an ANN-based soft-sensor to estimate the apparent viscosity of water-based drilling fluids," *Journal of Petroleum Science & Engineering*, vol. 150, pp. 69–73, 2017.

[5] L. Yao and Z. Ge, "Deep learning of semisupervised process data with hierarchical extreme learning machine and soft sensor application," *IEEE Transactions on Industrial Electronics*, vol. 65, no. 2, pp. 1490–1498, 2017.

[6] C. Cozin, F. E. C. Vicencio, F. A. de Almeida Barbuto et al., "Two-phase slug flow characterization using artificial neural networks," *IEEE Transactions on Instrumentation and Measurement*, vol. 65, no. 3, pp. 494–501, 2016.

[7] Z. Ge, "Review on data-driven modeling and monitoring for plant-wide industrial processes," *Chemometrics & Intelligent Laboratory Systems*, vol. 171, pp. 16–25, 2016.

[8] C. Shang, F. Yang, D. Huang, and W. Lyu, "Data-driven soft sensor development based on deep learning technique," *Journal of Process Control*, vol. 24, no. 3, pp. 223–233, 2014.

[9] R. Ouysse, "Bayesian model averaging and principal component regression forecasts in a data rich environment," *International Journal of Forecasting*, vol. 32, no. 3, pp. 763–787, 2016.

[10] P. Gottardo, M. Penasa, N. Lopez-Villalobos, and M. De Marchi, "Variable selection procedures before partial least squares regression enhance the accuracy of milk fatty acid composition predicted by mid-infrared spectroscopy," *Journal of Dairy Science*, vol. 99, no. 10, pp. 7782–7790, 2016.

[11] H. Zhang, S. Wang, D. Li, Y. Zhang, and J. Hu, "Edible gelatin diagnosis using laser-induced breakdown spectroscopy and partial least square assisted support vector machine," *Sensors*, vol. 19, no. 19, pp. 4225, 2019.

[12] B. Wang, S. Ch, S. Mathur, and J. Adamowski, "Estimation of in-situ bioremediation system cost using a hybrid Extreme Learning Machine (ELM)-particle swarm optimization approach," *Journal of Hydrology*, vol. 543, pp. 373–385, 2016.

[13] M. C. Xie, X. Han, S. Luan, L. I. Fang, and C. X. Wang, "Brain tumor segmentation using convolutional neural networks feature extraction in MRI images," *Journal of Qufu Normal University*, vol. 43, no. 9, pp. 1–10, 2019.

[14] M. Esmaeilpour, P. Cardinal, and A. Lameiras Koerich, "Unsupervised feature learning for environmental sound classification using Weighted Cycle-Consistent Generative Adversarial Network," *Applied Soft Computing*, vol. 86, pp. 105912, 2020.

[15] M. Jiao, D. Wang, and J. Qiu, "A GRU-RNN based momentum optimized algorithm for SOC estimation," *Journal of Power Sources*, vol. 459, pp. 228051, 2020.

[16] E. Heidari, M. A. Sobati, and S. Movahedirad, "Accurate prediction of nanofluid viscosity using a multilayer perceptron artificial neural network (MLP-ANN)," *Chemometrics and Intelligent Laboratory Systems*, vol. 155, pp. 73–85, 2016.

[17] Z. Shen, Y. Bi, Y. Wang, and C. Guo, "MLP neural network-based recursive sliding mode dynamic surface control for trajectory tracking of fully actuated surface vessel subject to unknown dynamics and input saturation," *Neurocomputing*, vol. 377, no. 15, pp. 103–112, 2020.

[18] Y. Wang and W. Gao, "Prediction of the water content of biodiesel using ANN-MLP: an environmental application," *Energy Sources, Part A: Recovery, Utilization, and Environmental Effects*, vol. 40, no. 8, pp. 987–993, 2018.

[19] X. Yuan, B. Huang, Y. Wang, C. Yang, and W. Gui, "Deep learning-based feature representation and its application for soft sensor modeling with variable-wise weighted SAE," *IEEE Transactions on Industrial Informatics*, vol. 14, no. 7, pp. 3235–3243, 2018.

[20] L. Liu, B. Li, and R. Guo, "Consensus control for networked manipulators with switched parameters and topologies," *IEEE Access*, vol. 9, pp. 9209–9217, 2021.

[21] K. Sun, S. H. Huang, S. H. Wong, and S. S. Jang, "Design and application of a variable selection method for multilayer perceptron neural network with LASSO," *IEEE Transactions on Neural Networks & Learning Systems*, vol. 28, no. 6, pp. 1386–1396, 2016.

[22] A. Rani, V. Singh, and J. R. P. Gupta, "Development of soft sensor for neural network based control of distillation column," *ISA Transactions*, vol. 52, no. 3, pp. 438–449, 2013.

[23] Z. Guo, W. Zhao, H. Lu, and J. Wang, "Multi-step forecasting for wind speed using a modified EMD-based artificial neural

network model," *Renewable Energy*, vol. 37, no. 1, pp. 241–249, 2012.

[24] E. Fock, "Global sensitivity analysis approach for input selection and system identification purposes-A new framework for feedforward neural networks," *IEEE Transactions on Neural Networks and Learning Systems*, vol. 25, no. 8, pp. 1484–1495, 2014.

[25] B.-H. Adil, G. Youssef, and E. Q. Abderrahim, "Hybrid method HVS-MRMR for variable selection in multilayer artificial neural network classifier," *International Journal of Electrical and Computer Engineering (IJECE)*, vol. 7, no. 5, pp. 2773–2781, 2017.

[26] J. F. D. Canete, P. D. Saz-Orozco, R. Baratti, M. Mulas, and A. Garcia-Cerezo, "Soft-sensing estimation of plant effluent concentrations in a biological wastewater treatment plant using an optimal neural network," *Expert Systems with Applications*, vol. 63, pp. 8–19, 2016.

[27] H. Sun, X. Deng, K. Wang, and R. Jin, "Logistic regression for crystal growth process modeling through hierarchical nonnegative garrote-based variable selection," *Iie Transactions*, vol. 48, no. 8, pp. 787–796, 2016.

[28] K. Sun, J. Liu, J.-L. Kang, S.-S. Jang, D. S.-H. Wong, and D.-S. Chen, "Development of a variable selection method for soft sensor using artificial neural network and nonnegative garrote," *Journal of Process Control*, vol. 24, no. 7, pp. 1068–1075, 2014.

[29] K. Sun, X. Wu, J. Xue, and F. Ma, "Development of a new multi-layer perceptron based soft sensor for SO2 emissions in power plant," *Journal of Process Control*, vol. 84, pp. 182–191, 2019.

[30] W. Pan, H. Dong, and Y. Guo, *DropNeuron: Simplifying the Structure of Deep Neural Networks*, vol. 12, pp. 160–172, 2016.

[31] S. K. Anbananthen, G. Sainarayanan, A. Chekima, and J. Teo, "Data mining using pruned artificial neural network tree (ANNT)," *Journal of Process Control*, vol. 1, pp. 1350–1356, 2006.

[32] P. Monika and D. Venkatesan, "DI-ANN clustering algorithm for pruning in MLP neural network," *Indian Journal of Ence & Technology*, vol. 8, no. 16, pp. 1, 2015.

[33] Y. Fan, B. Tao, Y. Zheng, and S.-S. Jang, "A data-driven soft sensor based on multilayer perceptron neural network with a double LASSO approach," *IEEE Transactions on Instrumentation and Measurement*, vol. 69, no. 7, pp. 3972–3979, 2020.

[34] L. Breiman, "Better subset regression using the nonnegative garrote," *Technometrics*, vol. 37, no. 4, pp. 373–384, 1995.

[35] T. F. Coleman and Y. Li, "An interior trust region approach for nonlinear minimization subject to bounds," *Siam Journal on Optimization*, vol. 6, no. 2, pp. 418–445, 1993.

[36] Y. Miche and A. Lendasse, "A faster model selection criterion for OP-ELM and OP-KNN: hannan-quinn criterion," *European Symposium on Esann*, vol. 9, pp. 177–182, 2009.

[37] E. Romero and J. M. Sopena, "Performing feature selection with multilayer perceptrons," *IEEE Transactions on Neural Networks*, vol. 19, no. 3, pp. 431–441, 2008.

[38] Y. Fan, B. Tao, Y. Zheng, and S.-S. Jang, "A data-driven soft sensor based on multilayer perceptron neural network with a double LASSO approach," *IEEE Transactions on Instrumentation and Measurement*, vol. 69, no. 7, pp. 3972–3979, 2019.

Hindawi
Mathematical Problems in Engineering
Volume 2021, Article ID 9965932, 14 pages
https://doi.org/10.1155/2021/9965932

Research Article

A Power Load Forecasting Model Based on FA-CSSA-ELM

Zuoxun Wang, Xinheng Wang, Chunrui Ma, and Zengxu Song

School of Electrical Engineering and Automation, Qilu University of Technology (Shandong Academy of Sciences), Jinan 250353, China

Correspondence should be addressed to Zuoxun Wang; wangzuoxun@126.com

Received 6 March 2021; Revised 30 March 2021; Accepted 10 April 2021; Published 24 April 2021

Academic Editor: Yi Qi

Accurate and stable power load forecasting methods are essential for the rational allocation of power resources and grid operation. Due to the nonlinear nature of power loads, it is difficult for a single forecasting method to complete the forecasting task accurately and quickly. In this study, a new combined model for power loads forecasting is proposed. The initial weights and thresholds of the extreme learning machine (ELM) optimized by the chaotic sparrow search algorithm (CSSA) and improved by the firefly algorithm (FA) are used to improve the forecasting performance and achieve accurate forecasting. The early local optimum that exists in the sparrow algorithm is overcome by Tent chaotic mapping. A firefly perturbation strategy is used to improve the global optimization capability of the model. Real values from a power grid in Shandong are used to validate the prediction performance of the proposed FA-CSSA-ELM model. Experiments show that the proposed model produces more accurate forecasting results than other single forecasting models or combined forecasting models.

1. Introduction

Nowadays, power loads have reached almost every corner of human society and have brought great convenience to mankind. And reasonable power loads planning will bring great convenience to human society, and wrong power loads planning will bring great loss to human society. Inaccurate power load forecasting will result in incorrect load planning and layout by the authorities. This will cause huge economic losses and wasted energy. Therefore, accurate forecasting of power loads has been a hot topic in power system planning. Since power loads cannot be stored on a large scale, this leads to low utilization of electric resources. Accurate power load forecasting results can provide correct feedback and decision-making for the power sector. It can also help achieve a reasonable dynamic balance between electricity production and electricity consumption. [1–5].

Initially, a series of traditional methods of forecasting power loads were proposed by many experts and scholars. Traditional methods include trend extrapolation [6, 7], exponential smoothing [8, 9], Kalman filtering [10], and ARIMA [11–13]. These traditional methods of forecasting electrical loads have the advantage of being simple to be calculated and easy to be implemented. However, traditional methods have the disadvantage of low prediction accuracy, which will cause management departments to be unable to make reasonable and accurate decisions. It also makes it difficult to play a key role in the planning and rational allocation of electrical loads.

With the continuous development of artificial intelligence, many researchers have realized the application potential of intelligent models in dealing with nonlinear and complicated problems. Elman proposed an intelligent model of the ELMAN [14]. Noble proposed an intelligent model of the support vector machine (SVM) [15]. Huang proposed an intelligent model of the extreme learning machine (ELM) [16]. Suykens and his partners proposed an intelligent model of the least squares support vector machine (LSSVM) [17]. Shi and his partners proposed an intelligent model of the recurrent neural networks (RNNs) [18].

Many experts have successfully applied intelligent models to complicated big data and nonlinear problems in power loads forecasting. A method of predicting short-term power loads using SVM had been proposed by Ye and his partners [19]. Using support vector machines can reflect the characteristics of important characteristics of power load to

establish a forecasting model. A new power load forecasting model had been proposed by Wei Li and his partners [20]. The training set was constructed using variational pattern decomposition, and then the decomposed data were fed into the ELM model to construct the prediction model. This forecasting model utilizes an extreme learning machine (ELM) combined with variational mode decomposition (VMD) to forecast power load models. An LSSVM-based model for power loads forecasting had proposed by Xuemei Li and his partners. The model was compared with a back propagation neural network (BPNN) and verified to have better prediction accuracy and generalization ability [21].

Nowadays, the prediction accuracy of a single intelligent forecasting model for power loads is no longer sufficient to meet the normal needs of the power system. So, many scholars have turned their attentions to swarm intelligence optimization algorithms [22]. The research shows that the swarm intelligence optimization algorithm has the characteristics of simple principle, easy realization, strong adaptability, and high efficiency. Therefore, swarm intelligence optimization algorithms are often used to optimize the parameters of a single power load forecasting model by scholars. Swarm intelligence optimization algorithms are mainly derived from the habits of organisms in nature. Although the capacity of a single individual is limited, populations can perform well when they work together. Common swarm intelligence optimization algorithms include the ant colony optimization (ACO) [23], the artificial bee colony algorithm (ABC) [24], the firefly algorithm (FA) [25], the bat algorithm (BA) [26], the cuckoo search (CS) [27], the grey wolf optimization (GWO) [28], the dragonfly algorithm (DA) [29], the whale optimization algorithm (WOA) [30], and the sparrow search algorithm (SSA). And SSA was a new swarm intelligence optimization algorithm proposed by Xue in 2020 [31].

As a result, a series of combinatorial models based on population intelligence optimization algorithms have been proposed by scholars to predict power loads. A method of forecasting short-term electricity loads using WOA optimized long- and short-term memory (LSTM) artificial neural networks was proposed by Haiyan [32]. A chaotic artificial bee colony algorithm to optimize the support vector regression (SVR) short-term power prediction model was proposed by Hong [33]. An improved grey wolf algorithm to optimize support vector machines for short-term power loads forecasting models was proposed by Jiang [34]. It can be found from the above research that the combined forecasting model can well meet the requirements of forecast accuracy and provide correct feedback and information for the power sector.

The SSA algorithm is a new swarm intelligence optimization algorithm, which simulates the foraging and antipredation behavior of sparrows, and is superior to particle swarm optimization (PSO) and GWO algorithms in terms of finding the best performance. The SSA algorithm, like other swarm intelligence algorithms, suffers from poor convergence accuracy and tends to fall into local optima. In this paper, Tent chaotic mapping is used to initialize the sparrow population. Chaos theory has been applied in many ways, especially to deal with nonlinear problems [35–38]. The initial population can be uniformly distributed in the solution space by using chaotic property. This will help the algorithm converge quickly and jump out of local optimality. And the firefly perturbation strategy is used to update the population position. The global optimization ability and convergence speed of the sparrow search algorithm are improved by using the characteristics of the firefly algorithm.

As a single-layer feedforward neural network (SLFN) [39], ELM has more powerful generalization ability than other traditional neural networks. And ELM is also faster than other neural network models while maintaining learning accuracy. This makes ELM ideal for problems with large amounts of data, such as power load forecasting. Therefore, the FA-CSSA algorithm is used to optimize the initial weights and thresholds of the ELM model. The powerful global search capability of the FA-CSSA algorithm is used to improve the generalization capability of the model and hence the predictive capability of the overall combined power loads forecasting model.

Therefore, this paper addresses the SSA algorithm, the ELM neural network model, and the FA-CSSA algorithm. A new FA-CSSA-ELM electric load forecasting model and the corresponding feedback mechanism for power supply are proposed. And the real load history data of a certain power grid in Shandong is used as the simulation data to verify the prediction performance of the model. In order to better illustrate the excellent performance and accuracy of the FA-CSSA-ELM combined power load forecasting model, in this paper, the prediction results are compared and discussed with those of three single prediction models and two combined prediction models, respectively. The results demonstrate that the FA-CSSA-ELM power load model possesses better prediction accuracy than the other five models.

2. Chaotic Sparrow Algorithm Improved by Firefly Algorithm

2.1. Sparrow Search Algorithm. The SSA algorithm is made up of three components: a spotter, a tracker, and a vigilante. Suppose there are N sparrows in a D-dimensional space. Then, the sparrow flock can be expressed as the following equation:

$$X = \left[x_1, \ldots, x_2, \ldots, x_N\right]^T. \tag{1}$$

Then, the position of the i-th sparrow in the D-dimensional search space can be expressed as the following equation:

$$X_i = \left[x_{i1}, \ldots, x_{id}, \ldots, x_{iD}\right], \tag{2}$$

where x_{id} is the position of the i-th sparrow in dimension d. So, the position update formula can be expressed as the following equation:

$$x_{id}^{t+1} = \begin{cases} x_{id}^{t} \cdot \exp\left(\dfrac{-i}{\partial \cdot T}\right), & R_2 < ST, \\ x_{id}^{t} + Q \cdot L, & R_2 \geq ST, \end{cases} \tag{3}$$

where t denotes the current number of iterations, T denotes the maximum number of iterations, ∂ is the random number between $[0, 1]$, Q is a random number subject to a normal distribution, L is a matrix of $1 \times d$ whose elements are all 1, R_2 denotes a guard value, ranging from $[0, 1]$, and ST is a safe value, ranging from $[(1/2), 1]$.

It is generally assumed that discoverers make up about 10–20% of the population, with the rest belonging to trackers. The tracker's position update formula can be expressed as the following equation:

$$x_{id}^{t+1} = \begin{cases} x_{id}^{t} \cdot \exp\left(\dfrac{xw_d^t - x_{id}^t}{i^2}\right), & i > \dfrac{n}{2}, \\ xb_d^{t+1} + \dfrac{1}{D}\displaystyle\sum_{d=1}^{D}\left(\text{rand}\{-1, 1\} \cdot \left|x_{id}^t - xb_d^{t+1}\right|\right), & i \leq \dfrac{n}{2}, \end{cases} \tag{4}$$

where xw_d^t denotes the worst position in dimension d of the t th iteration and xb_d^{t+1} denotes the best position. When $i > (n/2)$, it means that the population is short of food and needs to go elsewhere to forage. When $i \leq (n/2)$, it means that the tracker is predating near the optimal position xb.

The last guards are used for vigilant reconnaissance of the population and number 10–20% of the total population. Its position update formula can be expressed as the following equation:

$$x_{id}^{t+1} = \begin{cases} xb^t + \beta\left(x_{id}^t - xb_d^t\right), & f_i \neq f_g, \\ x_{id}^t + K\left(\dfrac{x_{id}^t - xw_d^t}{|f_i - f_w| + \mu}\right), & f_i = f_g, \end{cases} \tag{5}$$

where β is the step control parameter, a normally distributed random number with a mean of 0 and a variance of 1, K is a random number between $[-1, 1]$, μ is a very small constant that prevents the denominator from going to zero; here, in this paper, we take $10E-8$, and f_i is the current fitness, f_g is the best fitness, and f_w is the worst fitness.

The flowchart of sparrow algorithm operation is shown in Figure 1.

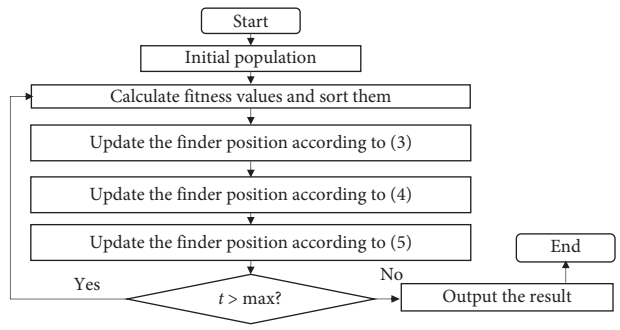

Figure 1: Flow chart of SSA algorithm operation.

2.2. Extreme Learning Machine. The extreme learning machine is an SLFN with faster learning speed and higher generalization capability. Assume that any N different training set (x_j, t_j), $x_j \in R^d, t_j \in R^m$, the mathematical model of SLFN with n hidden nodes can be defined as

$$\sum_{i=1}^{n} \beta_i g_i\left(x_j\right) = \sum_{i=1}^{n} \beta_i G_i\left(a_i, b_i, x_j\right), \quad j = 1, 2, \ldots, N, \tag{6}$$

where a_i is the vector of weights connecting the i-th hidden node to the input node, b_i is the threshold value of the i-th hidden node, β_i is the weight vector connecting the i-th hidden node to the output node, $g_i(x_j) = G_i(a_i, b_i, x_j)$ is the output function of the i-th hidden node, and $g(\bullet)$ is the sigmoid activation function.

Since SLFN can approach these N training samples with zero error, equation (6) can be further defined as the following equation:

$$\sum_{i=1}^{n} \beta_i G_i\left(a_i, b_i, x_j\right) = t_j, \quad j = 1, 2, \ldots, N, \tag{7}$$

where t_j is the output function. In addition, equation (7) can compactly express N equations as equation (8) which is given as follows:

$$H\beta = T, \tag{8}$$

$$H = \begin{bmatrix} G(a_1, b_1, x_1) & \cdots & G(a_n, b_n, x_1) \\ \vdots & \cdots & \vdots \\ G(a_1, b_1, x_N) & \cdots & G(a_n, b_n, x_N) \end{bmatrix},$$
$$\beta = \begin{bmatrix} \beta_1 \\ \vdots \\ \beta_n \end{bmatrix}_{n \times m}^{T}, \tag{9}$$
$$T = \begin{bmatrix} t_1 \\ \vdots \\ t_N \end{bmatrix}_{n \times N}^{T},$$

where H is the hidden layer output matrix of the network. SLFN has been shown to have universal approximation capability, and ELM network training process can be summarized as a nonlinear optimization problem. Its input weight a_i and hidden threshold b_i can be assigned randomly. Training SSFN is equivalent to finding the least squares solution $\widehat{\beta}$ for the linear system $H\beta = T$. The mathematical model of the least squares solution can be defined as

$$\widehat{\beta} = H^{+}T, \tag{10}$$

where H^{+} is the Moore–Penrose generalized inverse of the hidden layer output matrix and T is the expected output matrix.

2.3. Other Recommendations. In this paper, the SSA algorithm is optimized by Tent chaotic mapping strategy and firefly perturbation strategy, and an improved firefly chaotic sparrow algorithm is proposed. The FA-CSSA model uses the chaotic properties of the Tent mapping to initialize the population. The chaotic nature of the Tent mapping is used to make the initial population uniformly distributed in the solution space. And the firefly algorithm is used to update the optimal sparrow and sparrow flock position based on the principle that the fireflies with higher brightness in the search space can attract the fireflies with lower brightness to approach. Therefore, the chaotic mapping and firefly disturbance strategy can make up for the shortcomings of the SSA algorithm that it is easy to fall into the local optimum and can enhance the algorithm's global optimization ability and robustness.

2.3.1. Tent Chaos Mapping Strategy. It has been found that the goodness of the initial population profoundly affects the convergence process of the swarm intelligence optimization algorithm [39]. The SSA algorithm is a new swarm intelligence optimization algorithm proposed in 2020. Therefore, the SSA algorithm also suffers from the fact that the initial populations cannot be uniformly distributed in the solution space. This can lead to a lack of population diversity in the processing of the algorithm. So, the SSA algorithm has the disadvantage of low solution efficiency and insufficient global optimization capability when solving complex optimization problems.

As chaos is nonlinear, random, and ergodic [40], it can well allow the initial population to be traversed within the entire space. Therefore, this paper uses the strategy of chaotic mapping to initially optimize the SSA algorithm. In contrast to other types of chaotic mappings, the Tent chaotic mapping has a simple structure and the mapping presents a more uniform density. Tent chaos mapping distribution is shown in Figure 2, and Tent chaos mapping bifurcation diagram is shown in Figure 3. This indicates that Tent chaotic mappings have strong chaotic properties, ergodicity, and iteration speed. Therefore, this paper chooses the Tent chaotic map to avoid the SSA algorithm from falling into the local optimum in the iterative process.

Let the chaotic time series in the space of D dimensions be $x = \{x_n, n = 1, 2, \ldots, D\}$, and the Tent chaos mapping can be expressed as the following equation:

$$x_{n+1} = \begin{cases} 2x_n, & 0 \le x_n < 0.5, \\ 2(1 - x_n), & 0.5 \le x_n \le 1. \end{cases} \tag{11}$$

2.3.2. Firefly Disturbance Strategy. In the firefly disturbance strategy [25], the main purpose of the light emitted by fireflies is to act as a light-signal system to attract other individual fireflies. And all fireflies follow the following three points:

(1) All fireflies are attracted to fireflies that are brighter than them.

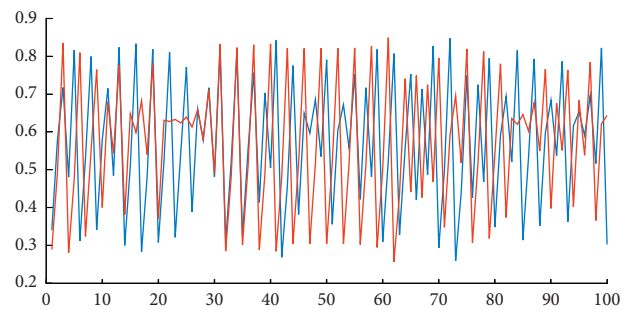

Figure 2: Tent chaos mapping distribution.

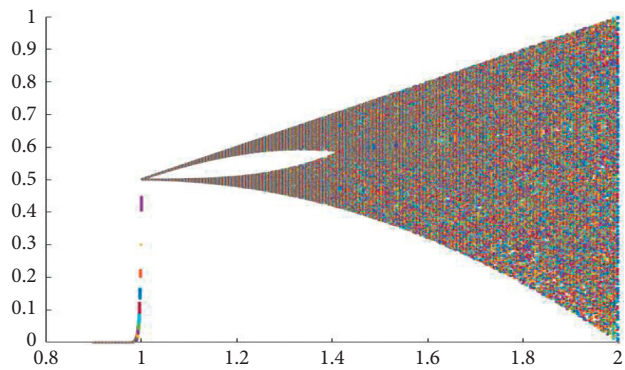

Figure 3: Tent chaotic mapping bifurcation diagram.

(2) The attractiveness of fireflies is directly proportional to their brightness. When a firefly approaches a firefly that is brighter than itself, the firefly's brightness decreases with distance.

(3) If no brighter firefly is found than the given one, then it will move randomly.

So, the formula for the relative luminosity of fireflies can be expressed as follows:

$$I = I_0 * e^{-\gamma r_{i,j}}. \tag{12}$$

The formula for the attractiveness of fireflies can be expressed as follows:

$$\beta = \beta_0 * e^{-\gamma r_{i,j}^2}. \tag{13}$$

The formula for updating the position of a firefly can be expressed as follows:

$$x_i(t+1) = x_i + \beta \times \left(x_j - x_i\right) + \alpha \times (\text{rand} - 0.5), \tag{14}$$

where I_0 is the maximum brightness of the firefly and proportional to the objective function value, γ is the light intensity absorption parameter, $r_{i,j}$ is the distance between fireflies i and j and is the maximum attraction, x_i and x_j are the spatial locations where fireflies i and j are located, respectively, α is a step factor in the range $[0, 1]$, and rand is a random number between $[0, 1]$.

The firefly perturbation strategy is used to update the positions of the optimal sparrows and sparrow flocks to improve the search capability of the algorithm. Finally, the

sparrow positions after the firefly perturbation strategy are compared with the sparrow positions without the firefly perturbation strategy. If the result is better, the sparrow positions are updated.

So, the flow chart of the operation of the FA-CSSA algorithm improved according to the Tent chaos mapping strategy and the firefly perturbation strategy is shown in Figure 4.

3. FA-CSSA-ELM Power Load Forecasting Model and Feedback Mechanism

3.1. The FA-CSSA-ELM Power Load Forecasting Model. The FA-CSSA algorithm is used to optimize the initial weights and thresholds of the ELM model to construct the FA-CSSA-ELM power load prediction model. The FA-CSSA algorithm has strong global search ability, which can improve the generalization ability of the model. And it can further improve the forecasting capability of the FA-CSSA-ELM power load forecasting model.

The specific forecasting steps of the FA-CSSA-ELM power load forecasting model can be expressed as follows:

(1) Divide the validation data into datasets and test sets.

(2) Construct the FA-CSSA-ELM prediction model. The SSA algorithm optimized by chaos mapping strategy and firefly disturbance strategy is used to find the optimal initial weight and threshold of the ELM model.

(3) The real historical data of a certain power grid in Shandong were used to verify the prediction performance of the FA-CSSA-ELM model and other comparison prediction models, and four performance index functions were used as qualitative comparison standards.

(4) The FA-CSSA-ELM power load forecasting model proposed is applied to the real power load transmission process. The accurate forecasting capability of the FA-CSSA-ELM load forecasting model is used to forecast real power load data. The forecast trends and results are used to provide feedback on the electricity consumption of each region to ensure maximum utilization of the electricity load. This can better achieve the purpose of saving energy and reducing consumption and reducing economic losses.

3.2. The Evaluation Functions. In order to judge the prediction effect of different competitive models more accurately and comprehensively, in this paper, the root mean square error (RMSE), mean absolute percentage error (MAPE), mean square error (MSE), and mean absolute error (MAE) are used to verify the results. Moreover, RMSE is highly sensitive to the accuracy of the prediction. MAPE is highly expressive of the prediction. The four evaluation functions are shown in Table 1.

3.3. Power Load Feedback System for Forecasting Models. Typically, the power load transmission process in this paper is shown in Figure 5. Firstly, the power plant transmits the power load through the 220 kV high-voltage transmission line to the first-stage substation for the first power load conversion. Then, the converted power load is transmitted through the 110 kV high-voltage transmission line to the secondary substation for the second power conversion. Finally, the power load of the second conversion will be transmitted to each electricity place. The proposed FA-CSSA-ELM power load prediction model is applied to the power load conversion process of the first-stage substation. Through real-time data update and accumulation in various places, the model can be continuously learned and updated, and the prediction accuracy of the model can be continuously improved, and the dynamic balance of power generation and power supply can be achieved. In this way, relevant departments can accurately predict the changing trend of power load and accurate power load value according to the history of power load. Through accurate prediction, we can not only give reasonable suggestions and guidance to relevant departments but also make the power load distribution more reasonable and maximize the use of power resources.

4. Simulation Experiments

In order to better verify the predictive performance of the FA-CSSA-ELM model proposed in this paper, the combined forecasting model FA-CSSA-ELM is compared with single competing models such as ELMAN, ELM, and SVM. In order to give a more comprehensive picture of the forecasting performance of the proposed FA-CSSA-ELM model, this paper also compares it with the two combined competing models WOA-ELM and PSO-ELMAN. The simulation experimental part consists of two parts: the data description section and the simulation experimental section. The data description section introduces the data used in the simulation experiments, as well as the specific way of dividing the training set and the test set. The experimental part consists of two parts, Experiment I and Experiment II, describing the specific steps of the predicted performance tests and analyzing the results of the simulated experiments.

4.1. Data Description Section

4.1.1. Presentation of Simulation Data. This paper uses real electrical load history data of four weeks from a power grid in Shandong in 2020 as simulation data. In order to predict the electrical load data more accurately, the frequency interval for collection in this paper is 5 minutes. A total of 8064 electrical load history data were measured for 288 electrical load history data per day. The power load time series is shown in Figure 6.

From Figure 6, this paper shows that the power load data are highly nonlinear and regular.

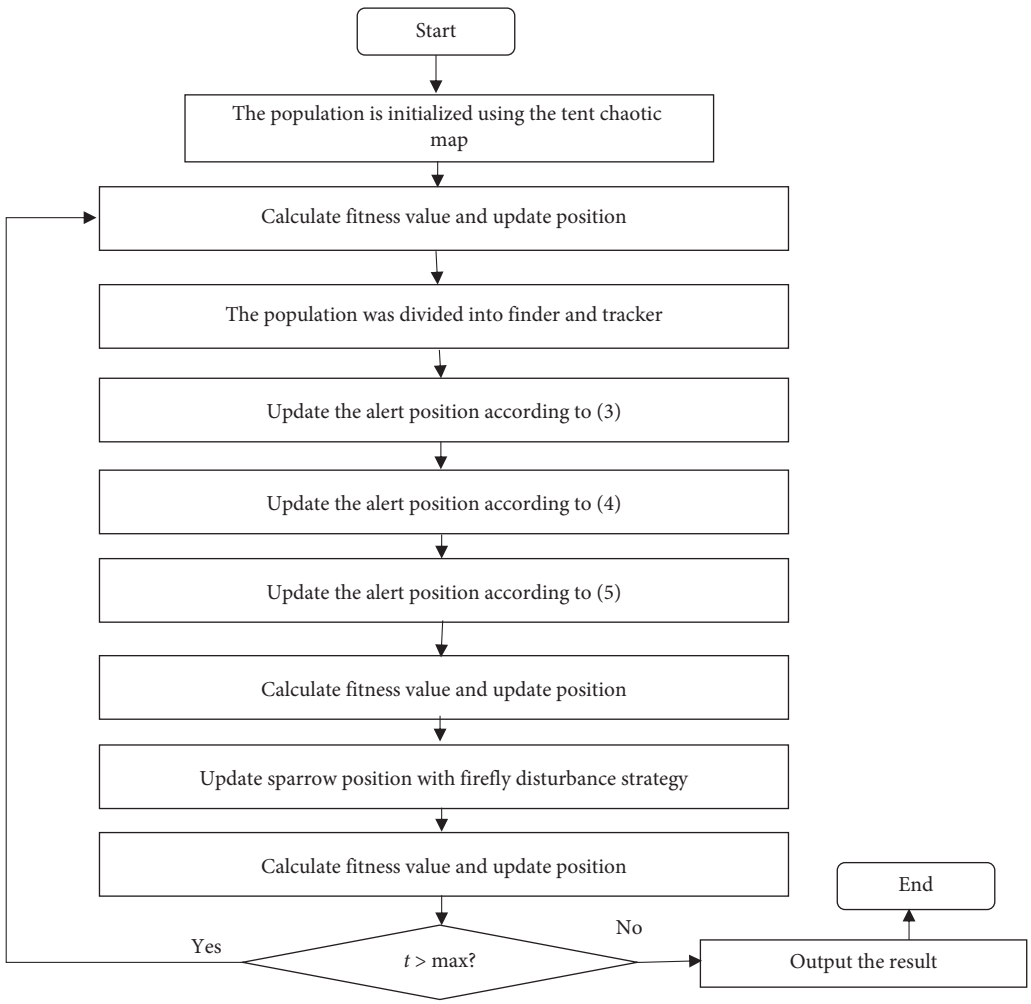

Figure 4: Flow chart of the FA-CSSA algorithm operation.

Table 1: Four types of evaluation functions.

Metrics	Definition	Equation
RMSE	The square root of average of the error squares	$\mathrm{RMSE} = \sqrt{(1/N)\sum_{i=1}^{N}(t_i - p_i)^2}$
MAPE	The average of absolute percentage error	$\mathrm{MAPE} = (100\%/N)\sum_{i}^{N}\lvert(t_i - p_i/t_i)\rvert$
MSE	The square root of the mean of the sum of squares of the errors	$\mathrm{MSE} = (1/N)\sum_{i=1}^{N}(t_i - p_i)^2$
MAE	The average value of the absolute error between the observed value and the true value	$\mathrm{MAE} = (1/N)\sum_{i=1}^{N}\lvert t_i - p_i\rvert$

t_i: i-th sample of expected output; p_i: i-th sample of predicted output; N: sample size.

4.1.2. Division of the Dataset. The dataset is divided into two sections: the training set and the test set. The training set is used to learn and train the model, and the test set is used to verify the training effect of the model. In order to make the distribution of power loads more rational and the forecasts more accurate, in this paper, the measured 8064 real power load history data of a power grid in Shandong Province were divided into 7 time series of data subsets. The 7 data subsets are created in the chronological order from Monday to Sunday. Each time series was recorded every 5 minutes for a total of 4 days. Each day has 288 data, and each set has 1152 data. By dividing the data in this way, the prediction units in this paper have been refined from months or weeks to a specific day. This not only improves the accuracy and relevance of the model predictions but also provides more reasonable suggestions for the allocation of power loads.

This paper divides the 8064 historical power load data into 7 subsets from Monday to Sunday. So, each subset has 1152 power load history data. In this paper, the data from the first three weeks are used as the test set data and the data from the last week are used as the validator data. For example, the test set for the first subset is the data for each Monday of the first three weeks, and the validator data are the data for Monday of the fourth week. The test set for the second subset is the data from Tuesday of the previous three weeks, and the validator data are the data from Tuesday of the fourth week. The remaining subsets of test and validation sets are divided according to this pattern.

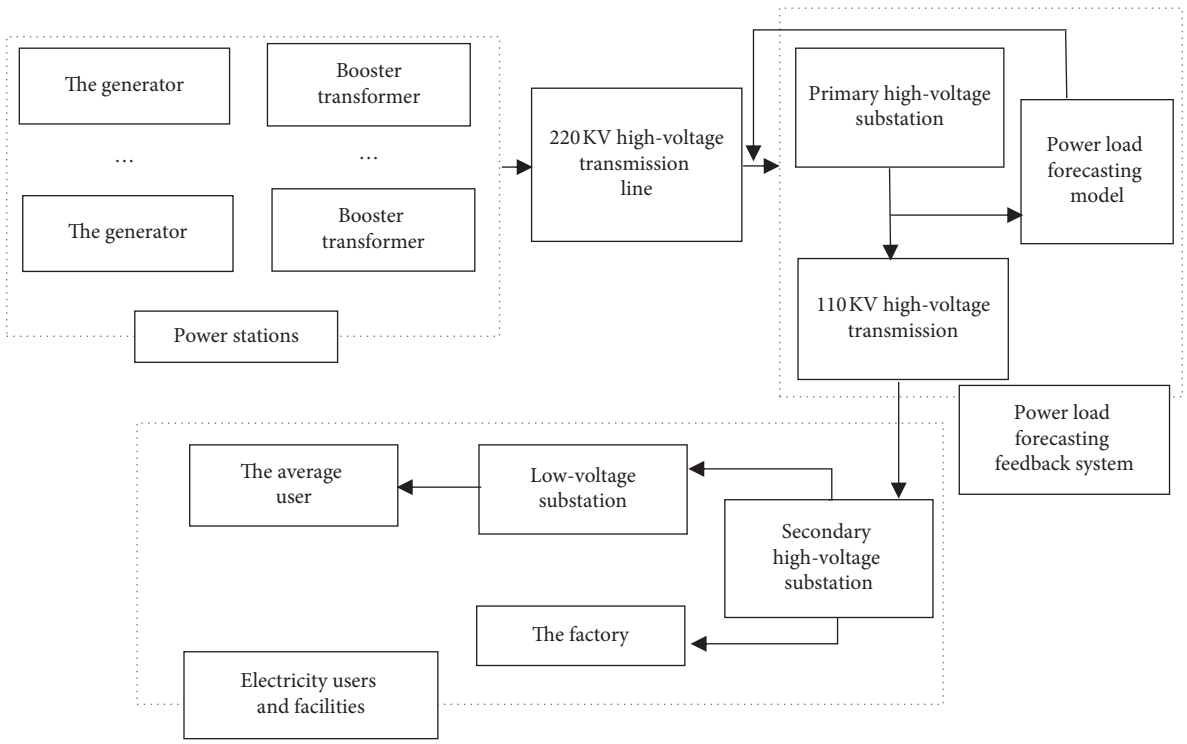

Figure 5: Electric load transfer process.

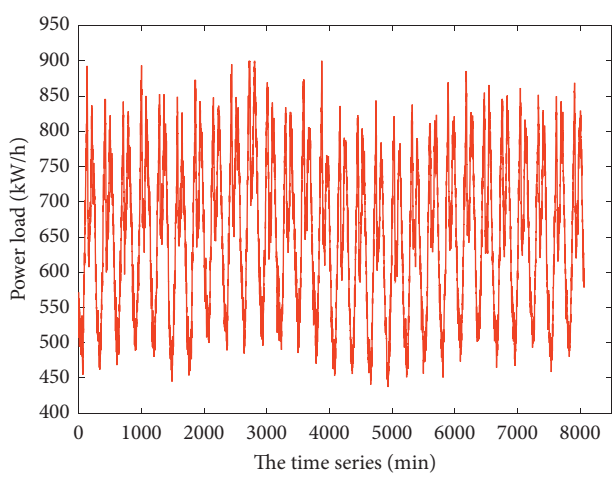

Figure 6: Real power load data for a grid in Shandong.

4.2. Simulation Experiments Section. The experimental simulation part introduces the prediction effect comparison between the FA-CSSA-ELM prediction model proposed in this paper and other competitive models.

4.2.1. Experiment I. The purpose of Experiment I is to compare the performance of the FA-CSS-ELM model with that of the single prediction model. And the single prediction models include ELMAN, ELM, and SVM. In order to make the data more accurate and representative, the data in the tables of this paper are calculated by averaging 20 operations. The metrics of the four evaluation functions compared with the single competing model are shown in Table 2 (the best data are highlighted in this paper).

A comparison of the data for the four indicators from the FA-CSSA-ELM model proposed in this paper with the single-competition model is shown in Table 2. The FA-CSSA-ELM model is the most effective, followed by the ELM single-competition model. And the SVM single prediction model is the least effective. Through data comparison, we can find that the FA-CSA-ELM model is superior to the single prediction model in all indicators. For a more visual observation, a histogram of the mean of the evaluation functions for these seven datasets is also plotted in this paper to represent it. And the histogram is shown in Figure 7.

Table 2: Experiment I: comparison of data with the evaluation function of a single competitive model.

Data	MSE	MAPE	RMSE	MAE
Monday				
ELMAN	1.5202	3.1632	3.1632	20.5353
ELM	0.9305	1.9381	1.9381	12.6597
SVM	5.7933	13.0061	13.0061	80.9685
FA-CSSA-ELM	0.77477	1.6099	1.6099	9.8266
Tuesday				
ELMAN	1.4905	3.1364	3.1364	20.2276
ELM	6.307	2.2570	2.2570	13.8804
SVM	5.7933	13.9705	13.9705	88.3321
FA-CSSA-ELM	0.8733	1.8208	1.8208	12.3912
Wednesday				
ELMAN	2.4602	5.1642	5.1642	33.698
ELM	1.3248	2.7226	2.7226	17.6342
SVM	5.307	10.9705	10.9705	67.3321
FA-CSSA-ELM	1.061	2.2299	2.2299	14.6999
Thursday				
ELMAN	1.8634	3.977	3.977	25.2004
ELM	1.3149	2.8083	2.8083	18.0642
SVM	6.3128	14.2424	14.2424	89.8527
FA-CSSA-ELM	1.118	2.3729	2.3729	15.6980
Friday				
ELMAN	1.3959	3.0618	3.0618	19.5877
ELM	1.0001	2.201	2.201	13.9655
SVM	5.7571	12.6769	12.6769	80.5392
FA-CSSA-ELM	0.7942	1.8056	1.8056	11.7099
Saturday				
ELMAN	1.674	3.646	3.646	23.0146
ELM	1.1409	2.4056	2.4056	15.4727
SVM	5.7579	13.1629	13.1629	83.5783
FA-CSSA-ELM	1.0377	2.2249	2.2249	14.5872
Sunday				
ELMAN	1.6556	3.536	3.536	22.5124
ELM	1.9696	2.4904	2.4904	15.9062
SVM	5.7579	13.1629	13.1629	83.5783
FA-CSSA-ELM	1.0326	2.1783	2.1783	14.0861

A comparison of the different competition model performance metric functions in Figure 7 shows that the FA-CSSA-ELM improved 72.29%, 99.8%, and 478.2% in MSE metrics compared with the other three single prediction models ELMAN, ELM, and SVM, respectively. The FA-CSSA-ELM improved by 80.3%, 18%, and 540% in the MAPE metric compared with the remaining three single prediction models ELMAN, ELM, and SVM, respectively. In the RMSE metric, the improvement is 77.8%, 14%, and 488% compared with the other three single forecasting models ELMAN, ELM, and SVM, respectively. In terms of MAE metric, the improvement is 77.2%, 15.6%, and 517% for ELMAN, ELM, and SVM, respectively. From the comparison data, the FA-CSSA-ELM model proposed in this paper is much more effective than the three representative single forecasting models compared.

4.2.2. Experiment II. The purpose of Experiment II is to compare the FA-CSSA-ELM model with other representative combinatorial competition models. The combined prediction models include WOA-ELM and PSO-ELMAN. In this paper, four performance indicators are used to verify the superiority of the model. And the evaluation function pairs of the three competitive models are shown in Table 3 (the best data are marked in bold in this paper). For a more intuitive view, a histogram of the mean values of the four evaluation functions for these seven datasets is also plotted in this paper. The histogram is shown in Figure 8.

It is shown in Figure 8 and Table 3 that the FA-CSSA-ELM prediction model proposed has superiority in all evaluation indicators, and it is more stable and has accurate prediction results in this paper. The PSO-ELMAN combined model, on the other hand, has the least satisfactory evaluation indexes and the lowest prediction accuracy. Although the WOA-ELM competition model also has excellent prediction results, it still does not surpass the FA-CSSA-ELM prediction model in the comparison of various evaluation indicators. Compared with the WOA-ELM model and PSO-ELMAN model, the MSE index of the FA-CSSA-ELM model increased by

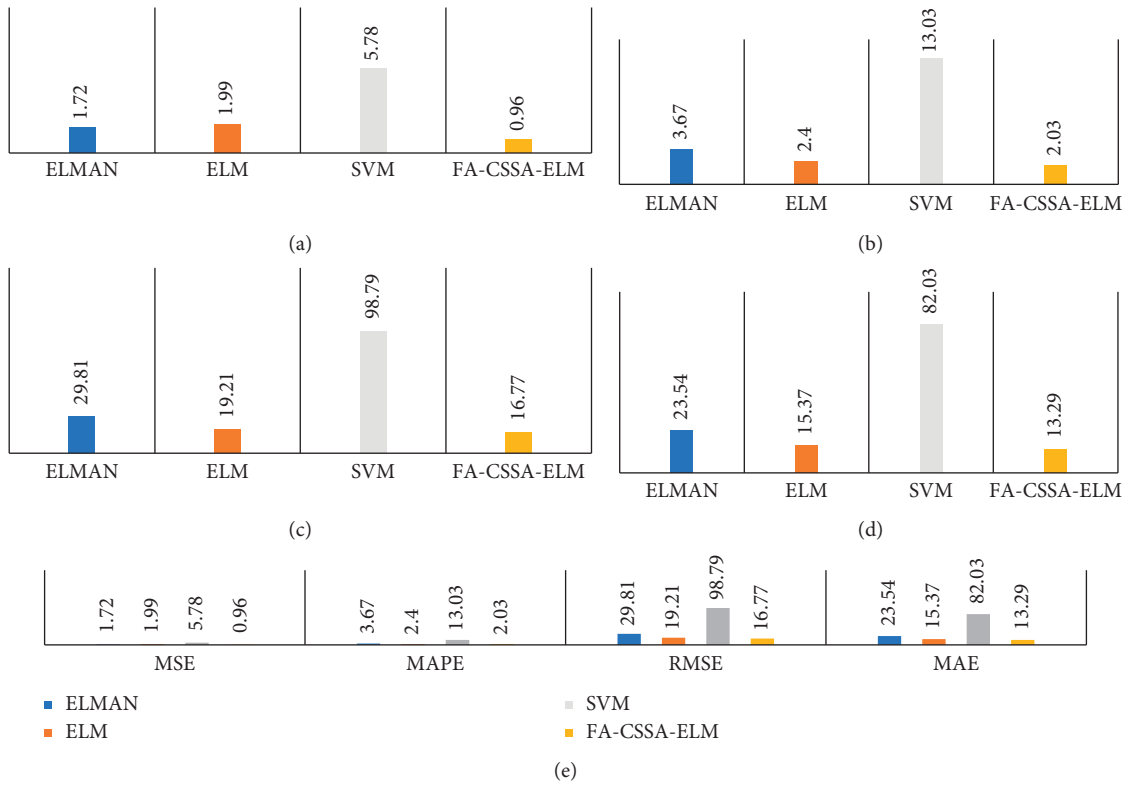

Figure 7: (a) Comparison chart of MSE data for four competitive models. (b) Comparison chart of MAPE data for four competitive models. (c) Comparison chart of RMSE data for four competitive models. (d) Comparison chart of MAE data for four competitive models. (e) Comparison diagram of MSE, MAPE, RMSE, and MAE of ELMAN, ELM, SVM, and FA-CSSA-ELM models.

Table 3: Experiment II: compared with the evaluation function of the combinatorial competition model.

Data	MSE	MAPE	RMSE	MAE
Monday				
WOA-ELM	0.82163	1.6683	13.9436	10.8239
PSO-ELMAN	1.5443	3.2796	26.2078	211148
FA-CSSA-ELM	0.77477	1.6099	13.8068	9.8266
Tuesday				
WOA-ELM	0.9408	1.9509	15.9538	12.9269
PSO-ELMAN	1.7102	3.6173	29.0235	22.9117
FA-CSSA-ELM	0.8733	1.8208	15.4092	12.3912
Wednesday				
WOA-ELM	1.1136	2.3014	18.9082	14.8435
PSO-ELMAN	1.7956	3.8768	30.4726	24.5816
FA-CSSA-ELM	1.061	2.2299	18.8049	14.6999
Thursday				
WOA-ELM	1.1359	2.3608	19.2711	15.3207
PSO-ELMAN	1.8188	3.8585	30.8664	24.3114
FA-CSSA-ELM	1.118	2.3559	18.7718	15.6980
Friday				
WOA-ELM	0.85777	1.8753	14.5568	11.8553
PSO-ELMAN	1.7447	3.9528	30.1052	24.7635
FA-CSSA-ELM	0.7942	1.8056	13.8266	11.7099
Saturday				
WOA-ELM	1.43121	2.3145	19.5556	15.0731
PSO-ELMAN	1.732	3.619	39.3924	22.9106
FA-CSSA-ELM	1.0377	2.2249	18.4252	14.5872
Sunday				
WOA-ELM	1.0807	2.2217	18.3403	14.09331
PSO-ELMAN	1.9889	4.3066	33.7536	27.6812
FA-CSSA-ELM	1.0326	2.1783	18.3226	14.0861

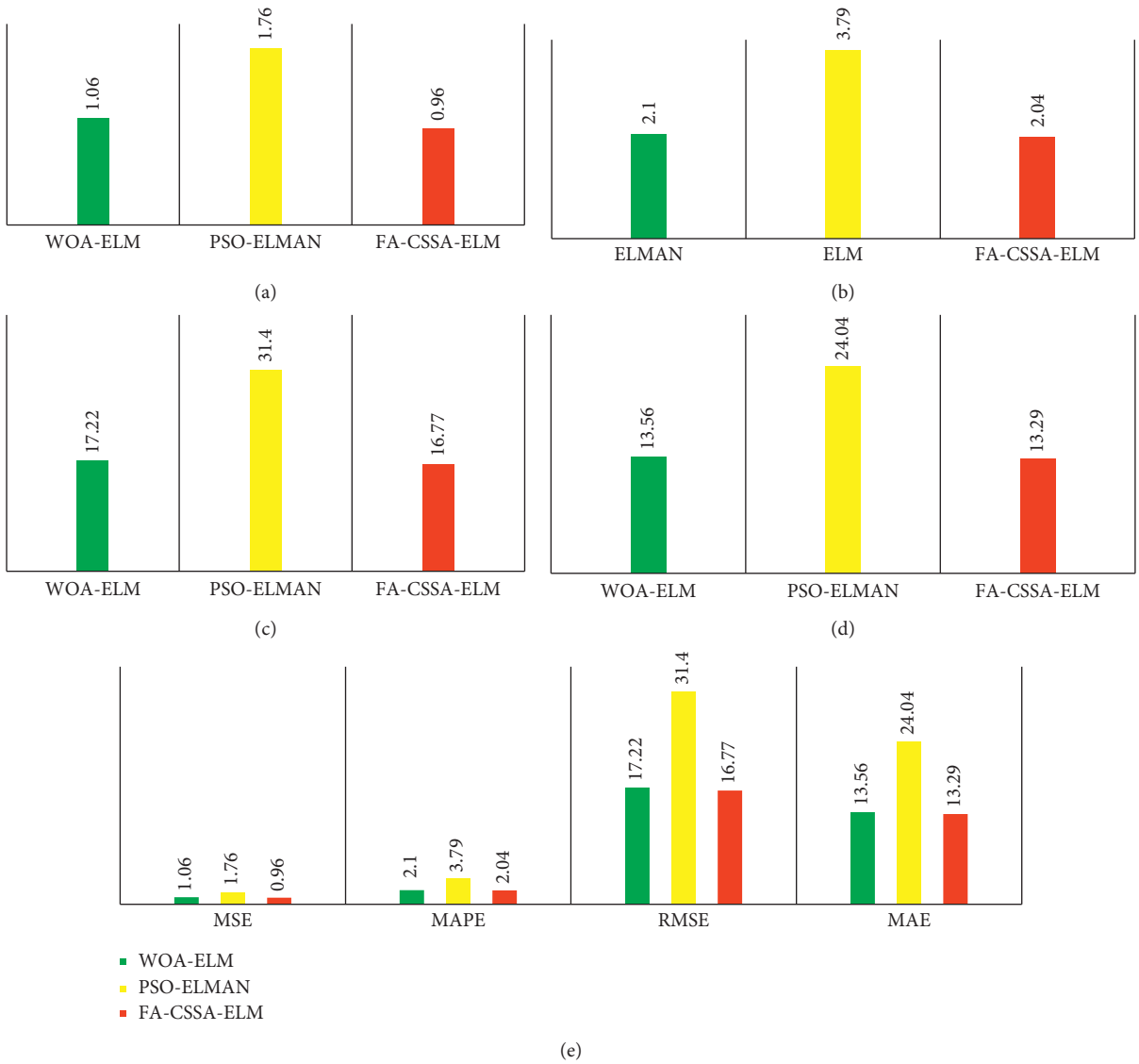

Figure 8: (a) Comparison chart of MSE data for three competitive models. (b) Comparison chart of MAPE data for three competitive models. (c) Comparison chart of RMSE data for three competitive models. (d) Comparison chart of MAE data for three competitive models. (e) Comparison diagram of MSE, MAPE, RMSE, and MAE of WOA-ELM, PSO-ELMAN, and FA-CSSA-ELM models.

10.2% and 87.3%, respectively. The MAPE index of the FA-CSSA-ELM model is increased by 3% and 86% compared with the WOA-ELM model and PSO-ELMAN model, respectively. Compared with WOA-ELM and PSO-ELMAN, the RMSE index of the FA-CSSA-ELM model increased by 2.6% and 89%, respectively. The MAE index of the FA-CSSA-ELM model compared with the WOA-ELM model and PSO-ELMAN model increased by 2.1% and 80.9%, respectively.

And this paper can also be more intuitively analyzed from the comparison graphs of the prediction effects of the six different competing models shown in Figure 9. The combined power load forecasting model is better than the single power load forecasting model in both accuracy and stability. Among the combined models, the FA-CSSA-ELM model proposed in this paper is the most superior. The FA-CSSA-ELM forecasting model outperforms the rest of the competing models in all evaluation metrics and has strong forecasting accuracy and stability. Therefore, the FA-CSSA-ELM power load forecasting model proposed in this paper can give accurate power forecasts and correct feedback to the authorities concerned.

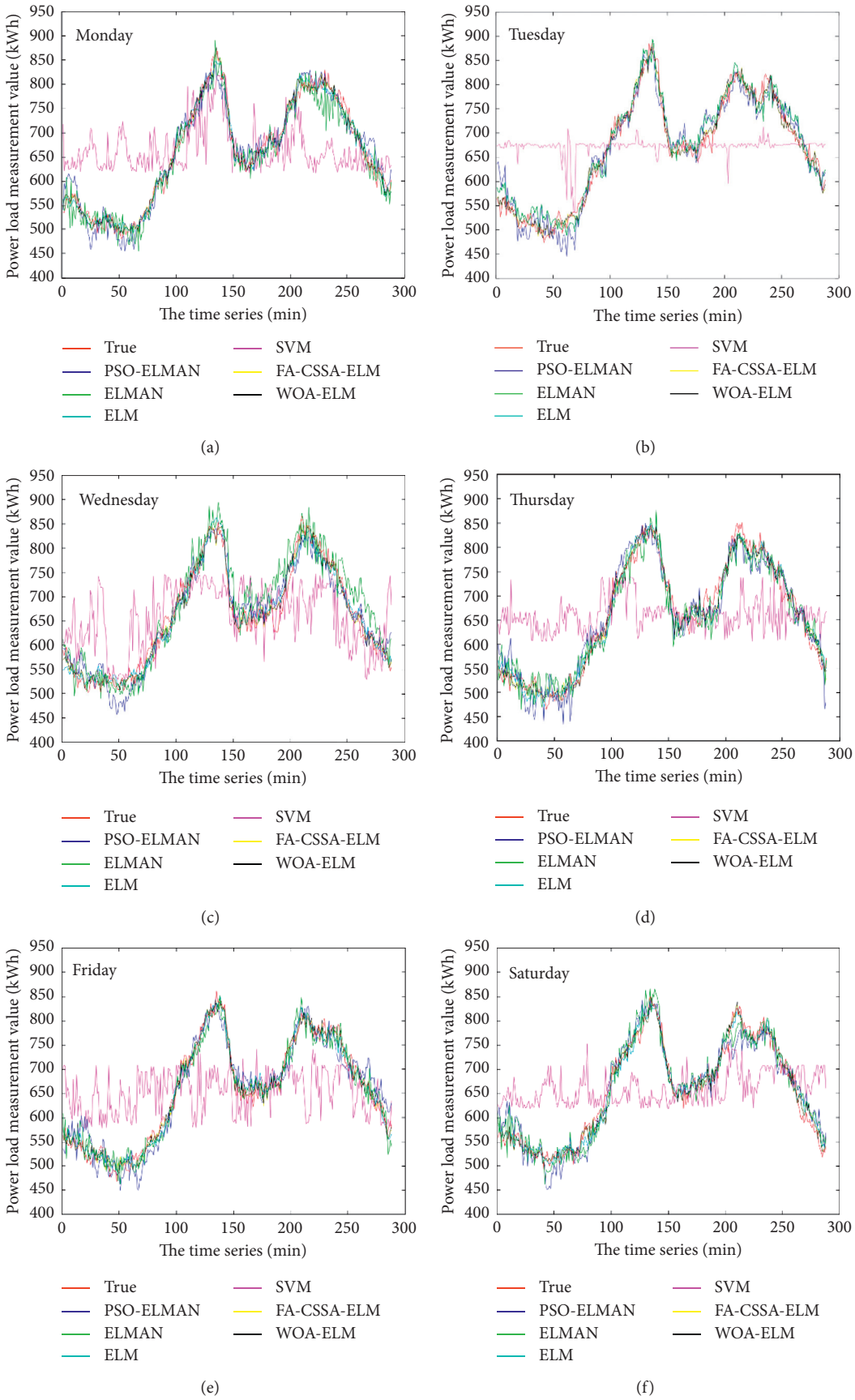

Figure 9: Continued.

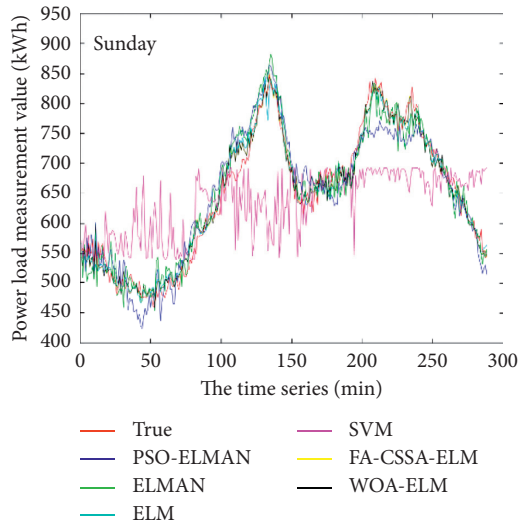

(g)

Figure 9: Forecast line chart of six competing models from Monday to Sunday.

5. Conclusion

In this study, we propose an FA-CSSA-ELM power load forecasting model to predict power loads accurately. First, this paper optimizes the SSA algorithm using the Tent chaos mapping strategy and the firefly perturbation strategy. Then, the constructed FA-CSSA algorithm is used to optimize the initial thresholds and weights of the ELM model. Finally, the FA-CSSA-ELM power load forecasting model is compared with three single forecasting models and two combined forecasting models. The forecasting effect is visualized through the 4 evaluation functions and the corresponding histograms. The following conclusions can be obtained through the simulation experimental validation of real power load data from a power grid in Shandong.

By comparing the FA-CSSA-ELM power load forecasting model with three typical single power load forecasting models, this paper finds that the FA-CSSA-ELM improved 72.29%, 99.8%, and 478.2% in MSE metrics compared with the other three single prediction models ELMAN, ELM, and SVM, respectively. The FA-CSSA-ELM improved by 80.3%, 18%, and 540% in the MAPE metric compared with the remaining three single prediction models ELMAN, ELM, and SVM, respectively. In the RMSE metric, the improvement is 77.8%, 14%, and 488% compared with the other three single forecasting models ELMAN, ELM, and SVM, respectively. In terms of MAE metric, the improvement is 77.2%, 15.6%, and 517% for ELMAN, ELM, and SVM, respectively. From the comparison data, the FA-CSSA-ELM model proposed in this paper has a much better prediction effect than the three representative single prediction models.

It can be found from Experiment I that the performance of the FA-CSSA-ELM prediction model is far superior to that of the three single prediction models. Then, WOA-ELM and PSO-ELMAN combination models are compared through Experiment II. Compared with the WOA-ELM model and PSO-ELMAN model, the MSE index of the FA-CSSA-ELM model increased by 10.2% and 87.3%, respectively. The MAPE index of the FA-CSSA-ELM model is increased by 3% and 86% compared with the WOA-ELM model and PSO-ELMAN model, respectively. Compared with WOA-ELM and PSO-ELMAN, the RMSE index of the FA-CSSA-ELM model increased by 2.6% and 89%, respectively. The MAE index of the FA-CSSA-ELM model compared with that of the WOA-ELM model and PSO-ELMAN model increased by 2.1% and 80.9%, respectively. This further indicates that the FA-CSSA-ELM power load forecasting model has higher forecasting accuracy and performance. The FA-CSSA-ELM prediction model can provide more accurate feedback to relevant departments. Relevant departments can guide the rational layout of the power system through accurate feedback so as to reduce the waste of power load and the economic loss of the industry.

Data Availability

No data were used to support this study.

Conflicts of Interest

The authors declare that they have no conflicts of interest.

Acknowledgments

This work was supported by Science, Education, and Industry Integration Innovation Pilot Project of Qilu University of Technology (Shandong Academy of Sciences) (2020KJC-ZD04), the Postgraduate Tutors' Guidance Ability Improvement Project of Shandong Province (SDYY17076), and the Empirical Research on Innovation of Cultivation Model of Control Graduate Students Based on System Synergy Theory (SDYY18151).

References

[1] G. Gross and F. D. Galiana, "Short-term load forecasting," *Proceedings of the IEEE*, vol. 75, no. 12, pp. 1558–1573, 1987.

[2] A. D. Papalexopoulos and T. C. Hesterberg, "A regression-based approach to short-term system load forecasting," *IEEE Transactions on Power Systems*, vol. 5, no. 4, pp. 1535–1547, 1990.

[3] B.-J. Chen, M.-W. Chang, and C.-J. Lin, "Load forecasting using support vector Machines: a study on EUNITE competition 2001," *IEEE Transactions on Power Systems*, vol. 19, no. 4, pp. 1821–1830, 2004.

[4] J.-F. Chen, W.-M. Wang, and C.-M. Huang, "Analysis of an adaptive time-series autoregressive moving-average (ARMA) model for short-term load forecasting," *Electric Power Systems Research*, vol. 34, no. 3, pp. 187–196, 1995.

[5] K. Lang, M. Zhang, Y. Yuan, and X. Yue, "Short-term load forecasting based on multivariate time series prediction and weighted neural network with random weights and kernels," *Cluster Computing*, vol. 22, no. S5, pp. 12589–12597, 2019.

[6] J. J. Xia, H. Qi, and Z. Q. Wang, "Combination forecasting of power load based on polynomial trend extrapolation and ARIMA model," *Advanced Materials Research*, vol. 546-547, pp. 357–362, 2012.

[7] Y. Wu, Z. Pan, X. Luo, J. Gao, and Y. Zhang, "A hybrid forecasting method of electricity consumption based on trend extrapolation theory and LSSVM," in *Proceedings of the 2016 IEEE PES Asia-Pacific Power and Energy Engineering Conference (APPEEC)*, pp. 2333–2337, Xi'an, China, October 2016.

[8] W. Christiaanse, "Short-term load forecasting using general exponential smoothing," *IEEE Transactions on Power Apparatus and Systems*, vol. PAS-90, no. 2, pp. 900–911, 1971.

[9] J. W. Taylor, "Short-term electricity demand forecasting using double seasonal exponential smoothing," *Journal of the Operational Research Society*, vol. 54, no. 8, pp. 799–805, 2003.

[10] H. Akçay and T. Filik, "Short-term wind speed forecasting by spectral analysis from long-term observations with missing values," *Applied Energy*, vol. 191, pp. 653–662, 2017.

[11] A. J. Conejo, M. A. Plazas, R. Espinola, and A. B. Molina, "Day-ahead electricity price forecasting using the wavelet transform and ARIMA models," *IEEE Transactions on Power Systems*, vol. 20, no. 2, pp. 1035–1042, 2005.

[12] T. Jakaša, I. Andročec, and P. Sprčić, "Electricity price forecasting — ARIMA model approach," in *Proceedings of the 2011 8th International Conference on the European Energy Market (EEM)*, pp. 222–225, Zagreb, Croatia, May 2011.

[13] Y. Wang, J. Wang, G. Zhao, and Y. Dong, "Application of residual modification approach in seasonal ARIMA for electricity demand forecasting: a case study of China," *Energy Policy*, vol. 48, pp. 284–294, 2012.

[14] J. L. Elman, "Finding structure in time," *Cognitive Science*, vol. 14, no. 2, pp. 179–211, 1990.

[15] W. S. Noble, "What is a support vector machine?" *Nature Biotechnology*, vol. 24, no. 12, pp. 1565–1567, 2006.

[16] G.-B. Huang, Q.-Y. Zhu, and C.-K. Siew, "Extreme learning machine: theory and applications," *Neurocomputing*, vol. 70, no. 1-3, pp. 2–501, 2006.

[17] J. A. K. Suykens and J. Vandewalle, "Least squares support vector machine classifiers," *Neural Processing Letters*, vol. 9, no. 3, pp. 293–300, 1999.

[18] H. Shi, M. Xu, and R. Li, "Deep learning for household load forecasting-A novel pooling deep RNN," *IEEE Transactions on Smart Grid*, vol. 9, no. 5, pp. 5271–5280, 2018.

[19] N. Ye, Y. Liu, and Y. Wang, "Short-term power load forecasting based on SVM," *World Automation Congress*, vol. 2012, pp. 47–51, Puerto Vallarta, Mexico, 2012.

[20] W. Li, C. Quan, X. Wang, and S. Zhang, "Short-term power load forecasting based on a combination of VMD and ELM," *Polish Journal of Environmental Studies*, vol. 27, no. 5, pp. 2143–2154, 2018.

[21] X. Li, Lv Jin-hu, L. Ding, G. Xu, and J. Li, "Building cooling load forecasting model based on LS-SVM," in *Proceedings of the 2009 Asia-Pacific Conference on Information Processing*, pp. 55–58, Shenzhen, China, July 2009.

[22] F. Yang, P. Wang, Y. Zhang, L. Zheng, and J. Lu, "Survey of swarm intelligence optimization algorithms," in *Proceedings of the 2017 IEEE International Conference on Unmanned Systems (ICUS)*, pp. 544–549, Beijing, China, October 2017.

[23] M. Dorigo, M. Birattari, and T. Stutzle, "Ant colony optimization," *IEEE Computational Intelligence Magazine*, vol. 1, no. 4, pp. 28–39, 2006.

[24] D. Karaboga and B. Akay, "A comparative study of artificial bee colony algorithm," *Applied Mathematics and Computation*, vol. 214, no. 1, pp. 108–132, 2009.

[25] X. S. Yang and X. He, "Firefly algorithm: recent advances and applications," *International Journal of Swarm Intelligence*, vol. 1, no. 1, pp. 36–50, 2013.

[26] X. S. Yang and A. Hossein Gandomi, "Bat algorithm: a novel approach for global engineering optimization," *Engineering Computations*, vol. 29, no. 5, pp. 464–483, 2012.

[27] R. Rajabioun, "Cuckoo optimization algorithm," *Applied Soft Computing*, vol. 11, no. 8, pp. 5508–5518, 2011.

[28] M. Seyedali, S. M. Mirjalili, and A. Lewis, "Grey wolf optimizer," *Advances in Engineering Software*, vol. 69, pp. 46–61, 2014.

[29] M. Seyedali, "Dragonfly algorithm: a new meta-heuristic optimization technique for solving single-objective, discrete, and multi-objective problems," *Neural Computing and Applications*, vol. 27, no. 4, pp. 1053–1073, 2016.

[30] M. Seyedali and A. Lewis, "The whale optimization algorithm," *Advances in Engineering Software*, vol. 95, pp. 51–67, 2016.

[31] J. Xue and B. Shen, "A novel swarm intelligence optimization approach: sparrow search algorithm," *Systems Science & Control Engineering*, vol. 8, no. 1, pp. 22–34, 2020.

[32] H. Wang, X. Lv, and X. Luo, "Short-term load forecasting of power grid based on improved WOA optimized LSTM," in *Proceedings of the 2020 5th International Conference on Power and Renewable Energy (ICPRE)*, pp. 54–60, Shanghai, China, September 2020.

[33] W.-C. Hong, "Electric load forecasting by seasonal recurrent SVR (support vector regression) with chaotic artificial bee colony algorithm," *Energy*, vol. 36, no. 91, pp. 5568–5578, 2011.

[34] F. Jiang, Z. Peng, and J. He, "Short-term load forecasting based on support vector regression with improved grey wolf optimizer," in *Proceedings of the 2018 Tenth International Conference on Advanced Computational Intelligence (ICACI)*, pp. 807–812, Xiamen, China, March 2018.

[35] X. YI, R. Guo, and Y. Qi, "Stabilization of chaotic systems with both uncertainty and disturbance by the UDE-based control method," *IEEE Access*, vol. 8, pp. 62471–62477, 2020.

[36] L. Liu, B. Li, and R. Guo, "Consensus control for networked manipulators with switched parameters and topologies," *IEEE Access*, vol. 9, pp. 9209–9217, 2021.

[37] T. Hou, Y. Liu, and F. Deng, "Finite horizon H2/H∞ control for SDEs with infinite Markovian jumps," *Nonlinear Analysis: Hybrid Systems*, vol. 34, pp. 108–120, 2019.
[38] R. Xu and F. Zhang, "ϵ-Nash mean-field games for general linear-quadratic systems with applications," *Automatica*, vol. 114, Article ID 108835, 2020.
[39] R. L. Haupt and S. E. Haupt, *Practical genetic algorithms*, Wiley, Hoboken, NJ, USA, 2004.
[40] E. Ott, C. Grebogi, and J. A. Yorke, "Controlling chaos," *Physical Review Letters*, vol. 64, no. 11, pp. 1196–1199, 1990.

Hindawi
Mathematical Problems in Engineering
Volume 2021, Article ID 5549775, 10 pages
https://doi.org/10.1155/2021/5549775

Research Article

Study on Nonlinear Dynamics and Chaos Suppression of Active Magnetic Bearing Systems Based on Synchronization

Shun-Chang Chang

Department of Mechanical and Automation Engineering, Da-Yeh University, No. 168 University Road, Dacun, Changhua 515006, Taiwan

Correspondence should be addressed to Shun-Chang Chang; changsc@mail.dyu.edu.tw

Received 21 January 2021; Revised 20 March 2021; Accepted 8 April 2021; Published 21 April 2021

Academic Editor: Renming Yang

This study employed a variety of nonlinear dynamic analysis techniques to explore the complex phenomena associated with a nonlinear mathematical model of an active magnetic bearing (AMB) system. The aim was to develop a method with which to assume control over chaotic behavior. The bifurcation diagram comprehensively explicates rich nonlinear dynamics over a range of parameter values. In this study, we examined the complex nonlinear behaviors of AMB systems using phase portraits, Poincaré maps, and frequency spectra. Furthermore, estimates of the largest Lyapunov exponent based on the properties of synchronization confirmed the occurrence of chatter vibration indicative of chaotic motion. Thus, the proposed continuous feedback control approach based on synchronization characteristics eliminates chaotic oscillations. Finally, some simulation results demonstrated the feasibility and efficiency of the proposed control scheme.

1. Introduction

Active magnetic bearings (AMBs) are widely used in rotating machinery and have high potential for machining applications. These noncontact bearings use magnetic forces to firmly hold the rotor and maintain separation between the rotor and the stationary components. In such a linear case study, the electromagnetic force is linearized about the operating point. In AMB systems, the occurrence of large unbalanced forces in rotor bearings can cause nonlinear motions of high amplitude. However, a closed-loop control system is required to stabilize the system by eliminating vibrations caused by disturbing forces. AMBs are regarded as inherently nonlinear due to nonlinearities of the electromagnetic forces. Accurate control of the system requires that designers account for the effects of nonlinearities. Thus, these complex nonlinear dynamics must be considered for in the design of AMB systems. Accordingly, in the present author's previous work [1], an experiment involving an unloaded symmetric rotor with a flexible coupler at one end and a bearing comprising two pairs of electromagnets at the other end (Figure 1) was conducted by applying a series of nonlinear electromagnetic forces to identify a nonlinear model of this system. Figure 2 illustrates the block diagram of the AMB control system along the horizontal direction. In the aforementioned study, we sought to predict these nonlinear dynamics by modifying the conventional identification technique based on the principle of harmonic balance to characterize the system with a higher degree of precision.

This model successfully captured the primary characteristics of the system by comparing the simulated frequency responses with those obtained experimentally [1]. However, theoretical analyses of this model to determine whether the nonlinear mathematical model derived experimentally can predict and characterize the dynamics of the physical system have not yet been undertaken. Various works have been carried out to study the chaotic motion in AMB systems [2–6]. But the chaotic motion that occurs when the rotor strikes the electromagnet that using the identification of a mathematical model for the AMB system has not been examined.

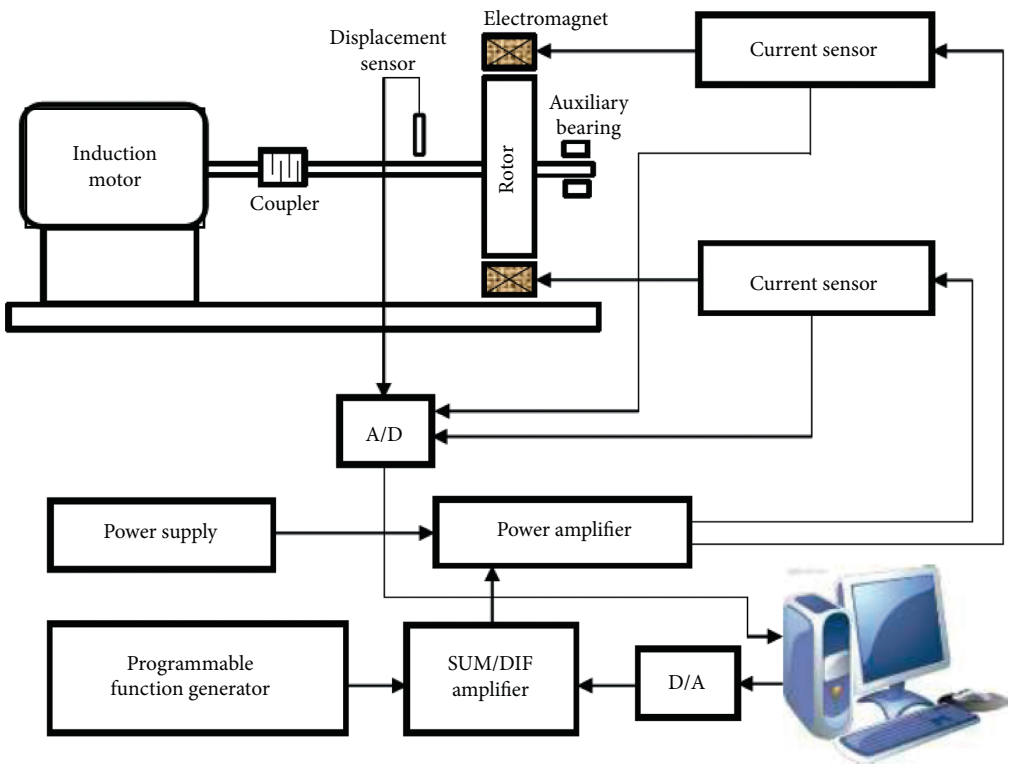

Figure 1: Schematic diagram of active magnetic bearing systems.

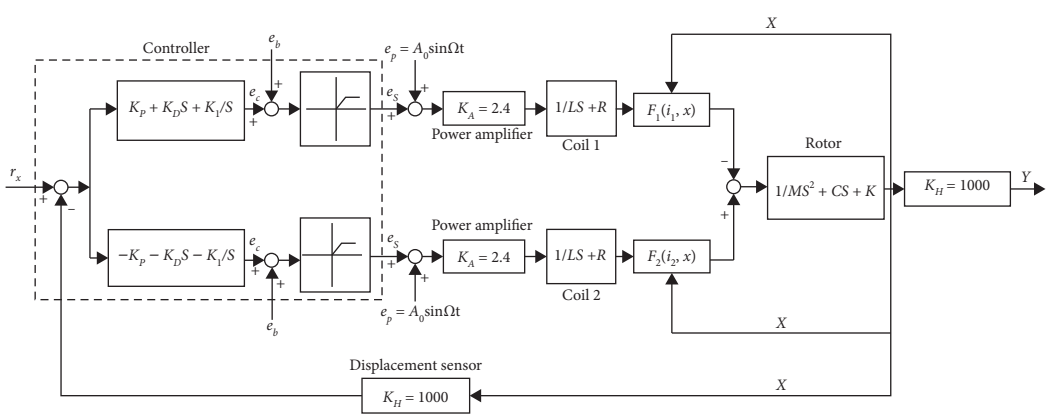

Figure 2: An overall block diagram of the AMB control system along the horizontal direction.

In this study, we used bifurcation diagrams, phase portraits, Poincaré maps, frequency spectra, and Lyapunov exponents to observe periodic orbits, bifurcation, and chaotic phenomena in an identified mathematical model of the AMB system. Across a broad range of parameters, the Lyapunov exponent offers the most powerful methods to measure the sensitivity of a dynamic system with regard to its initial conditions. This approach can be used to determine whether a system is susceptible to chaotic motion. The algorithms for computing Lyapunov exponents of smooth dynamic systems are well established [7–10]. However, a number of nonsmooth dynamic systems possess discontinuities, for example, discontinuities associated with dry friction, backlash, and saturation for which these algorithms cannot be applied directly. Numerous studies have developed procedures for the calculation of Lyapunov exponents associated with nonsmooth dynamic systems [11–13]. In this study, we adopted the method developed by Stefanski [13] for estimating the largest Lyapunov exponent for AMB systems with closed-loop control.

Several practical engineering problems involving chaos require control techniques to convert chaotic attractors into stable periodic orbits. Since the pioneering work of Ott et al. [14] on controlling chaos, various modified methods and other approaches have been proposed [15–22]. Improving the performance of a magnetic bearing system necessitates the transformation of chaotic motion into a steady-state periodic orbit by the state feedback control and the injection of dither signals [22]. Accordingly, a continuous feedback control method, based on the synchronization properties

proposed by Kapitaniak [18] and Pyragas [19], was used. Such schemes convert chaotic motion into stable motion by using feedback combined with a periodic external force. Simulation results demonstrate the efficacy of the proposed approach mechanism.

This paper is organized as follows. Section 2 describes an AMB system model and describes the complex dynamic behavior of a power system, which was elucidated using numerical analysis methods, such as bifurcation diagrams, phase portraits, Poincaré maps, and frequency spectra. Section 3 presents the Lyapunov exponent used to determine whether the system exhibits chaotic motion. A synchronization control technique for controlling chaos in the AMB system is described in Section 4. Conclusions are outlined in Section 5.

2. Overall Characteristics of AMB System: Simulations and Discussion

The resulting nonlinear model of the AMB system [1] is as follows:

$$\dot{x}_1 = x_2, \tag{1a}$$

$$\begin{aligned}\dot{x}_2 = &-d_1x_2 - d_2x_1 + d_3x_3 + d_4x_4 + d_5x_1^2 \\ &+ d_6x_1x_3 + d_7x_1x_4 + d_8x_3^2 + d_9x_4^2 + d_{10}x_1^3,\end{aligned} \tag{1b}$$

$$L\dot{x}_3 + Rx_3 = K_A\left(e_{c1} + A_0 \sin \Omega t\right), \tag{1c}$$

$$L\dot{x}_4 + Rx_4 = K_A\left(e_{c2} + A_0 \sin \Omega t\right), \tag{1d}$$

where

$$\begin{aligned}e_{c1} &= K_H\left(K_Px_1 + K_Dx_2 + K_I\int x_1\mathrm{d}t\right), \\ e_{c2} &= K_H\left(-K_Px_1 - K_Dx_2 - K_I\int x_1\mathrm{d}t\right),\end{aligned} \tag{2}$$

with the limitations

$$\begin{aligned}-3.5\ \mathrm{V} < e_{c1} < 6.5\ \mathrm{V}, \\ -3.5\ \mathrm{V} < e_{c2} < 6.5\ \mathrm{V}, \\ 0.0\ \mathrm{A} < x_3 < 2.0\ \mathrm{A}, \\ 0.0\ \mathrm{A} < x_4 < 2.0\ \mathrm{A},\end{aligned} \tag{3}$$

where x_1 is the displacement of the rotor around the equilibrium point, x_2 is the velocity of the rotor, x_3 and x_4 are coil currents oscillating around the bias current, e_{c1} and e_{c2} are the outputs of the proportional-integral-derivative controller to the two coils, $K_P = -55$, $K_D = -0.3$, and $K_I = -50$ are the control gains, K_A(=2.4) and K_H(=10000) represent the gains of the power amplifier and displacement sensor, and $A_0 \sin \Omega t$ is the forcing voltage generated by a programmable function generator. The procedures used to derive the other coefficients necessary for (1a)–(1d) are listed in Table 1.

Numerical simulations based on (1a)–(1d) were performed to clarify the characteristics of the proposed system.

Table 1: Identified results of parameters for the AMB system.

System parameter	Identified value
d_1	3.066133
d_2	4.3315×10^3
d_3	−5.5786683
d_4	6.5562
d_5	1.43371×10^7
d_6	-2.531×10^4
d_7	-4.53203×10^4
d_8	0.34514
d_9	−0.40171
d_{10}	-2.399816×10^{10}
L	0.0161203
R	14.3128231

In (1a)–(1d), the amplitude of the input excitation, A_0, equals 3.5 V. The commercial software package DIVPRK of IMSL [23] in Fortran subroutines for mathematics was used to solve these ordinary differential equations. The resulting bifurcation diagram is presented in Figure 3; this figure clearly demonstrates that the first period-doubling bifurcation occurred at approximately $\Omega = 19.5$ Hz and chaotic motion appears at approximately $\Omega = 18.63$ Hz. The period-doubling route to chaos has been observed in Figure 3. Additional details of the responses exhibited by the system are presented in Figures 4–7 , in which each type of response is characterized by time response, phase portrait, Poincaré map, and frequency spectrum. Figures 4(a)–4(d) prove that the T_f-period includes a constant term and the fundamental components. From Figures 5 and 6, we inferred that a cascade of period-doubling bifurcations produced a series of subharmonic components, revealing bifurcations with new frequency components at $1(\Omega/2)$, $(3\Omega/2)$, $(5\Omega/2)$, and so on. The essence of chaotic behavior can be described using Poincaré maps, which present an infinite set of points, referred to as a strange attractor. Chaotic motion also exhibits a broad continuous frequency spectrum. Thus, strange attractors and continuous-type Fourier spectra are generally regarded as strong indicators of chaos, as illustrated in Figures 7(a)–7(d).

3. Analysis of Chaotic Phenomena in AMB

The largest Lyapunov exponent is a useful diagnostic index of the chaotic system. Every dynamic system possesses a spectrum of Lyapunov exponents (λ), which determine length, area, and volume changes in phase space. In simple terms, Lyapunov exponents measure the rate of divergence (or convergence) between two adjacent orbits. Chaos can be identified simply by calculating the largest Lyapunov exponent, thereby determining whether nearby trajectories generally diverge ($\lambda > 0$) or converge ($\lambda < 0$). Any bounded motion in a system of at least one positive Lyapunov exponent is defined as chaotic, whereas nonpositive Lyapunov exponents indicate periodic motion. Numerous well-established algorithms are available for computing the Lyapunov spectrum of smooth dynamic systems [7–10]. However, these algorithms cannot be directly applied to

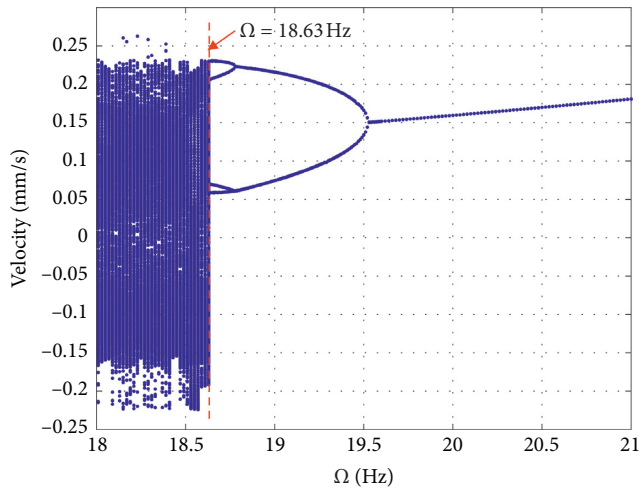

FIGURE 3: Bifurcation diagram of the system for $(A)_0 = 3.5$ V.

nonsmooth dynamic systems with discontinuities, such as dry friction, backlash, and saturation. In this study, we estimated the largest Lyapunov exponent in order to identify the onset of chaotic motion in AMB systems. Stefanski [13] proposed a simple method for estimating the largest Lyapunov exponent based on synchronization properties. Synchronization controls the response system by accessing the output of the drive system. Thus, the output of the response system asymptotically follows the output of the drive system. This method is described briefly in the following paragraph.

The dynamic system is decomposed into two subsystems, namely, a drive system

$$\dot{u} = f(u), \tag{4}$$

and a response system

$$\dot{v} = f(v). \tag{5}$$

Consider a dynamic system that is composed of two identical n-dimensional subsystems; a coupling coefficient d is applied only to the response system (5), while the drive system (4) remains unchanged. The first-order differential equations for such a system can be written as

$$\begin{aligned} \dot{u} &= f(u), \\ \dot{v} &= f(v) + d(u - v). \end{aligned} \tag{6}$$

The condition of synchronization is given by the following inequality:

$$d > \lambda_{\max}. \tag{7}$$

The smallest value of the coupling coefficient d in the synchronization, d_s, is assumed to equal the largest Lyapunov exponent, as follows:

$$d_s = \lambda_{\max}. \tag{8}$$

Equation (6) provides an augmented system, based on (1a)–(1d), as follows:

$$\dot{u}_1 = u_2, \tag{9a}$$

$$\begin{aligned} \dot{u}_2 = {} & -d_1 u_2 - d_2 u_1 + d_3 u_3 + d_4 u_4 + d_5 u_1^2 + d_6 u_1 u_3 \\ & + d_7 u_1 u_4 + d_8 u_3^2 + d_9 u_4^2 + d_{10} u_1^3, \end{aligned} \tag{9b}$$

$$L\dot{u}_3 + R u_3 = K_A (e_{c1u} + A_0 \sin \Omega t), \tag{9c}$$

$$L\dot{u}_4 + R u_4 = K_A (e_{c2u} + A_0 \sin \Omega t), \tag{9d}$$

$$\dot{v}_1 = v_2 + d(u_1 - v_1), \tag{10a}$$

$$\begin{aligned} \dot{v}_2 = {} & -d_1 v_2 - d_2 v_1 + d_3 v_3 + d_4 v_4 + d_5 v_1^2 + d_6 v_1 v_3 \\ & + d_7 v_1 v_4 + d_8 v_3^2 + d_9 v_4^2 + d_{10} v_1^3 + d(u_2 - v_2), \end{aligned} \tag{10b}$$

$$L\dot{v}_3 + R v_3 = K_A (e_{c1v} + A_0 \sin \Omega t) + d(u_3 - v_3), \tag{10c}$$

$$L\dot{v}_4 + R v_4 = K_A (e_{c2v} + A_0 \sin \Omega t) + d(u_4 - v_4), \tag{10d}$$

where

$$\begin{aligned} e_{c1u} &= K_H \left(K_P u_1 + K_D u_2 + K_I \int u_1 \mathrm{d}t \right), \\ e_{c2u} &= K_H \left(-K_P u_1 - K_D u_2 - K_I \int u_1 \mathrm{d}t \right), \\ e_{c1v} &= K_H \left(K_P v_1 + K_D v_2 + K_I \int v_1 \mathrm{d}t \right), \\ e_{c2v} &= K_H \left(-K_P v_1 - K_D v_2 - K_I \int v_1 \mathrm{d}t \right), \end{aligned} \tag{11}$$

with the following limitations:

$$\begin{aligned} & -3.5\ \mathrm{V} < e_{c1u} < 6.5\ \mathrm{V}, \\ & -3.5\ \mathrm{V} < e_{c2u} < 6.5\ \mathrm{V} \\ & \quad 0.0\ \mathrm{A} < u_3 < 2.0\ \mathrm{A} \text{ and } 0.0\ \mathrm{A} < u_4 < 2.0\ \mathrm{A}, \\ & -3.5\ \mathrm{V} < e_{c1v} < 6.5\ \mathrm{V}, \\ & -3.5\ \mathrm{V} < e_{c2v} < 6.5\ \mathrm{V}, \\ & \quad 0.0\ \mathrm{A} < v_3 < 2.0\ \mathrm{A} \text{ and } 0.0\ \mathrm{A} < v_4 < 2.0\ \mathrm{A}. \end{aligned} \tag{12}$$

In the next step, the largest Lyapunov exponent of the system under consideration was determined for the chosen parametric values, in an aforementioned manner. Figure 8 is a plot of the results of numerical calculations and shows the estimated largest Lyapunov exponents obtained using the synchronization method. All of the largest Lyapunov exponents were positive with regard to the forcing frequency ($\Omega \leq 18.63$ Hz), indicating that the system exhibited chaotic motion. These results help enhance our understanding of the chaos phenomenon in AMB systems under rotation.

4. Suppressing Chaos

Learning to predict the behaviors of a chaotic system provides a number of benefits, with the ultimate objective being to assume control over the system. Improving the performance of a dynamic system necessitates chaotic motion to be

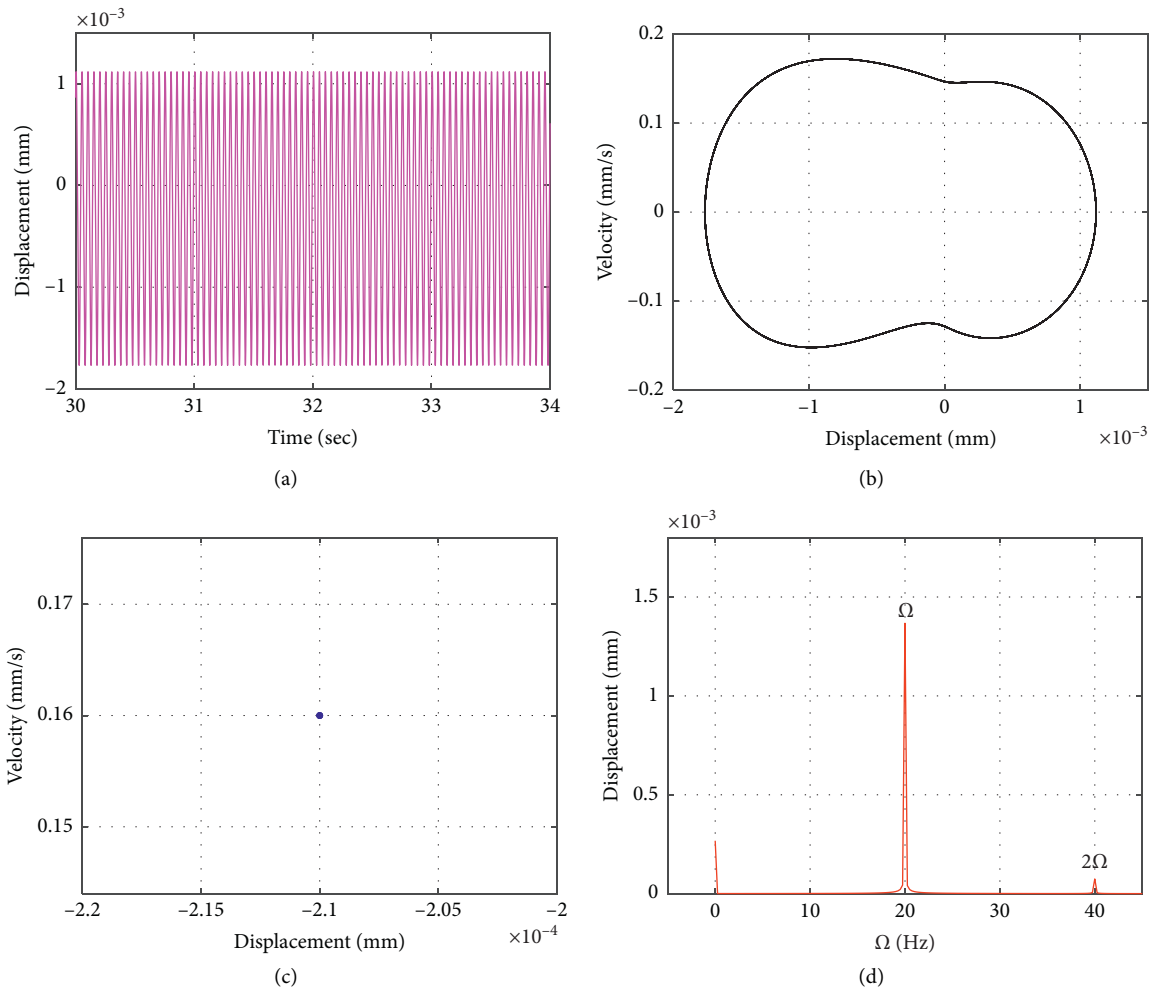

Figure 4: Period-one orbit for $\Omega = 20.0$ Hz: (a) time response; (b) phase portrait; (c) Poincaré map; (d) frequency spectrum.

converted into a stable periodic orbit. Therefore, suitable control methods must be developed. Kapitaniak [18] and Pyragas [19] have proposed simple and effective time-continuous control methods based on synchronization characteristics capable of converting chaotic motion into periodic motion. This method involves the construction of a feedback mechanism in conjunction with a specific time-continuous perturbation. Figure 9 is a plot of the proposed feedback-controlled loop with an external periodic perturbation. The technique is explained briefly in the following paragraph.

Consider an n-dimensional dynamic system,

$$\dot{p} = A(p), \tag{13}$$

$$\dot{q} = B(q) + F(t), \tag{14}$$

where $p(t), q(t) \in R^n$ denotes the state vector and $F(t)$ represents the input signal. System (14) without an input signal ($F(t) = 0$) is assumed to exhibit a strange attractor, whereas system (13) exhibits periodic motion. A periodic system is typically termed the drive system, whereas a chaotic system is called the response system. The strategy shown in Figure 9 is used to synchronize the two systems. The difference between signals $q(t)$ and $p(t)$ is utilized as a control signal:

$$F(t) = K[q(t) - p(t)], \tag{15}$$

where K represents the feedback gain.

When $\Omega_1 = 20$ Hz is selected in the drive system, the following equations reveal period-one motion.

$$\dot{p}_1 = p_2, \tag{16a}$$

$$\begin{aligned}\dot{p}_2 = {} & -d_1 p_2 - d_2 p_1 + d_3 p_3 + d_4 p_4 + d_5 p_1^2 + d_6 p_1 p_3 \\ & + d_7 p_1 p_4 + d_8 p_3^2 + d_9 p_4^2 + d_{10} p_1^3,\end{aligned} \tag{16b}$$

$$L\dot{p}_3 + R p_3 = K_A\left(e_{c1p} + A_0 \sin \Omega_1 t\right), \tag{16c}$$

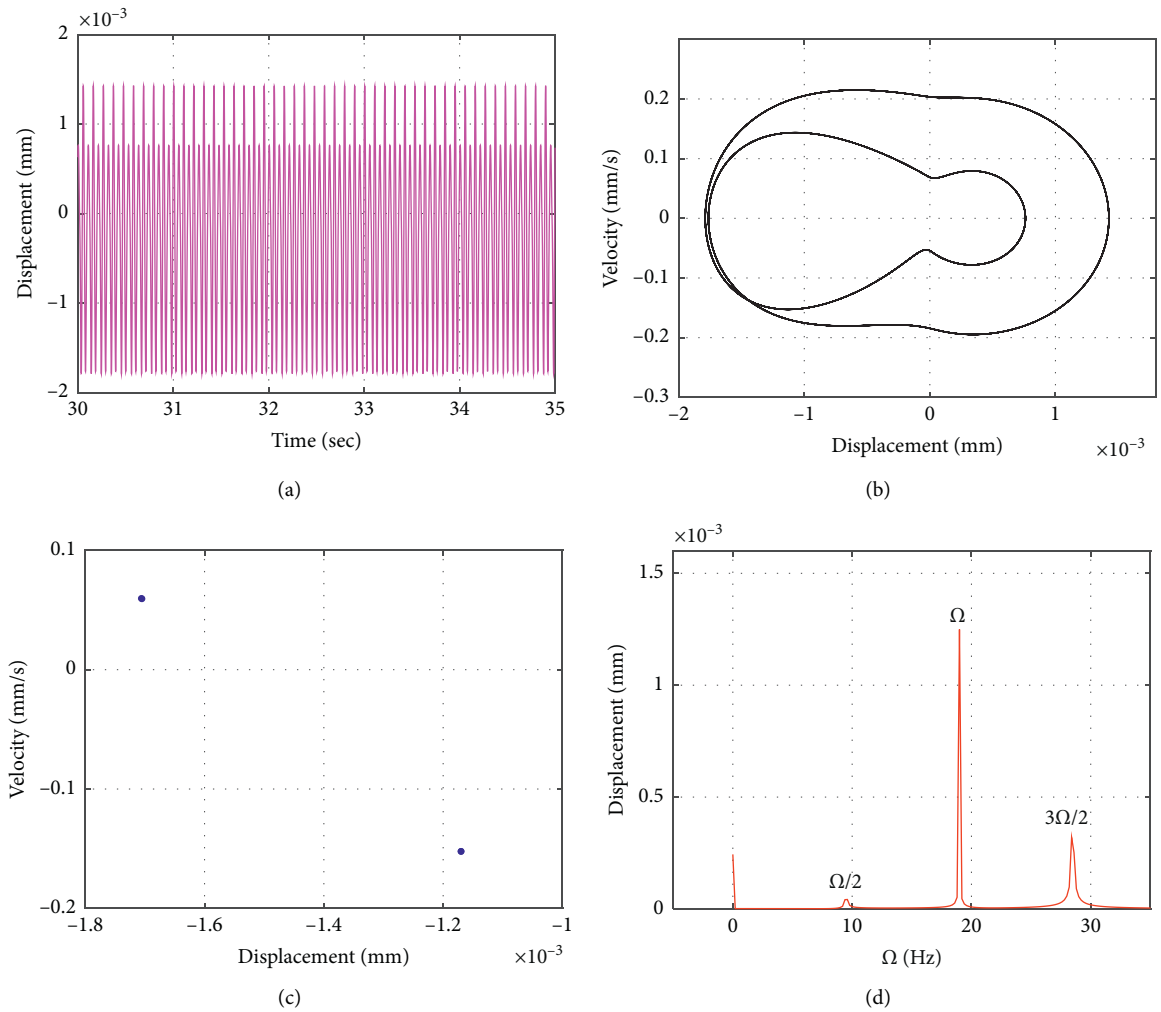

FIGURE 5: Period-two orbit for $\Omega = 19.0$ Hz: (a) time response; (b) phase portrait; (c) Poincaré map; (d) frequency spectrum.

$$L\dot{p}_4 + Rp_4 = K_A\left(e_{c2p} + A_0 \sin \Omega_1 t\right), \tag{16d}$$

where

$$\begin{aligned} e_{c1p} &= K_H\left(K_P p_1 + K_D p_2 + K_I \int p_1 \mathrm{d}t\right), \\ e_{c2p} &= K_H\left(-K_P p_1 - K_D p_2 - K_I \int p_1 \mathrm{d}t\right), \end{aligned} \tag{17}$$

with the following limitations:

$$\begin{aligned} -3.5\,\mathrm{V} < e_{c1p} < 6.5\,\mathrm{V}, \\ -3.5\,\mathrm{V} < e_{c2p} < 6.5\,\mathrm{V}, \\ 0.0\,\mathrm{A} < p_3 < 2.0\,\mathrm{A}, \\ 0.0\,\mathrm{A} < p_4 < 2.0\,\mathrm{A}. \end{aligned} \tag{18}$$

When $\Omega_2 = 18.2$ Hz is selected in the response system, the following equations reveal chaotic motion:

$$\dot{q}_1 = q_2, \tag{19a}$$

$$\begin{aligned} \dot{q}_2 = &-d_1 q_2 - d_2 q_1 + d_3 q_3 + d_4 q_4 + d_5 q_1^2 + d_6 q_1 q_3 \\ &+ d_7 q_1 q_4 + d_8 q_3^2 + d_9 q_4^2 + d_{10} q_1^3, \end{aligned} \tag{19b}$$

$$L\dot{q}_3 + Rq_3 = K_A\left(e_{c1q} + A_0 \sin \Omega_2 t\right), \tag{19c}$$

$$L\dot{q}_4 + Rq_4 = K_A\left(e_{c2q} + A_0 \sin \Omega_2 t\right), \tag{19d}$$

where

$$\begin{aligned} e_{c1q} &= K_H\left(K_P q_1 + K_D q_2 + K_I \int q_1 \mathrm{d}t\right), \\ e_{c2q} &= K_H\left(-K_P q_1 - K_D q_2 - K_I \int q_1 \mathrm{d}t\right), \end{aligned} \tag{20}$$

with the following limitations:

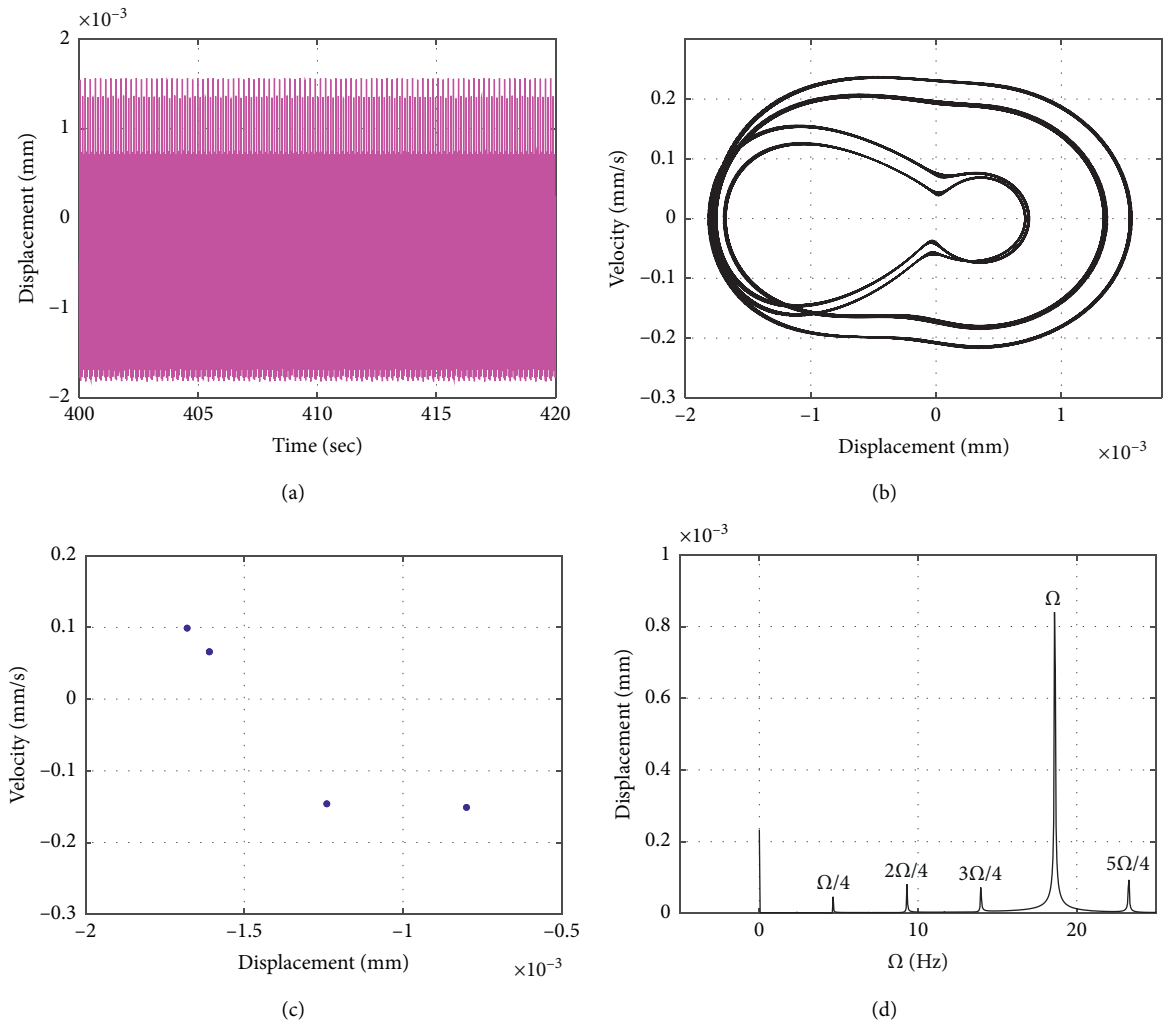

Figure 6: Period-four orbit for $\Omega = 18.63$ Hz: (a) time response; (b) phase portrait; (c) Poincaré map; (d) frequency spectrum.

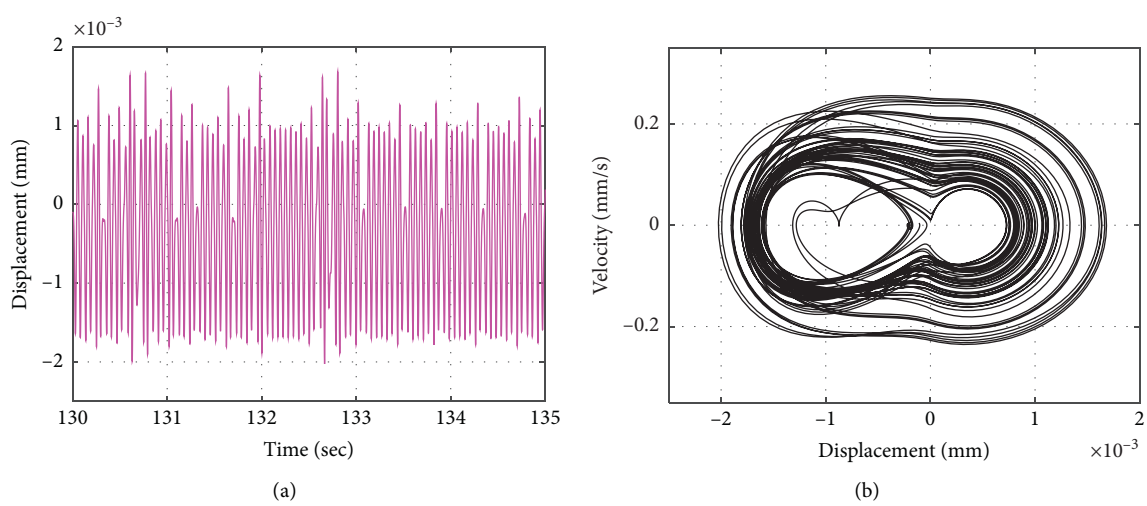

Figure 7: Continued.

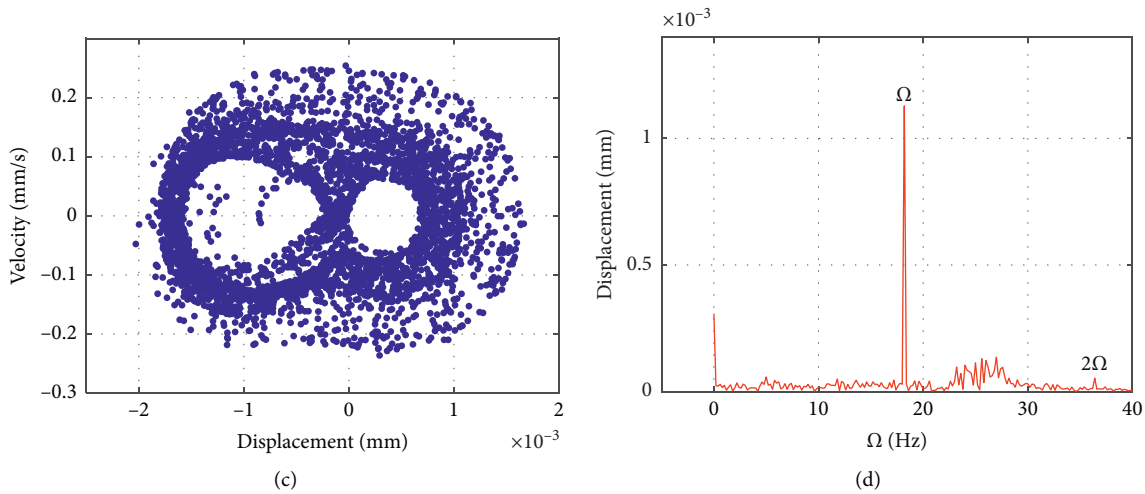

Figure 7: Chaotic motion for $\Omega = 18.2$ Hz: (a) time response; (b) phase portrait; (c) Poincaré map; (d) frequency spectrum.

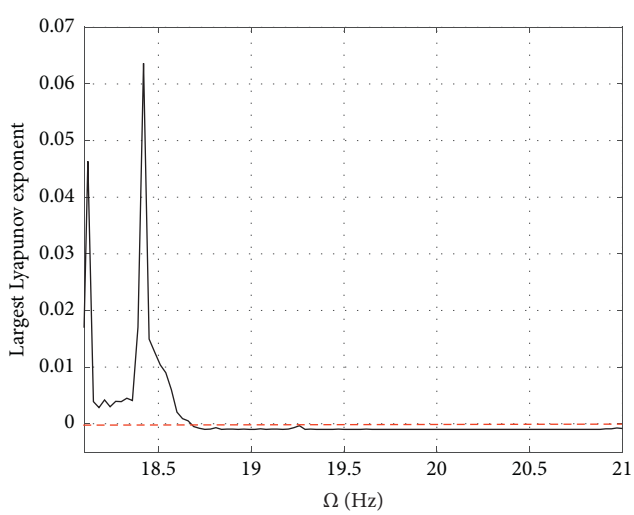

Figure 8: Evolutions of the largest Lyapunov exponent.

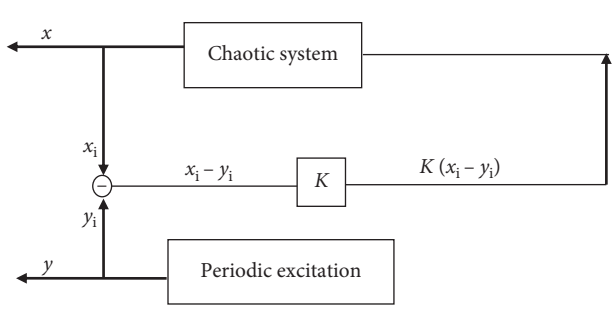

Figure 9: Block diagram of the continuous chaos control scheme.

$$\begin{aligned} &-3.5\ \text{V} < e_{c1q} < 6.5\ \text{V}, \\ &-3.5\ \text{V} < e_{c2q} < 6.5\ \text{V}, \\ &0.0\ \text{A} < q_3 < 2.0\ \text{A and } 0.0\ \text{A} < q_4 < 2.0\ \text{A}. \end{aligned} \tag{21}$$

Control signal (15) was introduced into (19a)–(19d) as a feedback control to synchronize (16a)–(16d) and (19a)–(19d). Control signal (15) was incorporated into (19a)–(19d), yielding the following coupled system, to achieve synchronization.

$$\dot{q}_1 = q_2 + K(q_1 - p_1), \tag{22a}$$

$$\begin{aligned} \dot{q}_2 = &-d_1 q_2 - d_2 q_1 + d_3 q_3 + d_4 q_4 + d_5 q_1^2 + d_6 q_1 q_3 \\ &+ d_7 q_1 q_4 + d_8 q_3^2 + d_9 q_4^2 + d_{10} q_1^3 + K(q_2 - p_2), \end{aligned} \tag{22b}$$

$$L q_3 + R q_3 = K_A\left(e_{c1q} + A_0 \sin \Omega_2 t\right) + K(q_3 - p_3), \tag{22c}$$

$$L \dot{q}_4 + R q_4 = K_A\left(e_{c2q} + A_0 \sin \Omega_2 t\right) + K(q_4 - p_4). \tag{22d}$$

Equation (22a)–(22d) exhibited chaotic motion when $K = 0$ and $\Omega_2 = 18.2$ Hz. The feedback gain K was adjusted to be between 0.0 and −3000 to convert the dynamics of system (22a)–(22d) from chaotic to periodic motion. Figure 10 presents the resulting bifurcation diagram, which comprehensively explains the dynamic behavior of the system over a range of feedback gains. Figure 10 clarifies that chaotic motion occurred in the region between $K = 0$ and $K = -120$. Stable periodic motion occurred when K decreased to below −120. When $K < -1000$, (22a)–(22d) display period-one motion. Accordingly, the synchronization was achieved in the AMB system by applying the control signal with $K < -1000$. When $t = 10$ s, the chaotic AMB system (19a)–(19d) can be synchronized by applying the control signal with $K = -1300$, as shown in Figure 11. Thus, this chaotic system can be managed using the control signal ($K = -1300$), such that chaotic motion is converted into period-one motion. Figure 11(a) presents the phase portrait of the controlled system, and Figure 11(b) plots the time response of displacement in which the synchronization control signal is injected after 10 s. Figure 12 presents the associated synchronization errors, $e_1 = q_1 - p_1$ and $e_2 = q_2 - p_2$. When the synchronization errors equal zeros,

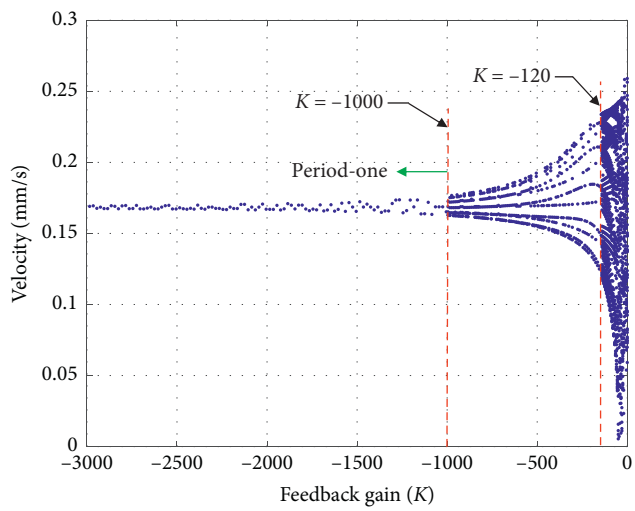

Figure 10: Bifurcation diagram of system with synchronization control, where K denotes feedback gain.

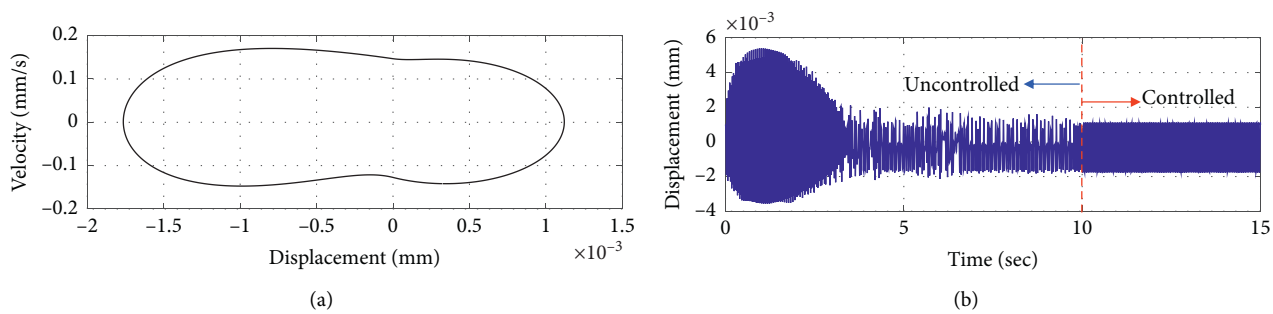

Figure 11: Transforming chaotic motion into period-one orbit at $K = -1300$ and $\Omega = 18.2$ Hz: (a) phase portrait of controlled system; (b) time responses of displacement. Synchronization control signal is introduced after 10 s.

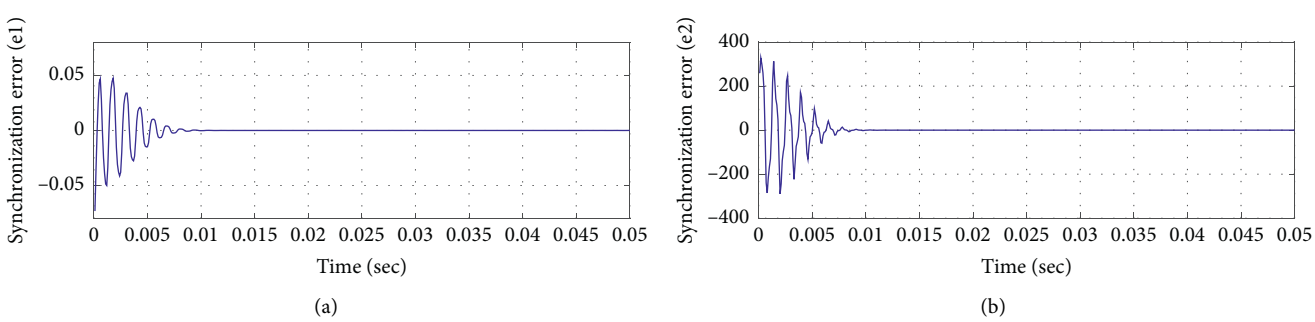

Figure 12: Synchronization errors associated with controlled system at $K = -1300$.

the synchronization is achieved. The control signal controlled the chaotic system, which converged to a stable equilibrium point. Therefore, the synchronization control method successfully suppressed chaotic motion and improved the chatter behavior of the AMB system. Thus, the performance of the AMB system could be improved considerably at high-speed rotations.

5. Conclusions

This work used an identified nonlinear model to explore global bifurcations and chaos control problem in AMB systems. Dynamic behaviors over the entire range of parameter values could be observed in a bifurcation diagram, which revealed that AMB systems exhibit period-doubling bifurcations and chaotic motions. The largest Lyapunov exponent, derived using the properties of synchronization, provided the most powerful approach for analyzing chaotic motion in a system. Controlling chaotic motion is an effective method to prevent chatter vibration in AMB systems. We propose a continuous feedback control method based on synchronization properties to suppress chaotic motion in AMB systems. Our analysis revealed that the proposed nonlinear model could predict the occurrence of global

bifurcations and chaos control in AMB systems. These results indicate that the proposed system has potential for application across a wide range of functions in the design of magnetic levitation systems. Furthering the development of magnetically levitated vehicles requires an understanding of their dynamic characteristics from the viewpoint of stability, safety, and ride quality at high speeds. We believe that studying the dynamics and controlling chaotic vibrations in the magnetically levitated systems will help to advance the development of magnetic transportation systems.

Data Availability

All data generated or analyzed during this study are included within this article.

Conflicts of Interest

The author declares that there are no conflicts of interest regarding the publication of this paper.

Acknowledgments

This research was supported by the Ministry of Science and Technology in Taiwan, Republic of China, under project number MOST 108-2221-E-212-010-MY3.

References

[1] S. C. Chang and P. C. Tung, "Nonlinear identification of a magnetic bearing system with closed loop control," *JSME International Journal Series C*, vol. 42, no. 4, pp. 982–990, 1999.

[2] W. Zhang and X. P. Zhan, "Periodic and chaotic motions of a rotor-active magnetic bearing with quadratic and cubic terms and time-varying stiffness," *Nonlinear Dynamics*, vol. 41, no. 4, pp. 331–359, 2005.

[3] W. Zhang, J. W. Zu, and F. X. Wang, "Global bifurcations and chaos for a rotor-active magnetic bearing system with time-varying stiffness," *Chaos, Solitons & Fractals*, vol. 35, no. 3, pp. 586–608, 2008.

[4] A. K. Mando, D. Yemélé, W. T. Sokamte, and A. Fomethe, "Structural static stability and dynamic chaos of active electromagnetic bearing systems: analytical investigations and numerical simulations," *Journal of Vibration and Control*, vol. 24, no. 24, pp. 5774–5793, 2018.

[5] W. S. Ma, W. Zhang, and Y. F. Zhang, "Stability and multi-pulse jumping chaotic vibrations of a rotor-active magnetic bearing system with 16-pole legs under mechanical-electric-electromagnetic excitations," *European Journal of Mechanics-A/Solids*, vol. 85, Article ID 104120, 2021.

[6] A. Kandil, M. Sayed, and N. A. Saeed, "On the nonlinear dynamics of constant stiffness coefficients 16-pole rotor active magnetic bearings system," *European Journal of Mechanics-A/Solids*, vol. 84, Article ID 104051, 2020.

[7] I. Shimada and T. Nagashima, "A numerical approach to ergodic problem of dissipative dynamical systems," *Progress of Theoretical Physics*, vol. 61, no. 6, pp. 1605–1616, 1979.

[8] A. Wolf, J. B. Swift, H. L. Swinney, and J. A. Vastano, "Determining lyapunov exponents from a time series," *Physica D: Nonlinear Phenomena*, vol. 16, no. 3, pp. 285–317, 1985.

[9] G. Benettin, L. Galgani, A. Giorgilli, and J.-M. Strelcyn, "Lyapunov Characteristic Exponents for smooth dynamical systems and for Hamiltonian systems; a method for computing all of them. part 1: Theory," *Meccanica*, vol. 15, no. 1, pp. 9–20, 1980.

[10] G. Benettin, L. Galgani, A. Giorgilli, and J.-M. Strelcyn, "Lyapunov Characteristic Exponents for smooth dynamical systems and for Hamiltonian systems; A method for computing all of them. part 2: numerical application," *Meccanica*, vol. 15, no. 1, pp. 21–30, 1980.

[11] P. C. Müller, "Calculation of lyapunov exponents for dynamic systems with discontinuities," *Chaos, Solitons & Fractals*, vol. 5, no. 9, pp. 1671–1681, 1995.

[12] N. Hinrichs, M. Oestreich, and K. Popp, "Dynamics of oscillators with impact and friction," *Chaos, Solitons & Fractals*, vol. 8, no. 4, pp. 535–558, 1997.

[13] A. Stefanski, "Estimation of the largest Lyapunov exponent in systems with impacts," *Chaos, Solitons & Fractals*, vol. 11, no. 15, pp. 2443–2451, 2000.

[14] E. Ott, C. Grebogi, and J. A. Yorke, "Controlling chaos," *Physical Review Letters*, vol. 64, no. 11, pp. 1196–1199, 1990.

[15] I. M. Ginarsa, A. Soeprijanto, and M. H. Purnomo, "Controlling chaos and voltage collapse using an ANFIS-based composite controller-static var compensator in power systems," *International Journal of Electrical Power & Energy Systems*, vol. 46, pp. 79–88, 2013.

[16] Z. Shen and J. Li, "Chaos control for a unified chaotic system using output feedback controllers," *Mathematics and Computers in Simulation*, vol. 132, pp. 208–219, 2017.

[17] S. M. A. Pahnehkolaei, A. Alfi, and J. A. Tenreiro Machado, "Chaos suppression in fractional systems using adaptive fractional state feedback control," *Chaos, Solitons & Fractals*, vol. 103, pp. 488–503, 2017.

[18] T. Kapitaniak, "Continuous control and synchronization in chaotic systems," *Chaos, Solitons & Fractals*, vol. 6, pp. 237–244, 1995.

[19] K. Pyragas, "Continuous control of chaos by self-controlling feedback," *Physics Letters A*, vol. 170, no. 6, pp. 421–428, 1992.

[20] X. Yi, R. Guo, and Y. Qi, "Stabilization of chaotic systems with both uncertainty and disturbance by the UDE-based control method," *IEEE Access*, vol. 8, pp. 62471–62477, 2020.

[21] N. A. Saeed and A. Kandil, "Two different control strategies for 16-pole rotor active magnetic bearings system with constant stiffness coefficients," *Applied Mathematical Modelling*, vol. 92, pp. 1–22, 2021.

[22] S. C. Chang, "Nonlinear dynamics and suppressing chaos in magnetic bearing system," *Mathematical Problems in Engineering*, vol. 2020, Article ID 6669941, 10 pages, 2020.

[23] IMSL, Inc., *User's Manual–IMSL Math/Library*, Valby, Denmark, 1989.

Hindawi
Mathematical Problems in Engineering
Volume 2021, Article ID 5516703, 8 pages
https://doi.org/10.1155/2021/5516703

Research Article

Dynamics Analysis and Fractional-Order Approximate Entropy of Nonlinear Inventory Management Systems

Tengfei Lei,[1] **Rita Yi Man Li**,[2] **and Haiyan Fu**[3]

[1]*Rattanakosin International College of Creative Entrepreneurship, Rajamangala University of Technology Rattanakosin, Rattanakosin, Bangkok, Thailand*
[2]*Department of Economics and Finance, Hong Kong Shue Yan University, Hong Kong, China*
[3]*Collaborative Innovation Center of Memristive Computing Application, Qilu Institute of Technology, Jinan 250200, Shandong, China*

Correspondence should be addressed to Haiyan Fu; fuhy413@126.com

Received 18 February 2021; Revised 17 March 2021; Accepted 29 March 2021; Published 8 April 2021

Academic Editor: Yi Qi

Inventory management is complex nonlinear systems that are affected by various external factors, including course human action and policy. We study the inventory management model under special circumstances and analyse the equilibrium point of the system. The dynamics of the system is analysed by means of the eigenvalue trajectory, bifurcations, chaotic attractor, and largest Lyapunov exponent diagram. At the same time, according to the definition of fractional calculus, the fractional approximate entropy is used to analyse the system, and the results are consistent with those of the largest Lyapunov exponent diagram, which shows the effectiveness of this method.

1. Introduction

Over the past few decades, chaos and its applications have attracted remarkable consideration in a variety of fields, including chemistry, ecology, and economy [1]. An economics management system is a typical discrete chaotic system, which has widely concerned scientists [2–8]. In 1993, Stiles and Levy proposed the concept of chaotic strategic management in [3]. In 1994, Feichtinger et al. [4] studied many chaotic systems in the field of management operations research, such as queuing system, inventory system, and planning and scheduling system. These systems are mainly characterised by the chaos of queue, inventory, and planning and scheduling under different management decision rules. Murphy [5] used the chaos theory as a model to study the management of public relations, such as problems and crises. After summarising the research status of chaos management, Joseph [6] pointed out that chaos management depends on change rules, which are a set of rules based on orderly or disorderly changes, adaptability, and new orderly emergence process.

The fractional calculus theory has a history of more than 300 years. Its history is almost the same as that of traditional integral calculus theory. Compared with an integer-order differential equation, a fractional-order differential equation has a memory effect [9–14]; therefore, it can describe these natural phenomena more accurately [9]. Many fractional-order chaotic systems, such as the fractional-order Lorenz system [15, 16] and the fractional-order Chen system [17, 18], have been studied [19]. However, most of the studies on chaos based on the theory of fractional calculus have been mainly limited to continuous-time chaotic systems, and the study of fractional-order discrete-time chaotic systems is insufficient. Thus, researchers turned their attention to apply the theory of discrete fractional calculus to discrete chaotic maps [20, 21]. It has been proven that there are abundant dynamical behaviours in the fractional chaotic maps [22–27]. All of the above studies are based on chaotic systems, and other fields of fractional order have not been studied.

Many scientists have conducted considerable research on the complexity of time series such as economic

management [8, 23–25]. Grassberger and Procaccia [28] used the GP algorithm to analyse the complexity of Hénon mapping, which was an early report on the complexity analysis of chaotic systems. Balasubramanian et al. [29] used the Lempel–Ziv algorithm and the ApEn algorithm to analyse the complexity of logistic mapping and used a complexity measure to distinguish among the different states of the system. In [30], the PE algorithm was used to analyse the complexity of chaotic pseudorandom sequences. In [31], the researchers analysed the randomness of discrete chaotic systems by using the SymEn algorithm and showed that discrete chaotic systems can be used as random sources. All of the above systems are based on the theory of integer-order differential information. Can we further extend them to the theory of fractional calculus?

In this paper, we propose a new special nonlinear inventory management system [32, 33]. The discretisation of the proposed system was performed using a Matlab simulation. The rest of this paper is organised as follows. In Section 2, the equilibrium point and the 0-1 test of the 2D inventory management nonlinear systems are presented. In Section 3, the bifurcation diagram, phase diagrams, and Lyapunov exponent spectrum are used to analyse the dynamics of the system. In Section 4, the fractional-order approximate entropy of 2D nonlinear inventory management systems is analysed. Finally, the obtained results are summarised in Section 5.

2. Nonlinear Inventory Management Model Description

2.1. 2D Inventory Management Model. Inventory management is an important part of enterprise organisation and management activities. A class of nonlinear inventory management systems is as follows [2]:

$$\begin{cases} x_{i+1} = s + pz_{i+1}, \\ y_{i+1} = qx_{i+1} + ry_i z_i, \\ z_{i+1} = 1 - x_i - y_i + z_i, \end{cases} \tag{1}$$

where s, p, q, and r are the system parameters, s represents the initial sales base, p represents the inventory fund transfer rate, q represents the product resource rate, r represents the inventory efficiency, x_i represents the resources for sales in the time period i, y_i represents the number of customers in the time period i, and z_i represents the inventory capital of the company in the time period i. After normalising the parameters of the inventory management model, we obtained the following: $0 < x_i < 1$, $0 < y_i < 1$, and $0 < z_i < 1/r$. Here, $p = 0.43$, $q = 0.38$, $s = 0.11$, and $r = 0.72$. The attractors of system (1) are shown in Figure 1.

The company had surplus inventory in stage i, and its main goal was to deal with this surplus inventory. At this time, the company shifted resources from production to sales. The new customers absorbed by the company in stage $i+1$ mainly depended on the direct investment in sales in stage i. In addition, some old customers had to be added to the total customer volume. If the company's inventory was insufficient and could not meet the requirements of the regular customers for timely pickup, some regular customers would disappear from the company's customer list. $x_i < 0$ indicates that the company had no resources available for sale. The absolute value of x_i implies that it had to borrow funds and promote production to supplement the sales resources, $y_i < 0$ denoted losing customers, and $z_i < 0$ denoted that the sales were very strong and the products were in short supply.

The problems of convenient calculation and original speed, in this paper, considers a special case of inventory management system, $P = 0$, that is, there is no transfer of resources. The mathematical model of inventory management (1) is rewritten as

$$\begin{cases} y_{i+1} = qs + ry_i z_i, \\ z_{i+1} = 1 - s - y_i + z_i, \end{cases} \tag{2}$$

where $0 < x_i < 1$, $0 < y_i < 1$, and $0 < z_i < 1/r$. The definition of the parameters is the same as in formula (1). Here, $q = 0.051$, $s = 0.58$, and $r = 0.72$. The attractors of system (2) are shown in Figure 2.

2.2. Equilibrium Stability Analysis. The fixed point of system (2) can be obtained by solving the following equations:

$$\begin{cases} y_i - qs + ry_i z_i = 0, \\ z_i - 1 - s - y_i + z_i = 0. \end{cases} \tag{3}$$

Apparently, the fixed point can be obtained by setting $A = \{(y_0, z_0) | y_0 = 1 - s,\ z_0 = (1 - s(1+q)/r(1-s))\}$. The Jacobian matrix J at the equilibrium set can be expressed as follows:

$$\mathbf{J} = \begin{bmatrix} \dfrac{1 - s(1+q)}{1-s} & r - rs \\ -1 & 1 \end{bmatrix}. \tag{4}$$

The systems' characteristic equation corresponding to matrix J can be written as follows:

$$\left(\lambda - 1 + \frac{qs}{1-s}\right)(\lambda - 1) + r - rs = 0. \tag{5}$$

From equation (7), we inferred that when $r < qs/(1-s)^2$, at the fixed point p_0, system (2) is unstable. When$r > qs/(1-s)^2$, at the fixed point p_0, system (2) is stable. When $r = qs/(1-s)^2$, system (2) is at the bifurcation point.

2.3. 0–1 Test. We implemented the 0-1 test method. The 0-1 test is a novel test approach to determine whether a given deterministic nonlinear dynamic system is chaotic. It was proposed by Sun et al. [31] and has already been successfully tested for integer-order chaotic systems [31] and fractional order chaotic systems with delay time [8]. If a set of discrete data $\varphi(n)$ $(n = 1, 2, 3, \ldots)$ represents a one-dimensional observable dataset obtained from the iterative, then the following two real-valued functions can be defined:

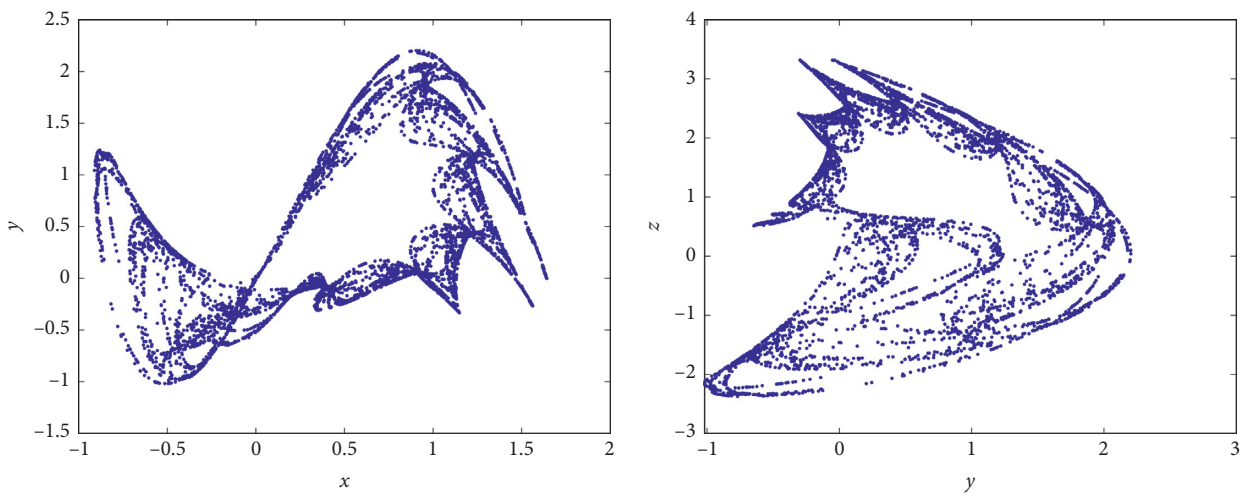

Figure 1: Attractors of system (1) with $p = 0.43$, $q = 0.38$, $s = 0.11$, and $r = 0.72$. (a) x-y phase and (b) y-z phase.

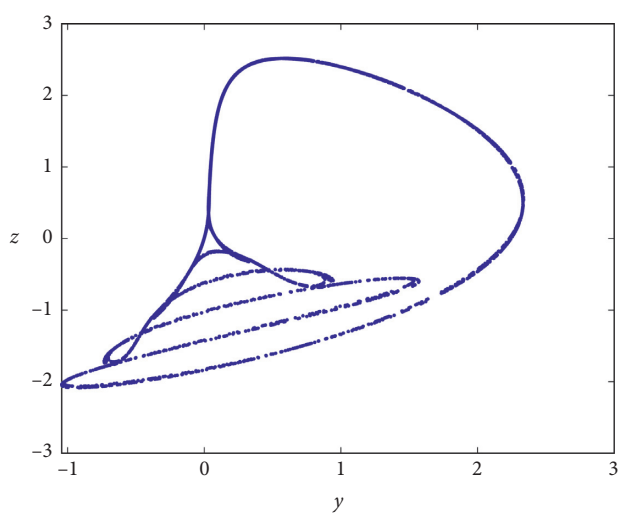

Figure 2: Attractors of system (2) from initial values (1.1, 0.1).

$$\left\{ p(n) = \sum_{i=1}^{n} \phi(i)\cos(\theta(i))s(n) = \sum_{i=1}^{n} \phi(i)\sin(\theta(i)), \right. \quad (6)$$

where $\theta(i) = i\omega + \sum_{j=1}^{i} \phi(j)$, plotting the trajectories in the p-s diagram. In any case, the trajectory in the p-s graph can provide a simple visual measurement. If the bounded trajectory in the p-s plots is a regular cloud slave, then the unbounded trajectory similar to Brownian motion indicates that the system is a chaotic system. This method was used to study the y and z sequence of the 2D system (2). Its parameters were the same as those shown in Figure 2. The obtained p-s diagram is shown in Figure 3; it can be seen that the system is chaotic.

3. Analysis of Dynamic Characteristics

3.1. Dynamics with q Varying. We fixed $s = 0.58$ and $r = 0.72$ and let the derivative order q vary from 0.05 to 0.08 with a step size of 0.0002 and the initial values of state variables $[y_0, z_0] = [1.1, 0.1]$. Figure 4(a) shows that, upon the variation of q, it was obvious that the system chaos and periodic variation were repeated and crossed and were not a process from period to chaos directly. Obviously, we observed that $q \in [0.05, 0.06) \cup [0.068, 0.074] \cup [0.077, 0.08]$ was in a chaos state and the other regions were in a chaotic state with periodic windows. Secondly, when $q \in [0.05, 0.06) \cup [0.068, 0.074] \cup [0.077, 0.08]$, the largest Lyapunov exponent (LLE) was positive; LLE was equal to 0 in the other regions, as shown in Figure 4(b).

3.2. Dynamics with r Varying. The chaotic system (2) had two system parameters besides q. In this study, the dynamic properties of the system parameters with r varied were analysed. Firstly, the bifurcation diagrams of the 2D system with $r \in [0.5, 0.75]$ were investigated, as shown in Figure 5(a). Obviously, we observed that $r \in [0.5, 0.55) \cup [0.68, 0.7]$ was in a chaos state and the other regions were in a chaotic state with periodic windows. Secondly, when $r \in [0.5, 0.55) \cup [0.68, 0.7]$, the LLE was positive; the LLE was equal to 0 in the other regions, as shown in Figure 5(b). Meanwhile, in eigenvalue trait of system (2) with r varying, as shown in Figure 6, r ranges from 0.5 to 0.75, and the eigenvalues are unstable, stable, and unstable processes, which are consistent with Figure 5. Eigenvalues are stable in the unit circle and unstable outside the unit circle.

For the case of $s = 0.58$, $q = 0.051$, and $r = 0.6$, the periodic state phase diagram is given in Figure 7(a) and its corresponding p-s plot is presented in Figure 7(c). For the case of $s = 0.58$, $q = 0.051$, and $r = 0.73$, the chaos state is shown in Figure 7(b) and the corresponding p-s plot is presented in Figure 7(d). Thus, the system had different states with different parameters, and chaos was verified.

4. Complexity Analysis of the System

Entropy measures the complexity of a time series by measuring the probability of generating new patterns in signals [34–36]. The greater the probability of signal generation is,

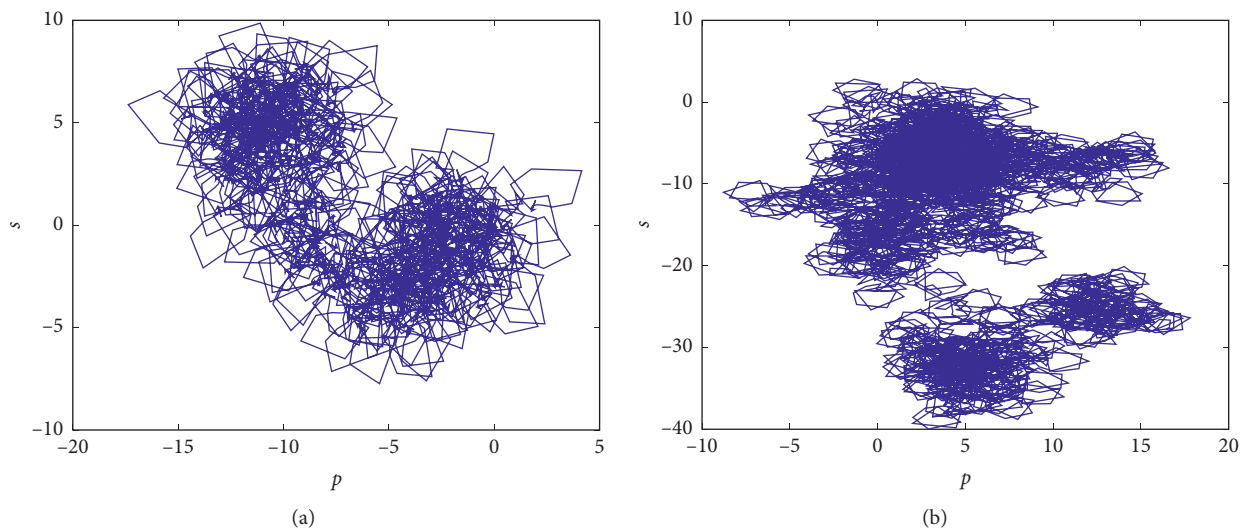

Figure 3: p-s phase diagrams of chaotic system (2) from initial values (1.1, 0.1). (a) p-s plot of y sequence. (b) p-s plot of z sequence.

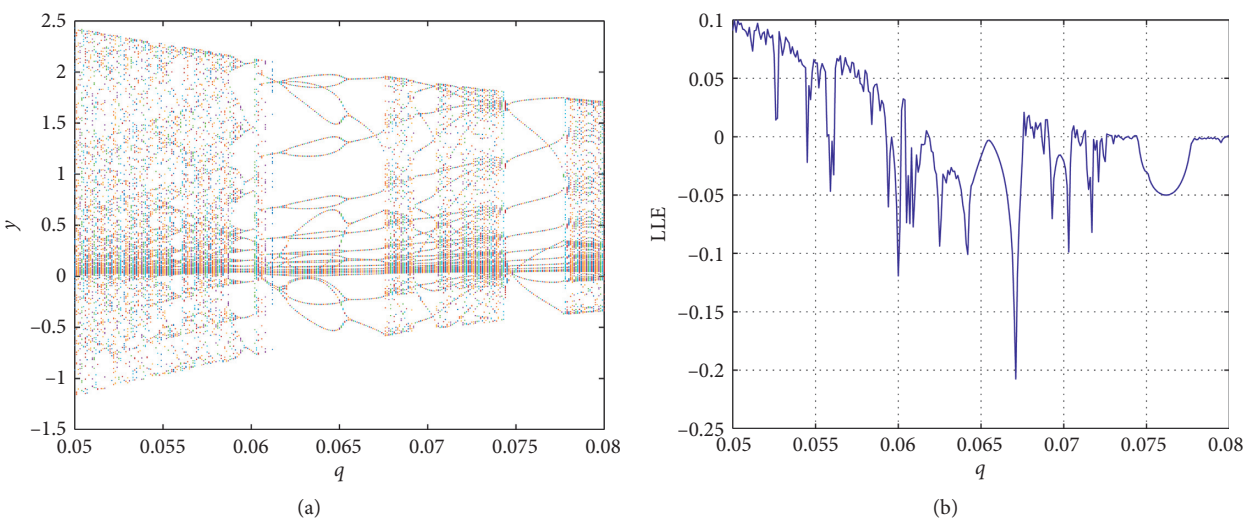

Figure 4: (a) Bifurcation diagram and (b) largest Lyapunov exponent (LLE) spectrum of system (2) with q varying.

the greater is the value of the complexity of the sequence [29, 30].

4.1. Fractional Entropy Calculation. Information entropy can be calculated for both continuous and discrete signals and is defined as follows:

$$H(p) = -c\sum_{i=1}^{n} P_i \ln P_i. \tag{7}$$

Let $c = 1$; then, according to the definition of a derivative,

$$\begin{aligned}\lim_{t\longrightarrow -1}\frac{d}{dt}\sum_{i=1}^{n}P_i^{-t} &= \lim_{t\longrightarrow -1}\sum_{i=1}^{n}\frac{d}{dt}P_i^{-t} = \lim_{t\longrightarrow -1}\sum_{i=1}^{n}P_i^{-t}\ln P_i \\ &= -\sum_{i=1}^{n}P_i\ln P_i.\end{aligned} \tag{8}$$

Comparing equation (7) with equation (8), we obtain the following:

$$H(p) = \lim_{t\longrightarrow -1}\frac{d}{dt}\sum_{i=1}^{n}P_i^{-t}. \tag{9}$$

According to [7], a fractional-order derivative can be defined as follows:

$$\begin{aligned}f^{\alpha}(x) = D_x^{(\alpha)}f(x) &= \lim_{h\longrightarrow 0}L\left(\frac{f^{\alpha}(x+h)-f^{\alpha}(x)}{(x+h)^{\alpha}-x^{\alpha}}\right) \\ &= \lim_{h\longrightarrow 0}\frac{\left(d\left(f^{\alpha}(x+h)-f^{\alpha}(x)\right)/d\left((x+h)^{\alpha}-x^{\alpha}\right)\right)}{\left(d\left((x+h)^{\alpha}-x^{\alpha}\right)/dh\right)} \\ &= \frac{f'(x)f^{\alpha-1}(x)}{x^{\alpha-1}}.\end{aligned} \tag{10}$$

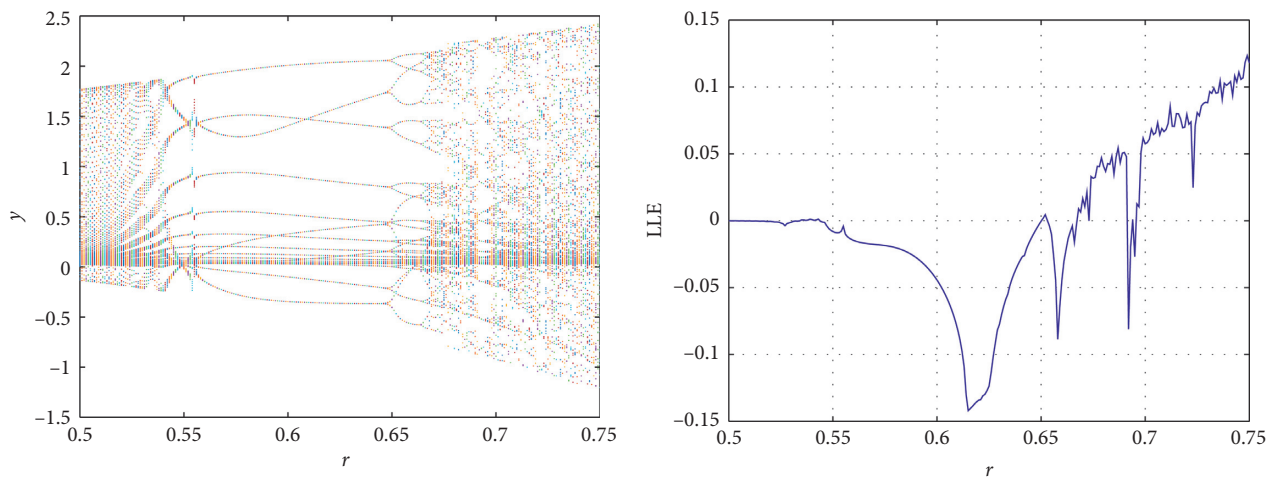

(a) (b)

Figure 5: (a) Bifurcation diagram and (b) largest Lyapunov exponent (LLE) spectrum of system (2) with r varying.

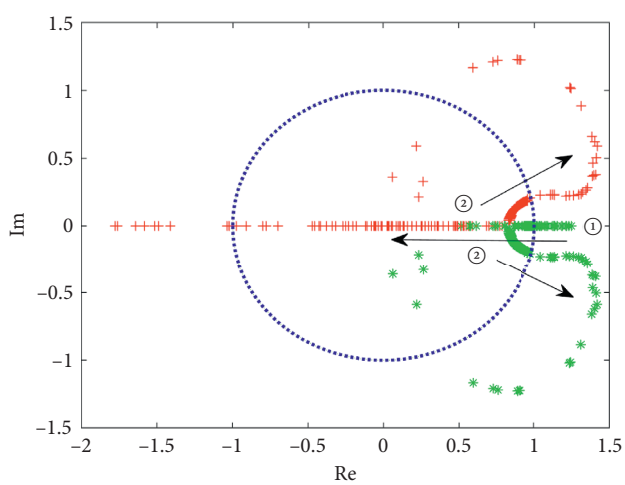

Figure 6: Eigenvalue trajectory of system (2) with r varying.

Equation (10) was used to first derive h, and then, we set $h \longrightarrow 0$ to seek the limit. On the basis of this fractional derivative, KARCI proposed the first type of fractional derivative [1, 3]:

$$H_i = D_t^{(\alpha)} P_i^{-t} = \sum_{i=1}^{n} \left| -p_i^{\alpha} p_i \ln p_i \right|. \tag{11}$$

When $\alpha \longrightarrow 1$, equation (11) cannot be degenerated into equation (7), so there is an error. The fractional entropy is thus redefined as follows:

$$\begin{aligned} H^{\alpha}(P) &= \lim_{t \longrightarrow -1} \sum_{i=1}^{n} D_x^{(\alpha)} P_i^{-t} = \lim_{t \longrightarrow -1} \sum_{i=1}^{n} \frac{\left(-P_i^{-t} \ln(P_i) P_i^{-t}\right)^{\alpha-1}}{t^{\alpha-1}} \\ &= \lim_{t \longrightarrow -1} \sum_{i=1}^{n} \frac{-P_i^{-t\alpha} \ln(P_i)}{t^{\alpha-1}} = \lim_{t \longrightarrow -1} \sum_{i=1}^{n} \frac{-P_i^{\alpha} \ln(P_i)}{(-1)^{\alpha-1}} \\ &= (-1)^{\alpha} \sum_{i=1}^{n} -P_i^{\alpha} \ln(P_i). \end{aligned} \tag{12}$$

When $\alpha \longrightarrow 1$, equation (12) can be degenerated into equation (7), but $0 < \alpha \leq 1$ and α is a complex number. Thus, if $(-1)^{-\alpha} = k_1 + ik_2$, $k_1, k_2 \in R$; then, $H^{\alpha}(P) = k_1 \sum_{i=1}^{n} P_i^{\alpha} \ln(P_i) + [k_2 \sum_{i=1}^{n} P_i^{\alpha} \ln(P_i)]$. If $k_2 = 0$, then $H^{\alpha}(p)$ is a real number. In practical applications, fractional entropy is redefined as follows:

$$H^{\alpha}(p) = \mathrm{Max}\left\{ k_1 \sum_{i=1}^{n} P_i^{\alpha} \ln(P_i) \right\}, k_2 \sum_{i=1}^{n} P_i^{\alpha} \ln(P_i). \tag{13}$$

4.2. Fractional-Order Approximate Entropy Calculation. Fractional-order entropy is combined with approximate entropy to obtain fractional-order approximate entropy (FAE). The specific steps are as follows.

In general, for the specific calculation method of the sample entropy of the time series $\{x(n)\}$ composed of N data items, the specific steps are as follows:

S1: according to the serial number to form a one-dimensional m vector sequence $\{X_m(1), \cdots, X_m(N-m+1)\}$, where $X_m(1) = \{x(i), x(i+1), \cdots, x(i+m-1)\}$, $1 \leq i \leq N-m+1$. These vectors are m consecutive x values starting from point 1.

S2: define the distance between $X_m(i)$ and $X_m(j)$, i.e., $d[X_m(i)\ X_m(j)]$, as the difference between the maximum absolute values of the corresponding elements.

S3: define the criterion of similarity r. Calculate the value of $d[X_m(i), X_m(j)] < r (1 \leq j \leq N-m, 1 \leq i \leq N-m)$ and its ratio to the total distance $N-m$, denoted as $B_i^m(r) = (B_i/(N-m-1))$.

S4: on the basis of equation (12), the average value of $B_i^m(r)$ can be calculated as follows:

$$B^m(r) = \frac{1}{N-m} \sum_{i=1}^{N-m} \left(-B_i^m(r)_i\right)^{\alpha} B_i^m(r) \ln B_i^m(r). \tag{14}$$

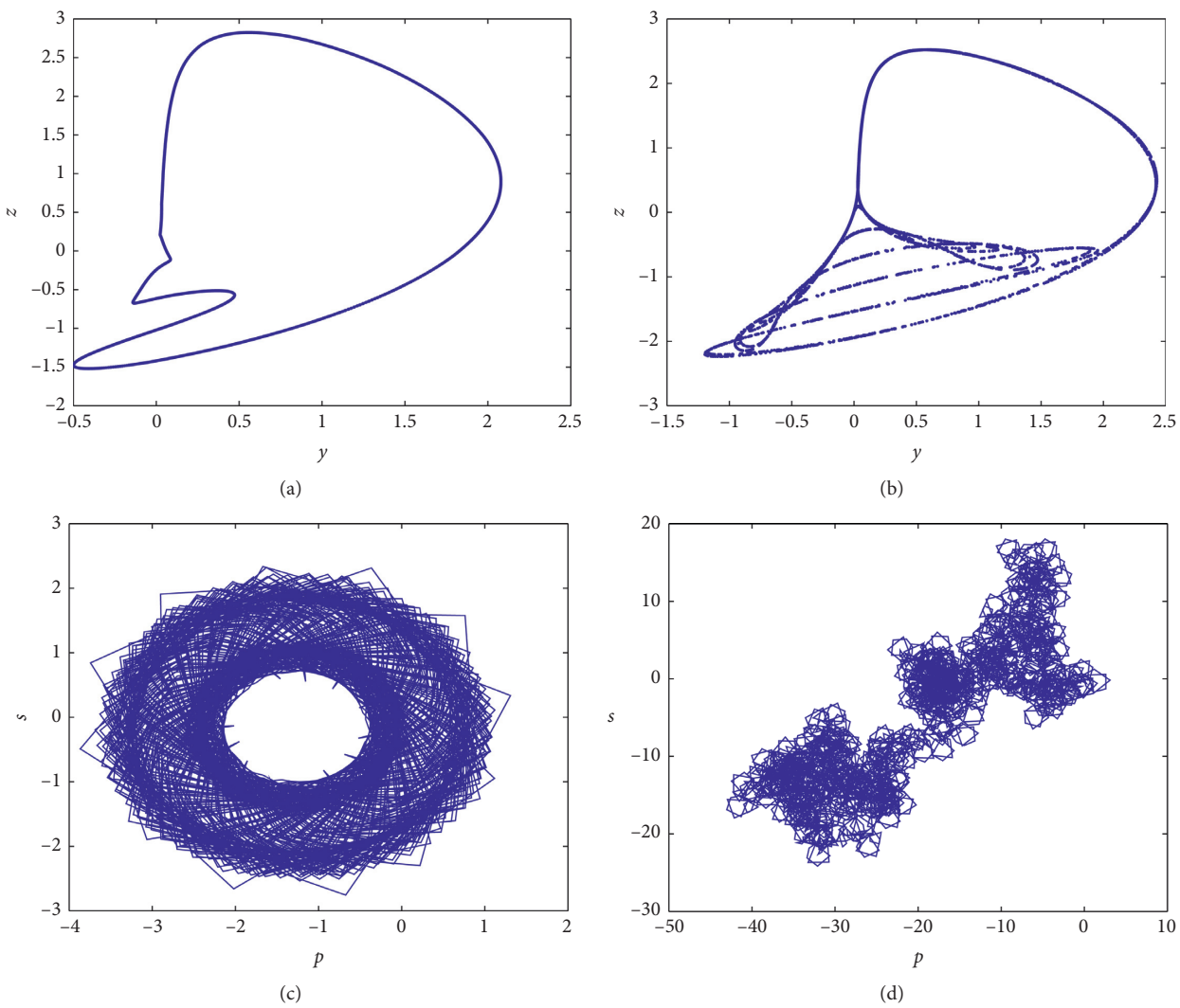

Figure 7: Phase diagrams and p-s plots of the systems with varying r: (a) y-z phase with $r = 0.6$, (b) y-z phase with $r = 0.73$, (c) p-s plots with $r = 0.6$, and (d) p-s plots with $r = 0.73$.

S5: similarly, change m to $m + 1$, and repeat S1 to S3 to obtain $A^m(r)$.

S6: theoretically, according to equation (13), the FAE complexity can be calculated as follows:

$$\mathrm{FAE}(m, r) = \max\{\mathrm{rel}(B^m(r) - \mathrm{A}^m(r)), \mathrm{imag}(B^m(r) - \mathrm{A}^m(r))\}. \tag{15}$$

4.3. Complexity Analysis. The FAE analysis results of the inventory management system with varying q and r values are shown in Figure 8. Here, the same parameter settings and step size are used as those in the corresponding bifurcation diagrams and LLE. As demonstrated in these FAE plots, the results matched the corresponding bifurcation diagrams well. When the system was chaotic, higher complexity measurement results were obtained, whereas when the system was nonchaotic, the measured results were relatively small. Obviously, FAE provided different information on the dynamics of the system from that obtained from the bifurcation diagrams. Thus, we could determine the complexity variation trend of the system clearly.

As it is well known and quite obvious, we do not need chaos in the inventory management system, at least in most cases. This implies that the system is unstable and the inventory management situation has become unpredictable. We diagnosed the status of the inventory management system by means of the complexity method using the time series.

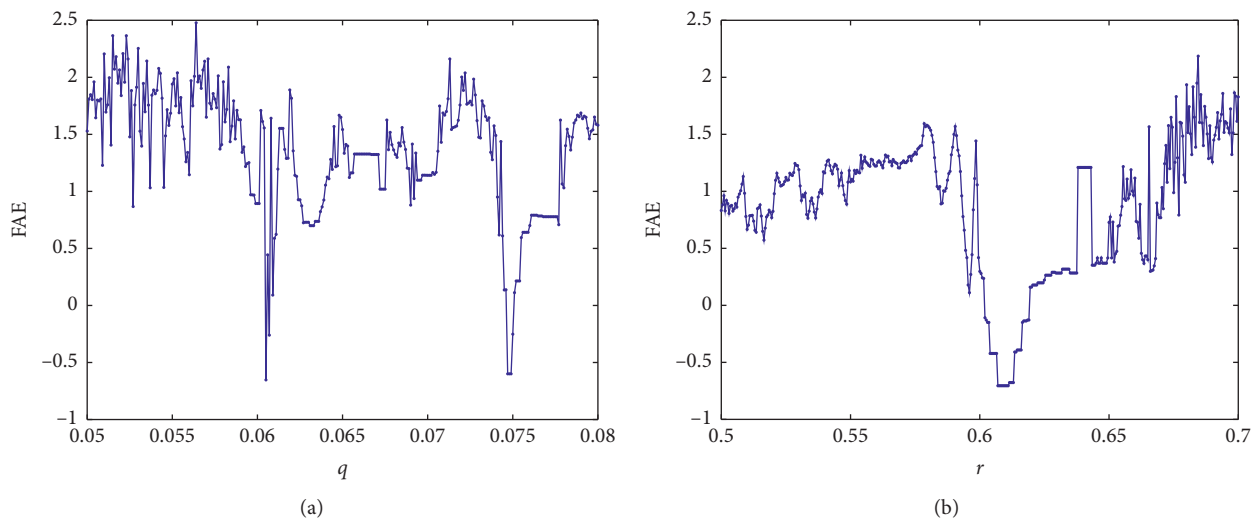

Figure 8: Fractional-order approximate entropy (FAE) of system (1) with (a) varying q and (b) varying r values.

5. Conclusion

In the present study, the dynamic behaviour of a nonlinear inventory management system was investigated. The different aspects of the dynamic behaviour of the system, including the phase diagrams and their corresponding *p-s* plots, bifurcation diagrams, LLE with parameters and FAE complexity with parameters, were studied. We found that chaos and different states could be observed with different parameter settings. Meanwhile, the AEP complexity showed the changes in the complexity of the system. It also showed that the system had a wide region of high complexity in the corresponding parameter planes.

Data Availability

The data used to support the findings of this study are available from the corresponding author upon request.

Conflicts of Interest

The authors declare that they have no conflicts of interest.

Acknowledgments

This work was supported the Major Scientific and Technological Innovation Projects of Shandong Province (Grant no. 2019JZZY010111), Natural Science Foundation of Shandong Province (Grant no. ZR2017PA008), Key Research and Development Plan of Shandong Province (Grant no. 2019GGX104092), and Science and Technology Plan Projects of Universities of Shandong Province (Grant no. J18KA381).

References

[1] A. T. Azar and S. Vaidyanathan, *Chaos Modeling and Control Systems Design*, Springer International Publishing, Berlin, Germany, 2015.

[2] J. P. Pinder, "Nonlinear dynamical systems and inventory management," *Managerial and Decision Economics*, vol. 17, no. 1, pp. 27–43, 1996.

[3] D. Levy, "Chaos theory and strategy :theory, application, an managerial implications," *Strategic Management Journal*, vol. 15, pp. 167–178, 1994.

[4] G. Feichtinger, C. H. Hommes, and W. Herold, "Chaos in a simple deterministic queueing system," *ZOR - Methods and Models of Operations Research*, vol. 40, no. 1, pp. 109–119, 1994.

[5] P. Murphy, "Chaos theory as a model for managing issues and crises," *Public Relations Review*, vol. 22, no. 2, pp. 95–113, 1996.

[6] E. C. Joseph, "Chaos & po stmodernism forecasting & futuring insights," Technical report, *Futurics, Summer-Fall*, pp. 1–12, 1994.

[7] Y. Ding and J. Cao, "Bifurcation analysis and chaos switchover phenomenon in a nonlinear financial system with delay feedback," *International Journal of Bifurcation & Chaos*, vol. 25, no. 12, pp. 2671–2691, 2015.

[8] S. Wang, S. He, A. Yousefpour, H. Jahanshahi, R. Repnik, and M. Perc, "Chaos and complexity in a fractional-order financial system with time delays," *Chaos, Solitons & Fractals*, vol. 131, 2020.

[9] R. Hilfer, *Applications of Fractional Calculus in Physics*, World Scientific Press, New Jersey, NJ, USA, 2001.

[10] X. Yi, R. Guo, and Y. Qi, "Stabilization of chaotic systems with both uncertainty and disturbance by the UDE-based control method," *IEEE Access*, vol. 8, no. 1, pp. 62471–62477, 2020.

[11] L. Liu, B. Li, and R. Guo, "Consensus control for networked manipulators with switched parameters and topologies," *IEEE Access*, vol. 9, pp. 9209–9217, 2021.

[12] R. Peng, C. Jiang, and R. Guo, "Stabilization of a class of fractional order systems with both uncertainty and disturbance," *IEEE Access*, vol. 9, p. 42697, 2021.

[13] R. Xu and F. Zhang, "ε-Nash mean-field games for general linear-quadratic systems with applications," *Automatica*, vol. 114, pp. 1–6, 2020.

[14] T. Hou, Y. Liu, and F. Deng, "Finite horizon H2/H∞ control for SDEs with infinite Markovian jumps," *Nonlinear Analysis: Hybrid Systems*, vol. 34, pp. 108–120, 2019.

[15] Y. Yu, H.-X. Li, S. Wang, and J. Yu, "Dynamic analysis of a fractional-order Lorenz chaotic system☆," *Chaos, Solitons & Fractals*, vol. 42, no. 2, pp. 1181–1189, 2009.

[16] S. B. He, K. H. Sun, and S. Banerjee, "Dynamical properties and complexity in fractional-order diffusionless Lorenz system," *The European Physical Journal Plus volume*, vol. 131, p. 254, 2016.

[17] J. G. Lu and G. Chen, "A note on the fractional-order Chen system," *Chaos, Solitons & Fractals*, vol. 27, no. 3, pp. 685–688, 2006.

[18] A. S. Hegazi and A. E. Matouk, "Dynamical behaviors and synchronization in the fractional order hyperchaotic Chen system," *Applied Mathematics Letters*, vol. 24, no. 11, pp. 1938–1944, 2011.

[19] Y. X. Xu, K. H. Sun, S. B. He et al., "Dynamics of fractional-order simplified unified system based on Adomian decomposition method," *The European Physical Journal Plus volume*, vol. 131, pp. 1–12, 2016.

[20] M. Edelman, "Fractional maps and fractional attractors part I: α-families of maps," *The interdisciplinary journal of Discontinuity Nonlinearity and Complexity*, vol. 1, no. 4, pp. 305–324, 2012.

[21] M. Edelman, "Fractional maps and fractional attractors. Part II: fractional difference caputo α- families of maps," *The Interdisciplinary Journal of Discontinuity, Nonlinearity, and Complexity*, vol. 4, no. 4, pp. 391–402, 2015.

[22] G.-C. Wu and D. Baleanu, "Discrete fractional logistic map and its chaos," *Nonlinear Dynamics*, vol. 75, no. 1-2, pp. 283–287, 2014.

[23] G.-C. Wu, D. Baleanu, and S.-D. Zeng, "Discrete chaos in fractional sine and standard maps," *Physics Letters A*, vol. 378, no. 5-6, pp. 484–487, 2014.

[24] A.-A. Khennaoui, A. Ouannas, S. Bendoukha, X. Wang, and V.-T. Pham, "On chaos in the fractional-order discrete-time unified system and its control synchronization," *Entropy*, vol. 20, no. 7, p. 530, 2018.

[25] Y. Liu, "Chaotic synchronization between linearly coupled discrete fractional Hénon maps," *Indian Journal of Physics*, vol. 90, no. 3, pp. 313–317, 2016.

[26] M. K. Shukla and B. B. Sharma, "Investigation of chaos in fractional order generalized hyperchaotic Henon map," *AEU - International Journal of Electronics and Communications*, vol. 78, pp. 265–273, 2017.

[27] Y. Ji, L. Lai, S. Zhong, and L. Zhang, "Bifurcation and chaos of a new discrete fractional-order logistic map," *Communications in Nonlinear Science and Numerical Simulation*, vol. 57, pp. 352–358, 2018.

[28] P. Grassberger and I. Procaccia, "Estimation of the Kolmogorov entropy from a chaotic signal," *Physical Review A*, vol. 28, no. 4, pp. 2591–2593, 1983.

[29] K. Balasubramanian, S. S. Nair, and N. Nagaraj, "Classification of periodic, chaotic and random sequences using approximate entropy and Lempel-Ziv complexity measures," *Pramana*, vol. 84, no. 3, pp. 365–372, 2015.

[30] E. H. Shen, Z. J. Cai, and F. J. Gu, "Mathematical foundation of a new complexity measure," *Applied Mathematics & Mechanics*, vol. 26, no. 9, pp. 1188–1196, 2005.

[31] K.-H. Sun, X. Liu, and C.-X. Zhu, "The 0-1 test algorithm for chaos and its applications," *Chinese Physics B*, vol. 19, no. 11, p. 110510, 2010.

[32] M. Sarkar and B. Sarkar, "Optimization of safety stock under controllable production rate and energy consumption in an automated smart production management," *Energies*, vol. 12, no. 11, p. 2059, 2019.

[33] J. Pinho, J. Resende, and I. Soares, "Capacity investment in electricity markets under supply and demand uncertainty," *Energy*, vol. 150, pp. 1006–1017, 2018.

[34] J. S. Richman and J. R. Moorman, "Physiological time-series analysis using approximate entropy and sample entropy," *American Journal of Physiology Heart & Circulatory Physiology*, vol. 278, no. 6, pp. 2039–2049, 2000.

[35] W. Chen, J. Zhuang, W. Yu, and Z. Wang, "Measuring complexity using FuzzyEn, ApEn, and SampEn," *Medical Engineering & Physics*, vol. 31, no. 1, pp. 61–68, 2009.

[36] S. Pincus, "Approximate entropy (ApEn) as a complexity measure," *Chaos: An Interdisciplinary Journal of Nonlinear Science*, vol. 5, no. 1, pp. 110–117, 1995.

Hindawi
Mathematical Problems in Engineering
Volume 2021, Article ID 5544063, 12 pages
https://doi.org/10.1155/2021/5544063

Research Article

Synchronization of Complex Dynamical Networks on Time Scales via Pinning Control

Fang-Di Kong [1,2] **and Jian-Ping Sun** [1,2]

[1] *College of Electrical and Information Engineering, Lanzhou University of Technology, Lanzhou 730050, China*
[2] *Department of Applied Mathematics, Lanzhou University of Technology, Lanzhou 730050, China*

Correspondence should be addressed to Jian-Ping Sun; jpsun@lut.edu.cn

Received 10 February 2021; Accepted 26 February 2021; Published 20 March 2021

Academic Editor: Yi Qi

In this paper, we are concerned with the synchronization problem of complex dynamical networks on time scales. Some pinning synchronization criteria, which combine main characteristics of time scales with main parameters of the pinning controlled network, are established. A numerical example is also included to verify the effectiveness of the results obtained.

1. Introduction

Many complex systems in nature and human societies can be modeled by complex dynamical networks with the nodes representing individuals in the system and the edges representing the interactions among them, such as social networks, food webs, the Internet, the World Wide Web, and neural networks (see [1] and the references therein). One of the most ubiquitous and significant phenomena in complex dynamical networks is the synchronization of all dynamical nodes in a network. Over the past decades, the synchronization has attracted considerable attention [2–9]. Control would be a necessary means to guide or force the complex dynamical network to realize synchronization if a given network is not self-synchronized or the synchronized state is not the desired one. At present, the control methods which are often used include adaptive control [10, 11], impulsive control [12], pinning adaptive control [13], pinning impulsive control [14], pinning feedback control [15–25], and so on [26–30]. Since pinning control only needs a small fraction of nodes to be dealt with, the synchronization of complex dynamical networks via pinning control has become a rather significant and interesting topic; see [13–27]. It is necessary to point out that most of the aforementioned discussions were aimed at the synchronization problem of continuous-time and discrete-time complex dynamical networks, respectively.

On the one hand, in some real-world systems, the interactions among individuals can take place at any time, maybe some continuous time intervals accompanying some discrete moments. On the other hand, the theory of time scales, a useful tool to deal with continuous and discrete analysis under a unified framework, was introduced by Hilger in his Ph.D. thesis [31]. With the development of the theory of time scales, the synchronization of complex dynamical networks on time scales has received increasing attention [32–40]. For example, in 2016, Liu and Zhang [35] studied the synchronization of linear complex dynamical networks on time scales via pinning impulsive control. In 2018, Lu et al. [39] considered finite-time synchronization of nonlinear complex dynamical networks on time scales via pinning impulsive control. In [40], Xiao, Lewis, and Zeng investigated event-based time-interval pinning control for complex networks on time scales.

Since time scale is an arbitrary nonempty closed subset of the real numbers, it has various forms such as the real numbers, the integers, the union of some closed intervals, and the union of some closed intervals and some discrete points. Therefore, complex dynamical networks on time scales have great complexity. Moreover, many existing

results for continuous-time or discrete-time complex dynamical networks cannot be simply generalized to complex dynamical networks on time scales [35, 40].

Motivated greatly by the abovementioned works, in this paper, we will study a complex dynamical network on time scales by applying pinning feedback control. Some sufficient conditions are derived to guarantee the complex dynamical network to realize synchronization when it is not self-synchronized or the synchronized state is not the desired one. The main contributions of this paper are listed as follows:

(i) In order to overcome the difficulties caused by nonlinear function $f(\cdot)$ in the complex dynamical network, we design some appropriate conditions

(ii) The pinning synchronization criteria established in our paper combine main characteristics of time scales with main parameters of the pinning controlled network (such as coupling strengths, coupling configuration matrix, and pinning feedback gain matrix)

(iii) Our results have revealed the discrepancies of the pinning synchronization between continuous-time and discrete-time complex dynamical networks

The rest of this paper is organized as follows. Some notations and supporting lemmas, and some foundational knowledge about time scales are simply enumerated in Section 2. In Section 3, the synchronization problem of a complex dynamical network on time scales is formulated. In Section 4, our main results are established. In Section 5, a numerical example is given to verify the effectiveness of the results obtained. Finally, conclusions are provided in Section 6.

2. Preliminaries

In this section, we will present some notations and lemmas, and some foundational knowledge on time scales which are needed later.

2.1. Notations and Supporting Lemmas. First, we define some notations as follows:

$\mathbb{N}_0$ is the set of all nonnegative integers

$\mathbb{Z}$ is the set of all integers

$\mathbb{R}$ is the set of all real numbers

$\mathbb{R}^n$ is the n-dimensional Euclidean space with the Euclidean norm $\|\cdot\|$

$\mathbb{R}^{m\times n}$ is the set of all $m\times n$ real matrices

$I_n \in \mathbb{R}^{n\times n}$ is the n-dimensional identity matrix

$\operatorname{diag}(d_1, d_2, \ldots, d_n)$ is the diagonal matrix with diagonal entries d_1 to d_n

The superscript "T" stands for the transpose of a matrix

For symmetric matrix $P \in \mathbb{R}^{n\times n}$, $\lambda_{\min}(P)$ and $\lambda_{\max}(P)$ denote the minimum and maximum eigenvalues of P, respectively

For symmetric matrices $P, Q \in \mathbb{R}^{n\times n}$, $P \geq Q\,(P \leq Q)$ means that $P - Q$ is positive semidefinite (negative semidefinite)

$\otimes$ denotes the Kronecker product

Lemma 1 (see [23]). *Suppose $A = (a_{ij})_{n\times n}$ is a real symmetric and irreducible matrix, in which $a_{ij} \geq 0\,(j \neq i)$ and $a_{ii} = -\sum_{j=1, j\neq i}^{n} a_{ij}$, and nonzero matrix $D = diag(d_1, d_2, \ldots, d_n)$ satisfies $d_i \geq 0\,(1 \leq i \leq n)$. Let $B = A - D$. Then, all the eigenvalues of B are less than 0.*

Lemma 2 (see [41]). *If $P, Q \in \mathbb{R}^{n\times n}$ are symmetric, $x \in \mathbb{R}^n$ is a nonzero vector, and $0 < a, b \in \mathbb{R}$, then*

(1) $P + Q$ is symmetric

(2) P^k is symmetric for $k = 1, 2, \ldots,$

(3) P is positive definite $\Leftrightarrow -P$ is negative definite

(4) P is positive definite $\Leftrightarrow$ there exists a positive definite matrix $S \in \mathbb{R}^{n\times n}$ such that $P = S^2$

(5) $\lambda_{\min}(P) \leq (x^T P x / x^T x) \leq \lambda_{\max}(P)$

(6) $\lambda_{\max}(aP + bQ) \leq a\lambda_{\max}(P) + b\lambda_{\max}(Q)$

Lemma 3 (see [41, 42]). *For matrices P, Q, R, and S with appropriate dimensions, we have the following properties:*

(1) $(\alpha P)\otimes Q = P \otimes (\alpha Q) = \alpha(P\otimes Q)$, where α is a constant

(2) $(P + Q)\otimes R = P\otimes R + Q\otimes R$

(3) $(P\otimes Q)(R\otimes S) = (PR)\otimes(QS)$

(4) $(P\otimes Q)^T = P^T \otimes Q^T$

(5) If P and Q are symmetric, then $P\otimes Q$ is symmetric

(6) For square matrices P and Q, every eigenvalue of $P\otimes Q$ arises as a product of eigenvalues of P and Q

Lemma 4 (see [43]). *Let $U = (\alpha_{ij})_{N\times N}$, $M \in \mathbb{R}^{n\times n}$, and $x = (x_1^T, x_2^T, \ldots, x_N^T)^T$, where $x_i = (x_{i1}, x_{i2}, \ldots, x_{in})^T \in \mathbb{R}^n$ and $y = (y_1^T, y_2^T, \ldots, y_N^T)^T$, where $y_i = (y_{i1}, y_{i2}, \ldots, y_{in})^T \in \mathbb{R}^n\,(i = 1, 2, \ldots, N)$. If $U = U^T$ and each row sum of U is zero, then*

$$x^T(U\otimes M)y = -\sum_{1\leq i<j\leq N} \alpha_{ij}\left(x_i - x_j\right)^T M\left(y_i - y_j\right). \quad (1)$$

2.2. Foundational Knowledge on Time Scales. In this section, some foundational definitions and lemmas on time scales are provided. For more details, one can refer to [44, 45].

Let $\mathbb{T}$ be a time scale; that is, $\mathbb{T}$ is a nonempty closed subset of $\mathbb{R}$. For each interval $\mathbb{I}$ of $\mathbb{R}$, $\mathbb{I}\cap\mathbb{T}$ is denoted by $\mathbb{I}_{\mathbb{T}}$. The properties of $\mathbb{T}$ are determined by the following three functions:

(1) The forward jump operator $\sigma(t) = \inf\{s \in \mathbb{T}: s > t\}, t \in \mathbb{T}$ (in this case, we put $\inf\varnothing = \sup\mathbb{T}$, where $\varnothing$ denotes the empty set)

(2) The backward jump operator $\rho(t) = \sup\{s \in \mathbb{T}: s < t\}, t \in \mathbb{T}$ (in this case, we put $\sup\varnothing = \inf\mathbb{T}$, where $\varnothing$ denotes the empty set)

(3) The graininess function $\mu(t) = \sigma(t) - t, t \in \mathbb{T}$

For $t \in \mathbb{T}$, if $\sigma(t) > t$, we say that t is right-scattered, while if $\rho(t) < t$, we say that t is left-scattered. Also, if $t < \sup\mathbb{T}$ and $\sigma(t) = t$, then t is called right-dense, and if $t > \inf\mathbb{T}$ and $\rho(t) = t$, then t is called left-dense. The set $\mathbb{T}^\kappa$ is derived from the time scale $\mathbb{T}$ as follows: if $\mathbb{T}$ has a left-scattered maximum m, then $\mathbb{T}^\kappa = \mathbb{T}\backslash\{m\}$. Otherwise, $\mathbb{T}^\kappa = \mathbb{T}$.

Definition 1. Let $f: \mathbb{T} \longrightarrow \mathbb{R}$. Define the function $f^\sigma: \mathbb{T} \longrightarrow \mathbb{R}$ by $f^\sigma(t) = f(\sigma(t))$ for all $t \in \mathbb{T}$, i.e., $f^\sigma = f \circ \sigma$.

Definition 2. Assume that $f: \mathbb{T} \longrightarrow \mathbb{R}$ is a function and let $t \in \mathbb{T}^\kappa$. Then, f is called differentiable at the point t if there exists a $\theta \in \mathbb{R}$ such that for any given $\varepsilon > 0$, there is an open neighborhood U of t such that

$$|[f(\sigma(t)) - f(s)] - \theta[\sigma(t) - s]| \le \varepsilon|\sigma(t) - s|, \quad s \in U. \tag{2}$$

In this case, θ is called the delta derivative of f at the point t and we denote it by $\theta = f^\triangle(t)$. Moreover, we say that f is delta differentiable (or in short: differentiable) on $\mathbb{T}^\kappa$ provided $f^\triangle(t)$ exists for all $t \in \mathbb{T}^\kappa$. The function $f^\triangle: \mathbb{T}^\kappa \longrightarrow \mathbb{R}$ is called the (delta) derivative of f on $\mathbb{T}^\kappa$. If $F^\triangle(t) = f(t)$, $t \in \mathbb{T}^\kappa$, then for any $a, b \in \mathbb{T}$, the integral is defined as follows:

$$\int_a^b f(t)\triangle t = F(b) - F(a). \tag{3}$$

Remark 1. If $\mathbb{T} = \mathbb{R}$, then $f^\sigma(t) = f(t)$ and $f^\triangle(t) = f'(t)$ is the usual derivative. If $\mathbb{T} = \mathbb{Z}$, then $f^\sigma(t) = f(t+1)$ is the forward shift and $f^\triangle(t) = \triangle f(t) = f(t+1) - f(t)$ is the usual forward difference.

Lemma 5. *If $f, g: \mathbb{T} \longrightarrow \mathbb{R}$ are differentiable at $t \in \mathbb{T}^\kappa$, then*

$$\begin{aligned}(fg)^\triangle(t) &= f^\triangle(t)g(t) + f^\sigma(t)g^\triangle(t) = f(t)g^\triangle(t) \\ &\quad + f^\triangle(t)g^\sigma(t).\end{aligned} \tag{4}$$

Lemma 6. *If $f: \mathbb{T} \longrightarrow \mathbb{R}$ is differentiable at $t \in \mathbb{T}^\kappa$, then $f^\sigma(t) = f(t) + \mu(t)f^\triangle(t)$.*

Definition 3. A function $f: \mathbb{T} \longrightarrow \mathbb{R}$ is called rd-continuous provided it is continuous at right-dense points in $\mathbb{T}$ and its left-sided limits exist (finite) at left-dense points in $\mathbb{T}$. The set of rd-continuous functions is denoted by $C_{rd}(\mathbb{T}, \mathbb{R})$.

Definition 4. We say that a function $p: \mathbb{T} \longrightarrow \mathbb{R}$ is regressive (positively regressive) provided

$$1 + \mu(t)p(t) \ne 0, \quad \text{for all } t \in \mathbb{T}^\kappa \, (1 + \mu(t)p(t) > 0 \text{ for all } t \in \mathbb{T}), \tag{5}$$

holds. The set of all regressive (positively regressive) and rd-continuous functions is denoted by $\mathscr{R}(\mathbb{T}, \mathbb{R})$ ($\mathscr{R}^+(\mathbb{T}, \mathbb{R})$).

Definition 5. If $p \in \mathscr{R}(\mathbb{T}, \mathbb{R})$, then we define the exponential function by

$$e_p(t, s) = \exp\left(\int_s^t \xi_{\mu(\tau)}(p(\tau))\Delta\tau\right), \quad \text{for } s, t \in \mathbb{T} \tag{6}$$

with the cylinder transformation $\xi_h(z)$ defined by

$$\xi_h(z) = \begin{cases} \dfrac{1}{h}\operatorname{Log}(1 + zh), & h > 0, \\ z, & h = 0, \end{cases} \tag{7}$$

where Log is the principal logarithm function.

Lemma 7. *Let $t_0 \in \mathbb{T}$, $y, f \in C_{rd}(\mathbb{T}, \mathbb{R})$, and $p \in \mathscr{R}^+(\mathbb{T}, \mathbb{R})$. Then,*

$$y^\Delta(t) \le p(t)y(t) + f(t), \quad \text{for all } t \in \mathbb{T}, \tag{8}$$

implies

$$y(t) \le y(t_0)e_p(t, t_0) + \int_{t_0}^t e_p(t, \sigma(\tau))f(\tau)\triangle\tau, \quad \text{for all } t \in \mathbb{T}. \tag{9}$$

Lemma 8 (see [40]). *For fixed $t_0 \in \mathbb{T}$, if $p < 0$ and $p \in \mathscr{R}^+(\mathbb{T}, \mathbb{R})$, then $e_p(t, t_0) \longrightarrow 0$ as $t \longrightarrow \infty$, $t \in \mathbb{T}$.*

Definition 6. Let A be an $m \times n$-matrix-valued function on $\mathbb{T}$. We say that A is rd-continuous on $\mathbb{T}$ if each entry of A is rd-continuous on $\mathbb{T}$. We say that A is differentiable on $\mathbb{T}$ provided each entry of A is differentiable on $\mathbb{T}$. In this case, we put $A^\triangle = (a_{ij}^\triangle)_{1 \le i \le m, 1 \le j \le n}$, where $A = (a_{ij})_{1 \le i \le m, 1 \le j \le n}$.

Lemma 9. *If A is differentiable at $t \in \mathbb{T}^\kappa$, then $A^\sigma(t) = A(t) + \mu(t)A^\triangle(t)$.*

Lemma 10. *Suppose A and B are differentiable $n \times n$-matrix-valued functions on $\mathbb{T}$. Then,*

(1) $(A + B)^\triangle = A^\triangle + B^\triangle$

(2) $(\alpha A)^\triangle = \alpha A^\triangle$ *if α is constant*

(3) $(AB)^\triangle = A^\triangle B + A^\sigma B^\triangle = AB^\triangle + A^\triangle B^\sigma$

Definition 7. An $n \times n$-matrix-valued function A on $\mathbb{T}$ is called regressive (with respect to $\mathbb{T}$) provided $I_n + \mu(t)A(t)$ is invertible for all $t \in \mathbb{T}^\kappa$, and the class of all such regressive and rd-continuous functions is denoted by $\mathscr{R}(\mathbb{T}, \mathbb{R}^{n\times n})$.

3. Problem Formulations

In the remainder of this paper, we always assume that $\mathbb{T}$ is a time scale with $0 \in \mathbb{T}$ and $\sup\mathbb{T} = \infty$.

Suppose that a complex dynamical network on $\mathbb{T}$ consists of N identical nodes, with each node being an

n-dimensional dynamical system. This complex dynamical network can be described as

$$x_i^{\triangle}(t) = f(x_i(t)) + \sum_{j=1, j\neq i}^{N} c_{ij} g_{ij} \Gamma\left(x_j(t) - x_i(t)\right), \quad t \in [0,\infty)_{\mathbb{T}}, i = 1,2,\ldots,N, \tag{10}$$

where $x_i(t) = (x_{i1}(t), x_{i2}(t), \ldots, x_{in}(t))^T \in \mathbb{R}^n$ is the state vector of the ith node at time t, $x_i^{\triangle}$ is the delta derivative of x_i on $[0,\infty)_{\mathbb{T}}$, $f\colon \mathbb{R}^n \longrightarrow \mathbb{R}^n$ is a vector function, the constant $c_{ij} > 0\,(1 \le i, j \le N, i \neq j)$ represents the coupling strength between node i and node j, $\Gamma \in \mathbb{R}^{n\times n}$ is the inner coupling matrix, and the coupling configuration matrix $G = (g_{ij})_{N\times N}$ represents the topological structure of the complex dynamical network and is defined as follows: if there exists a connection between node i and node $j\,(i \neq j)$, then $g_{ij} = g_{ji} = 1$; otherwise, $g_{ij} = g_{ji} = 0$; the diagonal elements of G are defined as

$$g_{ii} = -\sum_{j=1, j\neq i}^{N} g_{ij} = -\sum_{j=1, j\neq i}^{N} g_{ji}, \quad i = 1,2,\ldots,N, \tag{11}$$

and $c_{ii}\,(1 \le i \le N)$ satisfies

$$c_{ii} g_{ii} + \sum_{j=1, j\neq i}^{N} c_{ij} g_{ij} = c_{ii} g_{ii} + \sum_{j=1, j\neq i}^{N} c_{ji} g_{ji} = 0, \quad i = 1,2,\ldots,N. \tag{12}$$

Then, network (10) can be equivalently written in the following form:

$$x_i^{\triangle}(t) = f(x_i(t)) + \sum_{j=1}^{N} c_{ij} g_{ij} \Gamma x_j(t), \quad t \in [0,\infty)_{\mathbb{T}}, i = 1,2,\ldots,N. \tag{13}$$

In what follows, we always assume that network (13) is connected in the sense of having no isolated clusters, which means that the symmetric matrix G is irreducible, and the following condition is satisfied:

$$c_{ii} g_{ii} \Gamma \in \mathscr{R}(\mathbb{T}, \mathbb{R}^{n\times n}), \quad i = 1,2,\ldots,N. \tag{14}$$

Now, our goal is to control network (13) onto a solution of the uncoupled system

$$s^{\triangle}(t) = f(s(t)), \quad t \in [0,\infty)_{\mathbb{T}}, \tag{15}$$

that is,

$$\lim_{t\longrightarrow\infty} \left\| x_i(t) - s(t) \right\| = 0, \quad i = 1,2,\ldots,N. \tag{16}$$

Here, we assume that f is continuous and of such a nature that existence and uniqueness of solutions to dynamic equation (15) subject to $s(0) = s_0$ as well as their dependence on initial values is guaranteed.

To achieve the goal, we apply the pinning control strategy on a fraction of the nodes in network (13). Without loss of generality, let the first l nodes be selected to be pinned. The pinning controlled network can be described as follows:

$$\begin{aligned} x_i^{\triangle}(t) &= f(x_i(t)) + \sum_{j=1}^{N} c_{ij} g_{ij} \Gamma x_j(t) + u_i(t), \quad t \in [0,\infty)_{\mathbb{T}}, i = 1,2,\ldots,l, \\ x_i^{\triangle}(t) &= f(x_i(t)) + \sum_{j=1}^{N} c_{ij} g_{ij} \Gamma x_j(t), \quad t \in [0,\infty)_{\mathbb{T}}, i = l+1, l+2,\ldots,N, \end{aligned} \tag{17}$$

where $u_i(t) = -c_{ii} d_i \Gamma(x_i(t) - s(t)), \quad t \in [0,\infty)_{\mathbb{T}}, \quad d_i > 0$, and $c_{ii}(g_{ii} - d_i)\Gamma \in \mathscr{R}(\mathbb{T}; \mathbb{R}^{n\times n}), i = 1,2,\ldots,l$.

Remark 2. If $\mathbb{T} = \mathbb{R}$, then network (13) is reduced to the continuous-time network:

$$\dot{x}_i(t) = f(x_i(t)) + \sum_{j=1}^{N} c_{ij} g_{ij} \Gamma x_j(t), \quad t \in [0,\infty), i = 1,2,\ldots,N, \tag{18}$$

and pinning controlled network (17) can be described by

$$\begin{aligned} \dot{x}_i(t) &= f(x_i(t)) + \sum_{j=1}^{N} c_{ij} g_{ij} \Gamma x_j(t) + u_i(t), \quad t \in [0,\infty), i = 1,2,\ldots,l, \\ \dot{x}_i(t) &= f(x_i(t)) + \sum_{j=1}^{N} c_{ij} g_{ij} \Gamma x_j(t), \quad t \in [0,\infty), i = l+1, l+2,\ldots,N, \end{aligned} \tag{19}$$

where $u_i(t) = -c_{ii} d_i \Gamma(x_i(t) - s(t)), t \in [0,\infty)$, $d_i > 0$, $i = 1,2,\ldots,l$, and $s(t)$ is a solution of the system

$$\dot{s}(t) = f(s(t)), \quad t \in [0,\infty). \tag{20}$$

Remark 3. If $\mathbb{T} = \mathbb{Z}$, then network (13) is reduced to the discrete-time network:

$$\Delta x_i(t) = f(x_i(t)) + \sum_{j=1}^{N} c_{ij} g_{ij} \Gamma x_j(t), \quad t \in \mathbb{N}_0, i = 1, 2, \ldots, N, \tag{21}$$

and pinning controlled network (17) can be described by

$$\begin{aligned} \Delta x_i(t) &= f(x_i(t)) + \sum_{j=1}^{N} c_{ij} g_{ij} \Gamma x_j(t) + u_i(t), \quad t \in \mathbb{N}_0, i = 1, 2, \ldots, l, \\ \Delta x_i(t) &= f(x_i(t)) + \sum_{j=1}^{N} c_{ij} g_{ij} \Gamma x_j(t), \quad t \in \mathbb{N}_0, i = l+1, l+2, \ldots, N, \end{aligned} \tag{22}$$

where $u_i(t) = -c_{ii} d_i \Gamma (x_i(t) - s(t)), t \in \mathbb{N}_0$, $d_i > 0, i = 1, 2, \ldots, l$, and $s(t)$ is a solution of the system

$$\Delta s(t) = f(s(t)), \quad t \in \mathbb{N}_0. \tag{23}$$

Let $x(t) = (x_1^T(t), x_2^T(t), \ldots, x_N^T(t))^T \in \mathbb{R}^{nN}$, $F(x(t)) = (f^T(x_1(t)), f^T(x_2(t)), \ldots, f^T(x_N(t)))^T \in \mathbb{R}^{nN}$, $S(t) = \underbrace{(s^T(t), s^T(t), \ldots, s^T(t))}_{N}^{T} \in \mathbb{R}^{nN}$, $A = (c_{ij} g_{ij}) \in \mathbb{R}^{N \times N}$, and $D = \operatorname{diag}(c_{11} d_1, c_{22} d_2, \ldots, c_{ll} d_l, \underbrace{0, \ldots, 0}_{N-l})$. Then, we can write pinning controlled network (17) as

$$\begin{aligned} x^{\triangle}(t) &= F(x(t)) + (A \otimes \Gamma) x(t) - (D \otimes \Gamma) x(t) + (D \otimes \Gamma) S(t) \\ &= F(x(t)) + [(A - D) \otimes \Gamma] x(t) \\ &\quad + (D \otimes \Gamma) S(t), \quad t \in [0, \infty)_{\mathbb{T}}, \end{aligned} \tag{24}$$

and obtain the following error dynamical network:

$$z^{\triangle}(t) = F(x(t)) - F(S(t)) + [(A - D) \otimes \Gamma] z(t), \quad t \in [0, \infty)_{\mathbb{T}}, \tag{25}$$

where $z(t) = (z_1^T(t), z_2^T(t), \ldots, z_N^T(t))^T \in \mathbb{R}^{nN}$, $z_i(t) = x_i(t) - s(t) \in \mathbb{R}^n (i = 1, 2, \ldots, N)$, and $F(S(t)) = \underbrace{(f^T(s(t)), f^T(s(t)), \ldots, f^T(s(t)))}_{N}^{T} \in \mathbb{R}^{nN}$.

By [17], we know that A is a symmetric and irreducible matrix. So, it follows from Lemmas 1 and 2 that $\lambda_{\max}(A - D) < 0$ and $(A - D)^2$ is symmetric positive definite.

4. Pinning Synchronization Criteria for Complex Dynamical Networks on Time Scales

To derive the main results, first, we introduce a definition.

Definition 8 (see [2, 17, 46]). A function $\phi: \mathbb{R}^n \longrightarrow \mathbb{R}^n$ is said to be increasing if

$$(x - y)^T (\phi(x) - \phi(y)) \geq 0, \quad \text{for all } x, y \in \mathbb{R}^n. \tag{26}$$

Throughout this section, we always assume that the function $f: \mathbb{R}^n \longrightarrow \mathbb{R}^n$ satisfies Lipschitz condition; that is, there exists a constant $L > 0$ such that $\|f(x) - f(y)\| \leq L\|x - y\|$ holds for any $x, y \in \mathbb{R}^n$.

Theorem 1. *Suppose that there exists a constant $\mu^* \geq 0$ such that $\mu(t) \leq \mu^*$ for all $t \in \mathbb{T}$, Γ is symmetric and $\Gamma f(\cdot)$ is increasing. Then, the pinning controlled network (17) is synchronized, if there exists a constant function $\alpha \in \mathscr{R}^+(\mathbb{T}, (-\infty, 0))$ such that*

$$2LI_{nN} + 2(A - D) \otimes \Gamma + \mu^* \left[L^2 I_{nN} + (A - D)^2 \otimes \Gamma^2 \right] \leq \alpha I_{nN} \tag{27}$$

holds.

Proof. Construct the Lyapunov function $V(t) = z^T(t) z(t), t \in [0, \infty)_{\mathbb{T}}$. In view of Lemmas 3, 5, 6, 9, and 10, we can obtain the Δ-derivative of $V(t)$ along the trajectory (25):

$$\begin{aligned} V^{\triangle}(t) &= \left[\left(z^T(t)\right)^{\triangle} z(t) + \left(z^T\right)^{\sigma}(t) z^{\triangle}(t) \right] \\ &= \left(z^T(t)\right)^{\triangle} z(t) + \left(z^T(t) + \mu(t) \left(z^T(t)\right)^{\triangle} \right) z^{\triangle}(t) \\ &= 2 z^T(t) z^{\triangle}(t) + \mu(t) \left(z^{\triangle}(t)\right)^T z^{\triangle}(t) \\ &\leq 2 z^T(t) z^{\triangle}(t) + \mu^* \left(z^{\triangle}(t)\right)^T z^{\triangle}(t) \\ &= 2 z^T(t) \{ (F(x(t)) - F(S(t))) + [(A - D) \otimes \Gamma] z(t) \} + \mu^* \Big\{ (F(x(t)) - F(S(t)))^T \\ &\quad + ([(A - D) \otimes \Gamma] z(t))^T \Big\} \{ (F(x(t)) - F(S(t))) + [(A - D) \otimes \Gamma] z(t) \} \\ &= V_1(t) + V_2(t) + \mu^* [V_3(t) + V_4(t) + V_5(t)], \quad t \in [0, \infty)_{\mathbb{T}}, \end{aligned} \tag{28}$$

where

$$\begin{aligned}
V_1(t) &= 2z^T(t)(F(x(t)) - F(S(t))),\\
V_2(t) &= 2z^T(t)[(A-D)\otimes\Gamma]z(t),\\
V_3(t) &= (F(x(t)) - F(S(t)))^T(F(x(t)) - F(S(t))),\\
V_4(t) &= 2z^T(t)[(A-D)\otimes\Gamma](F(x(t)) - F(S(t))),\\
V_5(t) &= z^T(t)\left[(A-D)^2\otimes\Gamma^2\right]z(t).
\end{aligned} \tag{29}$$

On the one hand, since f satisfies Lipschitz condition, we get

$$\begin{aligned}
V_1(t) &= 2z^T(t)(F(x(t)) - F(S(t)))\\
&= 2\sum_{i=1}^{N} z_i^T(t)(f(x_i(t)) - f(s(t)))\\
&\le 2\sum_{i=1}^{N} \|z_i^T(t)\|\|f(x_i(t)) - f(s(t))\|\\
&= 2\sum_{i=1}^{N} \|(x_i(t) - (s(t))^T\|\|f(x_i(t)) - f(s(t))\|\\
&\le 2L\sum_{i=1}^{N} \|x_i(t) - s(t)\|^2\\
&= 2L\sum_{i=1}^{N} (x_i(t) - s(t))^T(x_i(t) - s(t))\\
&= 2Lz^T(t)z(t), \quad t\in[0,\infty)_{\mathbb{T}},
\end{aligned} \tag{30}$$

$$\begin{aligned}
V_3(t) &= (F(x(t)) - F(S(t)))^T(F(x(t)) - F(s(t)))\\
&= \sum_{i=1}^{N} (f(x_i(t)) - f(s(t)))^T(f(x_i(t)) - f(s(t)))\\
&= \sum_{i=1}^{N} \|(f(x_i(t)) - f(s(t)))\|^2\\
&\le L^2\sum_{i=1}^{N} \|(x_i(t)) - (s(t))\|^2\\
&= L^2\sum_{i=1}^{N} (x_i(t)) - (s(t))^T(x_i(t)) - (s(t))\\
&= L^2z^T(t)z(t), \quad t\in[0,\infty)_{\mathbb{T}}.
\end{aligned} \tag{31}$$

On the other hand, since $\Gamma f(\cdot)$ is increasing, by Lemma 4, we have

$$\begin{aligned}
V_4(t) &= 2z^T(t)[(A-D)\otimes\Gamma](F(x(t)) - F(S(t)))\\
&= 2\left[z^T(t)(A\otimes\Gamma)(F(x(t)) - F(S(t))) - z^T(t)\right.\\
&\quad \left.(D\otimes\Gamma)(F(x(t)) - F(S(t)))\right]\\
&= -2\left\{\sum_{1\le i<j\le N} c_{ij}g_{ij}(z_i(t) - z_j(t))^T\right.\\
&\quad \Gamma\left[(f(x_i(t)) - f(s(t))) - (f(x_j(t)) - f(s(t)))\right]\\
&\quad \left.+\sum_{i=1}^{l} z_i^T(t)c_{ii}d_i\Gamma(f(x_i(t)) - f(s(t)))\right\}\\
&= -2\left[\sum_{1\le i<j\le N} c_{ij}g_{ij}(x_i(t) - x_j(t))^T\right.\\
&\quad \Gamma(f(x_i(t)) - f(x_j(t)))\\
&\quad \left.+\sum_{i=1}^{l} c_{ii}d_i(x_i(t) - s(t))\Gamma(f(x_i(t)) - f(s(t)))\right]\\
&= -2\left[\sum_{1\le i<j\le N} c_{ij}g_{ij}(x_i(t) - x_j(t))^T\right.\\
&\quad (\Gamma f(x_i(t)) - \Gamma f(x_j(t)))\\
&\quad \left.+\sum_{i=1}^{l} c_{ii}d_i(x_i(t) - s(t))^T\right.\\
&\quad \left.(\Gamma f(x_i(t)) - \Gamma f(s(t)))\right], \quad \le 0, t\in[0,\infty)_{\mathbb{T}}.
\end{aligned} \tag{32}$$

So, it follows from (28), (30)–(32), and condition (27) that

$$\begin{aligned}
V^{\triangle}(t) &\le 2Lz^T(t)z(t) + 2z^T(t)[(A-D)\otimes\Gamma]z(t) + \mu^*\left\{L^2z^T(t)z(t) + z^T(t)\left[(A-D)^2\otimes\Gamma^2\right]z(t)\right\}\\
&= z^T(t)\left\{2LI_{nN} + 2(A-D)\otimes\Gamma + \mu^*\left[L^2I_{nN} + (A-D)^2\otimes\Gamma^2\right]\right\}z(t)\\
&\le \alpha V(t), \quad t\in[0,\infty)_{\mathbb{T}},
\end{aligned} \tag{33}$$

which together with Lemma 7 implies that

$$V(t) \le V(0)e_{\alpha}(t,0), \quad t\in[0,\infty)_{\mathbb{T}}. \tag{34}$$

At the same time, it follows from $\alpha\in\mathscr{R}^+(\mathbb{T},(-\infty,0))$ and Lemma 8 that

$$\lim_{t\longrightarrow\infty} e_\alpha(t,0) = 0. \tag{35}$$

In view of (34) and (35), we know that $V(t) \longrightarrow 0$ as $t \longrightarrow \infty$. This indicates that pinning controlled network (17) is synchronized. □

Theorem 2. *Suppose that there exists a constant $\mu^* \geq 0$ such that $\mu(t) \leq \mu^*$ for all $t \in \mathbb{T}$, Γ is symmetric, and $\Gamma f(\cdot)$ is increasing. Then, pinning controlled network (17) is synchronized, if*

$$\beta := \lambda_{\max}\left(2LI_{nN} + 2(A-D)\otimes\Gamma + \mu^*\left[L^2 I_{nN} + (A-D)^2\otimes\Gamma^2\right]\right) < 0, \quad \text{and } \beta \in \mathscr{R}^+(\mathbb{T},\mathbb{R}). \tag{36}$$

Proof. Construct the Lyapunov function $V(t) = z^T(t)z(t), t \in [0,\infty)_{\mathbb{T}}$. Similar to the proof of Theorem 1, we have

$$V^{\triangle}(t) \leq z^T(t)\left\{2LI_{nN} + 2(A-D)\otimes\Gamma + \mu^*\left[L^2 I_{nN} + (A-D)^2\otimes\Gamma^2\right]\right\}z(t), \quad t \in [0,\infty)_{\mathbb{T}}. \tag{37}$$

So, by (37) and Lemma 2, we get

$$\begin{aligned} V^{\triangle}(t) &\leq \lambda_{\max}\left(2LI_{nN} + 2(A-D)\otimes\Gamma \right.\\ &\quad \left. + \mu^*\left[L^2 I_{nN} + (A-D)^2\otimes\Gamma^2\right]\right)z^T(t)z(t) \\ &= \beta z^T(t)z(t) = \beta V(t), \quad t \in [0,\infty)_{\mathbb{T}}, \end{aligned} \tag{38}$$

which together with Lemma 7 implies that

$$V(t) \leq V(0)e_\beta(t,0), \quad t \in [0,\infty)_{\mathbb{T}}. \tag{39}$$

At the same time, it follows from $\beta < 0$, $\beta \in \mathscr{R}^+(\mathbb{T},\mathbb{R})$, and Lemma 8 that

$$\lim_{t\longrightarrow\infty} e_\beta(t,0) = 0. \tag{40}$$

In view of (39) and (40), we know that $V(t) \longrightarrow 0$ as $t \longrightarrow \infty$. This completes the proof. □

Corollary 1. *Suppose that there exists a constant $\mu^* \geq 0$ such that $\mu(t) \leq \mu^*$ for all $t \in \mathbb{T}$, Γ is symmetric positive definite, and $\Gamma f(\cdot)$ is increasing. Then, pinning controlled network (17) is synchronized, if*

$$\begin{aligned} \gamma &:= 2L + 2\lambda_{\max}(A-D)\lambda_{\min}(\Gamma) \\ &\quad + \mu^*\left[L^2 + \lambda_{\max}\left((A-D)^2\right)\lambda_{\max}\left(\Gamma^2\right)\right] \\ &< 0, \quad \text{and } \gamma \in \mathscr{R}^+(\mathbb{T},\mathbb{R}). \end{aligned} \tag{41}$$

Proof. Since $A-D$ is symmetric negative definite, Γ, Γ^2, and $(A-D)^2$ are symmetric positive definite, and by Lemmas 2 and 3, we get

$$\begin{aligned} &\lambda_{\max}\left(2LI_{nN} + 2(A-D)\otimes\Gamma + \mu^*\left[L^2 I_{nN} + (A-D)^2\otimes\Gamma^2\right]\right) \\ &\leq 2L + 2\lambda_{\max}(A-D)\lambda_{\min}(\Gamma) + \mu^*\left[L^2 + \lambda_{\max}\left((A-D)^2\right)\lambda_{\max}\left(\Gamma^2\right)\right] \\ &= \gamma. \end{aligned} \tag{42}$$

Similar to the proof of Theorem 2, we can prove that pinning controlled network (17) is synchronized. □

Corollary 2. *Suppose that there exists a constant $\mu^* \geq 0$ such that $\mu(t) \leq \mu^*$ for all $t \in \mathbb{T}$, $c_{ij} = c$, $\Gamma = I_n$, and $f(\cdot)$ is increasing. Then, pinning controlled network (17) is synchronized, if*

$$\begin{aligned} \xi &:= 2L + 2c\lambda_{\max}(G-D_1) \\ &\quad + \mu^*\left[L^2 + c^2\lambda_{\max}\left((G-D_1)^2\right)\right] < 0, \quad \text{and } \xi \in \mathscr{R}^+(\mathbb{T},\mathbb{R}), \end{aligned} \tag{43}$$

where $D_1 = diag(d_1, d_2, \ldots, d_l, \underbrace{0,\ldots,0}_{N-l})$.

When $\mathbb{T} = \mathbb{R}$, Theorem 2 yields the following result immediately.

Corollary 3. *Let Γ be symmetric. Then, pinning controlled network (19) is synchronized if*

$$\lambda_{\max}\left(LI_{nN} + (A-D)\otimes\Gamma\right) < 0. \tag{44}$$

Corollary 4. *Let $c_{ij} = c$ and Γ be symmetric positive definite. Then, pinning controlled network (19) is synchronized if*

$$c > \frac{-L}{\lambda_{\max}(G-D_1)\lambda_{\min}(\Gamma)}, \tag{45}$$

where $D_1 = diag(d_1, d_2, \ldots, d_l, \underbrace{0,\ldots,0}_{N-l})$.

Proof. In view of Lemma 1, it is easy to know that $\lambda_{\max}(G - D_1) < 0$. Now, the result follows from Lemmas 2, 3, and Corollary 3.

When $\mathbb{T} = \mathbb{Z}$, Theorem 2 yields the following result immediately. □

Corollary 5. *Suppose that Γ is symmetric and $\Gamma f(\cdot)$ is increasing. Then, pinning controlled network (22) is synchronized if*

$$-1 < \lambda_{\max}\left((2L + L)^2 I_{nN} + 2(A - D) \otimes \Gamma + (A - D)^2 \otimes \Gamma^2\right) < 0. \tag{46}$$

Corollary 6. *Suppose that $c_{ij} = c$, Γ is symmetric positive definite, and $\Gamma f(\cdot)$ is increasing. Then, pinning controlled network (22) is synchronized if*

$$\begin{aligned} &-1 < 2L + L^2 + 2c\lambda_{\max}(G - D_1)\lambda_{\min}(\Gamma) + c^2\lambda_{\max} \\ &\quad \left((G - D_1)^2\right)\lambda_{\max}\left(\Gamma^2\right) < 0, \end{aligned} \tag{47}$$

where $D_1 = diag(d_1, d_2, \ldots, d_l, \underbrace{0, \ldots, 0}_{N-l})$.

Remark 4. By comparing Corollaries 4 and 6, we find that the pinning synchronization criteria for discrete-time complex dynamical networks are different from those for continuous-time complex dynamical networks. For example, to achieve pinning synchronization, in the discrete-time case, the coupling strength needs to have an upper bound, while there is no requirement of upper bound for the coupling strength in the continuous-time case.

Obviously, the research of the synchronization problem for complex dynamical networks on time scales is more general. On the one hand, it provides a unified framework for continuous-time and discrete-time complex dynamical networks. On the other hand, it can give us a better insight into the differences of the pinning synchronization between continuous-time and discrete-time complex dynamical networks.

5. A Numerical Example

To verify the effectiveness of the results established in Section 4, we give a numerical example in this section.

Example 1. Consider the following complex dynamical network with ten nodes on $\mathbb{T}$:

$$\begin{aligned} x_i^{\Delta}(t) &= \begin{pmatrix} x_{i1}^{\Delta}(t) \\ x_{i2}^{\Delta}(t) \end{pmatrix} = \begin{pmatrix} 0.1\tanh(x_{i1}(t)) \\ 0.1\tanh(x_{i2}(t)) \end{pmatrix} \\ &\quad + \sum_{j=1}^{10} c_{ij} g_{ij} x_j(t), \quad t \in [0, \infty)_{\mathbb{T}}, i = 1, 2, \ldots, 10, \end{aligned} \tag{48}$$

where

$$G = \begin{pmatrix} -4 & 1 & 1 & 0 & 0 & 1 & 0 & 1 & 0 & 0 \\ 1 & -4 & 0 & 0 & 0 & 0 & 1 & 1 & 1 & 0 \\ 1 & 0 & -4 & 0 & 0 & 1 & 1 & 1 & 0 & 0 \\ 0 & 0 & 0 & -3 & 1 & 0 & 1 & 0 & 0 & 1 \\ 0 & 0 & 0 & 1 & -3 & 0 & 0 & 1 & 0 & 1 \\ 1 & 0 & 1 & 0 & 0 & -3 & 0 & 0 & 0 & 1 \\ 0 & 1 & 1 & 1 & 0 & 0 & -5 & 1 & 1 & 0 \\ 1 & 1 & 1 & 0 & 1 & 0 & 1 & -6 & 1 & 0 \\ 0 & 1 & 0 & 0 & 0 & 0 & 1 & 1 & -3 & 0 \\ 0 & 0 & 0 & 1 & 1 & 1 & 0 & 0 & 0 & -3 \end{pmatrix}. \tag{49}$$

Note that each isolated node of network (48) is a system described by

$$s^{\Delta}(t) = \begin{pmatrix} s_1^{\Delta}(t) \\ s_2^{\Delta}(t) \end{pmatrix} = \begin{pmatrix} 0.1\tanh(s_1(t)) \\ 0.1\tanh(s_2(t)) \end{pmatrix}, \quad t \in [0, \infty)_{\mathbb{T}}. \tag{50}$$

Obviously, G is a symmetric and irreducible matrix. Since $f\begin{pmatrix} u \\ v \end{pmatrix} = \begin{pmatrix} 0.1\tanh(u) \\ 0.1\tanh(v) \end{pmatrix}$ and $\Gamma = I_2$, it is easy to know that $f(\cdot)$ satisfies Lipschitz condition with $L = 0.1$ and $\Gamma f(\cdot) = f(\cdot)$ is increasing. Our objective is to synchronize network (48) onto the solution $s = (0, 0)^T$ of system (50) by applying pinning control strategy. For convenience, let $c_{ij} = c = 0.08$ in this example. Now, we consider the following three cases.

Case 1. Let $\mathbb{T} = \cup_{k=0}^{\infty}[k, k + 0.6]$.

From Figure 1, we find that network (48) cannot synchronize onto $s = (0, 0)^T$ without control.

In this case, since

$$\mu(t) = \begin{cases} 0, & t \in \bigcup_{k=0}^{\infty}[k, k + 0.6), \\ 0.4, & t = k + 0.6, \quad k \in \mathbb{N}_0, \end{cases} \tag{51}$$

it is easy to verify that $c_{ii}g_{ii}\Gamma = 0.08 g_{ii} I_2 \in \mathscr{R}(\mathbb{T}, \mathbb{R}^{2\times 2})$. Now, we apply pinning control to network (48) with $l = 5$ and feedback gain matrix $D = 0.08\,\mathrm{diag}(5, 7, 5, 2, 8, 0, 0, 0, 0, 0)$. By direct calculations, we know that $c_{ii}(g_{ii} - d_i)\Gamma = 0.08(g_{ii} - d_i)I_2 \in \mathscr{R}(\mathbb{T}, \mathbb{R}^{2\times 2}), i = 1, 2, \ldots, 5$,

$$\begin{aligned} \beta &:= \lambda_{\max}\left(2LI_{nN} + 2(A - D) \otimes \Gamma + \mu^* \left[L^2 I_{nN} + (A - D)^2 \otimes \Gamma^2\right]\right) \\ &= \lambda_{\max}(2 \times 0.1 I_{20} + 2(0.08G - D) \\ &\quad \otimes I_2 + 0.4\left[0.1^2 I_{20} + (0.08G - D)^2 \otimes I_2\right]) \\ &= -0.0023 < 0 \end{aligned} \tag{52}$$

and $\beta \in \mathscr{R}^+(\mathbb{T}, \mathbb{R})$. So, all the conditions of Theorem 2 are fulfilled. Hence, it follows from Theorem 2 that network (48) can realize pinning synchronization. In fact, Figure 2 also shows that the pinning synchronization is achieved.

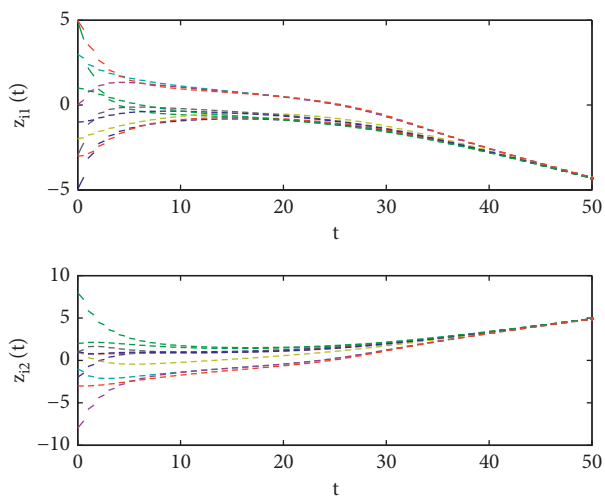

FIGURE 1: Errors z_{i1} and z_{i2} of network (48) without control, $c_{ij} = c = 0.08$, $\mathbb{T} = \cup_{k=0}^{\infty}[k, k+0.6]$.

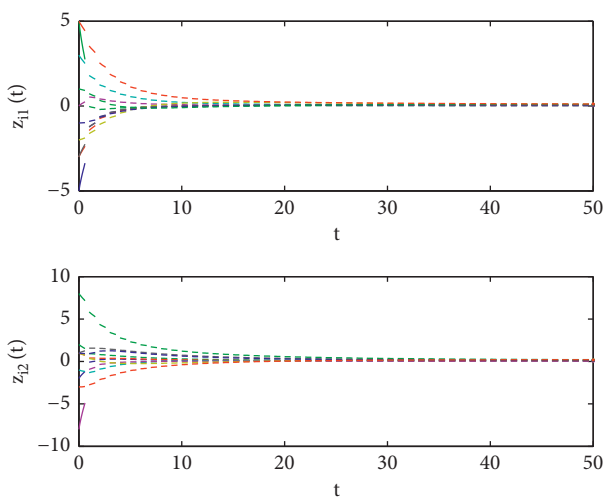

FIGURE 2: Synchronization errors z_{i1} and z_{i2} of network (48), $c_{ij} = c = 0.08$, $D = 0.08\,\mathrm{diag}(5, 7, 5, 2, 8, 0, 0, 0, 0, 0)$, $\mathbb{T} = \cup_{k=0}^{\infty}[k, k+0.6]$.

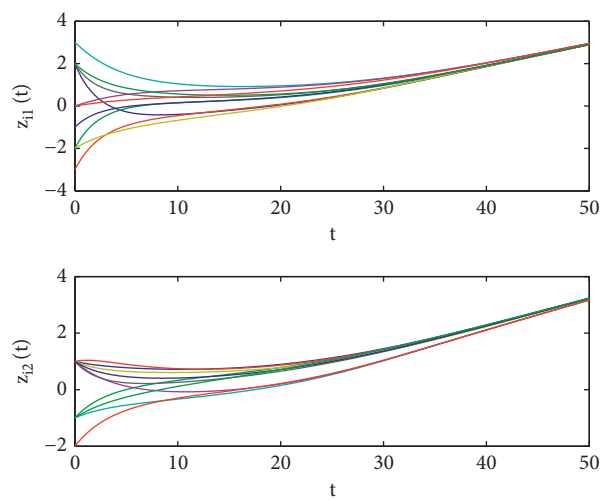

FIGURE 3: Errors z_{i1} and z_{i2} of network (48) without control, $c_{ij} = c = 0.08$, $\mathbb{T} = \mathbb{R}$.

Case 2. Let $\mathbb{T} = \mathbb{R}$.

From Figure 3, we find that network (48) cannot synchronize onto $s = (0, 0)^T$ without control.

In this case, since $\mu(t) \equiv 0$, it is easy to verify that $c_{ii}g_{ii}\Gamma = 0.08 g_{ii} I_2 \in \mathscr{R}(\mathbb{T}, \mathbb{R}^{2\times 2})$, $i = 1, 2, \ldots, 10$. Now, we apply pinning control to network (48) with $l = 6$ and feedback gain matrix $D = 0.08\,\mathrm{diag}(6, 8, 5, 3, 8, 9, 0, 0, 0, 0)$. By direct calculations, we know that $c_{ii}(g_{ii} - d_i)\Gamma = 0.08(g_{ii} - d_i)I_2 \in \mathscr{R}(\mathbb{T}, \mathbb{R}^{2\times 2})$, $i = 1, 2, \ldots, 6$, and $\lambda_{\max}(LI_{nN} + (A - D)\otimes\Gamma) = \lambda_{\max}(0.1 I_{20} + (0.08G - D)\otimes I_2) = -0.0299 < 0$. So, all the conditions of Corollary 3 are fulfilled. Hence, it follows from Corollary 3 that network (48) can realize pinning synchronization. In fact, Figure 4 also shows that the pinning synchronization is achieved.

Case 3. Let $\mathbb{T} = \mathbb{Z}$.

From Figure 5, we find that network (48) cannot synchronize onto $s = (0, 0)^T$ without control.

In this case, since $\mu(t) \equiv 0$, it is easy to verify that $c_{ii}g_{ii}\Gamma = 0.08 g_{ii} I_2 \in \mathscr{R}(\mathbb{T}, \mathbb{R}^{2\times 2})$, $i = 1, 2, \ldots, 10$. Now, we apply pinning control to network (48) with $l = 6$ and feedback gain matrix $D = 0.08\,\mathrm{diag}(6, 8, 5, 3, 8, 9, 0, 0, 0, 0)$. By direct calculations, we know that $c_{ii}(g_{ii} - d_i)\Gamma = 0.08(g_{ii} - d_i)I_2 \in \mathscr{R}(\mathbb{T}, \mathbb{R}^{2\times 2})$, $i = 1, 2, \ldots, 6$, and

$$\begin{aligned} -1 &< \lambda_{\max}\left(\left(2L + L^2\right)I_{nN} + 2(A - D)\otimes\Gamma + (A - D)^2\otimes\Gamma^2\right) \\ &= \lambda_{\max}\left(\left(2\times 0.1 + 0.1^2\right)I_{20} + 2(0.08G - D)\right. \\ &\quad \left.\otimes I_2 + (0.08G - D)^2\otimes I_2\right) \\ &= -0.0329 < 0. \end{aligned} \tag{53}$$

So, all the conditions of Corollary 5 are fulfilled. Hence, it follows from Corollary 5 that network (48) can realize pinning synchronization. In fact, Figure 6 also shows that the pinning synchronization is achieved.

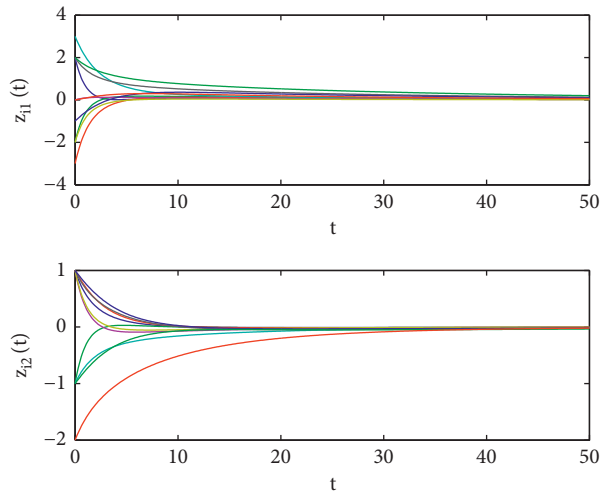

Figure 4: Synchronization errors z_{i1} and z_{i2} of network (48), $c_{ij} = c = 0.08$, $D = 0.08\,\mathrm{diag}(6, 8, 5, 3, 8, 9, 0, 0, 0, 0)$, $\mathbb{T} = \mathbb{R}$.

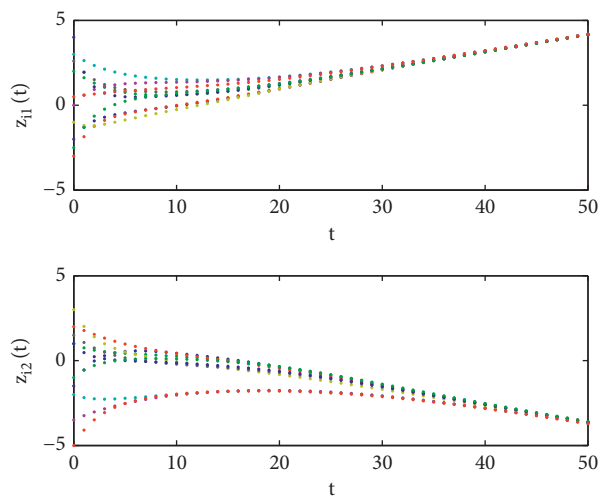

Figure 5: Errors z_{i1} and z_{i2} of network (48) without control, $c_{ij} = c = 0.08$, $\mathbb{T} = \mathbb{Z}$.

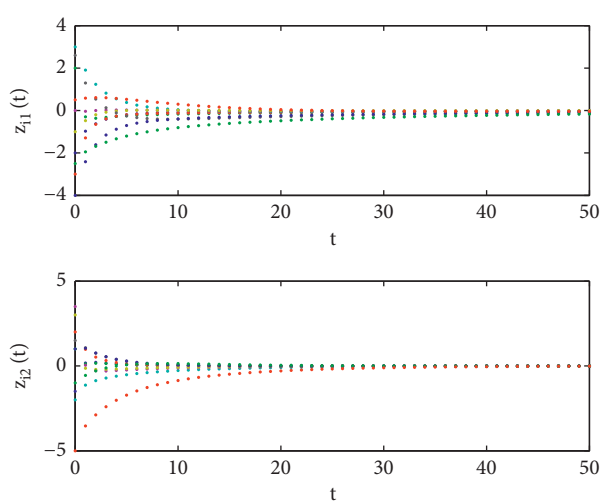

Figure 6: Synchronization errors z_{i1} and z_{i2} of network (48), $c_{ij} = c = 0.08$, $D = 0.08\,\mathrm{diag}(6, 8, 5, 3, 8, 9, 0, 0, 0, 0)$, $\mathbb{T} = \mathbb{Z}$.

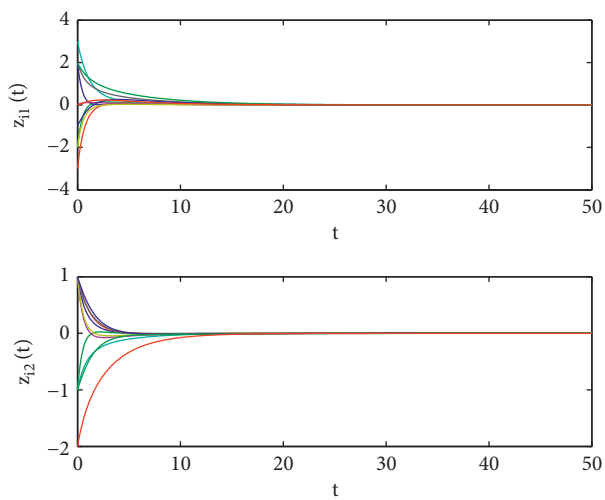

Figure 7: Synchronization errors z_{i1} and z_{i2} of network (48), $c_{ij} = c = 0.165$, $D = 0.165\,\mathrm{diag}(6, 8, 5, 3, 8, 9, 0, 0, 0, 0)$, $\mathbb{T} = \mathbb{R}$.

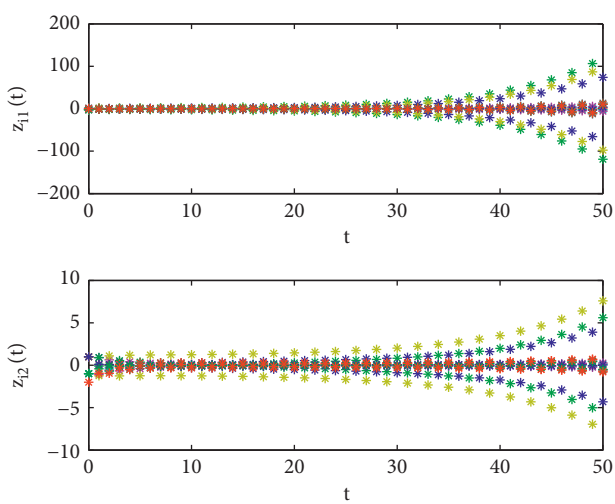

Figure 8: Errors z_{i1} and z_{i2} of network (48), $c_{ij} = c = 0.165$, $D = 0.165\,\mathrm{diag}(6, 8, 5, 3, 8, 9, 0, 0, 0, 0)$, $\mathbb{T} = \mathbb{Z}$.

Remark 5. To illustrate Remark 4, we choose $c_{ij} = c = 0.165$ in network (48). By numerical simulations, we find that network (48) can still realize pinning synchronization when $\mathbb{T} = \mathbb{R}$, see Figure 7. However, Figure 8 shows that network (48) cannot realize pinning synchronization when $\mathbb{T} = \mathbb{Z}$.

6. Conclusions

In this paper, we have investigated the synchronization problem of a complex dynamical network on time scales by pinning control strategy. The pinning synchronization criteria established combine main characteristics of time scales with main parameters of the pinning controlled network (such as the coupling strengths, the coupling configuration matrix, and the pinning feedback gain matrix). Our results have revealed the discrepancies of the pinning synchronization between continuous-time and discrete-time complex dynamical networks. A numerical example has also been given to verify the effectiveness of the theoretical results.

Data Availability

No data were used to support this study.

Conflicts of Interest

The authors declare that there are no conflicts of interest regarding the publication of this paper.

Acknowledgments

This work was supported by the National Natural Science Foundation of China (grant no. 11661049).

References

[1] S. H. Strogatz, "Exploring complex networks," *Nature*, vol. 410, no. 6825, pp. 268–276, 2001.
[2] C. W. Wu, *Synchronization in Coupled Chaotic Circuits and Systems*, World Scientific, Singapore, 2002.
[3] C. W. Wu, *Synchronization in Complex Networks of Nonlinear Dynamical Systems*, World Scientific, Singapore, 2007.
[4] W. Lu and T. Chen, "Synchronization analysis of linearly coupled networks of discrete time systems," *Physica D*, vol. 198, no. 1-2, pp. 148–168, 2004.
[5] C. Li and G. Chen, "Synchronization in general complex dynamical networks with coupling delays," *Physica A: Statistical Mechanics and its Applications*, vol. 343, pp. 263–278, 2004.
[6] Z. Li and G. Chen, "Global synchronization and asymptotic stability of complex dynamical networks," *IEEE Transactions on Circuits and Systems-II: Express Briefs*, vol. 53, no. 1, pp. 28–33, 2006.
[7] C. P. Li, W. G. Sun, and J. Kurths, "Synchronization of complex dynamical networks with time delays," *Physica A: Statistical Mechanics and its Applications*, vol. 361, no. 1, pp. 24–34, 2006.
[8] X. Li and G. Chen, "Synchronization and desynchronization of complex dynamical networks: an engineering viewpoint," *IEEE Transactions on Circuits and Systems-I*, vol. 50, no. 11, pp. 1381–1390, 2003.
[9] Z. Wu, "Synchronization of discrete dynamical networks with non-delayed and delayed coupling," *Applied Mathematics and Computation*, vol. 260, pp. 57–62, 2015.
[10] J. Zhou, J. Lu, and J. Lü, "Adaptive synchronization of an uncertain complex dynamical network," *IEEE Transactions on Automatic Control*, vol. 51, no. 4, pp. 652–656, 2006.
[11] Q. Zhang, J. Lu, J. Lü, and K. T. Chi, "Adaptive feedback synchronization of a general complex dynamical network with delayed nodes," *IEEE Transactions on Circuits and Systems-II: Express Briefs*, vol. 55, no. 2, pp. 183–187, 2008.
[12] G. Zhang, Z. Liu, and Z. Ma, "Synchronization of complex dynamical networks via impulsive control, *Chaos*," *An Interdisciplinary Journal of Nonlinear Science*, vol. 17, no. 4, p. 43126, 2007.
[13] J. Zhou, J.-a. Lu, and J. Lü, "Pinning adaptive synchronization of a general complex dynamical network," *Automatica*, vol. 44, no. 4, pp. 996–1003, 2008.
[14] J. Lu, J. Kurths, J. Cao, N. Mahdavi, and C. Huang, "Synchronization control for nonlinear stochastic dynamical

networks: pinning impulsive strategy," *IEEE Transactions on Neural Networks and Learning Systems*, vol. 23, no. 2, pp. 285–292, 2012.

[15] W. Yu, G. Chen, J. Lü, and J. Kurths, "Synchronization via pinning control on general complex networks," *SIAM Journal on Control and Optimization*, vol. 51, no. 2, pp. 1395–1416, 2013.

[16] X. F. Wang and G. Chen, "Pinning control of scale-free dynamical networks," *Physica A*, vol. 310, no. 3-4, pp. 521–531, 2002.

[17] X. Li, X. Wang, and G. Chen, "Pinning a complex dynamical network to its equilibrium," *IEEE Transactions on Circuits and Systems I: Regular Papers*, vol. 51, no. 10, pp. 2074–2087, 2004.

[18] T. Chen, X. Liu, and W. Lu, "Pinning complex networks by a single controller," *IEEE Transactions on Circuits and Systems I: Regular Papers*, vol. 54, no. 6, pp. 1317–1326, 2007.

[19] W. Yu, G. Chen, and J. Lü, "On pinning synchronization of complex dynamical networks," *Automatica*, vol. 45, no. 2, pp. 429–435, 2009.

[20] Q. Song and J. Cao, "On pinning synchronization of directed and undirected complex dynamical networks," *IEEE Transactions on Circuits and Systems I: Regular Papers*, vol. 57, no. 3, pp. 672–680, 2010.

[21] G. Chen, "Pinning control and synchronization on complex dynamical networks," *International Journal of Control, Automation and Systems*, vol. 12, no. 2, pp. 221–230, 2014.

[22] R. Cheng, M. Peng, and J. Zuo, "Pinning synchronization of discrete dynamical networks with delay coupling," *Physica A: Statistical Mechanics and its Applications*, vol. 450, pp. 444–453, 2016.

[23] Z. X. Liu, Z. Q. Chen, and Z. Z. Yuan, "Pinning control of weighted general complex dynamical networks with time delay," *Physica A: Statistical Mechanics and its Applications*, vol. 375, no. 1, pp. 345–354, 2007.

[24] H. Su and X. Wang, *Pinning Control of Complex Networked Systems: Synchronization, Consensus and Flocking of Networked Systems via Pinning*, Springer, Berlin, Germany, 2013.

[25] X. Wang and H. Su, "Pinning control of complex networked systems: a decade after and beyond," *Annual Reviews in Control*, vol. 38, no. 1, pp. 103–111, 2014.

[26] L. Y. Xiang, Z. X. Liu, Z. Q. Chen, F. Chen, and Z. Z. Yuan, "Pinning control of complex dynamical networks with general topology," *Physica A: Statistical Mechanics and its Applications*, vol. 379, no. 1, pp. 298–306, 2007.

[27] H. Zhang, K. Li, and X. Fu, "On pinning control of some typical discrete-time dynamical networks," *Communications in Nonlinear Science and Numerical Simulation*, vol. 15, no. 2, pp. 182–188, 2010.

[28] X. Yi, R. Guo, and Y. Qi, "Stabilization of chaotic systems with both uncertainty and disturbance by the UDE-based control method," *IEEE Access*, vol. 8, no. 1, pp. 62471–62477, 2020.

[29] R. Xu and F. Zhang, "ε-nash mean-field games for general linear-quadratic systems with applications," *Automatica*, vol. 114, Article ID 108835, 2020.

[30] L. Liu, B. Li, and R. Guo, "Consensus control for networked manipulators with switched parameters and topologies," *IEEE Access*, vol. 9, pp. 9209–9217, 2021.

[31] S. Hilger, *Ein Maßkettenkalkül mit anwendung auf zentrumsmannigfaltigkeiten*, Ph.D. thesis, Universität Würzburg, Würzburg, Germany, 1988.

[32] Q. Cheng and J. Cao, "Synchronization of complex dynamical networks with discrete time delays on time scales," *Neurocomputing*, vol. 151, pp. 729–736, 2015.

[33] X. Lu, Y. Wang, and Y. Zhao, "Synchronization of complex dynamical networks on time scales via Wirtinger-based inequality," *Neurocomputing*, vol. 216, pp. 143–149, 2016.

[34] A. Ogulenko, "Asymptotical properties of social network dynamics on time scales," *Journal of Computational and Applied Mathematics*, vol. 319, pp. 413–422, 2017.

[35] X. Liu and K. Zhang, "Synchronization of linear dynamical networks on time scales: pinning control via delayed impulses," *Automatica*, vol. 72, pp. 147–152, 2016.

[36] M. Syed Ali and J. Yogambigai, "Synchronization of complex dynamical networks with hybrid coupling delays on time scales by handling multitude Kronecker product terms," *Applied Mathematics and Computation*, vol. 291, pp. 244–258, 2016.

[37] M. Syed Ali and J. Yogambigai, "Synchronization criterion of complex dynamical networks with both leakage delay and coupling delay on time scales," *Neural Processing Letters*, vol. 49, no. 2, pp. 453–466, 2019.

[38] Z. Huang, J. Cao, and Y. N. Raffoul, "Hilger-type impulsive differential inequality and its application to impulsive synchronization of delayed complex networks on time scales," *Science China Information Sciences*, vol. 61, pp. 1–3, 2018.

[39] X. Lu, X. Zhang, and Q. Liu, "Finite-time synchronization of nonlinear complex dynamical networks on time scales via pinning impulsive control," *Neurocomputing*, vol. 275, pp. 2104–2110, 2018.

[40] Q. Xiao, F. L. Lewis, and Z. Zeng, "Event-based time-interval pinning control for complex networks on time scales and applications," *IEEE Transactions on Industrial Electronics*, vol. 65, no. 11, pp. 8797–8808, 2018.

[41] H. Lütkepohl, *Handbook of Matrices*, Wiley, New York, NY, USA, 1996.

[42] A. N. Langville and W. J. Stewart, "The Kronecker product and stochastic automata networks," *Journal of Computational and Applied Mathematics*, vol. 167, no. 2, pp. 429–447, 2004.

[43] Q. Cheng and J. Cao, "Global synchronization of complex networks with discrete time delays and stochastic disturbances," *Neural Computing and Applications*, vol. 20, no. 8, pp. 1167–1179, 2011.

[44] M. Bohner and A. Peterson, *Dynamic Equations on Time Scales: An Introduction with Applications*, Birkhäuser, Boston, MA, USA, 2001.

[45] M. Bohner and A. Peterson, *Advances in Dynamic Equations on Time Scales*, Birkhäuser, Boston, MA, USA, 2003.

[46] L. Chua and D. Green, "A qualitative analysis of the behavior of dynamic nonlinear networks: stability of autonomous networks," *IEEE Transactions on Circuits and Systems*, vol. 23, no. 6, pp. 355–379, 1976.

Hindawi
Mathematical Problems in Engineering
Volume 2021, Article ID 5572840, 16 pages
https://doi.org/10.1155/2021/5572840

Research Article

Complex Dynamics and Hard Limiter Control of a Fractional-Order Buck-Boost System

Bo Yan,[1] **Shaojie Wang**,[1] **and Shaobo He**[2]

[1]*College of Electrical and Information Engineering, Shaoyang University, Shaoyang 422000, China*
[2]*School of Physics and Electronics, Central South University, Changsha 410083, China*

Correspondence should be addressed to Shaobo He; heshaobo_123@163.com

Received 4 February 2021; Revised 27 February 2021; Accepted 4 March 2021; Published 19 March 2021

Academic Editor: Rongwei Guo

Chaos and control analysis for the fractional-order nonlinear circuits is a recent hot topic. In this study, a fractional-order model is deduced from a Buck-Boost converter, and its discrete solution is obtained based on the Adomian decomposition method (ADM). Chaotic dynamic characteristics of the fractional-order system are investigated by the bifurcation diagram, 0-1 test, spectral entropy (SE) algorithm, and NIST test. Meanwhile, the control of the fractional-order Buck-Boost model is discussed through two different ways, namely, the intensity feedback and the hard limiter control. Specifically, the hard limiter control can be realized using a current limiter in the circuit, where the current limiter device is applied to control the branch current. The results show that the proposed fractional-order system has complex dynamic behaviors and potential application values in the engineering field.

1. Introduction

The Buck-Boost converters are strongly nonlinear circuits [1–4] which can produce subharmonic, bifurcation, and chaos under certain conditions. At present, many researchers have investigated the chaos of the Buck-Boost converter systems [5–11]. For example, Wang et al. [10] investigated the mechanisms that lead to chaotic behaviors in the Buck-Boost power converter, and the existence of chaos is verified successfully by the Smale horseshoe, while Demirbaş et al. [11] investigated the bifurcation of the system with the material parameters and found a number of periodic windows. Obviously, chaos will lead to the instability of the converter via increasing the oscillation and producing the excessive irregular electromagnetic noise, which directly affects the operation quality and reliability of the converter. In fact, the Buck-Boost is a switched model, and control of the nonlinear switched systems is a challenging topic [12]. As a result, there are also many other reports about the chaos control of the Buck-Boost converters [13–15]. For instance, Sriramalakshmi et al. [15] analyzed the nonlinear phenomena and control of the current mode-controlled Buck-Boost converter. Meanwhile, complexity of nonlinear dynamical systems has aroused much interest of researchers [16, 17]. Therefore, an in-depth study of the complexity with the circuit parameters is still significant for the design and application of the Buck-Boost converter systems.

The fractional calculus was proposed at about the same time as the regular calculus. At present, since it can better describe those processes with time and the space memory effect, it has been accepted as a novel tool for building the mathematical models. Nowadays, the fractional calculus has extensive applications in the field of physics, engineering, and biology economics [18–20]. Generally, the nonlinear systems have more complex dynamical behaviors after the fractional calculus is introduced [21–24]. In fact, dynamics analysis of different kinds of fractional-order Buck-Boost systems has aroused concern from scholars [25–28]. However, these studies mainly focused on the modeling of fractional-order Buck-Boost systems. Currently, dynamics in different kinds of nonlinear systems have been investigated, such as memristor-based systems [29, 30] and chaotic systems [31, 32]. It is indicated that those systems have

abundant dynamic characteristics including the multistability and can be used for the image encryption applications. However, dynamics of the fractional-order Buck-Boost systems still need further study. Meanwhile, how to build an effective model is necessary for the applications of the fractional-order Buck-Boost system. In fact, He et al. [33] shows that, compared with other solution algorithms, the Adomian decomposition method (ADM) is more accurate, and the deduced solution can be used in the engineering applications. Thus, it can be employed to solve fractional-order Buck-Boost systems for further analysis and applications.

In 2008, Wu and Zhang [34] proposed an improved exponential delayed feedback controller to a Buck-Boost converter in the current mode. This exponential delayed feedback controller provides a new strategy for chaos control and for the switching law. As a matter of fact, control of chaos is important for the application of nonlinear systems [35]. On the other hand, although the chaotic systems can be applied in secret communications and information encryption [36, 37], there are few reports on applications of the Buck-Boost system in information security field. Motivated by the above discussions, we will explore the dynamics and control the potential application values of the fractional-order Buck-Boost system based on Wu and Zhang's model [34] by employing the ADM.

The rest of the study is organized as follows. In Section 2, the fractional-order Buck-Boost model which is a switching system is solved by employing the ADM. In Section 3, complexity of the fractional-order Buck-Boost system is investigated, and the existence of chaos is verified by the 0-1 test. A chaotic pseudorandom sequence generator is designed. In Section 4, control of chaos in the fractional-order Buck-Boost system is studied. Two different approaches are introduced. Finally, conclusion is made in Section 5.

2. The Fractional-Order Buck-Boost Model

2.1. Building the Fractional-Order Buck-Boost System. Wu and Zhang [34] designed a Buck-Boost converter in the current mode and found chaos in the proposed model. The circuit of the modified Buck-Boost converter is shown in Figure 1, and the description of the parameters is given in Table 1. In this enhanced Buck-Boost converter, there is an adjustment coefficient k which can be used to control the stability of the converter.

Let the Buck-Boost converter work in the continuous conductive mode, and the inductance current x_1 (i_L) and the capacitance voltage x_2 (u_c) be the system variables. According to on and off states of the power switch in the converter and based on Kirchhoff's law, the Buck-Boost converter system can be expressed as [34]

$$\begin{cases} \dot{x}_1 = \dfrac{1}{L}U_{\text{in}}, \\ \dot{x}_2 = -\dfrac{1}{RC}x_2, \end{cases} \begin{cases} \dot{x}_1 = -\dfrac{1}{L}x_2, \\ \dot{x}_2 = \dfrac{1}{C}x_1 - \dfrac{1}{RC}x_2. \end{cases} \tag{1}$$

Now, the Caputo fractional calculus, which is given by [38]

$$D_{t_0}^q f(t) = \frac{1}{\Gamma(1-q)} \int_{t_0}^{t} (t-\tau)^{-q} f'(\tau) \mathrm{d}\tau, \tag{2}$$

is introduced to the system, where $D_{t_0}^q$ is the Caputo derivative operator of order $q\,(0 < q \le 1)$, t_0 is the initial time, and $\Gamma(\cdot)$ is the Gamma function. Thus, the fractional-order Buck-Boost system is defined as

$$\begin{cases} D_{t_0}^q x_1 = \dfrac{1}{L}U_{\text{in}}, \\ D_{t_0}^q x_2 = -\dfrac{1}{RC}x_2, \end{cases} \tag{3}$$

$$\begin{cases} D_{t_0}^q x_1 = -\dfrac{1}{L}x_2, \\ D_{t_0}^q x_2 = \dfrac{1}{C}x_1 - \dfrac{1}{RC}x_2. \end{cases} \tag{4}$$

Although there are some research studies regarding the fractional-order Buck-Boost system, it is necessary to give more interpretations of the fractional-order Buck-Boost system [25–28]. Usually, we hold the opinion that the fractional-order calculus provides a more effective way for modeling of real systems, and the analysis results can reflect the dynamics of real systems better. Here, we hope that the fractional-order system could provide more information about the Buck-Boost circuit.

2.2. The Adomian Decomposition Method. As shown above, the systems have only linear items and a constant. To solve this system, the ADM [39–41] is employed, and the description of this algorithm is illustrated as follows.

For a given fractional-order linear system,

$$\begin{cases} D_{t_0}^q \mathbf{x}(t) = \Upsilon \mathbf{x} + \mathbf{g} \\ \dot{\mathbf{x}}(t_0^+) = \mathbf{x}_0, \end{cases}, \tag{5}$$

where $D_{t_0}^q$ is the Caputo definition, $\Upsilon\mathbf{x}$ is the linear terms in the system, and $q \in (0, 1]$. Its solution is given by [39]

$$\mathbf{x} = \sum_{i=1}^{\infty} \mathbf{x}^i = J_{t_0}^q \Upsilon \sum_{i=0}^{\infty} \mathbf{x}^i + J_{t_0}^q \mathbf{g} + \mathbf{x}_0. \tag{6}$$

Meanwhile, those decomposition items x^i $(i = 0, 1, \ldots, \infty)$ are calculated as [40, 41]

$$\begin{cases} \mathbf{x}^0 = J_{t_0}^q \mathbf{g} + \mathbf{x}_0, \\ \mathbf{x}^i = J_{t_0}^q \Upsilon \mathbf{x}^{i-1}, \quad i = 1, 2, \ldots, \infty. \end{cases} \tag{7}$$

When an infinite number of items is used, the solution is the exact solution. In this study, 11 decomposition items, namely, x^i $(i = 0, 1, \ldots, 10)$, are used.

2.3. Solution of the Fractional-Order Model. Let us focus on the nth sampling period; thus, $t \in (t_n, t_{n+1}]$. The initial value of this interval is $x_1(t_n)$ and $x_2(t_n)$.

Case 1. By employing the above ADM, the solution of equation (3) is given by

$$\begin{cases} x_1(t) = x_1(t_n) + \dfrac{U_{\text{in}}}{L}\dfrac{(t-t_n)^q}{\Gamma(q+1)}, \\ x_2(t) = x_2(t_n)\displaystyle\sum_{i=0}^{10}\kappa_2^i\dfrac{(t-t_n)^{\text{iq}}}{\Gamma(\text{iq}+1)}, \end{cases} \tag{8}$$

where

$$\begin{aligned} \kappa_2^i &= -\frac{1}{RC}\kappa_2^{i-1}, \\ \kappa_2^0 &= 1. \end{aligned} \tag{9}$$

When $t = t_{n+1}$, we can obtain the following discrete solution of the system, which is defined as

$$x(t_{n+1}) = f_1(x(t_n), h, q). \tag{10}$$

Case 2. By employing the above ADM, the solution of equation (4) is denoted as

$$\begin{cases} x_1(t) = x_1(t_n) + \displaystyle\sum_{i=1}^{10} c_1^i\dfrac{(t-t_n)^{\text{iq}}}{\Gamma(\text{iq}+1)}, x_2(t) = x_2(t_n) + \displaystyle\sum_{i=1}^{10} c_2^i\dfrac{(t-t_n)^{\text{iq}}}{\Gamma(\text{iq}+1)}, \end{cases} \tag{11}$$

where

$$\begin{cases} c_1^i = -\dfrac{1}{L}c_2^{i-1}, \\ c_2^i = \dfrac{1}{C}c_1^{i-1} - \dfrac{1}{RC}c_2^{i-1}, \end{cases} \tag{12}$$

$$c_1^0 = x_1(t_n),$$

$$c_2^0 = x_2(t_n).$$

So the following discrete solution is obtained:

$$\mathbf{x}(t_{n+1}) = f_2(\mathbf{x}(t_n), h, q). \tag{13}$$

Based on $x_1(t_n)$ and $x_2(t_n)$, the reference current for the inductance $I_{\text{ref}}(t_n)$, the boundary value of the inductance current $I_b(t_n)$, and the duty cycle $d(t_n)$ are calculated by [34]

$$\begin{cases} I_{\text{ref}}(t_n) = I_{\text{ref}} - e^{k(u_n - u_{n-1})} + 1, \\ I_b(t_n) = I_{\text{ref}}(t_n) - \dfrac{U_{\text{in}}T}{L}, \\ d(t_n) = L\dfrac{I_{\text{ref}}(t_n) - x_1(t_n)}{U_{\text{in}}T}. \end{cases} \tag{14}$$

When $x_1(t_n) < I_b(t_n)$, the power switch S is on during the whole sampling period, and the system is defined as Case 1. However, if $x_1(t_n) \geq I_b(t_n)$, the power switch S is on when $t \in (t_n, t_n + d_nT]$, while the power switch S is off when $t \in (t_n + d_nT, t_{n+1}]$. As a result, in this sampling period, the system is defined as Case 1 first and then become Case 2 in the rest part. Finally, the discrete model is built as follows.

$$\mathbf{x}(t_{n+1}) = \begin{cases} f_1(\mathbf{x}(t_n), T, q), \quad \text{if } x_1(t_n) < I_b(t_n), \\ f_2(f_1(\mathbf{x}(t_n), d(t_n)T, q), (1-d(t_n))T, q), \\ \quad \text{if } x_1(t_n) \geq I_b(t_n), \end{cases} \tag{15}$$

where $T = t_{n+1} - t_n$ is the length of the sampling period. Obviously, this is a switched discrete system. When the initial conditions $x_1(t_0)$ and $x_2(t_0)$ are given, states of the system can be observed.

3. Complexity of the Fractional-Order Buck-Boost System

3.1. Dynamics of the Fractional-Order Model. Let the simulation parameters be $U_{\text{in}} = 8\,\text{V}$, $R = 10\,\Omega$, $L = 0.3\,\text{mH}$, $C = 40\,\mu\text{F}$, and $T = 50\,\mu\text{s}$. Set the inductance reference current as $I_{\text{ref}} = 3\,\text{A}$. Phase diagrams with different derivative order q are shown in Figure 2. It is shown in Figure 2 that the states of the system are different with a different derivative order q. Especially, when $q = 0.95$, the system becomes a periodic system because there are only two points in the phase diagram.

Bifurcation diagrams of the system with different system parameters include the inductance reference current I_{ref}, the

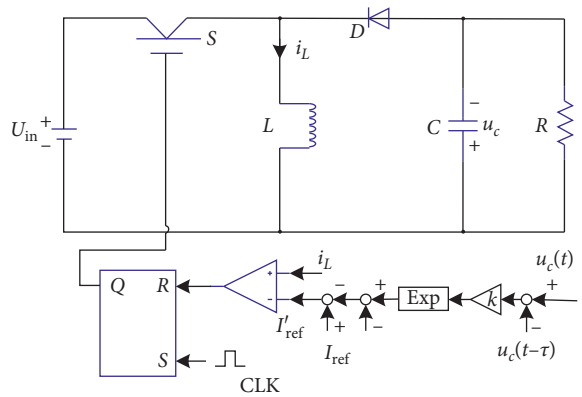

Figure 1: Circuit of the Buck-Boost converter.

Table 1: Description of the parameters in the Buck-Boost converter.

Symbol	Explanation
U_{in}	The input voltage of the converter
S	The power switch
D	The diode
L	The inductance
C	The capacitance
R	The load resistance
i_L	The inductive current
u_c	The capacitor voltage
I_{ref}	The inductance reference current
x_1 and x_2	The inductive current (i_L) and the capacitor voltage (u_c)
k	The intensity of feedback

inductance reference current L, the intensity of feedback k, and the derivative order q. Figure 3 shows the bifurcation diagrams with the inductance reference current I_{ref} under a different derivative order q. In Figure 3, I_{ref} varies from 0 to 4 with step size of 0.008 and $k = 0$. As shown in Figure 3, dynamics of the system with the variation of I_{ref} are different with a different derivative order q. Meanwhile, bifurcations versus different parameters are analyzed. Fix $k = 0$, $q = 0.9$, and $I_{ref} = 3$ A, and vary L from 2 mH to 5 mH with step size of 0.006. The analysis result is shown in Figure 4(a). Fix $q = 0.9$, $I_{ref} = 3$ A, and $L = 0.3$ mH, and vary parameter k from 0 to 5 with step size of 0.01. The bifurcation diagram with k is shown in Figure 4(b). Let $U_{in} = 8$ V, $L = 0.3$ mH, $R = 10\,\Omega$, $C = 40\,\mu$F, $k = 0$, and $T = 50\,\mu$s, and vary the derivative order q from 0.85 to 1, where the step size is 3×10^{-4}. As shown in Figure 4, the system has rich dynamics with those parameters. The systems can be chaotic and periodic with different parameters. For instance, when the intensity of feedback k is larger than 2, the system is periodic. It means that the system is nonchaotic, and k can be treated as a control parameter of the circuit.

3.2. 0-1 Test. The proposed system is a typical switched system, and Lyapunov exponents of the system cannot be calculated directly. In this study, the 0-1 test is employed to verify the existence of chaos.

If a set of one-dimensional observable data obtained from the iterative is represented by a set of multiscale discrete time series $\{x(n)\colon n = 1, 2, 3, \ldots,\}$, then the following two real valued sequences can be defined as [42, 43]

$$\begin{cases} p(n) = \sum_{j=1}^{n} x(j)\cos(\theta(j)), \\ s(n) = \sum_{j=1}^{n} x(j)\sin(\theta(j)), \end{cases} \tag{16}$$

where $\theta(j) = j\eta + \sum_{i=1}^{j}\varphi^{\sigma}(i)$, and $\eta \in [(\pi/5), (4\pi/5)]$. Usually, the state of the system can be identified by plotting the trajectories in the (p, s) plane. Figure 5 shows the (p, s) plots of the system with a different derivative order q, where the parameters are set as same as Figure 1, respectively. It shows that the system is chaotic when q =1, 0.95, and 0.9, while the system is periodic when $q = 0.85$. Thus, the existence of chaos is verified.

However, (p, s) plots can only be used to illustrate the state of the system under given parameters but cannot be used to show dynamics with the variation of parameters. Thus, it is necessary to deduce an index from the (p, s) plots. Fortunately, Gottwald and Melbourne [43] proposed a test which can be used to distill a binary quantity (K) from the power spectrum. Namely, if $K = 0$, the time series has regular dynamics, but if $K = 1$, the time series is chaotic.

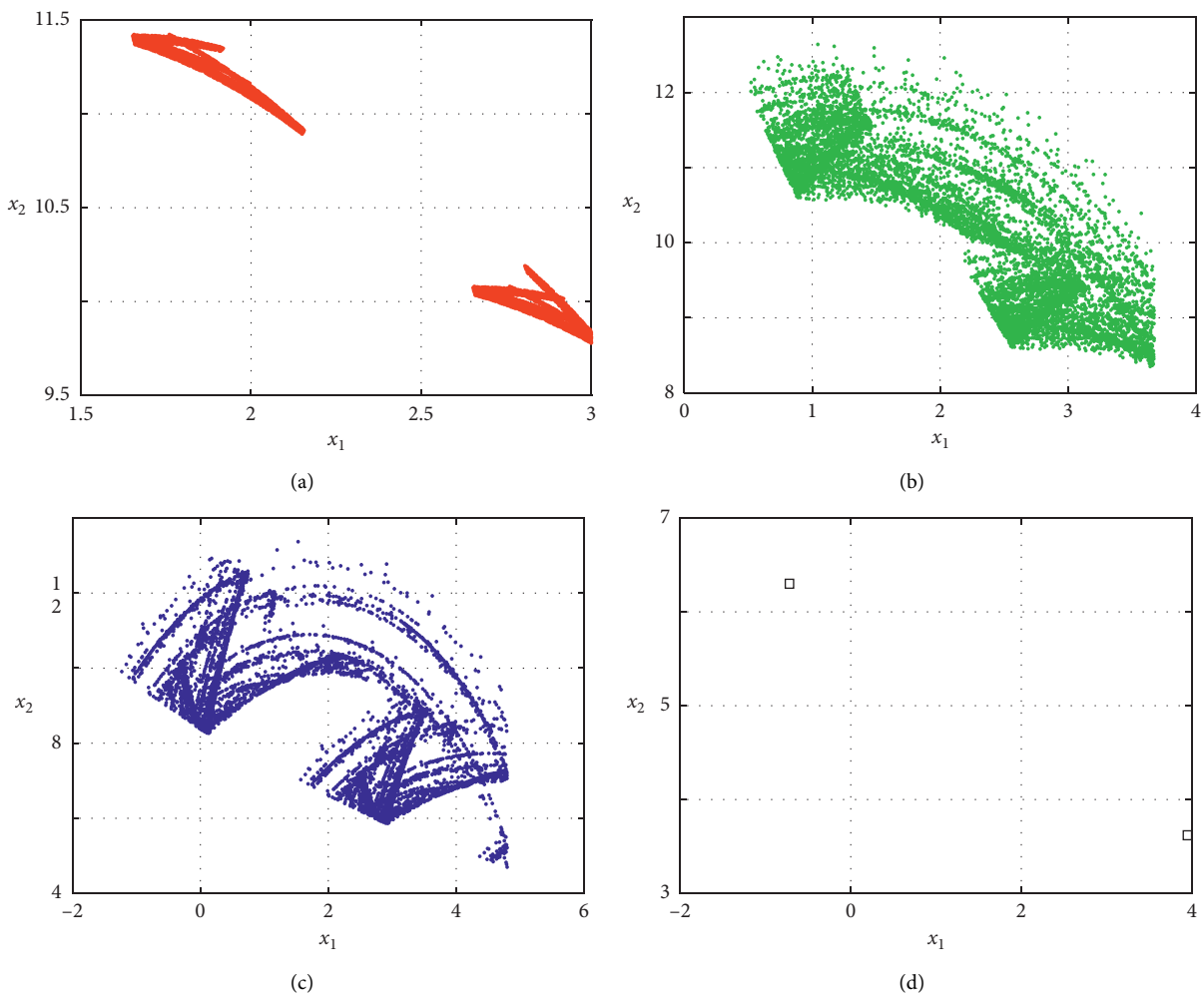

Figure 2: Phase diagrams of the fractional-order model. (a) $q = 1$, (b) $q = 0.95$, (c) $q = 0.9$, and (d) $q = 0.85$.

There are two steps for this quantity which are expanded as follows.

First, the mean square displacement is defined as [42, 43]

$$M(n) = \lim_{N\longrightarrow\infty} \frac{1}{N} \sum_{j=1}^{N} \left[(p(j+n) - p(j))^2 + (s(j+n) - s(j))^2 \right], \tag{17}$$

where $n \ll N$. In real applications, $n \leq (N/10)$ yields good results.

Second, the asymptotic growth rate K is defined as [42, 43]

$$K = \lim_{n\longrightarrow\infty} \frac{\log(M(n))}{\log(n)}. \tag{18}$$

Plots of K versus different parameters for the fractional-order Buck-Boost system are shown in Figure 6. Figures 6(a)–6(d) show the dynamics corresponding to the bifurcation diagrams as shown in Figure 3. And Figures 6(e)–6(g) are the corresponding analysis results of Figure 4 with the variation of parameters L, k, and q, respectively. It is shown in Figure 6 that chaos in the system is verified since K reaches to 1, and the K curves agree well with the bifurcation diagrams.

Moreover, K-value based contour plots of the fractional-order Buck-Boost system in different parameter planes is shown in Figure 7, where those parameter planes are divided as the 100×100 grid. The yellow color means that the system is chaotic when it takes parameters in those regions, while the rest parts mean that the system is nonchaotic. Meanwhile, it also shows that the system has wide regions for chaos in those parameter planes.

3.3. Complexity Analysis. Bifurcation diagrams, phase diagrams, (p, s) plot, and K curves are mainly used to analyze dynamics of the system but cannot show how the complexity of the system changes with the parameters. The spectral entropy (SE) [33] algorithm is employed to analyze complexity of the fractional-order Buck-Boost system, and details of this algorithm are presented as follows.

Given a time sequence of length N $\{x(n), n = 0, 1, 2, \ldots, N-1\}$, let $x(n) = x(n) - \overline{x}$, where $\overline{x}$ is the mean value of time series. Its corresponding DFT is defined by

$$X(k) = \sum_{n=0}^{N-1} x(n) e^{(-j2\pi nk/N)}, \tag{19}$$

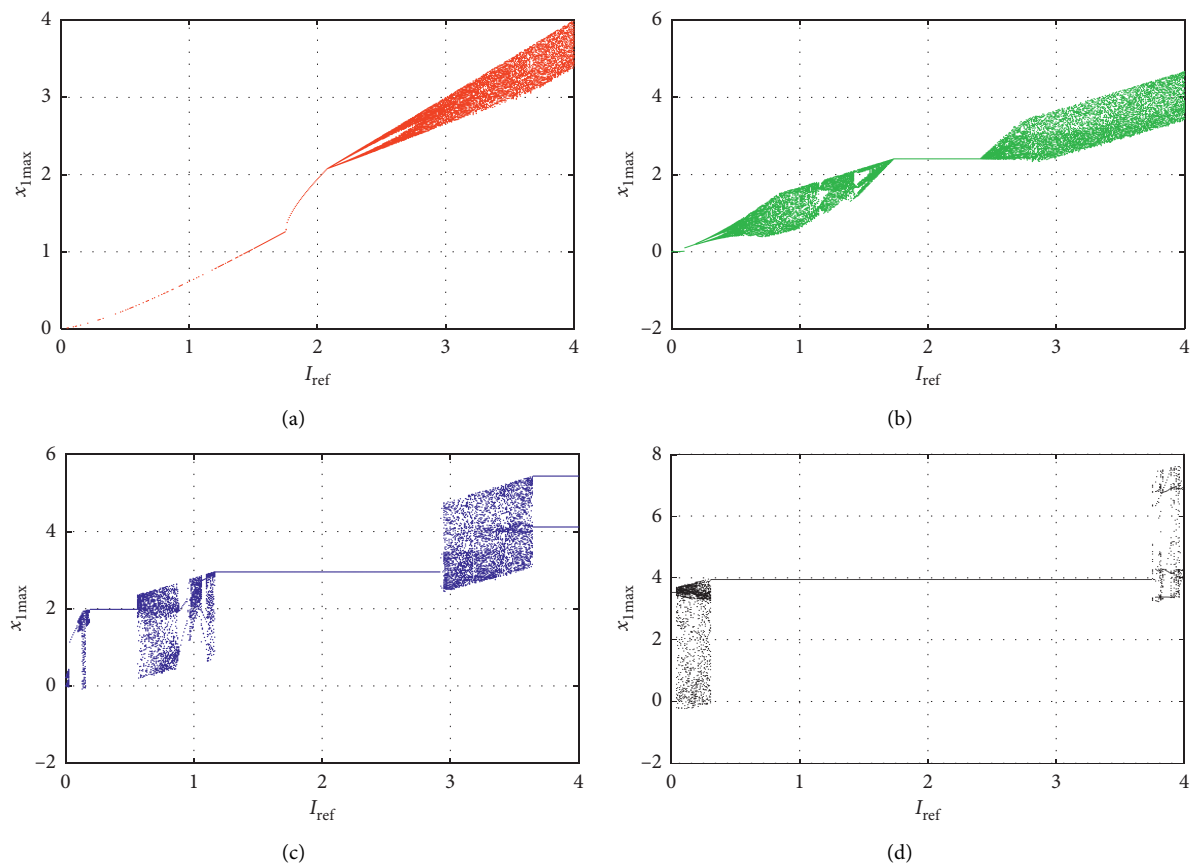

Figure 3: Bifurcation diagrams with the inductance reference current I_{ref} under different derivative orders q. (a) $q = 1$, (b) $q = 0.95$, (c) $q = 0.9$, and (d) $q = 0.85$.

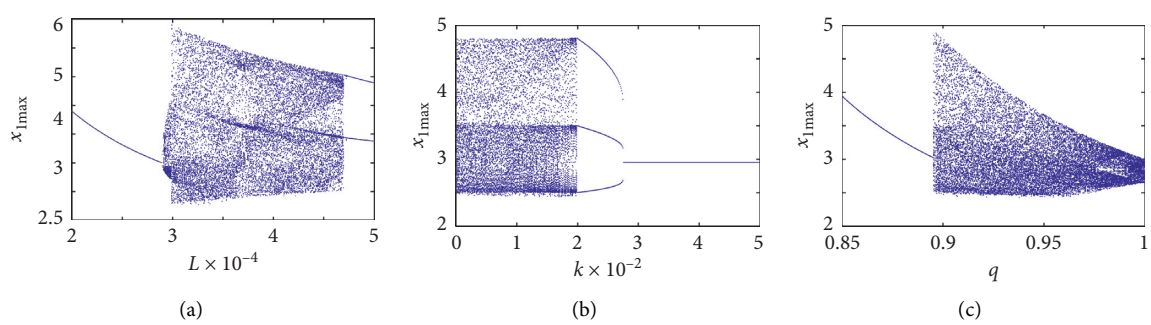

Figure 4: Bifurcation diagrams with the variation of different parameters. (a) L varying, (b) k varying, and (c) q varying.

where $k = 0, 1, \ldots, N-1$, and j is the imaginary unit. If the power of a discrete power spectrum with the k_{th} frequency is $|X(k)|^2$, then the "probability" of this frequency is defined as

$$P_k = \frac{|X(k)|^2}{\sum_{k=0}^{N/(2-1)} |X(k)|^2}. \tag{20}$$

When the DFT is employed, the summation runs from $k = 0$ to $k = (N/(2-1))$. The normalization entropy is denoted by [33]

$$SE(x^N) = \frac{1}{\ln(N/2)} \sum_{k=0}^{N/(2-1)} P_k \ln(P_k), \tag{21}$$

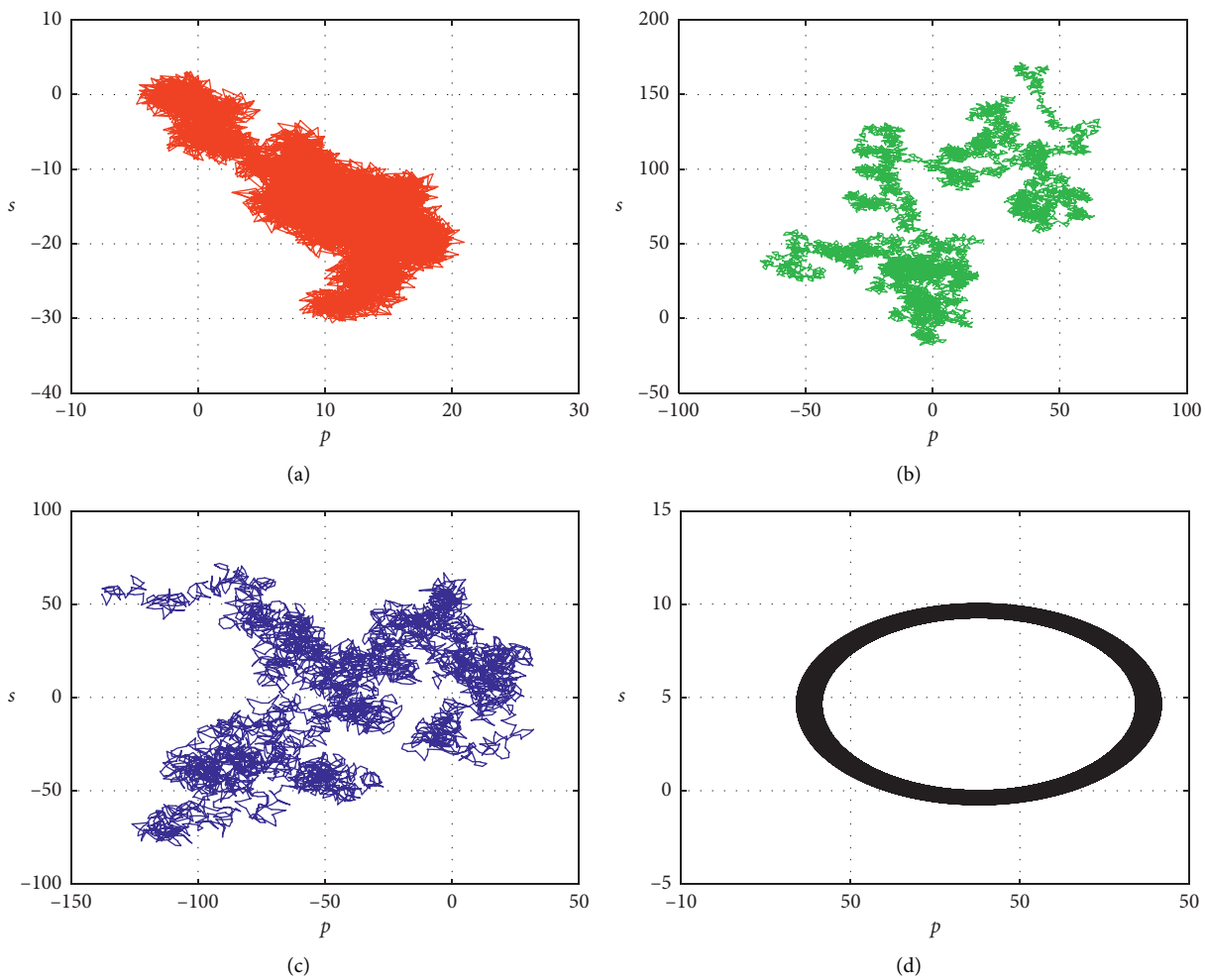

FIGURE 5: (p, s) plots of the fractional-order model. (a) $q = 1$, (b) $q = 0.95$, (c) $q = 0.9$, and (d) $q = 0.85$.

where $\ln(N/2)$ is the entropy of a completely random signal. Obviously, the more balanced the probability distribution is, the higher complexity (the larger entropy) the time series is. The larger measuring value means higher complexity and vice versa.

Using the same parameters, SE complexity of the fractional-order Buck-Boost system with different parameters is analyzed, and the results are shown in Figures 8 and 9. First, the SE analysis results have a high positive correlation with the corresponding bifurcation diagrams and 0-1 test results. As shown Figures 8 and 9, higher complexity is observed when the system is chaotic, but the nonchaotic states have lower complexity analysis results. Second, compared with the other methods in this study, SE complexity shows the variation tendency when the parameters vary.

3.4. Chaotic Pseudorandom Sequence Generator. Chaotic behaviors such as randomness, sensitive dependence on initial conditions, and ergodicity are important issues for the real applications. At present, there are many researchers focusing on the applications of chaos, such as chaos-based application of a novel no-equilibrium chaotic system with coexisting attractors [44], chaotic artificial neural networks for model memory in the brain [45], and a fractional-order chaotic system with an infinite number of equilibrium points located on a line and on a hyperbola [46]. Currently, designing chaos-based pseudorandom sequence generators has aroused much interest of researchers [33, 47–49]. Since the fractional-order Buck-Boost system has high complexity, it is a good model for designing the chaotic pseudorandom sequence generator.

In this section, by modifying our previously designed pseudorandom sequence generator [33], a pseudorandom bit generator is designed based on the fractional-order Buck-Boost system. The specific steps are given as follows.

Step 1. Set $U_{\text{in}} = 8\,\text{V}$, $R = 10\,\Omega$, $L = 0.3\,\text{mH}$, $C = 40\,\mu\text{F}$, $T = 50\,\mu\text{s}$, $I_{\text{ref}} = 4\,\text{A}$, $k = 0$,and $q = 0.95$. The initial value $\mathbf{x}_0 = [1, 2]$, $M = 0.125 \times 10^8 + 100$, and iterate the system 1000 times; then $n = 1000$, and thus, $\mathbf{x}_0 = [x_1(n), x_2(n)]$. Let $n = 1$.

Step 2. Iterate the system one time and then obtain the new value of data $= x_2(n+1)$ for the further calculation, where

$$\text{Data} = \text{round}\left(\text{data} \times 10^8\right). \tag{22}$$

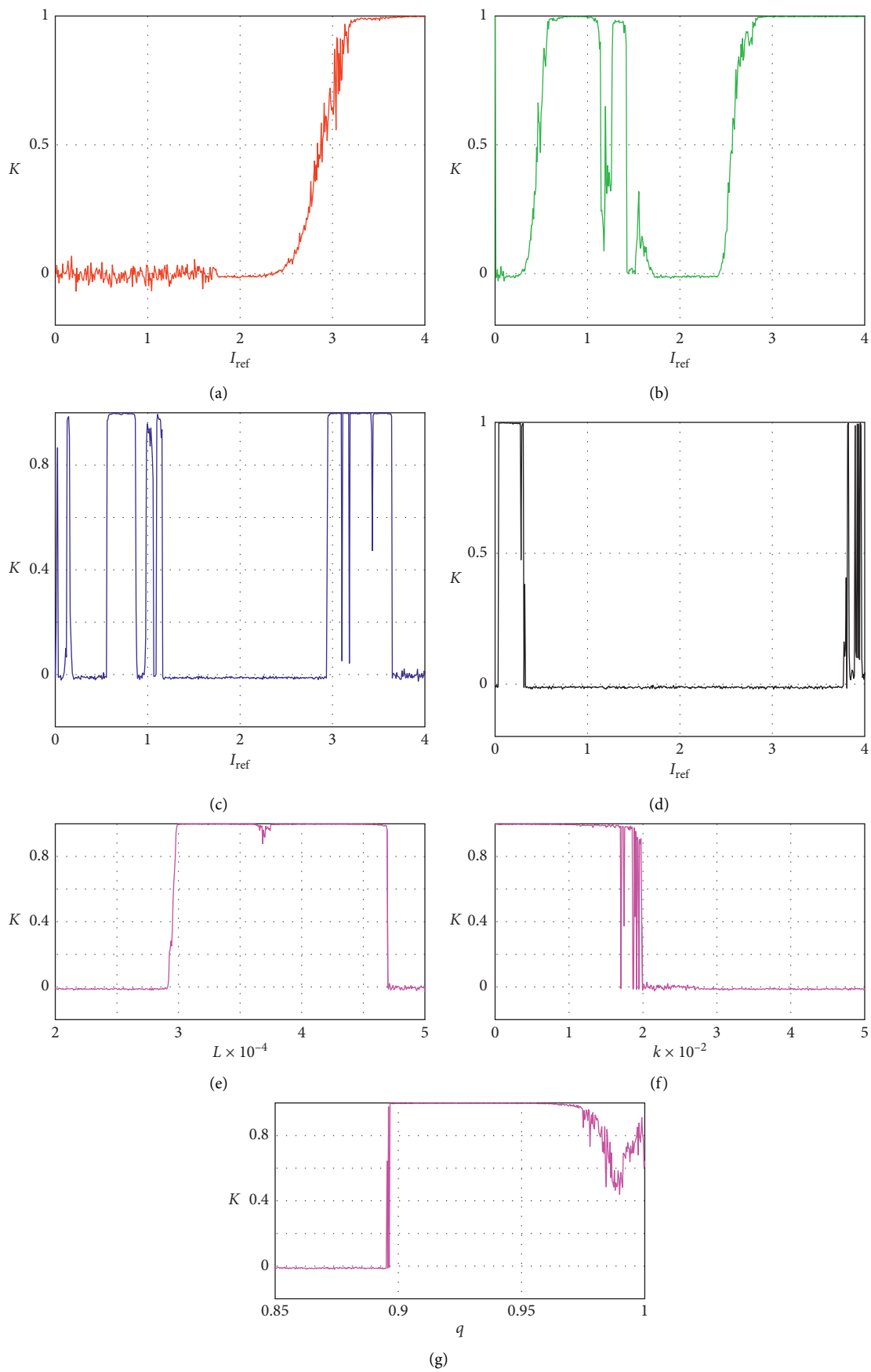

FIGURE 6: Plots of K versus different parameters for the fractional-order Buck-Boost system. (a) $q = 1$ and I_{ref} varying, (b) $q = 0.95$ and I_{ref} varying, (c) $q = 0.9$ and I_{ref} varying, (d) $q = 0.85$ and I_{ref} varying, (e) L varying, (f) k varying, and (g) derivative order q varying.

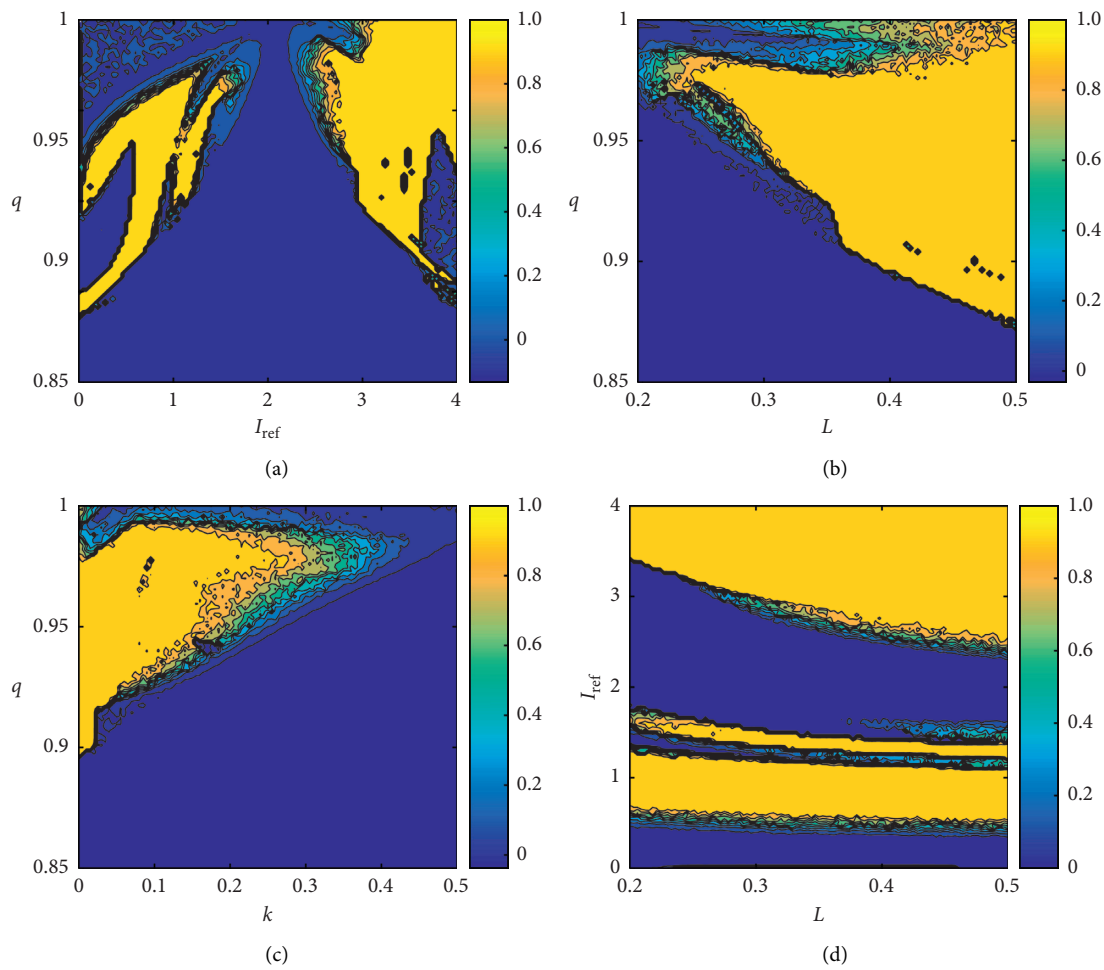

Figure 7: K value-based contour plots of the of fractional-order Buck-Boost system. (a) $q - I_{ref}$, (b) $q - L$, (c) $q - k$, and (d) $I_{ref} - L$.

Thus data are converted to as a 64-bit binary number $DB_{63} - DB_0$.

Step 3. Define $data_1 = DB_7 - DB_0$. Then, the 8-bit 0-1 sequence $data_1$ are saved in the target txt file.

Step 4. Set $n = n + 1$. If $n\%\,1000 = 0$, we define

$$\begin{cases} \Delta_1 = \dfrac{\left[x_1(n) \times 10^8\right]\%255}{100000}, \\ \Delta_2 = \dfrac{\left[x_2(n) \times 10^8\right]\%255}{100000}, \end{cases} \tag{23}$$

otherwise, $\Delta_1 = 0$ and $\Delta_2 = 0$, where $[\cdot]$ represents the round function. Now, set the initial condition for the next iterative as

$$\mathbf{x}_0 = \left[x_1(n) + \Delta_1, x_2(n) + \Delta_2\right]. \tag{24}$$

Step 5. Do Steps 2–4 in a loop until $n > M$.

As a result, a txt file which contains 10^8 more bits of "0" and "1" is obtained. In this section, the statistical test suite of NIST [50] is applied to test the randomness of the sequence.

The two indicators of the uniformity of p values and the proportion of passing sequences are used to check whether the targeting sequence passes the standard test or not. Here, the minimum uniformity of the p value is set as 0.0001. If all p values are larger than 0.0001 and the confidence interval satisfies

$$\left[(1-\alpha) - 3\sqrt{\frac{(1-\alpha)\alpha}{m}}, (1-\alpha) + 3\sqrt{\frac{(1-\alpha)\alpha}{m}}\right], \tag{25}$$

where m is the sample size and α is the given significance level, then the pseudorandom bit generator is determined to pass the standard test successfully.

One hundred pseudorandom sequences are tested, all of which are 10^6 bits long. For most tests, the confidence

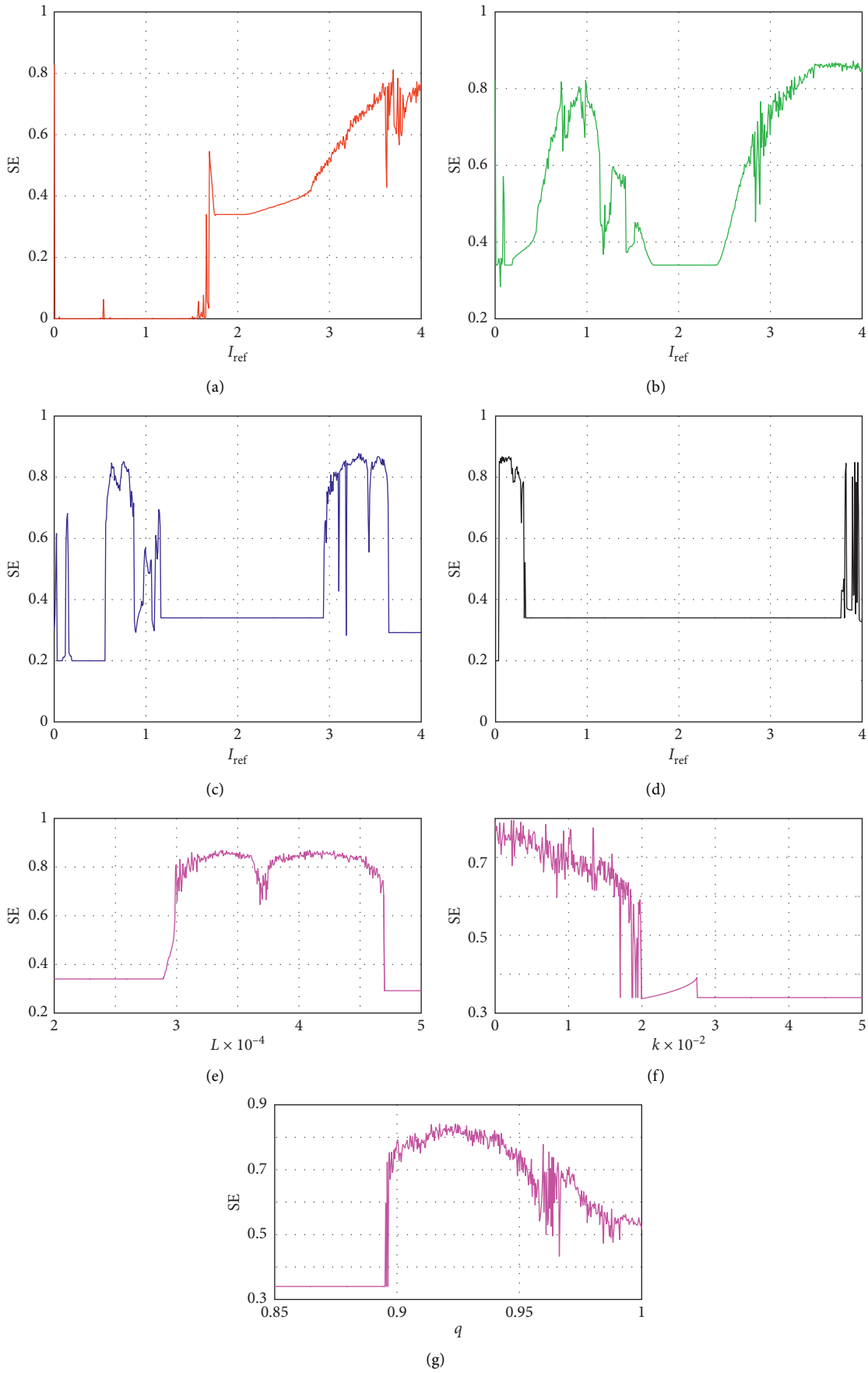

Figure 8: Plots of SE versus different parameters for the fractional-order Buck-Boost system. (a) $q = 1$ and I_{ref} varying, (b) $q = 0.95$ and I_{ref} varying, (c) $q = 0.9$ and I_{ref} varying, (d) $q = 0.85$ and I_{ref} varying, (e) L varying, (f) k varying, and (g) derivative order q varying.

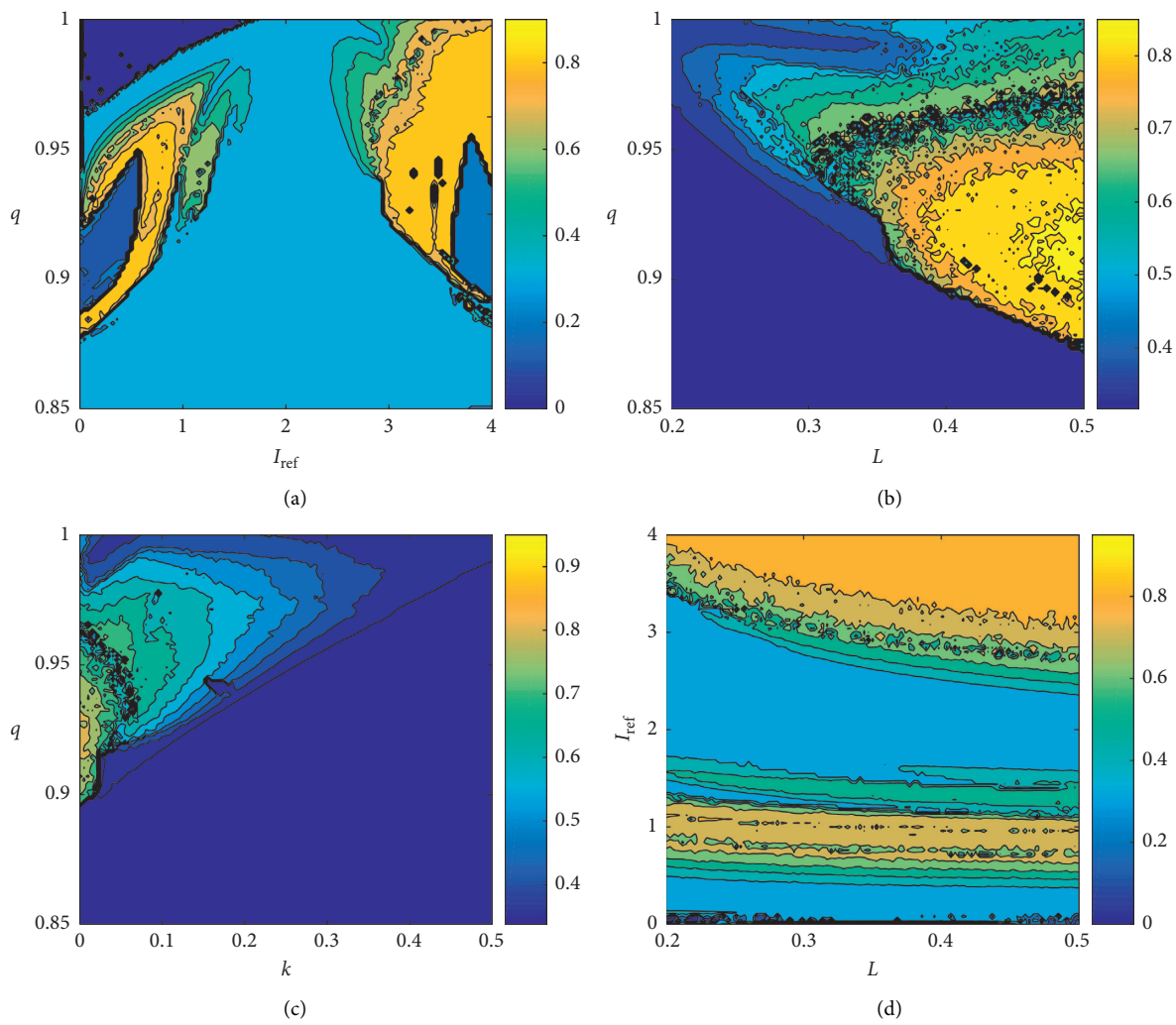

Figure 9: SE-based contour plots of the fractional-order Buck-Boost system. (a) $q - I_{ref}$, (b) $q - L$, (c) $q - k$, and (d) $I_{ref} - L$.

interval is [96.015%, 1] when $\alpha = 0.01$. For those items tested more than once (for example, N. O. Temp. is tested 148 times), we only chosen the worst results. The results are shown in Table 2. It can be seen that all p values are larger than 0.0001, and the computed proportion for each test lies inside the confidence interval. Obviously, the obtained chaotic pseudorandom sequence is random and can be used in the information security fields. And the fractional-order Buck-Boost system provides a good model for engineering applications.

4. Control of the Buck-Boost System

In the real applications, sometimes, it is deleterious when there appears chaos; then, we need to control the chaos [51]. However, in many cases, we need to use the chaos [36, 37]. In this section, the control of chaos in the fractional-order Buck-Boost system is discussed.

4.1. Control by the Intensity of Feedback k. In fact, there is no need to design an extra controller for the Buck-Boost circuit as shown in Figure 1. As shown in the above analysis results, in real applications, the values of different parameters should be chosen carefully. According to Figures 7 and 9, if parameters are chosen in those blue regions, the system is nonchaotic, and the behaviors of the circuit is under control. Moreover, if the parameters of circuit are given but it is chaotic, the system can be controlled by increasing the value of the intensity of feedback k. Here, a numerical simulation is carried out on the control of chaos of the circuit by changing the value of k. When $U_{in} = 8\,\text{V}$, $R = 10\,\Omega$, $L = 0.3\,\text{mH}$, $C = 40\,\mu\text{F}$, $T = 50\,\mu\text{s}$, $I_{ref} = 3\,\text{A}$, and $q = 0.9$, the system is chaotic for $k = 0$. In this case, we change the value of k as 0.1 (for the case $q = 0.9$) and 0.4 (for the case $q = 1$) when $t = 0.005\,\text{s}$. As shown in Figure 10, the system is chaotic at the beginning, but it becomes periodic when the value of k is changed.

As shown above, the control parameter can change the state of the system from chaos to periodic state. But it depends on how does the parameter affects dynamics of the system. As for the other parameters, they can be also used to control the state of the fractional-order Buck-Boost system. It should be noted out that the parameter control cannot

Table 2: NIST test result of the generated pseudorandom sequence.

	p value	Proportion (%)	Success
Frequency	0.779188	98	√
B. Frequency	0.514124	100	√
C. Sums (2)	0.319084	98	√
Runs	0.419021	98	√
Longest run	0.051942	97	√
Rank	0.366918	99	√
FFT	0.102526	100	√
N. O. Temp. (148)	0.003447	96	√
O. Temp.	0.534146	99	√
Universal	0.657933	100	√
App. Entropy	0.162606	99	√
R. Excur. (8)	0.327854	98.6	√
R. Excur. V. (18)	0.017912	97.3	√
Serial (2)	0.437274	99	√
L. Complexity	0.574903	100	√

make the system stable or make the system to a target state. Thus, we still need another reliable control method.

4.2. Hard Limiter Control. Hard limiter control is originally designed to control the dynamics of one-dimensional discrete maps. Specifically, Gueron [52] designed this controller to reformatting the dynamical behaviors of the discrete dynamical systems effectively. Based on the limiter control method, a one-dimensional chaotic map $x_{n+1} = f(x_n)$ becomes

$$f(x_n, \rho) = \min\{f(x_n), \rho\}, \tag{26}$$

where ρ is the value of the limiter. Recently, He et al. [53] introduced this method to control the dynamics of a fractional-order SIR epidemic model which is a two-dimensional model. For the Buck-Boost circuit, we can introduce a current limiter as shown in Figure 11 to control the dynamics of the whole circuit.

In Figure 11, the current limiter is actually a hard limiter controller. As a result, this is also a new application of the hard limiter controller. The new circuit with a hard limiter controller is rebuilt as follows.

First, let the model of Case 1 be given by

$$\begin{bmatrix} \tilde{x}_1(t_{n+1}, T) \\ \tilde{x}_2(t_{n+1}, T) \end{bmatrix} = f_1(\mathbf{x}(t_n), T, q). \tag{27}$$

In this case, the result is obtained based on the sample length of T.

Second, the model of Case 2 is defined as

$$\begin{bmatrix} \hat{x}_1(t_{n+1}) \\ \hat{x}_2(t_{n+1}) \end{bmatrix} = f_2\left(\begin{bmatrix} \min(\tilde{x}_1(t_{n+1}, d(t_n)T), \rho) \\ \tilde{x}_2(t_{n+1}, d(t_n)T) \end{bmatrix}, (1 - d(t_n))T, q\right), \tag{28}$$

where a hard limiter is used for $t \in (0t_n, t_n + d_nT]$.

Third, the hard limiter controlled model with limited variable x_1 is denoted as

$$\mathbf{x}(t_{n+1}) = \begin{cases} \begin{bmatrix} \min\{\tilde{x}_1(t_{n+1}, T), \rho\} \\ \tilde{x}_2(t_{n+1}) \end{bmatrix}, & \text{if } x_1(t_n) < I_b(t_n), \\ \begin{bmatrix} \min\{\hat{x}_2(t_{n+1}), \rho\} \\ \hat{x}_2(t_{n+1}) \end{bmatrix}, & \text{if } x_1(t_n) \geq I_b(t_n). \end{cases} \tag{29}$$

Obviously, the model is proposed based on the numerical simulation model as given by equation (15). There are two major reasons for this. One is that this numerical simulation model is a kind of equivalence of the original fractional-order Buck-Boost system. The second reason is that the hard limiter controller is proposed based on the discrete map.

Let $U_{\text{in}} = 8$ V, $R = 10\,\Omega$, $L = 0.3$ mH, $C = 40\,\mu$F, $T = 50\,\mu$s, $I_{\text{ref}} = 3$ A, $k = 0$, and $q = 0.9$, and the system is chaotic. Hard limiter control results of the fractional-order Buck-Boost system with ρ varying are shown in Figure 12. Bifurcation diagrams and the mean densities of the variables x_1 and x_2 show that the system has different states with the increase of the value of the limiter ρ. Here, the mean densities are the mean values of the variables. When the bifurcation diagram and its mean densities are overlapped, the system is convergent. Otherwise, the system is chaotic or periodic. It is shown in Figure 12 that the controlled system is convergent to the limiter ρ when $\rho < 2.4$. Meanwhile, it is verified in Figures 13(a) and 13(b) that the system is stable when $\rho = 1$ and $\rho = 2$. As for the variable x_1, it stabilizes at $x_1 = 1$ and 2, while the variable x_2 is convergent to zero. As shown in Figure 12, the system is periodic or chaotic when $\rho > 2.4$. It is also shown in Figures 13(c) and 13(d) that the controlled system is periodic for $\rho = 2.5$ and is chaotic for $\rho = 4.5$.

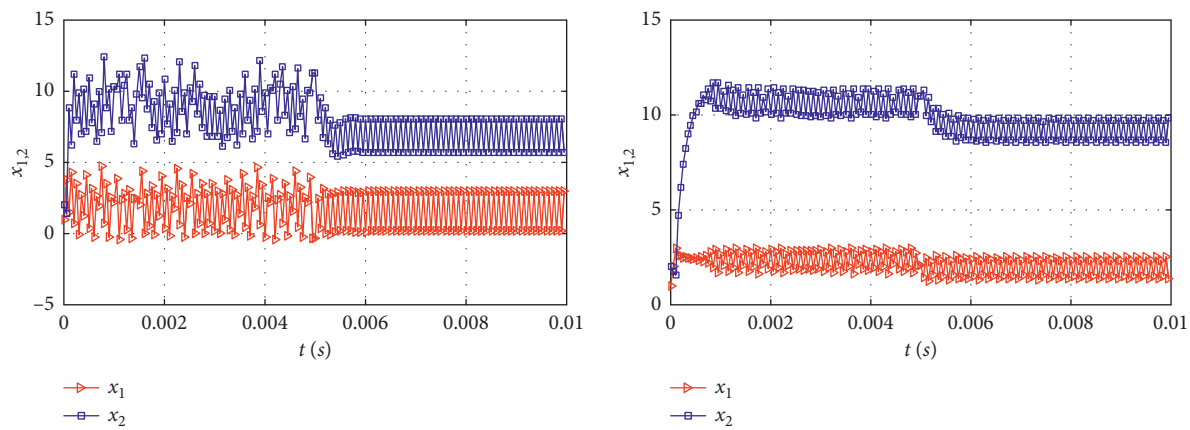

Figure 10: Plots of the fractional-order Buck-Boost system with regulable k. (a) $q = 0.9$ and k becomes to 0.1; (b) $q = 1$ and k becomes to 0.4.

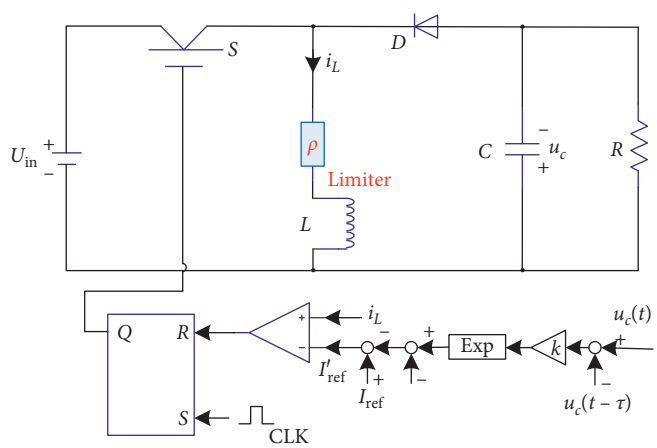

Figure 11: The Buck-Boost circuit with a limiter controller.

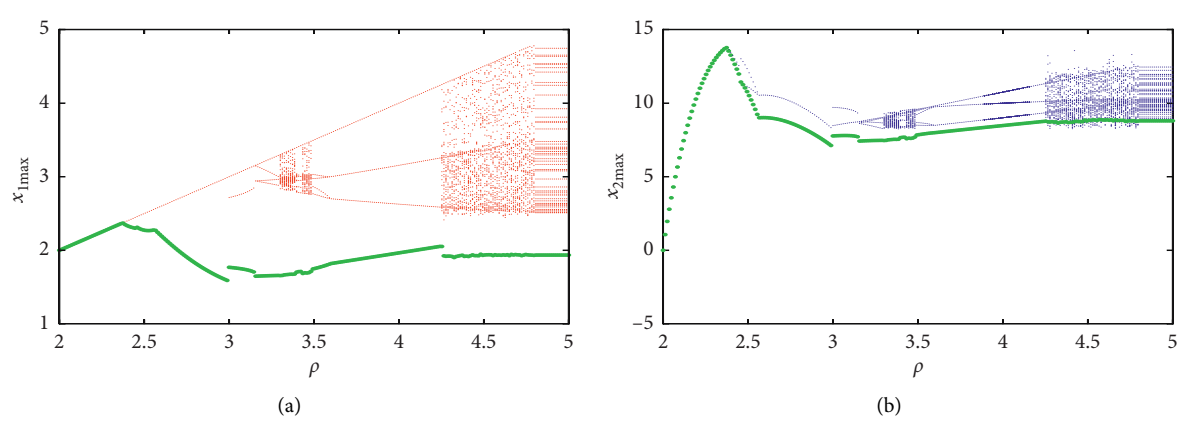

Figure 12: Hard limiter control results of the fractional-order Buck-Boost system with ρ varying. (a) Bifurcation diagram and mean densities of x_1. (b) Bifurcation diagram and mean densities with x_2.

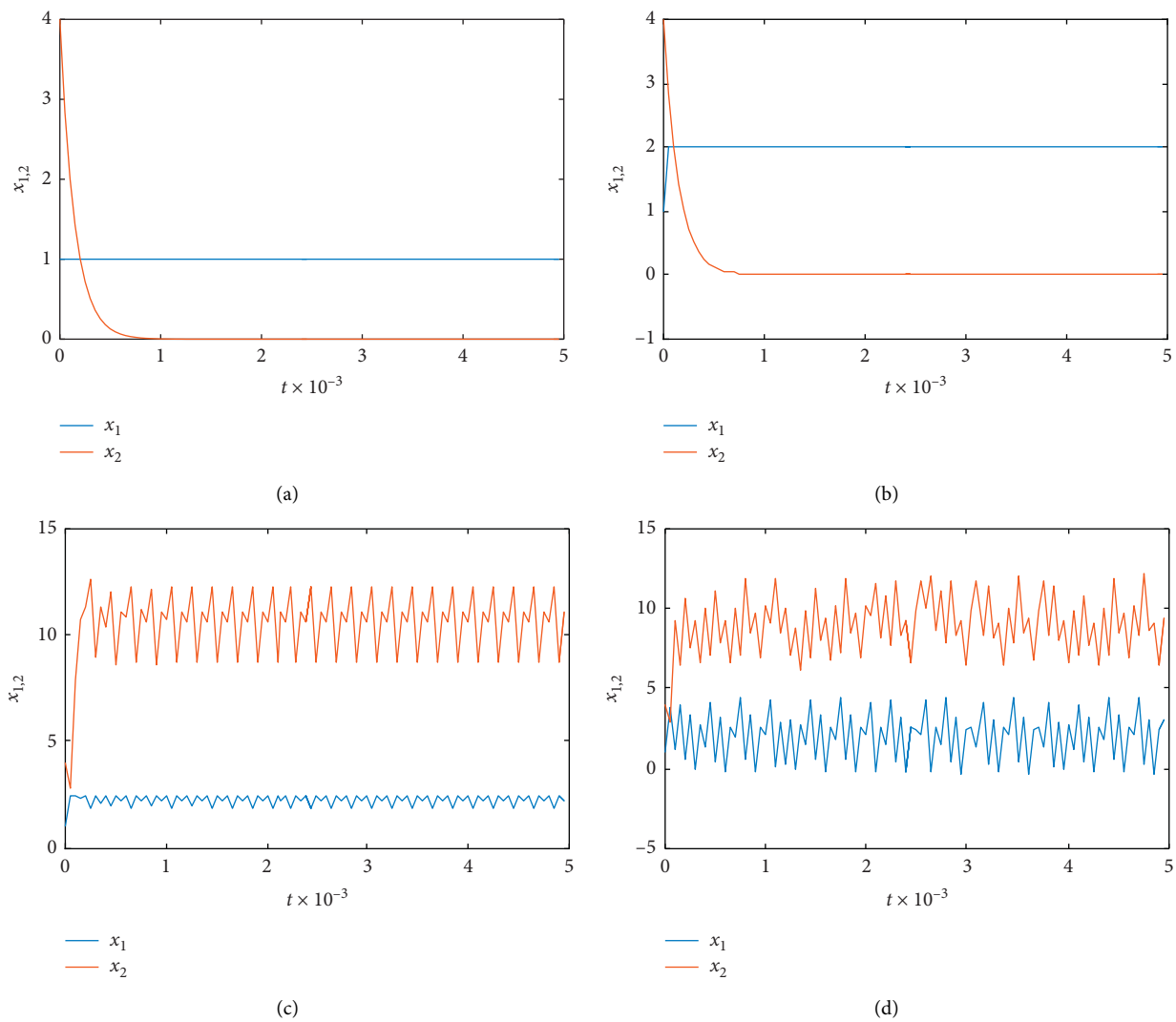

Figure 13: Hard limiter control results of the fractional-order Buck-Boost system with different ρ. (a) $\rho = 1$, (b) $\rho = 2$, (c) $\rho = 2.5$, and (d) $\rho = 4.5$.

According to above analysis, it is found that the hard limiter controller is effective for controlling the fractional-order Buck-Boost system. First, it is easy to realize in the real applications since we only need to add a current limiter in the circuit. Second, compared with the control by the intensity of feedback k, the hard limiter control is more flexible. The system can be controlled to convergent state, periodic state, and chaotic state by properly choosing a limiter ρ. Third, the hard limit controller is designed based on the obtained numerical model. In our opinion, the numerical solution is obtained from the system equation; thus, it also provides a model for analysis of the fractional-order Buck-Boost system. As for the hard limiter controller, it is designed for the discrete system, originally. Thus, it is reasonable to introduce the hard limiter controller to the numerical model of the system. Meanwhile, the proposed model can well explain the proposed circuit as shown in Figure 11. In conclusion, the hard limiter control can be related to the real situations and has a strong application prospect for controlling the Buck-Boost circuit.

5. Conclusions

In this study, a fractional-order Buck-Boost system is deduced and analyzed based on the Adomian decomposition method. Chaos, complexity, and application of this fractional-order Buck-Boost system are investigated, and methods including bifurcation diagram, the 0-1 test, and SE are introduced to carry out the study. According to the simulations and analyses, the following conclusions are obtained.

(1) The deduced fractional order has rich dynamics with different parameters, which means that the original

Buck-Boost converter could be chaotic if a set of proper parameters is given.

(2) As shown in those contour plots, the system has wide regions for chaos. The 0-1 test is an effective tool for detecting chaos, but SE shows more information on the variation tendency of the system with the variations of different parameters. Meanwhile, it shows that the generated pseudorandom sequence is random since it passes all the NIST tests.

(3) Chaos of the circuit can be controlled by adjusting the intensity of feedback k or by introducing a hard limiter controller.

Thus, this study extended the model of the Buck-Boost converter by introducing the fractional calculus. And it provides a good model for engineering applications in the information security field. Our next work is to investigate the hard limiter control of the circuit practically and to use this system for the information encryption.

Data Availability

The data used to support the findings of this study are included within the article.

Conflicts of Interest

The authors declare that there are no conflicts of interest.

Acknowledgments

This work was supported by the Hunan Provincial Department of Education General Project Fund (No. 18C0743), the Natural Science Foundation of China (Nos. 61901530, 62071496, and 62061008), and the Natural Science Foundation of Hunan Province (No. 2020JJ5767).

References

[1] E. Maali and B. Vahidi, "Double-deck buck-boost converter with soft switching operation," *IEEE Transactions on Power Electronics*, vol. 31, no. 6, pp. 4324–4330, 2016.

[2] S. Singh, N. Rathore, and D. Fulwani, "Mitigation of negative impedance instabilities in a DC/DC buck-boost converter with composite load," *Journal of Power Electronics*, vol. 16, no. 3, pp. 1046–1055, 2016.

[3] M. Salimi and S. Siami, "Cascade nonlinear control of dc-dc buck/boost converter using exact feedback linearization," in *Proceedings of the 2015 4th International Conference on Electric Power and Energy Conversion Systems (EPECS)*, pp. 1–5, IEEE, Sharjah, UAE, November 2015.

[4] M. K. Kavitha and A. Kavitha, "Nonlinear analysis of hysteretic modulation-based sliding mode controlled quadratic buck-boost converter," *Journal of Circuits, Systems and Computers*, vol. 28, no. 02, Article ID 1950025, 2019.

[5] A. El Aroudi, L. Benadero, E. Toribio, and S. Machiche, "Quasiperiodicity and chaos in the dc-dc buck-boost converter," *International Journal of Bifurcation and Chaos*, vol. 10, no. 02, pp. 359–371, 2000.

[6] K. W. E. Cheng, M. Liu, and J. Wu, "Chaos study and parameter-space analysis of the DC-DC buck-boost converter," *IEEE Proceedings-Electric Power Applications*, vol. 150, no. 2, pp. 126–138, 2003.

[7] M. R. Banaei and H. A. F. Bonab, "A high efficiency non-isolated buck–boost converter based on zeta converter," *IEEE Transactions on Industrial Electronics*, vol. 67, pp. 1991–1998, 2020.

[8] A. El Aroudi, L. Benadero, E. Toribio, and G. Olivar, "Hopf bifurcation and chaos from torus breakdown in a pwm voltage-controlled dc-dc boost converter," *IEEE Transactions on Circuits and Systems I: Fundamental Theory and Applications*, vol. 46, no. 11, pp. 1374–1382, 1999.

[9] J. D. Morcillo, D. Burbano, and F. Angulo, "Adaptive ramp technique for controlling chaos and subharmonic oscillations in DC-DC power converters," *IEEE Transactions on Power Electronics*, vol. 31, no. 7, pp. 5330–5343, 2016.

[10] Y. Wang, R. Yang, B. Zhang, and W. Hu, "Smale horseshoes and symbolic dynamics in the buck-boost DC-DC converter," *IEEE Transactions on Industrial Electronics*, vol. 65, no. 1, pp. 800–809, 2018.

[11] Ş. Demirbaş, H. Fidanboy, and E. Kurt, "Exploration of the chaotic behaviour in a buck–boost converter depending on the converter and load elements," *Journal of Electronic Materials*, vol. 45, pp. 3889–3899, 2016.

[12] M. P. Aghababa, "Stabilization of a class of cascade nonlinear switched systems with application to chaotic systems," *International Journal of Robust and Nonlinear Control*, vol. 28, no. 11, pp. 3640–3656, 2018.

[13] F. Yalcin, U. Arifoglu, I. Yazici, and K. Erin, "Robust single-phase inverter based on the buck-boost converter through an efficient hybrid control," *Iet Power Electronics*, vol. 13, no. 1, pp. 50–59, 2020.

[14] A. Kavitha and G. Uma, "Resonant parametric perturbation method to control chaos in current mode controlled dc-dc buck-boost converter," *Journal of Electrical Engineering and Technology*, vol. 5, no. 1, pp. 171–178, 2010.

[15] P. Sriramalakshmi, A. Kavitha, P. Sanjeevikumar, T. Sutikno, P. Kiran Maroti, and V. K. Ramachandaramurthy, "Control of chaos in a current mode controlled buck boost converter using weak periodic perturbation method," *International Journal of Power Electronics and Drive Systems (IJPEDS)*, vol. 8, no. 4, pp. 1467–1480, 2017.

[16] J. R. Sharma and D. Kumar, "A fast and efficient composite Newton-Chebyshev method for systems of nonlinear equations," *Journal of Complexity*, vol. 49, pp. 56–73, 2018.

[17] N. Giménez and G. Matera, "On the bit complexity of polynomial system solving," *Journal of Complexity*, vol. 51, pp. 20–67, 2019.

[18] S. G. Samko, A. A. Kilbas, and O. I. Marichev, *Fractional Integrals and Derivatives: Theory and Applications*, CRC, Boca Raton, FL, USA, 1993.

[19] H. Rudolf, *Applications of Fractional Calculus in Physics*, World Scientific, Singapore, 2000.

[20] H. Sun, Y. Zhang, D. Baleanu, W. Chen, and Y. Chen, "A new collection of real world applications of fractional calculus in science and engineering," *Communications in Nonlinear Science and Numerical Simulation*, vol. 64, pp. 213–231, 2018.

[21] B. Yan, S. He, and S. Wang, "Multistability in a fractional-order centrifugal flywheel governor system and its adaptive control," *Complexity*, vol. 2020, Article ID 8844657, 2020.

[22] S. Kumar, R. Kumar, C. Cattani, and B. Samet, "Chaotic behaviour of fractional predator-prey dynamical system," *Chaos, Solitons & Fractals*, vol. 135, Article ID 109811, 2020.

[23] S. He, K. Sun, and Y. Peng, "Detecting chaos in fractional-order nonlinear systems using the smaller alignment index," *Physics Letters A*, vol. 383, no. 19, pp. 2267–2271, 2019.

[24] S. Bendoukha and S. Abdelmalek, "The fractional chua chaotic system: dynamics, synchronization, and application to secure communications," *International Journal of Nonlinear Sciences and Numerical Simulation*, vol. 20, no. 1, pp. 77–88, 2019.

[25] Q. Zhidong, T. Juntao, P. Jin et al., "Fractional controller design of a dc-dc converter for pemfc," *IEEE Access*, vol. 8, pp. 120134–120144, 2020.

[26] A. G. Radwan, A. A. Emira, A. M. AbdelAty, and A. T. Azar, "Modeling and analysis of fractional order dc-dc converter," *ISA Transactions*, vol. 82, pp. 184–199, 2018.

[27] D. Vanitha and M. Rathinakumar, "Fractional order pid controlled pv buck boost converter with coupled inductor," *International Journal of Power Electronics and Drive Systems*, vol. 8, p. 1409, 2017.

[28] Y. Ningning, W. Chaojun, J. Rong, and L. Chongxin, "Modeling and characteristics analysis for a buck-boost converter in pseudo-continuous conduction mode based on fractional calculus," *Mathematical Problems in Engineering*, vol. 2016, Article ID 6835910, , 2016.

[29] Q. Lai, Z. Wan, L. K. Kengne, P. D. K. Kuate, and C. Chen, "Two-memristor-based chaotic system with infinite coexisting attractors," *IEEE Transactions on Circuits and Systems II: Express Briefs*, p. 1, 2020.

[30] Q. Lai, Z. Wan, P. D. Kamdem Kuate, and H. Fotsin, "Coexisting attractors, circuit implementation and synchronization control of a new chaotic system evolved from the simplest memristor chaotic circuit," *Communications in Nonlinear Science and Numerical Simulation*, vol. 89, Article ID 105341, 2020.

[31] Q. Lai, B. Norouzi, and F. Liu, "Dynamic analysis, circuit realization, control design and image encryption application of an extended Lü system with coexisting attractors," *Chaos, Solitons & Fractals*, vol. 114, pp. 230–245, 2018.

[32] Q. Lai, "A unified chaotic system with various coexisting attractors," *International Journal of Bifurcation and Chaos*, vol. 31, no. 01, Article ID 2150013, 2021.

[33] S. He, K. Sun, and H. Wang, "Complexity analysis and dsp implementation of the fractional-order lorenz hyperchaotic system," *Entropy*, vol. 17, no. 12, pp. 8299–8311, 2015.

[34] Z. Wu and X. P. Zhang, "Chaos control of buck-boost converter in current mode," *Proceedings of the CSU-EPSA*, vol. 30, no. 8, pp. 51–57, 2018.

[35] X. Yi, R. Guo, and Y. Qi, "Stabilization of chaotic systems with both uncertainty and disturbance by the ude-based control method," *IEEE Access*, vol. 8, pp. 62471–62477, 2020.

[36] L. M. Zhang, K. H. Sun, W. H. Liu, and S. B. He, "A novel color image encryption scheme using fractional-order hyperchaotic system and dna sequence operations," *Chinese Physics B*, vol. 26, Article ID 100504, 2017.

[37] F. F. Yang, J. Mou, C. F. Luo, and Y. H. Cao, "An improved color image encryption scheme and cryptanalysis based on hyperchaotic sequence," *Physica Scripta*, vol. 94, Article ID 085206, 2019.

[38] B. Dumitru, D. Kai, and S. Enrico, *Fractional Calculus: Models and Numerical Methods*, World Scientific, Singapore, 2012.

[39] G. Adomian and R. Rach, "Modified adomian polynomials," *Mathematical and Computer Modelling*, vol. 24, no. 11, pp. 39–46, 1996.

[40] R. Caponetto and S. Fazzino, "An application of adomian decomposition for analysis of fractional-order chaotic systems," *International Journal of Bifurcation and Chaos*, vol. 23, no. 03, Article ID 1350050, 2013.

[41] D. Cafagna and G. Grassi, "Bifurcation and chaos in the fractional-order chen system via a time-domain approach," *International Journal of Bifurcation and Chaos*, vol. 18, no. 07, pp. 1845–1863, 2008.

[42] I. Falconer, G. A. Gottwald, I. Melbourne, and K. Wormnes, "Application of the 0-1 test for chaos to experimental data," *SIAM Journal on Applied Dynamical Systems*, vol. 6, no. 2, pp. 395–402, 2007.

[43] G. A. Gottwald and I. Melbourne, "On the implementation of the 0-1 test for chaos," *SIAM Journal on Applied Dynamical Systems*, vol. 8, no. 1, pp. 129–145, 2009.

[44] Z. Wang, A. Akgul, V.-T. Pham, and S. Jafari, "Chaos-based application of a novel no-equilibrium chaotic system with coexisting attractors," *Nonlinear Dynamics*, vol. 89, no. 3, pp. 1877–1887, 2017.

[45] Z. Aram, S. Jafari, J. Ma, J. C. Sprott, S. Zendehrouh, and V.-T. Pham, "Using chaotic artificial neural networks to model memory in the brain," *Communications in Nonlinear Science and Numerical Simulation*, vol. 44, pp. 449–459, 2017.

[46] S. T. Kingni, V.-T. Pham, S. Jafari, and P. Woafo, "A chaotic system with an infinite number of equilibrium points located on a line and on a hyperbola and its fractional-order form," *Chaos, Solitons & Fractals*, vol. 99, pp. 209–218, 2017.

[47] R. Hamza, "A novel pseudo random sequence generator for image-cryptographic applications," *Journal of Information Security and Applications*, vol. 35, pp. 119–127, 2017.

[48] H. Xu, X. Tong, and X. Meng, "An efficient chaos pseudo-random number generator applied to video encryption," *Optik*, vol. 127, no. 20, pp. 9305–9319, 2016.

[49] A. A. Rezk, A. H. Madian, A. G. Radwan, and A. M. Soliman, "Reconfigurable chaotic pseudo random number generator based on fpga," *AEU-International Journal of Electronics and Communications*, vol. 98, pp. 174–180, 2019.

[50] A. Rukhin, J. Soto, and J. Nechvata, "A Statistical Test Suite for Random and Pseudorandom Number Generators for Cryptographic Applications," Technical Report, DTIC Document, 2001.

[51] G. Chen and X. Yu, *Chaos Control: Theory and Applications*, Springer Science, Berlin, Germany, 2003.

[52] S. Gueron, "Controlling one-dimensional unimodal population maps by harvesting at a constant rate," *Physical Review E*, vol. 57, no. 3, p. 3645, 1998.

[53] S. He and S. Banerjee, "Epidemic outbreaks and its control using a fractional order model with seasonality and stochastic infection," *Physica A: Statistical Mechanics and Its Applications*, vol. 501, pp. 408–417, 2018.

Hindawi
Mathematical Problems in Engineering
Volume 2021, Article ID 5512094, 15 pages
https://doi.org/10.1155/2021/5512094

Research Article

Adaptive Control of a New Chaotic Financial System with Integer Order and Fractional Order and Its Identical Adaptive Synchronization

Paul Yaovi Dousseh,[1] Cyrille Ainamon,[1] Clément Hodévèwan Miwadinou,[1,2] Adjimon Vincent Monwanou,[1] and Jean Bio Chabi Orou[1]

[1]*Laboratoire de Mécaniques des Fluides, de la Dynamique Non-linéaire et de la Modélisation des Systèmes Biologiques (LMFDNMSB), Institut de Mathématiques et de Sciences Physiques (IMSP), Porto-Novo, Benin*
[2]*Département de Physique, ENS-Natitingou, Université des Sciences, Technologies, Ingénierie et Mathématiques (UNSTIM), Abomey, Benin*

Correspondence should be addressed to Clément Hodévèwan Miwadinou; clement.miwadinou@imsp-uac.org

Received 19 January 2021; Revised 13 February 2021; Accepted 26 February 2021; Published 13 March 2021

Academic Editor: Yi Qi

In this paper, adaptive control and adaptive synchronization of an integer and fractional order new financial system with unknown constant parameters are studied. Based on Lyapunov's stability theory, an adaptive control law is designed to asymptotically stabilize the state variables of the system to the origin in integer and fractional order cases. By the same theory, an adaptive synchronization law is designed to perform the identical synchronization of the new financial system in the cases of integer and fractional order with unknown constant parameters. Numerical simulations are carried out in order to show the efficiency of the theoretical results.

1. Introduction

Fractional order derivatives are a subject over 300 years old, initiated by Leibniz's letter to L'Hospital [1, 2] and are a generalization of integer order derivatives But their applications in scientific fields are very recent and this is due to the lack of their physical interpretation. The difference between these fractional order derivatives and the integer order derivatives is that fractional order derivatives have the memory that turns out to be very useful when it comes to describing systems with memory and heredity properties. In the literature, several systems have been described using fractional order derivatives, we can cite the fractional order Liu system [3], the fractional order financial system [4], the fractional order glucose-insulin regulatory system [5], the fractional order Chua system [6], etc. Chaotic dynamical systems are first of all nonlinear systems, depending on several parameters and having an extreme sensitivity to initial conditions. These systems are found in many scientific fields including chemical, physical [6], economic [4], or biological [5]. This has led researchers from various horizons to take an interest in these types of systems, and especially the control of the chaos which intervenes and the synchronization of these systems with integer and fractional order. Chaos control in a dynamical system consists in designing a control law which stabilizes the system asymptotically on one of these unstable fixed points. In the literature, several methods have been proposed to achieve this goal. We have among others, the linear feedback control [7], adaptive control [8, 9], sliding mode control [10], Lyapunov-based nonlinear control [11], adaptive sliding mode control [12], etc. Recently, for the stabilization of dynamical systems, different results have been obtained in the literature in fields as diverse as varied. For example, see

[13], where authors proceeded to the stabilization of a class of chaotic systems when systems are subject to uncertainty and external disturbance by a new uncertainty and disturbance estimator- (UDE-) based control method. In [14], a novel distributed consensus algorithm based on the integration of sliding mode control scheme and (average) ADT method is proposed to solve consensus control problem in order to guarantee the stability of the closed-loop system. Also, in [15], the finite horizon control for a broad class of linear It ô stochastic differential equations (SDEs) with infinite Markovian jumps and (x, u, v)-dependent noise is done. The authors proposed the existence of the mixed control, a necessary and sufficient condition, which is represented by the solution of a countably infinite set of coupled generalized difference Riccati equations (GDREs).

The synchronization of integer and fractional order systems has also been widely discussed in the literature due to its applications in the field of communication [17, 18] for the secure transmission of information. Several approaches are used for the synchronization of chaotic systems such as synchronization via nonlinear control [19, 20], synchronization via active control [7, 21, 22], and adaptive synchronization [8, 9, 23]. The particularity of adaptive control and adaptive synchronization is that these unlike other controllers, which are used when the system's parameters are known, are used when the system's parameters are unknown.

In the field of economics, several models have been proposed [24, 25]. The study of dynamic behavior, and the control of chaos in financial and economic systems have also been approached in order to understand the dynamic behavior of these systems and stabilize them in order to eliminate undesirable behavior [10, 26–31]. In 2020, Liao et al. [32] presented a new model to take into account the interaction between the various state variables of the system. The numerical study of this model revealed that it presents complex dynamic behaviors such as period doubling and chaos [32]. It would therefore be interesting to control the chaos in this new financial system, in other words, to eliminate the undesirable behaviors of the system by considering the case where constant parameters of the system are unknown and also to carry out the identical adaptive synchronization of this new chaotic system. It is in this context that this work is part of which in order to control the chaotic behavior of the new financial system when the parameters are unknown; an adaptive control law will be designed to stabilize asymptotically at the origin the state variables of the integer and fractional order system. The case of the adaptive synchronization of the new financial system with integer and fractional order will also be discussed.

The organization of the rest of this paper is as follows: in Section 2, some concepts on fractional calculus and the description of the new financial system with integer and fractional order are given. The adaptive control of chaos in the new financial system based on Lyapunov's stability theory in the cases of integer order and incommensurate fractional order are done in Section 3. Section 4 deals with the adaptive synchronization of the new financial system in the cases of integer and incommensurate fractional order. Finally, the conclusion is discussed in Section 5.

2. Some Fractional Calculus Concepts and Model Description

The arbitrary order derivative, in other words, the fractional order derivative, is a generalization of the integer order derivative or the classical derivative. We generally meet in the literature three definitions of fractional order derivative [33]. In this paper, we will use the fractional order derivative in the sense of Caputo because with this derivative, the initial conditions take the same form as when the system is defined with integer order derivative.

The fractional order derivative in the sense of Caputo (C) is defined by

$$ {}_a^C D_t^q f(t) = \frac{1}{\Gamma(n-1)} \int_a^t (t-\tau)^{n-q-1} f^{(n)}(\tau) \mathrm{d}\tau, \quad n-1 < q < n, \tag{1} $$

where $\Gamma(\cdot)$is the gamma function and q is the order of the fractional derivative.

The fractional order derivative in the sense of Caputo has a certain number of properties defined as follows [33, 34].

Property 1. Suppose that $0 < q < 1$, then

$$ Dy(t) = D^{1-q} D^q y(t), \tag{2} $$

in which $D = (\mathrm{d}/\mathrm{d}t)$.

Property 2. When $q = 0$,

$$ D^0 y(t) = y(t). \tag{3} $$

Property 3. As in the case of the integer order derivative, the fractional order derivative in the sense of Caputo is a linear operator:

$$ D^q(\gamma x(t) + \delta y(t)) = \gamma D^q x(t) + \delta D^q y(t), \tag{4} $$

in which γ and δ are real constants.

Property 4. As in the case of the integer order derivative, the fractional order derivative in the sense of Caputo satisfies the additive index law, i. e.,

$$ D^{q_1} D^{q_2} y(t) = D^{q_2} D^{q_1} y(t) = D^{q_1+q_2} y(t), \tag{5} $$

with some reasonable constraints on the function$y(t)$.

In 2020, Liao et al. [32] presented a new financial model in order to take into account the interaction between the interest rate $x(t)$, the investment demand $y(t)$, and the price index $z(t)$. The system is defined as follows:

$$\begin{cases} \dfrac{\mathrm{d}x}{\mathrm{d}t} = \mathrm{d}z + (y - e)x, \\ \dfrac{\mathrm{d}y}{\mathrm{d}t} = -ky^2 - lx^2 + m, \\ \dfrac{\mathrm{d}z}{\mathrm{d}t} = -\gamma z - \delta x - \rho y, \end{cases} \tag{6}$$

where the parameters e, k, γ, m, l, ρ, and δ are constants. In [32], when $e = 0.3, k = 0.02, \gamma = 1, m = 1, l = 0.1, \rho = 0.05$, and $d = 1.2, \delta = 1$ and initial conditions (1.2, 1.5, 1.6) are considered, system (6) exhibits a chaotic behavior as shown in Figures 1(a)–1(d). When the initial conditions (0.2, 0.5, and 0.6) are considered, system (6) also presents a chaotic behavior [32].

The generalization of system (6), i.e., the fractional order version of the new financial system is also considered in this study. Classical derivatives (integer order) are replaced by fractional order derivatives as follows:

$$\begin{cases} D^{q_1} x = dz + (y - e)x, \\ D^{q_2} y = -ky^2 - lx^2 + m, \\ D^{q_3} z = -\gamma z - \delta x - \rho y, \end{cases} \tag{7}$$

where $q_i \in (0, 1)$ and $D^{q_i} = (\mathrm{d}^{q_i}/\mathrm{d}t^{q_i})\,(i = 1, 2, 3)$. If $q_1 = q_2 = q_3 = q$, then system (7) is said to be a commensurate order system; otherwise, it is said to be an incommensurate order system.

The new fractional order financial system is chaotic when the values of the above parameters are considered; the initial conditions $(1.2, 1.5, 1.6)$ and the orders $q_1 = 1, q_2 = 0.88$, and $q_3 = 1$ are considered.

The phase diagrams projected onto the phase planes (x, y), (x, z), and the time histories of the state variables $x(t)$ and $y(t)$ are shown in Figures 2(a)–2(d).

3. Adaptive Control of Chaos in a New Financial System

3.1. Integer Order Case. In this part, we will be interested in the design of an adaptive control law in order to globally stabilize the new integer order financial system.

3.1.1. Controller Design. To control the chaos in system (6), adaptive controllers are added to it. The new controlled financial system can therefore be written in the following form:

$$\begin{cases} \dot{x} = dz + (y - e)x + u_1, \\ \dot{y} = -ky^2 - lx^2 + m + u_2, \\ \dot{z} = -\gamma z - \delta x - \rho y + u_3, \end{cases} \tag{8}$$

in which $\dot{x} = (\mathrm{d}x/\mathrm{d}t)$, $\dot{y} = (\mathrm{d}y/\mathrm{d}t)$, and $\dot{z} = (\mathrm{d}z/\mathrm{d}t)$. The u_i, $(i = 1, 2, 3)$ are adaptive controllers which will be subsequently designed taking into account the state variables of the system and the estimation of the unknown constant parameters $d, e, k, l, m, \gamma, \delta$, and ρ of the system.

To allow the state variables of the system to converge asymptotically to the origin, we take the following adaptive control functions:

$$\begin{cases} u_1 = -yx - \hat{d}z + \hat{e}x - h_1 x, \\ u_2 = \hat{k}y^2 + \hat{l}x^2 - \hat{m} - h_2 y, \\ u_3 = \hat{\gamma}z + \hat{\delta}x + \hat{\rho}y - h_3 z, \end{cases} \tag{9}$$

in which $\hat{d}, \hat{e}, \hat{k}, \hat{l}, \hat{m}, \hat{\gamma}, \hat{\delta}$, and $\hat{\rho}$ are the estimation of the unknown constant parameters $d, e, k, l, m, \gamma, \delta$, and ρ, respectively, and h_i, $(i = 1, 2, 3)$ are positive constants.

By replacing the control law (9) in system (8), we have

$$\begin{cases} \dot{x} = (d - \hat{d})z - (e - \hat{e})x - h_1 x, \\ \dot{y} = -(k - \hat{k})y^2 - (l - \hat{l})x^2 + (m - \hat{m}) - h_2 y, \\ \dot{z} = -(\gamma - \hat{\gamma})z - (\delta - \hat{\delta})x - (\rho - \hat{\rho})y - h_3 z. \end{cases} \tag{10}$$

Let us define the estimation error of unknown parameters as follows:

$$\begin{cases} e_d = d - \hat{d}, \\ e_e = e - \hat{e}, \\ e_k = k - \hat{k}, \\ e_l = l - \hat{l}, \\ e_m = m - \hat{m}, \\ e_\gamma = \gamma - \hat{\gamma}, \\ e_\delta = \delta - \hat{\delta}, \\ e_\rho = \rho - \hat{\rho}. \end{cases} \tag{11}$$

By replacing equation (11) in system (10), we have

$$\begin{cases} \dot{x} = e_d z - e_e x - h_1 x, \\ \dot{y} = -e_k y^2 - e_l x^2 + e_m - h_2 y, \\ \dot{z} = -e_\gamma z - e_\delta x - e_\rho y - h_3 z. \end{cases} \tag{12}$$

For the design of the parameter update law which will allow to adjusting the parameter estimates, we use Lyapunov's stability theory.

For this, consider the Lyapunov quadratic function defined as follows:

$$V = \frac{1}{2}\left(x^2 + y^2 + z^2 + e_d^2 + e_e^2 + e_k^2 + e_l^2 + e_m^2 + e_\gamma^2 + e_\delta^2 + e_\rho^2\right), \tag{13}$$

which is a positive definite function on R^{11}.

The derivative with respect to time of equation (13) gives us

$$\begin{aligned} \dot{V} = {} & x\dot{x} + y\dot{y} + z\dot{z} + e_d\dot{e}_d + e_e\dot{e}_e + e_k\dot{e}_k \\ & + e_l\dot{e}_l + e_m\dot{e}_m + e_\gamma\dot{e}_\gamma + e_\delta\dot{e}_\delta + e_\rho\dot{e}_\rho, \end{aligned} \tag{14}$$

which specify that

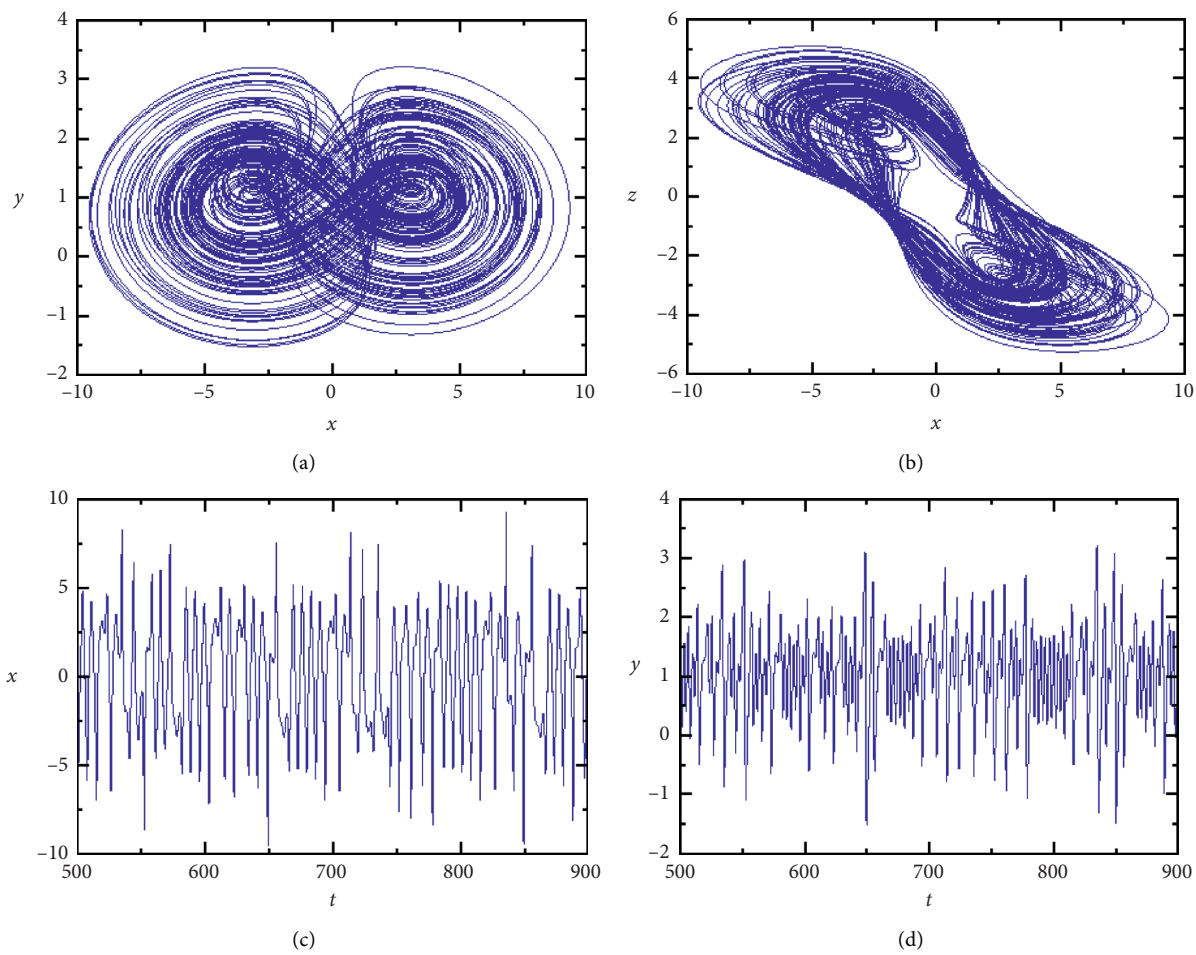

Figure 1: Phase diagrams and time histories of system (6): (a) projected onto x-y phase plane, (b) projected onto x-z phase plane, (c) time history of (x), and (d) time history of y.

$$\begin{cases} \dot{e}_d = -\dot{\hat{d}}, \\ \dot{e}_e = -\dot{\hat{e}}, \\ \dot{e}_k = -\dot{\hat{k}}\dot{e}_l = -\dot{\hat{l}}, \dot{e}_m = -\dot{\hat{m}}, \dot{e}_\gamma = -\dot{\hat{\gamma}}, \dot{e}_\delta = -\dot{\hat{\delta}}, \dot{e}_\rho = -\dot{\hat{\rho}}. \end{cases} \tag{15}$$

Using system (12) and equation (15), equations (14) becomes

$$\begin{aligned} \dot{V} = &-h_1x^2 - h_2y^2 - h_3z^2 + e_d(xz - \dot{\hat{d}}) \\ &+ e_e\left(-x^2 - \dot{\hat{e}}\right) + e_k\left(-y^3 - \dot{\hat{k}}\right) \\ &+ e_l\left(-yx^2 - \dot{\hat{l}}\right) + e_m(y - \dot{\hat{m}}) \\ &+ e_\gamma\left(-z^2 - \dot{\hat{\gamma}}\right) + e_\delta(-xz - \dot{\hat{\delta}}) \\ &+ e_\rho(-zy - \dot{\hat{\rho}}). \end{aligned} \tag{16}$$

From equation (16), we deduce that the estimated parameters update law is

$$\begin{cases} \dot{\hat{d}} = xz + h_4e_d, \\ \dot{\hat{e}} = -x^2 + h_5e_e, \\ \dot{\hat{k}} = -y^3 + h_6e_k, \\ \dot{\hat{l}} = -yx^2 + h_7e_l, \\ \dot{\hat{m}} = y + h_8e_m, \\ \dot{\hat{\gamma}} = -z^2 + h_9e_\gamma, \\ \dot{\hat{\delta}} = -xz + h_{10}e_\delta, \dot{\hat{\rho}} = -zy + h_{11}e_\rho, \end{cases} \tag{17}$$

in which $h_4, h_5, h_6, h_7, h_8, h_9, h_{10}$, and h_{11} are positive constants.

By replacing equation (17) in (16), we have

$$\begin{aligned} \dot{V} = &-h_1x^2 - h_2y^2 - h_3z^2 - h_4e_d^2 \\ &- h_5e_e^2 - h_6e_k^2 - h_7e_l^2 - h_8e_m^2 - h_9e_\gamma^2 \\ &- h_{10}e_\delta^2 - h_{11}e_\rho^2 < 0, \end{aligned} \tag{18}$$

which is the negative definite function on R^{11} for positive constants h_i, $(i = 1, \ldots, 11)$.

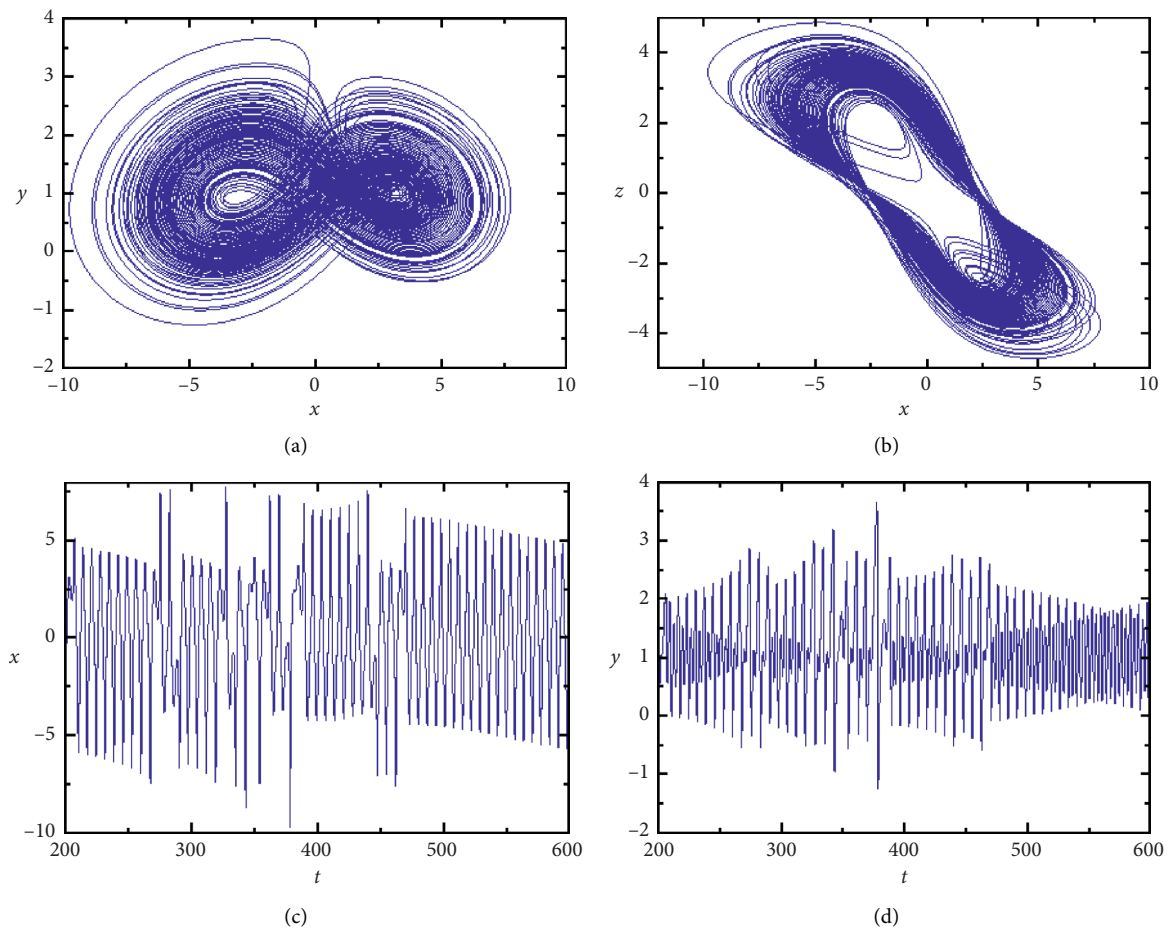

Figure 2: Phase diagrams and time histories of system (7) with $q_1 = 1, q_2 = 0.88$, and $q_3 = 1$: (a) projected onto x-y phase plane, (b) projected onto x-z phase plane, (c) time history of (x), and (d) time history of y.

So, we have found a function which verifies the Lyapunov stability theorem $(V > 0, \dot{V} < 0)$.

Thus, we have the following result.

Theorem 1. *The new financial system (8) with the unknown parameters is globally and asymptotically stabilized at the origin for all initial conditions by the adaptive law (9), where the update law of the parameters is given by (17) with h_i, $(i = 1, \ldots, 11)$ being positive constants.*

3.1.2. Simulation Results. In this part, we use the fourth-order Runge–Kutta algorithm to solve the new financial system (8) with the adaptive law (9) and the parameters update law (17). For the simulation, the time-step $h = 0.001$ is chosen. The initial conditions $(x(0), y(0), z(0)) = (1.2, 1.5, 1.6)$ are used. The parameters of the new financial system are chosen as follows:

$$e = 0.3, k = 0.02, \gamma = 1, m = 1, l = 0.1, \rho = 0.05, d = 1.2, \delta = 1. \tag{19}$$

For h_i, $(1, \ldots, 11)$ of the adaptive and update laws, we choose $h_i = 3$.

For the initial value of the estimated parameters, we assume the following values:

$$\hat{e}(0) = 3, \hat{k}(0) = 1, \hat{\gamma}(0) = 4, \hat{m}(0) = 3, \hat{l}(0) = 1, \hat{\rho}(0) = 2, \hat{d}(0) = 1, \hat{\delta}(0) = 3. \tag{20}$$

By applying the adaptive control law (9) and the parameter update law (17) to the new controlled financial system (8), the results of the numerical simulations are shown in Figures 3 and 4. From Figure 3, it can be seen that the state variables of the system converge asymptotically towards the origin (zero). Figure 4 shows the estimated parameters for

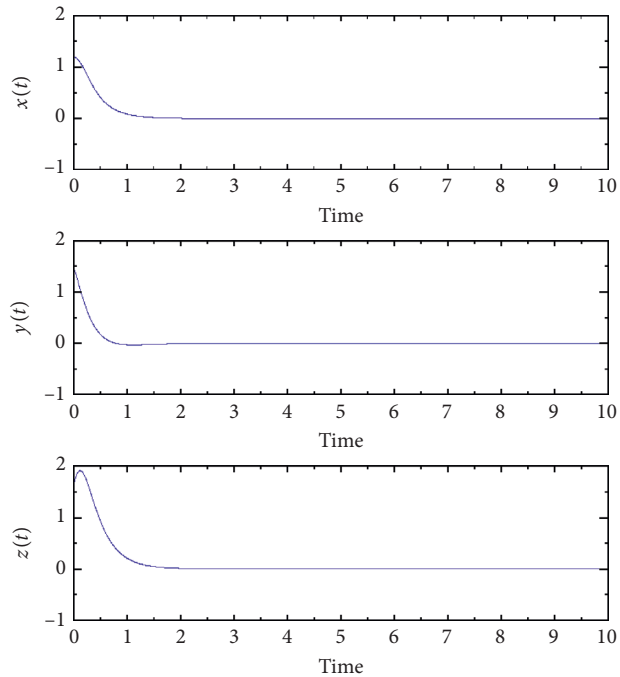

Figure 3: Time histories of the controlled integer order new financial system (8).

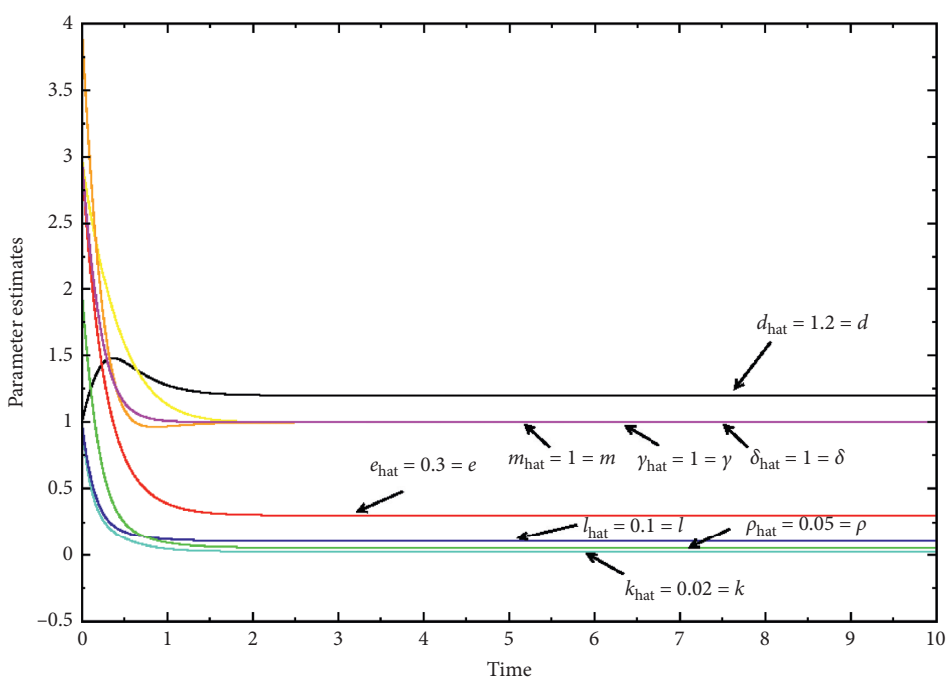

Figure 4: Parameter estimates for adaptive control in integer order case.

adaptive control in integer order case and, as it can be seen, these parameters converge towards the real values of the parameters of the system, i.e.,

$$e = 0.3, k = 0.02, \gamma = 1, m = 1, l = 0.1, \rho = 0.05, d = 1.2, \delta = 1. \tag{21}$$

3.2. Fractional Order Case. In this part, the adaptive control of the new fractional order financial system is performed to globally stabilize the new financial system with fractional order.

3.2.1. Controller Design. Consider the following new fractional order controlled financial system:

$$\begin{cases} D^{q_1} x = dz + (y - e)x + u_1, \\ D^{q_2} y = -ky^2 - lx^2 + m + u_2, \\ D^{q_3} z = -\gamma z - \delta x - \rho y + u_3, \end{cases} \tag{22}$$

in which the u_i, $(i = 1, 2, 3)$ are adaptive controllers which will be subsequently designed taking into account the sate variables of the system and the estimation of the unknown constant parameters $d, e, k, l, m, \gamma, \delta$, and ρ of the system.

To allow the states of the system to converge asymptotically to the origin, we take the following adaptive control functions:

$$\begin{cases} u_1 = -yx - \hat{d}z + \hat{e}x - h_1 D^{q_1 - 1} x + v_1, \\ u_2 = \hat{k}y^2 + \hat{l}x^2 - \hat{m} - h_2 D^{q_2 - 1} y + v_2, \\ u_3 = \hat{\gamma}z + \hat{\delta}x + \hat{\rho}y - h_3 D^{q_3 - 1} z + v_3, \end{cases} \tag{23}$$

in which $\hat{d}, \hat{e}, \hat{k}, \hat{l}, \hat{m}, \hat{\gamma}, \hat{\delta}$, and $\hat{\rho}$ are the estimation of the unknown constant parameters$d, e, k, l, m, \gamma, \delta$, and ρ, respectively. The h_i, $(i = 1, 2, 3)$ are positive constants and v_i, $(i = 1, 2, 3)$ are nonlinear functions that will be designed.

By replacing the control law (23) in system (22), we have

$$\begin{cases} D^{q_1} x = (d - \hat{d})z - (e - \hat{e})x - h_1 D^{q_1 - 1} x + v_1, \\ D^{q_2} y = -(k - \hat{k})y^2 - (l - \hat{l})x^2 + (m - \hat{m}) - h_2 D^{q_2 - 1} y + v_2, \\ D^{q_3} z = -(\gamma - \hat{\gamma})z - (\delta - \hat{\delta})x - (\rho - \hat{\rho})y. \end{cases} \tag{24}$$

With the estimation error of unknown parameters defined by equation (11), we obtain

$$\begin{cases} D^{q_1} x = e_d z - e_e x - h_1 D^{q_1 - 1} x + v_1, \\ D^{q_2} y = -e_k y^2 - e_l x^2 + e_m - h_2 D^{q_2 - 1} y + v_2, \\ D^{q_3} z = -e_\gamma z - e_\delta x - e_\rho y - h_3 D^{q_3 - 1} z + v_3. \end{cases} \tag{25}$$

For the design of the parameter update law which will allow to adjusting the parameter estimates, we use Lyapunov's stability theory.

For this, consider Lyapunov quadratic function defined as follows:

$$V = \frac{1}{2}\left(x^2 + y^2 + z^2 + e_d^2 + e_e^2 + e_k^2 + e_l^2 + e_m^2 + e_\gamma^2 + e_\delta^2 + e_\rho^2\right), \tag{26}$$

which is a positive definite function on R^{11}.

The derivative with respect to time of equation (26) gives us

$$\begin{aligned} \dot{V} &= x\dot{x} + y\dot{y} + z\dot{z} + e_d\dot{e}_d + e_e\dot{e}_e + e_k\dot{e}_k \\ &\quad + e_l\dot{e}_l + e_m\dot{e}_m + e_\gamma\dot{e}_\gamma + e_\delta\dot{e}_\delta + e_\rho\dot{e}_\rho, \\ &= xD^{1-q_1}D^{q_1}x + yD^{1-q_2}D^{q_2}y + zD^{1-q_3}D^{q_3}z \\ &\quad + e_d\dot{e}_d + e_e\dot{e}_e + e_k\dot{e}_k + e_l\dot{e}_l + e_m\dot{e}_m \\ &\quad + e_\gamma\dot{e}_\gamma + e_\delta\dot{e}_\delta + e_\rho\dot{e}_\rho. \end{aligned} \tag{27}$$

Taking into account system (25) and equation (15), equation (27) becomes

$$\begin{aligned} \dot{V} &= xD^{1-q_1}\left[e_d z - e_e x - h_1 D^{q_1 - 1} x + v_1\right] \\ &\quad + yD^{1-q_2}\left[-e_k y^2 - e_l x^2 + e_m - h_2 D^{q_2 - 1} y + v_2\right] \\ &\quad + zD^{1-q_3}\left[-e_\gamma z - e_\delta x - e_\rho y - h_3 D^{q_3 - 1} z + v_3\right] \\ &\quad - \dot{\hat{d}}e_d - \dot{\hat{e}}e_e - \dot{\hat{k}}e_k - \dot{\hat{l}}e_l - \dot{\hat{m}}e_m - \dot{\hat{\gamma}}e_\gamma \\ &\quad - \dot{\hat{\delta}}e_\delta - \dot{\hat{\rho}}e_\rho. \end{aligned} \tag{28}$$

From equation (28), we deduce that the estimated parameters update law is

$$\begin{cases} \dot{\hat{d}} = h_4 e_d, \\ \dot{\hat{e}} = h_5 e_e, \\ \dot{\hat{k}} = h_6 e_k, \\ \dot{\hat{l}} = h_7 e_l, \\ \dot{\hat{m}} = h_8 e_m, \\ \dot{\hat{\gamma}} = h_9 e_\gamma, \\ \dot{\hat{\delta}} = h_{10} e_\delta, \\ \dot{\hat{\rho}} = h_{11} e_\rho, \end{cases} \tag{29}$$

in which $h_4, h_5, h_6, h_7, h_8, h_9, h_{10}$, and h_{11} are positive constants.

From equation (28), we also deduce that the nonlinear functions v_i, $(i = 1, 2, 3)$ are given by

$$\begin{cases} v_1 = -e_d z + e_e x, \\ v_2 = e_k y^2 + e_l x^2 - e_m, \\ v_3 = e_\gamma z + e_\delta x + e_\rho y. \end{cases} \tag{30}$$

By replacing equations (29) and (30) in equation (28), we get

$$\begin{aligned}\dot{V} = &-h_1x^2 - h_2y^2 - h_3z^2 - h_4e_d^2 \\ &- h_5e_e^2 - h_6e_k^2 - h_7e_l^2 - h_8e_m^2 - h_9e_\gamma^2 \\ &- h_{10}e_\delta^2 - h_{11}e_\rho^2 < 0,\end{aligned} \tag{31}$$

which is a negative definite function on R^{11} for positive constants h_i, $(i = 1, \ldots, 11)$.

So, we have found a function which verifies the Lyapunov stability theorem $V > 0, \dot{V} < 0$.

Thus, we have the following result.

Theorem 2. *The new fractional order financial system (22) with the unknown parameters is globally and asymptotically stabilized at the origin for all initial conditions by the adaptive law (23) with the v_i, $(i = 1, 2, 3)$ given by (30) and where the parameters update law is given by (29) with h_i, $(i = 1, \ldots, 11)$ being positive constants.*

3.2.2. Simulation Results. In this part, we use the Adams-Bashforth-Moulton predictor-corrector method proposed by Diethelm et al. [35] to solve the new fractional order financial system (19.22) with the adaptive control law (23), the v_i, $(i = 1, 2, 3)$ given by (30), and the parameter update law given by (29). For the simulation, the time-step $h = 0.001$ is chosen. The initial conditions $(x(0), y(0), z(0)) = (1.2, 1.5, 1.6)$ are used. The orders q_i, $(i = 1, 2, 3)$ are taken as follows: $(q_1, q_2, q_3) = (1, 0.88, 1)$, i.e., the case of incommensurate order.

The parameters of the new financial system are chosen as follows:

$$e = 0.3, k = 0.02, \gamma = 1, m = 1, l = 0.1, \rho = 0.05, d = 1.2, \delta = 1. \tag{32}$$

For h_i, $(i = 1, \ldots, 11)$ of the adaptive and update laws, we choose $h_i = 3$.

For the initial value of the estimated parameters, we assume the following values:

$$\hat{e}(0) = 4, \hat{k}(0) = 2, \hat{\gamma}(0) = 3, \hat{m}(0) = 5, \hat{l}(0) = 2, \hat{\rho}(0) = 3, \hat{d}(0) = 7, \hat{\delta}(0) = 8. \tag{33}$$

By applying the adaptive law (23) and the parameters update law (29) to the new fractional order controlled financial system (22), the results of numerical simulations are shown in Figures 5 and 6. From Figure 5, it can be seen that the state variables of the system converge asymptotically towards the origin. Figure 6 shows the estimated parameters $\hat{d}, \hat{e}, \hat{k}, \hat{l}, \hat{m}, \hat{\gamma}, \hat{\delta}$, and $\hat{\rho}$ which, as it can be seen, converge towards the real values of the parameters of the system, i.e.,

$$e = 0.3, k = 0.02, \gamma = 1, m = 1, l = 0.1, \rho = 0.05, d = 1.2, \delta = 1. \tag{34}$$

4. Adaptive Synchronization of the Identical New Financial System

4.1. Integer Order Case. In this part, the identical adaptive synchronization of the new integer order financial system is achieved.

4.1.1. Analytical Results. Let us consider the master system as being the system described with index 1 and the slave system as being the system described with index 2. We have therefore, for the master system, the system

$$\begin{cases} \dot{x}_1 = dz_1 + (y_1 - e)x_1, \\ \dot{y}_1 = -ky_1^2 - lx_1^2 + m, \\ \dot{z}_1 = -\gamma z_1 - \delta x_1 - \rho y_1, \end{cases} \tag{35}$$

and for slave system, we have

$$\begin{cases} \dot{x}_2 = dz_2 + (y_2 - e)x_2 + u_1, \\ \dot{y}_2 = -ky_2^2 - lx_2^2 + m + u_2, \\ \dot{z}_2 = -\gamma z_2 - \delta x_2 - \rho y_2 + u_3, \end{cases} \tag{36}$$

in which u_1, u_2, u_3 are controllers to be designed so that system (36) synchronizes with system (35) and $d, e, k, l, m, \gamma, \delta$, and ρ are the unknown constant parameters of the system.

Let us define the error functions between the state variables of systems (36) and (35) as follows:

$$\begin{aligned} e_1 &= x_2 - x_1, \\ e_2 &= y_2 - y_1, \\ e_3 &= z_2 - z_1. \end{aligned} \tag{37}$$

From equation (37), we obtain the following error system:

$$\begin{cases} \dot{e}_1 = -ee_1 + de_3 + y_2x_2 - y_1x_1 + u_1, \\ \dot{e}_2 = -k\left(y_2^2 - y_1^2\right) - l\left(x_2^2 - x_1^2\right) + u_2, \\ \dot{e}_3 = -\gamma e_3 - \delta e_1 - \rho e_2 + u_3. \end{cases} \tag{38}$$

Let us define the adaptive control functions u_i, $(i = 1, 2, 3)$ as follows:

$$\begin{cases} u_1 = \hat{e}e_1 - \hat{d}e_3 - y_2x_2 + y_1x_1 - h_1e_1, \\ u_2 = \hat{k}\left(y_2^2 - y_1^2\right) + \hat{l}\left(x_2^2 - x_1^2\right) - h_2e_2, \\ u_3 = \hat{\gamma}e_3 + \hat{\delta}e_1 + \hat{\rho}e_2 - h_3e_3, \end{cases} \tag{39}$$

in which $\hat{d}, \hat{e}, \hat{k}, \hat{l}, \hat{m}, \hat{\gamma}, \hat{\delta}$, and $\hat{\rho}$ are the estimates of the parameters $d, e, k, l, m, \gamma, \delta$, and ρ, respectively, and h_i, $(i = 1, 2, 3)$ are positive constants.

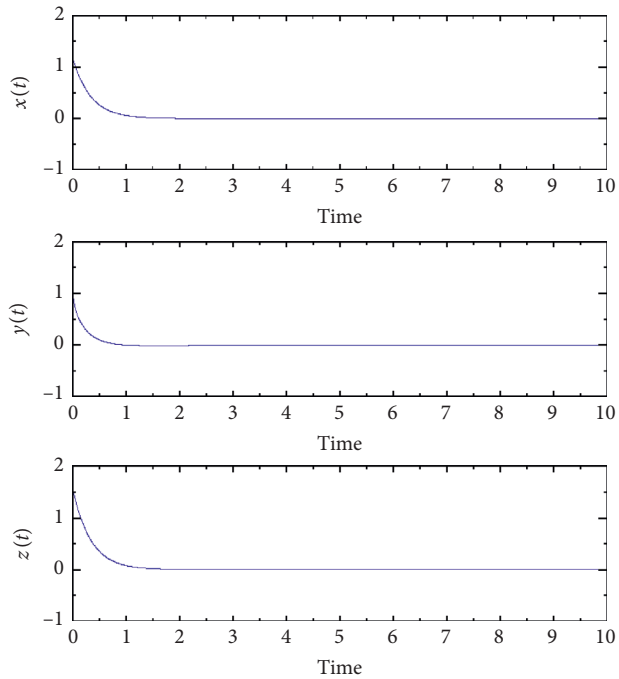

Figure 5: Time histories of the controlled fractional order new financial system (22).

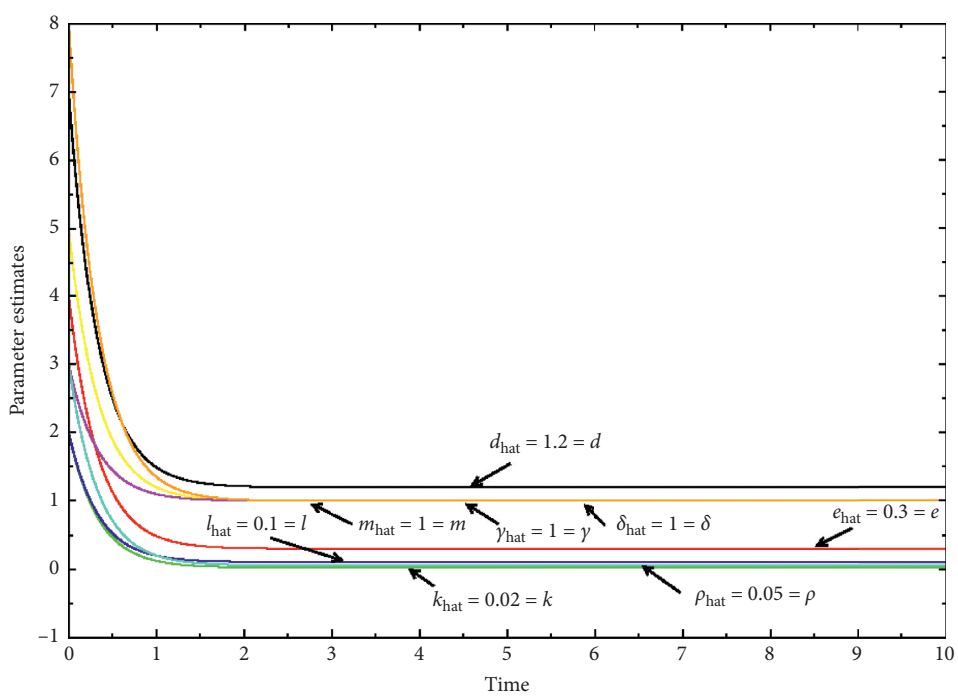

Figure 6: Parameter estimates for adaptive control in fractional order case.

By replacing the control law (39) in (38), we have

$$\begin{cases} \dot{e}_1 = -(e-\widehat{e})e_1 + (d-\widehat{d})e_3 - h_1e_1, \\ \dot{e}_2 = -(k-\widehat{k})\left(y_2^2 - y_1^2\right) - (l-\widehat{l})\left(x_2^2 - x_1^2\right) - h_2e_2, \\ \dot{e}_3 = -(\gamma-\widehat{\gamma})e_3 - (\delta-\widehat{\delta})e_1 - (\rho-\widehat{\rho})e_2 - h_3e_3. \end{cases} \quad (40)$$

Define the estimation error of unknown parameters as follows:

$$\begin{cases} e_d = d - \widehat{d}, \\ e_e = e - \widehat{e}, \\ e_k = k - \widehat{k}, \\ e_l = l - \widehat{l}, \\ e_m = m - \widehat{m}, \\ e_\gamma = \gamma - \widehat{\gamma}, \\ e_\delta = \delta - \widehat{\delta}, \\ e_\rho = \rho - \widehat{\rho}. \end{cases} \quad (41)$$

By substituting equation (41) in system (40), system (40) becomes

$$\begin{cases} \dot{e}_1 = -e_ee_1 + e_de_3 - h_1e_1, \\ \dot{e}_2 = -e_k\left(y_2^2 - y_1^2\right) - e_l\left(x_2^2 - x_1^2\right) - h_2e_2, \\ \dot{e}_3 = -e_\gamma e_3 - e_\delta e_1 - e_\rho e_2 - h_3e_3. \end{cases} \quad (42)$$

For the design of the parameter update law which will allow to adjusting the parameter estimates, we use Lyapunov's stability theory.

For this, consider the quadratic Lyapunov function defined as follows:

$$V = \frac{1}{2}\left(e_1^2 + e_2^2 + e_3^2 + e_d^2 + e_e^2 + e_k^2 + e_l^2 + e_m^2 + e_\gamma^2 + e_\delta^2 + e_\rho^2\right), \quad (43)$$

which is a positive definite function on R^{11}.

The derivative with respect to time of equation (43) gives us

$$\begin{aligned} \dot{V} = {} & e_1\dot{e}_1 + e_2\dot{e}_2 + e_3\dot{e}_3 + e_d\dot{e}_d + e_e\dot{e}_e \\ & + e_k\dot{e}_k + e_l\dot{e}_l + e_m\dot{e}_m + e_\gamma\dot{e}_\gamma + e_\delta\dot{e}_\delta + e_\rho\dot{e}_\rho. \end{aligned} \quad (44)$$

Using system (42) and equation (15), equation (44) becomes

$$\begin{aligned} \dot{V} = {} & -h_1e_1^2 - h_2e_2^2 - h_3e_3^2 + e_e\left(-e_1^2 - \dot{\widehat{e}}\right) \\ & + e_d\left(e_1e_3 - \dot{\widehat{d}}\right) + e_k\left[-e_2\left(y_2^2 - y_1^2\right) - \dot{\widehat{k}}\right] \\ & + e_l\left[-e_2\left(x_2^2 - x_1^2\right) - \dot{\widehat{l}}\right] + e_\gamma\left(-e_3^2 - \dot{\widehat{\gamma}}\right) \\ & + e_\delta\left(-e_3e_1 - \dot{\widehat{\delta}}\right) + e_\rho\left(-e_3e_2 - \dot{\widehat{\rho}}\right) - \dot{\widehat{m}}e_m. \end{aligned} \quad (45)$$

From equation (45), we deduce that the estimated parameters update law is

$$\begin{cases} \dot{\widehat{d}} = e_1e_3 + h_4e_d, \\ \dot{\widehat{e}} = -e_1^2 + h_5e_e, \\ \dot{\widehat{k}} = -e_2\left(y_2^2 - y_1^2\right) + h_6e_k, \\ \dot{\widehat{l}} = -e_2\left(x_2^2 - x_1^2\right) + h_7e_l, \\ \dot{\widehat{m}} = h_8e_m, \\ \dot{\widehat{\gamma}} = -e_3^2 + h_9e_\gamma, \\ \dot{\widehat{\delta}} = -e_3e_1 + h_{10}e_\delta, \\ \dot{\widehat{\rho}} = -e_3e_2 + h_{11}e_\rho, \end{cases} \quad (46)$$

in which $h_4, h_5, h_6, h_7, h_8, h_9, h_{10}$, and h_{11} are positive constants.

By replacing equation (46) in equation(45), we get

$$\begin{aligned} \dot{V} = {} & -h_1e_1^2 - h_2e_2^2 - h_3e_3^2 - h_4e_d^2 - h_5e_e^2 \\ & - h_6e_k^2 - h_7e_l^2 - h_8e_m^2 - h_9e_\gamma^2 - h_{10}e_\delta^2 - h_{11}e_\rho^2 < 0, \end{aligned} \quad (47)$$

which is a negative definite function on R^{11} for positive constants h_i, $(i = 1, \ldots, 11)$.. So, we have found a function which verifies the Lyapunov stability theorem $(V > 0, \dot{V} < 0)$.

Thus, the error functions converge globally and asymptotically towards zero for all initial conditions. The synchronization of the states of the identical systems (35) and (36) is therefore complete. So, we have the following result.

Theorem 3. *The identical financial systems (35) and (36) with unknown parameters are globally and asymptotically synchronized for all initial conditions by the adaptive control law (39) where the parameters update law is given by (46) and the h_i, $(i = 1, \ldots, 11)$ are positive constants.*

4.1.2. Simulation Results. In this part, we use the fourth-order Runge--Kutta algorithm to solve the two identical financial systems (35) and (36) with the adaptive control law (39) and the parameters update law (46). For the simulation, the time-step $h = 0.001$ is chosen. The initial conditions for the master system are $(x_1(0), y_1(0), z_1(0)) = (1.2, 1.5, 1.6)$ and for the slave system, $(x_2(0), y_2(0), z_2(0)) = (0.2, 0.5, 0.6)$.

The parameters of the new financial system are chosen as follows:

$$e = 0.3, k = 0.02, \gamma = 1, m = 1, l = 0.1, \rho = 0.05, d = 1.2, \delta = 1. \quad (48)$$

For the h_i, $(i = 1, \ldots, 11)$ of the adaptive and update laws, we choose $h_i = 3$.

For the initial value of the estimated parameters, we assume the following values:

$$\begin{aligned} & \widehat{e}(0) = -1, \widehat{k}(0) = 2, \widehat{\gamma}(0) = 0.5, \\ & \widehat{m}(0) = 4, \widehat{l}(0) = 2, \widehat{\rho}(0) = 3, \\ & \widehat{d}(0) = 7, \widehat{\delta}(0) = -0.5. \end{aligned} \quad (49)$$

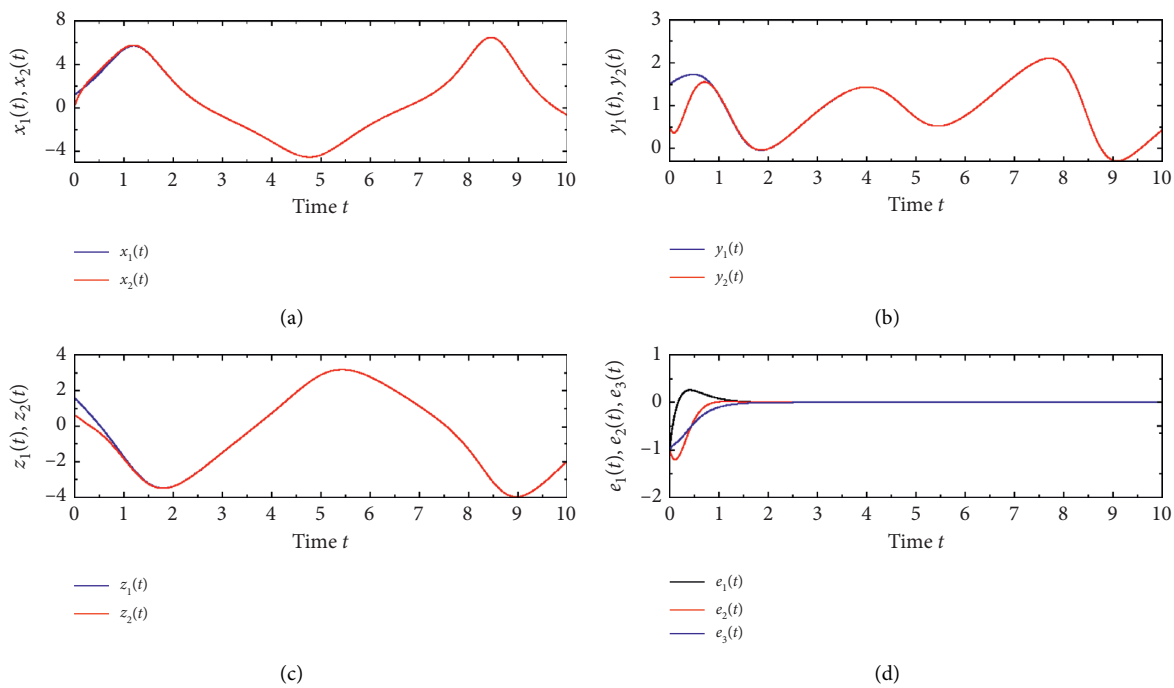

FIGURE 7: (a–c) Time evolutions of the master and slave systems state variables (x_1, x_2), (y_1, y_2), (z_1, z_2), respectively, in integer order case and (d) time evolution of the error functions e_1(black line), e_2(red line), and e_3(blue line).

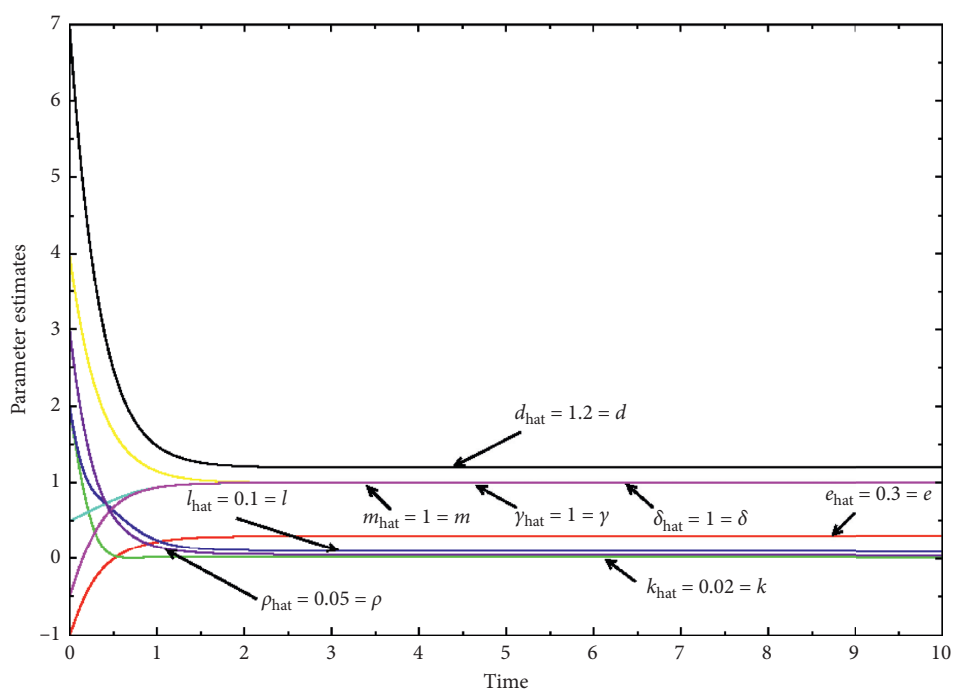

FIGURE 8: Parameter estimates for adaptive synchronization in integer order case.

By applying the adaptive control law (39) and the parameter update law (46) to the new controlled financial system (36), the results of the numerical simulations are shown in Figures 7(a)–7(d) and 8. From Figures 7(a)–7(c), it can be seen that the state variables of the slave and master systems are synchronized. Figure 7(d) shows the error system which eventually converges to zero. Finally, Figure 8 shows the estimated parameters $\hat{d}, \hat{e}, \hat{k}, \hat{l}, \hat{m}, \hat{\gamma}, \hat{\delta}$, and $\hat{\rho}$ which, as it can be seen, converge towards the real values of the parameters of the system, i.e.,

$$e = 0.3, k = 0.02, \gamma = 1, m = 1, l = 0.1, \rho = 0.05, d = 1.2, \delta = 1. \tag{50}$$

4.2. Fractional Order Case. In this part, the identical adaptive synchronization of the new fractional order financial system is achieved.

4.2.1. Analytical Results. Let us consider the master system as being the system described with index 1 and the slave system as being the system described with index 2. We have therefore for the master system, the system

$$\begin{cases} D^{q_1} x_1 = dz_1 + (y_1 - e)x_1, \\ D^{q_2} y_1 = -ky_1^2 - lx_1^2 + m, \\ D^{q_3} z_1 = -\gamma z_1 - \delta x_1 - \rho y_1, \end{cases} \tag{51}$$

and for slave system, we have

$$\begin{cases} D^{q_1} x_2 = dz_2 + (y_2 - e)x_2 + u_1, \\ D^{q_2} y_2 = -ky_2^2 - lx_2^2 + m + u_2, \\ D^{q_3} z_2 = -\gamma z_2 - \delta x_2 - \rho y_2 + u_3, \end{cases} \tag{52}$$

where u_1, u_2, u_3 are controllers to be designed so that system (52) synchronizes with system (51) and $d, e, k, l, m, \gamma, \delta$, and ρ are the unknown constant parameters of the system.

Let us define the error functions between the state variables of systems (2) and (51) as follows.

$$\begin{aligned} e_1 &= x_2 - x_1, \\ e_2 &= y_2 - y_1, \\ e_3 &= z_2 - z_1. \end{aligned} \tag{53}$$

From equation (53), we get the following error system:

$$\begin{cases} D^{q_1} e_1 = -ee_1 + de_3 + y_2 x_2 - y_1 x_1 + u_1, \\ D^{q_2} e_2 = -k\left(y_2^2 - y_1^2\right) - l\left(x_2^2 - x_1^2\right) + u_2, \\ D^{q_3} e_3 = -\gamma e_3 - \delta e_1 - \rho e_2 + u_3. \end{cases} \tag{54}$$

Let us define the adaptive control functions u_i, $(i = 1, 2, 3)$.

$$\begin{cases} u_1 = \hat{e} e_1 - \hat{d} e_3 - y_2 x_2 + y_1 x_1 - h_1 D^{q_1 - 1} e_1 + v_1, \\ u_1 = \hat{k}\left(y_2^2 - y_1^2\right) + \hat{l}\left(x_2^2 - x_1^2\right) - h_2 D^{q_2 - 1} e_2 + v_2, \\ u_3 = \hat{\gamma} e_3 + \hat{\delta} e_1 + \hat{\rho} e_2 - h_3 D^{q_3 - 1} e_3 + v_3, \end{cases} \tag{55}$$

in which $\hat{d}, \hat{e}, \hat{k}, \hat{l}, \hat{m}, \hat{\gamma}, \hat{\delta}$, and $\hat{\rho}$ are the estimates of the parameters $d, e, k, l, m, \gamma, \delta$, and ρ, respectively, h_i, $(i = 1, 2, 3)$ are positive constants, and v_i, $(i = 1, 2, 3)$ are nonlinear functions that will be designed. By replacing the control law (55) in (54), we get

$$\begin{cases} D^{q_1} e_1 = -(e - \hat{e})e_1 + (d - \hat{d})e_3 - h_1 D^{q_1 - 1} e_1 + v_1, \\ D^{q_2} e_2 = -(k - \hat{k})\left(y_2^2 - y_1^2\right) - (l - \hat{l})\left(x_2^2 - x_1^2\right) - h_2 D^{q_2 - 1} e_2 + v_2, \\ D^{q_3} e_3 = -(\gamma - \hat{\gamma})e_3 - (\delta - \hat{\delta})e_1 - (\rho - \hat{\rho})e_2 - h_3 D^{q_3 - 1} e_3 + v_3. \end{cases} \tag{56}$$

With the estimation error of unknown parameters defined by equation (41), we obtain

$$\begin{cases} D^{q_1} e_1 = -e_e e_1 + e_d e_3 - h_1 D^{q_1 - 1} e_1 + v_1, \\ D^{q_2} e_2 = -e_k\left(y_2^2 - y_1^2\right) - e_l\left(x_2^2 - x_1^2\right) - h_2 D^{q_2 - 1} e_2 + v_2, \\ D^{q_3} e_3 = -e_\gamma e_3 - e_\delta e_1 - e_\rho e_2 - h_3 D^{q_3 - 1} e_3 + v_3. \end{cases} \tag{57}$$

For the design of the parameter update law which will allow to adjusting the parameter estimates, we use Lyapunov's stability theory.

For this, consider the quadratic Lyapunov function defined as follows:

$$V = \frac{1}{2}\left(e_1^2 + e_2^2 + e_3^2 + e_d^2 + e_e^2 + e_k^2 + e_l^2 + e_m^2 + e_\gamma^2 + e_\delta^2 + e_\rho^2\right), \tag{58}$$

which is a positive definite function on R^{11}. The derivative with respect to time of equation (58) gives us

$$\begin{aligned} \dot{V} &= e_1 \dot{e}_1 + e_2 \dot{e}_2 + e_3 \dot{e}_3 + e_d \dot{e}_d + e_e \dot{e}_e \\ &\quad + e_k \dot{e}_k + e_l \dot{e}_l + e_m \dot{e}_m + e_\gamma \dot{e}_\gamma + e_\delta \dot{e}_\delta + e_\rho \dot{e}_\rho, \\ &= e_1 D^{1-q_1} D^{q_1} e_1 + e_2 D^{1-q_2} D^{q_2} e_2 \\ &\quad + e_3 D^{1-q_3} D^{q_3} e_3 + e_d \dot{e}_d + e_e \dot{e}_e + e_k \dot{e}_k \\ &\quad + e_l \dot{e}_l + e_m \dot{e}_m + e_\gamma \dot{e}_\gamma + e_\delta \dot{e}_\delta + e_\rho \dot{e}_\rho. \end{aligned} \tag{59}$$

Taking into account system (57) and equation (15), equation (59) becomes

$$\begin{aligned} \dot{V} &= e_1 D^{1-q_1}\left[-e_e e_1 + e_d e_3 - h_1 D^{q_1 - 1} e_1 + v_1\right] \\ &\quad + e_2 D^{1-q_2}\left[-e_k\left(y_2^2 - y_1^2\right) - e_l\left(x_2^2 - x_1^2\right)\right. \\ &\quad \left. - h_2 D^{q_2 - 1} e_2 + v_2\right] + e_3 D^{1-q_3}\left[-e_\gamma e_3 - e_\delta e_1\right. \\ &\quad \left. - e_\rho e_2 - h_3 D^{q_3 - 1} e_3 + v_3\right] - \dot{\hat{d}} e_d - \dot{\hat{e}} e_e - \dot{\hat{k}} e_k \\ &\quad - \dot{\hat{l}} e_l - \dot{\hat{m}} e_m - \dot{\hat{\gamma}} e_\gamma - \dot{\hat{\delta}} e_\delta - \dot{\hat{\rho}} e_\rho. \end{aligned} \tag{60}$$

From equation (60), we deduce that the estimated parameters update law is

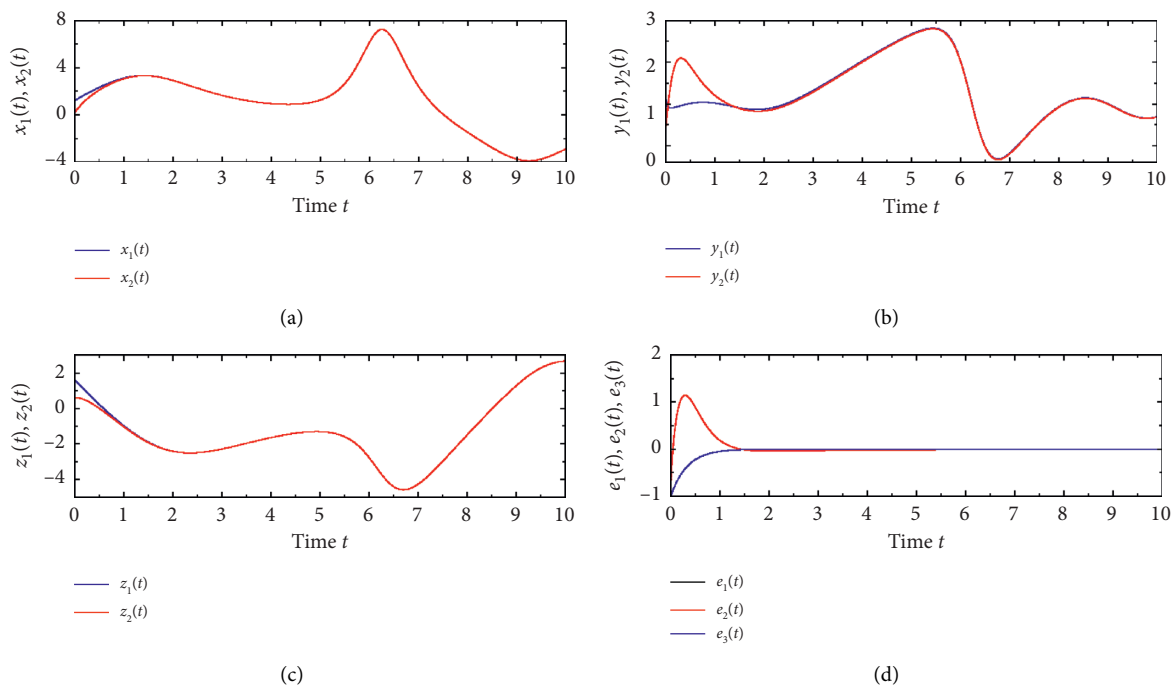

FIGURE 9: (a–c) Time evolutions of the master and slave systems state variables (x_1, x_2), (y_1, y_2), (z_1, z_2), respectively, in fractional order case and (d) time evolution of the error functions e_1(black line), e_2(red line), and e_3(blue line).

$$\begin{cases} \dot{\hat{d}} = h_4 e_d, \\ \dot{\hat{e}} = h_5 e_e, \\ \dot{\hat{k}} = h_6 e_k, \\ \dot{\hat{l}} = h_7 e_l, \\ \dot{\hat{m}} = h_8 e_m, \\ \dot{\hat{\gamma}} = h_9 e_\gamma, \\ \dot{\hat{\delta}} = h_{10} e_\delta, \\ \dot{\hat{\rho}} = h_{11} e_\rho, \end{cases} \tag{61}$$

where $h_4, h_5, h_6, h_7, h_8, h_9, h_{10}$, and h_{11} are positive constants.

From equation (60), we also deduce that the nonlinear functions v_i, $(i = 1, 2, 3)$ are given by

$$\begin{cases} v_1 = e_e e_1 - e_d e_3, \\ v_2 = e_k\left(y_2^2 - y_1^2\right) + e_l\left(x_2^2 - x_1^2\right), \\ v_3 = e_\gamma e_3 + e_\delta e_1 + e_\rho e_2. \end{cases} \tag{62}$$

By replacing equations (61) and (62) in (60), we get

$$\begin{aligned} \dot{V} = &-h_1 e_1^2 - h_2 e_2^2 - h_3 e_3^2 - h_4 e_d^2 - h_5 e_e^2 \\ &- h_6 e_k^2 - h_7 e_l^2 - h_8 e_m^2 - h_9 e_\gamma^2 - h_{10} e_\delta^2 \\ &- h_{11} e_\rho^2 < 0, \end{aligned} \tag{63}$$

which is a negative definite function on R^{11} for positive constants h_i, $(i = 1, \ldots, 11)$. So, we have found a function which verifies the Lyapunov stability theorem $(V > 0, \dot{V} < 0)$.

Thus, the error functions converge globally and asymptotically towards zero for all initial conditions. The synchronization of the states of the identical systems (51) and (52) is therefore complete. So, we have the following result:

Theorem 4. *The identical financial systems (51) and (52) with unknown parameters are globally and asymptotically synchronized for all initial conditions by the adaptive control law (55) with v_i, $(i = 1, 2, 3)$ given by (62), and where the parameters update law is given by (61) and the h_i, $(i = 1, \ldots, 11)$ are positive constants.*

4.2.2. Simulation Results. In this part, we use the Adams-Bashforth-Moulton predictor-corrector method proposed by Diethelm et al. [35] to solve the two identical fractional order systems (51) and (52) with the adaptive control law (55), the v_i, $(i = 1, 2, 3)$ given by (62), and the law for updating the parameters is given by (61). For the simulation, the time-step $h = 0.001$ is chosen. The initial conditions for the master system are $(x_1(0), y_1(0), z_1(0)) = (1.2, 1.5, 1.6)$ and for the slave system, $(x_2(0), y_2(0), z_2(0)) = (0.2, 0.5, 0.6)$ are used. The orders q_i, $(i = 1, 2, 3)$ are taken as follows $(q_1, q_2, q_3) = (1, 0.88, 1)$, i.e., the case of incommensurate order.

The parameters of the new fractional order financial system are chosen as follows:

$$e = 0.3, k = 0.02, \gamma = 1, m = 1, l = 0.1, \rho = 0.05, d = 1.2, \delta = 1. \tag{64}$$

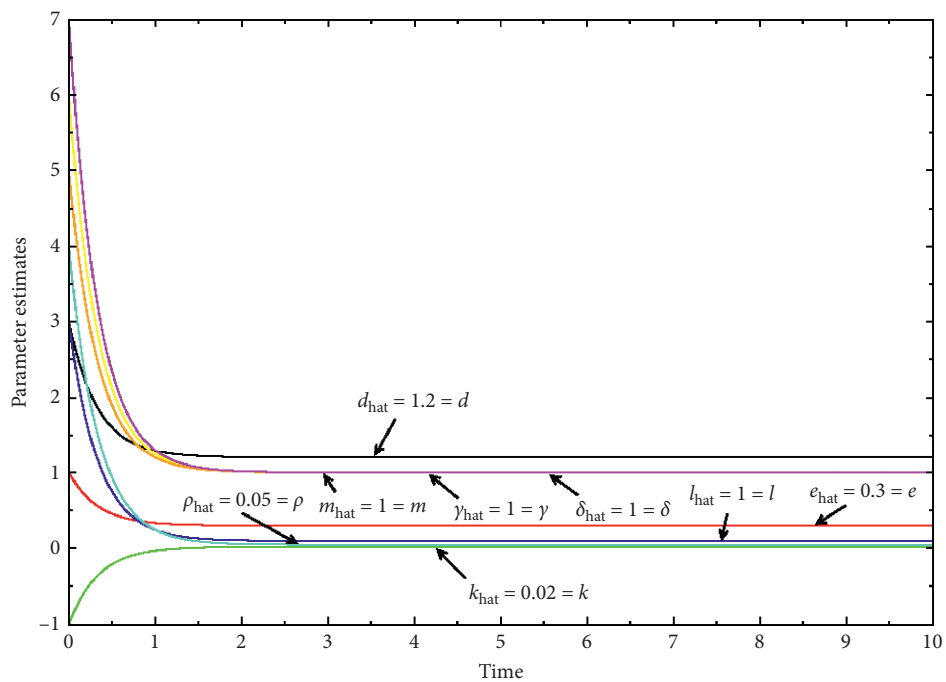

Figure 10: Parameter estimates for adaptive synchronization in fractional order case.

For h_i, $(i = 1, \ldots, 11)$ of the adaptive and update laws, we choose $h_i = 3$.

For the initial value of the estimated parameters, we assume the following values:

$$\widehat{e}(0) = 1, \widehat{k}(0) = -1, \widehat{\gamma}(0) = 5, \widehat{m}(0) = 6, \widehat{l}(0) = 3, \widehat{\rho}(0) = 4, \widehat{d}(0) = 3, \widehat{\delta}(0) = 7. \tag{65}$$

By applying the adaptive control law (55) and the parameter update law (61) to the new controlled fractional-order financial system (52); the results of numerical simulations are shown in Figures 9(a)–9(d) and 10. From Figures 9(a)–9(c), it can be seen that the state variables of the master and slave systems are synchronized. Figure 9(d) shows the error system which eventually converges to zero. Finally, Figure 10 shows the estimated parameters $\widehat{d}, \widehat{e}, \widehat{k}, \widehat{l}, \widehat{m}, \widehat{\gamma}, \widehat{\delta}$, and $\widehat{\rho}$ which, as it can be seen, converge towards the real values of the parameters of the system, i.e.,

$$e = 0.3, k = 0.02, \gamma = 1, m = 1, l = 0.1, \rho = 0.05, d = 1.2, \delta = 1. \tag{66}$$

5. Conclusions

In this paper, the adaptive control and the adaptive synchronization of a new financial system with unknown constant parameters were studied in the cases of integer and fractional order. The adaptive control law and the adaptive synchronization law were designed based on Lyapunov's stability theory and on the adaptive control theory. The laws have been designed in the cases of integer and incommensurate fractional order system.

The proposed adaptive control technique is effective for chaos control and synchronization of the new financial system when the constant parameters of the system are unknown. Numerical simulations are carried out to prove the efficiency of the control and synchronization techniques designed in this work.

Data Availability

No data were used to support this study.

Conflicts of Interest

The authors declare that they have no conflicts of interest.

Acknowledgments

The authors thank IMSP-UAC and the German Academic Exchange Service (DAAD) for financial support under the programme "In-Country/In-Region Scholarship Programme."

References

[1] K. B. Oldham and J. Spanier, *The Fractional Calculus*, Academic Press, New York, NY, USA, 1974.

[2] B. Ross, "Fractional calculus and its applications," *Lecture Notes in Mathematics*, Vol. 457, Springer-Verlag, New York, NY, USA, 1975.

[3] V. Daftardar-Gejji and S. Bhalekar, "Chaos in fractional ordered Liu system," *Computers & Mathematics with Applications*, vol. 59, no. 3, pp. 1117–1127, 2010.

[4] W.-C. Chen, "Nonlinear dynamics and chaos in a fractional-order financial system," *Chaos, Solitons & Fractals*, vol. 36, no. 5, pp. 1305–1314, 2008.

[5] K. Rajagopal, A. Bayani, S. Jafari, A. Karthikeyan, and I. Hussain, "Chaotic dynamics of a fractional order glucose-insulin regulatory system," *Frontiers of Information Technology & Electronic Engineering*, vol. 21, no. 7, pp. 1108–1118, 2019.

[6] T. T. Hartley, C. F. Lorenzo, and H. Killory Qammer, "Chaos in a fractional order Chua's system," *IEEE Transactions on Circuits and Systems I: Fundamental Theory and Applications*, vol. 42, no. 8, pp. 485–490, 1995.

[7] Q. Jia, "Chaos control and synchronization of the Newton-Leipnik chaotic system," *Chaos, Solitons & Fractals*, vol. 35, no. 4, pp. 814–824, 2008.

[8] M. T. Yassen, "Adaptive control and synchronization of a modified Chua's circuit system," *Applied Mathematics and Computation*, vol. 135, no. 1, pp. 113–128, 2003.

[9] V. Sundarapandian, "Adaptive control and synchronization of a generalized Lotka-Volterra system," *International Journal of Bioinformatics & Biosciences*, vol. 1, no. 1, pp. 1–12, 2011.

[10] S. Dadras and H. R. Momeni, "Control of a fractional-order economical system via sliding mode," *Physica A: Statistical Mechanics and Its Applications*, vol. 389, no. 12, pp. 2434–2442, 2010.

[11] U. E. Kocamaz, A. Göksu, H. Taşkin, and Y. Uyaroğlu, "Control of chaotic two-predator one-prey model with single state control signals," *Journal of Intelligent Manufacturing*, pp. 1–10, 2020.

[12] A. Hajipour and H. Tavakoli, "Dynamic analysis and adaptive sliding mode controller for a chaotic fractional incommensurate order financial system," *International Journal of Bifurcation and Chaos*, vol. 27, no. 13, p. 14, 2017.

[13] X. Yi, R. Guo, and Y. Qi, "Stabilization of chaotic systems with both uncertainty and disturbance by the UDE-based control method," *IEEE Access*, vol. 8, no. 1, pp. 62471–62477, 2020.

[14] L. Liu, B. Li, and R. Guo, "Consensus control for networked manipulators with switched parameters and topologies," *IEEE Access*, vol. 9, pp. 9209–9217, 2021.

[15] T. Hou, Y. Liu, and F. Deng, "Finite horizon H2/H∞ control for SDEs with infinite Markovian jumps," *Nonlinear Analysis: Hybrid Systems*, vol. 34, pp. 108–120, 2019.

[16] R. Xu and F. Zhang, "-Nash mean-field games for general linear-quadratic systems with applications," *Automatica*, vol. 114, pp. 1–4, 2020.

[17] R. Hilfer, *Applications of Fractional Calculus in Physics*, World Scientific, Hackensack, NJ, USA, 2001.

[18] R. He and P. G. Vaidya, "Implementation of chaotic cryptography with chaotic synchronization," *Physical Review E*, vol. 57, no. 2, pp. 1532–1535, 1998.

[19] J. H. Park, "Chaos synchronization of a chaotic system via nonlinear control," *Chaos, Solitons & Fractals*, vol. 25, no. 3, pp. 579–584, 2005.

[20] L. Huang, R. Feng, and M. Wang, "Synchronization of chaotic systems via nonlinear control," *Physics Letters A*, vol. 320, no. 4, pp. 271–275, 2004.

[21] S. Bhalekar and V. Daftardar-Gejji, "Synchronization of different fractional order chaotic systems using active control," *Communications in Nonlinear Science and Numerical Simulation*, vol. 15, no. 11, pp. 3536–3546, 2010.

[22] H. N. Agiza and M. T. Yassen, "Synchronization of Rossler and Chen chaotic dynamical systems using active control," *Physics Letters A*, vol. 278, no. 4, pp. 191–197, 2001.

[23] T.-l. Liao, "Adaptive synchronization of two Lorenz Systems," *Chaos, Solitons & Fractals*, vol. 9, no. 9, pp. 1555–1561, 1998.

[24] H. Yu, G. Cai, and Y. Li, "Dynamic analysis and control of a new hyperchaotic finance system," *Nonlinear Dynamics*, vol. 67, no. 3, pp. 2171–2182, 2012.

[25] J.-h. Ma and Y.-s. Chen, "Study for the bifurcation topological structure and the global complicated character of a kind of nonlinear finance system, I," *Applied Mathematics and Mechanics*, vol. 22, no. 11, pp. 1240–1251, 2001.

[26] M. S. Abd-Elouahab, N. E. Hamri, and J. Wang, "Chaos control of a fractional order financial system," *Mathematical Problems in Engineering*, vol. 2010, Article ID 270646, 18 pages, 2010.

[27] I. Hernández, C. Mateos, J. Núñez, and Á. F. Tenorio, "Lie theory: applications to problems in mathematical finance and economics," *Applied Mathematics and Computation*, vol. 208, no. 2, pp. 446–452, 2009.

[28] S. A. David, J. A. T. Machado, D. D. Quintino, and J. M. Balthazar, "Partial chaos suppression in a fractional order macroeconomic model," *Mathematics and Computers in Simulation*, vol. 122, pp. 55–68, 2016.

[29] J. Yang, E. Zhang, and M. Liu, "Bifurcation analysis and chaos control in a modified finance system with delayed feedback," *International Journal of Bifurcation and Chaos*, vol. 26, no. 06, 2016.

[30] A. Hajipour and H. Tavakoli, "Analysis and circuit simulation of a novel nonlinear fractional incommensurate order financial system," *Optik*, vol. 127, no. 22, pp. 10643–10652, 2016.

[31] X. Zhao, Z. Li, and S. Li, "Synchronization of a chaotic finance system," *Applied Mathematics and Computation*, vol. 217, no. 13, pp. 6031–6039, 2011.

[32] Y. Liao, Y. Zhou, F. Xu, and X.-B. Shu, "A study on the complexity of a new chaotic financial system," *Complexity*, vol. 2020, Article ID 8821156, 5 pages, 2020.

[33] I. Podlubny, *Fractional Differential Equations*, Academic Press, New York, NY, USA, 1999.

[34] I. Petrás, *Fractional-order Nonlinear Systems: Modeling, Analysis and Simulation*, Springer Science & Business Media, Berlin, Germany, 2011.

[35] K. Diethelm, N. J. Ford, and A. D. Freed, "A predictor-corrector approach for the numerical solution of fractional differential equations," *Nonlinear Dynamics*, vol. 29, no. 1–4, pp. 3–22, 2002.

Hindawi
Mathematical Problems in Engineering
Volume 2021, Article ID 6647074, 8 pages
https://doi.org/10.1155/2021/6647074

Research Article

Trajectory Data Compression Algorithm Based on Motion State Changing

Shuo Zhang,[1] Jian Zhang,[1] and Lin Qi[1,2]

[1]*Beijing Information Science and Technology University, Beijing 100192, China*
[2]*Beijing World Urban Circular Economy System (Industry) Collaborative Innovation Center, Beijing 100192, China*

Correspondence should be addressed to Lin Qi; qilin@bistu.edu.cn

Received 22 December 2020; Revised 30 January 2021; Accepted 9 February 2021; Published 28 February 2021

Academic Editor: Rongwei Guo

The trajectory information generated by the moving object plays an important role in studying the object movement. In this paper, a trajectory data compression algorithm based on the motion state changing is proposed to reduce trajectory data storage space and increase compression speed, which can accurately show the motion state and trajectory characteristics. This study has certain significance for the exploration of mass traffic data and the planning of traffic network. Combining the angle threshold with the velocity threshold of a moving object, the key data points are found and the redundant information is removed. Subsequently, the compressed trajectory is obtained. The experimental results show that the new algorithm can help to improve compression efficiency. The compressed trajectory has high similarity with the original trajectory in movement tendency.

1. Introduction

With the development of economy and technology, mobile devices and global positioning system are popular in various industries [1, 2]. In particular, data collection and storage of trajectory information with the characteristics of time, location, speed, and direction are showing high-speed growth. Currently, how to compress and dispose the GPS data is becoming a hot spot. In 1973, David Douglas and Thomas Peucker presented a classical Douglas–Peucker algorithm to preferentially delete some points by means of information loss in iterative calculations. Afterwards, this algorithm was improved by many scholars. Hershberger John implemented the Douglas–Peucker algorithm for line simplification [3], and Jin et al. studied near-linear time approximation algorithms for curve simplification by reducing the time complexity [4]. In addition, Keogh proposed the Opening Window (OPW) algorithm based on the same algorithm in which the trajectory is simplified by iterative information loss. This algorithm cannot track information of the whole iteration; it is based on the concept of "open window" in which the algorithm "window" contains only a portion of track point iteration. Then, it keeps updating the track information in the "window" until the whole track simplification is completed. This algorithm can be synchronized with online track compression [5]. The sliding window algorithm [6] is similar to the open window algorithm, the main idea of which is to start from the track start, initialize a sliding window size of 1, and gradually expand the window, thereby adding subsequent trajectory points. After connecting the first path point within the window and the last track point, the resulting segment is considered as segment approximation. Sliding window algorithm is used to calculate the approximate vertical line segment with the original track Euclidean distance; if the distance is less than the predetermined distance threshold, then continue to increase the sliding window. This process is repeated until the error is within the window. However, the above-mentioned algorithm uses less track information using GPS time information. For this situation, Meratnia proposed a Top-Down Time Ratio algorithm [7]. This algorithm uses synchronous Euclidean distance (SEDm) in place of the vertical distance, which takes into account the time information from GPS track information. Coclite et al. [8] proposed using the road network of semantic information instead of track points to store compressed track objects and

performed experimental studies in 2012. Yeh et al. used the oppressed road network link information in conjunction with information of the mobile objects' time to enter and leave the track [9]. This largely highly compressed the data storage. Threshold algorithm is another type of algorithm proposed by Al-Hussaeni et al. [10]. This algorithm is based on the moving object speed and direction at locus points to predict binding region threshold set at a point that may exist. Location prediction is decided by retaining or removing the points. Threshold algorithm deletes redundant indicator points based on speed and direction, and the algorithm takes into account the state trajectory, but the area to predict the next big point will possibly cause more points to delete. However, it can achieve a high compression ratio and has led to track trends and similar characteristics. Based on the above reasons, this paper constructs new indicators based on speed and angle, namely, the weighted combination of both thresholds to find the key points, and through statistical sampling to find the most appropriate threshold.

2. Compression Algorithm Based on Angle Threshold

The data used in this study are the taxi GPS positioning data of a Chinese megacity. The objective of the data compression algorithm is to show the trajectory form of taxi movement with the least GPS data.

Suppose there are n taxi tracks. X_i represents i track, and each track has m^i dots. A point of each track contains time, position, speed, and direction of rate in the GPS. X_i^j represents j point of i track, where $j = 1, \cdots, m_i$, and $X_i^j = (t_i^j, x_i^j, y_i^j, v_i^j, \theta_i^j)$. Five components of X_i^j represent time, longitude, latitude, speed, and speed direction in j point of i track.

Due to fewer data points collected for each track, the data storage and calculating speed will be greatly affected. Therefore, the track can be compressed to find key points and remove redundant data on the premise that there is no loss of essential feature track [11–14]. In order to reduce the data amount, it is necessary to find the retained or removed data point indicators. From an intuitive point of view, when the velocity of a track point of direction change is large, it indicates that the vehicle is traveling or changing its track due to road change or incidental situation [15]. Thus, this paper first considers the speed direction (angle) as a screening data point indicator.

θ_α is defined as the angle threshold, which is used to eliminate the trajectory points which are less than the angle threshold, and the scope of angle threshold is greater than 5 and less than 20. $\Delta\theta_i^{j,j+1} = |\theta_i^{j+1} - \theta_i^j|$ represents the absolute value of the change in the direction of the velocity values of two adjacent points in i track. If $\Delta\theta_i^{j,j+1} \le \theta_\alpha$, X_i^j is deleted; if $\Delta\theta_i^{j,j+1} > \theta_\alpha$, X_i^j is retained.

According to this principle, from the first point of a track, successive points will be tested backwards to get a compressed trajectory. In order to reflect the effect of compression, the compression ratio is defined as follows:

$$Y_i^{\theta_\alpha} = \frac{m_i - m_i^H}{m_i}, \tag{1}$$

where $Y_i^{\theta\alpha}$ represents the compression rate of i track with angle threshold θ_α and m_i and m_i^H represent, respectively, the number of track points in i track before and after compression [16].

Angle threshold θ_α is defined, respectively, as 5, 10, 15, and 20 in this paper. In nearly a month, running track (an example of the sample database shown in Table 1) of 2000 taxis in Beijing is verified, indicating that, with an increase in θ_α, the average compression rate increases.

With the increase in the angle threshold, the change of the average compression rate of 2000 taxis is shown in Figure 1. It can be seen from Figure 1 that the average compression rate is more than 45% and the time efficiency is improved greatly. However, since only the information point of view is considered, some points with an important feature of the information have been deleted so that the original motion trajectory trend has changed; for example, the license plate number "669148" taxi track is shown in Figure 2.

In Figure 2, with the angle threshold values of 5, 10, 15, and 20, four figures are shown before and after compression of the taxi track; the red trace is the original track and the blue trace is the track after compression. It is obvious that the significant changes in movement trend between points A and B before and after compression have taken place as shown in Figure 2; the main reason is that the locus points between points A and B are all deleted. In order to avoid the deletion of some key data points, the compression ratio is usually reduced. Therefore, we need to add a new threshold to filter the key data points that need to be retained. Thus, the information in the locus points contain the speed at different time periods; in addition, the size of the rate of change reflects whether there is traffic congestion or smooth, and it reveals the trajectory of internal features. If the speed is the only indicator, the situation with the angle threshold control of key points is bound to arise, which can get a higher compression ratio [17]. But it will lose some points that reflected track trends, and the characteristics of the track cannot be fully demonstrated by the rest of the points. For these reasons, this paper, used the two indicators angle and speed as the key points of track [18–20].

3. Compression Algorithm Based on Angle and Speed Threshold

Speed threshold is defined asv_α, which is used to eliminate the trajectory points which are less than the speed threshold, and the scope of the speed threshold is greater than 5 and less than 20. $\Delta v_i^{j,j+1} = |v_i^{j+1} - v_i^j|$ represents the absolute value of

Table 1: Example of the sample database.

Plate number	Time	Longitude	Latitude	Speed	Direction (angle)
669148	20121130044746	116.134	39.642	0	194
669148	20121130001657	116.373	39.987	25	184
669148	20121130001751	116.373	39.984	54	166
669148	20121130001845	116.374	39.98	47	164
669148	20121130001940	116.375	39.976	0	168
669148	20121130002033	116.375	39.974	43	186
669148	20121130002126	116.374	39.967	23	268
669148	20121130002219	116.365	39.967	60	268

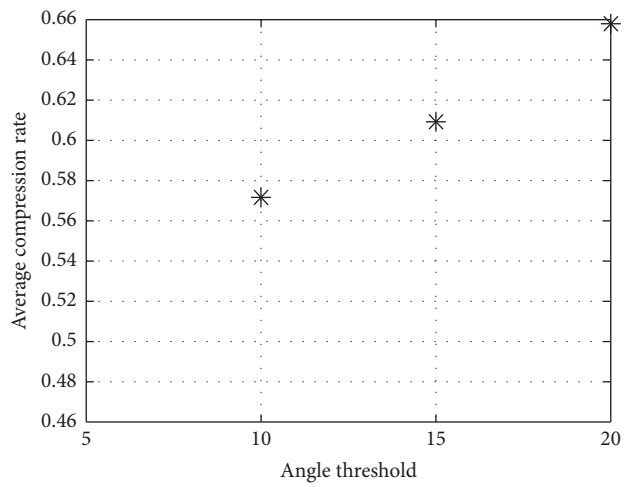

Figure 1: The trend of the average compression rate with the angle threshold.

the change in the speed of the velocity values of two adjacent points in i track. These points that meet the limit of angle threshold and speed threshold are deleted, namely, if $\Delta\theta_i^{j,j+1} \le \theta_\alpha$ and $\Delta v_i^{j,j+1} \le v_\alpha$, $X_i^j$is deleted, or else, X_i^j is retained.

According to this principle, from the first point of a track, successive points will be tested backwards to get a compressed trajectory. The track is still referred to be X_i^H in the case not to cause confusion. Simultaneously, the compression ratio is defined as follows:

$$Y_i^{\theta_\alpha, v_\alpha} = \frac{m_i - m_i^H}{m_i}, \tag{2}$$

where m_i is as defined above and m_i^H is the number of compressed track points in the angle and speed threshold control.

Angle threshold θ_α is defined, respectively, as 5, 10, 15, and 20, and the speed threshold $v_\alpha$is defined, respectively, as 5, 10, 15, 20, 25, and 30 in this paper. Thus, 30 combinations are obtained.

As shown in Figure 3, track trends of A and B points before and after compression are well preserved in this method. In Figure 3, tracks are shown in the last small picture with grid before and after compression when $\theta_\alpha = 25$ and $v_\alpha = 30$. In addition, two encircled points, respectively, in Figure 3 are points A and B in Figure 2. It is very intuitive that motion trends of point A and point B were retained well even in the larger threshold, but the compression ratio of this algorithm is lower. The average compression ratio of 2000 taxi track trends with the angle and speed threshold values at the same time is shown in Figure 4. Thus, the highest value of compression ratio is about 50% and the lowest value is only about 20%. We have paid more attention to keeping contrail features and being stringent to take data points so that a few points meet the speed and angle threshold. Besides, it leads to a situation that the similarity of the track shape is higher, but the compression rate is lower. When the angle and velocity threshold values change, the compression ratio also changes in size as shown in Figure 4.

4. Compression Algorithm of Trajectory Data Based on Motion State Change

Assuming a new index, the weighted threshold value for velocity and angle, so as to obtain higher compression ratio and retain important information after compression [21], the index is marked as θv_α. Making $\Delta\theta v_i^{j,j+1} = \alpha_1 \Delta\theta_i^{j,j+1} + \alpha_2 \Delta v_i^{j,j+1}$, where$\Delta\theta_i^{j,j+1}$ and α_2 are the weights of $\Delta\theta_i^{j,j+1}$ and $\Delta v_i^{j,j+1}$, respectively. If $\Delta\theta v_i^{j,j+1} \le \theta v_\alpha$, X_i^j is deleted; else, $X_i^j$is retained.

Using the mathematical model established above, each data point of the vehicle trajectory data is screened in turn, and the key data points left by the screening are used to form the compressed vehicle trajectory. Without a disordered case, mark the compressed trajectory as X_i^H, and the

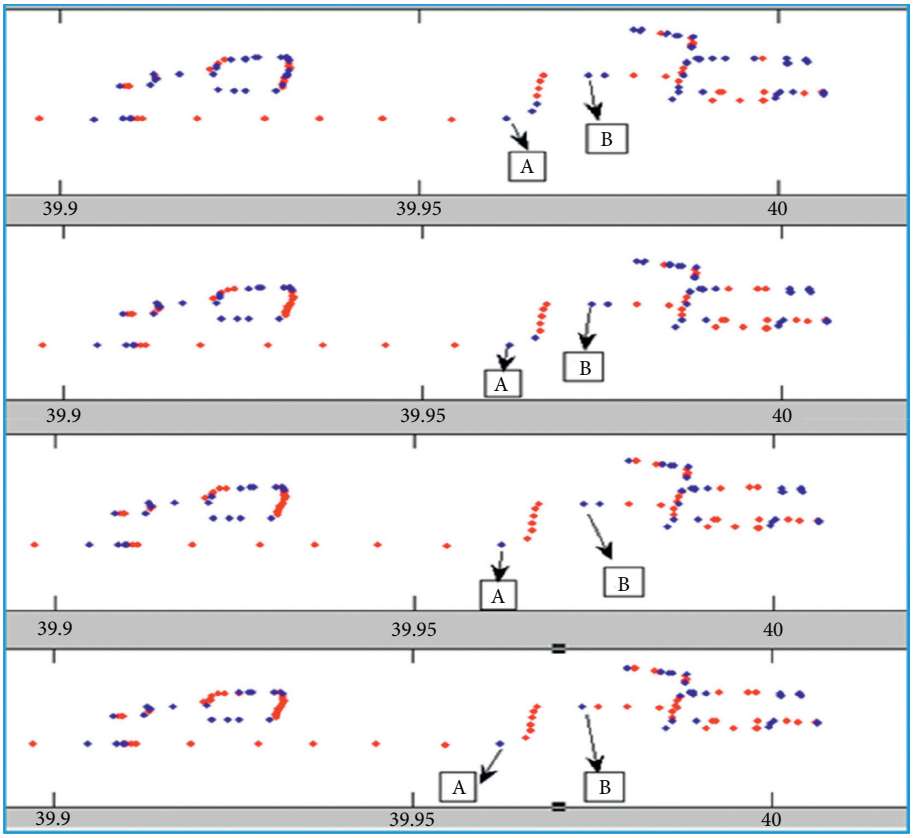

Figure 2: Trajectory map before and after compression at different angles.

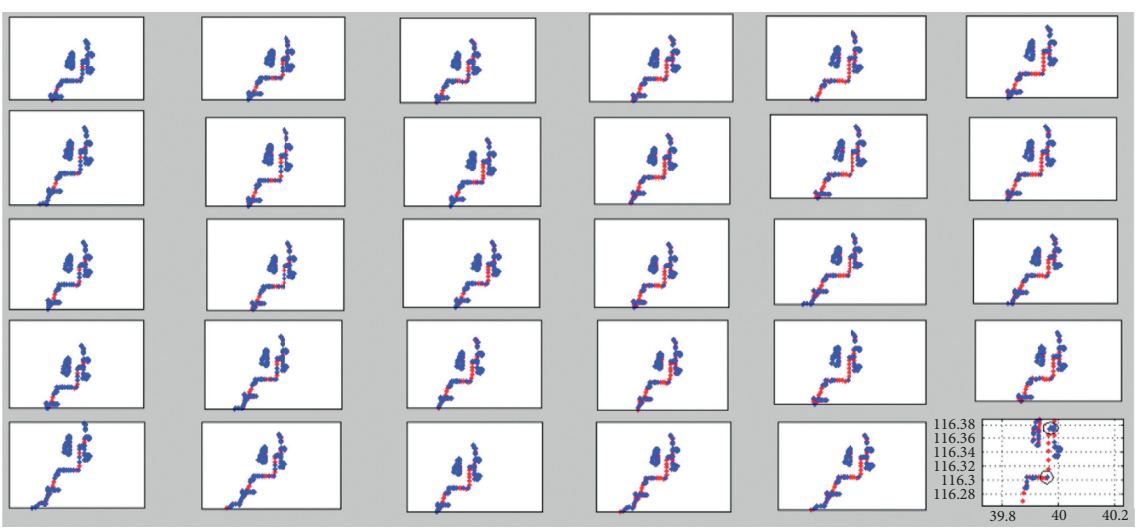

Figure 3: Trajectory map before and after compression at different angles and speeds.

compression ratio is defined as $Y_i^{\theta v_\alpha} = ((m_i - m_i^H)/m_i)$, but m_i as primary. Under the control of the weighted threshold value for velocity and angle, m_i^H is the number of trajectory points compressed [22].

Reduced trajectory was not only considering efficiency, but it was also guaranteeing the compressed trajectory as well as the original trajectory. In order to reflect the similarity of the two trajectories before and after compression, the diversity of the two trajectories is defined. D_i represents the absolute difference of i track before and after compression. Owing to the concern about kinetic trend changes before and after compression [23], area of the shadow that the compression trajectory and the original trajectory are surrounded by was not too large, as shown in Figure 5.

In Figure 5, the red line represents the point of original trajectory data and the blue line represents the point of

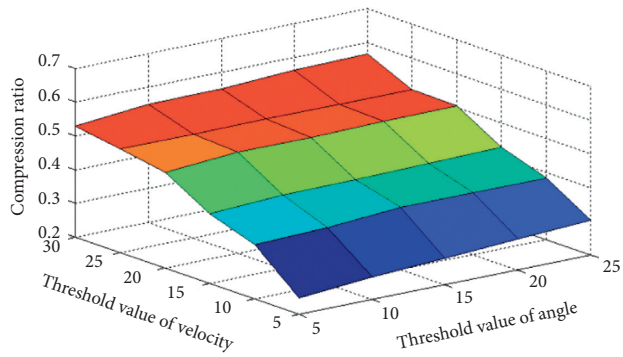

Figure 4: The change of angle threshold and velocity threshold leads to the change trend of compression ratio.

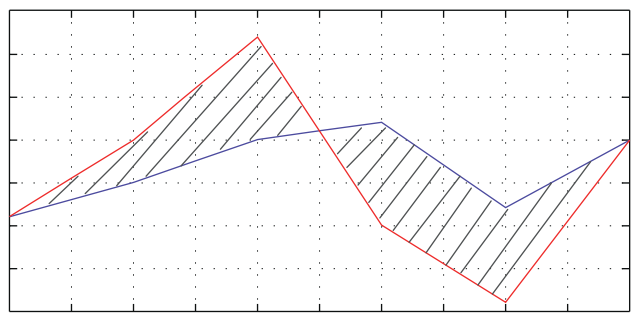

Figure 5: The area of the shadow that the compression trajectory and the original trajectory are surrounded by.

Table 2: Average compression ratio and average relative diversity of different threshold values and weights.

Threshold value	Weight 1	Weight 2	The average compression ratio	The average relative diversity	1 − the average relative diversity	$P = 1 -$ the average compression ratio + (1 − the average relative diversity)
	0.1	0.9	0.4398	0.24087042	0.75912958	1.198929583
	0.2	0.8	0.40601504	0.00037894	0.99962106	1.405636094
	0.3	0.7	0.39849624	0.00040007	0.99959993	1.398096167
	0.4	0.6	0.39097744	0.00040175	0.99959825	1.390575697
10	0.5	0.5	0.41353384	0.00040171	0.99959829	1.413132124
	0.6	0.4	0.42481203	0.00034475	0.99965525	1.424467279
	0.7	0.3	0.33082707	0.00031865	0.99968135	1.330508419
	0.8	0.2	0.4962406	0.09109596	0.90890404	1.405144641
	0.9	0.1	0.4962406	0.09514899	0.90485101	1.401091612
	0.1	0.9	0.5	0.28109667	0.71890333	1.218903331
	0.2	0.8	0.48872181	0.00076605	0.99923395	1.487955751
	0.3	0.7	0.5112782	0.0004619	0.9995381	1.510816294
	0.4	0.6	0.5037594	0.0004616	0.99953841	1.503297804
15	0.5	0.5	0.52255639	0.00069379	0.99930621	1.521862599
	0.6	0.4	0.54887218	0.09412948	0.90587052	1.454742699
	0.7	0.3	0.39473684	0.00040175	0.99959825	1.39433509
	0.8	0.2	0.59398496	0.09527842	0.90472158	1.49870654
	0.9	0.1	0.59398496	0.09526771	0.90473229	1.498717254
	0.1	0.9	0.5977	0.28465153	0.71534847	1.313048474
	0.2	0.8	0.57894737	0.24425466	0.75574534	1.33469271
	0.3	0.7	0.54511278	0.00076575	0.99923425	1.544347035
	0.4	0.6	0.57894737	0.09443527	0.90556473	1.484512094
20	0.5	0.5	0.60150376	0.09413002	0.90586998	1.507373736
	0.6	0.4	0.62030075	0.09418688	0.90581312	1.526113872
	0.7	0.3	0.4962406	0.00046169	0.99953831	1.49577891
	0.8	0.2	0.64285714	0.09532709	0.90467291	1.547530049
	0.9	0.1	0.64285714	0.09532786	0.90467214	1.547529287

Table 2: Continued.

Threshold value	Weight 1	Weight 2	The average compression ratio	The average relative diversity	1 − the average relative diversity	$P = 1 -$ the average compression ratio + (1 − the average relative diversity)
	0.1	0.9	0.6429	0.32357906	0.67642094	1.319320939
	0.2	0.8	0.62781955	0.29011079	0.70988921	1.337708762
	0.3	0.7	0.62406015	0.09759624	0.90240376	1.526463914
	0.4	0.6	0.64661654	0.09760408	0.90239592	1.549012461
25	0.5	0.5	0.67293233	0.09854359	0.90145641	1.574388742
	0.6	0.4	0.67293233	0.09635091	0.90364909	1.576581419
	0.7	0.3	0.52631579	0.00069379	0.99930621	1.525621997
	0.8	0.2	0.68421053	0.09780954	0.90219046	1.586400983
	0.9	0.1	0.68421053	0.1019832	0.8980168	1.582227325
	0.1	0.9	0.7406	0.57247657	0.42752343	1.16812343
	0.2	0.8	0.70300752	0.38568571	0.61431429	1.317321811
	0.3	0.7	0.71428571	0.3400506	0.6599494	1.374235114
	0.4	0.6	0.69548872	0.09853923	0.90146077	1.596949488
30	0.5	0.5	0.69172932	0.09963609	0.90036391	1.592093231
	0.6	0.4	0.71804511	0.10238604	0.89761396	1.615659076
	0.7	0.3	0.58646617	0.09413012	0.90586988	1.492336042
	0.8	0.2	0.69924812	0.10209319	0.89790681	1.597154926
	0.9	0.1	0.69924812	0.10209311	0.89790689	1.597155012

compressed trajectory data. If key points are selected properly, the shaded area would be as small as possible. Based on the above considerations, define

$$D_i = \left| \sum_{j-1}^{m_i-1} \left(y_j + y_{j+1}\right)\left|x_{j+1} - x_j\right| - \sum_{k-1}^{m_i^H-1} \left(y_k^H + y_{k+1}^H\right)\left|x_{k+1}^H - x_k^H\right| \right| = S_i - S_i^H, \tag{3}$$

where S_i is the area of the original trajectory surrounding the horizontal axis and S_i^H is the area of the compressed trajectory surrounding the horizontal axis.

Because of the different lengths of the original trajectory, the difference between the two tracks is called relative diversity, to be called $D_i' = (D_i/S_i)$. Taking $\theta v_\alpha = 10$, 15, 20, 25, and 30 and $(\alpha_1, \alpha_2) = (0.1, 0.9)$, (0.2, 0.8), (0.3, 0.7), (0.4, 0.6), . . ., (0.9, 0.1) as weights, the experiments of 2000 trajectories were run. According to various values, the average trajectory compression ratio was calculated and the average relative diversity was reckoned. The group that had a high average compression rate and a low average relative diversity as final thresholds and last weights was selected. Test results are shown in Table 2. In order to conveniently determine the threshold value and weights, choose by the size of $P = 1 -$ the average compression ratio + (1 − the average relative diversity). As is shown in Table 1, when $\theta v_\alpha = 30$, P-values for different situations are maximum. So 30 and 0.6, 0.4 were determined as threshold value and weights. At the moment, the average compression ratio was greater than 71%, the average relative diversity was only 10%, and the similarity of the original trajectory and the compressed trajectory was approximately 90%.

5. Conclusions and Discussion

Exploring the law of vehicle trajectory data can uncover some important road network information, which can provide effective decisions and suggestions for reducing road congestion and planning of traffic routes. To explore the value of object trajectory information, we study a vehicle trajectory data compression algorithm based on the change of motion state. The advantage of the algorithm is that the vehicle trajectory data compression rate is high, and the vehicle motion state and trajectory characteristics can be displayed as accurately as possible. In the research process of the algorithm, we use the GPS data of taxi track to do a lot of experiments to explore the impact of speed threshold and angle threshold on the track data compression rate. According to the experimental results, we propose a threshold combination algorithm, which improves the data compression rate by changing the threshold parameters and makes the compressed data clearly show the characteristics of vehicle trajectory. Reference values are as follows:

(1) Angle threshold is defined, respectively, as 5, 10, 15, and 20 in this paper. In nearly a month, running track of 2000 taxis in Beijing is verified, when the average compression rate is more than 45%. However, some points with an important feature of the information have been deleted so that the original motion trajectory trend has changed. Obviously, it is unscientific to only use the angle threshold to screen out the key data points in the vehicle trajectory; therefore, we need to add a new threshold to screen out the key data points that need to be retained. Thus, the information about the locus points contains the

speed at different times; in addition, the size of the rate of change reflects whether there is traffic congestion or smooth, and it reveals the trajectory of internal features. If the speed is the only indicator, the situation with the angle threshold control of key points is bound to arise, which can get a higher compression ratio. But it will lose some points that reflected track trends, so that the characteristics of the track cannot be fully demonstrated by the rest of the points.

(2) Angle threshold is defined, respectively, as 5, 10, 15, and 20, and speed threshold is defined, respectively, as 5, 10, 15, 20, and 25; the highest value of compression ratio is about 50%, and the lowest value is only about 20%. We have paid more attention to keeping contrail features and being stringent to take data points so that a few points meet the speed and angle threshold. Besides, it leads to a situation that the similarity of the track shape is higher, but the compression rate is lower.

(3) Using speed threshold and angle threshold to set a new index so as to obtain higher compression ratio and retain important information after compression, the index setting and parameter selection can be obtained through a large number of experiments. Angle threshold and velocity threshold are controlled by parameters so that reduced trajectory was not only considering efficiency but also guaranteeing the compressed trajectory as well as the original trajectory. Finally, the vehicle trajectories before and after compression are presented and similarity analysis is carried out.

Data Availability

The data presented in this study are available upon request from the corresponding author.

Conflicts of Interest

The authors declare that they have no conflicts of interest regarding the publication of this paper.

Acknowledgments

This research was funded by the Project of Promoting the Connotative Development of Beijing Information Science and Technology University (521201090A).

References

[1] C. L. Meehan, D. V. Cacciola, and M. Khosravi, "Monitoring field lift thickness using compaction equipment instrumented with global positioning system (GPS) technology," *Geotechnical Testing Journal*, vol. 36, no. 5, pp. 755–767, 2013.

[2] S. Khan, P. Maini, and K. Thanasupsin, "Car-following and collision constraint models for uninterrupted traffic: reexamination using high-precision global positioning system data," *Transportation Research Record: Journal of the Transportation Research Board*, vol. 1710, no. 1, pp. 37–46, 2000.

[3] L. Zhao and G. Shi, "A trajectory clustering method based on Douglas-Peucker compression and density for marine traffic pattern recognition," *Ocean Engineering*, vol. 172, pp. 456–467, 2019.

[4] K. Jin, J. Li, H. Wang, B. Zhang, and N. Zhang, "Near-linear time approximation schemes for geometric maximum coverage," *Theoretical Computer Science*, vol. 725, pp. 64–78, 2018.

[5] S. Khan, P. Maini, and K. Thanasupsin, "Stability control and turning algorithm of an alpine skiing robot," *Sensors*, vol. 19, no. 17, 2019.

[6] W. Song, R. Zhang, Y. Yao, Y. Liu, and Y. Hu, "PPP sliding window algorithm and its application in deformation monitoring," *Scientific Reports*, vol. 6, no. 1, pp. 149–158, 2016.

[7] H. Alborzi and H. Samet, "Execution time analysis of a top-down R-tree construction algorithm," *Information Processing Letters*, vol. 101, no. 1, pp. 6–12, 2006.

[8] G. M. Coclite, M. Garavello, and B. Piccoli, "Traffic flow on a road network," *SIAM Journal on Mathematical Analysis*, vol. 36, no. 6, pp. 1862–1886, 2006.

[9] A. G. O. Yeh, T. Zhong, and Y. Yue, "Hierarchical polygonization for generating and updating lane-based road network information for navigation from road markings," *International Journal of Geographical Information Science*, vol. 29, no. 9, pp. 1509–1533, 2015.

[10] K. Al-Hussaeni, B. C. M. Fung, F. Iqbal, G. G. Dagher SafePath, and E. G. Park, "SafePath: differentially-private publishing of passenger trajectories in transportation systems," *Computer Networks*, vol. 143, pp. 126–139, 2018.

[11] R. Mahbubani, P. Schwaller, and J. Zurita, "Erratum to: closing the window for compressed dark sectors with disappearing charged tracks," *Journal of High Energy Physics*, vol. 2017, no. 6, pp. 1–22, 2017.

[12] C. L. Meehan, D. V. Cacciola, and M. Khosravi, "Robust multi-scale ship tracking via multiple compressed features fusion," *Signal Processing: Image Communication*, vol. 31, pp. 76–85, 2015.

[13] X. Yi, R. Guo, and Y. Qi, "Stabilization of chaotic systems with both uncertainty and disturbance by the UDE-based control method," *IEEE Access*, vol. 8, no. 1, pp. 62471–62477, 2020.

[14] X.-J. Shen, L. Mu, Z. Li, H.-X. Wu, J.-P. Gou, and X. Chen, "Large-scale support vector machine classification with redundant data reduction," *Neurocomputing*, vol. 172, pp. 189–197, 2015.

[15] H. Mahdin and J. Abawajy, "An approach for removing redundant data from RFID data streams," *Sensors*, vol. 11, no. 10, pp. 9863–9877, 2011.

[16] E. Kotter, A. Roesner, J. Torsten Winterer et al., "Evaluation of Lossy data compression of chest X-rays: a receiver operating characteristic study," *Investigative Radiology*, vol. 38, no. 5, pp. 243–249, 2003.

[17] N. K. Kasumov, "Data positioning as an instrument of constructive data compression," *Automatic Control and Computer Sciences*, vol. 46, no. 5, pp. 223–231, 2012.

[18] L. Liu, B. Li, and R. Guo, "Consensus control for networked manipulators with switched parameters and topologies," *IEEE Access*, vol. 9, pp. 9209–9217, 2021.

[19] R. Xu and F. Zhang, "ε -Nash mean-field games for general linear-quadratic systems with applications," *Automatica*, vol. 114, pp. 1–6, 2020.

[20] W. Wang, Y. He, J. Liu, and S. Gombault, "Constructing important features from massive network traffic for lightweight intrusion detection," *IET Information Security*, vol. 9, no. 6, pp. 374–379, 2015.

[21] T. Hou, Y. Liu, and F. Deng, "Finite horizon H2/H∞ control for SDEs with infinite Markovian jumps," *Nonlinear Analysis: Hybrid Systems*, vol. 34, pp. 108–120, 2019.

[22] S. Ke, J. Gong, S. Li, Q. Zhu, X. Liu, and Y. Zhang, "A hybrid spatio-temporal data indexing method for trajectory databases," *Sensors*, vol. 14, no. 7, pp. 1290–3005, 2014.

[23] L. Chen, M. Lv, Ye Qian, G. Chen, and J. Woodward, "A personal route prediction system based on trajectory data mining," *Information Sciences*, vol. 181, no. 7, pp. 1264–1284, 2010.

Hindawi
Mathematical Problems in Engineering
Volume 2021, Article ID 5558757, 12 pages
https://doi.org/10.1155/2021/5558757

Research Article

Financial Imbalance Risk and Its Control Strategy of China's Pension Insurance Contribution Rate Reduction

Peng Jing, Cai Chang, Heng Zhu, and Qiuming Hu

School of Insurance, Southwestern University of Finance and Economics, Chengdu 611130, China

Correspondence should be addressed to Qiuming Hu; hqiuming@263.net

Received 25 January 2021; Revised 15 February 2021; Accepted 20 February 2021; Published 28 February 2021

Academic Editor: Rongwei Guo

Within the context of China's Urban Employees' Basic Pension Insurance (UEBPI), this paper constructs an actuarial model to analyze the financial imbalance risk of contribution rate reduction and to investigate the possibility of further reducing the contribution rate. It is found that the UEBPI fund would show financial imbalance risk in 2024 if the contribution rate is 16%, and no control strategy is introduced. In the case of single strategy (the collection system reform, delay of retirement age, or the introduction of external finance), the financial sustainability of the UEBPI fund could be improved to some extent, whereas the financial imbalance risk remains huge. In the case of a package of control strategies being implemented, the UEBPI fund could be able to continue its operation until 2060, and the contribution rate can be further reduced by 0–4 percentage. Therefore, the implementation of a package of control strategies presents a prerequisite for controlling the financial imbalance risk and further reducing the contribution rate.

1. Introduction

The contribution rate of China's social insurance is among the highest in the world, particularly the Urban Employees' Basic Pension Insurance (UEBPI). According to "Social Security Programs Throughout the World: Africa, 2015" released by the U.S. Social Security Administration (https://catalog.data.gov/dataset/social-security-programs-throughout-the-world-africa-2015), the contribution rate of China's social insurance and pension insurance ranked 16th and 11th among 175 countries or regions, respectively. Several reasons contribute to this high contribution rate, including the high transition cost, the low dependency ratio, the imperfect contribution incentive mechanism, and the improper management of the fund.

At present, China's economy has entered a new stage characterized by the transformation from rapid growth to high-quality development. According to current policies, the employers contribute 30% of employees' wages to social insurance, which brings a negative impact to their business operations. To lighten the contribution burden, the Chinese government has reduced the contribution rate for several times since 2015. However, those reductions are mainly for employment injury insurance and unemployment insurance. For the pension insurance with the heaviest contribution burden among five social insurances, the contribution rate is reduced by only one percentage. Due to the fact that the reduction is relatively low, more and more employers call for further reduction. In view of this, the Chinese government reduced the UEBPI contribution rate for employers from 19% to 16% in May 2019, emphasizing that the reduction is a long-term institutional arrangement and should adapt to the new normal economic development.

The policy objective of lowering the UEBPI contribution rate is to lighten the burdens on employers, while it also results in the reduction of the pension fund's income. Although the accumulated surplus of China's UEBPI fund has reached more than 5 trillion RMB in 2019, which could support the contribution rate reduction in the short term, the financial sustainability of the fund would be threatened in the long run. It can be seen from Figure 1 that the income from the collection was lower than the total expenditure since 2014, and the gap between these two even reached 662.80 billion RMB in 2019. In addition, according to the

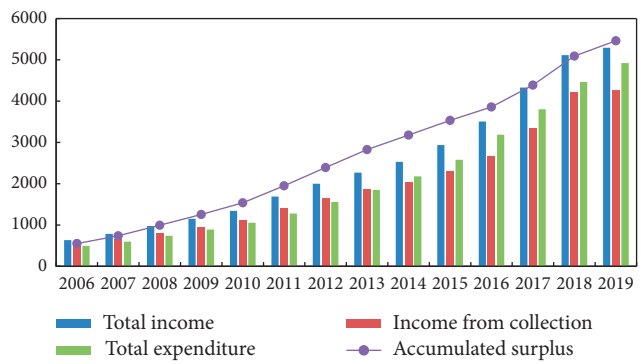

Figure 1: Financial balance of the UEBPI fund in 2006–2019 (unit: billion RMB; source: Statistical Bulletin on the Development of Human Resources and Social Security, http://www.mohrss.gov.cn/gkml/ghtj/tj/ndtj/).

data of Figure 1, we can calculate that the annual growth rate of total expenditure and total income of the UEBPI fund are 19.47% and 17.93%, indicating that the fund may have hidden the financial imbalance risk. Previous studies generally concluded that the current arrangement of the UEBPI fund was not sustainable in the long term with the rapid growth of population aging (Liu et al. [1]; Luo et al. [2]), suggesting that the contribution rate reduction will enhance the financial imbalance risk. To achieve the goal of reducing the contribution rate without cutting the pension benefit, the following questions must be answered first, i.e., how much financial imbalance risk exists in the UEBPI fund, and how to mitigate the risk by settling control strategies?

In recent years, the Chinese government has carried out a series of reforms to finance the UEBPI fund, including implementing the two-child policy, encouraging market-oriented investment, and establishing the pension benefit adjustment mechanism. Though these reforms could enhance the financial sustainability, it is unlikely to completely settle the problem of inadequate solvency of pension funds (Xie et al. [3]; Zeng and Yu [4]). Meanwhile, the Chinese government also considers extending the mandatory retirement age and implementing the collection system reform. On the premise of the sustainable operation of the UEBPI fund, is it possible to further reduce the contribution rate in the process of pension system reforms? The answers to the question can provide a quantitative basis for the government to further reduce the UEBPI contribution rate.

The remaining part of this paper is organized as follows. Section 2 reviews the literature. Section 3 constructs an actuarial model to analyze the financial imbalance risk and calculates the contribution rate under actuarial equivalence. Section 4 describes the parameters and assumptions. Section 5 presents the prediction results in several scenarios. Section 6 reports the results of sensitivity analysis. Section 7 concludes the paper.

2. Literature Review

In the 1990s, the concept of sustainable development was introduced into the reform of the pension system. Many countries set their ultimate goal of the pension system reform to achieve sustainable development (World Bank [5]). Holzmann and Hinz [6] emphasized that sustainability referred specifically to financial sustainability. In most countries, pension system is confronted with great challenges due to population aging. Therefore, considerable literature is prepared to assess the financial sustainability of pension funds (Blake and Mayhew [7]; Rauh and Novymarx [8]; Billig and Ménard [9]; Metzger [10]). Bongaarts [11] found that the pension fund in most OECD countries would not be sufficient with an aging population because of the Pay-As-You-Go (PAYG) system. Sin [12] found that China's UEBPI fund would have an annual deficit after 2030 and the amount of the accumulated deficit would increase on yearly basis. In this case, to maintain the balance between the fund's income and expenditure, the contribution rate should increase to 37%. To enhance the financial sustainability and alleviate the financial imbalance risk of the pension system, multiple studies have proposed many optimization strategies, such as postponing the mandatory retirement age, lowering the growth rate of pension benefits, relaxing the childbearing policy, and increasing the return on investment of the fund (Belolipetskii and Lepskaya [13]; Heeringa and Bovenberg [14]; Liu and Sun [15]).

In general, existing literature on the pension insurance contribution rate mainly focuses on three aspects. First, from the perspective of fund balance, some literature constructed an actuarial model to predict the financial status and the feasible extent of contribution rate reduction. Second, from the perspective of cost-benefit comparison, some literature empirically analyzed the impact of the contribution rate on employers' behavior. Third, from the perspective of general equilibrium, some literature established an overlapping generation model to estimate the impact of the contribution rate on several essential economic outcomes.

Pension insurance contributions present the main income source of the pension fund; therefore, lowering the contribution rate will inevitably reduce the fund's income and further bring negative impact on the sustainability of the fund. Whiteford and Whitehouse [16] suggested that the premise for the reduction of the contribution rate was to consolidate the contribution base. Lin [17] found that a contribution rate of 16.47% was required to achieve the vertical financial balance of China's UEBPI fund from 2008 to 2050. Jing and Hu [18] pointed out that the contribution rate could be kept within 14.64%–16.14% if a combination of policy reforms was performed. Zeng et al. [19] found that the two-child policy could decrease the contribution rate in the short term, while postponing the retirement age could result in a reduction in the rate by 0.30–0.43 percentage every two years before 2050. Guo and Zhang [20] believed that there was little room for further reduction of the contribution rate in the short term. To obtain a reduction of the rate in the long run, they advised implementing the collection system reform. Zeng et al. [21] found that the contribution rate could be reduced by 0.57–1.50 percentage between 2020 and 2030 provided that the tax authorities collected pension insurance contributions.

Pension insurance contribution presents a chief component of enterprises' operating costs. The reduction of the

contribution rate may result in a decrease of the enterprises' labor costs and an increase in cash flow, thus changing their business behaviors. According to Kugler and Kugler [22], enterprises' employment behavior is associated with the cost and benefit of the pension contribution. Their study showed that an increase in the contribution rate may lead to the reduction of formal employment. Iturbe-Ormaetxe [23] reached a similar conclusion. Ma et al. [24] found that the increase of one percent of the pension insurance contribution rate would reduce employment by 0.8%. Chaudhry et al. [25] and Saez et al. [26] found that increasing the contribution rate would reduce the cash flow and squeeze the R&D expenditures, which is unfavorable for the improvement of production efficiency. Based on the data of Chinese industrial enterprises, Tang and Feng [27] found that the increase of the contribution rate would increase the capital-labor ratio.

Pension insurance contributions profoundly affect personal interests. The changes in the contribution rate may lead to the adjustments of individuals' decision-making behavior, thereby affecting the economic growth through labor supplies and the accumulation of physical and human capital. Ehrlich and Kim [28] found that a higher contribution rate encouraged a lower fertility rate and leaded to a decrease in private savings. Yew and Zhang [29] showed that when parents' preference for their children's utility was greater than that for the number of children, pension insurance would improve social welfare by reducing the fertility rate and increasing human capital. Fanti and Gori [30] illustrated that a lower contribution rate would accumulate physical capital and increase the economic growth rate. Peng et al. [31] showed there was an optimal combinatorial relationship between the pension insurance contribution rate and the tax rate on public education. By increasing public investment in education, it is possible to maintain the pension replacement rate and economic growth rate, while reducing the contribution rate in the meantime.

In summary, existing literature has deeply analyzed the pension insurance contribution rate from different perspectives. However, there is still room for improvement. Firstly, most of the existing studies only focus on one particular pension system reform, and few pieces of literature investigate the impact of multiple reforms on the financial sustainability of pension funds. Secondly, the actuarial model adopted in most studies fails to classify the pension participants, and their assumptions on parameters make no difference between regulation and practice into account. Accordingly, we aim to construct an actuarial model with reasonable parameter assumptions to predict the financial sustainability of China's UEBPI fund in several scenarios. Based on the calculated contribution rate under actuarial equivalence, we also attempt to investigate whether the contribution rate could be further reduced.

3. Methodology

3.1. Actuarial Model. In 1997, after the State Council proposed the issue "Decision on Establishing a Unified Basic Pension System for Enterprise Employees," the Chinese government established a public pension program with a social pooling account and an individual account. In 2005, the State Council issued "Decision on Improving the Enterprise Employees' Basic Pension System," which changed the method to calculate pension benefits. According to the time when employees entered the labor market and employees worked until retiring and the implementation of the above two documents, we classify pension participants into four categories, including "old people," "older middle-aged people," "younger middle-aged people," and "young people". The "old people" refers to those who had retired before 1998. The "older middle-aged people" refers to those who started work before 1998 and retired before 2006. The "younger middle-aged people" refers to those who started work before 1998 and retired or will retire after 2006. The "young people" refers to those who started work after 1998. Besides, the current statutory retirement age in China is 60 for males, 55 for female carders, and 50 for female workers, indicating that we should consider the differences in employees' gender and occupation. The purpose of classifying pension participants is to predict the income and expenditure of pension funds more accurately. Finally, we decide to construct the actuarial model combined with the stabilization of chaotic systems and control theory (Yi et al. [32]; Liu et al. [33]).

The pension fund's income (referred to income from the collection) is the multiplication of the number of contributors, contribution base, collection rate, and contribution rate. Thus, the t-year pension fund's income, I_t, is given by

$$I_t = \sum_{i=1}^{4}\sum_{j=1}^{3}\sum_{x=a^j}^{b^j-1} N_{t,x}^{i,j} \times w_t \times \rho_t \times (\theta+\sigma) = \sum_{i=1}^{4}\sum_{j=1}^{3}\sum_{x=a^j}^{b^j-1} N_{t,x}^{i,j} \times \left[w_{t_0-1} \times \prod_{s=t_0}^{t} (1+k_s) \right] \times \rho_t \times (\theta+\sigma). \quad (1)$$

In equation (1), $i = 1$–4 refers to "old people," "older middle-aged people," "younger middle-aged people," and "young people," respectively. $J = 1$–3 refers to male, female carder, and female worker, respectively. a^j is the initial contributory age, b^j is the retirement age, and $N_{t,x}^{i,j}$ is the number of contributors aged x at year t who belong to the ith and jth group. w_t represents the contribution base, k_t represents the growth rate of contribution base, ρ_t represents the collection rate. θ and σ are the contribution rates of employers and employees, respectively, t_0 refers to the year in which the actuarial analysis begins. Note that, the above equation is a general form. Under the current retirement age in China, except for the "old people," "older middle-aged people," and part of the "younger middle-aged people," the

remaining "younger middle-aged people" and all of the "young people" still need to pay for it in 2020. After 2037, only the "young people" need to pay for the contributions.

The pension fund's expenditure consists of basic pension benefits, transitional pension benefits, and individual account pension benefits. According to the regulation of UEBPI, the "old people" can only receive basic pension benefits, the "older middle-aged people" and "younger middle-aged people" can receive three kinds of pension benefits, the "young people" can receive basic pension benefits and individual account pension benefits.

The expenditure of basic pension benefits equals the multiplication of the number of retired members, payment base, payment ratio, and adjustment factor. Thus, the expenditure of basic pension benefits, $E_{t,A}$, is given by

$$E_{t,A} = \sum_{i=1}^{4}\sum_{j=1}^{3}\sum_{x=b^j}^{c^j} N_{t,x}^{i,j} \times A_{t,x}^{i,j} \times m_{t,x}^{i,j} \times \prod_{s=t-x+b^j}^{t} (1+g_s). \quad (2)$$

In equation (2), c^j refers to the maximum age of survival, $A_{t,x}^{i,j}$ refers to the payment base of basic pension benefits for members aged x at year t who belong to the ith and jth group, $m_{t,x}^{i,j}$ is the corresponding payment ratio, and g_t is the growth rate of basic pension benefits. According to the pension benefits adjustment in practice, we assume that the growth rates of basic pension benefits, transitional pension benefits, and individual account pension benefits are the same.

The expenditure of transitional pension benefits equals the multiplication of the number of retired "older middle-aged people" and "younger middle-aged people", payment base, payment ratio, admitted number of years of contributory service, and adjustment factor. Thus, the expenditure of transitional pension benefits, $E_{t,B}$, is given by

$$E_{t,B} = \sum_{i=2}^{3}\sum_{j=1}^{3}\sum_{x=b^j}^{c^j} N_{t,x}^{i,j} \times B_{t,x}^{i,j} \times n_{t,x}^{i,j} \times TI_{t,x}^{i,j} \times \prod_{s=t-x+b^j}^{t} (1+g_s). \quad (3)$$

In equation (3), $B_{t,x}^{i,j}$ refers to the payment base of transitional pension benefits for members aged x at year t who belong to the ith and jth group, $n_{t,x}^{i,j}$ is the corresponding payment ratio, and $TI_{t,x}^{i,j}$ is the admitted number of years of contributory service before the establishment of the individual account, $TI_{t,x}^{i,j} = 1998 - (t - x + a^j)$.

The expenditure of individual account pension benefits depends on the number of retired "older middle-aged people," "younger middle-aged people," and "young people," their accumulated balance of the individual account, and adjustment factor. Thus, the expenditure of individual account pension benefits, $E_{t,C}$, is given by

$$E_{t,C} = \sum_{i=2}^{4}\sum_{j=1}^{3}\sum_{x=b^j}^{c^j} N_{t,x}^{i,j} \times \frac{\sum_{s=a^j}^{b^j-1} w_s \times \sigma_t \times (1+i_s)^{b^j-s-1}}{v_t^{i,j}} \times 12 \times \prod_{s=t-x+b^j}^{t} (1+g_s). \quad (4)$$

In equation (4), i_t refers to the nominal interest rate of individual account at year t, $v_t^{i,j}$ is the number of expected months issuing individual account pension benefits for members who belong to the ith and jth groups at year t.

The current surplus of the pension fund equals the income minus the expenditure in the current year. The accumulated surplus of the pension fund equals the sum of last year's accumulated surplus, accrued interest, and the current surplus. At year t, the current surplus CS_t and the accumulated surplus AS_t are as follows:

$$\begin{aligned} CS_t &= I_t - E_t = I_t - \left(E_{t,A} + E_{t,B} + E_{t,C}\right), \\ AS_t &= AB_{t-1} \times (1+r_t) + CS_t, \end{aligned} \quad (5)$$

where r_t is the return on investment of the pension fund at year t. According to the amount of accumulated surplus, r_t takes different values. When the accumulated surplus is positive, r_t is the actual rate of return on investment. When the accumulated surplus is negative, $r_t = 0$. By judging the symbol of accumulated surplus, we can evaluate the financial imbalance risk of pension funds. If $AS_{t-1} > 0$ and $AS_t < 0$, the fund will show financial imbalance risk at year t.

3.2. Contribution Rate under Actuarial Equivalence Principle. Although China adopts an integrated account that combines a social pooling account and an individual account, a PAYG system is executed in practice. Due to the high transition cost, the Chinese government has to use part of individual account funds to fill the gap in the pooling account, which directly induces the problem of "empty account". Under the PAYG system, the government decides the annual fund's income based on its expenditure and then determines the contribution rate according to the number of contributors and the contribution base. However, it is inadvisable to change the contribution rate frequently because of the menu cost. Therefore, the pension fund should satisfy the vertical financial balance, and the vertical financial balance means that accumulated income equals accumulated expenditure during a certain period, which is given by

$$\sum_{t=t_0}^{t_T}\left[I_t \times \prod_{s=t}^{t_T}(1+r_s)\right] + AS_{t_0-1} \times \prod_{t=t_0}^{t_T}(1+r_t) = \sum_{t=t_0}^{t_T}\left[E_t \times \prod_{s=t_0}^{t_T}(1+r_s)\right], \quad (6)$$

where t_T is the year of termination of actuarial analysis. Substituting equation (1)–(4) in equation (6), we could calculate the contribution rate under the actuarial equivalence principle and then decide whether it is possible for further reduction and its extent. This paper focuses on the employers' contribution rate, and the actuarial balance rate, $\widehat{\theta}$, is

$$\hat{\theta} = \frac{\sum_{t=t_0}^{t_T}\left[E_t \times \prod_{s=t_0}^{t_T}(1+r_s)\right] - AS_{t_0-1} \times \prod_{t=t_0}^{t_T}(1+r_t)}{\sum_{t=t_0}^{t_T}\left[\sum_{i=1}^{4}\sum_{j=1}^{3}\sum_{x=a^j}^{b^j-1} N_{t,x}^{i,j} \times w_t \times \rho_t \times \prod_{s=t}^{t_T}(1+r_s)\right]} - \sigma. \tag{7}$$

If $\widehat{\theta} \geq \theta$, there is no space for the contribution rate reduction. If $\widehat{\theta} < \theta$, the employers' contribution rate can be reduced by $\theta - \widehat{\theta}$.

4. Parameters Setting

4.1. Demographic Parameters.

(1) Urban population: Based on China's sixth census in 2010 and 1% mini census in 2015, we rearrange the population data into different cohorts. Firstly, we predict the number of urban and rural births with the estimation of the total fertility rate, fertility pattern, and sex ratio at birth. Secondly, we forecast the number of urban and rural deaths with the assumption of life expectancy and mortality. Lastly, considering the amount of rural-urban migration, we obtain the urban population by age and gender in each future year.

According to China's sixth census (http://www.stats.gov.cn/tjsj/pcsj/rkpc/6rp/indexch.htm), the total fertility rate in 2010 is 1.18, among which urban and rural are 0.98 and 1.44, respectively. Due to the phenomenon of concealment and omission during the census, existing literature applies different methods to adjust the total fertility rate, which is considered to be 1.4–1.5 (Cai [34]; Chen and Yang [35]). We assume that the total fertility rate is 1.45 and is 1.23 times higher than the original one. The resulted adjusted total fertility rates for urban and rural are 1.205 and 1.771. The two-child policy implemented in 2016 will have a great impact on the fertility rate. A survey conducted by China Women's Federation and Beijing Normal University showed that the proportion of families with one child having an intention to bear a second child was 20.5%. Using the "4-2-1" family microscopic simulation model, we found that the urban total fertility rate is $0.795 \times 1.205 + 0.205 \times 2 = 1.368$ and the rural total fertility rate is $0.795 \times 1.771 + 0.205 \times 2 = 1.81$. As for other demographic parameters, the fertility pattern is the same with 1% mini census. The sex ratio to birth is assumed to decrease by 0.3 per year, until 107. Life expectancies are from the "World Population Prospects 2019," mortality rates by age and gender are estimated using Far Eastern life table. The amount of migration from rural to urban follows Jiang [36].

(2) Urban employed population: With the urban population and employment rate from 1% mini census, assuming that female carders account for 20% of all female employers, we can calculate the urban employed population by age, gender, and occupation.

(3) The number of UEBPI participants: According to "Statistical Bulletin on the Development of Human Resources and Social Security 2019" (http://www.mohrss.gov.cn/gkml/ghtj/tj/ndtj/202009/t20200911_385449.html), the number of UEBPI participants is 434.88 million, among which the number of contributors and retirees is 311.77 million and 123.11 million. To estimate the number of UEBPI participants by age and gender, we assume that the age structure of contributors is consistent with that of urban employees, and the age structure of retirees is consistent with that of the urban elderly. With mortality rates by age and gender, we can estimate the number of the "old people," "older middle-aged people," "younger middle-aged people," and "young people" by age, gender, and occupation.

Figure 2 shows the trends in four kinds of UEBPI participants from 2020 to 2060. The number of "old people," "older middle-aged people," and "younger middle-aged people" gradually decreases year by year, while the number of "young people" gradually increases year by year. As a result, the number of total UEBPI participants increases first and then decreases to a turning point of 2052.

4.2. Policy Parameters.

(1) Contribution rate, contribution base, and collection rate: At present, China's UEBPI contribution rates of employers and employees are 16% and 8%, and the legal contribution base is last year's average wage. Driven by interests, most employers desire and require avoidance of paying pension insurance contributions, resulting in the situation where the actual contribution base is much lower than the legal one. Statistics dates show that the actual contribution base accounts for only 65% of the legal contribution base in recent years. According to the "China Statistical Yearbook" (http://www.stats.gov.cn/tjsj/ndsj/), the average wage growth rate is approximately equal to the economic growth rate. Considering that China's economic growth rate will

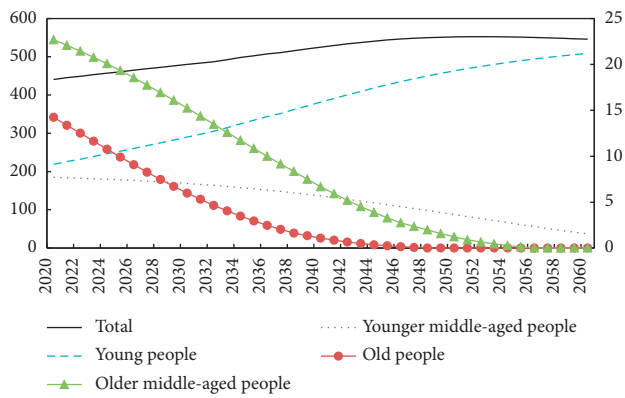

Figure 2: Trends in four kinds of UEBPI participants (unit: million).

gradually slow down, we assume that the growth rate of the legal contribution base is 6.5% in 2020, which will reduce by 0.5 percentage every five years, till it reaches 2%.

(2) Initial contributory age, retirement age, and the maximum age of survival: According to current employment features and population census in China, we assume that employees enter the labor market at the age of 22, and the maximum age of survival is 100. That is to say, pension participants' initial contributory age is 22, and they receive pension benefits till 100. According to the current retirement age policy formulated in the early 1950s in China, the age of male is 60, for female, the age of carder is 55, and the age of worker is 50.

(3) Pension payment ratio: The basic pension payment ratios for "old people" and "older middle-aged people" are 70% and 20%, while the basic pension payment ratios for "younger middle-aged people" and "young people" are related to their contributory years at retirement, 1% for each contributory year. According to the current retirement age policy, the basic pension payment ratios are 38% for male, 33% for female carders, and 28% for female workers. The number of expected months issuing individual account pension benefits is 139 for male, 170 for female carders, and 195 for female workers. The transitional pension payment ratio for "older middle-aged people" and "younger middle-aged people" is 1.2%.

(4) Growth rate of pension benefits: "The Social Insurance Law of the People's Republic of China" requires setting up a mechanism to adjust pension benefits, and raising pension benefits according to the growth rate of employees' wages and inflation rate. Therefore, we assume that the growth rate of pension benefits is $g = \pi + \alpha\lambda$, where π is the inflation rate, λ is the growth rate of wage, and α is the economic sharing factor. Based on pension benefits adjustment in practice, we assume that the inflation rate is 2%, and the economic sharing factor is 0.5.

(5) Return on investment and nominal interest rate of the individual account: China's UEBPI fund is either invested in national debt or reserved in the commercial bank before 2016, resulting in the return on investment to be less than 2%. Form 2017, the pension fund could be invested in financial markets, but the investment scale is still small. Therefore, we assume the return on investment to be 3%. Based on the regulations of UEBPI, the nominal interest rate of individual account should consider the growth rate of wage and the balance of pension funds and should not be lower than the one-year deposit rate. Based on the nominal interest rate of individual account in recent years, we assume it to be 5%.

5. Prediction Results

5.1. Baseline Scenario: No Strategy Intervention. In the baseline scenario, we predict the income, expenditure, current surplus, and accumulated surplus of the UEBPI fund when the contribution rate is 19% and 16%, respectively, assuming that there is no strategy intervention. The prediction results are summarized in Table 1. The baseline scenario serves as the reference for the analysis of optimization scenarios.

It can be seen from Table 1 that when the contribution rate is 19%, the fund's income increases from 4965.61 billion RMB in 2020 to 22387.59 billion RMB in 2060, with an annual average growth rate of 3.85%. Meanwhile, the fund's expenditure increases from 5295.18 billion RMB in 2020 to 56664.13 billion RMB in 2060, with an annual average growth rate of 6.13%. We can find that with the changes in the income and expenditure, the fund will experience an annual deficit from 2020 and reach 36764.05 billion RMB in 2060. However, according to "Statistical Bulletin on the Development of Human Resources and Social Security 2019," the accumulated surplus of the UEBPI fund was 5462.30 billion RMB in 2019. Based on the return on investment and the annual deficits, it is calculated that the fund will be exhausted in 2025, and the accumulated deficit will be as high as 568681.59 billion RMB in 2060. It means that in the baseline scenario of the contribution rate 19%, the UEBPI fund could last for only 5 years (2020–2024), and the fund will become unsustainable since 2025. While under the contribution rate of 16%, the reduction of income and the maintenance of expenditure will cause the UEBPI fund to be exhausted in 2024, and the accumulated deficit is 629455.86 billion RMB in 2060, indicating that the contribution rate reduction will lead to a greater risk of financial imbalance.

Based on the predicted results of the contribution rate 16%, we calculate the actuarial balance rate that could maintain the vertical financial balance from 2020 to 2060 using equation (7), which is 43.34%, a number far beyond 16%. It shows that there is no feasible space for the decrease of pension insurance contribution rate. Therefore, the question is how to maintain the vertical financial balance of the UEBPI fund with contribution rate reduction? In recent years, among all the proposed arrangements related to the improvement of the financial sustainability of the UEBPI

Table 1: Financial balance of the UEBPI fund in baseline scenario (unit: billion RMB).

Year	$\theta = 19\%$				$\theta = 16\%$			
	I_t	E_t	CS_t	AS_t	I_t	E_t	CS_t	AS_t
2020	4965.61	5295.18	−329.57	5296.60	4413.87	5295.18	−881.31	4744.86
2021	5252.18	5821.01	−568.82	4886.67	4668.61	5821.01	−1152.40	3734.81
2022	5548.84	6335.77	−786.93	4246.34	4932.30	6335.77	−1403.47	2443.38
2023	5856.37	6972.37	−1116.00	3257.72	5205.66	6972.37	−1766.71	749.97
2024	6144.44	7746.27	−1601.82	1753.64	5461.73	7746.27	−2284.54	−1512.07
2025	6461.68	8484.21	−2022.54	−216.29	5743.71	8484.21	−2740.50	−4252.57
2030	8229.43	12769.50	−4540.08	−17527.33	7315.05	12769.50	−5454.46	−25723.88
2035	10438.51	18216.50	−7777.99	−50020.81	9278.68	18216.50	−8937.82	−63476.43
2040	13042.81	24724.94	−11682.13	−100086.68	11593.61	24724.94	−13131.33	−120181.58
2045	16017.97	32264.41	−16246.44	−171920.97	14238.20	32264.41	−18026.22	−200229.55
2050	18299.96	41209.25	−22909.29	−272709.16	16266.63	41209.25	−24942.62	−310667.63
2055	20407.20	49539.54	−29132.35	−406713.52	18139.73	49539.54	−31399.81	−455516.57
2060	22387.59	56664.13	−34276.54	−568681.59	19900.08	56664.13	−36764.05	−629455.86

fund by the Chinese government, the two-child policy is implemented. However, we still need other risk control strategies, such as implementing the collection system reform, postponing the retirement age, and introducing external finance. Therefore, we analyze the impacts of the said three risk control strategies on alleviating the financial imbalance risk of the UEBPI fund. It should be noted that the following content is analyzed when the contribution rate is 16%.

5.2. Optimization Scenario 1: Implementing the Collection System Reform. Pension insurance contributions are collected in three methods, namely, "collected by tax authorities," "collected by social security department," and "collected by tax authorities on behalf of social security department." By 2018, 5, 15, and 17 of 37 contributory districts in China adopted the above three methods, respectively. Collection system reform refers to "collected by tax authorities," which means the tax authorities are responsible for determining the contribution base and collecting the contributions.

Contribution evasion is one of the major issues in pension collection management. According to the "China Enterprise Social Insurance White Paper 2018" (https://www.51shebao.com/article/detail/2957), only 27% of the enterprises pay the compliant contributions. It was verified by many studies that "collected by tax authorities" would increase the collection rate (Barrand et al. [37]; Enoff and Mckinnon [38]). Based on China's provincial panel data, Zeng et al. [21] found that the collection rate could be increased by 20.3–25.2 percentage if the contributions were collected by the tax authorities. Gillion [39] pointed out that the collection rate in both eastern and central European countries is 70%–80%, and these countries usually adopt the method of "collected by tax authorities." It is assumed that the collection rate will increase to 75% or 85% after the collection system reform, namely, the optimization scenario 1.

It can be seen from Table 2 that, with the increase of the collection rate, the earliest year of the accumulated deficit is delayed. When the collection rate reaches 75%, the earliest year of the accumulated deficit is 2026. However, the number of years with the current deficit is not changed. When the collection rate is as high as 85%, the earliest year of the accumulated deficit is 2029, and the earliest year of the current deficit is 2023. Compared with the baseline scenario, with the collection system reform, the sustainable operation of the fund is extended by 2–5 years, and the amount of accumulated deficit in 2060 is decreased by 11.89%–23.84%. However, the fund still shows a large accumulated deficit. To achieve the vertical financial balance, the actuarial balance rate has to be 36.49% with a collection rate of 75%, or 31.26% with a collection rate of 85%. In this case, the collection system reform cannot effectively solve the problem associated with financial imbalance risk.

5.3. Optimization Scenario 2: Postponing the Retirement Age. The current retirement age policy in China was adopted at the beginning of the 1950s, when the life expectancy was less than 45 years. However, the life expectancy is more than 77 years in recent years and is expected to continue to grow in the future. The Chinese government proposed to delay the retirement age in 2013 and emphasized several times that the policy would be implemented. However, the detailed scheme has not been announced yet. Raising the retirement age will contribute to the full use of human resources and enhancement of the sustainability of pension funds. Due to its feasibility and effectiveness, the policy of postponing the retirement age is favored by many countries (Borsch-Supana et al. [40]). Table 3 shows the reforms based on the retirement age policy in four representative countries. To deal with the resistance to the implementation of this policy, all of these countries choose to gradually raise the retirement age.

Based on the experiences in developed countries and the situation in China, two schemes are designed for postponing the retirement age. Scheme 1: Raise the retirement age for female workers, female carders, and males from 2022, 2032, and 2042, respectively. The retirement age is delayed by one year every two years, so that the retirement age will rise to 65 in 2051. Scheme 2: Raise the retirement age for female workers, female carders, and males from 2022 at the same time. The retirement age is delayed by one year every two

Table 2: Financial balance of the UEBPI fund in optimization scenario 1.

Scenario	Collection rate (%)	Years of the current deficit	Years of the accumulated deficit	Accumulated deficit in 2060 (billion RMB)	Actuarial balance rate (%)
Baseline scenario	65	2020–2060	2024–2060	629455.86	43.34
Optimization	75	2020–2060	2026–2060	554624.52	36.49
scenario 1	85	2023–2060	2029–2060	479372.09	31.26

Table 3: Reforms in the retirement age policy of representative countries.

	Before reform	After reform	Detailed scheme
U.S.	Male: 65 years Female: 65 years	Male: 67 years Female: 67 years	From 2003, postponing two months each year, till 67 years in 2017
U.K.	Male: 65 years Female: 60–65 years	Male: 68 years Female: 68 years	From 2016 to 2018, female increases to 65 years. From 2034 to 2036, both male and female increase to 67 years, and increase to 68 from 2044 to 2046.
Germany	Male: 65 years Female: 65 years	Male: 67 years Female: 67 years	From 2012, postponing one month each year, till 66 years in 2023. Form 2023, postponing two months each year, till 67 years in 2029.
Australia	Male: 65 years Female: 60 years	Male: 67 years Female: 67 years	From 1995, female postpones six months every 1.5 years, till 65 years in 2017. From 2018, both and male and female postpone six months every 1.5 years, till 67 years in 2022.

years, thereby reaching 65 in 2051, 2041, and 2031 for the above three subgroups of pension participants. Please be noted that we choose 2022 as the first year to implement the policy of postponing the retirement age; this is because the Ministry of Human Resources and Social Security of the People's Republic of China emphasizes that the policy would be implemented in 2022. And we predict the financial sustainability of pension funds in optimization scenario 2.

It can be seen from Table 4 that postponing the retirement age has an insignificant impact on the number of years for current deficit or accumulated deficit. The main reason is that the policy starts in 2022, and the growth rate of the number of contributors cannot compare with that of the population aging. However, the policy may take effect with time, thereby narrowing the gap between pension fund's income and expenditure, and further resulting in a substantial decrease in the accumulated deficit. Intuitively, postponing the retirement age increases the number of contributors, decreases the number of retirees, extends the contributory years, and reduces the years of receiving benefits. Thus, it leads to more income and less expenditure. If we take a step forward, postponing the retirement age brings impacts to other factors as well. Firstly, it would increase the pension replacement rate, which may result in more expenditure. Secondly, given the growth rate of wage, it would be favorable to raise the wage at the time of retirement, which leads to a higher payment base. Therefore, the impact of postponing the retirement age on the financial sustainability of the UEBPI fund is uncertain. According to Table 4, compared with the baseline scenario, the amount of accumulated deficit in 2060 is decreased by 46.15% under Scheme 1 and 50.59% under Scheme 2, and the corresponding actuarial balance rate is reduced by 14.46 and 15.01 percentage, respectively. To sum up, postponing the retirement age would significantly improve the financial sustainability of the UEBPI fund. However, the fund still faces a high risk of financial imbalance, and there is no space for the reduction of the contribution rate.

5.4. Optimization Scenario 3: Introducing External Finance. As one of the major financing sources for the UEBPI fund, the government is responsible for maintaining its financial balance. Although China's UEBPI system does not stipulate the government's contribution responsibility, the government still provides fiscal subsidies to the provinces with an annual deficit in funds. Zheng [3] suggested that fiscal subsidy should be fixed at a certain level, so that the pension system could achieve a balanced development by itself. According to "Statistical Bulletin on the Development of Human Resources and Social Security," the fiscal subsidy accounted for 18%–21% of the UEBPI fund's expenditure from 2015 to 2019, with an average value of 20.17%. Apart from the fiscal subsidy, the transfer of state-owned capital and the use of national social security funds also present key financing sources. To mitigate the impact of population aging on the pension fund, the State Council asked the state-owned enterprises to transfer 10% of their earnings in terms of shares and profits to fill the funding gap. Based on the data from "Finance Year Book of China," we calculate that the state-owned capital available to be transferred to the UEBPI fund is 104.98 billion RMB in 2018 and 116.07 billion RMB in 2019, accounting for 2.36% of the fund's expenditure. The national social security fund is a reserve fund to supplement the pension fund gap during the peak period of population aging. According to the scale of the national social security fund and its investment return, it is supposed to afford at least 1% of the annual expenditure of the UEBPI fund. Therefore, we assume that the external finance accounts for 23.5% of the UEBPI fund's expenditure in each future year.

As shown in Table 5, the earliest year of the current deficit and the accumulated deficit is 2023 and 2030, respectively. The amount of accumulated deficit in 2060 is 365175.33 billion RMB, and the actuarial balance rate is 31.14%. Compared with the baseline scenario, with external finance, the time for financial imbalance risk is delayed by 6 years, the accumulated deficit is lowered by

Table 4: Financial balance of the UEBPI fund in optimization scenario 2.

Scenario	Retirement age	Years of the current deficit	Years of the accumulated deficit	Accumulated deficit in 2060 (billion RMB)	Actuarial balance rate (%)
Baseline scenario	Current	2020–2060	2024–2060	629455.86	43.34
Optimization scenario 2	Scheme 1	2020–2060	2024–2060	338934.25	28.88
	Scheme 2	2020–2060	2025–2060	311009.23	28.33

Table 5: Financial balance of the UEBPI fund in optimization scenario 3.

Scenario	Percentage of external finance	Years of the current deficit	Years of the accumulated deficit	Accumulated deficit in 2060 (billion RMB)	Actuarial balance rate (%)
Baseline scenario	0	2020–2060	2024–2060	629455.86	43.34
Optimization scenario 3	23.5%	2023–2060	2030–2060	365175.33	31.14

41.99%, and the actuarial balance rate is reduced by 12.20 percentage. It indicates that the introduction of external finance will improve the sustainability of the UEBPI fund. However, the fund is still confronted with a huge financial imbalance risk.

5.5. Optimization Scenario 4: Combinatorial Optimization. The results of 1–3 optimization scenarios show that the above three strategies are available to decrease the financial imbalance risk. According to the scale of the accumulated deficit and the actuarial balance rate, the effects of the above three strategies from high to low are postponing the retirement age, introducing external finance, and implementing the collection system reform. However, the accumulated deficit of the UEBPI fund in 2060 is still large. In that case, we combine any two of the above three strategies or all of them, namely, the optimization scenario 4. The forecasting results are shown in Table 6.

It can be seen from Table 6 that, with the combination of any two strategies, the financial sustainability of the UEBPI fund is significantly improved. Besides, the fund could last 7–34 years on a sustainable basis; that is, 3–30 years longer than that in the baseline scenario. In the case with all the three strategies being implemented, the fund can almost maintain its financial sustainability till 2060, its accumulated surplus in 2060 is between −15.80 trillion RMB and 210.42 trillion RMB, and the actuarial balance rate is 12.00%–16.36%. To maintain the vertical financial balance from 2020 to 2060, the contribution rate could be further reduced by 0–4 percentage. Therefore, it is a prerequisite to implement a package of strategies to control the financial imbalance risk and to provide space for contribution rate reduction.

6. Sensitivity Analysis

To examine the robustness of the above conclusions and provide suggestions for China's UEBPI system reform, we further analyze the sensitivity of three parameters, namely, the return on investment of the fund, the growth rate of pension benefits, and the nominal interest rate of the individual account. Results of the sensitivity analysis are summarized in Table 7.

Keeping other parameters constant, if the return on investment increases by one percentage, that is, from 3% to 4%, the conclusions remain hold. In specific, first, in the baseline scenario with no strategy intervention, the fund could only be sustainably operated until 2023. Second, by implementing the collection system reform only, if the collection rate increases from 65% to 75%–85%, the fund could last for additional 2–5 years. Third, by postponing the retirement age only, the fund could only last for an additional 0–1 year under both the schemes. Fourth, by introducing external finance only, the fund could last for additional 6 years. Fifth, with the combination of any two strategies, the fund could last for additional 3–31 years. Sixth, in the case that the three strategies are implemented at the same time, the fund will almost not have an accumulated deficit before 2060, and the contribution rate is available for a further reduction of 0–4.42 percentage.

Keeping other parameters constant, if the economic sharing factor in the pension benefits growth formula decreases by 0.25, that is, from 0.5 to 0.25, the conclusions remain unchanged. The financial sustainability of the UEBPI fund enhances in each scenario, indicating that a decrease in the growth rate of pension benefits may lead to the decrease of financial imbalance risk. In the case that the all the three strategies are implemented, the actuarial balance rate is 9.80%–13.46%, which means the contribution rate could be further reduced by 2.54–6.20 percentage.

Keeping other parameters constant, if the nominal interest rate of the individual account decreases by one percentage, that is, from 5% to 4%, the conclusions are also right. The results also show that the reduction of the nominal interest rate could decrease the financial imbalance risk. More importantly, if the three strategies are implemented together, the actuarial balance

Table 6: Financial balance of the UEBPI fund in optimization scenario 4.

Collection rate (%)	Postponing retirement age scheme	Percentage of external finance	Years of the accumulated deficit	Accumulated deficit in 2060 (billion RMB)	Actuarial balance rate (%)
65	N/A	0	2024–2060	629455.86	43.34
75	Scheme 1	0	2027–2060	249290.03	23.97
85	Scheme 1	0	2031–2060	158865.11	20.21
75	Scheme 2	0	2035–2060	214709.35	21.75
85	Scheme 2	0	2053–2060	109071.36	18.25
75	N/A	23.5%	2035–2060	288430.07	25.92
85	N/A	23.5%	2042–2060	208173.54	21.93
65	Scheme 1	23.5%	2032–2060	119880.02	20.10
65	Scheme 2	23.5%	2054–2060	80229.67	18.15
75	Scheme 1	23.5%	2059–2060	15798.01	16.36
85	Scheme 1	23.5%	N/A	−127517.14	13.49
75	Scheme 2	23.5%	N/A	−61898.57	14.67
85	Scheme 2	23.5%	N/A	−210417.53	12.00

Table 7: Results of the sensitivity analysis of three parameters.

Collection rate (%)	Postponing retirement age scheme	Percentage of external finance	Return on investment		Growth rate of pension benefits		Nominal interest rate	
			Years of the accumulated deficit	Actuarial balance rate (%)	Years of the accumulated deficit	Actuarial balance rate (%)	Years of the accumulated deficit	Actuarial balance rate (%)
65	N/A	0	2024–2060	41.96	2024–2060	37.47	2024–2060	42.19
75	N/A	0	2026–2060	35.30	2027–2060	31.41	2026–2060	35.50
85	N/A	0	2029–2060	30.21	2031–2060	26.77	2029–2060	30.38
65	Scheme 1	0	2024–2060	28.47	2025–2060	24.51	2024–2060	28.17
65	Scheme 2	0	2025–2060	25.64	2027–2060	22.57	2025–2060	25.67
65	N/A	23.5%	2030–2060	30.06	2032–2060	26.66	2030–2060	30.26
75	Scheme 1	0	2027–2060	23.61	2029–2060	20.18	2027–2060	23.34
85	Scheme 1	0	2032–2060	19.89	2039–2060	16.87	2032–2060	19.66
75	Scheme 2	0	2035–2060	21.16	2053–2060	18.50	2035–2060	21.18
85	Scheme 2	0	2054–2060	17.73	N/A	15.38	2055–2060	17.75
75	N/A	23.5%	2035–2060	24.99	2040–2060	22.03	2035–2060	25.16
85	N/A	23.5%	2043–2060	21.11	2051–2060	18.50	2042–2060	21.26
65	Scheme 1	23.5%	2033–2060	19.76	2057–2060	16.76	2033–2060	19.56
65	Scheme 2	23.5%	2055–2060	17.60	N/A	15.28	2055–2060	17.65
75	Scheme 1	23.5%	2060	16.06	N/A	13.46	N/A	15.88
85	Scheme 1	23.5%	N/A	13.23	N/A	10.94	N/A	13.07
75	Scheme 2	23.5%	N/A	14.19	N/A	12.17	N/A	14.23
85	Scheme 2	23.5%	N/A	11.58	N/A	9.80	N/A	11.61

rate will be 11.61%–15.88%, indicating that the contribution rate could be further reduced by 0.12–4.39 percentage.

7. Concluding Remarks

Combined with the regulation and reform tendency of China's UEBPI, we construct an actuarial model to analyze the financial imbalance risk of contribution rate reduction in several scenarios and examine the feasible ways to further reduce the contribution rate. The main findings are as follows. First, in the baseline scenario with no strategy intervention, the UEBPI fund will have accumulated deficits since 2024 and the actuarial balance rate is 43.34% between 2020 and 2060. It indicates that the fund is confronted with a high risk of financial imbalance, and there is no space for further reduction of the rate. Second, in the scenarios with single strategy implemented (the collection system reform, delay of retirement age, or the introduction of external finance), the financial sustainability of the UEBPI fund could be improved to some extent. However, the financial imbalance risk remains huge, and therefore limits the space for contribution rate reduction. Third, in the scenario with the combination of any two said strategies, the fund could be operated on a sustainable basis until 2027 at least, but the actuarial balance rate is still greater than 16%. In the case that all the three strategies are implemented, the fund will almost not have an accumulated deficit before 2060, and the contribution rate can be further reduced by 0–4 percentage. Fourth, whether we choose to increase the return on investment or decrease the growth rate of pension benefits and the nominal interest rate, these strategies will help to alleviate the financial imbalance risk of the UEBPI fund.

Based on the above conclusions, we put forward several policy recommendations for the control of the financial

imbalance risk of the UEBPI fund. The first is to implement the collection system reform quickly. If the information system of tax authorities is applied to pension insurance contribution collection, it would be possible to avoid contribution evasion, and to increase the collection rate. The second is to carry out the postponing retirement age policy as soon as possible. The retirement age should gradually be raised and should be set differently based on the employees' sex and occupation. It is also plausible to provide a buffer period, so that individuals could be adapted to this policy. The third is to broaden financing sources for the pension system. On the one hand, it is necessary to clarify the specific responsibility of the government in the pension system and determine the scale of fiscal subsidies as a certain percentage of the fund's expenditure. On the other hand, it is advisable to speed up the process of transferring state-owned capital to pension funds and continue to enrich the fund's income. Fourthly, some possible strategies also included strengthening the investment management capabilities of pension funds, relaxing restrictions on the investment scope and ratio, establishing a reasonable pension benefits adjustment mechanism, and lowering the nominal interest rate of the individual account.

Data Availability

All the data are available from National Bureau of Statistics at http://www.stats.gov.cn/tjsj/ndsj/ and the Statistical Bulletin on the Development of Human Resources and Social Security at http://www.mohrss.gov.cn/gkml/ghtj/tj/ndtj/.

Conflicts of Interest

The authors declare that they have no conflicts of interest.

Acknowledgments

This study was supported by the National Natural Science Foundation of China (72004183) and the Fundamental Research Funds for the Central Universities (JBK2103001).

References

[1] X. Liu, Y. Zhang, L. Fang, Y. Li, and W. Pan, "Reforming China's pension scheme for urban workers: liquidity gap and policies' effects forecasting," *Sustainability*, vol. 7, pp. 10876–10894, 2015.

[2] Z. Q. Luo, Z. Y. Chen, and A. Lu, "A study on the effects of population factors on the payment balance of basic pension insurance funds in China," *Forecasting*, vol. 29, no. 2, pp. 42–46, 2010.

[3] Y. Xie, X. Zhang, H. Lv, and X. Guo, "The new fertility policy and the actuarial balance of China urban employee basic endowment insurance fund based on stochastic mortality model," *Mathematical Problems in Engineering*, vol. 2020, Article ID 3596384, 12 pages, 2020.

[4] Y. Zeng and B. Yu, "Tackling China's pension fund payment crisis: will the 'Two-Child Policy' be the answer? An example with the basic pension insurance program for urban employees," *China Economist*, vol. 5, no. 1, pp. 20–36, 2015.

[5] World Bank, *Averting the Old-Age Crisis: Policies to Protect the Old and Promote Growth*, The World Bank, Washington, DC, USA, 1994.

[6] R. Holzmann and R. Hinz, *Old-Age Income Support in the 21st Century: An International Perspective on Pension Systems and Reform*, The World Bank, Washington, DC, USA, 2005.

[7] D. Blake and L. Mayhew, "On the sustainability of the UK state pension system in the light of population ageing and declining fertility," *The Economic Journal*, vol. 116, no. 6, pp. 286–305, 2006.

[8] J. D. Rauh and R. Novymarx, "Policy options for state pension systems and their impact on plan liabilities," *Journal of Pension Economics and Finance*, vol. 10, no. 2, pp. 173–194, 2011.

[9] A. Billig and J. C. Ménard, "Actuarial balance sheets as a tool to assess the sustainability of social security pension systems," *International Social Security Review*, vol. 66, no. 2, pp. 31–52, 2013.

[10] C. Metzger, "An actuarial balance sheet of the Swiss old-age pension scheme," *International Social Security Review*, vol. 71, no. 1, pp. 25–49, 2018.

[11] J. Bongaarts, "Population aging and the rising cost of public pensions," *Population and Development Review*, vol. 30, no. 1, pp. 1–23, 2004.

[12] Y. Sin, *China Pension Liabilities and Reform Options for Old Age Insurance*, World Bank Working Paper, vol. 2005-1, 2005.

[13] A. A. Belolipetskii and M. A. Lepskaya, "A mathematical model of pension fund operation and methods of fund stability analysis," *Computational Mathematics and Modeling*, vol. 29, no. 2, pp. 233–243, 2018.

[14] W. L. Heeringa and A. L. Bovenberg, "Generational impacts of demographic changes in Pay-as-you-go pension schemes: measurement and application to The Netherlands," *De Economist*, vol. 160, no. 1, pp. 1–16, 2012.

[15] T. Liu and L. Sun, "Pension reform in China," *Journal of Aging Society Policy*, vol. 28, no. 1, pp. 15–28, 2016.

[16] P. Whiteford and E. Whitehouse, "Pension challenges and pension reforms in OECD countries," *Oxford Review of Economic Policy*, vol. 22, no. 1, pp. 78–94, 2006.

[17] B. Lin, "Impact of population ageing on China's old-age insurance system for urban employees," *Chinese Journal of Population Science*, vol. 24, no. 1, pp. 84–92, 2010, in Chinese.

[18] P. Jing and Q. Hu, "The Potential cutting extent for social pooling contribution rate of state basic pension scheme for enterprise employees," *Chinese Journal of Population Science*, vol. 31, no. 1, pp. 21–33, 2017, in Chinese.

[19] Y. Zeng, N. Liu, and J. Gao, "The decreasing space of China's basic pension insurance for urban employees and the effect on public expenditures," *Journal of Finance and Economics*, vol. 44, no. 12, pp. 70–84, 2018, in Chinese.

[20] Y. Guo and Y. Zhang, "Can stringent contribution collection reduce contribution rate of basic social pension insurance for urban employees?" *Insurance Studies*, vol. 26, no. 2, pp. 101–113, 2019, in Chinese.

[21] Y. Zeng, S. Li, and X. Li, "Research on the influence of tax authority's full responsibility of collecting social security fee on the space of reducing the contribution rate of pension insurance," *Public Finance Research*, vol. 41, no. 2, pp. 96–112, 2020, in Chinese.

[22] A. Kugler and M. Kugler, "Labor market effects of payroll taxes in developing countries: evidence from Colombia," *Economic Development and Cultural Change*, vol. 57, no. 2, pp. 335–358, 2009.

[23] I. Iturbe-Ormaetxe, "Salience of social security contributions and employment," *International Tax and Public Finance*, vol. 22, no. 5, pp. 1–19, 2015.
[24] S. Ma, X. Meng, and L. Gan, "Effect to pension on employment and firm average wage," *China Economic Quarterly*, vol. 3, no. 3, pp. 969–1000, 2014, in Chinese.
[25] N. Chaudhry, H. Yong, and V. Chris, "How does the funding status of defined benefit pension plans affect investment decisions of firms in the United States?" *Journal of Business Finance and Accounting*, vol. 141, no. 23, pp. 4513–4525, 2016.
[26] E. Saez, B. Schoefer, and D. Seim, "Payroll taxes, firm behavior, and rent sharing: evidence from a young workers' tax cut in Sweden," *American Economic Review*, vol. 109, no. 5, pp. 1717–1763, 2019.
[27] J. Tang and J. Feng, "Do social security contributions affect the capital-labor ratio: evidence from China," *Economic Research Journal*, vol. 65, no. 11, pp. 87–101, 2019.
[28] I. Ehrlich and J. Kim, "Social security and demographic trends: theory and evidence from the international experience," *Review of Economic Dynamics*, vol. 10, no. 1, pp. 55–77, 2007.
[29] S. L. Yew and J. Zhang, "Optimal social security in a dynastic model with human capital externalities, fertility and endogenous growth," *Journal of Public Economics*, vol. 93, no. 3, pp. 605–619, 2009.
[30] L. Fanti and L. Gori, "Economic growth and stability with public Pay-as-you-go pensions and private intra-family old-age insurance," *Research in Economics*, vol. 66, no. 3, pp. 219–229, 2012.
[31] H. Peng, H. Qiu, C. Zhu, and A. Li, "Pension contribution rate, public educational investment and pension replacement rate," *The Journal of World Economy*, vol. 41, no. 12, pp. 148–168, 2018.
[32] X. Yi, R. Guo, and Y. Qi, "Stabilization of chaotic systems with both uncertainty and disturbance by the UDE-based control method," *IEEE Access*, vol. 8, no. 1, pp. 62471–62477, 2020.
[33] L. Liu, B. Li, and R. Guo, "Consensus control for networked manipulators with switched parameters and topologies," *IEEE Access*, vol. 9, no. 1, pp. 9209–9217, 2021.
[34] Y. Cai, "China's new demographic reality: learning from the 2010 census," *Population and Development Review*, vol. 39, no. 3, pp. 371–396, 2013.
[35] W. Chen and S. Yang, "China's fertility in 2010: an indirect estimation using brass P/F ratio method," *Population Research*, vol. 38, no. 6, pp. 16–24, 2014, in Chinese.
[36] Y. Jiang, "Study on the intergenerational balance of China's pension system for urban employees," *World Economic Papers*, vol. 27, no. 1, pp. 58–69, 2009, in Chinese.
[37] P. Barrand, S. G. Ross, and G. Harrison, "Integrating a unified revenue administration for tax and social contribution collections: experiences of Central and Eastern European countries," *IMF Working Papers*, WP/04/237, 2004.
[38] L. D. Enoff and R. Mckinnon, "Social security contribution collection and compliance: improving governance to extend social protection," *International Social Security Review*, vol. 64, no. 4, pp. 99–119, 2011.
[39] C. Gillion, *Social Security Pensions: Development and Reforms*, International Labor Organization, Geneva, Switzerland, 2000.
[40] A. Börsch-Supana, K. Härtla, and A. Ludwiga, "Aging in Europe: reforms, international diversification and behavioral reactions," *American Economic Review*, vol. 104, no. 5, pp. 224–229, 2014.